Bubble Coalescence in a Range of Fluids: Surface and Viscous Effects

by

Kathryn Tse

A thesis submitted to the Faculty of Engineering
of The University of Birmingham
for the degree of
Doctor of Philosophy

School of Chemical Engineering
The University of Birmingham
Birmingham B15 2TT
UNITED KINGDOM

June 2000

Abstract

An in-depth investigation has been carried out into the use of a coalescence cell as a predictive tool for determining the coalescence behaviour in larger scale process apparatus. Within the cell, conditions can be manipulated to allow separate examination of the influences of system and operating parameters. The study has demonstrated that a much broader range of coalescence behaviour can be observed in the cell, beyond the step change commonly reported in the literature, by altering the range and combination of operating parameters (such as gas flow rate and nozzle separation distance). Coalescence behaviour was investigated in a range of well-defined fluids of differing viscosities, including several pure liquids (water, propan-1-ol and silicone fluid), solutions of various electrolyte (Na_2SO_4, $MgSO_4$, KI, HNO_3), *n*-alcohol (propan-1-ol) and non-polar solute (glycerol, sucrose, PPG) species and additionally, for a range of gas types (air, nitrogen, hydrogen and xenon). In all systems, coalescence behaviour was observed to be heavily dependent on operating parameters such as the contact pressure and temperature, which could moderate the influences of the gas-liquid system itself. To enable comparisons with the results obtained in the cell, the coalescence behaviour in laboratory-scale bubble columns was assessed. Observations were made of a previously unreported coalescence dependent break-up mechanism. Responses observed in the coalescence cell were seen to approach trends observed in the small-scale systems, despite being attributed to very different influences. As a general diagnostic tool, use of the cell is disadvantaged by the degree of rigour which must be applied to both experiments and the subsequent interpretation of results; however, as an analytical tool for investigating the coalescence process, the cell shows potential for advancing the current state of knowledge.

Acknowledgements

I wish to thank my supervisors Professor A. W. Nienow and Dr C. M. McFarlane for their advice and assistance over the duration of this project. Thanks also to Dr T. M. Martin, of DSM (Netherlands), for his constant support and enthusiasm over this time.

For financial support, I am indebted to the sponsorship of The University of Birmingham and DSM (Netherlands).

Thanks to Mr R. Badham, Mr T. Eddleston, Mr J. Homer and Mrs K. Dyster for the technical support and friendship they have provided.

For the loan of the Kodak Ekta-Pro High Speed Camera from the EPSRC Instrument Pool, I wish to thank Mr A. T. Walker for technical support and unfailing helpfulness.

I would like to acknowledge the contribution of Mr S. Palmer who worked on the project during his MSc.

Thanks to all my friends and colleagues who have provided lively discussion, encouragement and support over this time, especially Ms L. Boon, Mr K. Gezork, Dr C. Man, Dr S. Munaweera and Mr A. Nixon. Many thanks also to Dr A. W. Pacek, Dr S. Stocks and Dr E. Thwaites for helpful discussions and moments of insight.

Table of Contents

List of Figures

Chapter 2

List of Tables

Chapter 7

Nomenclature

Roman Symbols

A	Hamaker constant	[Nm]
a	area	[m^2]
B	retarded van der Waals coefficient	[Nm]
c, C	concentration	[$moldm^{-3}$]
c_t, C_{trans}	'transition' concentration	[$moldm^{-3}$]
D	Diffusion coefficient	[m^2s^{-1}]
d, D	diameter	[m]
d_{10}	arithmetic mean bubble diameter	[m]
d_{32}	Sauter mean bubble diameter	[m]
d_{43}	volume moment mean bubble diameter	[m]
E	surface elasticity	[Nm^{-1}]
f	frequency	[s^{-1}]
F	force	[N]
G	Gibbs interaction energy	[J]
h	film thickness	[m]
h_c	critical film thickness at which rupture occurs	[m]
M	molecular weight	[$gmol^{-1}$]
n	number of bubbles in class	[-]
N	total number of bubbles in distribution	[-]
P	pressure	[Nm^{-2}]
ΔP	pressure difference	[Nm^{-2}]
q(x)	probability density function	[-]
Q(x)	cumulative distribution function	[-]
Q	flow rate	[$mlmin^{-1}$]
R	ideal gas constant	[$Jg^{-1}mol^{-1}K^{-1}$]
r	radius	[m]

Re_b	Bubble Reynolds Number = $\frac{\rho U_b D_b}{\mu}$	[-]
Re_d	particle Reynolds Number	[-]
Re_{trans}	Reynolds Number at 'transition' concentration	[-]
t	time	[s]
t_b	bubble lifetime	[s]
t_c	coalescence time	[s]
t_{con}	contact time, for a non-coalescent event	[s]
T	temperature	[°C]
u_s	superficial gas velocity	[ms^{-1}]
U	rise velocity	[ms^{-2}]
$\overline{U}$	average rise velocity	[ms^{-2}]
v	velocity	[ms^{-1}]
v_{int}	interfacial velocity	[ms^{-1}]
V_R	Reynolds velocity of thinning	[ms^{-1}]
x	class size of distribution	[-]
z	ionic valency	[-]

Greek Symbols

ε	hold-up	[-]
η	number of events	[-]
λ	collision efficiency	[-]
μ	dynamic viscosity	[$Nm^{-2}s$]
Π	disjoining pressure	[Nm^{-2}]
ρ	density	[kgm^{-3}]
σ	surface tension	[Nm^{-1}]
τ	contact time	[s]
ω	coalescence frequency measured in bubble column	[s^{-1}]
ω_{cell}	coalescence frequency measured in coalescence cell	[%]

Subscripts

b	bubble
c	continuous phase
d	dispersed phase
g	gas phase
l	liquid phase
trans	'transition'
z	height up column

Chapter 1
Introduction

Processes involving the dispersion of one or more gases into a liquid are commonplace throughout the processing industries, for example, in many chemical reactions and biochemical fermentations. In each case, the dispersion of gas through the liquid leads to the formation of multi-phase systems, which are often characterised by complex flow patterns.

The nature of the dispersion is crucially dependent on the ultimate aim of the process. For example, in many systems, it is desirable to maximise the interfacial area between the gas and liquid phases and to ensure that bubbles reside in the bulk sufficiently long to allow for mass transfer to occur prior to disengagment. These requirements suggest a dispersion of small bubbles is desirable, although if the dispersion is too fine, bubbles will fail to disengage readily. Conversely, in systems which aim for phase separation, maximising contact areas is no longer the primary concern, rather rapid disengagement of the dispersed gases from the liquid is required, thereby necessitating larger bubble sizes which coalesce readily. Often, effective operation of a process requires consideration of both aspects, such that dispersion is required in one part of the process and phase separation further downstream.

In these process applications, therefore, control of the bubble size distribution is necessary to achieve the process aim. This in turn, depends on the equilibrium between bubble coalescence and break-up occurring in the bulk fluid. In addition to the effects of process variables, such as gas flow rate and for mechanically agitated systems, impeller speed, this equilibrium will depend on the nature of the gas-liquid interfaces and the interactions between the bubbles themselves. The constant collisions between bubbles in dynamic systems may lead to coalescence, whereas interactions between the bubbles and fluid stresses may result in bubble break-up. Whilst bubble break-up is mainly determined by local hydrodynamic considerations (such as the micro scale of turbulence, Prince and Blanch, 1990a), coalescence is a complex phenomenon, which depends not only on local flow conditions, (which determine collision velocities and bubble densities), but is also crucially influenced by the nature of the gas-liquid interface itself. Although coalescence may be thermodynamically favourable (due to the reduced surface area to volume ratios that result), the process may be resisted by the energetic considerations of the gas-liquid interface such that following a

collision, bubbles will separate without coalescing. For this reason, a better understanding of the coalescence process would appear to be a fundamental step in controlling bubble size distributions. Consequently, considerable efforts have gone into investigating the physical mechanisms of coalescence and the influence of process conditions, with the ultimate aim of integrating the information into design and modelling considerations for improved reactor performance.

1.1 Motivation

Despite intensive research into bubble coalescence, the current state of knowledge only allows systems to be broadly categorised as either fully coalescing or coalescence repressed. Within each of these categories, however, are a wide range of observed behaviours that currently resist further classification. Bubble sizes in coalescing systems are generally much larger than those observed in coalescence repressed systems (Marrucci and Nicodemo, 1967), as the maximum bubble size is determined by the coalescence break-up equilibrium and not the initial bubble size, as in coalescence repressed systems. However, coalescing liquids generally include only pure liquids and very dilute solutions, which are of limited use in industrial processes. Within the larger category of coalescence repressed systems, the system behaviour appears to be very dependent on the type of process equipment (for example, agitated vessel or bubble column) and the flow regime under which the process is operated (homogeneous or heterogeneous, Zahradnik et al., 1995, 1987). Additional research is necessary to investigate these systems, to determine whether further classifications is possible and to enable system behaviour to be more easily interpreted.

The mechanism of coalescence repression is still the subject of considerable debate, although almost all studies acknowledge the extremely complex interactions between the many aspects of surface phenomena which influence one or all stages of the process. In addition to the influences arising from the native gas-liquid system, the type of processing equipment and hence the system hydrodynamics, exerts a significant influence on the coalescence behaviour observed. For all these reasons, it is most unlikely that a single variable, which dictates the extent of coalescence in a process system, will ever be identified. Therefore, it is of immediate interest to develop a test system that shows direct relevance to the behaviour of larger process systems and can accurately indicate the degree of coalescence behaviour occurring in such a system. In the first instance, such an objective is probably best achieved

by developing a test system which would enable the effects of the gas and liquid properties to be studied separately from the complex hydrodynamic considerations.

Ideally, such a test system would operate under a range of well-defined and controlled conditions. To ensure maximum applicability, such simplified conditions would need to be linked directly to the various operating regimes observed in process equipment. One such approach would be to observe isolated contact and coalescence events, although it must be demonstrated that the information obtained is directly relevant to the same process occurring under the myriad of influences present in operating systems. Indeed, this is an approach which has been used in several studies reported in the literature (Lessard and Zieminski, 1971, Zahradnik et al., 1987, 1995, 1997, 1999, Oolman and Blanch, 1986, amongst others) where pairs of bubbles are contacted in apparatus known as a coalescence cell. According to the literature, such equipment is simple to use, provides results which require little interpretation and are very effective at determining the point at which systems become seriously coalescence inhibited.

1.2 Aims of this Study

The aim of this study therefore, was to thoroughly investigate the use of a simple coalescence cell, as a tool for predicting the responses of various systems to a variety of operating conditions. Previous studies reported in the literature have focussed largely on utilising similar equipment under a narrow range of operating conditions and many have not demonstrated applicability of the equipment to the behaviour of larger scale process systems. Consequently, this study aimed to extend the range of conditions which could be investigated in the cell. It was of particular interest to extend the narrow range of gas flow rates investigated previously (bubble frequencies up to 5 s^{-1}, Drogaris and Weilland, 1983) to significantly higher values, in an attempt to approximate the highly turbulent conditions of agitated vessels and bubble columns operating under the heterogeneous regime. Whereas previous coalescence cell studies have aimed to observe either bulk system behaviour or the small-scale behaviour of individual bubble pairs, this study aimed to combine the two approaches to provide an improved understanding of how the coalescence process is affected by system hydrodynamics.

The first objective in the study was to validate the cell behaviour, which was achieved through a series of investigations into the coalescence behaviour of pure liquids, considering

effects of surface tension and liquid viscosity. Following this, the study aimed to investigate the coalescence behaviour of solutions, once again considering especially the effects of solutes on the nature of the gas-liquid interface and liquid viscosity. To achieve the aim of investigating both bulk system and small-scale coalescence behaviour, supplementary high-speed video studies was used to provide a high level of scrutiny for both coalescence and non-coalescence events, making the study unique in the literature. The final project objective was to extend the coalescence cell studies to observations of in-situ coalescence in small bubble columns to demonstrate the usefulness of the cell as an indicator of behaviour in dynamic systems.

1.3 Layout of Thesis

The study begins with a detailed review of the current understanding of the coalescence process (Chapter 2), considering both possible mechanisms and the consequences of bubble coalescence on system behaviour. Following this, Chapter 3 discusses the experimental methods and materials used in the study. A detailed examination of the use of the coalescence cell is conducted in Chapter 4, which specifically addresses the need to define operating parameters rigorously, as a result of the complexity inherent in the practical application of the experimental equipment. These considerations are then extended to discussions of coalescence cell studies with model fluids. To provide well defined operating systems, experiments were carried out with inviscid liquids (solutions of electrolytes and a surface-active species, Chapter 5) and in viscosity modified solutions (Chapter 6). Finally, in Chapter 7, the results of studies in bubble columns are presented as an insight into the coalescence process in dynamic systems and attempts made to link the observed behaviour with that previously seen in the coalescence cell. Conclusions from the study and suggestions for further work are presented in Chapter 8.

Chapter 2
Bubble Coalescence: A Review

There is an enormous body of work in the literature concerning coalescence in gas-liquid systems, which encompasses mathematical models of the various sub-processes to experimental studies in the most specialised of contacting equipment. The current review considers the mechanism of bubble coalescence and identifies the important physical processes (Section 2.1), before examining the various modelling approaches to the sub-processes and to coalescence in a turbulent environment (Section 2.2) before finally reviewing experimental studies of coalescence (Section 2.3).

2.1 The Process Of Bubble Coalescence

Bubble coalescence is generally accepted to be a three-step process (Figure 2.1), influenced by a combination of hydrodynamic and surface chemical parameters.

1. In the first instance, two bubbles approach each other to within a distance between 10 - 100μm. The contact surfaces flatten and a thin film forms between the two. This step is controlled by the hydrodynamics of the bulk liquid phase (Oolman and Blanch, 1986) and depends on the extent of energy dissipation in the system.
2. Thinning occurs as liquid drains from the intervening film until it is about 100 nm thick. Initially film drainage occurs under the influence of gravity and suction due to capillary forces arising from surface curvature at the edges of the film. However, once the film thickness reduces to about 100 nm, the effect of intermolecular forces between surface molecules become significant. Van der Waals attractions will increase the rate of drainage whereas repulsion arising from electrostatic double layers will decrease it. If the

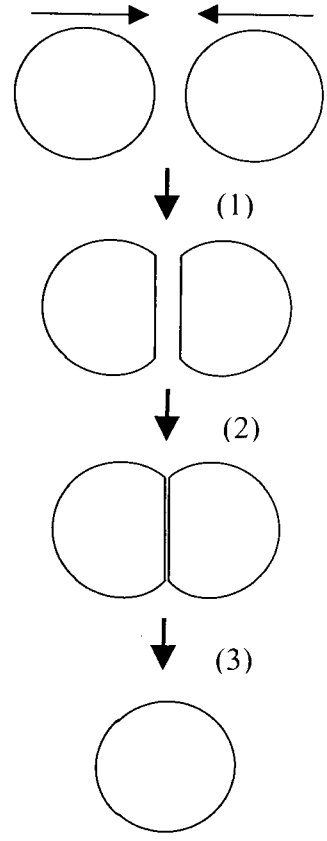

Figure 2.1

The process of coalescence: (1) contact (2) film drainage (3) film rupture.

forces due to border suction, van der Waals attraction and double layer repulsion equilibrate, the film becomes 'meta-stable' and further thinning will occur only slowly. Conversely, if attractive forces predominate, the film becomes unstable, collapsing at a thickness between 50 - 100nm (Vrij, 1966).

3. As the film reaches a thickness of approximately 10 nm it collapses, rupturing via an instability mechanism. Unstable films will rupture spontaneously once a characteristic 'critical thickness' is reached.

Film drainage is considered to be slow and is therefore the rate-controlling step in the process, as film rupture is very rapid. Coalescence will only occur if the two bubbles remain in contact for longer than the time required for the film to thin to the rupture thickness. If the contact time is less than the drainage time, the bubbles will separate without coalescing.

What factors influence the coalescence process? Obvious influences are those which will affect conditions at the gas-liquid interface (and hence the rate of film thinning), but there will also be considerable influences from the process parameters, system hydrodynamics and physical properties of the reacting phases, all of which will affect the nature of the bubble-bubble collision.

Chesters (1991) considered the physicochemical hydrodynamics of coalescence process in fluid-liquid dispersions by dividing the flow into internal and external fields, as shown schematically in Figure 2.2. The influence of system hydrodynamics and the physical properties of the bulk liquid are represented by the external flow, which determines bubble velocities and hence the collision frequency, force and contact time for a bubble-bubble pair. In turn, the collision force and contact time provide the boundary conditions for the draining film between the bubbles, represented by the internal flow, which is characterised by deformation of the approaching surfaces and where sufficient time is available, by rupture and confluence. It is generally assumed that the internal flow is most influenced by surface chemical phenomena. The framework outlined in Figure 2.2 usefully identifies the primary influences on coalescence process, but it is now necessary to consider how each of these primary factors is in turn influenced by the system parameters and physical properties.

2.1.1 Bubble-Bubble Collisions

Bubble-bubble collisions arise from a variety of mechanisms, depending on the nature of the

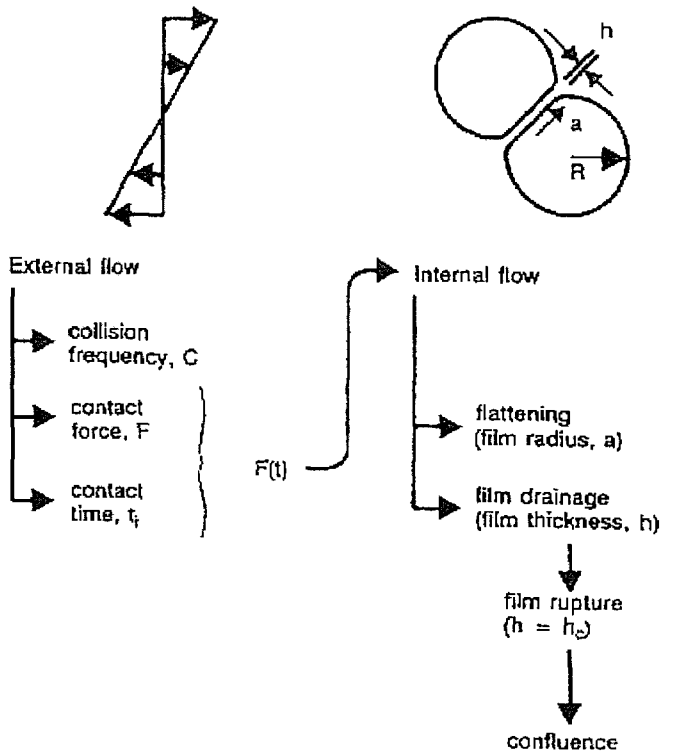

Figure 2.2

Conceptual framework for the coalescence process (Chesters, 1991)

gas-liquid system. Prince and Blanch (1990b), reporting on bubble coalescence and break-up in a bubble column, identify collisions arising from turbulence, buoyancy and laminar shear flow. In addition, the influence of wake induced collisions must be considered, especially in viscous liquids. Of course, collision rates will be also affected by parameters such as the bubble density, thereby increasing as the gas throughput of the system increases.

Prince and Blanch (1990b) assume the predominant cause of bubble collisions in turbulent systems to be the turbulence eddies, with both the collision rate and contact time estimated from Kolmogoroff's theory. Eddies of the inertial sub-range are considered to be responsible for the random motion of bubbles, as those smaller than the bubble length contain insufficient energy to affect bubble motion, whilst those much larger will transport groups of bubbles with little relative motion.

Collisions due to buoyancy arise due to differences in the rise velocities of bubbles of different sizes. Larger bubbles rise faster than smaller ones and consequently collisions will occur between bubbles rising at different rates.

Bubble collisions can also arise from the development of gross circulation patterns within a vessel, which enable bubbles in a region of high liquid velocity to collide with bubbles in a slower section of the velocity field. This mechanism of laminar shear becomes important in bubble columns operating under heterogeneous conditions (Prince and Blanch, 1990b); the non-uniform gas hold-up results in a circulation profile enabling two bubbles of the same size and rise velocity but in different regions of the velocity field to collide.

In addition, Otake et al. (1977) and Stewart (1995) both report the importance of wake induced collisions on bubble coalescence under multi-bubble conditions and a large number of studies (Narayanan et al. (1974), Crabtree and Bridgwater (1971), de Nevers and Wu (1971), amongst others) demonstrate the prominent role of this mechanism for two successive bubbles in viscosity enhanced solutions. Wake induced collisions occur when a trailing bubble is drawn into the wake of a leading bubble and due to the decrease in drag force experienced, accelerates, rising with an increased velocity until the two bubbles collide. The collision may result in either coalescence or break-up, depending on several variables, including the collision geometry (Miyahara et al. 1991).

The dominant collision mechanism will depend on the type of flow and also on the dimensions of the bubbles. The value of the particle Reynolds number ($Re_d = \rho d_p v/\mu$) can be used to quantify the type of flow close to the bubble surface and also the intensity of the force responsible for collision (Chesters, 1991). For $Re_d << 1$, viscous forces govern the collision mechanism and laminar shear will be the most important mechanism, but for $Re_d >> 1$ inertial forces dominate and the majority of collisions arise from the bulk turbulence. Both mechanisms are functions of the gas flow rate in the system; as this increases the relative contribution of buoyancy will diminish. Contributions from wake induced collisions become increasingly important as the continuous phase becomes more viscous and decrease in highly turbulent systems (Narayanan et al., 1974).

The type of flow also affects the force and duration of the bubble-bubble collision. During a viscous collision, bubbles are brought together by the bulk flow, rotate around each other and separate if coalescence does not occur. In inertial collisions however, the virtual absence of viscous dissipation means that colliding bubbles will bounce. Kinetic energy is converted into surface energy during the film formation process and in the absence of coalescence, will

be reconverted as the bubbles bounce apart (Chesters, 1991). The force of contact depends on the inclination of the speed vectors, not on the exact separation; it is largest when bubbles collide head on. The duration of a bubble-bubble contact is dependent on both bubble size and turbulent intensity; high levels of turbulence increase the probability of separation while contact area increases with increasing bubble size. Levich (1962) developed an expression for the contact time from dimensional considerations:

$$\Omega \quad \frac{r^{\frac{2}{3}}}{H^{\frac{1}{3}}} \tag{2.1}$$

where τ is the contact time between two bubbles, r is the bubble radius and ε is the energy dissipation rate per unit mass.

In Section 2.2, where approaches to modelling coalescence processes are reviewed, expressions for the collision efficiency will be examined. This term provides a measure of the number of collisions that give rise to a coalescence event, obviously it will be a function of contact time between bubbles and the time required for coalescence.

2.1.2 Film Thinning

As film rupture is considered to be extremely rapid, the rate-determining step in the coalescence process is the rate of thinning of the liquid film between two contacting bubbles. Thinning relies on a balance of forces to control the movement of the liquid inside the film, at the interface and in the bulk flow and is a function of both the bulk liquid and surface properties. Initially any film that forms between two colliding bubbles will be relatively thick and drainage will take place primarily through gravitational flow of liquid throughout the film. However, once the film thins to a thickness of some several hundred nanometers, drainage due to gravitational flow becomes negligible and further thinning will be controlled by the capillary pressure and interactions arising from molecules adsorbed at the interface.

The primary force promoting film thinning is the capillary (Laplace) pressure, which is induced by variations in the curvature of the gas-liquid interface (Oolman and Blanch, 1986a). The film between two contacting bubbles is very close to flat at the centre and the pressure at this point equals the excess pressure inside the bubbles. However, due to the curvature of the bubble surfaces at the edges of the film, the pressure in the bulk liquid outside the film will be less than at the centre by the amount:

$$\partial P_c \quad \frac{2\varsigma}{r} \tag{2.2}$$

for equal sized bubbles of radius, r. Consequently, liquid will be sucked from the film into the bulk. When the film thickness is greater than the distance over which intermolecular forces operate (about 100nm) the Laplace pressure is the principal negative contribution to the disjoining pressure exerted on the film.

The concept of a disjoining pressure $\Pi(h)$ was introduced by Derjaguin and Kussakov (1939) and defined as:

$$3 \quad h \quad \frac{\partial G(h)}{\partial h} \tag{2.3}$$

where $G(h)$ is the Gibbs energy of interaction per unit area of the film of thickness, h. The disjoining pressure is the net force per unit area acting normal to the film surfaces. For a thin film between two bubbles it can be defined as "the difference between the pressure on the interlayer surface (P_l) and the pressure in the bulk phase (P_o) from which the interlayer extends" (Derjaguin et al., 1987):

$$3 \quad h \quad P_l \quad P_o \tag{2.4}$$

If $\Pi(h)$ is positive there is a net tendency to disjoin the film such that the two surfaces experience repulsion and a stable film is created. When $\Pi(h)$ is negative, the two interfaces attract one another due to intermolecular forces which act to reduce the film thickness. A film must drain to a thickness of approximately 100nm before the negative disjoining pressure become significant enough to destabilise the film. In the presence of a positive disjoining pressure, the film does not rupture but reaches an equilibrium thickness of about 100nm (the metastable films of Vrij, 1966). The net value of $\Pi(h)$ contains contributions from several components, principally $\Pi_{vw}(h)$ due to van der Waals forces and $\Pi_e(h)$ arising from double layer interactions although there are also contributions from other non-hydrodynamic sources such as steric and solvation effects.

2.1.2.1 van der Waals Interactions

Van der Waals forces are long-range, attractive intermolecular forces which originate from electrostatic interactions. Three types exist of which London dispersion forces are the most significant. Dispersion forces exist between all molecules and are caused by the polarisation of one molecule by instantaneous changes in the charge distribution of a neighbouring

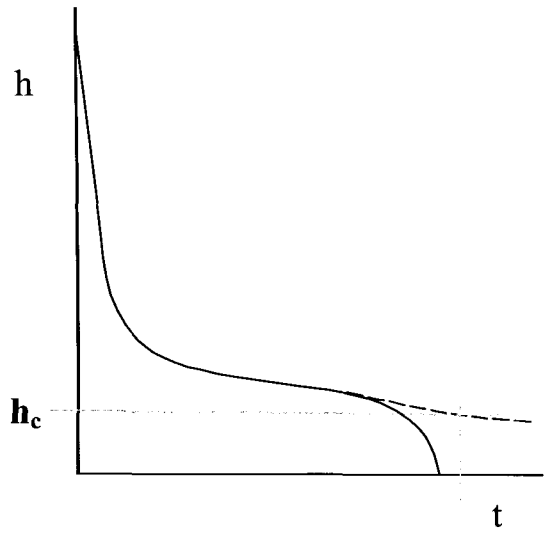

Figure 2.3

The influence of van der Waals forces on film thinning. Solid line: actual thinning behaviour. Dashed line: behaviour in the absence of van der Waals forces. h_c is the film thickness at point of rupture. (from Chesters, 1991).

molecule. The interaction energy between individual molecules is very short range, varying with the inverse of the sixth power of the intermolecular distance. However, the forces are not additive; in a group of molecules the dispersion forces are greater than the sum of the constituent parts and consequently will be effective over a larger distance (up to 100nm) and will tend to decay much less rapidly than the interactions between individual molecules. For a film formed between two bubbles, the van der Waals forces will favour film thinning as the contribution of these interactions to the disjoining pressure is always negative, acting to draw the interfaces together and thus tending to destabilise the thinning film. The forces increase rapidly with decreasing film thickness and eventually become sufficiently strong enough to result in instability and film rupture. The contribution of the van der Waals interactions to the disjoining pressure on a thin film of thickness h, can be represented as:

$$3_{vw} \qquad \frac{A}{6\Sigma h^3} \qquad (2.5)$$

where A is the Hamaker constant, which corresponds to the interactions of the bulk-phase molecules with film molecules (Edwards et al., 1991). At distances beyond about 100nm the van der Waals attraction is retarded and becomes:

$$3_{vw} \qquad \frac{B}{h^4} \qquad (2.6)$$

where B is the retarded van der Waals coefficient. Figure 2.3 (from Chesters, 1991) shows the effect of van der Waals forces on film thickness; in their absence the lifetime of a film would be much greater. The influence of van der Waals interactions on film thinning has been qualitatively examined by Hahn et al. (1985) and Chen et al. (1984), both of whom predict an increase in the coalescence time as the strength of the van der Waals forces decreases.

2.1.2.2 Electrostatic Double Layer Interactions

In electrolyte solution, the dissociated ions and their mixing due to random thermal motion will result in an electrical double layer forming at the gas-liquid interface. Ions adsorbed on the surface will generate a net surface charge which will attract a layer of oppositely charged ions (counter-ions) and repel ions of like charge (co-ions), resulting in a potential formed across the interface. This is shown schematically in Figure 2.4. The double layer consists of two parts: an inner Stern layer and an outer diffuse layer. The Stern layer contains ions which are specifically adsorbed (albeit temporarily) to the surface through electrostatic and/or van der Waals interactions strong enough to overcome thermal agitation (Shaw, 1980). It is separated from the diffuse region by the Stern plane, which lies approximately an hydrated

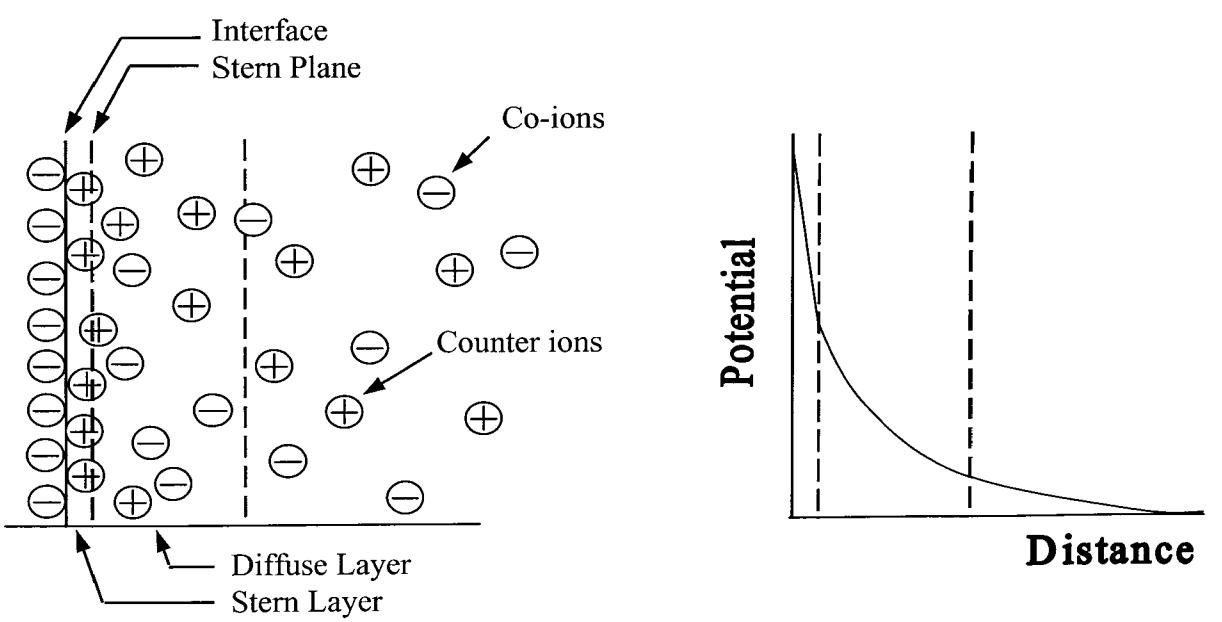

Figure 2.4

A schematic representation of the electric double layer, showing both the inner Stern layer and outer diffuse layers. Note that the potential decreases to zero over the distance of the double layer, such that at a finite distance the number of counter ion is equal to the number of co-ions. (Adapted from Shaw, 1980)

ion radius from the surface. In the diffuse layer ions are distributed according to the influences of electrostatic forces and random thermal motion, such that close to the Stern layer there is an excess of counter-ions over co-ions as a result of the surface charge but that at increasing distance from the surface the numbers of counter and co-ions become equal and electrical neutrality is restored. This distance is known as the Debye length $1/\kappa$, and includes contributions from both the ion valency and concentration.

As the film between two bubbles thins to dimensions where intermolecular forces become significant (about 100nm), the electrostatic double layers at each surface will repel the opposing surface. Consequently, the contribution of the electrostatic double layer to the disjoining pressure ($\Pi_e(h)$) is always positive, tending to stabilise the film and retard coalescence. As the concentration of an electrolyte solution is increased, the electrostatic double layer becomes compressed as a result of the inverse dependence of the Debye length on concentration ($1/\kappa$ also decreases with increasing valency) and two surfaces are able to approach more closely before repulsion occurs. Derjaguin and Kussakov (1939) measured the equilibrium film thickness for air bubbles in electrolyte solution and found values of 90 and 50nm respectively for bubble in 0.01 and 0.1M KCl solution. The effects of electrostatic double layer forces on bubble coalescence have been qualitatively examined by Chen et al. (1988) who demonstrate that it is the relative magnitude of both electrostatic double layer repulsion and van der Waals attractions which is important in determining the time to film rupture, or in the case of a stable film, the equilibrium film thickness. Experimental data from Li and Slattery (1988), clearly shows the strong influence of concentration on electrostatic double layer repulsion; coalescence times for equal sized bubbles at an interface decreased from greater than 200 seconds in 0.025M KCl to about 38 seconds in 0.05M KCl solution.

It must be noted however, that although the electrostatic double layer is seen to exert some influence on the film thinning process, there are other more important influences. Considerations of the electrostatic double layer do not account for the fact that bubbles in concentrated electrolyte solution are unlikely to coalesce in dynamic systems, such as bubble columns. Indeed, the rate of thinning is very much reduced in concentrated solutions, where the double layer would be expected to be compressed, than in weak electrolyte solutions, where it is expected to be larger.

2.1.2.3 Steric Interactions

Coalescence is also inhibited in the presence of surfactants, some of which are species of extremely high molecular weight. When these species are adsorbed at the interface, film thinning is retarded as a result of the steric interactions which arise from the presence of such large molecules. The presence of such large molecules at the interface is also a primary contributor to the surface viscosity of the system.

In addition to the effects of interfacial forces, the rate of film thinning will be influenced by properties of the bulk flow (such as viscosity and the density difference between the two phases) and factors affecting the properties of the gas-liquid interface (including surface tension gradients and surface viscosity). In addition, diffusional processes such as diffusion of solute from the bulk liquid to the film or from the film to the gas-liquid interface may be considered to influence the thinning rate.

2.1.2.4 Interfacial Mobility

The mobility of the interface exerts the greatest influence on the flow conditions in the gap between two colliding bubbles and consequently on the rate of film thinning. As two bubbles

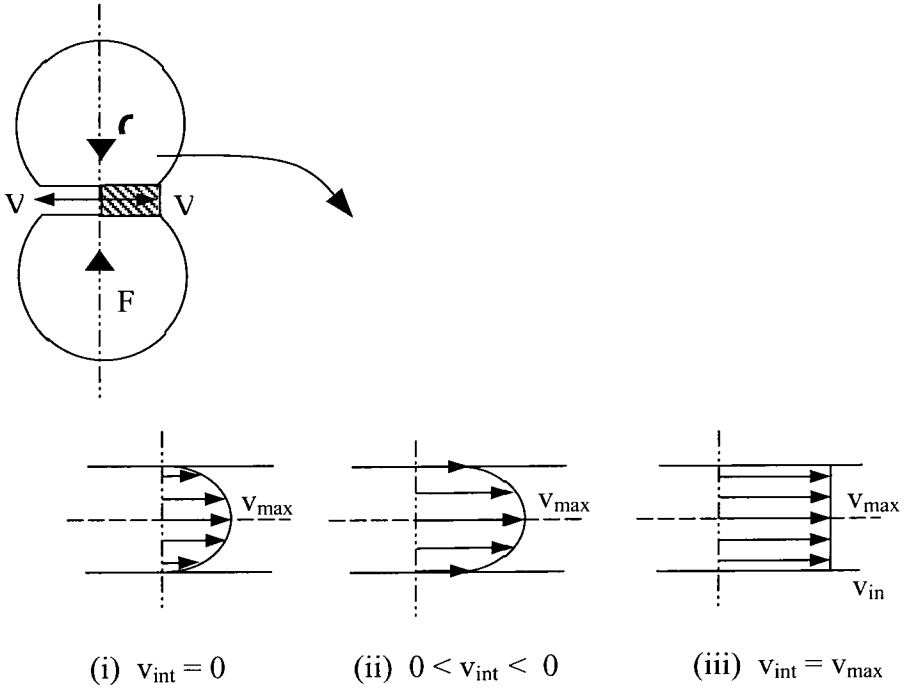

Figure 2.5

Variations in surface mobility: (i) immobile: parabolic flow profile, velocity at the interface is zero. (ii) partially mobile: flow profile is superposition of plug flow and parabolic flow profiles, velocity at the interface has some intermediate velocity between zero and v_{max}. (iii) fully mobile: plug flow profile, velocity at the interface equals velocity at the mid-plane. (adapted from Man, 1999).

approach, the resulting radial flow in the gap exerts a shear stress tangential to each surface, causing tangential motion of the interface and the flow inside the film. The velocity of the flow reaches a maximum at the mid-plane of the film, irrespective of the degree of interface mobility. When no resistance exists to oppose the radial flow in the film, the interface is fully mobile, a plug flow profile is established and the rate of film thinning is fastest. If a resistance to shear stress exists, the velocity of flow at the interface no longer equals the velocity at the mid-plane of the film. When the velocity at the interface is zero, the surface is considered immobile, the velocity profile is parabolic and the rate of thinning will be slowest. Partially mobile interfaces also exist where the flow in film can be described by the superposition of plug and parabolic flow profiles; for these systems surface properties strongly influence the rate of thinning. These variations in interface mobility are shown schematically in Figure 2.5.

Lee and Hodgson (1968) were the first to identify the importance of interface mobility on film flow by allowing that an interface could be fully mobile, of retarded mobility or completely immobile. Film flow was shown to be much slower and consequently drainage (and coalescence) times much longer, in systems with immobile interfaces. Figure 2.6 graphically demonstrates the influence of surface mobility on the film thickness.

What factors are important in determining the degree of interfacial mobility in a system? In a

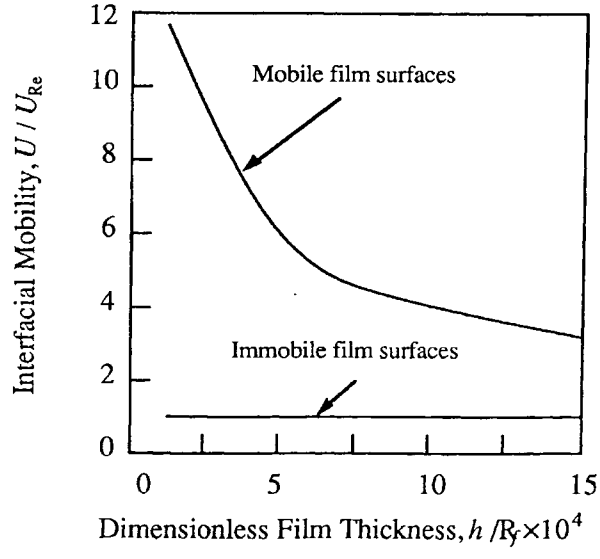

Figure 2.6

Theoretical values for the interfacial mobility versus dimensionless film thickness. Upper curve corresponds to completely mobile surfaces, with no resistance to drainage. Lower curve applies to limiting case of completely rigid surfaces. [Interfacial Mobility is a non-dimensional group determined from the relative magnitude of the approach velocity (U) and immobile drainage velocity (Reynolds velocity, U_{Re})]. (from Edwards, 1991)

liquid-liquid dispersion, the principal factor controlling interfacial mobility is the ratio of the dispersed to continuous phase viscosity μ_d/μ_c; interfaces are considered mobile for values of $\mu_d/\mu_c << 1$ and immobile for $\mu_d/\mu_c >> 1$. In a gas-liquid dispersion however, μ_d/μ_c is always $<< 1$ and so immobilisation of the gas-liquid surface generally only occurs in the presence of a third component. When a surfactant is present in one or both surfaces of the film (including impurities) radial interfacial tension gradients $d\sigma/dr$, are established. These produce a shear stress which opposes the direction of the liquid flow and the surface velocity is then reduced or halted completely (Lee and Hodgson, 1968). Completely immobile interfaces exist when the surface shear stresses due to flow within the film are exactly opposed by the interfacial tension gradients set up because of the surface expansion at the centre of the film. When the amount of surfactant is insufficient to provide the critical interfacial tension difference or if, through surface transport (for an insoluble surfactant) or diffusion (for species soluble in one or both phases) surfactant can be transported to the film to relax the interfacial tension gradients, interface mobility is increased. Theoretical models investigating the effect of surface tension gradients on surface mobility and coalescence time have been developed by Jeelani and Hartland (1994) and Lin and Slattery (1982), amongst others, where expressions for the coalescence time contain a contribution from the number of immobile surfaces, n_i, which includes the influence of the radial interfacial tension gradient, $d\sigma/dr$.

The magnitude of the radial surface tension gradients formed is influenced by factors such as the surface diffusion and the adsorption kinetics of the surfactant species. Interface mobility increases (and consequently film thinning time decreases) with increasing surface diffusion and for a higher rate of surfactant adsorption from the dispersed phase. The surface tension gradients are relieved by the amount of surfactant which diffuses back into the film. Radoëv et al. (1974), developed a model to quantitatively investigate the effects of diffusion; surface diffusion was found to increase the velocity of thinning beyond the value predicted by the Reynolds (1886) equation (which assumes zero velocity at the interface) with the effect becoming more important at decreasing film thicknesses and for more surface active surfactants. The influence of bulk and surface diffusion has also been considered by Li (1996); when the rate of mass transfer to the surface is controlled by diffusion in the liquid film, the effect of bulk diffusion was found to be negligible with respect to that of surface diffusion (except in the instance of a very slow draining film (Edwards et al., 1991)).

Immobile surfaces are caused by large surface tension gradients and small diffusion coefficients; mobility increases with increasing values of the diffusion coefficient.

The mobility of a surface is also strongly affected by the surface viscosity. Large surface viscosities result in immobile surfaces and slow rates of thinning; where the surface tension gradients and surface viscosities are negligible, the film thinning rate will be fastest. Two types of surface viscosity exist: the surface shear viscosity, which opposes a change in shape of a surface and the dilational (dilatational) surface viscosity, which opposes a change in the area of a surface element. In a thin liquid film, the dilational surface viscosity is several orders of magnitude larger than the surface shear viscosity and consequently, is the principal influence on the rate of drainage (Barber and Hartland, 1976). Hahn and Slattery (1985, 1986) developed a model to quantify the effects of surface viscosity (both surface shear and dilational): for both the case of sufficiently large surface viscosities and small bubbles and for small surface viscosities and large bubbles, no influence of surface viscosity is observed and interfaces are respectively immobile and mobile. For a large intermediate range of viscosities and bubble sizes, the coalescence time was strongly influenced by both variables such that the predictions of Chen et al. (1984) made assuming immobile interfaces (film thinning times increase with increasing bubble radius, continuous phase viscosity, density difference and decreasing van der Waals forces) were found to be moderated or reversed. The analysis of Li (1988) showed that both surface viscosities and surface tension gradients must be considered in developing an expression for the film thinning time.

2.1.2.5 Deformability

In a bubble-bubble collision, the bubbles deform to form a disc of liquid between the two. As the amount of deformation increases, the area of contact increases, resulting in an increase in the volume of film required to drain to reach the critical thickness. In a turbulent system the increased drainage time would affect the coalescence probability by causing a decrease in the coalescence efficiency (see Section 2.2.6). The amount of deformation undergone by a bubble increases with size such that the influence of deformation is less significant for small bubbles owing to the large excess pressure required. To deform a bubble of diameter d, a pressure in excess of $2\sigma/r$ is required; consequently, an increase in diameter constitutes an increase in the degree of deformability.

Although at first the bubble surfaces flatten on contact, this is quickly followed by the formation of a dimple. Consequently, whilst the film is initially thinnest at the centre, dimple formation causes the thinning process to be discontinuous so that the thinnest portion of the film occurs at the rim and centre becomes thickest. As the bubble diameter decreases, the dimpling effect at the centre of the film is reduced and the film more nearly approaches the plane parallel disc model (Lee and Hodgson, 1968). Jeelani and Hartland (1991) developed a model to determine the effect of approach velocity on coalescence which predicts film area will increase over time to a maximum value before then decreasing as the bubble regains a spherical shape. The area of the film increases as the initial approach velocity or applied force increases. However, the time required for the area of the film to attain its maximum and zero values increases with the applied force but decreases with the initial approach velocity (Jeelani and Hartland, 1991). Kirkpatrick and Lockett (1974) defined three types of coalescence depending upon the approach velocity of the bubble(s): at low velocities the rate of increase of the film with time is sufficiently slow to allow the film to drain to the rupture thickness before the bubble comes to rest. At large velocities, the film area increases rapidly with time so that there is insufficient time for the film to drain to the rupture thickness before the bubbles come to rest. The strain energy stored in the deformed bubbles then tends to reverse the bubble motion and the contact film starts to thicken (Kirkpatrick and Lockett, 1974). In this instance, it is likely that bubbles will bounce apart and coalescence will only occur if renewed contact is made.

2.1.3 Critical Thickness For Rupture

The final step in the process of bubble coalescence involves the rupture of the thin film at some 'critical' film thickness. Vrij (1966) defined two types of liquid film: metastable and unstable (transient), which rupture by different mechanisms. Metastable films form when border suction, van der Waals attractions and double-layer repulsion forces equilibrate and appear to rupture in an irregular manner, due to external disturbances such as thermal shocks, vibrations or the presence of foreign particles. For films thicker than 10 nm, a high activation energy is necessary for the rupture of the film through the formation of a nucleus (hole) to occur. Consequently, spontaneous rupture is unlikely to take place except in very thin metastable films. In contrast, unstable films always rupture spontaneously at some characteristic 'critical' thickness, often several hundred nanometers.

Vrij (1964) used light scattering to show that the surfaces of thin liquid film are slightly corrugated because of thermal fluctuations. Scheludko (1962, 1967) considered that the deformations grow spontaneously in amplitude. Surface tension acts against the corrugations, whereas van der Waals forces favour disproportionation of the film into thick and thin parts. At the critical thickness the film becomes unstable with respect to these surface deformations and although the increase in surface area causes an associated increase in surface free energy, the total free energy of the film decreases due to the van der Waals attractions. An expression was proposed for the critical film thickness, h_c:

$$h_c = \left(\frac{3K\Lambda_c^2}{64\sigma} \right)^{\frac{1}{4}} \tag{2.7}$$

where K is a constant proportional to the Hamaker constant ($A = 6\pi K$) and Λ_c is the wavelength of a certain surface deformation.

Vrij (1966) and Vrij and Overbeek (1967) related the critical wavelength, Λ_c to the Gibbs energy of interaction as a function of film thickness, $G(h)$. Corrugations with wavelengths larger than a critical value will grow spontaneously due to van der Waals forces and cause the film to thin rapidly and then break

$$\Lambda_c = \left[\frac{-2\pi^2\sigma}{\left(d^2G/dh^2\right)} \right]^{\frac{1}{2}} \tag{2.8}$$

where σ is the surface tension. $G(h)$ may include contributions from van der Waals attractions and electrical double-layer and steric repulsion forces. Corrugations with wavelengths below this critical value will 'fluctuate' around a metastable equilibrium; when the wavelength exceeds the value of Λ_c, the fluctuations will grow in amplitude making the film unstable and ultimately resulting in film rupture. The effect of these thickness fluctuations increases as a film thins. Initially when the film is still thick and the rate of drainage is rapid, the thickness fluctuations will grow only slowly. However, as the film thins and the rate of drainage slows, the fluctuations will become more rapid until the critical thickness is reached, at which point the fluctuations grow so fast the film breaks. The growth rate of fluctuations beyond the critical wavelength depends on the viscosity of the liquid.

Values for the critical thickness can be determined from plotting the draining and breaking times of the film as a function of the film thickness; h_c is determined from the minimum total

time for film thinning. In addition, Virj and Overbeek (1964) derived an expression for the critical thickness at which rupture occurs:

$$h_c = 0.267\left(\frac{A^2 r^2}{6\pi\sigma\Delta P}\right)^{\frac{1}{7}} \tag{2.9}$$

where A is the Hamaker constant and ΔP is the pressure difference between the film. When values calculated for the critical film thickness were compared to experimentally determined values, reasonable comparisons (of the same order of magnitude) were obtained. Interestingly, thickness fluctuations in a film have been visualised by Cahn (1965) and show a pattern of interconnected 'hills and gullies'. Film rupture is assumed to start along one of the gullies.

2.2 MODELS FOR BUBBLE-BUBBLE COALESCENCE

2.2.1 Modelling Collision Dynamics

In almost all models for coalescence and certainly in all the models proposed for coalescence in turbulent systems, it is assumed that bubble collisions are binary events. However, there are a number of experimental observations that suggest coalescence could occur through a cluster type mechanism. The nature of the collision step was the focus of a study by Stewart et al. (1993) wherein models were developed for both binary and cluster coalescence and the results of each compared with experimentally determined bubble size distributions.

Stewart et al. (1993) dismiss the commonly made analogy of bubble collisions with the kinetic theory of gases (as per Coulaloglou and Tavlarides (1977), amongst others), on the grounds that bubbles do not collide, they 'only come into contact while moving generally in the same direction'. In addition they claim the in-line wake coalescence mechanism is defeated by deceleration of the fluid which prevents bubbles from following in the wake centre-line of an ascending bubble. Consequently it will only occur between bubbles generated in line from the same orifice. Small-scale turbulence is also considered to prevent coalescence; as the colliding liquid packets decelerate, the entrained bubbles will be kept out of the vicinity of the event (Stewart et al., 1993).

Binary coalescence was modelled by both geometric and exponential distributions, assuming the events are completely random and independent and where the probability of a specific

coalescence is determined by the number of ways to combine two given bubble sizes divided by the total number of binary combinations possible in the existing distribution (Stewart et al., 1993). Non-binary cluster coalescence was modelled by assuming that coalescence occurs between clusters of bubbles, not pairs; the dependence on the number of bubbles was found to change from linear (binary) to quadratic. The distribution function for the cluster model was found to correspond exactly to the *Pareto* distribution function [this is qualitatively similar to an exponential distribution, although with a much slower decay thus giving a 'long-tailed one-sided distribution' (Lloyd, 1980)]. Comparisons with experimental data showed that except for studies where an equilibrium between coalescence and break-up rates had been obtained, size distributions compared much more closely with the predictions of the Pareto model for cluster dynamics than with the exponential distribution of binary coalescence. The binary coalescence model in all cases failed to account for the large tail of the distributions at higher bubble volumes (in the model, the smallest bubbles have the highest coalescence probability). The Pareto distribution showed a good match over the range of bubble sizes as it assigns a small (but non-zero) probability to the coalescence of very large bubbles. From the comparisons, the authors conclude that coalescence in bubble swarms is not a binary process, but occurs through simultaneous coalescence of bubble clusters. However, these theoretical predictions should be compared with experimental observations of coalescence in dynamic systems discussed in Section 2.3.4, where only binary coalescence events have been reported.

2.2.2 Modelling Coalescence Times

A number of theoretical models have been developed to quantify the process of bubble coalescence, for which the primary differences are in the assumptions made about the mobility of the film surface during film thinning. The principal results of these developments are examined here. In addition to those models developed specifically in terms of bubble coalescence, there is also an extensive literature on the stability of thin films wherein a large number of complex film thinning models have been developed to investigate the influence of specific parameters, such as van der Waals interactions, electric double layer forces, surface viscosity and interface mobility. The results of these models are not reviewed in the following section (primarily due to their focus on the discrete influence of individual variables), although the qualitative trends from these studies have formed the basis of the discussion presented in Section 2.1.2.

The parameter usually chosen to describe the process (both theoretically and experimentally) is the 'coalescence time', which is defined as the time between the first contact of the bubble pair and the subsequent coalescence. Although such a parameter will contain contributions from both the film thinning and film rupture stages of the process, it does not allow for the influences of the bubble collision. Sagert et al. (1976b) define a coalescence time t_c, which consists of three parts:

$$t_c = t_s + t_i + t_b \tag{2.10}$$

where t_s is the time required for the film to stretch from the initial thickness to a final thickness, t_i is a correction for the inertial force on the liquid film and t_b represents the lifetime of the film at the final thickness before rupture (assumed to be typically about 10 nm).

2.2.2.1 Coalescence Times in Pure Liquids

In pure liquids coalescence occurs very rapidly as the composition of the gas-liquid interface is identical to that in the bulk liquid, thereby eliminating surface tension gradients. Consequently, the liquid draining from the film will not encounter any resistance at the interface and thinning will proceed by an inertially controlled mechanism.

Chesters and Hofman (1982) modelled the coalescence of gas bubbles in pure (inviscid) liquids, assuming an almost parallel-sided film with fully mobile surfaces. An approximate coalescence time was predicted:

$$t_c = \frac{r^2 \rho v}{\sigma} \tag{2.11}$$

where v is the relative approach velocity of the two bubbles and r the bubble radius. For the case of unequally sized bubbles, r can be replaced with r_{eq} where:

$$\frac{1}{r_{eq}} = \frac{1}{2(r_1 + r_2)} \tag{2.12}$$

and r_1 and r_2 are the radii of the two bubbles. Values for r_{eq}/r_1 vary from 1 for two equal sized bubbles to 2 ($r_2 = \infty$), such that coalescence of a bubble with a free interface is equivalent to coalescence of equal sizes bubbles of twice the radius.

In addition, the model predicted deviations from plane parallel geometry as the bubble surfaces flatten, with a dimple developing around the edge of the film. The dimple forms at small thickness and rapidly becomes the point of rupture (even in the absence of van der Waals forces) due to the presence of very large velocities and pressure gradients. The model

also predicted that bubbles would bounce apart before coalescence is completed, if the relative approach velocities are sufficiently large (Weber numbers of approximately unity). For coalescence in pure, viscous liquids the coalescence process is retarded. The total film thinning time for a pure (inviscid) liquid was predicted to be of the order of 10^{-2} to 10^{-3} seconds.

Coalescence of bubbles in pure liquids is not the most commonly encountered situation and therefore a number of models have been developed to allow for the determination of coalescence times in solutions containing solutes.

2.2.2.2 The Liquid Phase Diffusion Model

Marrucci (1969a) developed a model where the rate of film thinning is governed by the rate of diffusion of the solute into the liquid of the film. Two possible mechanisms were identified for film thinning; via laminar flow of the liquid in the film with respect to the bubble surfaces or via a uniform expansion of the bubble surfaces with stretching of the liquid between them. The first mechanism is restricted to systems with immobile interfaces where the liquid can be considered to drain from between the bubble surfaces as from between two flat plates (Reynolds equation). The model however, was based on a system with fully mobile bubble surfaces, in which case laminar flow can be neglected with respect to the stretching of the film as a whole. An expression was derived to allow the concentration of solute at which a mobile surface becomes immobile (called the transition concentration, c_t) to be calculated:

$$c_t = 0.084 \nu RT \left(\frac{\sigma A^2}{r} \right)^{\frac{1}{3}} \left(\frac{d\sigma}{dc} \right)^{-2} \qquad (2.13)$$

where ν is the number of ions produced upon dissociation of the solute, R is the ideal gas constant, T is temperature, σ is the surface tension, r is the bubble radius and A is the Hamaker constant for the liquid.

Film thinning was considered to occur in two stages. Initially the film drains rapidly until a 'quasi-equilibrium' thickness is reached, at which point the build up in surface tension balances the pressure difference across the film and the interfaces become immobilised. Further thinning follows, although much more slowly, at a rate governed by the diffusion of solute from the bulk into the edge of the film.

The driving force for film thinning is the pressure difference between the liquid of the film and that in the bulk phase. At any point in time and in the absence of inertial effects, this pressure difference (ΔP) will be balanced by a difference in the surface tension ($\Delta\sigma$) and the force balance across a film of uniform thickness h can be written:

$$h\Delta P = 2\Delta\sigma \tag{2.14}$$

During the initial stage of film thinning the solute concentration at the surface is considered to be in equilibrium with that in the film. For a positively adsorbed solute (most surface active species), the increase in surface area which accompanies the film thinning will result in a decreased solute concentration in both the liquid of the film and at the film surface, thereby increasing the surface tension. The first stage of thinning stops when the increase in surface tension is balanced by the internal pressure in the film, i.e. when the force balance equation 2.14 is dynamically satisfied. At this transition point, the 'quasi-equilibrium' thickness, the surfaces of the film change from mobile to immobile.

A value for the overall internal pressure, ΔP, was obtained by summing the effects of the capillary pressure and van der Waals forces (neglecting effects arising from electrical double layer forces):

$$\Delta P = \frac{2\sigma}{r} + \frac{A}{6\pi h^3} \tag{2.15}$$

The first term on the right hand side is the effect of capillary pressure, the second accounts for the effects of the van der Waals forces (A is the Hamaker constant). In the absence of van der Waals attractions, there would always be a film thickness at which the mass balance effect compensates the capillary pressure and no further thinning would occur (see Figure 2.3).

To obtain an expression for the difference in surface tension $\Delta\sigma$, a mass balance was carried out over a film of thickness h and area s, assuming equilibrium between solute in the surface and the bulk:

$$\Delta\sigma = \frac{1}{vh}\left(\frac{2c_1}{RT}\right)\left(\frac{d\sigma}{dc}\right)^2 = \frac{c'}{h} \tag{2.16}$$

where

$$c' = \frac{2a_1}{RT}\,\frac{d\sigma}{da_1}\,\frac{d\sigma}{dc_1}\,\frac{1}{1 + \dfrac{x_1V_1}{x_2V_2}} \tag{2.17}$$

which is a fixed quantity for a given solution concentration and where a_1 is the activity of the surface active species, c_1 is the concentration, x_1 and x_2 are the molar fractions of the surface active species and solvent, respectively and V_1 and V_2 are the molar volumes of the two components.

The force balance then becomes:

$$(kh_o)^2 + \frac{1}{kh_o} = \frac{c'rk^2}{\sigma} \qquad (2.18)$$

where

$$k = \left(\frac{12\pi\sigma}{Ar}\right)^{\frac{1}{3}} \qquad (2.19)$$

and h_o is the 'quasi-equilibrium' thickness which represents the transition point between a fully mobile and immobile surface. Figure 2.7 shows a plot of $c'rk^2/\sigma$ as a function of kh: the curve has a minimum at $kh = 0.793$, $c'rk^2/\sigma = 1.89$, which arises from the effect of the van der Waals interactions. The existence of the minimum predicts different behaviour for systems with values for $c'rk^2/\sigma$ above or below a critical value of 1.89.

An expression was developed to predict the order of magnitude of the thinning time required to reach the 'quasi-equilibrium' thickness h_o and values were found to vary from 10^{-7} to 10^{-3} seconds. These values were considered negligible in relation to the entire time required for coalescence. It was shown that for systems where $c'rk^2/\sigma < 1.89$, coalescence occurs almost instantaneously and no quasi-equilibrium film forms; this is the case for pure liquids and some dilute solutions. For those systems where $c'rk^2/\sigma > 1.89$, a 'quasi-equilibrium' thickness exists and the time required for the film to reach this (irrespective of the initial film thickness) is negligible with respect to the total coalescence time. It is the time required for the second stage of film thinning, from the quasi-equilibrium thickness to the point of rupture which determines the coalescence time.

The second stage of thinning involves further drainage of the film beyond the 'quasi-equilibrium' thickness to the point of rupture by a diffusion controlled process occurring at the edges of the film, arising due to the concentration gradient which exists between the liquid in the film and the bulk. This diffusion process alters the surface tension and consequently

the film must stretch further to maintain the balance of forces. A mass balance was derived for this process:

$$\frac{d(\Delta c_1)}{dt} = -\frac{2D}{xr}\Delta c_1 + \frac{c'}{d\sigma/dc_1}\frac{d}{dt}\left(\frac{1}{h}\right) \qquad (2.20)$$

where Δc_1 is the concentration difference between the film and the bulk liquid, D is the diffusion coefficient, x is the length at the edge of the film over which the concentration gradient develops. The first term on the right hand side is the contribution of the diffusion process whereas the second represents the change in solute concentration with time due to the film stretching. Both the concentration difference, Δc_1 and film thickness, h are functions of time and also related by the force balance. In addition, for a two component system at a fixed temperature, the surface tension can be considered a unique function of the concentration of one component, for small solute concentrations:

$$\Delta\sigma = \frac{d\sigma}{dc_1}\Delta c_1 = \frac{d\sigma}{dc_2}\Delta c_2 \qquad (2.21)$$

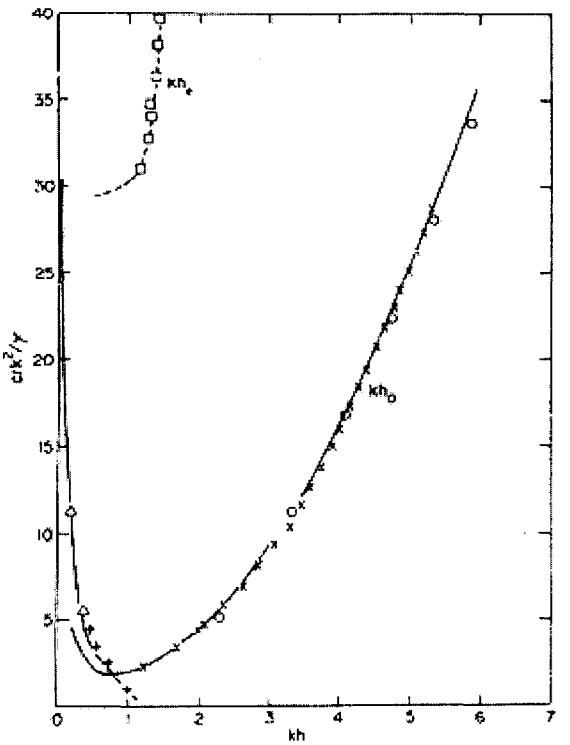

Figure 2.7

Dimensionless concentration parameter, $c'rk^2/\sigma$ as a function of film thickness. h_o is the quasi-equilibrium film thickness predicted by Marrucci (1969a); the right hand side of the curve is the physical solution to Equation 2.18. The minimum is due to the action of van der Waals interactions, beyond this limiting value no quasi-equilibrium thickness occurs and coalescence is instantaneous. h_e is the equilibrium film thickness predicted by Sagert and Quinn (1978a), taking into account the effect of the electrostatic double layer; below a value of 28.5, thinning is not hindered by double layer repulsion. (from Oolman and Blanch, 1986a).

If this expression, together with that for the internal pressure (Equation 2.15) is substituted into the mass balance and the resulting equation integrated between the quasi-equilibrium thickness and the thickness at which rupture occurs, an expression can be derived for the coalescence time.

The dimensionless concentration parameter, $c'rk^2/\sigma$, is important as a measure of the relative contributions of the film stretching and solute diffusion times to the total coalescence time. At high values of $c'rk^2/\sigma$, the slow diffusion step is rate controlling whereas for smaller values it is the time required for the film to thin to the quasi-equilibrium thickness which determines the coalescence time.

2.2.2.3 Modifications to the Liquid Phase Diffusion Model

Sagert and Quinn (1976b, 1978) extended the Marrucci model to incorporate the repulsive effects of electrostatic forces in addition to the effects of capillary and van der Waals forces. The expression for the overall internal pressure then becomes:

$$\Delta P = \frac{2\sigma}{r} + \frac{A}{6\pi h^3} - bC_{el}\exp(-\kappa h) \qquad (2.22)$$

where C_{el} is the total electrolyte concentration, κ is the Debye reciprocal length and the constant b contains contributions from the ion valency (Z), the double layer potential at the interface (Φ_o) and the Faraday constant (F). This expression was then used together with the mass balance derived by Marrucci (1969a) to generate an expression for the coalescence time. The results from the modified model were compared to those predicted by the original by plotting the parameter $c'rk^2/\sigma$ against kh. The inclusion of electrostatic interactions had little effect at distances typical of the quasi-equilibrium thickness. However, in the second stage of thinning, (from the 'quasi-equilibrium' thickness to the point of rupture), the inclusion of electrostatic repulsion resulted in the formation of an equilibrium thickness, h_e at which point the internal pressure, ΔP reaches zero and all thinning stops (see Figure 2.7). This point is defined as:

$$\frac{2\sigma}{r} + \frac{A}{6\pi h_e^3} = bC_{el}\exp(-\kappa h_e) \qquad (2.23)$$

When thinning stops, the coalescence time is then determined by the inherent breaking times of the equilibrium thickness film, as predicted from the expressions for film rupture

developed by Vrij (1966). A value of $(c'rk^2/\sigma)_{crit}$ was determined below which ΔP never becomes zero and film thinning proceeds according to the Marrucci model, with little effect from electrostatic repulsion. Above $(c'rk^2/\sigma)_{crit}$ the equilibrium thickness is smaller than the 'quasi-equilibrium ' thickness proposed by Marrucci (1969a) and so film thinning stops as the film reaches the equilibrium thickness, h_e. The existence of the critical value was ascribed to the short range and relatively large magnitude of the electrostatic forces.

Oolman and Blanch (1986a), observed that if diffusion occurred only at the outer edges of the film, localised film thinning would occur which would cause sharp changes in the film curvature. Surface tension forces would resist these changes and tend to flatten the surface, thereby reducing the total surface energy. Consequently, it was concluded that thinning of the film beyond the quasi-equilibrium thickness would be better represented by a mechanism which would allow for simultaneous thinning over the entire radial dimension of the film. The net pressure variation along the radial length of the film and the net surface tension force acting along the film are given by Equation 2.15 and 2.16 respectively, both as derived by Marrucci (1969a). Once again the film thinning was considered to consist of two distinct regimes, an initial inertially controlled regime which is followed by viscous thinning once the bubble surfaces become immobile. By assuming that the inertial and viscous thinning processes could be decoupled, an expression was developed to describe the rate of film thinning for a plane parallel film geometry and flat velocity profile:

$$\frac{dh}{dt} = \left\{\frac{8}{r_d \rho_l}\left[\frac{-4c}{RT}\left(\frac{d\sigma}{dc}\right)^2 + h^2\left(\frac{2\sigma}{r} + \frac{A}{6\pi h^3}\right)\right]\right\}^{\frac{1}{2}} \qquad (2.24)$$

where r_d is the radius of the liquid disc between the coalescing bubbles, ρ_l is the liquid phase density and h is the film thickness. This expression for the rate of film thinning was combined with the equations for ΔP and $\Delta\sigma$ and the entire expression numerically integrated over the radial dimensions of the film to give the solute concentration at which the thinning transition occurs (proportional to $(d\sigma/dc)^{-2}$) and also an expression for the coalescence time.

Prince and Blanch (1990a) modified the Marrucci model to include the effects of inertia and 'retarded' van der Waals attractions. The solute concentration at which a surface becomes immobilised is then:

$$c_t = 1.18\nu\left(\frac{B\sigma}{r}\right)^{\frac{1}{2}} RT\left(\frac{d\sigma}{dc}\right)^{-2} \tag{2.25}$$

where B is the retarded van der Waals coefficient. The term used to account for the contributions of the van der Waals forces to the internal pressure was revised after evaluating the distances over which the forces were applied. The term used by Marrucci (1969a), applies over much shorter distances than those generally associated with film thinning: at approximately 10 nm (the film thickness at the point of rupture) there is a transition from normal to retarded van der Waals interactions (Prince and Blanch, 1990a). The expression for the internal pressure is then:

$$\Delta P = -\left(\frac{2\sigma}{r} + \frac{B}{h^4}\right) \tag{2.26}$$

The inclusion of inertial terms into the force balance is reflected in the numerical coefficient of Equation 2.25. The effect is an increase in the solute concentration required to inhibit coalescence; that is, inertia favours coalescence. Good agreement was found between the theoretical values calculated for the transition concentrations using the modified model with the experimental data reported by Marrucci (1969a) and Lessard and Zieminski (1971).

None of the models considered so far allow for the influence of factors such as surface diffusion, diffusion of the film liquid into the gas bubbles (important for a volatile liquid phase) or changes in the shape of the film and the bubble. A number of alternative models have been developed which aim to examine these influences.

2.2.2.3 Gas Phase Diffusion Models

In developing the liquid phase diffusion model, Marrucci (1969a) made the assumption, amongst others, that there was no mass transfer to or from the gas phase. Nicodemo et al. (1972) found a good fit between the model and experimental data for bubbles in electrolyte solution but observed large discrepancies between predicted and measured coalescence times for bubbles in solutions of *n*-alcohols. It was proposed that the same 'quasi-equilibrium' state would be achieved but that there would be an important contribution to the concentration gradient from diffusion of the solute through the gas phase into the film. Sagert et al. (1976b) analysed this proposed model by assuming that the gas in the bubble had the same partial pressure of alcohol as in equilibrium over the bulk liquid. Provided the mole fraction of the

active component is small, then activities can be assumed to be equal to concentrations. The mass balance (Equation 2.20) then becomes:

$$\frac{d}{dt}(\Delta c) = -\frac{2}{h}\frac{D}{x}\Delta c + \frac{2c}{RT}\left(\frac{d\sigma}{dc}\right)\frac{d}{dh}\left(\frac{1}{h}\right) \tag{2.27}$$

where h is the film thickness, D is the diffusion coefficient, x is the diffusion distance, c is the concentration of solute and Δc is the concentration difference. Following Marrucci (1969a), the expression for the coalescence time then becomes:

$$\frac{Dt}{x} = \frac{2\pi}{3\sqrt{3}}\frac{r}{RT\sigma}\left(\frac{12\pi\sigma}{Ar}\right)^{\frac{1}{3}}\left(\frac{d\sigma}{dc}\right)^{2} c \tag{2.28}$$

where r is the bubble radius and A the Hamaker coefficient. Using the modified model, Sagert et al. (1976b) calculated the diffusion distance, the 'quasi-equilibrium' thickness and the final film thickness at rupture for aqueous solutions of ethanol and n-amyl alcohol. The values obtained for the diffusion distances were found to be considerably higher than both the quasi-equilibrium thickness and final rupture thickness, which was considered unrealistic. Film thinning times predicted by the model were much shorter than those experimentally observed, leading to the conclusion that gas-phase mass transfer was very rapid and that other factors must be rate controlling.

Oolman and Blanch (1986a) developed a model to predict the concentration at which the bubble surfaces become immobilised in solutions of volatile surfactant. It was assumed that the rate of film thinning was controlled by the rate of replenishment of the surfactant from the gas phase, so that the surface concentration remains constant, thereby eliminating surface tension gradients. Surfactant is depleted from a stretching film at a rate equal to the rate of generation of new surface multiplied by the concentration of surfactant on the surface. The rate of replenishment is therefore:

$$\frac{\Gamma_i d\ln s}{dt} = \left(\frac{d\ln h}{dt}\right)\left(\frac{c_i}{RT}\right)\left(\frac{d\sigma}{dc}\right) \tag{2.29}$$

where Γ_i is the surface excess and c_i is the concentration of component i. Equating this expression with the rate at which surfactant molecules diffuse from the bulk gas of the bubble to the film surface gives:

$$\left(\frac{d\ln h}{dt}\right)\left(\frac{c_i}{RT}\right)\left(\frac{d\sigma}{dc}\right) = -k_g\Delta\sigma\left(\frac{d\sigma}{dc}\right)^{-1}\left(\frac{\gamma_i P_i}{P}\right)\left(\frac{M_l}{\rho_l}\right) \tag{2.30}$$

where k_g the gas phase mass transfer constant, γ_i is mole fraction of component i in the gas phase, P_i the partial pressure of component i, M_l the molecular weight of the liquid and ρ_l the liquid density. Combining this expression with the force balance:

$$\frac{2\Delta\sigma}{h} = \frac{2\sigma}{r} + \frac{A}{6\pi h^3} \tag{2.31}$$

leads to an expression which can be integrated to give the rate at which the film thins. When solved for dimensionless parameters, the equation predicts initial rapid thinning, which slows as the concentration driving force decreases with decreasing film thickness before finally accelerating rapidly as the van der Waals forces become significant.

The predictive equation developed to determine the concentration of surfactant at which the surface changes from mobile to immobile can be written:

$$c_t = 0.9tk_g\left(\frac{Ar}{12\pi\sigma}\right)^{\frac{1}{3}}\left(\frac{2\sigma}{r}\right)\left(\frac{d\sigma}{dc}\right)^{-2} RT\left(\frac{\gamma_i P_i}{P}\right)\left(\frac{M_l}{\rho_l}\right) \tag{2.32}$$

An expression was also developed to determine the upper limit for the value of the gas-phase mass transfer coefficient, $k_g = P(2\pi MRT)^{1/2}$, where M is the molecular weight of the surfactant species.

2.2.2.4 The Dynamic Surface Tension Model

Andrew (1960) investigated the foaming capacity of a two component mixture and developed a criterion for determining the mixture composition for maximum foaming based on surface elasticity concepts. The elastic forces were considered to result from the rise in the dynamic surface tension above the static value as the film undergoes steady uniform expansion. As the film stretched the surface tension increases. This is due to a decrease in the solute concentration at the surface caused by slow diffusion of solute from the bulk liquid and consequently the surface tension increases. Mass transfer of solute to the surface was considered to occur by convective diffusion normal to the surface, with no mass transfer occurring between the gas and liquid phases. For a pseudo-steady state (no accumulation or depletion of solute) in an element of volume over time, an equation was derived for the change in surface tension:

$$\Delta\sigma = \frac{c\left(d\sigma/dc\right)^2}{RT\left(\frac{2D}{\pi S}\right)^{\frac{1}{2}} - \left(\frac{d\sigma}{dc}\right) - \left(\frac{d^2\sigma}{dc^2}\right)c} \tag{2.33}$$

where S is the surface expansion rate per unit area and defined

$$S = \left(\frac{1}{s}\right)\left(\frac{ds}{dt}\right) = -\frac{1}{h}\frac{dh}{dt} \tag{2.34}$$

for an element of surface area, s and for the case when the film is considered to stretch elastically.

Sagert et al. (1976b) used this expression for $\Delta\sigma$ in the development of a coalescence model based on the assumption that as the film was stretched, surface area was created more rapidly than the rate at which solute could diffuse to the surface and maintain the equilibrium surface excess. This model differs from those previously considered in that there is no inherent prediction of a final rupture thickness. Consequently, the total coalescence time becomes the sum of the time required for the film to stretching from an initial to final thickness t_s and the time required for the film to rupture, which is determined separately.

Following Marrucci (1969a), the force balance over a film segment is given by Equation 2.14. The expression used for the excess internal pressure in the film, ΔP contained contributions from the capillary pressure, Hamaker forces and electrostatic double layer repulsive forces, as given in Equation 2.22. When expressions for ΔP, S (Equation 2.34) and $\Delta\sigma$ are substituted into the force balance, an expression is developed for the time required for the film to stretch from infinite thickness to a final thickness, which can be numerically integrated to give t_s as a function of the final film thickness, h_f. As inertial effects were neglected in the development of the expression for t_s, a third contribution to the overall coalescence time was developed to represent inertial influences on the film thinning, t_i:

$$t_i = \frac{r_d}{2v}\ln\left(\frac{h_i}{h_f}\right) \tag{2.35}$$

where r_d is the radius of the film between two coalescing bubbles (determined from photographic images) and v is the velocity of the film between them. A final estimation of the coalescence time can be made from the minimum time in a plot of $(t_s + t_i + t_b)$ against film thickness.

2.2.2.5 The Surface Immobility Model

The models reviewed so far have only allowed for the gas-liquid surface to be either fully mobile (no velocity variation across the depth of the film) or beyond a critical solute

concentration, immobile (velocity at the surface is zero). In an investigation into the coalescence times of H_2S and CO_2 bubbles in water, Sagert and Quinn (1976b) developed a model which allowed for partially mobile interfaces and the subsequent effect on film thinning. As in the development of the dynamic surface tension model, the overall coalescence time is defined as the sum of the film stretching time and rupture time, which are both determined separately.

In this model, a single expression was used to summarise the rate of film thinning for the three possible interface combinations: flow between two immobile interfaces (where the rate of thinning is given by the Reynolds equation (Equation 2.39)), a mobile and an immobile interface and two mobile interfaces:

$$\frac{dh}{dt} = \frac{8\pi F h^3}{3\phi\mu s_d^2} \tag{2.36}$$

where F is the force acting on the interface, h is the film thickness, μ is the viscosity of the bulk liquid, s_d is the contact area of the interfaces and ϕ is the surface immobility parameter, defined as:

$$\phi = \frac{2n_i}{(3-n_i)} \tag{2.37}$$

where n_i is the number of immobile interfaces. Values of ϕ lie between 0 (for two mobile interfaces) and 4 (two immobile interfaces) with no restriction to integer values; in addition, as the film thins, the values of ϕ are found to change, generally decreasing with time (Barber and Hartland, 1976). From Marrucci (1969a), the force acting on the interface is considered as the product of the contact area, s_d and the internal pressure in the film, ΔP, which was expressed as the sum of the capillary pressure and Hamaker forces, as given by Equation 2.15 (the effects of electrostatic repulsion were neglected). The expression for film thinning then becomes:

$$\frac{dh}{dt} = 8h^3 \frac{\left(\frac{2\sigma}{r} + \frac{A_h}{6\pi h^3}\right)}{3\phi\mu r_d^2} \tag{2.38}$$

where A is the Hamaker constant and r_d is the radius of the liquid film disc (determined from photographic images). Integration of Equation 2.38 allowed values of t_s, the time required for the film to stretch to a final thickness h_f, to be calculated for a given value of ϕ in order to generate of family of thinning curves (t_s against h_f) for different values of ϕ. The film rupture

time t_b, was calculated during the approach of Ruckenstein and Jain (1974) and the overall coalescence time was then determined as the minimum in the sum of (t_s + t_b) plotted as a function of the film thickness, h_f.

In their investigation the authors were concerned with developing a model to determine the coalescence time in the presence of highly volatile surfactants, where no surface tension gradients exist in the film due to rapid replenishment from the gas phase. Thus film mobility is only influenced by the total concentration of surfactant present and the magnitude of the shear stress at the interface. Values for n_i were found by comparing the model values to the experimental data and adjusting n_i to give a good fit over the range of film thicknesses. This feedback determination of a critical parameter somewhat limits the usefulness of the model in predicting coalescence times in the absence of experimental data.

2.2.2.6 General Expressions for Film Thinning

The classic expression for film thinning is the Reynolds (1886) solution for the drainage velocity between two plane parallel plates:

$$V_R = -\frac{dh}{dt} = \frac{8h^3\Delta P}{3\mu r_d^{\,2}} \tag{2.39}$$

where V_R is the Reynolds velocity of thinning, h is the film thickness, ΔP is the excess pressure on the film and r_d is the radius of the film. Direct application of this equation results in predicted thinning times much longer than those observed experimentally (Cain and Lee, 1985 and Pashley and Craig, 1997), especially so at smaller film thicknesses. Despite this, many models have been developed from modifications to the Reynolds equation.

Chesters (1991), investigating coalescence in pure liquids, used the Reynolds equation to develop film thinning equations for the case of deformable particles with immobile surfaces (applicable to solutions containing surfactants):

$$-\frac{dh}{dt} \approx \frac{8\pi\sigma^2 h^3}{3\mu r^2 F} \tag{2.40}$$

It can be seen from this expression that increasing the collision force decreases the rate of thinning, suggesting that in this case coalescence is favoured by gentle collisions. This arises from the interdependence between the collision force, F and film radius, r_d:

$$F \approx \pi r_d^2 (2\sigma / r) \tag{2.41}$$

Separate expressions were also developed for the case of deformable particles with partially mobile or fully mobile surfaces. The rate of thinning between partially mobile surfaces was determined assuming quasi-steady creeping flow in the film (and therefore negligible variation in velocity across the film):

$$-\frac{dh}{dt} \approx \left[2\frac{(2\pi\sigma/r)^{\frac{3}{2}}}{\pi\mu_d F^{\frac{1}{2}}} \right] h^2 \qquad (2.42)$$

For fully mobile surfaces, the rate of thinning is controlled by the resistance of the film to deformation, which corresponds to viscous control and acceleration, where the rate is inertially controlled. An expression for the rate of film thinning, containing both viscous and inertial terms was developed; in the viscous limit ($\mu \rightarrow \infty$) this expression integrates to:

$$h = h_o \exp\left(- \frac{t}{t_{ch}} \right) \qquad (2.43)$$

where t_{ch} is some characteristic time scale, given by:

$$t_{ch} = \frac{3\mu r}{2\sigma} \qquad (2.44)$$

When thinning is inertially controlled, the drainage expression integrates to:

$$h = h_o \exp\left(-\frac{t}{t_{ch}} \right) \qquad (2.45)$$

where t_{ch} is now given by:

$$t_{ch} = \frac{\rho v r^2}{8\sigma} \qquad (2.46)$$

In both cases, the rate of thinning has become independent of the film radius and hence (as a result of Equation 2.41), the collision force.

2.3.1 Modelling Coalescence In Turbulent Conditions

The coalescence models presented so far have all been restricted to the contact of two bubbles under idealised conditions. In order to model bubble coalescence in a dynamic system expressions must be obtained to determine the influence of bubble-bubble collisions, in addition to the influences of film thinning and rupture processes. In studies of liquid-liquid coalescence, a common approach has been to determine the coalescence frequency for a

system, which is defined as the product of the collision frequency and coalescence efficiency. The collision frequency is often modelled by analogy to the collisions between molecules as in the kinetic theory of gases (Coulaloglou and Tavlarides, 1977). Expressions for the coalescence efficiency term contain contributions from the contact and coalescence times where the coalescence time is considered the time for film drainage. This approach to coalescence in turbulent systems has not been widely adopted for gas-liquid dispersions, where studies in dynamic systems have generally been restricted to qualitative determination of coalescence rates from bubble size data and gas hold-up measurements (see Section 2.3).

Chesters (1991) considered bubbles in turbulent flow for pure, inviscid liquids, such that the film drainage occurs between two fully mobile interfaces. The coalescence time was considered to be equivalent to the time required for the film to thin to the critical thickness for rupture and was expressed as:

$$t_c \propto 0.5\frac{\rho u_{rel}^2 r}{\sigma} \tag{2.47}$$

where ρ is the liquid density, u_{rel} is the relative velocity of the centres of the colliding bubbles, r is the bubble radius and σ is the surface tension. The collision time, τ, was defined as the time from the onset of flattening to the point at which the motion of the bubbles is arrested and expressed as:

$$\tau \approx \left[\frac{\rho r^3}{2\sigma}\right]^{\frac{1}{2}} \tag{2.48}$$

Coalescence was considered to occur only if the interaction time exceeded the coalescence time, thus allowing the probability of coalescence occurring during a collision (or coalescence frequency, ϖ) to be expressed as a function of the ratio t_c/τ:

$$\varpi \approx \exp\left(\frac{-t_c}{t_i}\right) \approx \exp\left[-\left(\frac{\rho u_{rel}^2 r}{\sigma}\right)^{\frac{1}{2}}\right] \tag{2.49}$$

As observed experimentally (Duineveld, 1994, Kirkpatrick and Lockett, 1974 and Farooq, 1972), the model suggests that large bubbles with a high relative velocity are less likely to coalesce as they will bounce apart before the film can thin to the critical thickness for rupture.

Prince and Blanch (1990b), developed a model to determine the bubble coalescence and break-up rates in a bubble column by considering the overall coalescence rate to be the

product of the collision rate and collision efficiency (equivalent to coalescence efficiency). The collision rate was modelled by assuming that the (binary) collisions arising from turbulence, buoyancy and laminar shear were cumulative. An expression was developed for the turbulent collision rate as a function of bubble size, concentration and velocity (the bubble velocity was assumed to be the turbulent eddy velocity of the length scale of the bubbles). It was also assumed that the bubble sizes lie in the inertial sub-range. Buoyant collisions were modelled in terms of the bubble concentration and velocity, where the velocity was equal to the rise velocity of the bubbles and therefore a function of the bubble size, bulk liquid density, surface tension and gravity. The collision rate due to laminar shear was expressed in terms of bubble size, concentration and the average shear rate in the column, which was evaluated by averaging the local shear rate over the radial dimensions of the column.

Following Coulaloglou and Tavlarides (1977), the collision efficiency, λ, was modelled as a function of the contact time between bubbles and the coalescence time:

$$\lambda = \exp\left(\frac{-t_c}{\tau}\right) \tag{2.50}$$

where t_c is the coalescence time and τ is the contact time for two bubbles. To determine the coalescence time the authors used the film thinning expression developed by Oolman and Blanch (1986a), together with values for the initial film thickness and final thickness at rupture taken from the literature. The contribution of van der Waals interactions to the rate of film thinning was neglected to allow for an analytical solution to the model. It was claimed that although this may result in an overestimation of the coalescence time, it would be partially offset as the effect of approach velocities, shown to be important by Kirkpatrick and Lockett (1974), (and which would tend to increase coalescence times) was also neglected. The contact time of the bubbles was estimated as a function of the bubble size and the energy dissipation per unit mass, using the approach of Levich (1962) as given in Equation 2.1.

Finally, the overall coalescence rate in the system was obtained by summing the coalescence rate for each bubble pair and dividing by two, in order to avoid counting coalescence between bubble pairs twice. A brief analysis of coalescence rates in electrolyte solutions concluded that coalescence is unlikely to occur if the solute concentration exceeds a critical value, c_t, which can be calculated from Equation 2.25 (Prince and Blanch, 1990a). For concentrations exceeding this critical value the gas-liquid surface is immobilised by surface tension gradients

so that the rate of film thinning exceeds the bubble contact time and in these systems the coalescence efficiency is taken to be zero. Results generated by the model for coalescence in distilled water compared favourably with experimental data but when the model was extended to coalescence in electrolytic solutions, predicted and observed results were not comparable. Aspects of the modelling identified for further consideration were the particle contact times, effect of approach velocities on coalescence and the assumption of plane parallel flow and constant film radius during film thinning.

Lee et al. (1987), have also proposed a theoretical model to describe bubble break-up and coalescence in a turbulent gas-liquid dispersion, where bubble coalescence is again modelled in terms of the product of collision rate, coalescence efficiency and number densities of bubbles. The expression for the collision rate follows Coulaloglou and Tavlarides (1977), in assuming that the collision mechanism in a locally isotropic turbulent flow field is analogous to molecular collisions in the kinetic theory of gases and is modelled as a function of bubble size, concentration and velocity. Once again, bubbles are considered to be lie in the inertial sub-range with a velocity proportional to the turbulent eddy velocity. Only binary collisions were considered to give rise to coalescence.

The expression for the coalescence efficiency was determined as a function of the coalescence time and mean contact time, as given in Equation 2.50 (but with the contact time τ, replaced with the mean contact time $\bar{\tau}$). The mean contact time for two bubbles of sizes d_1 and d_2 was estimated by assuming it was proportional to the characteristic period of velocity fluctuations of an eddy of size $d_1 + d_2$ and consequently a function of the turbulent energy dissipation rate and bubble diameters. Coalescence time was considered to be the sum of the film thinning and rupture times. Two mechanisms were identified for film thinning; inertial or viscous force controlled. The expressions used for the rate of thinning in each case were those developed by Sagert and Quinn (1976a). The authors proposed an general expression for the rupture time of a film based on the expressions developed by Ruckenstein and Jain (1974), for rupture in a pure liquid and in the presence of a surface active agent (upper bound only) which contained contributions from the surface tension, bulk liquid viscosity, and surface immobility parameter. The coalescence time was estimated by taking the minimum in the sum of the film thinning and rupture times plotted as a function of the final film thickness.

Analysis of the model in terms of the influence of bubble size, energy dissipation rate per unit mass and surface immobility parameter showed the coalescence efficiency initially decreases with increasing bubble size before reaching a minimum and then increasing at each energy dissipation rate examined. This was attributed to the increase in both coalescence time and mean contact time as the bubble size increases. In the small bubble region the influence of size is stronger on the coalescence time than the contact time, this is reversed at larger bubble sizes. In all cases coalescence efficiency was found to decrease with increasing energy dissipation rate per unit mass, due to the decrease in mean contact time. Coalescence efficiency was also reduced as the surface immobility parameter increased, a result of the increase in coalescence times. The surface immobility parameter was found to exert a strong influence on the coalescence frequency: at low values where coalescence frequency increased with both bubble size and energy dissipation rate, the collision rate term was considered to dominate. However, at higher values of the surface immobility parameter, the coalescence frequency was found to decrease with increasing energy dissipation rate and to pass through a minimum bubble diameter and it was concluded that the coalescence efficiency term was now predominant.

In a theoretical analysis based on fluid mechanics, Thomas (1981) predicted a minimum bubble size stable against coalescence, which can be determined by considering the rate of energy dissipation in a turbulent two-phase system, ε. In the development the (equi-sized) bubble surfaces were considered immobile so that the film drainage was as between rigid planes. The time required for the film to thin to the rupture thickness is:

$$t_d = \frac{3}{32\pi}\mu F\left(\frac{d}{\sigma h_f}\right)^2 \qquad (2.51)$$

where F is the force pressing the bubbles together, d is the bubble diameter and h_f is the film thickness at the point of rupture. To develop the expression for the force applied to the bubbles it was considered that coalescence was due to eddies of the inertial sub-range (buoyancy effects were neglected as a consequence of the intensity of agitation). The force is therefore a function of the bulk liquid density, the bubble size and the energy dissipation rate per unit mass:

$$F \approx \rho\varepsilon^{\frac{2}{3}}d^{\frac{8}{3}} \qquad (2.52)$$

It was assumed that coalescence would only occur if the time for film drainage was less than the characteristic time-scale for the bubble-bubble collision (the contact time, τ), as given in

Equation 2.1 (Levich, 1962). Combining the expressions for the film drainage time, the applied force and the contact time, it was concluded that coalescence is not likely to occur unless $d < d_{crit}$, where:

$$d_{crit} \approx 2.4\left(\frac{\sigma^2 h^2}{\mu\rho\varepsilon}\right)^{\frac{1}{4}} \tag{2.53}$$

so that d_{crit} gives the size of the smallest bubble stable against coalescence. Experimental support for the model was claimed from the studies of Shinnar et al. (1961, 1960, 1957) who investigated liquid-liquid dispersions in which the predominant factor for determining drop size was considered to be coalescence prevention due to turbulence. It was found that below a critical value of the energy dissipation rate per unit mass, a minimum drop size stable against coalescence was observed to exist. In addition, the mean droplet size was found to be proportional to $\varepsilon^{-1/4}$ as suggested in Equation 2.53. This study has made little impact in the literature.

In a recent study of bubble coalescence and break-up in bubble columns, Colella et al. (1999) presented a model which accounts for the physics of freely rising bubble (including wake interactions, bubble swarm velocity and bubble shape), in which the predominant influences are the 'Wake' effect and the 'Shape' effect. The Wake effect is due to the fact that a bubble rising in a liquid determines the hydrodynamics in a portion of space at its rear, making it a primary mechanism for bubble-bubble interactions (Stewart, 1995 and Miyhara et al., 1991). The Shape effect allows for the fact that bubbles in a dynamic system are not generally spherical and that the shape can influence break-up (allowing easier formation of a neck) and coalescence (determining the amount of liquid in the film). The authors claim that the analogy with the kinetic theory of gases is inappropriate, as it considers bubbles interacting only through collisions and fails to allow for the influence of bubble wakes. The probabilistic approach of previous models (Chesters, 1991, Prince and Blanch, 1990b and Lee et al., 1987) is not considered valid, as coalescence times are usually an order of magnitude smaller than the contact time. In addition, it is claimed that the important effects of bubble shape have been ignored in the models previously developed.

In the model, the population balance equation is expressed as a series of differential equations evaluated for up to N discretised bubble classes and their respective radial positions, with terms allowing for the birth and death of bubbles due to coalescence and break-up. Once

again, coalescence was considered to be a binary process. The collision frequency is expressed as the product of the bubble concentration of each bubble class at that radial position, the relative velocities of the bubbles and a ratio expressing the probability of one bubble being in the wake of another. The coalescence efficiency is considered proportional to the average draining velocity (determined using a proportionality constant equivalent to the reciprocal of the relative velocity), which allows the coalescence efficiency to approach unity as the bubble diameter decreases. In line with experimental observations (Duineveld, 1994, Kirkpatrick and Lockett, 1974) the resultant expression predicts that bubbles will bounce as their relative velocity increases. Validation of the model with experimental data (from three different air-water systems) showed excellent agreement between measured and predicted trends.

2.3 Experimental Studies of Coalescence

Experimental studies into bubble coalescence fall broadly into two categories: those in which coalescence is observed directly under controlled hydrodynamic conditions and in-situ studies under dynamic conditions where coalescence behaviour is examined indirectly through measurements of bubble size distributions and gas hold-up values.

Bubbles have been observed to coalesce in stagnant liquids under a variety of geometries. Two adjacent bubbles can be formed simultaneously at parallel, vertical nozzles, (Lessard and Zieminski, 1971, Nicodemo et al., 1972, Sagert and Quinn, 1978, Oolman and Blanch, 1986a) or from two horizontal opposing nozzles (Zharadnik et al., 1998, 1995, 1987 and Martin, 1996). In these studies the parameters most often reported are the coalescence time, coalescence frequency and solute concentration corresponding to 50% coalescence in the system (variously called the transition or critical concentration). Coalescence times have also been determined by studying contact between a rising bubble and a free interface, (Doubliez, 1991, Farooq, 1972, Hodgson and Lee, 1969, Allan et al., 1969); such studies have also been used to observe changes in film thickness over time and the thickness at the point of rupture. (often using optical interference techniques). Studies on the interactions of two freely moving bubbles (DeKee et al., 1986, 1990, Crabtree and Bridgwater, 1971, De Nevers and Wu, 1971) have generally focused on quantifying the influence of bubble wakes on coalescence and are usually restricted to observing bubbles rising in-line in viscous liquids.

Although the film thinning times observed in stagnant liquids cannot be directly applied to coalescence rates on account of their more complex hydrodynamic environments, such studies provide a great deal of information about the way in which the liquid film between the bubbles thins and ruptures. In addition, studies in coalescence cells allow the complex interactions governing the coalescence process to be decoupled, so that it becomes possible to investigate separately the influence of variables such as bubble size, surface tension, surface age and the collision force and angle on the rate of coalescence.

In studies carried out in bubble columns and agitated vessels, the coalescence behaviour is investigated indirectly by measuring parameters such as the bubble size distribution and gas hold up of the system. However, both these parameters are influenced by physical properties of the system in addition to the coalescence behaviour; bubble sizes and the bubble size distribution are strongly influenced by the type of orifice and gas flow rate and the gas hold-up of a system is affected by the bubble density, the bubble rise velocities and the liquid viscosity. Care must be taken therefore in interpreting the results of the many studies carried out in order to obtain useful information about bubble coalescence in dynamic systems.

2.3.1 The Transition Concentration

In the development of liquid phase diffusion model (Section 2.2.2.1) Marrucci (1969a), introduced the concept of a transition concentration as the concentration of solute required in order to arrest the drainage of the thin film and prevent the almost instantaneous coalescence that occurs in pure liquids. Experimental evidence for the transition concentration has been obtained in both aqueous solutions of electrolytes and organic solutes, where the amount of coalescence observed in a system has been found to decrease dramatically over a very narrow concentration range.

2.3.1.1 Electrolyte Solutions

The transition concentration was first identified experimentally by Lessard and Zieminski (1971) who investigated the effect of inorganic electrolytes on bubble coalescence in aqueous solutions. Pairs of air bubbles were formed on adjacent vertical nozzles and a 'percent coalescence' (defined as the ratio of coalescing bubbles to the overall number of contacting pairs and henceforth referred to as the coalescence frequency) was determined for each solution. In pure water and dilute electrolyte solutions the coalescence frequency was 100%. However, at a concentration characteristic for each electrolyte, a distinct reduction in the

coalescence frequency was observed over a narrow concentration range. A critical concentration, analogous to the transition concentration, c_{trans}, was defined as that corresponding to 50% coalescence. Values of c_{trans} were smallest for the higher valency ion combinations and largest for the univalent electrolytes; they varied from 0.03 – 0.06M (for 3-1 ($AlCl_3$) and 2-2 ($MgSO_4$)) to 0.16 - 0.23M (for 1-1 combinations (LiCl, NaCl, NaBr, KCl)), as can be seen in Figure 2.8. By plotting coalescence frequency against ionic strength for each solution, c_{trans} was found to correspond to an ionic strength of 0.2 for all solutions. The authors proposed a combined charge-viscosity mechanism for coalescence inhibition, where the charge effects accounted for the valence dependence observed and the viscosity effect allowed for the temperature dependence reported. It was suggested that the ions influence the water structure in and around the surface layers of the bubbles, (depending on whether they were structure formers or structure breakers) and thereby retarding film drainage.

Similar observations had been made by Foulk and Miller (1921) who used a similar two bubble set-up to investigate 'film formation' (the absence of instantaneous coalescence) in solutions of electrolytes and mixtures of electrolytes and surface active species. Once again, rapid coalescence was observed in pure liquid and dilute solutions, but as the electrolyte

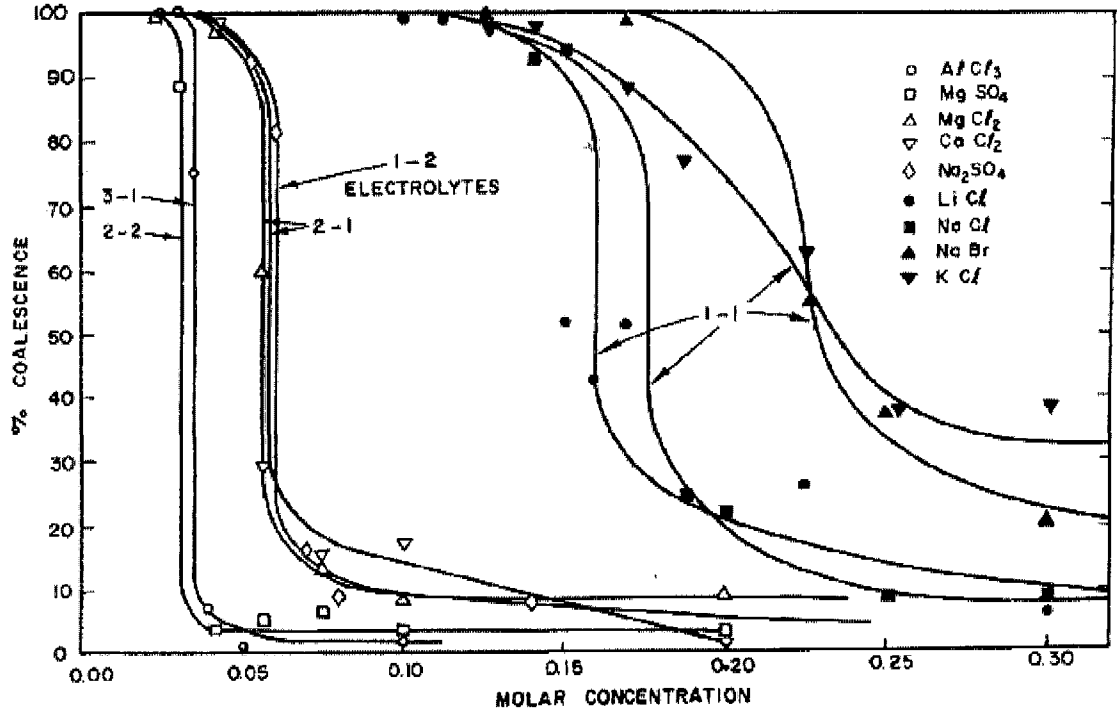

Figure 2.8

Plot of percentage coalescence against concentration for the range of electrolytes tested by Lessard and Zieminski (1971). Note the transition (critical) concentration at which there is a step change in coalescence behaviour for each electrolyte species.

concentration increased the amount of coalescence decreased sharply. However, in some mixtures of positively and negatively adsorbed solutes, rapid coalescence was still observed, even at high concentrations. It was also reported that solutions of cane sugar and sulfuric acid foam only at certain concentrations. The authors suggested 'film formation' depended on the difference between the static and dynamic surface tensions: when this difference is large coalescence is inhibited, whereas when the two values are similar (no difference in concentration in the surface layer and the bulk liquid) coalescence is rapid, as in a pure liquid. Correlation between '% film formation' and the difference between static and dynamic surfaces tension was extremely good.

Further studies of the transition concentration (c_{trans}) in aqueous electrolyte solutions have been carried out using pairs of vertically formed bubbles (Prince and Blanch, 1990a, Oolman and Blanch, 1986a) and bubbles formed at opposing nozzles (Zahradnik et al., 1999a, b, 1998, 1995, 1987). In each case experimental values for c_{rans} were compared to predicted values for the electrolyte concentration required to immobilise the gas-liquid interface, calculated using expressions reviewed in Section 2.2.1. Table 2.1 summarises the range of experimental data for a selection of electrolytes, together with values predicted using the various

Electrolyte	Transition Concentration (mol l^{-1})	
	Experimental	Calculated
$MgSO_4$	$0.032^{(1,)}$, $0.036^{(4)}$	$0.042^{(3,\ \blacktriangledown)\ (4,\ \blacktriangledown)}$
$MgCl_2$	$0.055^{(1)}$,	$0.056^{(3,\ \blacktriangledown)}$
$BaCl_2$	$0.037^{(4)}$	$0.039^{(4,\ \blacktriangledown)}$
Na_2SO_4	$0.051^{(4)}$, $0.061^{(1)}$	$0.05^{(2,\ \clubsuit),\ (4,\clubsuit)}$, $0.061^{(3,\ \blacktriangledown)}$, $0.089^{(4,\clubsuit)}$
$CaCl_2$	$0.055^{(1)}$, $0.056^{(4)}$	$0.053^{(4,\ \blacktriangledown),}$ $0.055^{(3,\ \blacktriangledown)}$
LiCl	$0.16^{(1)}$,	$0.16^{(3,\ \blacktriangledown)}$
NaOH	$0.084^{(4)}$	$0.078^{(4,\ \blacktriangledown)}$
NaCl	$0.145^{(4)}$, $0.175^{(1)}$	$0.15^{(4,\ \blacktriangledown)}$, $0.175^{(3,\ \blacktriangledown)}$
NaBr	$0.22^{(1)}$,	$0.22^{(3,\ \blacktriangledown)}$
KCl	$0.202^{(4)}$, $0.23^{(1)}$	$0.13^{(2,\ \clubsuit)}$, $0.196^{(3,\ \blacktriangledown)}$, $0.209^{(4,\ \blacktriangledown)}$
KI	$0.38^{(4)}$	$0.38^{(2,\clubsuit),\ (4,\clubsuit)}$, $0.58^{(3,\ \blacktriangledown),\ (4,\ \blacktriangledown)}$

Reference (1)	Lessard and Zieminski (1971)	Equation (♣)	Marrucci (1969a)
Reference (2)	Oolman and Blanch (1986a)	Equation (♥)	Prince and Blanch (1990a)
Reference (3)	Prince and Blanch (1990a)		
Reference (4)	Zahradnik et al., (1995)		

Table 2.1

Summary of experimental and predicted values for transition concentrations in electrolyte solutions.

expressions for c_{trans}. As can be seen, both equations give satisfactory predictions, given the variation in experimental values obtained.

In a recent study, Craig et al. (1993) investigated the effect of electrolytes on coalescence using a simple bubble column. The coalescence frequency was determined by measuring the amount of light transmitted, assuming that 100 % coalescence corresponded to the signal for pure water and 0 % coalescence to the concentration at which no further change in signal was measurable. As in the two bubble studies, a transition concentration (corresponding to 50 % coalescence) was observed for a large number of electrolytes. However, a significant number of species showed no coalescence inhibiting effect, these included the mineral acids and various organic electrolyte species. From the results, the authors devised a combination rule for the anions and cations investigated, assigning a 'property' of α or β to each, such that combinations $\alpha\alpha$ or $\beta\beta$ exhibited coalescence inhibition, whereas combinations of $\alpha\beta$ or $\beta\alpha$ had no effect (Figure 2.9). For the coalescence preventing salts a correlation with ionic strength was observed, as noted by Lessard and Zieminski (1971). The existence of a transition concentration was also demonstrated for the sugars glucose, fructose and sucrose. Explanations for coalescence inhibition based on surface tension effects, viscous effects and electrostatic repulsion were dismissed in lieu of a possible correlation of the coalescence prevention effects of various electrolytes with their ability to reduce the hydrophobic force of

	CATIONS								
	β	α	α	α	α	α	α	β	α
ANIONS	H^+	Mg^{2+}	Na^+	Ca^{2+}	K^+	NH_4^+	Cs^+	Me_4N^+	Li^+
OH^-	✗	I. Sol		I. Sol	✓				
Cl^-	✗	✓	✓	✓	✓	✓		✗	✓
Br^-	✗		✓		✓		✓		
NO_3^-	✗		✓	✓	✓	✓		Unavail	✓
ClO_3^-	Unavail	Unavail	✗	Unavail	I. Sol	Unavail	I. Sol	Unavail	Unavail
SO_4^{2-}	✗	✓	✓	I. Sol		✓			✓
ClO_4^-	✓	✗	✗	Unavail	I. Sol	✗	I. Sol	Unavail	Unavail
CH_3COO^-	✓	✗	✗		✗	✗	✗	✓	
Oxalate $^{2-}$	✗	I. Sol	I. Sol	I. Sol	✓	I. Sol	Unavail	Unavail	

Combining Rules: αα or ββ gives ✓ αβ or βα gives ✗

I. Sol=Insufficiently soluble Unavail=Salt unavailable

Addition of salt: Prevents coalescence ✓ Has no effect on coalescence ✗

Figure 2.9

The effect of electrolytes on bubble coalescence (Craig et al., 1993)

attraction between two bubbles. (This is a long-range force, about 10 to 100 times greater in magnitude than the van der Waals attractive force, see Section 2.3.1.3).

2.3.1.2 Solutions of Surface Active Species

The existence of a transition concentration has also been confirmed for surface active species. Oolman and Blanch (1986a), observed bubble pair coalescence in a number of pure liquids, solutions of electrolytes and surfactants and in two microbial broths and attempted to correlate their experimental results with theoretical models.

It was predicted that the coalescence behaviour of solutions of organic species would differ from that observed in electrolyte solutions, as the vapour pressure of the organic species would allow replenishment of the surfactant in the film, due to diffusion from the gas phase. In addition, it was claimed that as the higher molecular weight molecules would not equilibrate rapidly with an interface, chemical equilibrium between the bulk and the surface of the film could no longer be assumed. Surfactants investigated in this work included a range of *n*-alcohols (C_1 to C_5), *n*-amyl alcohol, *n*-butyric acid and sodium dodecyl sulfate. For the higher molecular weight species, a very sharp transition between coalescing and non-coalescing systems was observed; for solutions containing methanol and ethanol this transition region was much broader (Figure 2.10).

Experimental data was compared with two sets of predicted values, the first calculated using liquid phase diffusion theory of Marrucci (1969a) and the second using the volatile surfactant theory developed by the authors. Good agreement was observed between experimental and the Marrucci values for sodium dodecyl sulfate (ionic species, no vapour pressure), but for the remaining solutes the difference between measured and predicted values increased with vapour pressure. Better agreement was observed between experimental values and the volatile surfactant theory, although in all cases there was a consistent deviation from theory, which was attributed to the inaccuracy of parameters used in predicting the transition concentration.

In their study, the coalescence frequency was measured in a number of fermentation broths and in the uninoculated growth media. As in the solutions of organic surfactants, a sharp transition in coalescence frequency was observed. No coalescence was observed in the undiluted broths. As the ionic concentration in the growth media was below the predicted

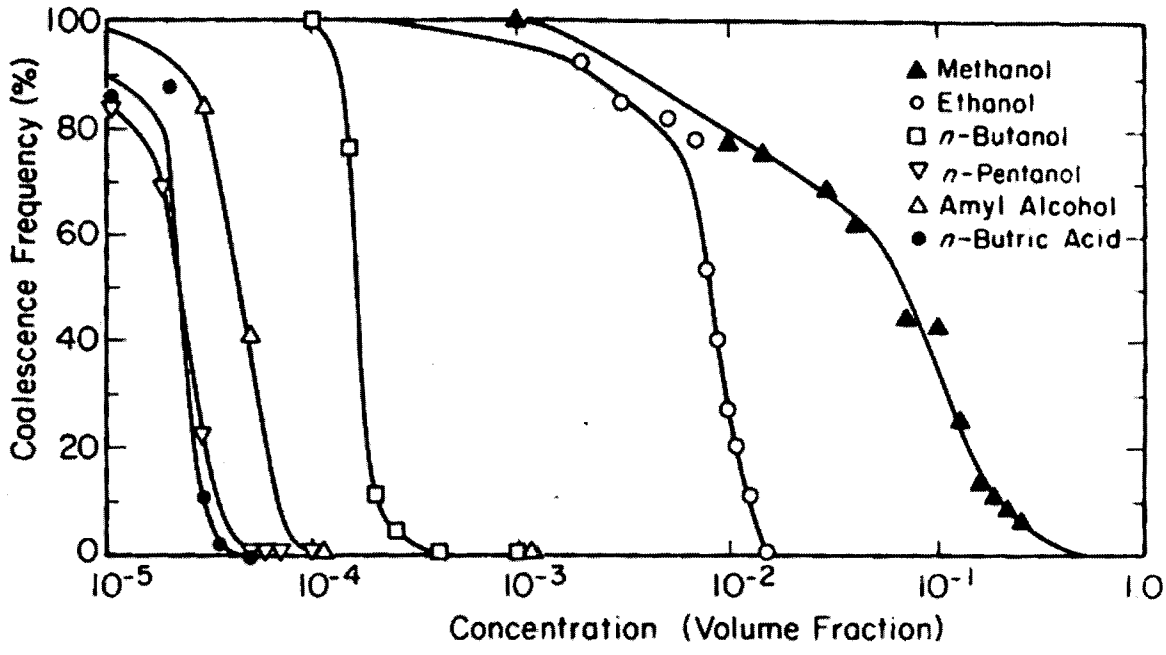

Figure 2.10

Plot of coalescence frequency against concentration for aqueous solutions of organic surfactants. Note the sharp change in coalescence frequency for higher alcohols compared to the broad transitions observed for methanol and ethanol (from Oolman and Blanch, 1986a).

inhibitory level, inhibition was considered a result of the surface activity of the organic substrates and metabolic products. The transition concentration was found to decrease from the initial growth media to the final broth, suggesting that the metabolic products were more surface active than the substrates. Microbial cells appeared to have no influence on the coalescence process as no significant variations were observed between the filtered and unfiltered broths.

Drogaris and Weiland (1983) measured the coalescence times for bubble pairs in aqueous solutions of *n*-alcohols and fatty acids. Again bubbles in very dilute solutions were observed to coalesce at the moment of contact but at increased surfactant concentrations a sharp transition from 100 % to 0 % coalescence was noted. The transition concentration decreased with increasing surfactant chain length and values were approximately an order of magnitude greater for *n*-alcohols than for fatty acids of the same carbon chain length. Values increased with increasing bubble size and decreased with increasing bubble frequency. The sharp change in coalescence behaviour with increasing chain length was explained in terms of a change in the relationship between the drainage and rupture times of the intervening film. For the low molecular weight alcohols and fatty acids, the time required for film rupture is negligible and coalescence times are approximately equal to the film drainage times. However, as the chain length increases, increased dampening of the film surfaces means the

contribution of the film rupture time to the overall coalescence time can no longer be neglected.

2.3.1.3 Explanations for the Transition Concentration

Marrucci (1969a) attributed the transition concentration to the establishment of surface tension gradients caused by film stretching. Indeed, the parameter common to the many of the models for coalescence time (including the liquid phase diffusion model and its modifications, the gas diffusion model of Oolman and Blanch (1986a) and the dynamic surface tension theory of Andrew (1960) and Sagert et al., (1976a)) is the change in surface tension with concentration $d\sigma/dc$ (or $[d\sigma/dc]^{-2}$ as it appears in the expressions for transition concentration). It is only in the surface immobility model (Sagert and Quinn, 1978) that the rate of decrease of thinning is ascribed to some other factor, in this instance, the surface immobilisation.

Experimental evidence reported in the literature as to the correlation of $d\sigma/dc$ with the transition concentration is not consistent. Zahradnik et al. (1998) report good correlation of the transition concentrations for both alcohols and electrolytes as a function of the term $[\sigma^n(d\sigma/dc)^{-2}]$, where n = 1/3 and ¼ (or 1/6) for solutions of alcohols or electrolytes respectively. Christenson and Yaminsky (1995) re-interpret the results of Craig et al. (1993) in terms of surface elasticity, E. This parameter determines the response of the interface to mechanical disturbance and can be related to the quantity $d\sigma/dc$ (also known as the surface activity) through the expression:

$$E = \frac{4c[d\sigma / dc]^2}{kTD^*} \qquad 2.54$$

where k is the Boltzmann constant, T, the temperature and D^* a measure of the thickness of the interface. Measured values for the transition concentration (from Craig et al., 1993) are plotted against values for $[d\sigma/dc]^{-2}$ in Figure 2.11; the correlation coefficient is 0.92 and as can be seen, low transition concentrations are associated with high film elasticity. Christenson and Yaminsky (1995) claim that those electrolytes which do not exhibit a transition concentration are those for which the concentration would have to exceed the solubility limit in order to give the same elasticity. Table 2.2 shows that electrolytes which have no effect on bubble coalescence have very small values of $[d\sigma/dc]^2$. Generally the

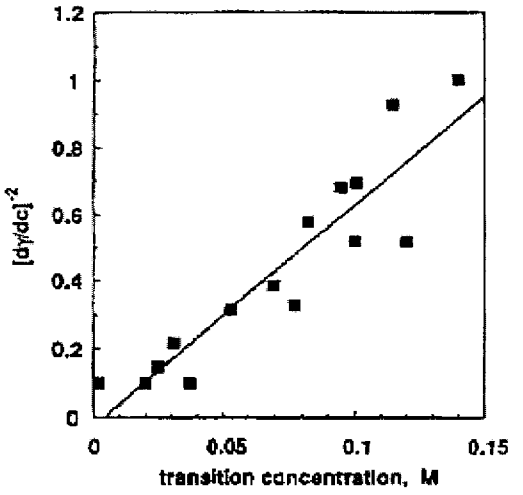

Figure 2.11

Plot of the inverse of elasticity factor $(d\sigma/dc)^{-2}$ against the transition concentration (From Craig et al. 1993) for the following: CH_3COOH, $MgSO_4$, Li_2SO_4, $(NH_4)_2SO_4$, $CaCl_2$, KOH, $HClO_4$, NaCl, KBr, $LiNO_3$, NH_4Cl, $NaNO_3$, KNO_3, KCl and NH_4NO_3. Least-squares fit with slope = 6.5, intercept = -0.03 and correlation coefficient = 0.92. (Christenson and Yaminsky, 1995).

electrolyte	$d\gamma/dc \approx \Delta\gamma/c$ (1 M)	$(d\gamma/dc)^2$	transition concn
$CaCl_2$	3.2	10	yes
NaCl	1.6	2.6	yes
$(CH_3)_4NCl$	0.6	0.4	no
$NaClO_3$	0.55	0.3	no
CH_3COOK	0.45	0.2	no
HCl	−0.3	0.1	no
HNO_3	−0.8	0.6	no
$(COOH)_2$	−0.85	0.7	no
$HClO_4$	−1.6	2.6	yes
CH_3COOH	−3.2	10	yes

Table 2.2

Surface activity ($d\sigma/dc$) and coalescence behaviour in aqueous electrolyte solutions. (Christenson and Yaminsky, 1995).

transition from one type of electrolyte to the other occurs when the value of $[d\sigma/dc]^2$ falls below −1 $(mNm^{-1}M^{-1})^2$ (Pashley and Craig, 1997).

However, Weissenborn and Pugh (1996) claim that the correlation between values for the transition concentration (from Craig et al, 1993) and $[d\sigma/dc]^{-2}$ is only mediocre (0.74, see Figure 2.12). In addition, it is claimed that it is inconceivable that such small surface tension differences in the film could generate sufficient flow of liquid to slow film drainage/rupture and hence bubble coalescence (Weissenborn and Pugh, 1996). Instead, several other mechanisms are discussed including hydration forces and interfacial attraction arising from the presence of microscopic bubbles.

Hydration forces are short-range repulsive forces, which have been observed between approaching hydrophobic surfaces. Experiments carried out by Pashley (1981) observed the existence of hydration forces between mica surfaces in solutions of KBr above concentrations of about 10^{-4} M (transition concentration 0.83 M, Craig et al., 1993) but not in HCl solutions, even at high concentrations (Craig et al. (1993) report no transition for HCl at concentrations below 1 M). However, Weissenborn and Pugh (1995) note that the rupture thicknesses

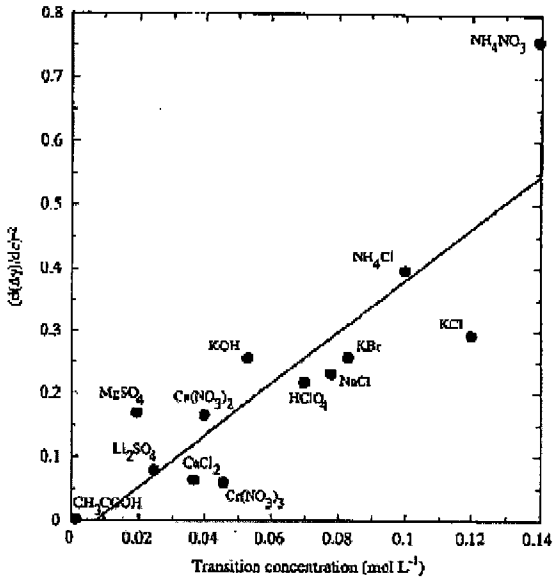

Figure 2.12

Correlation between $[d(\Delta\sigma)/dc]^{-2}$ and bubble coalescence transition concentration taken from Craig et al., 1993. Correlation coefficient = 0.74. (Weissenborn and Pugh, 1996).

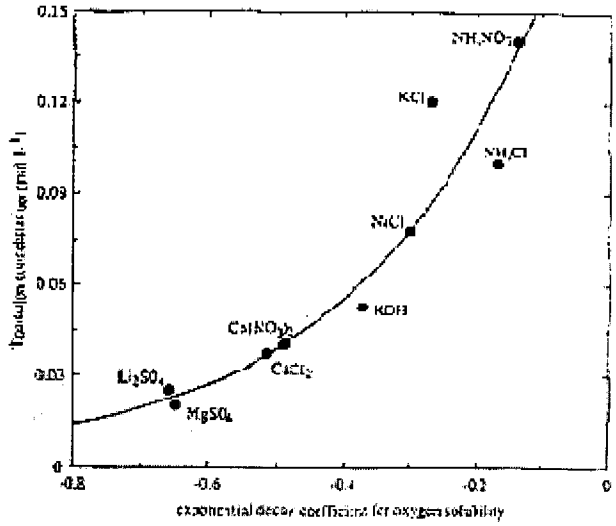

Figure 2.13

Correlation between transition coalescence (from Craig et al., 1993) and exponential decay coefficient for oxygen. Correlation coefficient = 0.95. (Weissenborn and Pugh, 1995).

reported by Cain and Lee (1985) for bubbles in solutions of KCl (see Section 2.3.2) are much larger than the range over which any conceivable hydration force could operate.

Craig et al. (1993) observed that explanations for the transition concentration cannot be based on surface tension changes at the interface, nor on viscosity effects, as suggested by Lessard and Zieminski (1971). Repulsion due to electrostatic forces was also discounted due to the short range and weak magnitude of such forces. Pashley and Craig (1997) observe that at the rupture thicknesses reported by Doubliez (1991), (about 110 nm for bubbles in water) the van der Waals forces are negligible. Consequently, it was proposed that coalescence in water is due to an attractive hydrophobic force, sufficiently long-range (between 10 – 100 nm) and strong enough (10 - 100 times stronger than van der Waals forces) to overcome the hydrodynamic repulsion between two bubbles. In coalescence inhibited solutions this force is much reduced. A mechanism for the origin of the force was proposed based on surface-induced adsorption and nucleation of dissolved gases in water.

Experimental support for the effect of electrolytes on the hydrophobic attraction is conflicting. Measurements (between methylated silica surfaces) in solutions of NaCl and $NaClO_3$ have been reported (Craig et al. 1993) and the results found to correlate with the effects of the two salts on coalescence (in NaCl, a coalescence inhibitor, the magnitude of the force is much

reduced, whereas in $NaClO_3$, which shows no effect on coalescence, it is equivalent to that in water). It has also been observed that higher valence electrolytes are more effective than univalent species in reducing the strength of the hydrophobic force (the decay length is unaffected) (Tsao et al., 1993). However, it has also been reported (Parker et al., 1994) that electrolytes have only a minor effect on hydrophobic force, except at very high concentrations where the force of attraction is found to increase slightly. In addition, Wood and Sharma (1995) report that the range of the interaction depends very much on the nature of the surface preparation, such that it is much shorter for truly hydrophobic surfaces, such as bubbles (approximately 10 nm) and independent of electrolyte concentration.

In addition to hydration forces, Weissenborn and Pugh (1995) also considered that coalescence could arise through a bridging interaction, mediated by microscopic bubbles adsorbed onto the macroscopic bubble surfaces, which would result in perturbations in the water structure at this point. It was proposed that these perturbations could be related to the effect of electrolyte concentration on the dissolved gas concentration; good correlation was reported between the transition concentrations reported by Craig et al. (1993) and the gas solubility (see Figure 2.13, Weissenborn and Pugh 1995). Inhibition of coalescence would therefore be linked with a decrease in dissolved gas concentration in electrolyte solution (and a consequent decrease in the number of microscopic bubbles), thus weakening the bridging attraction.

2.3.2 Measuring Coalescence Times and Film Thicknesses

In experimental terms the coalescence (or rest) time is defined as the time taken from the initial bubble-bubble contact to the point of film rupture. Usually a range of coalescence times is observed for a particular system and although individual coalescence times are not reproducible, a distribution of coalescence times is obtained when sufficient measurements are made, which is generally reproducible (Palermo, 1991). Coalescence times are most often determined using photographic methods, although some recent studies report the use of optical interference methods. Interferometric techniques have been often applied to follow the change in film thickness with time (especially for studies of a single bubble coalescing with an interface), although high-speed camera studies have also been reported.

Coalescence times in pure solutions were measured by Oolman and Blanch (1986a) for two bubbles formed adjacently in water, propyl acetate, iso-butanol, *n*-propanol, glycerol and

carbopol solution. Values for the coalescence times varied from a few milliseconds in water (5.0 ms) and the organic species (the shortest time observed for propyl actate, 2.7 ms) to 100 ms in glycerol. The experimental data was compared with that calculated from the authors' model and that of Chesters and Hofman (1982), (Equation 2.11 of this work); although both models gave reasonable agreement for the insvicid solutions, neither accurately predicted the very large increase in coalescence time observed for bubbles in glycerol. Farooq (1972), investigating coalescence of single bubbles with an interface found coalescence times were strongly dependent on the bubble size; bubbles larger than 0.5 mm bounced before coalescing, thereby greatly increasing the coalescence time.

Data for coalescence times in aqueous electrolyte solutions has been reported by several authors (Cain and Lee, 1985, Nicodemo et al., 1972 and Marrucci et al., 1969b). Nicodemo et al. (1972) and Marrucci et al. (1969b) observed that for a specific electrolyte the coalescence time increased with solution concentration and that the rate of increase in time was greater in solutions of Na_2SO_4 than in solutions of KOH. Values ranged from a few milliseconds for very dilute solutions to several hundred milliseconds as the concentration increased. For each solution the coalescence time versus solute concentration curve could be divided into two distinct regions, which were interpreted by the authors as corresponding to regions of inertially controlled thinning (dilute solutions) and the formation of a quasi-equilibrium film thickness (more concentrated solutions).

Cain and Lee (1985) determined the coalescence times and film thickness during drainage for two air bubbles formed in a series of KCl solutions, by measuring changes in reflected light intensity as the film drained. No film was formed between bubbles in 0.1 M KCl solution. In 0.5 M solution, the coalescence time was approximately 420 ms and the film ruptured at a thickness between 75 and 95 nm. The coalescence time increased to about 600 ms for bubbles in 1 M solutions, although the rupture thickness decreased to between 55 and 75 nm. Interestingly, visual observations of the film during thinning did not show any non-uniformity of thickness (considering the formation of a dimple observed by Allen et al., 1969) and films were observed to be essentially plane parallel. Experimental values for thinning times were compared with model predictions; the rate predicted by the rigid interface model of Reynolds (1886) was found to be too slow and although the model of Radoëv (1969) showed good agreement at small film thicknesses, the initial rate of thinning was too rapid. Experimental values for the thickness at rupture were compared with the theoretical values predicted by Vrij

and Overbeek (1968), (Equation 2.9 of this work); experimental values were found to be twice those predicted.

Several studies have been carried out into the coalescence times of bubbles in aqueous solutions of various surfactants. Bubbles in solutions of *n*-alcohols and fatty acids have been studied by Ueyama et al. (1993), Drogaris and Weiland (1983) and Sagert et al. (1976b); Babak et al. (1996), Kim and Lee (1987) and Yang and Maa (1983) have observed coalescence times in ionic surfactant solutions.

Coalescence time data for bubbles in solutions of *n*-alcohols are reported to range from a few tenths of a millisecond to several hundred milliseconds. As in electrolyte solutions there is a increase with increasing solute concentration; in addition Drogaris and Weilland (1983) report the existence of an asymptotic (maximum) coalescence time beyond which solute concentration has no effect, this maximum value increases with increasing carbon number. All studies observed a systematic increase in coalescence time for an increase in chain length of the solute molecule. Drogaris and Weiland (1983) also reported much greater coalescence times for fatty acids than for *n*-alcohols with an equal number of carbon atoms; this difference was attributed to the higher polarity of the carboxyl group and consequently, an increased affinity for the surface over the bulk. Coalescence times increase with increasing bubble size (Drogaris and Weilland, 1983). The influence of surface age and approach velocity has been investigated by Ueyama et al. (1993). Coalescence times were observed to increased with the age of the bubbles, the effect being greater at higher concentrations. As the bubble age approached zero the coalescence time was observed to approach a value characteristic of the bulk concentration. In contrast with the results of Kirkpatrick and Lockett (1974) and Farooq (1972), coalescence times were observed to be largely independent of the approach velocity of the bubbles, although a much smaller range of velocities was investigated (the maximum velocity being less than half the threshold value identified by Kirkpatrick and Lockett, 1974).

Both Drogaris and Weilland (1983) and Sagert et al. (1978) observed that coalescence times for low molecular weight species (up to *n*-pentanol) were proportional to the alcohol concentration. For most of the higher molecular weight species however, times were found to be to proportional to the square of the concentration. Drogaris and Weilland (1983) demonstrated a correlation between the coalescence time and change in surface tension with concentration and found that for a given solution, coalescence times were proportional to both

the surface excess concentration (calculated from the Gibbs or Langmuir isotherms) and the square of the bubble diameter.

Sagert et al. (1978, 1976a, b), compared experimental results with theoretical predictions generated from the coalescence models discussed in Section 2.2.2.4 and 2.2.2.5. High-speed film was used to measure coalescence times for nitrogen bubbles formed adjacently in solutions of alkyl ammonium bromides (Sagert and Quinn, 1976b) and solutions of *n*-alcohols (Sagert et al., 1978). Coalescence times for the alkyl ammonium bromides were found to increase with increasing solution concentration and ranged from about 5 to 500 ms. Both sets of experimental data were compared with the predictions of the liquid phase diffusion model (Marrucci, 1969a) and the dynamic surface tension model. A good fit was obtained with Marrucci (1969a) model for the solutions of low molecular weight alkyl bromides (ammonium bromide and tetramethylammonium bromide). However, for the solutions of *n*-alcohols the dynamic surface tension model gave better agreement, correctly identifying the order of alcohols in stabilising films (coalescence decreases as molecular weight increases). The dimensionless parameter $c'rk^2/\sigma$ was used to give an indication of the stability and immobility of the films and hence the nature of the coalescing system. The liquid phase diffusion model was found to apply for values of $c'rk^2/\sigma$ between 0 - 10, whereas for values above 400 (providing viscous effects are negligible) the dynamic surface tension model was most applicable. For values of $c'rk^2/\sigma$ between 10 - 400, neither model predicted experimental results accurately.

Yang and Maa (1983) used high-speed photography to investigate the effects of various surfactants (*n*-octanol, sodium lauryl sulfate, sodium lauryl benzene sulfonate) on the coalescence of nitrogen bubble pairs. Once again, systems were found to change from fully coalescing to non-coalescing over a very narrow concentration range, although coalescence was inhibited at much smaller concentrations than in electrolyte solutions (less than 2 ppm for n-octanol and less than 1ppm for sodium lauryl benzene sulfonate). Depending on the concentration of solute, the coalescence times measured varied from 1 – 500 ms. Coalescence restraining was attributed to large $d\sigma/dc$ values, caused by the local depletion of surfactant and consequent increase in surface tension at the point where the gas-liquid interface is stretched. It was also suggested that adsorption of the high molecular weight species may

cause the bubble surface to become slightly immobile, resulting in a large change in the coalescence time.

Coalescence times in aqueous solutions of surfactants and polymers were also measured by Babak et al. (1996) who again report the existence of a critical concentration corresponding to the transition from unstable (lifetimes of several seconds) to stable (lifetimes greater than 1000 s) foam films. The value of the critical concentration was reported to depend on the concentration of electrolyte, pH, compression force (and film surface area) and temperature.

In one of the few studies to investigate bubble coalescence in gases aside from air (or nitrogen), Sagert and Quinn (1976a) measured coalescence times for H_2S and CO_2 bubbles formed on adjacent nozzles in water. Both gases are considered surface active as they result in lower surface tensions compared to air-water. Coalescence times for CO_2 bubbles were small (average values 1 – 3 ms) at pressures below 2 MPa, but increased with pressure to 20 ms at 3.4 MPa (this compares with nitrogen bubbles, where the coalescence times measured were in the range 1.5 ± 0.5 ms and independent of pressure). Times for H_2S bubbles were also measured as a function of pressure; values were much larger than for CO_2, especially at higher pressures, increasingly linearly from about 8 ms to in excess of 100 ms. The authors demonstrated a linear correlation between coalescence time and activity for H_2S and suggested that coalescence times would increase as the saturation pressure of a system is approached.

In addition to the above two bubble studies, several studies have measured coalescence times and changes in film thickness by observing the interactions of a single bubble with a free interface. Doubliez (1991) carried out a series of experiments in water and solutions of methanol and ethanol. As Farooq (1972) and Kirkpatrick and Lockett (1974) reported, bubbles greater than a certain size tended to oscillate at the interface before coalescing, the number of bounces being greater in solutions of alcohol than water. For a 0.25 mm diameter bubble in water, coalescence times were of the order of 1 – 2 ms, with film thicknesses at rupture ranging from 110 to 435 nm. In solutions of alcohol the coalescence times were increased, primarily due to increased bouncing. In all cases, the thinning curves showed three stages: a fast drainage, a reduced rate and arrest of thinning and finally a thickening of the film (Doubliez, 1991). Interestingly, rupture was generally observed to occur during the final

stage when the film thickness was increasing and never occurred at thicknesses below 80 nm (in all liquids).

2.3.3 Coalescence Studies In Bubble Columns

As has been discussed previously, coalescence and therefore the bubble size and gas hold-up in a bubble column is strongly dependent on system properties. It is well known that bubbles tend to coalescence faster in pure liquids, whereas the addition of electrolytes or surfactants leads to the suppression of bubble coalescence resulting in a lower average bubble size and higher gas hold-up and interfacial area.

2.3.3.1 Coalescing Systems (Pure Liquids)

Air-water systems are used as the benchmark system for the design of bubble columns and consequently numerous studies are reported in the literature. Although less extensively reported, studies in pure organic liquids (not mixtures) show similar influences. In both cases the primary influence on the bubble size is the flow regime (hold-up increases with gas velocity) and a definite effect of gas distributor.

Bach and Pilhofer (1978) measured gas hold-up as a function of superficial gas velocity in a number of different organic liquids (butan-1,3-diol, ethylene glycol, tetrabromomethane and *n*-octanol) over a range of temperatures (283 – 333 K). Hold-up was observed to decrease with increasing liquid viscosity, although no effect of surface tension was observed. The most important parameter was found to be the liquid kinematic viscosity; for liquids with the same kinematic viscosity (and similar densities), differences in gas hold-up were negligible and a plot of relative bed expansion against kinematic viscosity (for a constant gas flow rate) gave a linear correlation. For comparison a number of experiments were carried out with glycerol-water mixtures; these showed an initial increase in hold-up with glycerol concentration (and consequently with increasing viscosity) and the existence of distinct maxima in the hold-up curves.

Studies of gas hold-up in mixtures of organic liquids show considerable differences to the behaviour observed in pure liquids, most notably that gas content appears to pass through a maximum, which varies according to mixture composition. Bhaga et al. (1971) measured the gas hold-up in binary mixtures for different gases. For all mixtures, the gas hold-up was higher than that observed for the pure components and passed through a maximum, although

the composition at which this occurred varied. Bubble sizes in the mixtures were considerably smaller than in the pure liquids. The decrease in hold-up either side of the maximum values was attributed to bubble coalescence, confirmed through visual observation. The effect of temperature and gas properties was also investigated: increasing temperature caused a decrease in gas hold-up in the middle range, with the effect more pronounced at higher gas flow rates (no effect of temperature was observed for pure liquids). Hold-up increased with gas molecular weight, with the largest increase observed for pure liquids; smaller bubbles were formed with denser gas. The increase in hold-up observed for the binary mixtures was discussed in terms of the formation of surface tension gradients ($d\sigma/dc$) arising from surface elasticity considerations, although the important influence of gas density on bubble formation was also recognised.

2.3.3.2 Coalescence Inhibited Systems

It is well known that the average bubble size in solutions of electrolytes or surface active species is much smaller than those observed in comparable systems of pure liquids; a fact which is attributed to the inhibition of bubble coalescence in these solutions. The increase in interfacial area observed in these coalescence inhibited systems generally results in increased values for the gas hold-up.

Marrucci and Nicodemo (1967) used a photographic technique to measure bubble sizes in electrolyte solutions. For all electrolytes, the average bubble size was found to decrease asymptotically to a common value, which was independent of gas flow rate (Figure 2.14). The concentration at which this asymptotic value was reached differed for the various electrolytes and could be correlated with the transition concentrations reported by Lessard and Zieminski (1971) in their two bubble experiments. For the five electrolytes used with equal anion and cation valences (KCl, KOH, KI, KNO_3, $CuSO_4$) the mean bubble size was shown to be depend on the change of surface tension with solute concentration ($d\sigma/dc$). Dilute solutions of ethanol behaved in a similar manner to the electrolyte solutions, although the asymptotic diameter was reached at a much lower concentration. Visual observation showed that the primary influence on bubble size was the type of distributor plate and that the influence of gas flow rate and electrolyte concentration was secondary. The greatest amount of coalescence was observed to occur near the distributor plate and this appeared to determine the ultimate size of bubbles in the column, as throughout the remainder bubble sizes were approximately uniform.

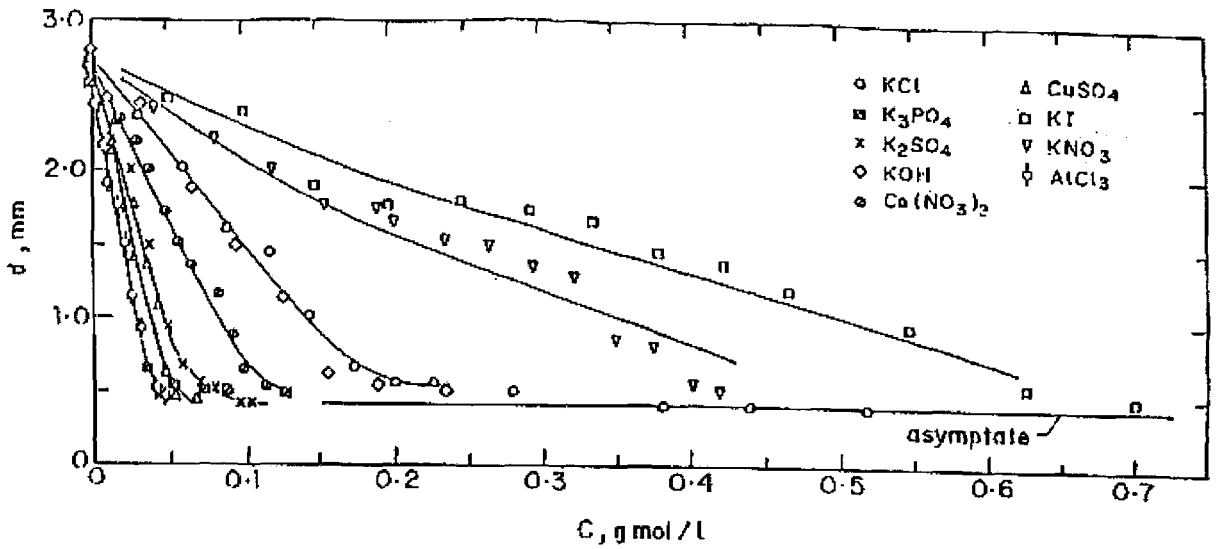

Figure 2.14

Average bubble diameter as a function of electrolyte concentration (u = 0.5cms^{-1}, plate porosity = 8μ), showing the asymptotic bubble diameter approached by all electrolytes solutions. (from Marrucci and Nicodemo, 1967).

Bubble sizes in air-sparged electrolyte solutions have also been measured by Zieminski and Whittemore (1971) who combined the results with gas hold-up measurements to determine interfacial areas for the dispersions. 3-2, 3-1 and 1-3 electrolytes ($Al_2(SO_4)_3$, $AlCl_3$, Na_3PO_4) showed the greatest increase in interfacial area for the smallest concentration, whereas much higher concentrations were required for the 1-1 electrolytes to show much smaller effects. The influence of valence and concentration was accounted for by correlating the interfacial area with ionic strength (Figure 2.15).

Marrucci and Nicodemo (1967) attributed the coalescence restraining effects (of both electrolytes and alcohols) to the presence of an electrical double layer, resulting in a surface potential. Zieminski and Whittemore (1971) point out that this is unlikely to be correct; for solutions of equal concentration, KCl is much more effective than KI at preventing coalescence, despite the fact that KI produces a higher surface charge. [Chaudhuri and Hofman (1994) offer an alternative interpretation of the results, in terms of the liquid phase diffusion model (Section 2.2.2.1); at solute concentrations above the 'critical' value, electrostatic double layer repulsive force balances the van der Waals attractions, resulting in the existence of an equilibrium thickness and hence suppressing coalescence.] Instead, Zieminski and Whittemore (1971) suggest that the degree of coalescence depends on ion - water interactions (such as the degree of order produced) and the presence of charges at the bubble surface. It was suggested that ions which are structure makers will increase the rigidity of the surface film and thus decreases coalescence. A similar explanation was

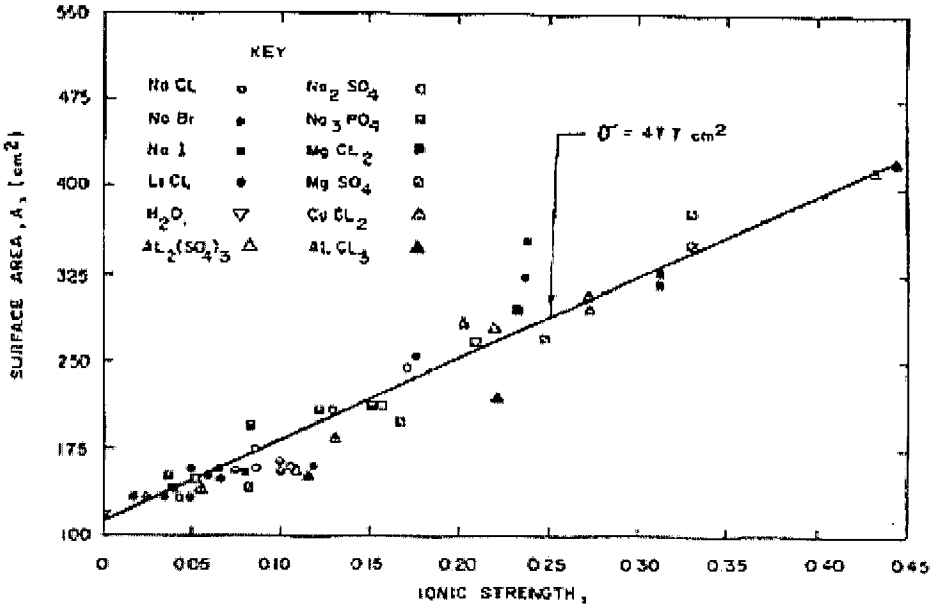

Figure 2.15

Zieminski and Whittemore (1971); correlation of interfacial area with ionic strength.

proposed by Lessard and Zieminski (1971) to explain transition concentrations observed in electrolyte solutions.

Keitel and Onken (1982b) measured bubble size distributions in various solutions of electrolytes and organic solutes using a photoelectric probe. For electrolyte solutions, the Sauter mean diameter d_{32}, was found to correlate with ionic strength, with a maximum decrease of a factor of four (correspondingly, Zieminksi and Whittemore (1971) observed a maximum increase in interfacial area of the same amount). The Sauter mean diameter and gas hold-up for aqueous solutions of alcohols, glycols, ketones and carboxylic acids were plotted as a function of the logarithm of the solute concentration (Figure 2.16). A critical concentration c_o, was defined above which coalescence inhibition became significant, causing a measurable decrease in the mean bubble size. For each homologous series a linear relation was found between the logarithm of c_o and the number of carbon atoms; values of c_o decreased with increasing solute chain length, before approaching a limiting value at high molecular weights beyond which the effectiveness of the solute in inhibiting coalescence became independent of molecular size. The observation of a limiting bubble size correlated well with the observations of Drogaris and Weiland (1983) of an asymptotic maximum coalescence time with increasing solute concentration. For the same number of carbon atoms, c_o values increased (and coalescence inhibition decreased) in the order monocarboxylic acids < *n*-alcohols < glycols < ketones. It was also observed that there was no simple correlation

between coalescence inhibition and gas hold-up; for solutions of electrolytes and monocarboxylic acids the increase in hold-up was negligible despite the decrease in bubble size measured.

In studies reviewed so far, gas velocities have been low and systems therefore restricted to operating within the homogenous (bubbly flow) regime. Zahradnik et al. (1987, 1995), measured hold-up in aqueous solutions of electrolytes and alcohols, in a column operating under both homogeneous and heterogeneous regimes. For all solutions hold-up increased continuously in the column (no step-wise change as in a coalescence cell) and maximum values for hold-up were obtained at concentrations close to the transition concentration; increasing the electrolyte/alcohol concentration beyond this value had little effect. For alcohol solutions, the effect on hold-up decreased with decreasing gas flow rate, being greatest in the heterogeneous regime but negligible at very low gas velocities. In contrast, the influence of electrolytes was greatest in the homogeneous and transition bubbling regimes, but only moderate in the heterogeneous bubbling regime where the dominant influence appeared to be macro-scale turbulence. A good correlation was observed when the values for gas hold-up in alcohol solutions were plotted against the logarithm of the bubble coalescence ratio (ψ), suggesting the possible existence of a relationship, $\varepsilon_G = \psi\varepsilon_G$ (Zahradnik et al., 1987). For electrolyte solutions, the absolute increase in bed voidage was found to be

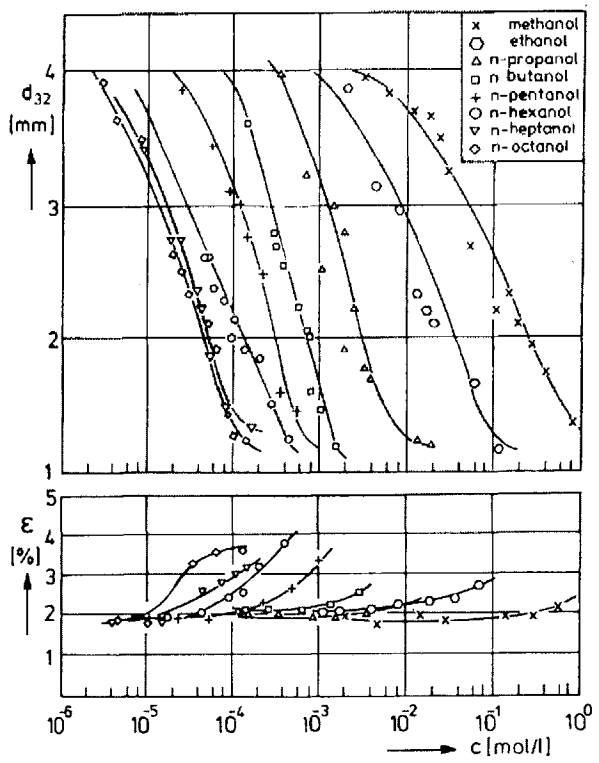

Figure 2.16

Sauter mean diameter, d_{32} and gas hold-up , ε for air-water versus concentrations of *n*-alcohols. (Keitel and Onken, 1982b).

independent of the type of electrolyte, varying only with the mode of primary gas dispersion.

2.3.3.3 Viscous Systems

The importance of viscosity on bubble coalescence in pure liquids was demonstrated by Bach and Pilhofer (1978), who observed that there was a general decrease in gas hold-up with increasing liquid viscosity. With increasing liquid viscosity one tends to observe shift towards a bimodal bubble size distribution (Lee and Patel, 1983) where coalescence is promoted with respect to large bubbles such that a number of very large bubbles are formed (which have a short residence time) whilst at the same time, large numbers of very small bubbles (less than 1 mm in diameter) are retained in the dispersion due to their impeded rise velocity. It is generally accepted that the coalescence promotion observed for medium to large bubbles is due to the increased contributions of wake-induced collisions through which bubbles are drawn into the wake of a leading bubble, resulting in prolonged contact times and therefore increased probability of coalescence. The importance of wake induced coalescence has been demonstrated by Stewart (1995) and Otake et al. (1977) and in two bubble studies by DeKee et al. (1990, 1986), Narayanan et al. (1974) and Crabtree and Bridgwater (1971), amongst others.

Aqueous solutions of glycerol provide a convenient (Newtonian) model liquid and are often used to investigate the effect of viscosity. In contrast with pure liquids, no simple decrease in hold-up with viscosity is observed. Instead, several authors (Zahradnik et al., 1987, Bach and Pilhofer, 1978) report that hold-up increases in solutions of intermediate concentration (and thus moderate viscosity). Bach and Pilhofer (1978), observed that this increase is greatest for the heterogeneous bubbling regime. Maximum values for hold-up occurred in mixtures of moderate viscosity (between 1.5 and 6mPas) whereas for viscosities beyond 50 mPas hold-up remained constant (and much decreased). Likewise, Zahradnik et al. (1987) reported no change in gas hold-up in very dilute solutions (less than 1%); in concentrated solutions however, hold-up was decreased relative to the air-water system. Studies in a coalescence cell supported these observations; coalescence frequency approached unity for the more concentrated (and viscous) solutions but tended towards 0.1 for solutions of intermediate concentration (Zahradnik et al., 1987). Calderbank (1965) claimed that the extent of bubble coalescence was largely determined by the liquid viscosity; in a CO_2-water/glycerol system a critical viscosity of 70 mPas was observed above which coalescence was very rapid leading to a large decrease in hold-up and interfacial area.

Zahradnik et al. (1999a, b, 1998) have recently investigated gas hold-up and transition concentrations in viscous solutions of saccharose and xanthan containing either electrolytes or alcohols. Transition concentration for alcohols in fully coalescent solutions of saccharose (Newtonian) and xanthan (non-Newtonian) were of the same order as those observed in aqueous solutions and showed a very similar dependence on carbon chain length ($c_t = n_c^{-7}$). In contrast, no change in coalescence frequency was observed for electrolytes in saccharose solution (up to 3 M) and in xanthan solutions values for the transition concentrations were much higher than those observed in aqueous solution. The effect of alcohol addition on gas hold-up was evaluated in the homogeneous bubbling regime for increasing concentrations of saccharose (and hence increasing viscosity); all showed an increase in hold-up with increasing alcohol concentration, with the influence greatest in highly viscous solutions (beyond 100 mPas). As in the coalescence cell, coalescence inhibition increased significantly with carbon chain length. Whereas flow in the unmodified saccharose solutions was found to be extremely non-uniform, the addition of small amounts of alcohol was found to significantly improve the radial uniformity. In addition no influence of the distributor plate was observed in the unmodified solutions; on the addition of alcohol however hold-up was increased for the smaller orifice diameters and the homogeneous bubbling regime extended.

2.3.3.4 The Influence of Gas Properties

Generally increasing the gas density is considered to give the same results as increasing the system pressure. However, whilst it is usually reported that an increase in pressure gives higher values for hold-up, there is some inconsistency in the literature as to the effect of gas density. Hikita et al. (1980) investigated several non-air systems (H_2, CO_2, CH_4, C_3H_8 and mixtures of H_2 and N_2) using a single nozzle sparger and developed a correlation for gas hold-up which included the physical properties of the gas phase. It was concluded that although small, the effects of gas density and viscosity on gas hold-up could not be considered negligible. Craig et al. (1993) investigated the effect of gas on the transition concentration in electrolyte solutions and also observed a small but definite change with gas density (the transition concentration occurred earlier in high density gases). Bhaga et al. (1971), in their study of organic liquid mixtures observed a definite influence of gas type, with an increase in gas hold-up and decrease in bubble size as the gas density increased.

In contrast, Akita and Yoshida (1973) measured the hold-up in water of air, O_2, He and CO_2 and concluded the effect of gas density was negligible though it was observed that hold-ups

with He were slightly decreased at higher gas velocities. Clark (1990) measured hold-up in a slurry bubble column at elevated pressures and found lower values for N_2 than for H_2, (except at higher gas velocities) in spite of the fourteen-fold increase in gas density. It was concluded that hold-up is not dependent on gas density, but rather on some other pressure dependent property (the gas bubble surface tension was suggested).

2.3.3.5 Effects of Temperature and Pressure

Despite the fact that most industrial processes operate at increased temperature and pressure, the majority of bubble column studies have been carried out at ambient temperature and pressures. Studies reported in the literature for both temperature and pressure effects are not fully consistent.

Bhaga et al. (1971) included temperature effects in their investigations of hold-up in organic liquid mixtures, carrying out experiments at 298 and 333 K. Very little effect of temperature was observed for pure liquids; for mixtures however, an increase in temperature resulted in a decrease in gas-hold-up, which was especially pronounced at high gas velocities. Grover et al. (1986) investigated the effect of temperature (303 – 353 K) on gas hold-up in air-water and air-electrolyte solution bubble columns. In the air-water system, hold-up decreased substantially with increasing temperature up to a particular temperature, beyond which the effect was marginal. In electrolyte solutions however, the influence of temperature was more complex: at lower gas velocities hold-up increased with temperature, but at higher velocities, it was observed to decrease with temperature. Similar observations were made by Lessard and Zieminski (1971) who note an increase in percentage coalescence with increasing temperature for air bubbles in seawater. In contrast Craig et al. (1993) conducted experiments in solutions of NaCl and $MgSO_4$ at temperatures from 280 to 323 K and noted a slight reduction in the coalescence frequency. Correspondingly, Zou et al. (1988), studying hold-up in air-water, air-alcohol and air-5% NaCl solution, report that gas hold-up always increases (and average bubble size decreases) with temperature. The effect of temperature was ascribed to its influence on vapour pressure and not its effect on parameters such as density, viscosity and surface tension.

Lin et al. (1998) studied the effects of temperature and pressure on a nitrogen-organic liquid column and observed that gas hold-up increases with both increasing temperature (generally) and pressure. The temperature effect was considered to result from decreased liquid viscosity

and surface tension, leading to a smaller average bubble size, although a secondary, (competing) effect of increasing gas density was recognised. Over a range of temperatures, the bubble size was observed to decrease and the bubble size distributions narrow with increasing pressure. This was considered to arise from a reduction in the maximum stable bubble size combined with a decrease in coalescence efficiency as the system pressure increased. The decrease in coalescence efficiency was considered to result from a reduction in the bubble collision rate together with an increase in film thinning rates (increasing pressure results in an increased liquid viscosity and a reduction in surface tension). The increase in hold-up was considered to result from the smaller bubble size and narrowed bubble size distribution coupled with reduced rise velocities.

Jiang et al. (1995) report that although gas hold-up increases with pressure up to 10 MPa, beyond this point the hold-up is largely unaffected by system pressure. The effect of increased pressure was principally to reduce the fraction of large bubbles in the column, thereby decreasing the average bubble size and narrowing the size distribution. Wilkinson and van Dierendonck (1990) also observed an increase in gas hold-up (and decrease in average bubble size) with increasing pressure but claimed this was due to the influence of gas density on bubble break-up rather than bubble formation. A study in electrolyte solutions (Wilkinson et al., 1994) showed the increase in gas hold-up with increasing pressure was more pronounced at higher gas velocities, and in all cases resulted in values much higher than in pure liquids. It was concluded that the influence of electrolyte and gas density on hold-up are synergistic.

2.3.4 Observations Of Coalescence In-Situ

Observations of bubble interactions and coalescence in-situ have proved important for elucidating the primary mechanisms of approach and contact that precede bubble coalescence (or break-up).

Many studies have focused on the influence of bubble wakes on interactions between two bubbles rising in line, which become especially important in viscosity modified solutions. Crabtree and Bridgwater (1971) conclude that increasing liquid viscosity promotes coalescence between two vertically aligned bubbles rising in Newtonian solutions, although the wake effects of the leading bubble diminish with distance such that beyond a critical value interaction no longer occurs. Bubble shape and size are also reported to influence the

coalescence process. Narayanan et al. (1974) identified five classes of bubble wakes, based on the bubble Reynolds numbers (see Figure 2.17); the wakes with the greatest influence on coalescence are those of classes III and IV. Although wakes of class I and II favour coalescence with a trailing bubble, their influence is effective only over small separations. Class V wakes are very unstable and their influence on coalescence is small due to the unsystematic configuration of the wake.

Studies on interactions within a bubble swarm have been carried out by Stewart (1995) and Otake et al. (1977), both of which emphasise the importance of the bubble wake in coalescence. Stewart (1995), investigating pulsed planar swarms of 10-20 bubbles rising in low viscosity, aqueous solutions of sucrose, reported that only a very small number of events collisions resulted in coalescence (~3 %), approximately half as many as resulted in break-up (~6.5 %). Wake-induced collisions were observed to be the driving force and sole mechanism for bubble interaction as no bubble approached another without being drawn into a leading bubble wake. Coalescence (or break-up) only occurred after (not during) collisions and only when certain geometrical arrangements were achieved (see Figure 2.18). All the coalescence events observed were binary and occurred between bubbles of approximately similar size. Time scales were very short, with many events occurring within 30 ms and all within 100 ms. Unlike the accepted mechanism for coalescence, requiring bubbles to remain in contact until

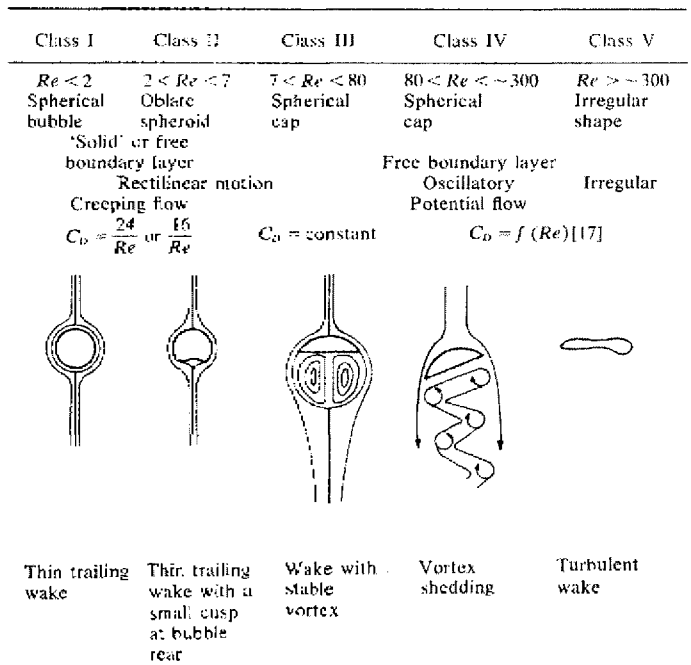

Figure 2.17

The five classifications for bubble wakes identified by Narayanan et al. (1974).

the film thins sufficiently to allow rupture, the 'interface penetration' (Stewart, 1995) appeared to be instantaneous, with confluence being the longest part of the process. Clusters of bubbles formed when several bubbles were captured in the wake of another or in rapid sequence and the close proximity of bubbles was found to promote coalescence, resulting in the formation of large cap bubbles.

Otake et al. (1977) report that coalescence only occurs when the two bubbles come within a critical distance of each other, (approximately 3 to 4 times the leading bubble diameter), at which point the influence of the leading bubble wake becomes noticeable. In addition, it was observed that coalescence requires that greater than half of the projected area of the trailing bubble overlaps with that of the leading bubble at this critical distance. If not, bubble break-up would occur. This corresponds with the observations of Mao and Core (1993) who report that for coalescence to occur, the trailing bubble must be drawn into the centre-line of the leading bubble wake. Consequently, coalescence is also much influenced by the oscillations of the freely rising bubbles (and the associated shape changes) which affect the wake geometry. Although both Otake et al. (1977) and Mao and Core (1993), observe that the relative sizes of the bubbles strongly influenced the coalescence process, the detail is not consistent. Otake et al. (1977) note that coalescence generally only occurred when the leading bubble was larger than the trailing bubble, as it was easier to satisfy the geometrical (overlap) requirements. Mao and Core (1993) however, observed that when the leading bubble is small, it is entrained in the fluid surrounding the larger bubble and is swept behind, in effect becoming the trailing bubble, before coalescence occurs. Mao and Core (1993)

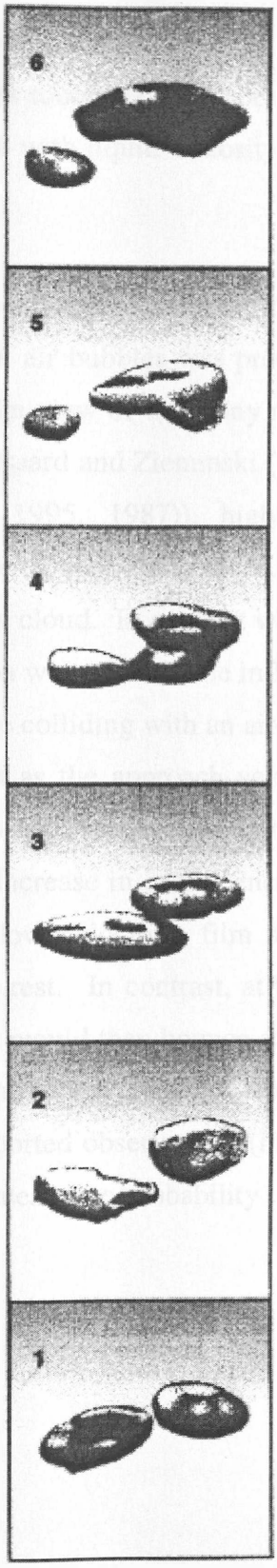

Figure 2.18

Simultaneous break-up and coalescence showing the influence of bubble wake and position on bubble interaction (from Stewart, 1995)

confirm the wake dependence of the process by injecting bubbles simultaneously but 0.5cm apart; although the bubbles influenced each other (and sometimes touched), coalescence did not occur. Otake et al. (1977), ascribe the increase in coalescence with liquid viscosity to the increased stability of the bubble wakes in viscous liquids.

The influence of approach velocity on coalescence was demonstrated by Kirkpatrick and Lockett (1974), using an experimental set-up in which a cloud of air bubbles was prevented from rising up a column by down-flowing water. Surprisingly, (in view of the many reports of virtually instantaneous coalescence for air bubbles in water (Lessard and Zieminski (1971), Oolman and Blanch (1986a) and Zahradnik et al. (1998, 1995, 1987)), high-speed photography revealed an almost complete absence of coalescence in the bubble cloud. This was attributed to the large approach velocities of the bubbles in the cloud. In contrast with the observations of Stewart (1995) and Otake et al. (1977), no mention was made of the influence of bubble wakes in coalescence. Experiments with a single bubble colliding with an air-water surface showed that at low velocities coalescence was rapid but as the approach velocities increased, the coalescence time also increased, principally as a consequence of bubble bouncing. A mathematical model was developed to explain the increase in coalescence time with increasing approach velocities. It was postulated that at low velocities, film rupture would occur before the two approaching bubbles are brought to rest. In contrast, at higher velocities the bubbles stop moving before film rupture occurs and would then bounce apart as a result of the stored strain energy, thus increasing the total coalescence time. Predictions made using the model were found to compare favourably with reported observations (Farooq, 1972) correlating bubble size (and therefore rise velocity) with coalescence probability.

Chapter 3
Experimental Equipment and Methods

In this study, investigations into bubble coalescence have been carried out using two different experimental approaches. The first set of experiments concentrated on observing two bubble coalescence in the controlled environment of a coalescence cell. Results from these experiments provided information about the influence of various factors on the coalescence process, as the experimental design allowed a number of system parameters to be altered. In the second type of experiment, investigations were carried out in the dynamic environment of a bubble column, where coalescence was monitored indirectly through the determination of bubble size data and bubble size distributions. In addition, a limited number of high-speed video studies were carried out in order to monitor coalescence events in-situ.

3.1 TWO BUBBLE STUDIES

All two-bubble studies were carried out in a coalescence cell, similar in design to that used by Zahradnik et al., (1999, 1995, 1987) where bubbles were contacted from two horizontally opposing nozzles. This contrasts with the apparatus used by Lessard and Zieminski (1971) and Drogaris and Weilland (1983), amongst others where bubbles where contacted from vertical oriented nozzles and not constrained by the apparatus geometry. Table 3.1 provides a summary of the geometries used in the two bubble investigations reported in the literature.

As can be seen, by far the majority of the work has been carried out using vertically oriented nozzles, with the bubbles generated at very low flow rates. Under these circumstances, the fluid dynamics may be reasonably expected to be quite different from those experienced by bubbles colliding from horizontally opposing nozzles; this should be especially true at higher flow and hence bubble formation rates. The parameter most commonly reported in these studies is the coalescence time, which is taken as the time from the first moment of contact to the film rupture point and in almost all cases, is determined using photographic methods. Lessard and Zieminski (1971), Oolman and Blanch (1986a) and Zahradnik et al. (1995, 1987) however have reported coalescence frequencies (ratio of coalescing bubble pairs to contacting bubble pairs).

Reference	System	Nozzle Orientation/ Separation (mm)	Nozzle Diameter (mm)	Gas Flow Rate ($ml min^{-1}$)	Bubble Frequency (s^{-1})
Marrucci et al. (1969b)	Air & Aq. Electrolyte Sol^n	Vertical / 0.8	0.8	1.98	0.38
Lessard & Zieminski (1971)	Air & Aq. Electrolyte Sol^n	Vertical / -	D_b = 3.6		1.8 – 2.6
Nicodemo et al. (1972)	Air & Aq. Electrolyte /Alcohol Sol^n	Vertical / 0.8	0.8	1.98	0.38
Sagert & Quinn (1976b)	Air/N_2 & Aq. Alcohol Sol^n	Vertical / 1.1	1.1	2.0	-
Sagert & Quinn (1976a)	CO_2/H_2S & Water	Vertical / 1.1	1.1	2.0	-
Sagert & Quinn (1978)	N_2 & Aq. Tetra-alkylammonium Bromide Solutions	Vertical / 1.1	1.1	2.0	0.4 – 4
Drogaris & Weilland (1983)	Air & Aq. Alcohol/ Fatty Acid Sol^n	Angled 30°/	0.5 – 2.7	-	0.01 – 5
Yang & Maa (1984)	N_2 & Surfactant Sol^n	Vertical / 1.0	2.0	-	0.5 – 2.0
Chaung et al. (1984)	N2 & Aq. Amyl Alcohol Sol^n	Vertical / adjustable	-	-	0.09 – 1.0
Oolman & Blanch (1986a)	Air & Aq. Sol^n (Electrolyte/ Alcohol/ Glycerol/ Carbopol/ Surfactant) Air - Microbial Broth	Vertical / 1.5	0.9	0.8 – 4.0	0.67 – 4.0
Zharadnik et al. (1995, 1987)	Air & Aq. Electrolyte/Alcohol Sol^n	Horizontal / 3.5	1.6	1.13	0.75
Ueyama et al. (1993)	Air & Aq. *n*-Alcohol & Surfactant Sol^n	Vertical / adjustable	D_b = 3.4	-	-
Cattaneo (1995)	Air & Aq. Na_2SO_4 / PPG Sol^n	Horizontal / 4 – 6	1.6	5 - 280	1 - 25
Zharadnik et al. (1999)	Air & Aq. Electrolyte/Alcohol & Sucrose Sol^n	Horizontal / 3.5	1.6	1.13	0.75

Table 3.1 (preceding page)
Summary of the configurations of two bubble experiments reported in the literature.

3.1.1 Equipment

3.1.1.1 The Coalescence Cell

The cell was constructed from window glass cut to size and assembled with silicone sealant. Figure 3.1(a) gives a representation of the cell and dimensions; the internal volume of the cell was 2.1 dm^3. The cell was surrounded on the two narrow sides and on the base by a water jacket which enabled contents to be maintained at a constant operating temperature during experiments. The front and rear sides of the cell remained unjacketed in order to allow for clear observation of events inside the cell. In addition, the rear face of the cell was sandblasted to reduce reflection and to ensure the video camera was focused on events occurring at the nozzles. The water jacket was connected through copper piping sealed into the vessel near the top of the two sides and connected with silicone tubing to a water-bath (model LTD6 from Grant Instruments (Cambridge) Ltd., UK) which had precision temperature control of ± 0.1°C. The temperature of the cell contents was measured using a mercury thermometer (accuracy ± 0.5°C) and over the duration of a typical experiment was found to remain within this limit.

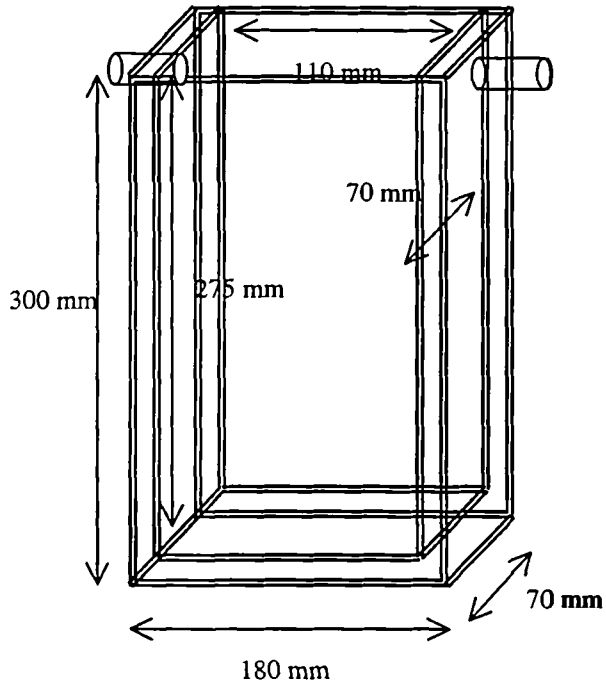

Figure 3.1(a)
The coalescence cell, showing dimensions.

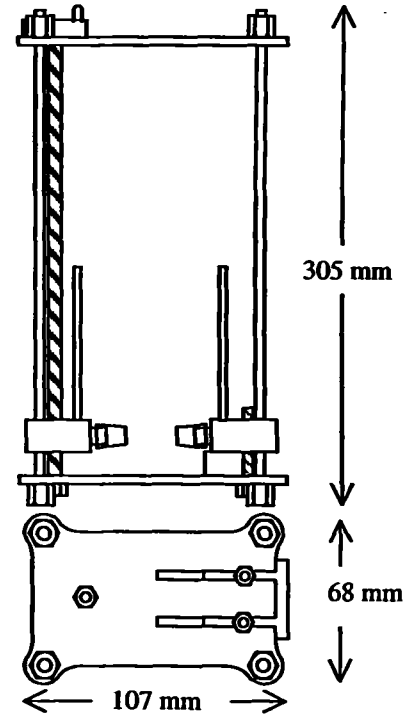

Figure 3.1(b)
The stainless steel frame.

The second part of the coalescence cell consisted of a stainless steel frame (Figure 3.1(b)) which had two adjustable mountings for the nozzles, allowing the geometry to be altered in both the horizontal and vertical directions. For this work, all bubble pairs were generated in the same plane, with no variations in vertical alignment. One of the nozzles was attached to two of the frame pillars and although vertically adjustable through winding the vertical thread, was fixed in the horizontal position. The second nozzle was attached with two bolts to the base of the frame and maintained at a height of 10 mm through the use of a spacing block. The inter-nozzle distance was varied by moving the horizontally adjustable nozzle, setting the distance with a set of Vernier calipers.

For experiments the stainless steel frame was inserted into the cell and the working height of sample liquid was added to give an inclusive volume of 1 dm^3. Care was taken to ensure the cell and contents were always completely level before use.

3.1.1.2 Nozzles

Following on from development work carried out by Cattaneo (1995) polypropylene nozzle extensions were attached to the end of each of the stainless steel nozzles. These extensions were created from 1 ml polypropylene syringes. The end of the syringe was cut off at a distance of 8 mm from the narrow end (measured using Vernier calipers) and using a 5 mm stainless steel reamer, the inside was drilled out to a distance of 5 mm from the cut edge, to allow for mounting onto the stainless steel nozzles. Dimensions of the finished nozzle extensions are given in Figure 3.2. The internal diameter of the nozzle extension was 2 mm, outer diameter 3.8 mm.

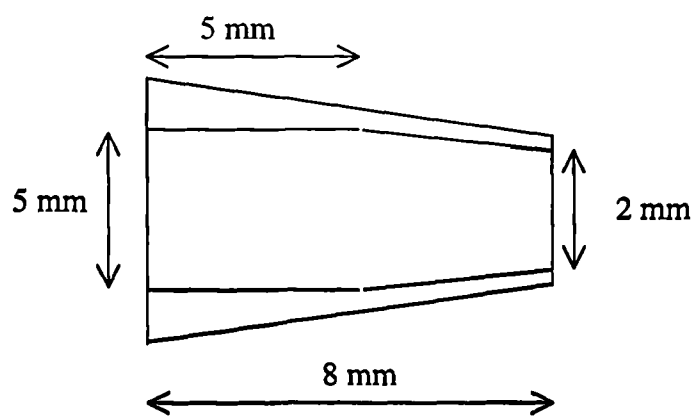

Figure 3.2

Dimensions of the polypropylene nozzle extensions attached to the stainless steel frame.

3.1.2 Experimental Set-Up

In this work the coalescence cell was integrated into a continuous flow system which ideally resulted in the constant formation of synchronised bubble pairs. A general schematic of the final experimental set-up used is shown in Figure 3.3.

Compressed gas [1] is delivered at a pressure of $2.1*10^{-2}$ kgcm^{-2} through the use of secondary pressure regulation with a mercury manometer [2]. The gas is filtered through a 0.2 μm filter [3] and passed through a saturator [4] filled either with water (when the test fluids contained no volatile substances) or the test fluid (in the case of volatile additions). In the section following the saturator, the gas supply is split into two separate flows. Each passes through a 2 dm^3 buffer tank [5], designed to suppress any pressure fluctuations in the gas flow. Flow control is achieved through the use of needle valves [6] in conjunction with a pair of gas flow meters [7]. The gas then passed through a pair of 150mm long capillary tube [8] (glass, internal diameter 0.8 mm) designed to induce an increased pressure drop across the system and promote the synchronous formation of bubbles, before being connected to the stainless steel frame [9]. All tubing in the systems was silicone rubber tubing (4.8 mm internal diameter, 1.6 mm wall thickness). Throughout the set-up efforts were taken to ensure that tubing lengths were kept to a practical minimum and that the path lengths for both the gas

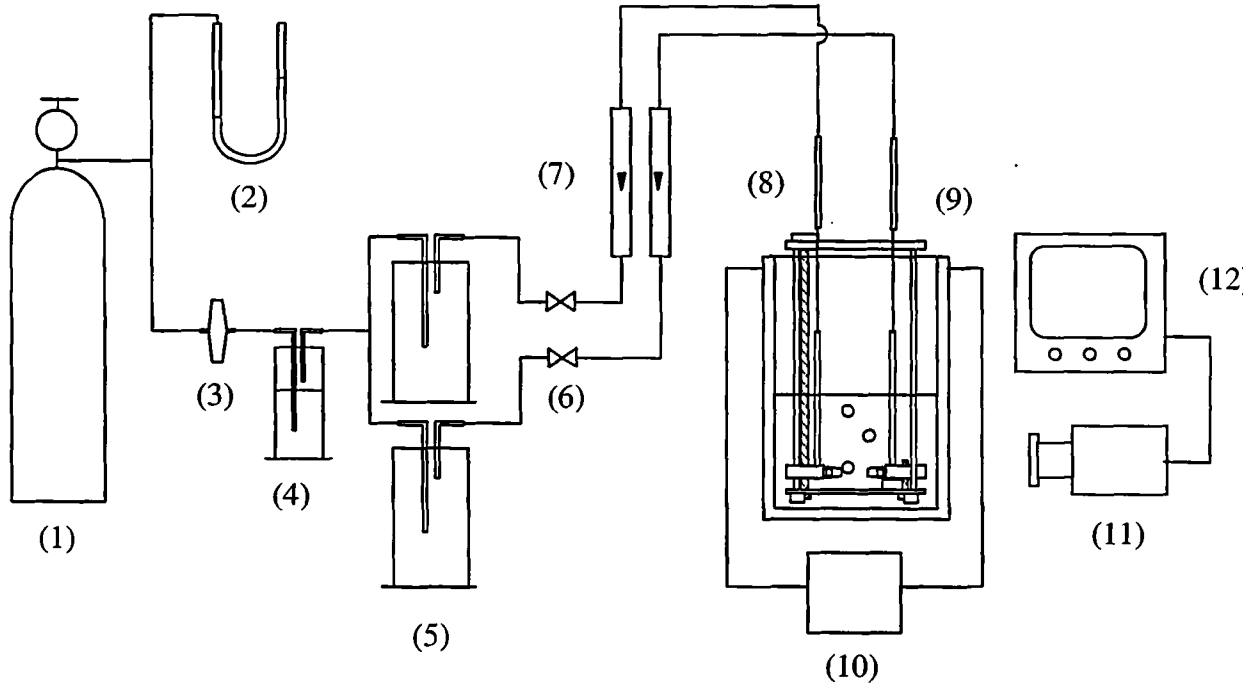

Figure 3.3

Schematic diagram of the experimental set-up: (1) Gas cylinder, (2) Mercury manometer, (3) 0.2μm filter, (4) Saturator, (5) Buffer tank, (6) Needle valve, (7) Flow meter, (8) Glass capillary tube, (9) Coalescence cell with stainless steel frame, (10) Water-bath, (11) Panasonic NV-M40 movie camera, (12) Television.

flow routes identical. Events occurring at the nozzles were filmed using a Panasonic NV-M40 VHS movie camera [11], using VHS videotape.

3.1.2.1 Promoting Synchronous Bubbling

Although there are a number of studies reported in the literature using experimental set-ups similar to the one described in this work, virtually none of the workers have mentioned the necessity of synchronising the bubble pairs and the concomitant difficulties. However, it has become obvious from this work that for a two-bubble system, synchronous bubble formation is neither trivial nor easily achieved. Consequently, a large amount of work in this study has been devoted to the pursuit of synchronous bubbling and many modifications were made to the both the experimental set-up and gas feed combinations before the configuration shown in Figure 3.3 was adopted.

In the original experimental set-up a mercury manometer was used to regulate the system pressure and the gas was filtered before being passed through the saturator directly to the coalescence cell. The range of gas flows investigated was much wider than for the final experimental set-up: two pairs of Model RGT Platon flow meters (5 to 100 $mlmin^{-1}$ and 50 to 500 $mlmin^{-1}$, Platon Instrumentation, UK) were used to measure over the range 10 to 300 $mlmin^{-1}$. Although care was taken to try to ensure the flow rates through the two nozzles was the same, bubble synchronicity had not been yet considered to be a crucial factor.

However, it soon became obvious that synchronous bubble formation over the duration of the experiment was extremely important. Painstaking efforts to ensure minimum possible tubing and identical paths (equal length and running parallel to ensure the same geometry) did not provide a solution. The addition of a pair of needle valves (which replaced those attached to the flow meters) was also unable to provide the expected level of fine control necessary to produce synchronicity across the flow range. Following Miyahara and Takahashi (1986), a buffer tank (1 dm^{-3}) was inserted into the set-up just downstream from the filter and a pair of capillary tubes (glass, length 150 mm, internal diameter 0.8 mm) was used to replace the final length of silicone rubber tubing immediately preceding the coalescence cell. Although there was a noticeable improvement in the bubble-pair synchronicity at intermediate flow rates, at very high flow rates (200 to 300 $mlmin^{-1}$) it was even more difficult to synchronise the pairs.

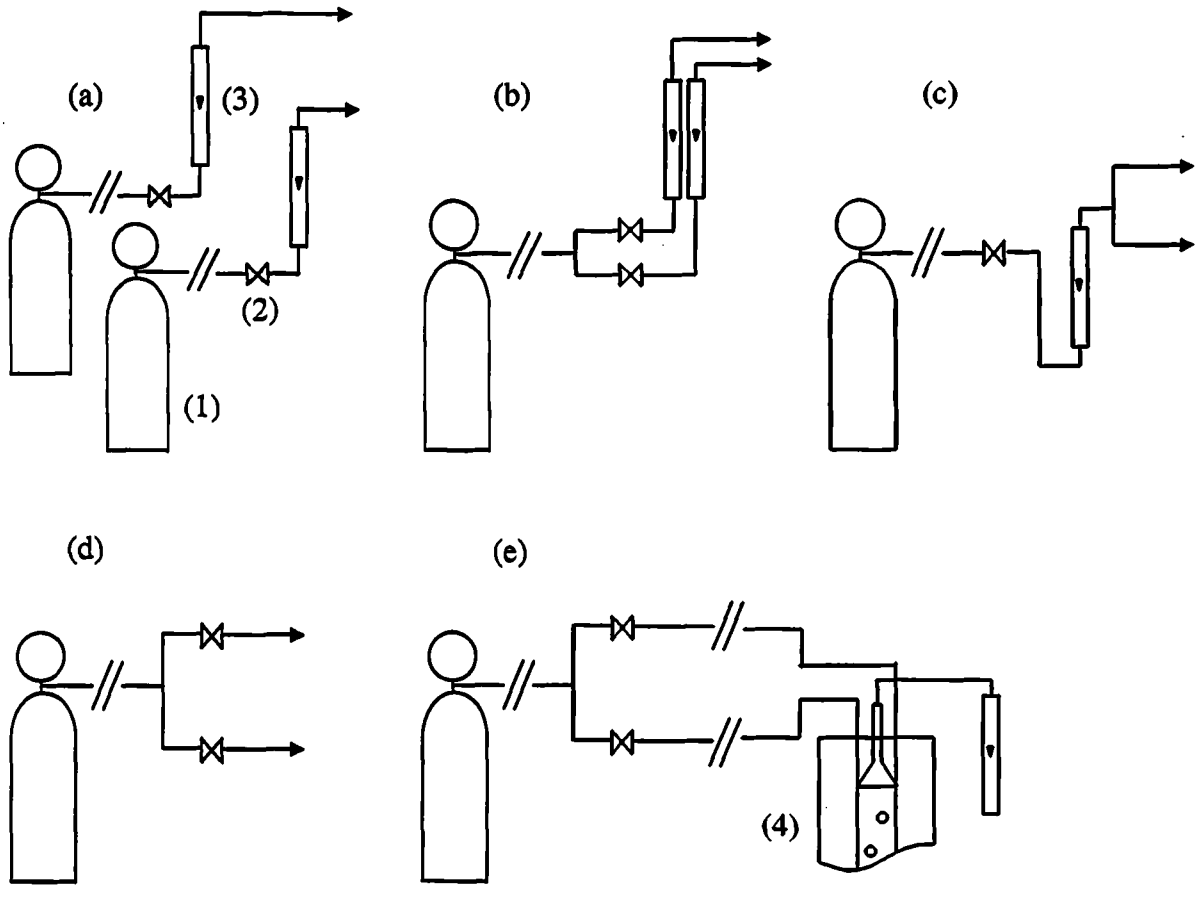

Figure 3.4

Combinations of needle valves and flow meters tested for flow measurement and synchronous bubble formation, (1) gas cylinder, (2) needle valve, (3) flow meter, (4) coalescence cell.

As a result it was decided not to carry out experiments at flow rates in excess of 100 $mlmin^{-1}$ and to extend the flow rate range towards the low flow region. The introduction of soap film flow meters into the experimental set-up allowed for the first indication that synchronous bubbling depended on several factors, of which accurate flow control was merely one (see Chapter 4).

Various gas feed configurations were also tested by altering the combination of gas supply, needle valves and flow meters to investigate the effect on the synchronicity of the system. These changes were generally restricted to the low gas velocities (1 to 5 $mlmin^{-1}$) where in addition to improving synchronisation, it was also hoped to decrease the amount of time required for the measurement and setting of the flow rates. In Figure 3.4 the five combinations that were investigated are shown schematically.

As the original (non-synchronous) experiments were carried out using a single gas supply, it was thought that using separate supply sources for each nozzle (3.4 (a)) might improve the synchronicity. Results failed to show significant differences and a single gas supply was used for all subsequent experiments. Figure 3.4 (b) shows the gas feed configuration, which gave the best synchronisation across the flow range, 4 to 20 $mlmin^{-1}$. However, use of this configuration for the lowest flow rates involved very tedious measurements due to the feedback nature of the flow meters. Consequently, configuration 3.4 (c) was tested, where the flow rate was set to double the required value and then split in two just prior to reaching the coalescence cell. At the lowest flow rate investigated (1 $mlmin^{-1}$) this resulted in the alternating formation of bubbles, although at higher flow rates (> 4 $mlmin^{-1}$), this did not occur. It was then decided to run the experiment with needle valves only to control the flow at 1 and 2 $mlmin^{-1}$, (3.4 (d)) and determine the exact flow rate from the bubble size and frequency. Attempts to use configuration 3.4 (e) to measure flow rates at 1 and 2 $mlmin^{-1}$ were unsuccessful and abandoned on account of erratic film formation within the collecting funnel.

3.1.2.2 Gas Flow Regulation

For synchronous bubble formation in the coalescence cell, it is obvious that the gas flow rates through each nozzle should be identical. As this work aimed to investigate, amongst other parameters, the effect of gas flow rate on coalescence frequency, it was necessary to measure a wide range of gas flow rates at a low system pressure. As no single piece of flow metering apparatus was available that would span such a range (1 to 100 $mlmin^{-1}$), three different methods were used for flow regulation involving two different types of flow meter to cover the required range.

For air and nitrogen flow rates between 20 and 100 $mlmin^{-1}$, a pair of 5 to 100 $mlmin^{-1}$ flow meters (Model GTV, Platon Instrumentation, UK) were inserted in-line and the gas flow regulated using two Ermeto™ needle valves, downstream of the flow meters. For both gases, the flow meters were calibrated with a wet type gas flow meter (Alexander Wright & Co. (Westminster) Ltd., 250 cm^3 per revolution). The same wet type gas flow meter was used to directly control the gas flow rates between 20 and 100 $mlmin^{-1}$ for the experiments using hydrogen and xenon.

For flows from 4 to 20 mlmin^{-1} a pair of soap film flow meters were constructed 'in-house' from 5 ml Pyrex™ pipettes. As the design of the flow meters did not allow for them to be placed in-line, it was planned to switch the gas flow from cell to flow meter and vice versa, using a combination of screw clamps to act as a crude three way valve. However, it became apparent that the flow meters tended to act as a gas reservoir, resulting in non-synchronous bubble formation further downstream, irrespective of whether the gas flows through each nozzle were identical. Consequently, flow measurement and control was achieved by re-routing the gas from the coalescence cell to flow through the flow meters. The flow was then regulated by determining the time required for a soap film to travel 5 ml. Once a stable flow had been maintained at the required flow rate for a minimum of three measurements, the flow meters were bypassed and the flow re-directed to the coalescence cell. Re-measurement of the gas flow after a typical low flow experiment showed no change in the rate despite the reconnection of tubing that was necessary for re-routing.

The soap film flow meters were also initially used to set the flow rates at 1 and 2 mlmin^{-1}, but the feedback nature of the regulation meant that this was an exceptionally tedious process. In consequence, it was decided that as these flow rates corresponded approximately to 45 and 100 bubbles per minute respectively, for these two flow rates no flow meters would be introduced into the set-up and instead the needle valves would be adjusted to give the required number of bubbles per minute.

The very low system pressure used in this work, together with the low range of flow rates to be measured, meant that it was difficult to find needle valves that provided sufficiently fine control. During the development of the experimental set-up three brands of needle valves were tested: Drallim type 1500 miniature valves (Drallim Industries Ltd., UK), Series 2300 metering valves with micrometer handles from Hoke (Hoke International, Middlesex, UK) and the Ermeto™ needle valves. The final experimental set-up shown in Figure 3.3 was achieved using the Ermeto™ needle valves, which were found to provide the best level of control at the lowest flow rates.

3.1.3 Experimental Procedure

Before experiments were carried out all components of the cell and the saturator bottles and buffer tanks were disassembled and thoroughly washed. The cleaning procedure used in this work was developed from the experience of previous workers (Cattaneo, 1995 and Man,

1998). Cleaning was considered a crucial step in the experimental procedure as the presence of minute amounts of impurities in the experimental system will affect the composition of the bubble surfaces and may give rise to unreliable results. Details are provided in Appendix C.

The experimental procedure was then as follows:

1. The empty cell was connected to the water-bath using silicone rubber tubing (6.3 mm internal diameter, 3.2 mm wall thickness) and the water jacket filled. Inversion of the cell was necessary to avoid the entrapment of air pockets in the water jacket.
2. The saturator was filled with 150 ml of test solution.
3. The cell and frame were rinsed with a small amount of the test fluid.
4. The test solution was introduced into the vessel such that the combined volume (including the frame) was about 1 dm^3. This volume gave a liquid height of 100 mm above the nozzles, which previous work (Cattaneo, 1995) had determined as optimum for bubble synchronisation. (Experiments carried out in this work showed very little influence of static head within a liquid height of 100 – 150 mm).
5. The cell was covered to present the introduction of foreign particles into the test solution and left to equilibrate to temperature, which was maintained at $\pm$0.5C of the target value. A mercury thermometer was placed inside the cell to measure the temperature of the cell contents for the duration of each experiment.
6. While the cell contents were equilibrating, the gas supply was turned on and the pressure of the system brought up to $2.1*10^{-2}$ $kgcm^{-2}$.
7. Once the test solution had reached the required temperature, the glass capillary tubes were connected to the stainless steel frame using short lengths of silicone rubber tubing. Depending on the flow rate required, the experimental set-up consisted of either (i) needle valves only (ii) needle valves and soap film flowmeters or (iii) needle valves and 'Platon' flowmeters. In addition, for experiments using with hydrogen and xenon, a further means of flow regulation was employed, using the Alexander Gasometer (case (iv)).
   (i) For flow rates of 1 to 2 $mlmin^{-1}$: the flow rate though one nozzle was set at the required bubbling rate, with no flow through the other nozzle. After the required bubbling rate had been set, the second nozzle was brought on-line until the bubbling rates though the two nozzles were equal.
   (ii) For flow rates of 4 to 20 $mlmin^{-1}$: the soap film flow meters were inserted into the experimental set-up, downstream from the needle valves. The gas flow

was then diverted from the coalescence cell and passed through the flow meters. Flow rates were set for each nozzle individually, by measuring the time required for a soap film to travel the distance equivalent to 5 ml, as marked on the pipette. Once the desired flow rate had been set and found to be stable (a minimum of three consecutive readings) the flow meters were removed from the set-up and the flow re-directed though the coalescence cell. Visual observation was used to check that the bubbles formed synchronously at the nozzles.

(iii) For flow rates of 20 to 100 $mlmin^{-1}$: the set-up was re-configured to include the Platon flow meters, placed in-line upstream of the needle valves. The flow rates were set individually for each of the nozzles and visual observation (using the video camera) used to assess the synchronicity of the flows.

For those experiments where a range of flow rates were investigated, the flow rates were incrementally increased from 1 to 100 $mlmin^{-1}$. Between each change over of flow meter the gas supply to the cell was stopped, in order to avoid unnecessary aeration of the test fluid.

8. Once the required flow rates had been set, the system was allowed to stabilise for five to ten minutes (less time was required for the higher flow rates). During this period the synchronisation of the system was assessed by filming a test piece and using the frame-by-frame option on the camera to view the recording. If the system appeared synchronised, the experiment was recorded; conversely if the bubbles appeared

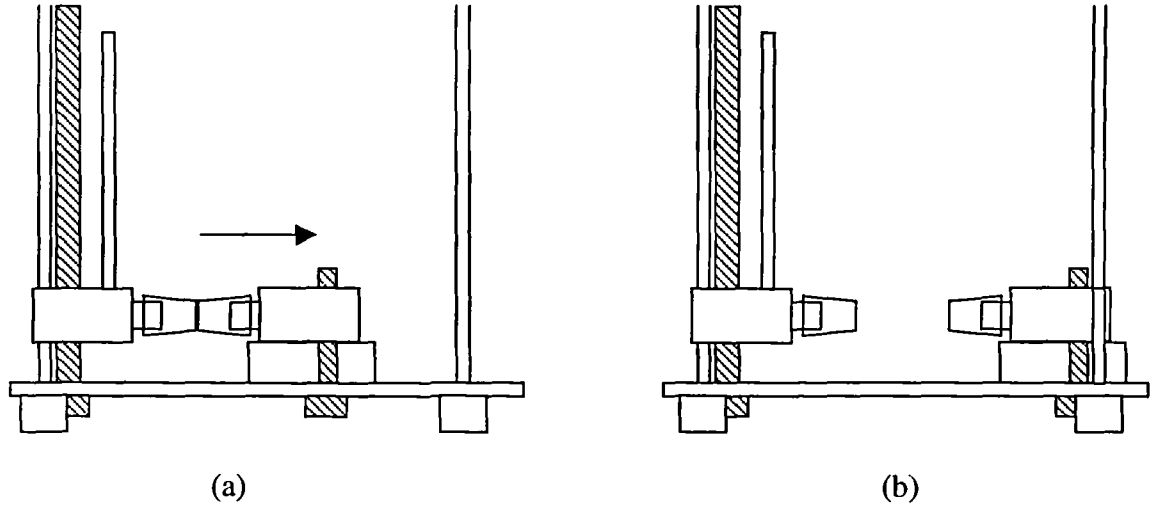

Figure 3.5

Schematic diagram showing the method for setting the nozzle separation in the cell (a) the nozzles are aligned vertically by eye with the extensions touching (b) the right hand nozzle is moved outwards to give the desired horizontal spacing.

unsynchronised, the flow rates would be reset according to step 7 and re-tested.

3.1.4 Data Acquisition

All experiments were recorded on Super Standard Grade video cassettes using a Panasonic NV-M40 video camera. The camera had a frame rate of 50 frames per second (0.02 seconds between pictures) and was equipped with shutter speed control from 1/60 and 1/8000 seconds. The shutter speed which offered the best balance between a fully resolved picture and the need for an exterior light source, was found to be 1/2000 seconds; this was used for all experiments. The camera was also equipped with a 'macro' facility which enabled the area of interest to be studied close up, with the lens 40 - 60 mm from the cell wall. This gave bubble diameters between 15 to 30 mm on screen. Due to the shutter speed used it was necessary to provide lighting in addition to the ambient lighting of the laboratory. A 1000 Watt halogen Wotan™ lamp was placed at an angle of 45° to the cell and at a distance of 1 m (to minimise heating of the cell contents). To improve the resultant image a sheet of black card was placed behind the rear face of the cell. A typical video image acquired using this set-up is shown in Figure 3.6. Experiments were filmed for a sufficiently long to ensure a minimum of 250 contacting pairs was recorded. Due to the wide flow range investigated, this could vary from one minute (high flow rate, fully coalescing conditions) to half an hour (for very low flow rates in coalescence inhibited fluids), which was arbitrarily set as the maximum film time.

Coalescence time data was obtained using a Kodak EktaPro EM high-speed video camera, borrowed from the EPSRC Engineering Instrument Pool. This had a frame rate of up to 1000 frames per second with the full aspect ratio, although this could be increased to 6000 frames per second with an accompanying decrease in picture size to 1/6 full screen size. A set of MonoZoom lenses (Cambridge Instruments, New York, USA) were used to magnify events occurring at the nozzles. The 0.5x objective used for the majority of two-bubble studies had a field depth 0.21 - 4.5 mm, with the actual magnification range between 8.9 - 62.4 times.

3.1.5 Data Analysis

All data was recorded on SHS video cassettes and analysed using image analysis equipment and a Panasonic AG – 7355 video recorder, both of which allowed frame-by-frame playback of images. This was especially important for analysing results taken at high gas flow rates and for those using the high-speed camera.

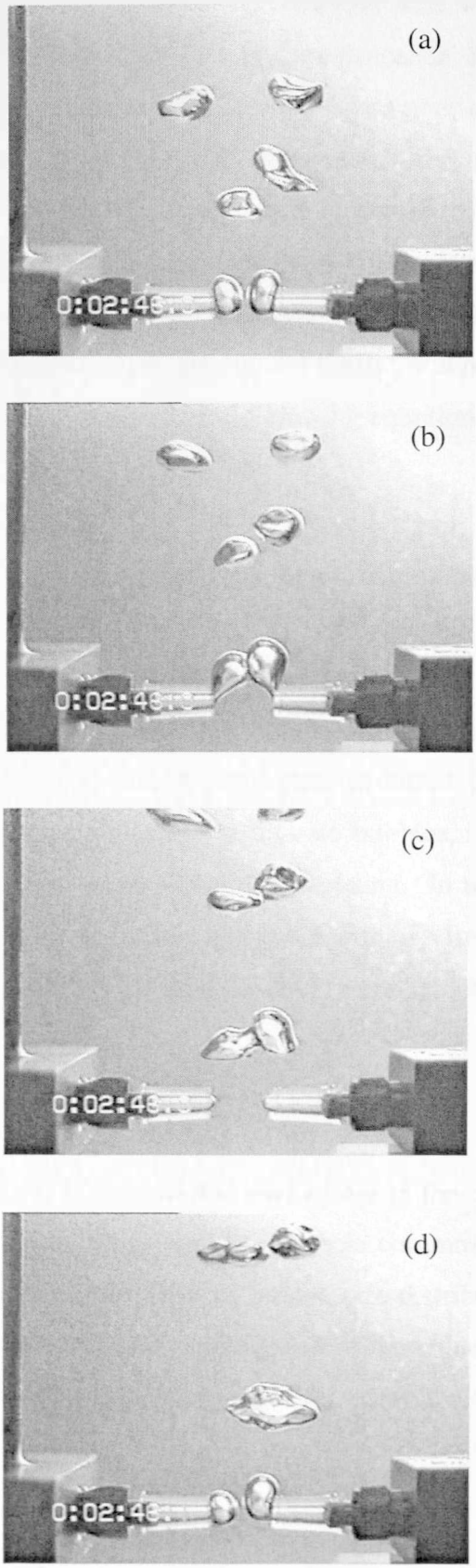

Figure 3.6

Typical sequence of images acquired with the Panasonic video camera (frame rate 50 s^{-1}), showing a coalescence event in 0.1 M Na_2SO_4. Air flow rate 100 $mlmin^{-1}$. Nozzle distance, 4 mm. Time between frames is 20 ms.

The coalescence frequency, bubble frequency and bubble size were determined from the Panasonic video recordings (50 $frames^{-1}$). The coalescence frequency was measured manually using hand-held tally counters to determine the number of coalescing bubble pairs as a percentage of 250 contacting pairs (Chapter 4 contains a discussion about the subtleties inherent in this variable). Bubble frequencies were estimated by counting the number of bubbles formed over a set time interval (one minute for flow rates of 1 and 2 $mlmin^{-1}$, 30 seconds for flow rates from 4 to 10 $mlmin^{-1}$ and over 15 second intervals for flow rates in excess of 10 $mlmin^{-1}$). Bubble sizes were determined either by direct measurement from the video images (for bubble diameters), or from the following equation:

$$V_b = \frac{Q_g}{f_b} \tag{3.1}$$

where V_b is the bubble volume, Q_g the gas flow rate and f_b the bubble frequency.

Contact and coalescence times were determined from the Kodak EktaPro EM high-speed video recordings. This involved counting the number of frames from the initial contact between the two bubbles to the frame before film rupture occurred, in the case of coalescence, or from the point of contact to the separation of the two bubbles, in the case of contact time and then multiplying by the frame rate used for the recording. In addition to the coalescence time, the diameter of the contact area was measured directly from the frame before film rupture, to provide an estimate of the film area (assumed to be circular).

3.2 STUDIES IN BUBBLE COLUMNS

In addition to the controlled coalescence studies carried out in the coalescence cell, a limited amount of work was carried out in laboratory-scale bubble columns. The data acquired from these investigations was resolved in the form of bubble size distributions and mean diameter values, which could then be used to give an indication of the coalescence behaviour of each system. In addition, high-speed video camera was used to investigate bubble-bubble interactions in the columns.

3.2.1 Equipment

Laboratory-scale bubble columns were constructed from borosilicate glass, using sintered discs of Pyrex ™ glass as the distributor plates. The discs were of porosity grade 0, 1 and 2 (using the classification system provide by the manufacturer) and complied with requirements

of ISO 4793 in terms of pore size distribution. The discs were of diameter 50 mm and thickness 5 mm, details are given in Table 3.2. Each porous plate was fused into a 50 mm diameter glass tube which was then annealed at 650 °C for the minimum time, in order to prevent alterations to the pore size distribution of the plate. The finished dimensions of the columns are shown in Figure 3.7(a). In addition, a fourth column was constructed with a sintered plate of porosity grade 2, and the column encased in a water jacket to allow for temperature control. Dimensions are shown in Figure 3.7(b).

Porosity Grade	*Pore Index (μm)*	*ISO Designation (μm)*
0	>160 ≤ 250	P250
1	>100 ≤ 160	P160
2	>40 ≤ 100	P100

Table 3.2
Pore size distributions for the sintered glass discs used in the bubble columns.

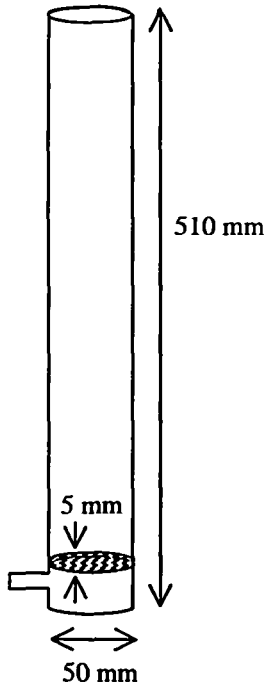

Figure 3.7 (a)
Laboratory-scale bubble column, showing dimensions.

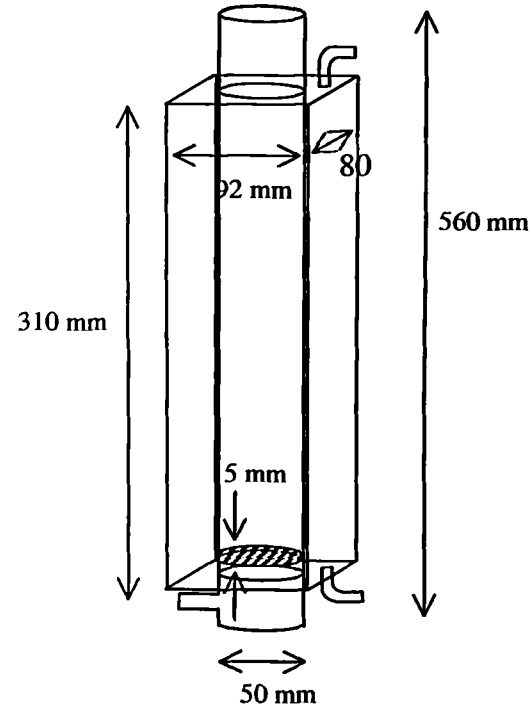

Figure 3.7 (b)
Laboratory-scale bubble column with water jacket for temperature control, showing dimensions.

3.2.2 Experimental Set-Up

Figure 3.8 is a schematic representation of the experimental set-up for the study of bubble size distributions in bubble columns. As for the coalescence cell studies, compressed gas [1] is delivered at a pressure of $2.1*10^{-2}$ kgcm^{-2} through the use of secondary pressure regulation with a mercury manometer [2]. The gas is filtered through a 0.2 μm filter [3] and then passed through a saturator [4] to a 2 dm^3 buffer tank [5]. The flow rate is measured with an in-line Model GTF Platon flow meter, (Platon Instrumentation, UK) [7] and controlled by a needle valve, [6] before sparging into the bubble column [8]. All tubing in the systems was silicone rubber tubing (4.8 mm internal diameter, 1.6 mm wall thickness). An advanced video technique (see Section 3.2.4) was used to observe events in the bubble column.

3.2.3 Experimental Procedure

Equipment was cleaned before use and between experiments, following the cleaning protocol outlined in Appendix C. Experiments were carried out as follows:

1. The column was connected to the water-bath using silicone rubber tubing (6.3 mm internal diameter, 3.2 mm wall thickness) and the water jacket filled (column number 4 only).
2. The saturator was filled with 150 ml of test solution.

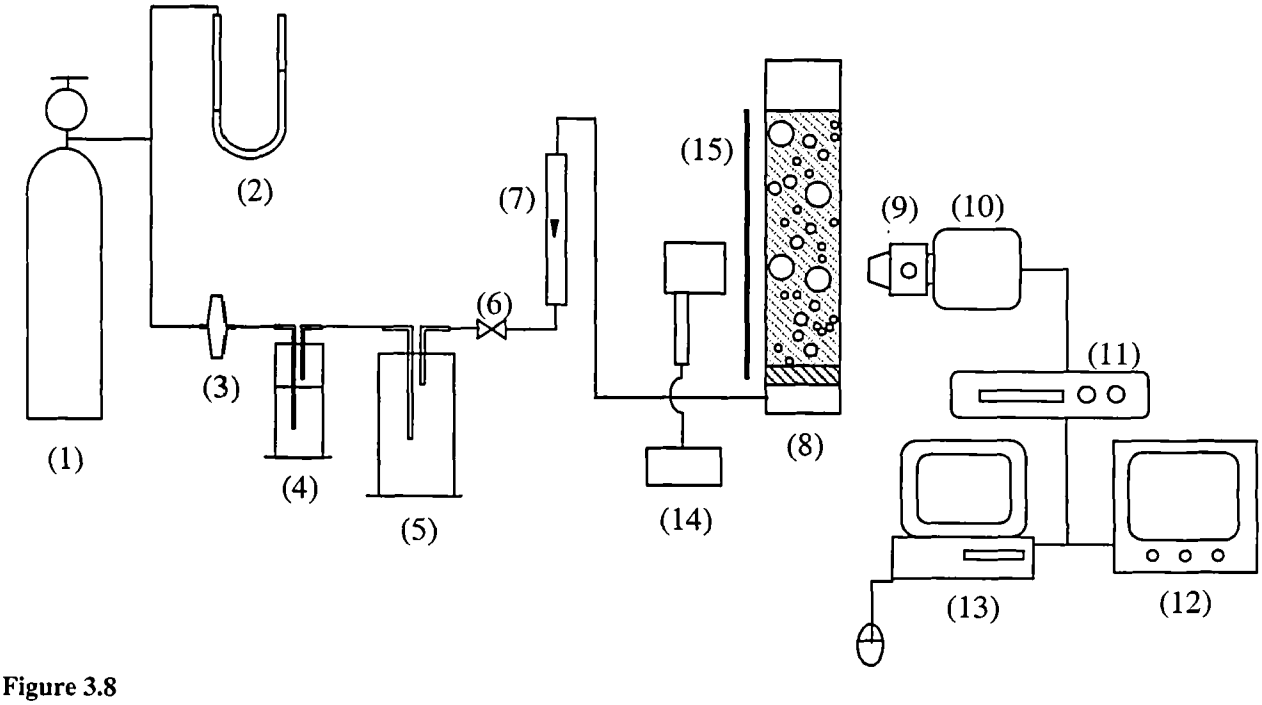

Figure 3.8

Schematic diagram of the experimental set-up: (1) gas cylinder, (2) mercury manometer, (3) 0.2μm filter, (4) saturator, (5) buffer tank, (6) needle valve, (7) flowmeter, (8) bubble column, (9) stereomicroscope, (10) Panasonic F15 HS camera, (11) video recorder, (12) monitor, (13) computer, (14) stroboscope and strobe light, (15) Light diffuser.

3. The column was rinsed with a small amount of test fluid and then inserted into the test rig using silicone tubing (5.6 mm internal diameter, 1.6 mm wall thickness) to connect to the outlet of the flow meter. It was then filled with the test solution to give a liquid height of 250 mm above the distributor plate. A screw clamp was used to prevent the test solution draining through the sparger into the flow meter.
4. The solution was covered to prevent the introduction of foreign particles and left to equilibrate to temperature. In the case of the non-jacketed columns, the test solutions were brought up to the working temperature (25 °C) before use.
5. Once the test fluid had reached the required temperature, the gas supply was turned on and the system pressure brought up to $2.1 * 10^{-2}$ kgcm^{-2}. The screw clamp was then removed from the silicone tubing and the flow rate set to give an equivalent superficial velocity of 1, 2 or 3 cms^{-1}.
6. The flow was allowed to develop for a short period. During this time the focus of the camera was checked and a test piece filmed to check the quality of the images. Once the flow had fully developed short video recordings were made at four points over the column height: at the distributor plate and at distances of 20 mm, 100mm and 200 mm above (the last equivalent to 50 mm below the unaerated liquid height).

3.2.4 Data Acquisition

Bubble size data was acquired using the advanced video technique described in detail in Pacek et al. (1994). Although originally developed to monitor drop sizes in stirred liquid-liquid dispersions, the technique has been used successfully by Machon et al. (1997) and Martin (1996) to observe bubble sizes in stirred gas-liquid dispersions. Adopting the technique to measure bubble sizes in bubble columns required very few modifications and the set-up is shown in Figure 3.8. Bubbles were recorded using an Olympus stereo microscope, model SZ 6045 TR (Olympus Optical Co., (UK) ltd.), [9] with variable magnification, connected to a Panasonic F15 HS video camera [10] (frame rate 50 s^{-1}). Images were recorded on Super VHS video cassettes using a Panasonic AG-5700 SVHS video recorder [11]. When used in an agitated vessel, the light source is provided by a strobe light placed inside the vessel. For this work a Phillips PR 9112/13 strobe lamp connected to a Phillips PR 9113/00 stroboscope, [14] and set at 50 s^{-1}, was placed directly behind the column at a distance of about 50 mm. A single sheet of 90 gm^{-2} tracing paper, [15] was placed between the column and the strobe light to diffuse the light source and ensure clear images were obtained. In addition, the sides and front and rear edges of the jacketed column were masked

with black tape to restrict the amount of ambient light entering and decrease the amount of reflection.

High-speed studies of bubble interactions in the column were carried out using the Kodak EktaPro EM video camera also used to monitor events in the coalescence cell. For these experiments, a frame rate of 1000 frames per second was used (images were full screen size). The camera was equipped with a MonoZoom lens (Cambridge Instruments ltd., New York, USA) and a 0.5x objective, as previously described.

3.2.5 Data Analysis

Bubble sizes were measured directly from the video images of the experiments, using a Gateway 2000 Pentium-90 MHz computer. This was equipped with a digitising card (Screen Machine II from FAST Electronic GmbH, Munich, Germany) which allowed the video images to be converted frame by frame, into digital images. For this work data was not acquired from sequential images in order to avoid measuring bubbles which may have become entrained in the flow more than once. Instead, the first frame in every second of filming was digitised. Typically 30 frames were required to give the statistical minimum of 500 bubble measurements. Bubble sizes were measured using a software package developed 'in-house' (Droplet Detection System Version 1.5). Size distributions and mean values were then calculated using DOS based drop-measuring software, also developed in-house ('DropDis') and manipulated using the Windows based data analysis package Sigmaplot ^{TM}. Further details of the method for bubble size measurement and data analysis are given in Appendix D.

3.3 MATERIALS

All aqueous solutions in this work were made up using de-ionised water, prepared by a reverse osmosis system (Elga ltd., UK) and with a typical conductivity between 0.05 and 0.1 μScm^{-1}. Table 3.3 summarises the chemical additives used in the experiments and Table 3.4 details the properties of the gases used.

Chemical	Supplier	Molecular Weight ($gmol^{-1}$)	Grade
Glycerol	BDH	92.9	AnalaR (99.5%)
Magnesium Sulfate Heptahydrate	BDH	246.48	AnalaR (99.5%)
Nitric Acid	BDH	63.02	AnalaR
Potassium Iodide	Reidel-de Haen	166.00	(99 – 100.5%)
Propan-1-ol	BDH	60.10	AnalaR (99.5%)
Sodium Sulfate Anhydrous	BDH	142.04	AnalaR (99.5%)
Sodium Chloride	BDH	58.44	AnalaR (99.5%)
Sucrose	BDH	342.30	AnalaR (99.5%)
Silicone Fluid (200/3cS)	BDH (Dow Corning)	-	-

Table 3.3

Summary of chemical additives used in experiments.

Gas	*Supplier*	*Grade*	*Density ($kg\ m^{-3}$) (20 °C, 1 Atm)*
Air	BOC	High Purity	1.2928
Hydrogen	BOC	High Purity 99.995%	0.0898
Nitrogen	BOC	Oxygen Free 99.998%	1.2507
Xenon	BOC	99.993%	5.7168

Table 3.4

Summary of gases used in experiments.

3.4 SUPPLEMENTARY EXPERIMENTAL METHODS

This section reports the supplementary experimental methods, which were used to provide supporting data for the experiments carried out in the coalescence cell and bubble columns.

3.4.1 Viscosity Measurements

Viscosity measurements were required for the coalescence cell experiments carried out with glycerol solutions and were measured at temperatures of 10°C, 15°C, 25°C, and 50°C. For all solution concentrations below 8 M, measurements were made using a Contraves RM-30 viscometer, using the double concentric cylinder apparatus and a shear rate range from 108 to 1711 s^{-1}, as this allowed for accurate measurement of the relatively low viscosities. For solution concentrations above 8 M (and including 8 M at 10°C), measurements were made either in the Contraves RM-30 (shear rates from 41.7 to 662 s^{-1}) or a Bohlin Visco 88-BV viscometer (shear rates from 383 to 595 s^{-1}), using concentric cylinder apparatus. In both instruments, temperature control was effected externally through the use of a water-bath (model W14 Grant Instruments (Cambridge) ltd., UK) which provided temperature control to ± 0.1°C. The temperature of experimental solutions was checked with a mercury thermometer (± 0.5 C) prior to measurements being carried out.

3.4.2 Density Measurements

Measurements of density were made using a 25 ml density bottle, the volume of which was accurately determined using water at 25°C. All solutions were incubated at the experimental temperature for approximately one hour prior to measurement of density.

3.4.3 Measurements of Dynamic Surface Tension

Measurements of dynamic surface tension were considered important in this work, given that the influence of solutes may be expected to be manifest during periods of surface expansion. Consequently, a Lauda MPT1 Maximum Bubble Pressure meter was used to determine the change in surface tension with bubble lifetime. To allow measurements to be made over a range of temperatures, temperature control was provided by a circulating water-bath (TE-7 Tempette from Tecam ltd., UK) which controlled to ± 0.5°C. The water-bath temperature was checked using a mercury thermometer (± 0.5 C) prior to measurements being carried out.

The Lauda MPT1 Maximum Bubble Pressure meter comprises of two components: a bubble detector (MPT 1E) linked to a test capillary unit (MPT 1M), both controlled from a computer using a DOS based program supplied with the instrument. Measurements are made by forcing air though a thin capillary of known diameter, into the liquid for which the surface tension is to be measured. During this process, the instrument records the gas pressure in the capillary,

which increases from some initial value to a maximum, corresponding to the point at which the bubble is hemispherical: The maximum bubble pressure occurs when the bubble diameter is equal to that of the capillary and the surface tension at this point can be calculated using the Laplace equation:

$$\bar{\sigma} = r_c \frac{\Delta P}{2} \qquad (3.2)$$

The process is repeated over a range of gas flow rates (3.7 to 107.8 mms^{-1}) to allow the surface expansion rate at the time of maximum pressure and the maximum bubble pressure for each flow rate to be calculated. The instrument is also able to determine the value of equilibrium surface tension, i.e. that which would result if the gas-liquid interface had an infinitely long time to equilibrate with the bulk solution.

The manufacturer claims a measurement error of ± 0.1 mNm^{-1} for this instrument. However, problems were encountered with adequate cleaning, as successful operation of the instrument greatly depends on system cleanliness. In addition, multiple test runs carried out with water and ethanol to ascertain the reproducibility of measurements suggest that the operating error is closer to ± 0.5 mNm^{-1}. As a consequence, the instrument was not used extensively and all results are reported only as an indication of the overall trend in surface tension behaviour with changing surface expansion rates.

Chapter 4
Using the Coalescence Cell

Experimental apparatus similar to the coalescence cell used in this study can be found in several works reported in the literature (see Table 3.1). However, in the vast majority of these studies, the focus of the work has been on collecting data to allow the determination of a single parameter such as coalescence frequency or coalescence time in various aqueous solutions. Few studies (for example, Drogaris and Weilland, 1983) have extended the work beyond this basic outline and exploited the capabilities of such equipment to potentially generate information on the independent influences of parameters such as bubble pair orientation (and contact angle), bubble formation rate, bubble size, contact force and contact duration on the coalescence process for a bubble pair.

In the following chapter, the details of working with the coalescence cell are explored and the various problems with the equipment are highlighted and discussed in light of their influence on the results obtained. Initially the experimental parameters are considered and definitions proposed for the primary working variable, called variously in the literature, the 'percentage coalescence' or 'coalescence frequency'. Following this, aspects of the apparatus which influence the measured value of this variable are discussed and the validity of several possible interpretations are explored. Questions of experimental reproducibility are addressed and the experimental limitations of the equipment are considered.

4.1 Experimental Parameters

In a dynamic system, bubble-bubble collisions can be envisaged to occur under a variety of conditions; from the (wake induced) in-line contact between a rising and following bubble pair to collisions between bubbles contacting in the horizontal plane. Depending on the nature of the flow fields entraining the bubbles, the duration and contact pressure of the collisions will vary. In order to estimate the effects of parameters such as contact angle and pressure on collision and coalescence, the current equipment was designed to allow independent investigation of several possible parameters.

It was envisaged that with minimal modification to the cell, the effects of both vertical (as in Lessard and Zieminski, 1971 and Oolman and Blanch, 1986a) and horizontal (as in Zarahdnik et al., 1998, 1995, 1987) bubble orientation could be investigated and the effects of bubble contact angle quantified. Altering the gas flow rates through the nozzles would allow the effect of bubble generation rate to be determined over a wide range of values. In addition, bubble size could be altered both as a function of gas flow rate and also independently, through the use of different nozzle attachments. A combination of various nozzle separation distances and different gas flow rates would also allow a variety of contact forces and contact times to be investigated.

One of the outcomes of this in-depth study was to highlight the extreme care and meticulous attention to detail which is required, not only in using the coalescence equipment but also in interpreting the results. During the work, aspects of system behaviour were discovered which had serious repercussions on the experimental possibilities which could be realistically achieved with the cell (Section 4.2). Consequently, all the experimental work was restricted to using nozzles fixed in the horizontally-opposing geometry and with only small variations in inter-nozzle spacing (4 – 8 mm). In addition, independent investigation of the effect of bubble size, through the use of differently sized nozzles was not carried out, although bubble sizes were altered as a consequence of the various gas flow rates used.

4.1.1 *Defining the Coalescence Frequency*

In previous studies using a coalescence cell, the primary parameter reported has been the coalescence frequency or percentage coalescence. This value is defined in the work of Lessard and Zieminski (1971) as "the number of coalescing pairs [divided] by the total number of pairs contacted". Similarly, Zahradnik et al. (1987) define a "bubble coalescence ratio" as the "ratio of coalescing bubble pairs to the overall number of pairs generated in a given time period", although this is altered to the "number of coalescing bubble pairs [per] one hundred bubble pairs contacted" in Zahradnik et al. (1998). All of these phrases appear simple and well defined, with an immediate assessment of the experimental descriptions suggesting that the work should be easy to replicate. However, during the present study it was realised that the above definitions are deceptively straightforward, failing to allow for the many subtleties which can be observed in the coalescence cell. Obviously, coalescence events are influenced by the conditions under which the experiments are carried out (bubble formation rate and nozzle separation distance, for

example), but they are also heavily dependent on the liquid phase investigated, to the extent that far less nuances are possible when interpreting data for events occurring in a pure (and therefore fully coalescent) liquid.

Even an in-depth look at experimental methods reported in the literature provides no indication of the range of complex phenomena which have been observed in this work. Firstly, there is no mention of the necessity for synchronisation of the bubble flows, nor of the difficulty in achieving this; Zahradnik et al. (1998), note only that "pairs of bubbles were generated simultaneously". Although synchronicity may not be a critical factor for the work carried out using vertically oriented nozzles (not a view supported by the present work), it is difficult to understand how such an important aspect of the system could have been omitted in describing work with horizontally oriented nozzles, such as reported here. In addition, none of the literature studies provide a definition for what constitutes a contact event between two bubbles, nor a discussion of the subtle variations possible. The present work, however, suggests both factors are critical aspects of the experimental system and that, in order to generate useful results it is vital to determine a clear and precise definition for the parameter, 'coalescence frequency'.

In a system where bubbles are formed at horizontally-opposing nozzles, it is possible to envisage five different types of event.

a) Two bubbles form simultaneously at either nozzle and grow until the point of contact, when they coalesce. They continue to grow and finally detach from both nozzles simultaneously as a single large bubble (Figure 4.1(a)).
b) Two bubbles form simultaneously at the nozzles, grow until the point of contact but do not coalesce. Growth continues until the bubbles detach from the nozzles and rise up as a bubble pair (Figure 4.1(b)).
c) The bubbles are not synchronised and grow at different rates. The leading bubble detaches from the nozzle before the following bubble has grown sufficiently to contact and the bubbles never touch. (Figure 4.1(c)).
d) Although the bubbles grow in an unsynchronised fashion, the leading bubble has not detached from the nozzle before the following bubble grows sufficiently large enough to contact. Such

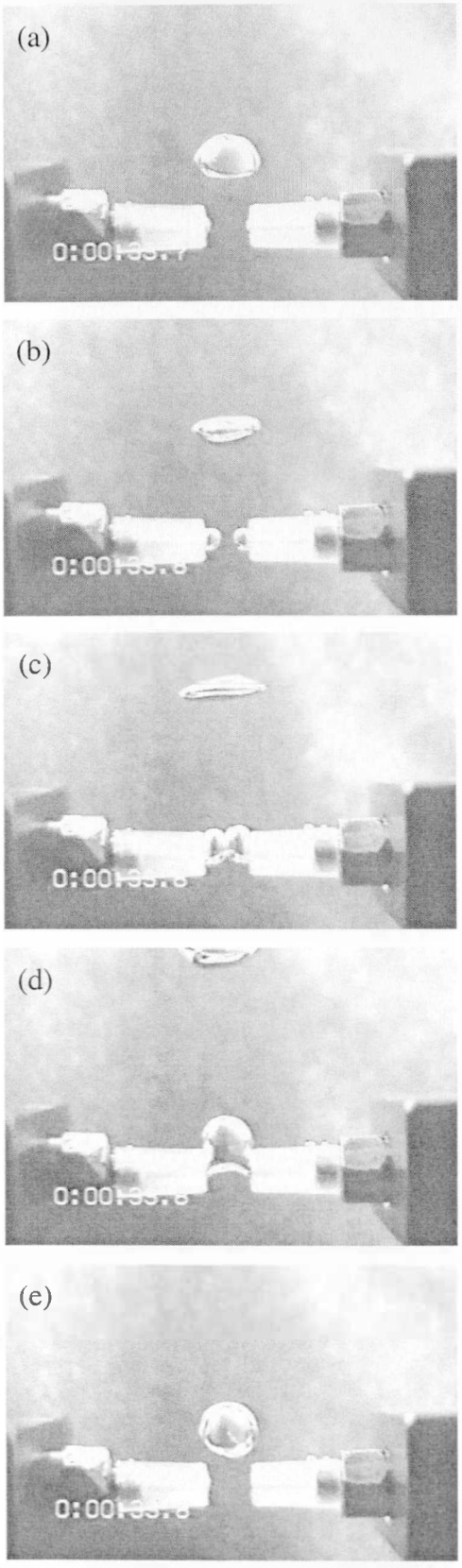

Figure 4.1(a)

Fully synchronised bubble pair, which coalesces following face-to-face contact. 0.03 M Na_2SO_4, nozzle distance 4 mm, air flow rate 30 $mlmin^{-1}$.

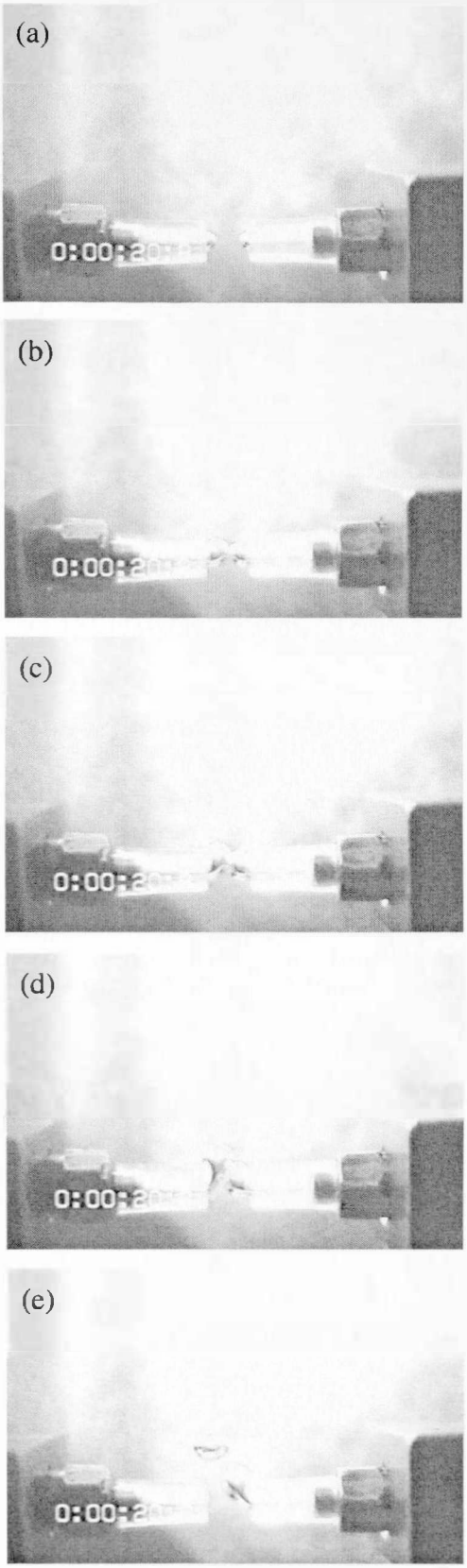

Figure 4.1(b)

Fully synchronised bubble pair which does not coalesce despite face-to-face contact. 0.04 M Na_2SO_4, nozzle distance 4 mm, air flow rate 6 $mlmin^{-1}$.

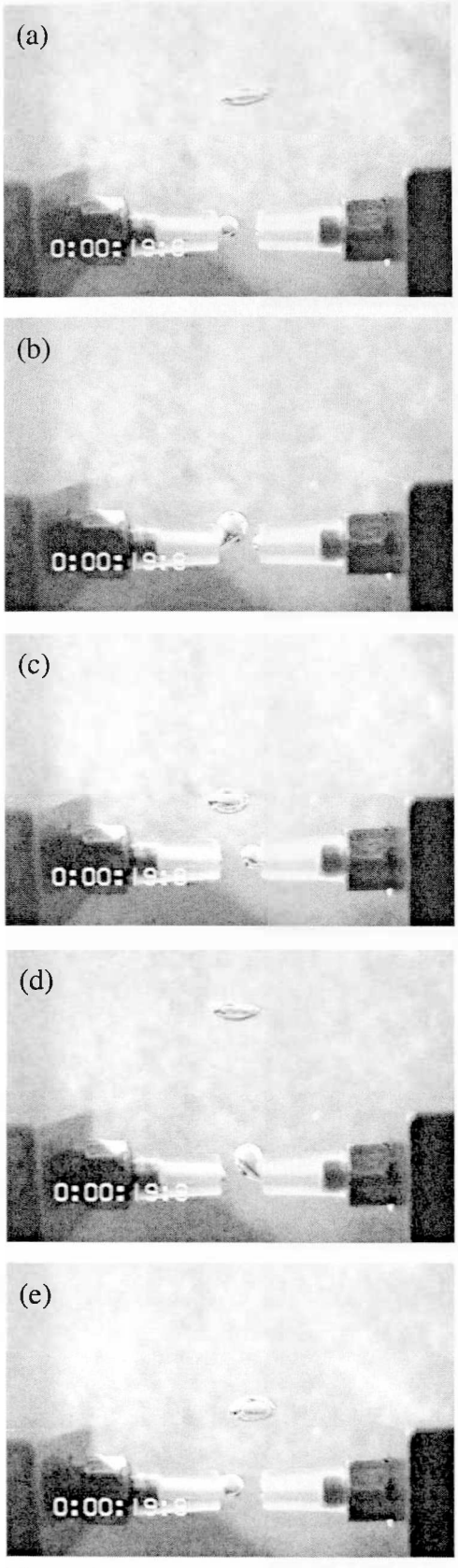

Figure 4.1(c)

Bubble formation is completely non-synchronous, resulting in a lack of contact between the two bubbles and subsequently, no coalescence. 0.04 M Na_2SO_4, nozzle distance 4 mm, air flow rate 8 $mlmin^{-1}$.

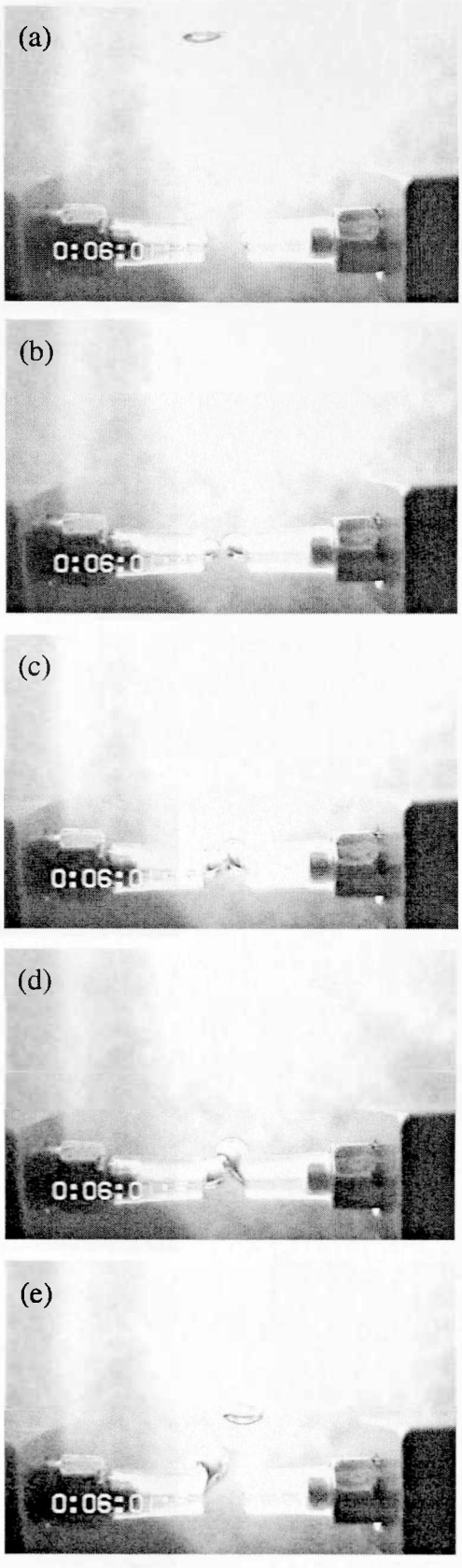

Figure 4.1(d)

Bubbles formation is not synchronised and subsequent contact is not face-to-face. No coalescence is observed. 0.04 M Na_2SO_4, nozzle distance 4 mm, air flow rate 6 $mlmin^{-1}$.

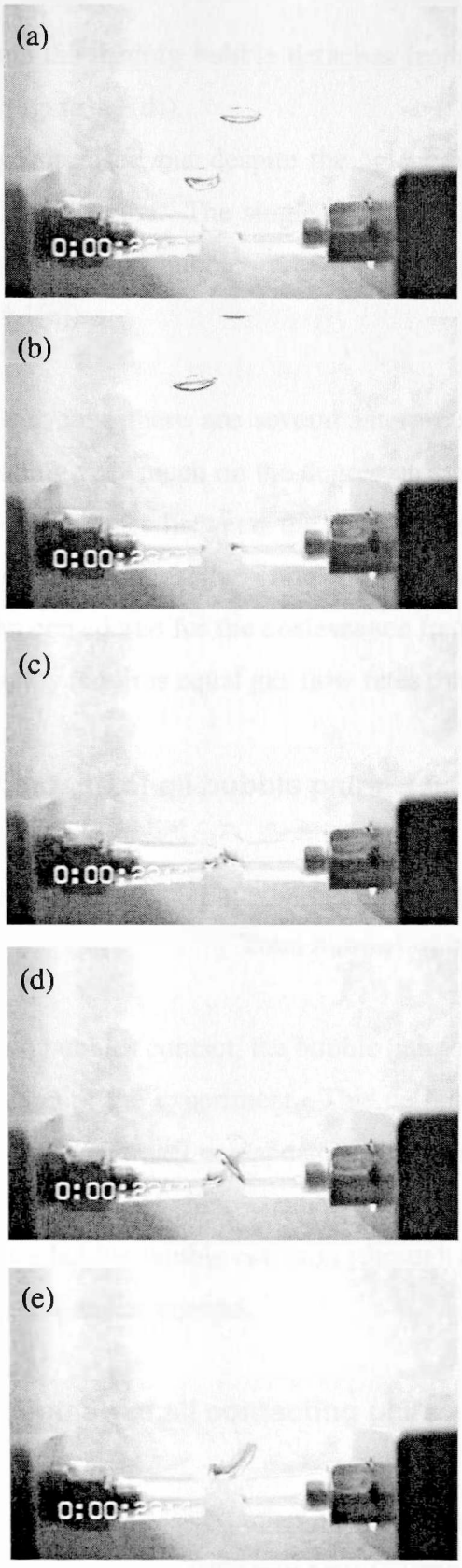

Figure 4.1(e)

Despite non-synchronous bubble formation and 'glancing' contact coalescence occurs. 0.04 M Na_2SO_4, nozzle distance 4 mm, air flow rate 10 $ml min^{-1}$.

a contact is 'glancing' and the leading bubble detaches from the nozzle without coalescing with the trailing bubble (Figure 4.1(d)).

e) The bubble pair is unsynchronised but despite the 'glancing' nature of the contact made between the two, coalescence occurs. The single large bubble detaches from the nozzles in an uneven fashion and further bubble growth from the nozzles is subsequently unsynchronised (Figure 4.1(e)).

As a result of these possible events, there are several interpretations for a parameter such as coalescence frequency, depending very much on the degree on synchronisation in the system and consequently, the nature of the contact between the two bubbles. These factors are in turn, further influenced by parameters such as the contact force and liquid composition. Three working definitions have been considered for the coalescence frequency in this work, as outlined below. For each of them to apply requires equal gas flow rates through both nozzles.

- **Definition 1: as a percentage of all bubble pairs**

$$\text{Coalescence Frequency, } \omega_{cell}' = \frac{\text{Number of bubble pairs coalescing}}{\text{Total number of bubble pairs}}$$

Irrespective of whether the two bubbles contact, the bubble pair is included in the total number of pairs generated over the duration of the experiment. This definition recalls that of Zahradnik et al. (1987). Although bubble-bubble contact is mandatory for coalescence to occur, the use of this definition may not be as flawed as on first consideration, as it may provide a means for quantifying the probability of a bubble-bubble collision (through the likelihood of approach) and hence the initial stage in the coalescence process.

- **Definition 2: as a percentage of all contacting pairs**

$$\text{Coalescence Frequency, } \omega_{cell}'' = \frac{\text{Number of bubble pairs coalescing}}{\text{Total number of bubble pairs contacting}}$$

Only bubble pairs which contact are included in the data analysis, but any touch between the two, however slight and irrespective of the plane of contact, is considered valid. In this work, this definition has also included bubble pairs which coalesce after detaching from the nozzles, although it excludes coalescence arising as a consequence of wake induced contacts (which are ignored for the purposes of this study). This is the definition closest to that proposed by Zahradnik et al. (1998) and Lessard and Zieminski (1971). Although it cannot provide information regarding the likelihood of a bubble-bubble contact, it may be considered the most accurate reflection of the events occurring in free flow where contacts occur without geometrical constraints.

- **Definition 3: as a percentage of selected contacting pairs**

Coalescence Frequency,

$$\omega_{cell}''' = \frac{\text{Number of bubble pairs coalescing after contact at angle} \geq \theta}{\text{Total number of bubble pairs contacting at angle} \geq \theta}$$

where θ is an angle measured from the vertical, midway between the opposing nozzles. The advantage of this definition is that it can be manipulated (through the value of θ chosen) to reflect the influence of contact angle on coalescence. As the present work has been carried out with horizontally opposing bubble pairs, setting the value of θ at 90° (± 10°) would allow the influence of collisions in the horizontally plane only to be investigated. In applying this definition then, bubble pairs contacting at an angle beyond 90° would be disregarded, irrespective of whether they generate a coalescence event.

How do the values generated from each of the definitions compare? Before considering this question, two further (although interdependent) issues must be addressed; the definition of a bubble-bubble contact and the effects of bubble synchronisation in the coalescence cell.

4.1.2 *What Constitutes a Contact Event?*

The necessity of characterising a contact event can only be avoided when the first definition for coalescence frequency is applied; the use of either of the others requires a clear and unambiguous interpretation. In addition, it is closely related to the discussion which follows, concerning the importance of bubble synchrony on the coalescence frequency. Studies in the literature emphasise the importance of the wake induced contact events that are so well observed in two-bubble systems (Crabtree and Bridgwater (1971), de Nevers and Wu (1982) and which are considered to be the predominant mode of bubble-bubble collisions in free flow (Miyahara et al. 1993, Stewart, 1995). However, as described in Chapter 7, high speed video studies of bubbles in bubble columns show very few purely wake driven coalescence events, as compared with a large number of coincidental contacts arising through the random motion of bubbles. In these events as in the cell, coalescence is observed to occur following contacts in a wide variety of geometries. The imposition of geometrical constraints on the contact event (as suggested by the third definition) should therefore be considered further only as a method for elucidating extra information from the coalescence cell data. In this study therefore, any touch between two bubbles, irrespective of the plane of approach, is considered to constitute a contact event.

4.2 The Importance of Synchrony

The three definitions proposed for the coalescence frequency suggest that the impact of bubble synchrony cannot be underestimated. Initially it was considered that obtaining full synchrony was merely a case of setting identical flow rates through both nozzles and carefully aligning the nozzles in the stainless steel frame. However, it has become evident during this study that bubble synchronisation depends, in an interrelated fashion, on a combination of the following parameters: the nature of the liquid phase, gas flow rate (and hence the bubble formation rate) and nozzle separation distance.

4.2.1 *Synchronous Systems*

In a fully coalescent fluid, provided that the two gas feed rates are the same and the geometry of the system allows contact between the two bubbles (sufficiently small nozzle separation) bubbles pairs were always found to be synchronised. Two typically synchronous systems are shown in

Figure 4.2, one at a very low flow rate in 0.03 M Na_2SO_4 and one at a much higher flow rate in 0.1 M Na_2SO_4. Bubbles are formed at the two orifices at the same time (4.2(i), (vii)) and grow at the same rate (4.2(ii), (x)), such that they are very similar in size at the point of contact (4.2(iii), (viii)). The amount of deformation which occurs at the point of contact depends heavily on the gas feed rate; at low values bubbles will just touch before coalescing (4.2(iii)) such that the amount of deformation (and hence the area of the thin film) will be minimal, whereas at higher gas feed rates, the bubbles are forced together ensuring a much larger contact area between the two (4.2(viii)). Once coalescence occurs, bubble growth continues until buoyancy forces cause the now single bubble to detach from the nozzles (4.2(vi), (ix)). In synchronous systems, the bubble will tend to detach from the each of the nozzles simultaneously, thus ensuring that further bubble growth from the nozzles is also synchronised. Fully synchronised systems are generally obtained in pure liquids and for those solutions where the solute concentration is below the 'transition' value. In both instances, the gas velocity is immaterial (provided it is the same for both nozzles) and synchronous bubbling is maintained over the entire flow range investigated. The further regulation of synchronised bubble growth by the coalescence event itself through a 'feedback' mechanism (even detachment from the nozzles ensures following bubbles grow at the same rate) is an important aspect of the system. It is also interesting to observe that following a perturbation in the flow from one nozzle (actual flow rate unaltered), the system will self-synchronise such that it becomes fully synchronised (and fully coalescing) once again. Although bubbles will initially be generated out of phase, after a period of time they will begin to approach each other. Once two bubbles are sufficiently close to contact, however slight, the leading bubble will 'pull' the trailing bubble into line, resulting in coalescence and causing subsequent bubble growth to be synchronised. Systems which tend to be fully coalescing are less sensitive to small differences in the gas flow rates between the nozzles and consequent out-of phase formation within a bubble pair.

4.2.2 *Non-Synchronous Systems*

Non-synchronous systems are observed in solutions containing solute at a concentration at, or in excess of the 'transition' value and tend to show much greater variation in contact events than synchronous systems. An example is shown in Figure 4.3. In this example bubbles form at the

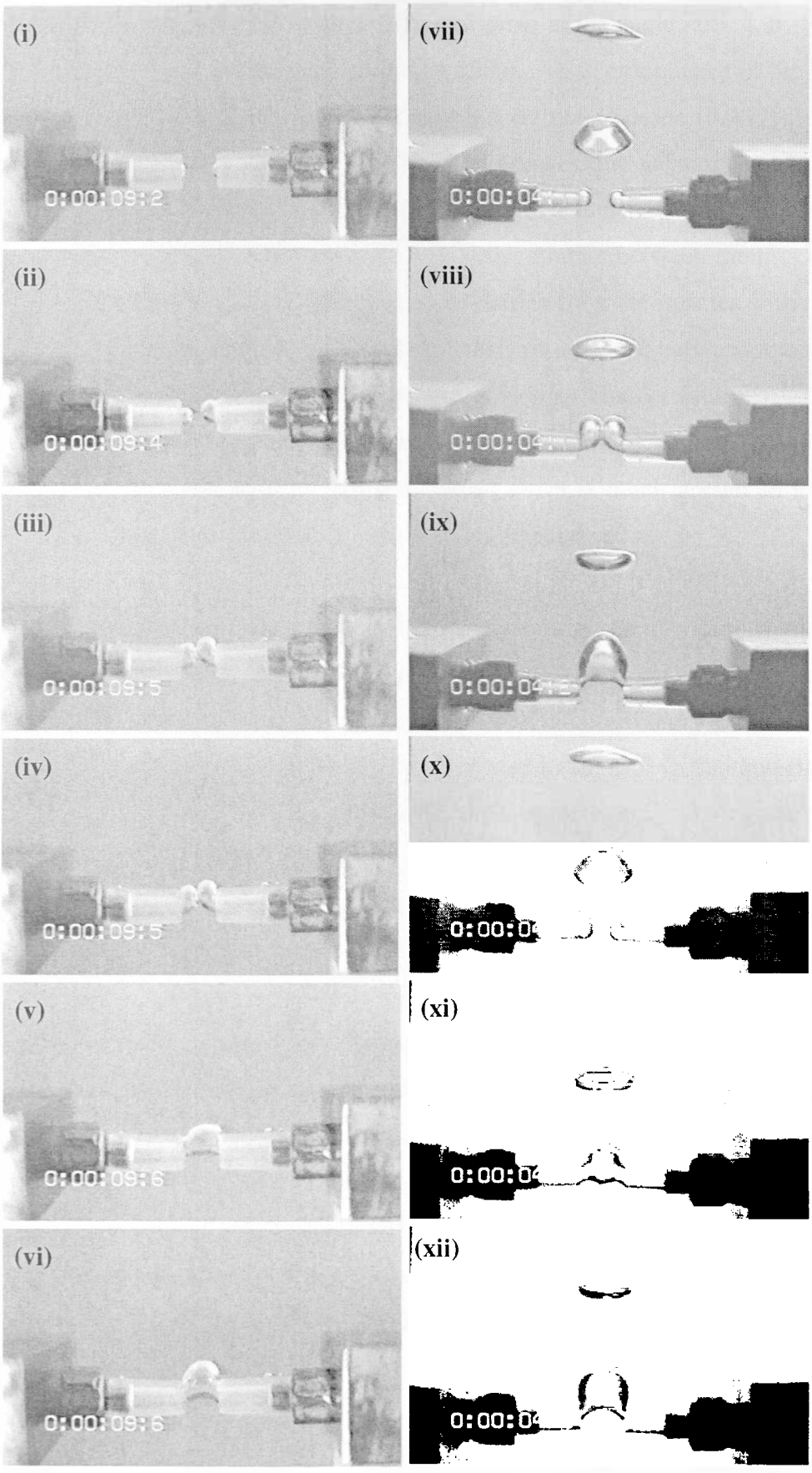

Figure 4.2

Two examples of synchronous systems obtained under quite different conditions.

(i) – (vi) 0.03 M Na_2SO_4. Air flow rate = 1 $mlmin^{-1}$. Nozzle separation 4 mm.

(vii) – (xii) 0.1 M Na_2SO_4. Air flow rate = 50 $mlmin^{-1}$. Nozzle separation 6 mm.

In both cases, bubbles are very similar in size at the moment of contact and such contacts are generally face-to-face.

two orifices at the same time (4.3(i)) and grow at the same rate (4.3(ii)), such that they are very similar in size at the point of contact (4.2(iii)). As a consequence of the low flow rate the bubbles remain in contact for a protracted time but do not coalesce (4.3(iv)). The bubbles continue to grow until they detach unevenly from the nozzles due to buoyancy forces (4.3(v)), which then results in the further growth form the nozzles being unsynchronised. As the unsynchronised bubbles grow sufficiently large (4.3 (vi)) the contact between them is different from that in the previous event and the bubbles grow and detach from the nozzles without coalescing. Following the onset of non-synchronous bubbling, the loss of phase between the bubbles is amplified, until the bubbles form at different times and no longer contact (4.3(vii)). Given sufficient time the system will cycle back into phase and bubble-bubble contact is re-established. As is evident from this sequence, the need to define a contact event is much greater in a non-synchronous system due to the greater variety of events that can be observed.

Is the much diminished coalescence frequency observed in solutions with concentrations at, or in excess of the 'transition' value, the result of the loss of synchrony; or is this loss of synchrony a manifestation of system behaviour and merely a contributory factor to the low values recorded for the coalescence frequency? The first step to answering this question is to consider whether synchrony is intrinsic to a successful coalescence event. During the study, observations have shown that although coalescence can occur from the slightest of contacts, the likelihood of a coalescence event is greater following the face-to-face contacts which result from complete synchrony. This is most probably the result of the increased contact time which follows a fully synchronised contact between bubbles at the same stage of the growth cycle and which subsequently favours film thinning to the point of rupture (although at flow rates where the bubble pair are subject to significant deformation, face-to-face contacts will also increase the contact area between two bubbles). Non-synchronous contacts are generally of a much shorter duration, occurring as they do between bubbles at different stages of the growth phase. However, it is important to note that not all fully synchronised contacts will generate a coalescence event; as shown in Figure 4.4, in solutions with concentrations at, or in excess of the 'transition' value, coalescence can also be repressed despite good synchronisation.

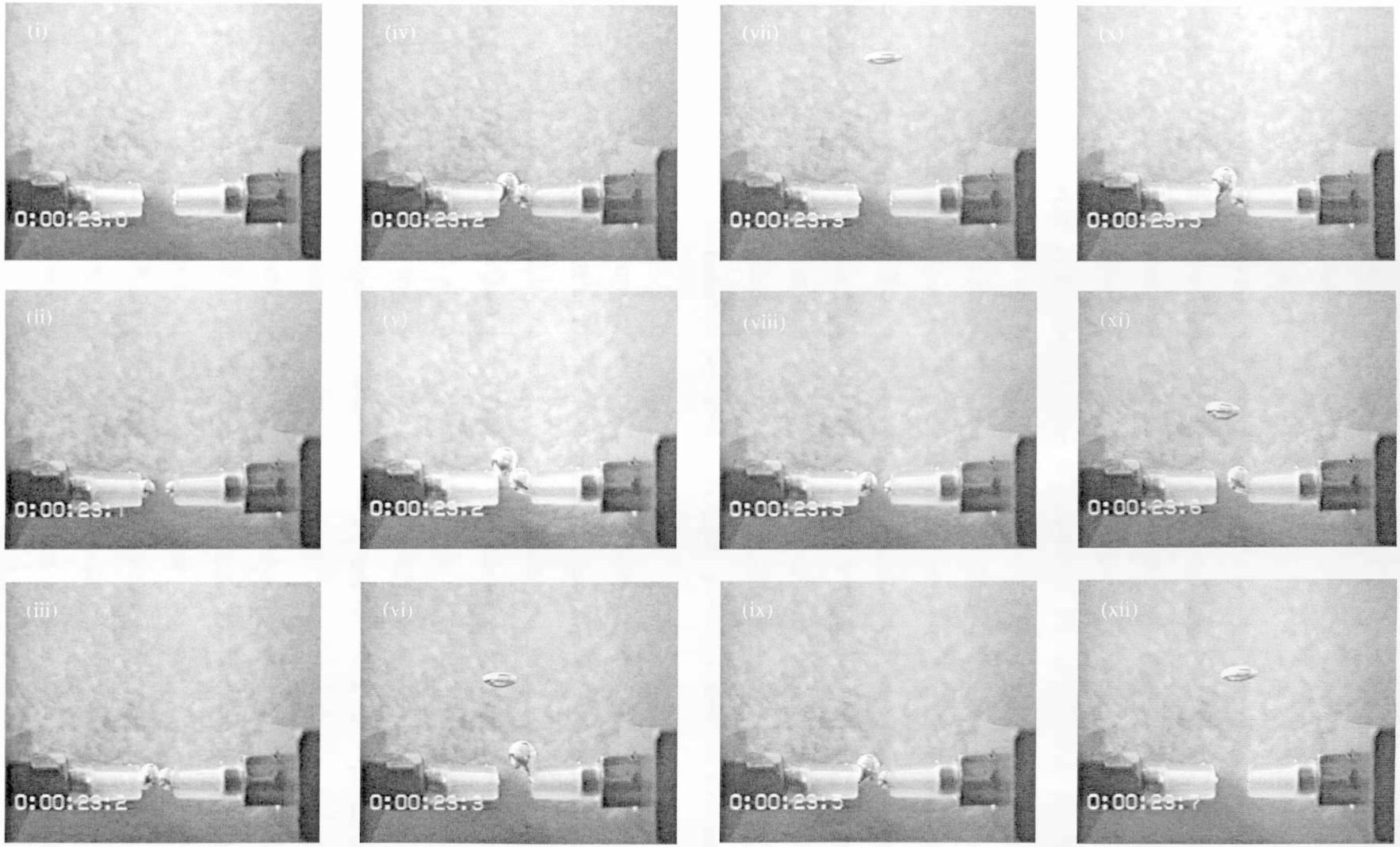

Figure 4.3

Non-synchronous bubbling in 0.06M Na_2SO_4, Q = 4 mlmin^{-1}. (i) - (iii) bubbles are initially synchronised and similar sizes at point of contact, but after contact, left hand bubble slips over opposing bubble (iv) and detaches first (v), causing further bubble growth to be non-synchronous (viii) - (xii).

Once sufficiently out-of-phase, bubble pairs increase the degree of non-synchronisation in a self-amplifying fashion as the bubble formation from one nozzle promotes the rise and detachment of the bubble at the opposing nozzle. Visual observations appear to show that the premature detachment and rise of the leading bubble of an out-of-phase pair results in an increase in the rate of growth, rise and detachment due to buoyancy considerations of the trailing bubble. Although this cannot rigorously be ascribed to wake effects (as the flow behind the leading bubble will not be well formed), the effect of a pressure drop behind the leading bubble, caused by the displacement of liquid as the bubble rises, is suspected. For this reason, one tends to observe phases of bubbling, where initially bubbles form simultaneously and contact for a certain length of time before the bubbles become sufficiently out of phase such that no contact occurs. After a period of interlacing without contact, the interval between non-contacting bubbles diminishes as the bubbles cycle back into contact before a coalescence event triggers the simultaneous formation of a bubble pair, allowing the pattern to re-establish. Cycling of synchronous and asynchronous bubble formation has been reported for bubbles formed at adjacent orifices over a range of gas flow rates (Ruzicka et al., 2000, 1999), which suggests once again, that consistently synchronised bubble formation is not solely dependent on having identical flow rates.

Although a diminished number of face-to-face contacts are obtained in a poorly synchronised system, the low values for coalescence frequency are augmented by the extreme rigidity of the bubble surfaces generated in coalescence repressed solutions. The surface rigidity is obvious in Figure 4.4 (0.04 M Na_2SO_4, Q_g = 10 mlmin^{-1}) where two well synchronised bubbles, despite being held in contact for a significant period of time (73 ms), do not coalesce. The contact between the two bubbles is only broken when the left hand bubble slips over the bubble on the right (maintaining contact) before detaching from the nozzle. As a consequence of the premature detachment of the left-hand bubble from the nozzle, subsequent bubble formation is uneven, leading to a loss of synchrony. It seems appropriate to consider the effect of surface elasticity ($E \propto c(d\sigma/dc)^2$) as a potential cause of this surface rigidity (Hofmeier et al., 1995, Christenson and Yaminsky, 1995), as this provides a measure of the resistance of the surface to mechanical stresses and hence rupture. Electrostatic double layer repulsion should not be a predominant consideration, as the electrolyte concentrations investigated in this work constitute 'concentrated solutions', at which the double layer is compressed and operates only over a very short range. It

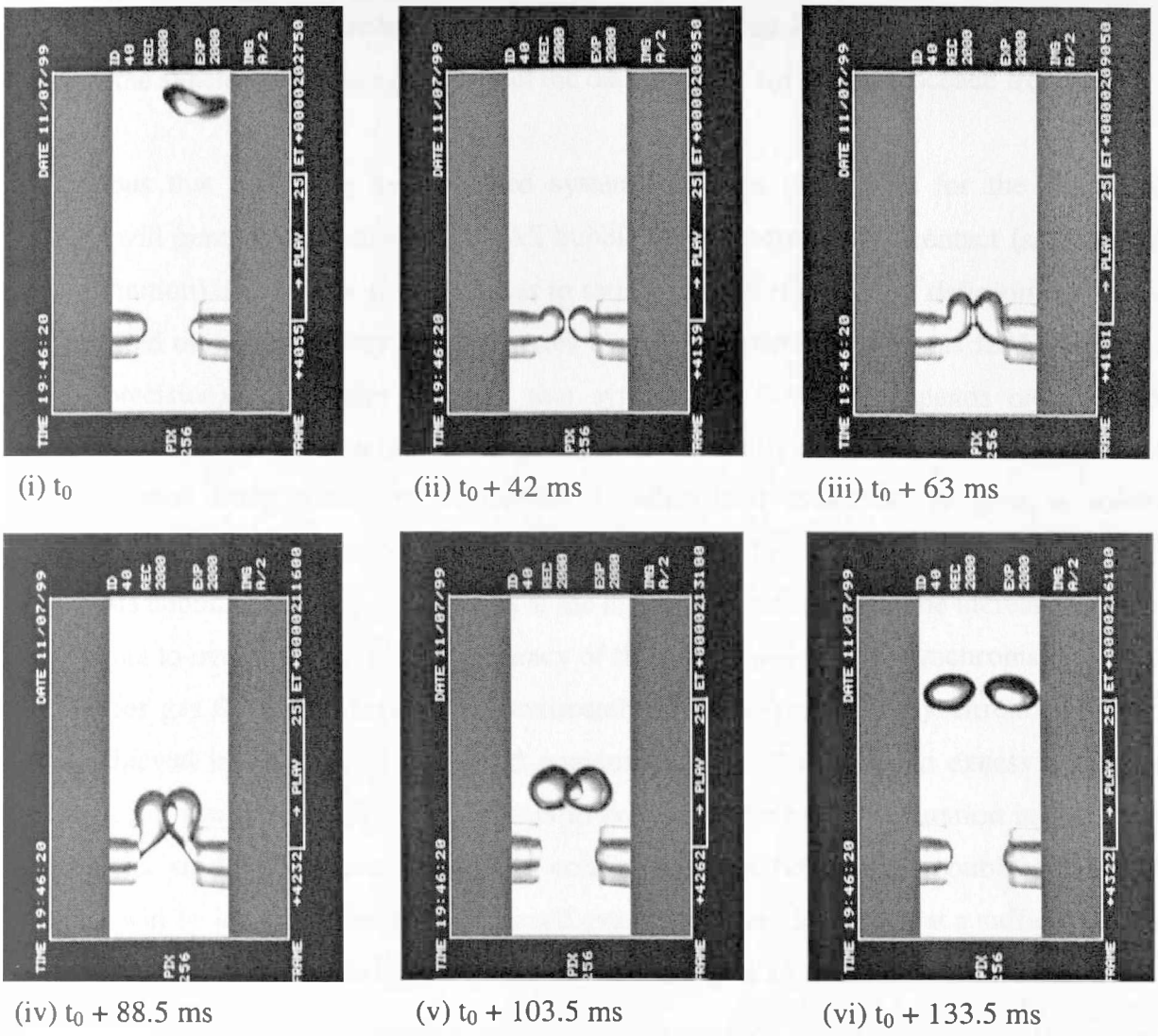

Figure 4.4

High-speed video pictures showing a full face-to-face contact between two bubbles in 0.04M Na_2SO_4, that does not result in coalescence despite the protracted contact time (73 ms). Flow rate 10 $mlmin^{-1}$ (equivalent bubble frequency ~ 8 s^{-1}), nozzle distance 4mm.

may be however, that the electrostatic double layers acts as a 'trigger' for the loss of synchronicity by causing a slight shift in the contact angle of the bubbles which is subsequently amplified through further bubbling, until the system is non-synchronised.

From these considerations, it can be seen that low coalescence frequency values are not solely the result of poor bubble pair synchronisation, although loss of synchrony certainly exerts an additional contribution.

4.2.3 Implications of Synchronisation on Coalescence Frequency

How does the synchrony of the system affect the data obtained for the coalescence frequency?

It is obvious that in a fully synchronised system, all three definitions for the coalescence frequency will generate the same result. All bubble pairs generated will contact (satisfying the second definition) and at such an angle so as to satisfy the criteria for third definition. From the studies carried out with the very low flow rates especially (where the two gas feed rates can be set with precision), it becomes apparent that synchronous bubbling depends on more than identical flows; a system which is initially synchronised and fully coalescing (water) will become non-synchronous once sufficient electrolyte is added and dissolved to give a solution concentration at, or in excess of the 'transition' value. In such a solution, the onset of synchronous bubbling can only be achieved at the higher flow rates, where the increased collision force appears to overcome the natural tendency of the bubble pairs to 'de-synchronise'. Broadly speaking, for gas flow rates between approximately 30 and 60 $mlmin^{-1}$, synchronous bubbling will be achieved irrespective of the liquid composition. At flow rates in excess 60 $mlmin^{-1}$, maintenance of synchronous bubbling appears to depend on the nozzle separation in the system; if this is too small (and consequently the contact pressure between the bubbles too high), synchrony will be lost as the bubbles are forced over each other. However, at a sufficiently large nozzle separation, synchronous bubbling can be observed up to a flow rate of 100 $mlmin^{-1}$.

Consequently, it is obvious that the need for a precise definition for the coalescence frequency becomes imperative for low flow rate experiments with solution concentrations at, or beyond the transition value. In Figure 4.5 the three definitions are investigated by applying each to determine the coalescence frequencies for 0.04M sodium sulfate solutions, over a range of flow rates.

As can be seen, values obtained using the first definition (as a percentage of all bubble pairs) result in much lower coalescence frequencies than the other two definitions. This is especially so at the lower flow rates, where the degree of synchrony is lower. With increasing gas flow rate, the degree of synchronisation also increases, such that all bubble pairs contact and values approach those obtained using the second definition. Although in-situ coalescence events are

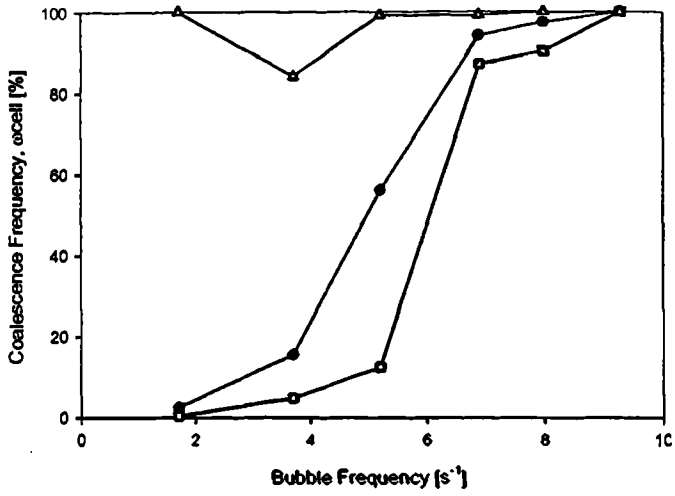

Figure 4.5

Analysing results with the three possible definitions for coalescence frequency, ω_{cell}. —□— Definition 1, —●— Definition 2, —△— Definition 3 (see page 95, 96). 0.04 M Na_2SO_4, Q_g = 2 – 12 mlmin^{-1}, corresponding to bubble frequency 1.7 to 9.3 s^{-1}. Nozzle separation 4 mm.

unlikely to occur if there is no contact between two bubbles, this definition may reflect the probability of approach and thus the overall coalescence probability, as stated previously. In non-synchronous systems, where an intrinsic feature of the system appears to be the intermittent but persistent loss of synchrony, it may be supposed that in free flow, bubbles in coalescence repressed solutions will exhibit a diminished number of bubble-bubble contacts than observed in fully coalescent systems. As noted in Chapter 7, fewer contacts are indeed observed in bubble columns containing concentrated electrolyte solutions than in water (for the same superficial gas flow rate); although it is not possible to attribute this directly to a diminished approach tendency, as there are other pronounced differences, such as the degree of oscillation during free rise, which is much greater for air bubbles in water.

The second definition classifies any touch between two bubbles as a contact. In comparison with the first definition, values for the coalescence frequency are increased, especially at the lower flow rates, where many bubble pairs never contact. When compared to the results obtained using the third definition, however, the values are much lower, perhaps as a result of very slight contacts that occur in a non-synchronous system. It must be noted however, that coalescence events have been observed to occur from the slightest of touches between a bubble pair. In terms of applying the results of the experiment to process systems, this second definition is the most useful as an indication of the coalescence frequency. Coalescence events are unlikely to arise if there is no contact (as reflected in first definition), but there is also no guarantee in situ that bubble-bubble contacts will be as substantial as those suggested by third definition.

Coalescence frequency values obtained using the third definition (contact angle 90° ± 10°) are the largest of all three analyses (and required the longest analysis time). Two factors contribute to these increased values. Firstly, the increased contact times for face-to-face contacts increase the time available for film rupture and therefore coalescence. The second factor, however, is a reflection of the need to observe a representative number of events. At the very lowest flow rates, it was difficult to measure a sufficiently large number of events, due to the restraints imposed by the definition and the poor degree of bubble pair synchrony. Consequently, the data points at gas flow rates 2 and 4 $mlmin^{-1}$ (bubble frequencies 1.7 and 3.7 s^{-1}) represent only 12 and 42 events respectively; both far short of the 250 considered to be representative. Although this definition allows for the effects of contact angle on coalescence frequency to be investigated, (depending on the value of θ chosen), the need to collect very large amounts of data to provide a representative sample which will also satisfy the contact criteria (especially in non-synchronous systems) makes it unfavourable. In addition, visual observations of bubble behaviour in bubble columns with non-viscous solutions do not show a preference for bubble-bubble collisions in the horizontal plane (Chapter 7). Rather bubbles are observed to coalesce following contacts in a variety of geometries, which suggests that for overall relevance, this definition reflects unnecessary 'over-interpretation' of the experimental data.

4.3 Sample Size and Experimental Reproducibility

In establishing the experimental method for this work, it was necessary to determine the number of contact events which constitutes a representative sample, although it is obviously desirable to minimise the time for analysis of a single experiment by counting as few events as possible. Additionally, the minimum sample size changes with the nature of the system; much smaller samples are required to accurately assess a coalescing (synchronised) system, than a non-synchronous one. In the literature the issue has only been addressed by Zahradnik et al. (1987), who considered that 100 events were sufficiently representative, although no explanation for this is provided. For this work, the validation procedure was carried out by initially counting 100 consecutive contacts to determine the coalescence frequency, before increasing this incrementally to 1000 events. The results are shown in Figure 4.6, where the coalescence frequency is shown as a function of the sample size for three combinations of sodium sulfate concentration and

bubble frequency ($f_b \sim 0.8\ s^{-1} \equiv Q_g \sim 1$ mlmin^{-1}, $f_b \sim 7\ s^{-1} \equiv Q_g \sim 15$ mlmin^{-1}). For the fully coalescing systems (0.02 M sodium sulfate), the coalescence frequency is constant, regardless of sample size, as expected. For the solution concentrations 0.04 M and 0.08 M, it can be seen that irrespective of bubble frequency, the value for the coalescence frequency becomes approximately constant at a sample size approaching 300 events. When sample sizes greater than this are counted, the difference between two consecutive values of the coalescence frequency is less than 10%. Consequently, it was concluded that in order to obtain an accurate assessment of the system, not less than 250 events should be counted.

In addition to the number of events, at higher gas flow rates ($Q_g > 30$ mlmin^{-1}, equivalent to $f_b \sim 12\ s^{-1}$) in electrolyte solutions with concentrations in excess of the 'transition' value, the onset of macro-scale bubbling patterns means that the interval over which the sample is gathered becomes important. Due to the high bubble frequencies in these systems, the required 250 events can be observed over a very small time period (10 – 20 s). However, as the bubbling patterns tend to persist for much longer periods of time (> 30 s), it is difficult to determine a representative value for the coalescence frequency by merely counting 250 consecutive bubble pairs, due to the short time span this encompasses. Consequently, for these systems a revised approach to the data analysis was developed wherein the 250 events were split into groups of 50 bubbles, counted at 20 seconds intervals throughout the experiment, to ensure an more accurate assessment of the nature of the system.

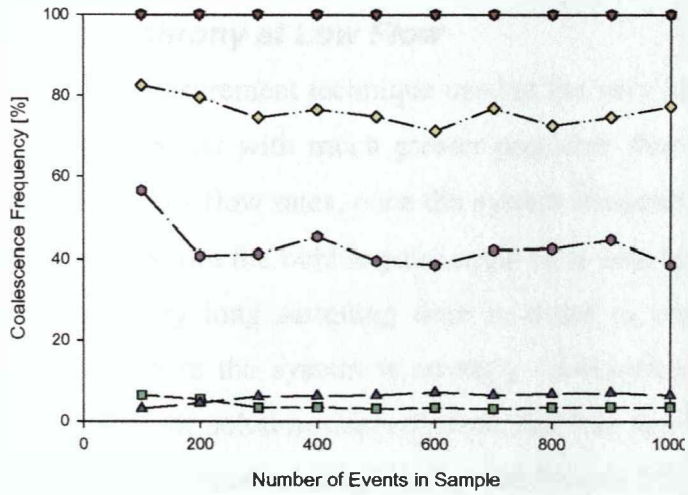

Figure 4.6

Determining the minimum representative sample size; 0.02M, $f_b \sim 0.8\ s^{-1}$, $f_b \sim 7\ s^{-1}$, 0.04M, f_b Q $\sim 0.8\ s^{-1}$, $f_b \sim 7\ s^{-1}$, 0.08M, $f_b \sim 0.8\ s^{-1}$, $f_b \sim 7\ s^{-1}$.

In light of the experimental aspects considered so far, it should not be surprising that reproducibility also shows a dependence on bubble synchronisation. The issue is only briefly addressed in the literature, with Lessard and Zieminksi (1971) quoting an error in their coalescence frequency values of ± 2 % and Yang and Maa (1984), noting only that their system was 'highly reproducible'. Figure 4.7 shows the results of three experimental runs over a range of flow rates for a fully coalescent system (water, 4.7(a)); in two solutions with sodium sulfate concentrations approaching (0.05 M) and in excess of the transition concentration (0.1 M), (as determined by Zahradnik et al., 1987), 4.7(b) for flow rates from 10 $mlmin^{-1}$ to 75 $mlmin^{-1}$ and in solutions of 0.04 M Na_2SO_4 for the much lower flow rates from 2 to 12 $mlmin^{-1}$ (4.7(c)). Graphs are plotted in terms of the corresponding bubble frequencies. As can be seen, a system that is fully coalescing is also perfectly reproducible. For non-synchronous systems, there is a fair degree of reproducibility, especially in the trends obtained over the higher range of flow rates investigated, although for each flow rate, there is an error of the order of ± 15% in the absolute values of the coalescence frequency measured. At lower flow rates a similar degree of reproducibility in the overall trends is observed, although the individual error increases to approximately ± 30%. At these low flow rates the contact pressure exerted on the bubbles is insufficient to force a non-synchronous bubble pair together and consequently, contacts are observed to occur in a wider variety of geometries than at the higher flow rates.

4.4 Experimental Limitations: Effect of Flow Rate

4.4.1 Synchrony at Low Flow

Due to the measurement technique used at the very low flow rates (soap film flow meters), these flows could be set with much greater precision than the higher gas flow rates. However, as a result of the low flow rates, once the system becomes non-synchronous, a considerable period of time passes before the bubble pairs cycle back into synchronous formation. Experimentally, this requires a very long sampling time in order to capture a sufficiently representative sample, especially where the system is strongly coalescence repressed. As a consequence, for some combinations of solution concentration and gas flow rate, data cannot be presented due to the lack of a representative sample of events having been observed; this is especially the case with the measurements of coalescence times, using the high speed video camera.

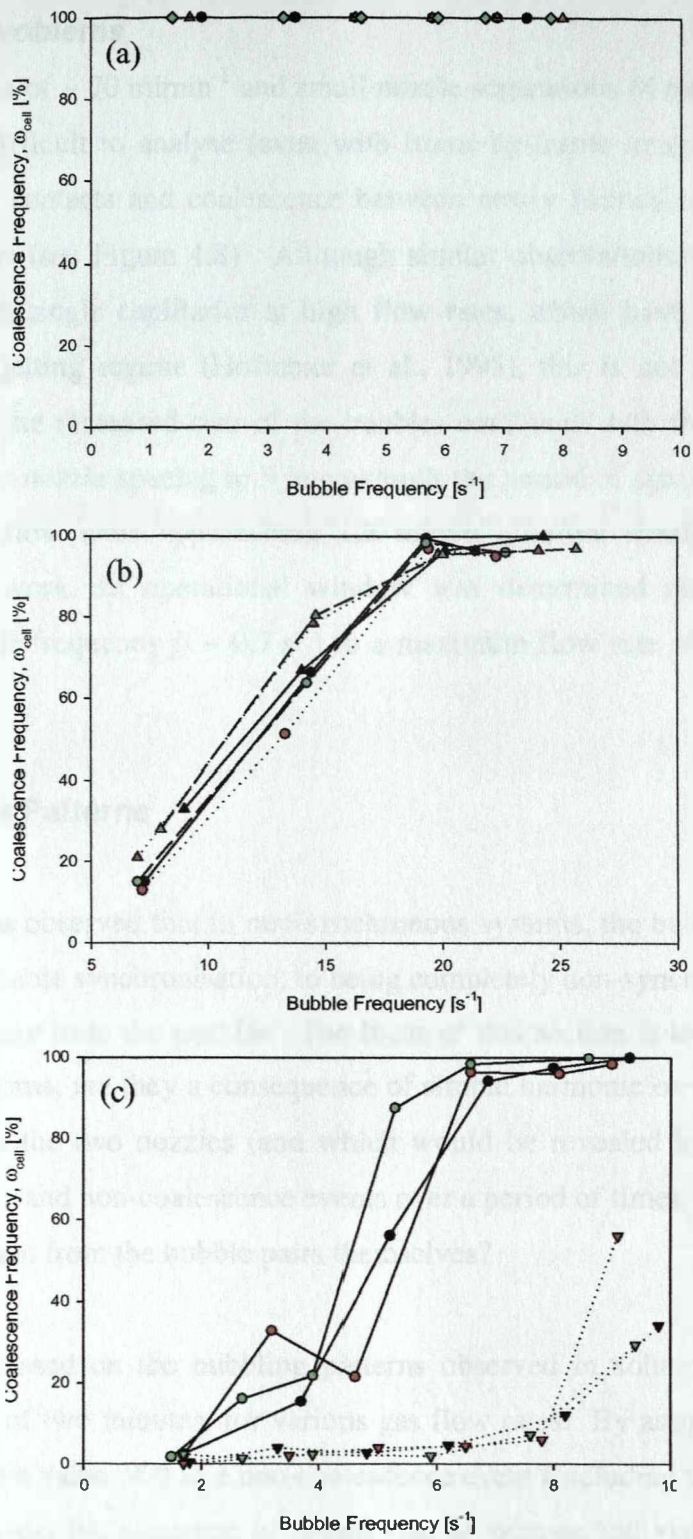

Figure 4.7

The degree of experimental reproducibility depends on the nature of the system and the flow rate range under investigation. (a) Water, three separate trials; good reproducibility of both coalescence and bubbling frequencies. (b) Medium to high air flow rates (10 – 75 $mlmin^{-1}$) for three separate trials; ●, ●, ○ 0.05M Na_2SO_4; ▼, ▼, ▽ 0.1M Na_2SO_4, average error ± 15% (c) Low flow rates (2 – 12 $mlmin^{-1}$) for three separate trials: ●, ●, ○ 0.04M Na_2SO_4, ▼, ▼, ▽ 0.08M Na_2SO_4, average error ± 30%.

4.4.2 High Flow Problems

At flow rates in excess of ~ 70 mlmin^{-1} and small nozzle separations (4 mm), the bubbling mode becomes extremely difficult to analyse (even with frame-by-frame image analysis), due to the existence of multiple contacts and coalescence between newly formed bubbles and previously coalesced bubble pairs (see Figure 4.8). Although similar observations have been made about chaotic bubbling from single capillaries at high flow rates, which have been attributed to the establishment of the jetting regime (Hofmeier et al., 1995), this is not the case in this work. Rather it arises from the increased size of the bubbles combined with the close spacing of the nozzles; increasing the nozzle spacing to 5 mm extends the period of synchronous bubbling (and full coalescence) to flow rates approaching 120 mlmin^{-1}, before similar behaviour is again observed. For this work, an operational window was determined ranging from 1 mlmin^{-1} (equivalent to a bubble frequency f_b ~ 0.7 s^{-1}) to a maximum flow rate of 75 mlmin^{-1} (f_b ~ 20 – 23 s^{-1}).

4.5 Coalescence Patterns

In section 4.2.2, it was observed that in non-synchronous systems, the bubble pairs tend to cycle from periods of reasonable synchronisation, to being completely non-synchronous, such that they are generated alternately from the nozzles. The focus of this section is to investigate the source of these bubbling patterns; are they a consequence of simple harmonic oscillation due to unequal gas flow rates though the two nozzles (and which would be revealed by the repetition of the patterns of coalescence and non-coalescence events over a period of time), or do they arise from a more random interaction from the bubble pairs themselves?

The investigation focussed on the bubbling patterns observed in solutions of 0.04 M sodium sulfate, over a period of two minutes, for various gas flow rates. By assigning a value of 1 to a coalescence event and a value of 0 to a non-coalescence event (including the formation of a non-synchronous bubble pair) the sequence of events can be represented visually, as a function of time, as shown in Figures 4.9(a) to (d). Each line on the bar graphs indicates a coalescence event. It is clear that the number of coalescence events increases with an increase in air flow rate. None of the graphs show a simple repeating pattern that might indicate the bubbling cycles alter as a

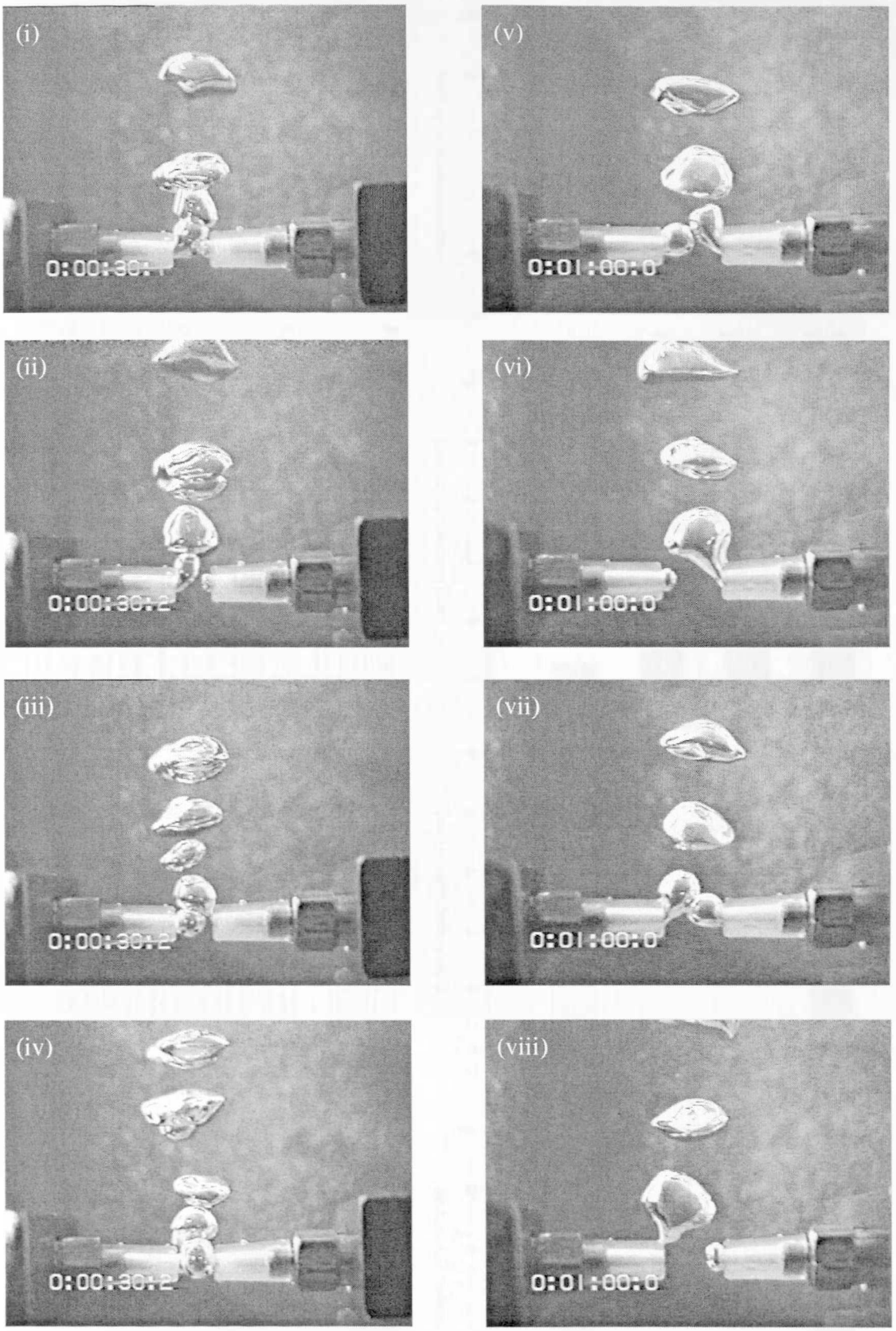

Figure 4.8

(i) to (iv) Chaotic bubbling is observed at high flow rates (Q = 100 mlmin^{-1}) in 0.06M Na_2SO_4 due to the small nozzles separations (4mm). (v to viii) Increasing the nozzle distance to 6mm, prolongs the regime of synchronous bubbling at high flow rates (Q = 100 mlmin^{-1}). Time between frames is 20 ms.

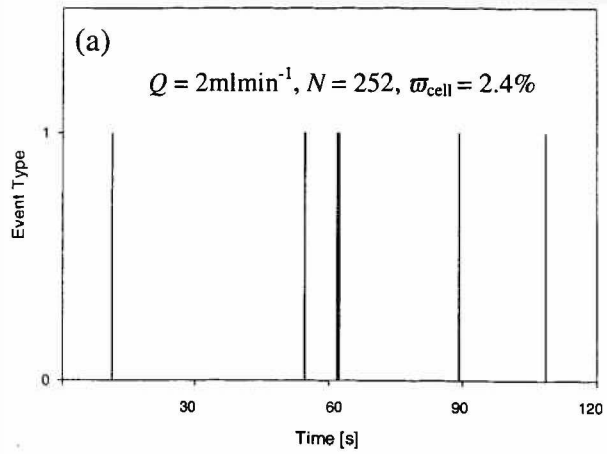
(a)
$Q = 2\text{mlmin}^{-1}$, $N = 252$, $\varpi_{cell} = 2.4\%$
Event Type
Time [s]

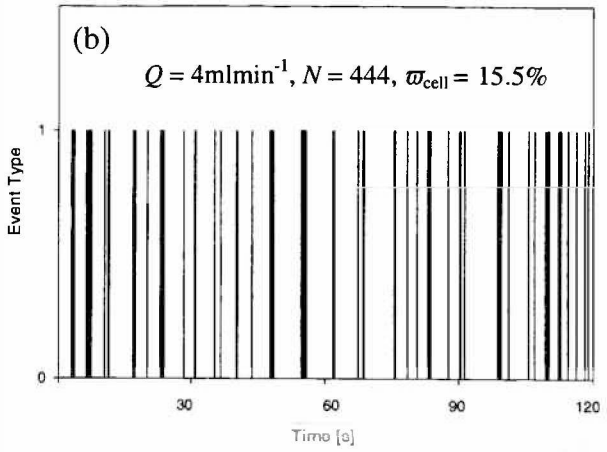
(b)
$Q = 4\text{mlmin}^{-1}$, $N = 444$, $\varpi_{cell} = 15.5\%$
Event Type
Time [s]

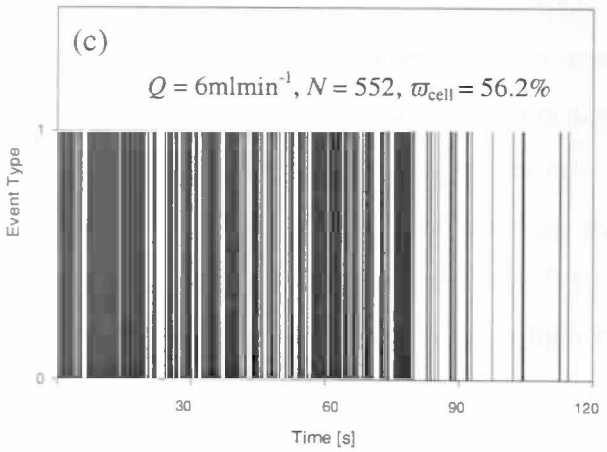
(c)
$Q = 6\text{mlmin}^{-1}$, $N = 552$, $\varpi_{cell} = 56.2\%$
Event Type
Time [s]

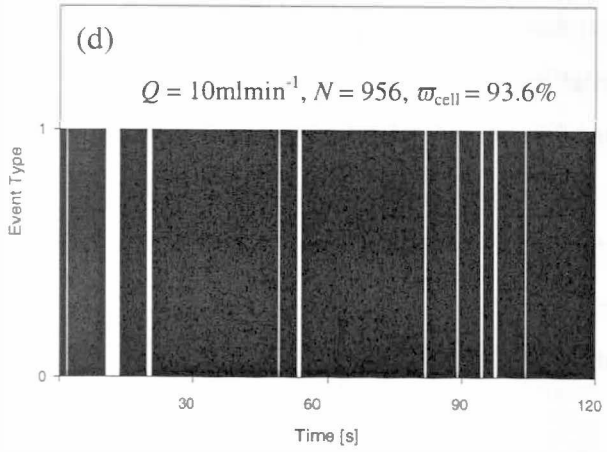
(d)
$Q = 10\text{mlmin}^{-1}$, $N = 956$, $\varpi_{cell} = 93.6\%$
Event Type
Time [s]

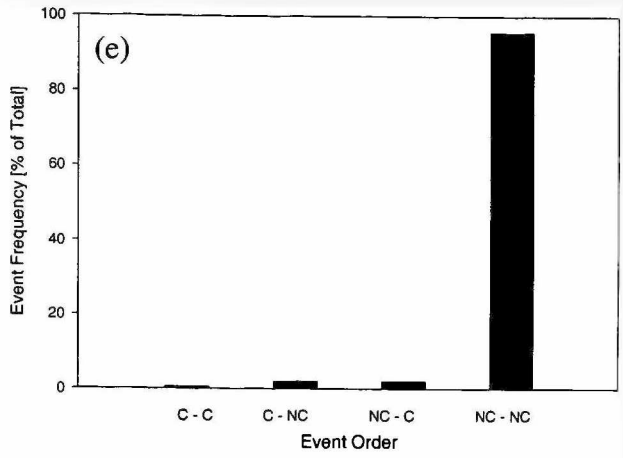
(e)
Event Frequency [% of Total]
C - C
C - NC
NC - C
NC - NC
Event Order

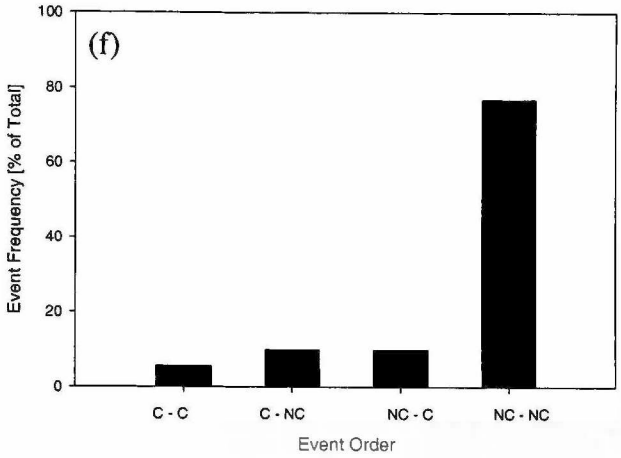
(f)
Event Frequency [% of Total]
C - C
C - NC
NC - C
NC - NC
Event Order

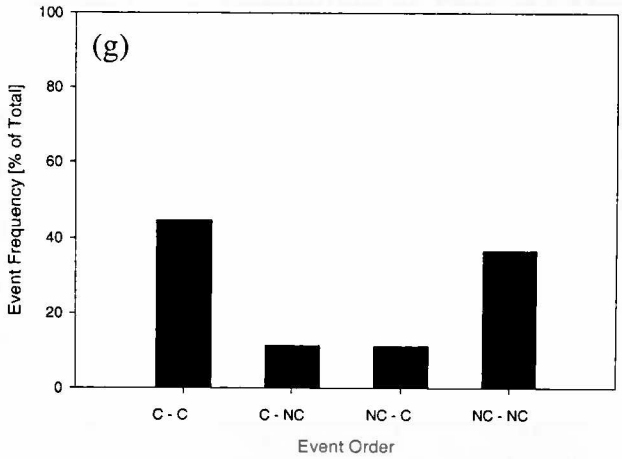
(g)
Event Frequency [% of Total]
C - C
C - NC
NC - C
NC - NC
Event Order

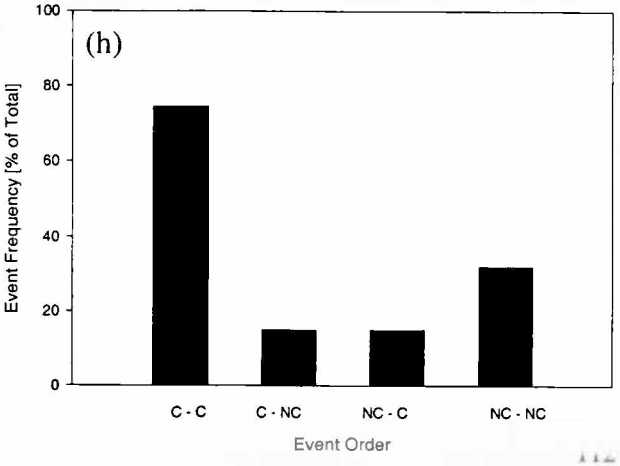
(h)
Event Frequency [% of Total]
C - C
C - NC
NC - C
NC - NC
Event Order

Figure 4.9 (page 23)

Visualising the coalescence patterns observed in solutions of 0.04M Na_2SO_4 with increasing flow rate. For graphs (a) to (d) each line on the bar graphs represents a coalescence event (and consequently, each space a non-coalescing event (including non-synchronous bubble pairs)). In graphs (e) to (h), the event order observed in each system is shown: C-C corresponds to coalescence followed by coalescence, C-NC to coalescence followed by non-coalescence, NC-C to non-coalescence followed by coalescence and NC-NC to non-coalescence followed by non-coalescence.

result of simple harmonic oscillation between the two gas flow rates. However, it is interesting to observe that as the number of coalescence events increases, these tend to occur in clusters; this is especially noticeable at Q_g = 6 mlmin^{-1}, where the system initially appears coalescence dominated, before long intervals of non-coalesce are observed towards the end of the measurement interval.

This tendency of the system for like events to follow like is clearly illustrated in Figures 4.9(e) to (h) where the event order (coalescence/coalescence, coalescence/non-coalescence, non-coalescence/coalescence or non-coalescence/non-coalescence) observed for each system is shown. The proportionally greater occurrence of like-like events is readily seen, demonstrating that the system tends to favour either coalescence or non-coalescence, rather than switching continuously between states. This is completely contrary to the observations of Yang and Maa (1984), who note regular alternation between coalescence and non-coalescence events at coalescence frequencies of 50%. The tendency becomes exaggerated in concentrated electrolyte solutions at high gas flow rates (in excess of ~ 30 mlmin^{-1}), where macro-scale bubbling patterns can be observed, with the system moving through distinct periods of coalescence and non-coalescence. These patterns appear to result from a freak event which perturbs the system, giving rise to a new 'steady-state' behaviour, which persists until further disruption switches the mode of bubbling once again.

Similarities can be drawn between the interdependence of the individual bubbling nozzles and the known chaotic behaviour of a double oscillatory system. Attempting to prove that the system under consideration was indeed subject to chaotic behaviour has proved beyond the scope of this project, given that the very large amount of data which would be required for such a task must be manually collected and reduced. However, it may provide a means of quantifying the seemingly random bubbling modes observed in the cell, especially in light of the observation of Ruzicka et al. (2000, 1999), in their studies of bubbling through adjacent orifices from a common plenum.

The use of twin laser beams to accurately assess the time difference between bubble formation and detachment from the nozzles, combined with a visual assessment of the event occurring (thereby assessing the degree of interaction between the nozzle streams) would provide one possible method of collecting the required volume of data within a reasonable time frame.

4.5.1 Flow Patterns

Attempts were made to visualise the flow patterns present in the liquid between two approaching bubbles through the use of a He-Ne laser, diffracted through a glass rod to create a laser sheet. Flow following particles of neutral density were added to the cell contents and tracked with a video camera. Although the flow patterns could be followed clearly, the structure of the stainless steel frame prevented the laser sheet from illuminating the area of interest, between the nozzle spacing and consequently only the flow patterns in the bulk liquid could be seen.

4.6 Parameters Determined From High Speed Studies

The use of high-speed video enables the coalescence process to be examined with a greater degree of scrutiny than provided by the collection of bulk system data, such as coalescence frequencies. In addition to being used to determine coalescence times, the high speed video was used to determine supporting data such as the contact time (for non-coalescence events), film area and bubble lifetime, all of which was useful in allowing in-depth observation of the process. As noted in Chapter 3, each of the parameters was determined from analysis of the video images; all measurements were made manually, as was all data reduction.

Coalescence times were measured by counting the number of frames from the initial contact between the two bubbles to the frame just prior to film rupture and then compensating for the frame rate used to capture the images. For those instances where two contacting bubbles did not coalesce, contact times were determined corresponding to the time between the initial contact and subsequent separation of the two bubbles. This parameter can provide a significant degree of information about the system behaviour. Not only will the contact time change with gas flow rates (as this increases, two bubbles will remain in contact for shorter periods of time), but it will obviously depend on the degree of synchronisation of the contacting bubble pair. For those

bubbles which are synchronised and contact face-to-face, contact times will be longer than in situations where there is only a glancing touch between a non-synchronous bubble pair. However, in this study contact times are used only to provide a means of comparison between coalescence and non-coalescing events, not as an indication of the overall system behaviour.

In addition to the effect on contact time, increasing gas flow rates cause the area of the film between two contacting bubbles increases, as a result of the larger bubbles and the subsequent greater degree of deformation. Measurements of the coalescence time over a range of gas flow rates however do not allow for the very significant differences in contact area which can be observed. Even for a specific flow rate, the contact areas between bubbles pairs are not always constant, despite unchanged conditions, due largely to the different degrees of synchrony with which bubbles pairs may contact. To allow comparisons to be made for events at different gas flow rates, some compensation for the differing film areas was required. This was achieved by calculating a 'coalescence rate', defined as contact area (a) thinned over a given coalescence time (t_c). In order to calculate this parameter, the diameter of the intervening film was measured directly from the frame just preceding film rupture and used to estimate the film area at this time, which was assumed to be circular. This parameter is especially useful at higher gas flow rates when the contact area between two contacting bubbles is much greater. Although the method does not account for the changes in contact area with time (which is a noticeable feature of colliding bubbles at the higher gas flow rates, where the bubbles are forced together and continue to grow before coalescence occurs), it does provide a means of assessing the effects of contact pressure on coalescence, independent of the contact area.

Finally, the video images were also used to obtain the bubble age at contact, which is defined as the age of the bubble at the point of initial contact. It was determined by measuring the time from when the hemispherical bubble surface was first observed at the nozzle opening to the moment of first contact with the opposing bubble (i.e. the starting point for the coalescence time measurement).

One of the most notable features of the bubbles formed in water and in low concentration electrolyte solutions is the considerable amount of oscillation of the newly formed surfaces,

which increase in magnitude as the bubbles grow. As a result, after a bubble pair becomes sufficiently large enough for opposing bubbles to touch, the initial contact may be broken and renewed as the surfaces continue to oscillate before coalescence occurs (Figure 4.10). [This is not the same as 'bouncing' of the bubbles after contact which is sometimes observed in electrolyte solutions as overall, the bubble continues to move in the same direction.] As a result, there are two possible values which correspond to the coalescence time. In the first case, it corresponds to the time from the initial contact to the point of film rupture and as such obviously includes any renewed contacts (and the non-contact time between). The second interpretation would be the time from the final contact time to the point of rupture. Obviously, when film rupture occurs directly following the initial contact, the two interpretations of coalescence time generate the same value. Of the two measures, the second is the one that most closely corresponds to the generally accepted mechanism of bubble-bubble contact, film thinning and subsequent rupture, as it involves a single, unique contact area. When the coalescence time is measured from the moment of the initial touch, no account is made of the fact that the actual film area may change as contact between the two bubble surfaces is renewed. For those systems where surface oscillations are significant, it is also possible to determine an additional parameter, closely linked to the two measures of coalescence time. This is the 'number of contacts' which is defined as the number of contacts between bubbles prior to coalescence. Obviously, for those system where coalescence occurs directly following the initial contact, the value of this parameter will be unity; in those systems where contact is renewed several times, it will have a much greater value.

Surface oscillations are generally only observed when bubbles form at the low gas flow rates. Under these conditions, the bubbles form slowly at the nozzles, giving rise to long bubble lifetimes and the degree of oscillation significantly affects the nature of the contact between the two. The oscillations are not observed at higher gas flow rates, when the rate of surface expansion is much more rapid and appears to dominate any independent movement of the surface. The effects of surface oscillation should not just be considered an artefact of the experimental set-up. High speed video studies of dispersions in bubble columns (Chapter 7) show bubbles continuously oscillating during free rise (this is especially prominent in water) and the importance of continually renewed contacts between colliding bubbles can be confirmed

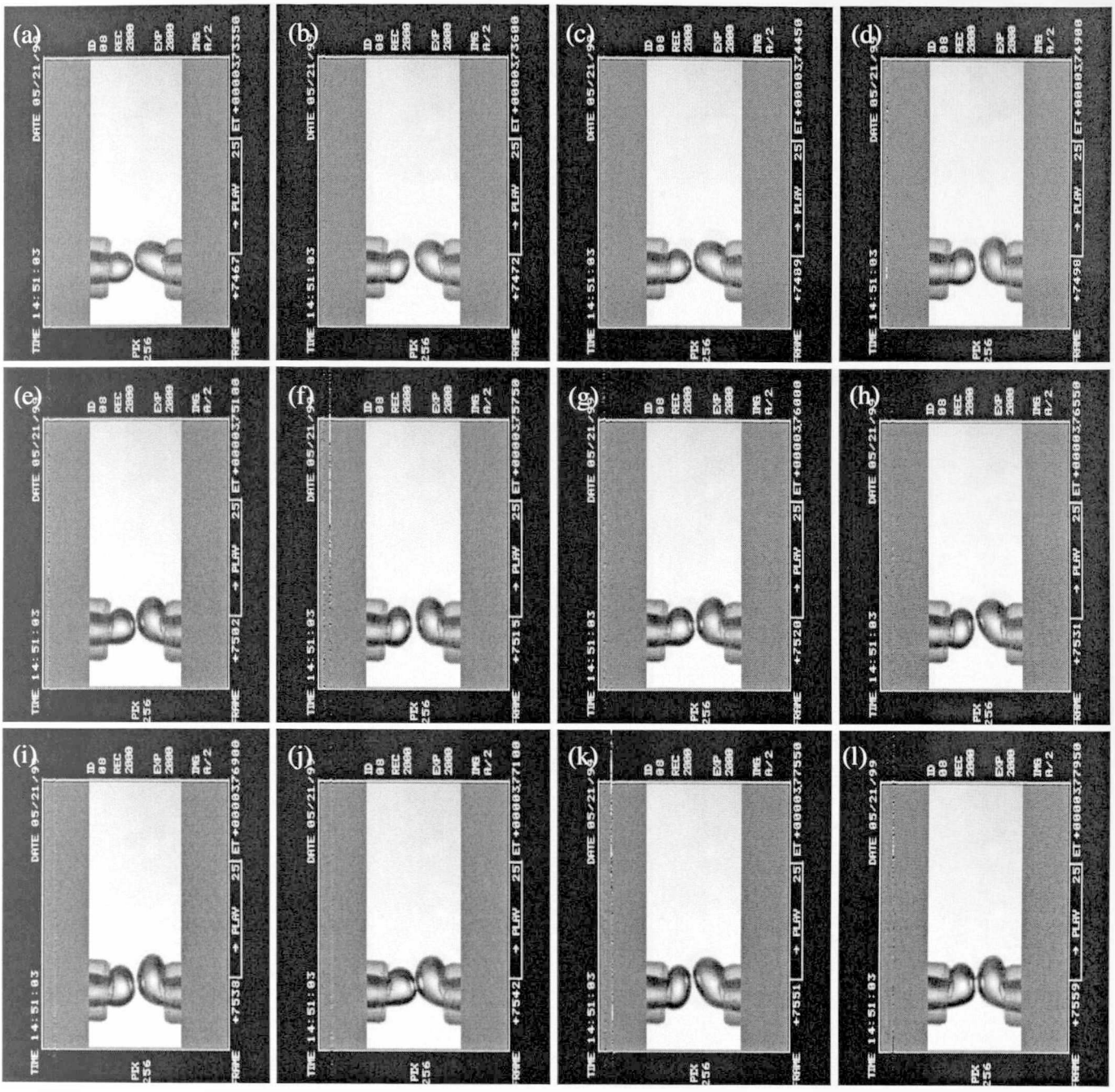

Figure 4.10

Air bubbles in water at 10°C, showing multiple renewed contacts as a consequence of the prominent surface oscillations. In this example, 10 separate contacts are made before the bubbles coalesce.

Time between frames: (a) $t = 0$ ms, (b) $t = +2.5$ ms, (c) $t = +11$ ms, (d) $t = +15.5$ ms, (e) $t = +17.5$ ms, (f) $t = +24$ ms, (g) $t = +26.5$ ms, (h) $t = +32$ ms, (i) $t = +35.5$ ms, (j) $t = +37.5$ ms, (k) $t = +42$ ms and (l) $t = +46$ ms.

(sequence continues on following page ...).

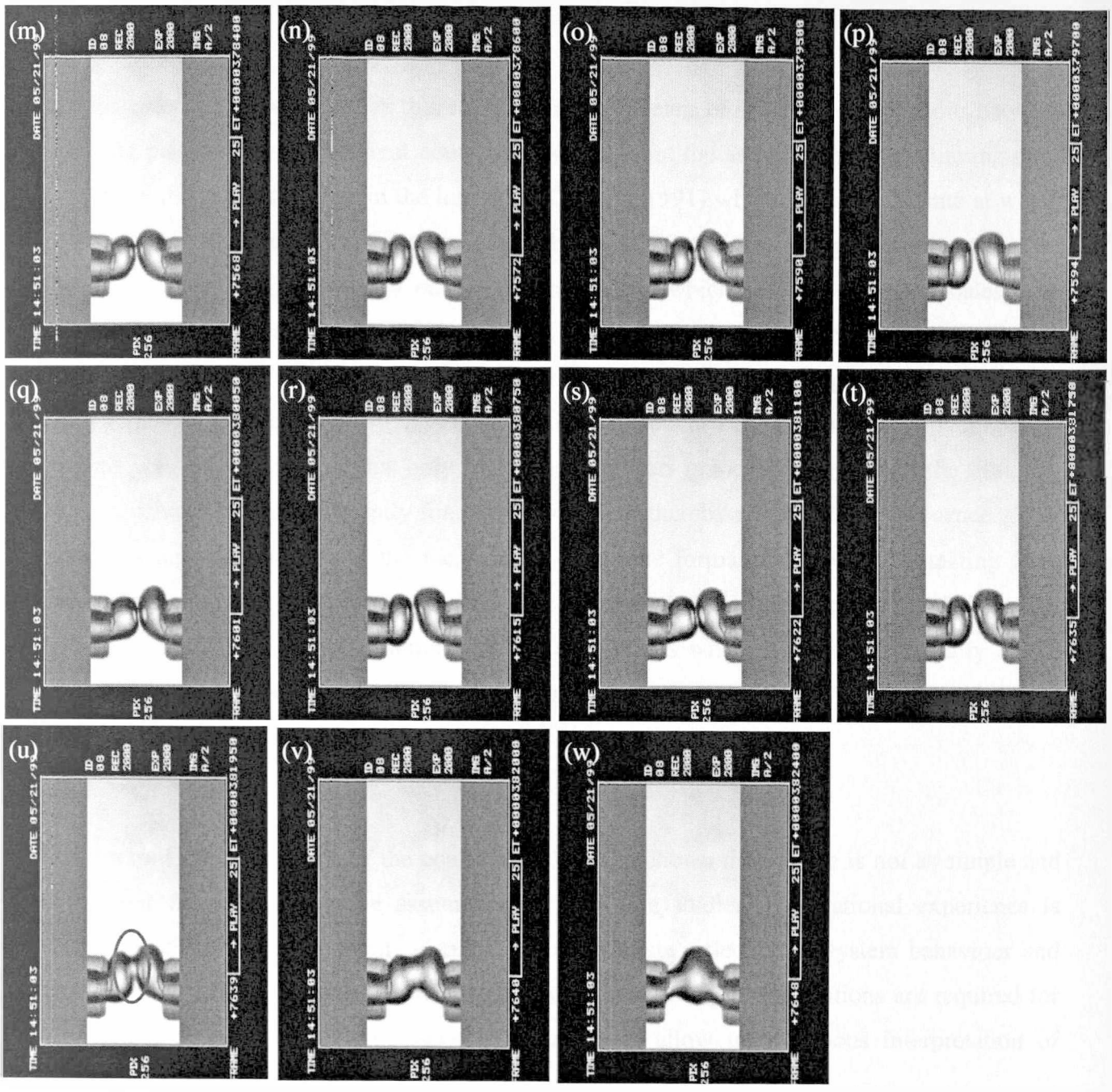

Figure 4.10 (cont.)

Air bubbles in water at 10°C, showing multiple renewed contacts as a consequence of the prominent surface oscillations. In this example, 10 separate contacts are made before the bubbles coalesce.

Time between frames: (m) $t = +50.5$ ms, (n) $t = +52.5$ ms, (o) $t = +61.5$ ms, (p) $t = +63.5$ ms, (q) $t = +67$ ms, (r) $t = +74$ ms, (s) $t = +77.5$ ms, (t) $t = +84$ ms, (u) frame directly after the moment of film rupture, $t = +86$ ms, (v) $t = +86.5$ ms and (w) $t = +90.5$ ms.

(... sequence continued from preceding page).

visually (and which may perhaps account for the low number of coalescence events observed, even in pure systems).

The 'coalescence rate' was used in this study solely as a means of allowing comparisons between contacting pairs with very different contact areas. It is not the same as the film thinning rates proposed in the various models in the literature (Chester, 1991) which consider the rate at which the thickness of the intervening film changes with time. The validity of a parameter such as the 'coalescence rate' depends greatly on the mechanism by which film rupture and coalescence occurs. If, as proposed in many of the models for coalescence (Marrucci, 1969a, Sagert and Quinn, 1976b) the entire film must thin to the critical thickness at which rupture may occur, then such a parameter should provide a degree of consistency between coalescence times over a range of events. However, it may be that only film thinning occurs in localised regions of the film, any one of which could thin sufficiently for rupture to occur, thereby resulting in coalescence. This scenario is not dissimilar from the mechanism of dimple formation between contacting fluid particles as suggested by Allan et al. (1961). For such a mechanism, compensating for the different contact areas within a number of collision events will be of reduced validity as the thinning times should be largely independent of the contact area.

4.7 Conclusions

- An in-depth assessment of the coalescence cell has shown that its use is not as simple and straightforward as may be assumed from literature studies. Operational experience is required to ensure the results obtained are an accurate reflection of system behaviour and free from experimental artefact. In addition, clear and explicit definitions are required for parameters such as the coalescence frequency to allow unambiguous interpretation of coalescence cell data.
- A definition for coalescence frequency has been selected which provides the best balance between the need for accurate representation of the coalescence behaviour of a system and rigorous data acquisition methods. The definition is:

$$\text{Coalescence Frequency, } \omega_{cell}'' = \frac{\text{Number of bubble pairs coalescing}}{\text{Total number of bubble pairs contacting}}$$

where any touch between bubbles in a pair, irrespective of contact angle, constitutes a contact event.

- Synchronous bubbling is a system dependent variable, influenced by the nature of the liquid phase, gas flow rate and rate of bubble formation and nozzle separation distance for two equal gas feed rates.

  In pure liquids and dilute solutions of electrolytes, bubble pairs are fully synchronised, even at the lowest gas flow rates. For all solutions, irrespective of electrolyte concentration, synchronous bubbling can be obtained within the range of gas flow rates 30 – 60 $mlmin^{-1}$. However, at high gas flow rates and small nozzle separations, synchronised bubbling is not maintained, even in pure liquids and dilute solutions.
- To ensure a sufficiently representative sample, the number of contacting events observed should not be less than 250 events. For high gas flow rates (> 30 $mlmin^{-1}$) in concentrated electrolyte solutions, these 250 events should be split into discrete groups to ensure sampling occurs over a sufficiently long time period to avoid the influence of macro-scale bubbling patterns.
- Reproducibility of experimental results is very dependent on the degree of synchronisation between bubble pairs. For fully coalescing (always synchronised) systems, results are fully reproducible. For coalescence repressed systems, experimental reproducibility is flow rate dependent: for flow rates from 10 to 75 $mlmin^{-1}$, the average experimental error is ± 15 %; at flow rates 1 to 12 $mlmin^{-1}$, the average error increases to ± 30 %. In each case however, good reproducibility of general trends is observed.
- In order to minimise the experimental artefact which occurs for a combination of high gas flow rates and small nozzle separations, an operational window has been established in this study, such that all experiments are carried out within the limits of gas flow rates between 1 and 75 $mlmin^{-1}$.
- Coalescence patterns do not show any consistent repetitions between the occurrence of coalescing and non-coalescing/non-contacting events. Analysis shows a system preference for like events to follow like, rather than alternating behaviour.
- Parameters determined from high-speed video analysis have been defined for the purpose of this study; these include coalescence time, contact times, bubble lifetime and

'coalescence rate'. This last parameter is defined as the contact area divided by the coalescence time and is used solely to account for difference between contacting bubbles due to influences of gas flow rate and the degree of synchronisation between the bubble pair.

- Surface oscillations are a prominent feature of bubbles formed in water and low concentration electrolyte solutions at low gas flow rates. These significantly influence the nature of the coalescence events and subsequently, the values of parameters measured.

Chapter 5
The Coalescence Cell and Inviscid Liquids

The previous chapter examined the basic considerations that arise from the application of the coalescence cell as a tool for investigating coalescence behaviour. Following this introduction to the cell, this chapter reports results from experiments carried out in a range of inviscid liquids, ranging from pure fluids to solutions of electrolytes and short chain alcohols. In each case, the macro-scale data obtained from direct observation of the coalescence behaviour is accompanied by coalescence time measurements acquired using high-speed video. Section 5.1 reports on experiments carried out in water and propan-1-ol, both pure liquids, where the focus is on the effect of temperature on the coalescence times as determined through high-speed video studies. In section 5.2, results are presented for experiments conducted in electrolyte solutions of varying concentration, followed by the results of experiments with solutions of propan-1-ol (section 5.3). Finally, in section 5.4, the effects of increasing gas density are investigated for solutions of magnesium sulfate and propan-1-ol. All the data acquired has been analysed in accordance with the definitions outlined in the preceding chapter.

5.1 Pure Liquids

Pure liquids are the quintessential 'fully coalescing' systems, which tend to generate low gas hold-ups and large bubble sizes in process systems, irrespective of the gas dispersion system. This is largely due to the absence of the surface tension gradients which in multi-component systems work to resist surface expansion and retard the rate of film drainage between two contacting bubbles. Consequently, in pure systems coalescence can occur on a very rapid time scale (1 – 10 ms, according to Chesters and Hofman, 1982). However, in spite of these extremely short coalescence times, Stewart (1995) has observed very few coalescence events in dynamic dispersions of air and water. Likewise, in Chapter 7 of this work, high-speed video studies of coalescence in bubble columns show that very few of the many bubble-bubble contacts result in coalescence. Generally it is considered that coalescence will occur when contact time exceeds the time required for film drainage and rupture; although in these in-situ studies, the contact times have been observed to be on average, greater than coalescence times reported in the literature (Sagert and Quinn, 1978, 1976a, b). It is well known that coalescence in pure systems is very sensitive to the presence of impurities and it

may be that the low number of coalescence events observed were due to contamination of the gas-liquid interfaces by surface-active impurities, causing surface tension gradients, decreasing surface mobility and hence slowing the rate of film thinning.

In this study the coalescence cell has been used to investigate coalescence times in two pure liquids; water and propan-1-ol, over a range of gas flow rates (and therefore range of bubble frequencies and sizes), using various gases. The absence of surface active species to adsorb at the interface suggested that effects of surface age should remain negligible over the range of bubble life-times, allowing the effect of contact pressure and increased contact area to be qualified.

5.1.1 Water

The experiments carried out with water were used to provide a baseline for the investigations into coalescence in electrolyte and alcohol solutions, in addition to acting as an assessment of system cleanliness and the equality of the two gas feeds. Materials and methods used are fully described in Chapter 3. A coalescence frequency of 100% was always observed, irrespective of the gas flow rate (1 – 50 $mlmin^{-1}$), gas type (air, hydrogen or xenon) or nozzle distances (4 to 6 mm), although for the combinations of very high gas flow rate and small nozzle separation, chaotic coalescence was observed as in electrolyte solutions (Figure 4.8) such that coalescence often occurred between vertically aligned bubbles or between previously coalesced bubbles and newly formed ones. The fully coalescing nature of the system confirms the absence of impurities and validates the cleaning protocols outlined in Appendix C.

Coalescence times studies were carried out using high speed video for air, hydrogen and xenon bubbles in water, again to provide a baseline for later studies but also to allow a means of comparison with previously reported studies. In addition, experiments with air and water were carried out at three different temperatures (10°C, 25°C and 50°C) as a means of manipulating the bulk properties of surface tension and viscosity (Table 5.1). The results of these three sets of experiments with air are presented in Figure 5.1 (where each data point represents the mean of 25 measurements). Measurements were carried out as discussed in Chapter 3. In Figure 5.1 the mean coalescence times and 'coalescence rates' are shown as functions of the mean bubble lifetime (from t_b ~20 ms, equivalent to gas flow rate 50 $mlmin^{-1}$, to t_b ~1200 ms at flow rates of 1 $mlmin^{-1}$). A third parameter, the mean number of contacts is

	T = 10°C	T = 25°C	T = 50°C
Surface Tension [mNm^{-1}]	74.23	71.97	67.94
Viscosity [mPas]	1.307	0.894	0.547

Table 5.1

Effect of temperature on bulk properties of water. Data from 'Handbook of Chemistry and Physics', 74th Edition, 1993, Lide, D. R., Ed.

also shown; this is an important indication of the system behaviour and influences the values of the coalescence time (as discussed in Chapter 4).

Prior to examining the graphs in Figure 5.1, it is useful to consider the factors which may affect coalescence time (and 'coalescence rate') as the gas flow rates through the nozzles increase and the fluid dynamics in the cell are altered. As the bubbles are formed in a pure liquid, considerations of surface age and complications from differential diffusion rates of solute to the surface are not relevant (excepting the effects of surface-active contaminants, which may be present). At the low gas flow rates used initially, the bubbles form slowly at the nozzles and are subject to significant oscillations, which affect the nature of the contact between the two (Figure 4.10). These surface oscillations are not observed at higher gas flow rates, when the rate of surface expansion is much more rapid and dominates any independent movement of the surface.

Additional factors which may affect film thinning and hence coalescence times are contact pressure and area. Due to the constant nozzle separation, the increase in bubble size, which accompanies higher gas flows, will increase the contact pressure between two (fully synchronised) bubbles, hence accelerating the rate of film thinning. However, as the two bubbles are forced together, the amount of deformation will also increase such that the contact area between the two becomes larger and a greater film area that must be required to thin down to the rupture thickness. Although the bubbles formed at higher flow rates do not show pronounced surface oscillations, when these do occur, the increased contact area tends to also decrease the likelihood of fully renewed contacts as observed at slower gas feed rates, although there still may be a shift in the actual contact area. Consequently it is obvious that there are a number of interacting factors which can be expected to exert opposing influences on the rate of film thinning and hence the coalescence time, as the gas flow rate increases.

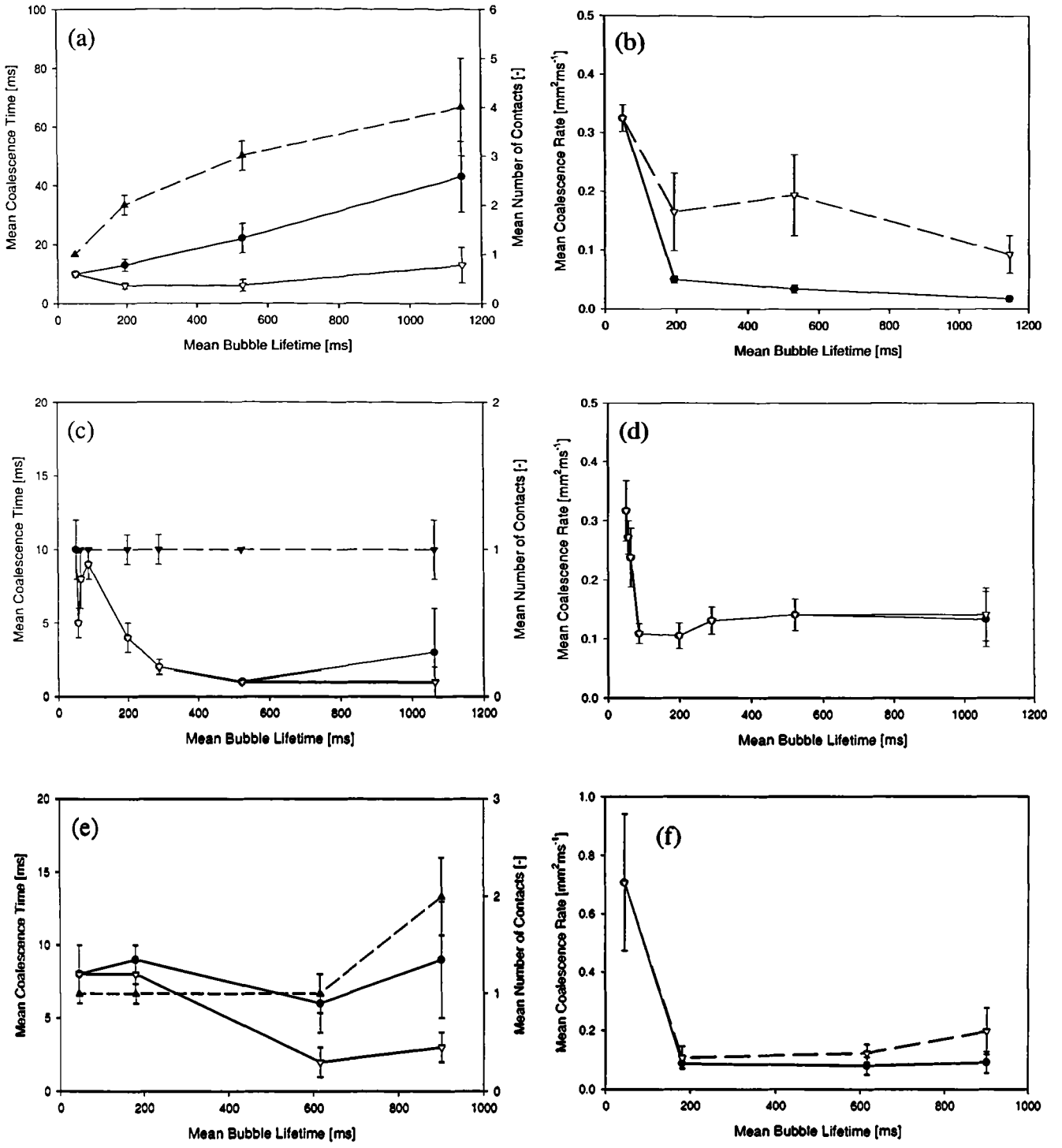

Figure 5.1

Mean coalescence times for air bubbles in water at temperatures (a), (b) 10°C, (c), (d) 25°C and (e), (f) 50°C, error bars show 95% confidence levels (from 25 measurements). For (a), (c) and (e) —●— coalescence time from initial contact, —▽— coalescence time from last contact and —▲· number of contacts. For (b), (d) and (f) —●— thinning rate from initial contact and —▽· thinning rate from last contact.

In all the experiments, one of the most noticeable aspects of the coalescence time data is the variability under a single set of conditions (shown by the wide 95% confidence levels), especially at the lowest gas flow rates. Although in some cases the error bars are reduced by compensating for the contact area between the two bubbles (calculating the 'coalescence rate'), a considerable degree of scatter remains for others, notably in experiments at 10°C and 50°C.

At 25°C (Figure 5.1(c)) the effects of surface oscillation are minimal, such that the majority of bubbles coalesce after the initial contact. The only exception is at the lowest flow rate (Q_g = 1 mlmin^{-1}, bubble lifetime, t_b ~1300 ms) for which the coalescence times from initial and final contact are different. Overall, there is an increase in mean coalescence times with decreasing bubble lifetime (corresponding to increasing gas flow rate) up to t_b ~ 100 ms (Q_g = 30 mlmin^{-1}). Beyond this, the sharp fall in coalescence times may be related to the lower average contact area measured in this region (1.3 mm^2 compared to 1.9 mm^2 at t_b ~ 65 ms (Q_g = 40 mlmin^{-1}) and 2.9 mm^2 at t_b ~ 50 ms (Q_g = 50 mlmin^{-1}).

In fact, measurements of coalescence times do not account for differences in contact areas between two bubbles, which may arise from increased deformation or degrees of bubble pair synchronisation. Rather, as discussed in Chapter 4, this can be achieved by calculating a mean 'coalescence rate' (a/t_c). [As noted previously (Section 4.6), this is completely different from the film thinning rate dh/dt quoted in the literature.] It is used in this work solely as a means of normalising the coalescence time in relation to the contact area between two bubbles, as this changes significantly with increasing gas flow rate.

Figure 5.1(d) shows that the mean coalescence rate (a/t_c) remains essentially constant until gas flow rates exceed 20 mlmin^{-1} (t_b ~ 90ms), beyond which there is a substantial increase. This suggests that for this system, it is only at gas feed rates beyond 20 mlmin^{-1} that contacting bubbles are squeezed together with sufficiently increased pressure to substantially accelerate the rate at which film thinning occurs (and notwithstanding the increased film area). Prior to this, the influence of gas flow rate appears to be virtually negligible. This is quite interesting as the consistent increase in bubble size with gas flow rate will cause an increase in contact area, which may be expected to slow the rate of film thinning in the absence of (compensating) increased contact pressures. It is the first of several indications

that the rate of film thinning may not be inextricably linked with area of the film between two bubbles.

For air bubbles in water at 10°C (Figures 5.1(a) and (b)), the effect of surface oscillations on the contact mode is considerable, particularly at the lower gas flow rates (greater bubble lifetimes) where bubbles were observed to make up to five renewed contacts before coalescing. Due to the multiple contacts, there are significant differences between the two values measured for the coalescence time and 'coalescence rate'. It was only at the highest flow rate, 50 mlmin^{-1} (t_b ~ 50 ms) that bubbles always coalesced directly following the initial contact. Not unexpectedly, coalescence times measured from first contact are longer and correspondingly, the mean 'coalescence rates' smaller. In addition, for the lower flow rates the coalescence times determined from the final moment of contact are much longer than those measured at 25°C, although values at 10 and 50 mlmin^{-1} (t_b ~ 200 and 50 ms) are virtually the same. Despite the increased coalescence times at 1 and 2 mlmin^{-1} (t_b ~ 1100 and 500 ms), the mean 'coalescence rates' are not significantly smaller than comparable values at 25°C, due largely to the increased contact areas observed at 10°C (for Q_g = 1 mlmin^{-1}, 0.58mm^2 compared to 0.13mm^2 at 25°C).

At the highest temperature, 50°C, multiple contacts arising from surface oscillations are only generally observed at the lowest flow rate, although for flow rates of both 1 and 2 mlmin^{-1}, there are significant differences between the two coalescence time values recorded (Figure 5.1(e)). As at 25°C, there is a general increase in coalescence times with increasing air flow rate, up to air flow rate of 10 mlmin^{-1} (t_b ~ 200 ms). Coalescence rates, when measured from the final contact, show a small decrease as the gas flow rate increases from 1 to 2 mlmin^{-1} (bubble lifetimes decrease from ~ 900 to 600 ms), although values calculated at flow rates of 2 mlmin^{-1} (t_b ~ 600) and 10 mlmin^{-1} (t_b ~ 200 ms) are similar. As the gas flow rate increases to 50 mlmin^{-1} (t_b ~ 50 ms) coalescence rates increase significantly. With the exception of the values calculated for the highest flow rate, coalescence rates are essentially the same as at 25°C. This is quite surprising, considering that a primary consequence of increasing the temperature is to alter the liquid viscosity, which many of the film thinning models (see Chapter 2) predict should impact significantly on the rate of drainage.

Following the experiments with air and water, bubbles of hydrogen and xenon were contacted in water, over a range of gas flow rates (1 – 50 mlmin^{-1}, t_b ~ 1200 – 50 ms^{-1}), at a temperature of 25°C. The results of these experiments are shown in Figure 5.2, which once again shows the mean values for coalescence times, coalescence rates and number of contacts as functions of the bubble lifetime.

It is readily observed that the greatest difference between the two sets of experiments is in the number of contacts prior to coalescence. Once again, these are caused by surface oscillations and are observed to be much more frequent in hydrogen–water than in xenon-water systems. As a consequence, in the hydrogen-water systems there is a significant difference between the two values measured for the coalescence times, except for those obtained at the highest flow rate where once again, coalescence was observed to occur directly following the initial contact. Coalescence times measured from the final contact remain essentially constant with

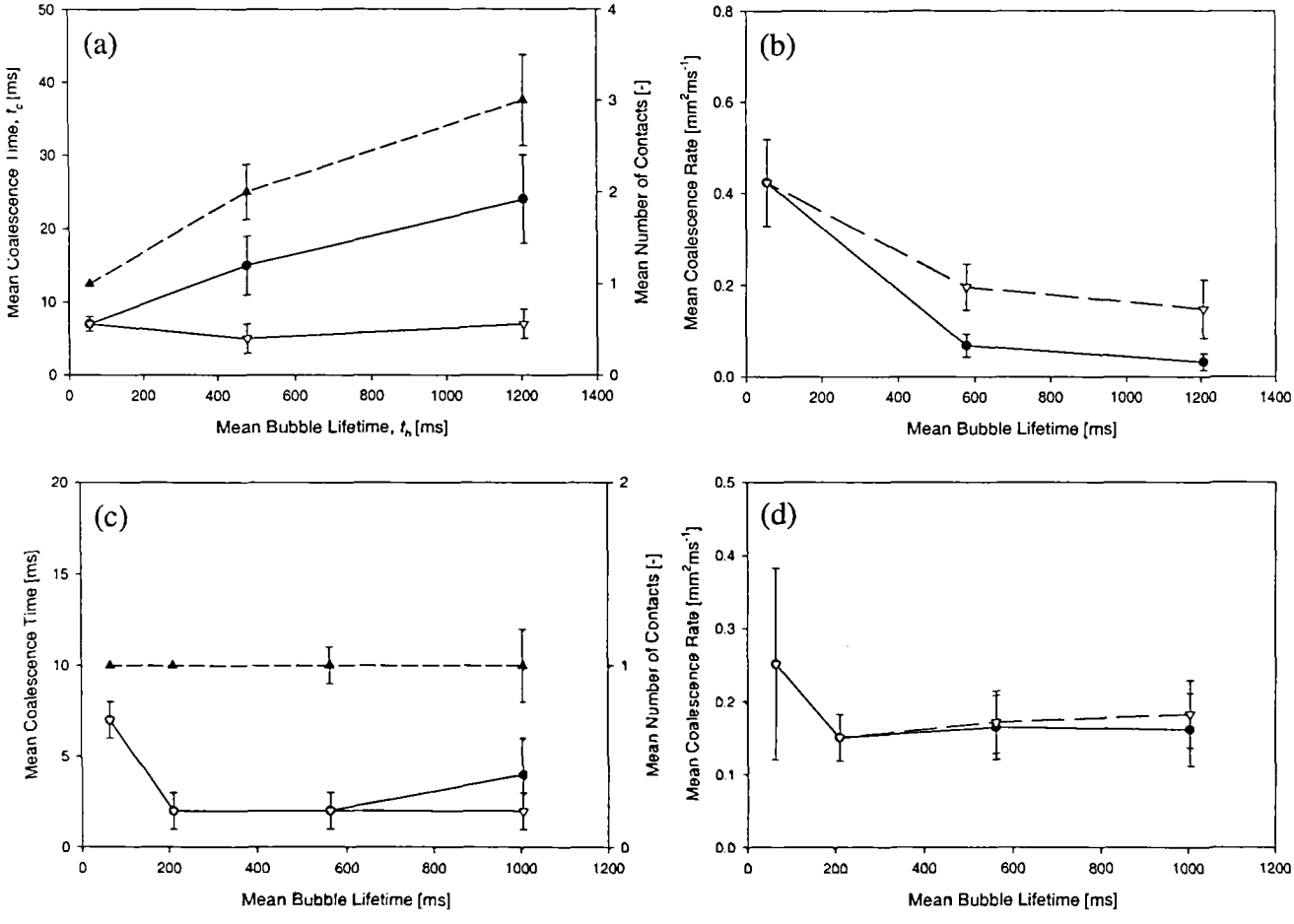

Figure 5.2

Mean coalescence times and coalescence rates for (a), (c) hydrogen and water and (b), (d) xenon and water, with error bars giving 95% confidence levels. For (a), (c) —●— coalescence time from initial contact, —▽— coalescence time from last contact and —▲· number of contacts. For (b), (d) —●— thinning rate from initial contact and —▽· thinning rate from last contact.

increasing gas flow rate, although there is a significant increase in the rate of film drainage and hence the coalescence rates measured at the highest gas flow rate (50 $mlmin^{-1}$, $t_b \sim 50$ ms) due to the much larger contact areas measured (2.73 mm^2 compared to 0.52 mm^2 at Q_g = 1 $mlmin^{-1}$). In contrast, bubbles of xenon in water were almost always observed to coalesce following the initial contact; the absence of pronounced surface oscillations was noticeable, with the bubbles appearing much more rigid and less prone to oscillations even during the very slow growth at the lowest gas flows. The coalescence times in the xenon-water system show a similar behaviour to the air-water system at 25°C, with no change over the lower gas flow rates and then a significant increase in coalescence time at 50 $mlmin^{-1}$. Coalescence rates follow the same trend, with mean values slightly higher than those measured for air-water.

5.1.2 Propan-1-ol

Experiments with propan-1-ol were carried out with air at two different gas flow rates, 10 and 50 $mlmin^{-1}$ and at two different temperatures (10°C and 25°C, see Table 5.2 for values of viscosity and surface tension at these temperatures). Due to the much lower surface tension, the bubbles formed in propan-1-ol tended to be much smaller than equivalent bubbles in water, such that at flow rates below 10 $mlmin^{-1}$ no contact was made between bubbles in a synchronous pair, even at the smallest nozzle distance used in this work (4 mm). For those flow rates at which bubble pairs were sufficiently large enough to contact, systems were 100% coalescing. Once again, this suggests the absence of surface-active impurities in the system and confirms the efficacy of the cleaning used in this study. Results for the mean coalescence times and coalescence rates are presented in Table 5.3 where they are compared to those for water under similar conditions (taking only the time from final contact to film rupture).

	T = 10°C	T = 25°C
Surface Tension [mNm^{-1}]	24.48	23.32
Viscosity [mPas]	2.92	1.19

Table 5.2

Effect of temperature on bulk properties of propan-1-ol. Data from 'Handbook of Chemistry and Physics', 74th Edition, 1993, Lide, D. R., Ed., except for viscosity for Propan-1-ol at 10°C, taken from 'The Data Book of the Viscosity of Liquids', 1989, Viswanath and Narajan.

Q (mlmin^{-1})	Parameter	Propan-1-ol		Water	
		$T = 10°C$	$T = 25°C$	$T = 10°C$	$T = 25°C$
10	$\bar{t}_c$ [ms]	14 (±2)	5 (±0.4)	6 (±1)	4 (±1)
	$\bar{a}/t_c$ [mm^{2}ms^{-1}]	0.082 (±0.013)	0.128 (±0.016)	0.165 (±0.066)	0.105 (±0.022)
50	$\bar{t}_c$ [ms]	13 (±0.05)	9 (±1)	10 (±1)	10 (±2)
	$\bar{a}/t_c$ [mm^{2}ms^{-1}]	0.304 (±0.012)	0.355 (±0.024)	0.325 (±0.023)	0.317 (±0.051)

Table 5.3

Mean coalescence times and coalescence rates for air bubbles in propan-1-ol and water at temperatures of 10°C and 25°C. Values in parentheses represent the 95% confidence limits.

No pronounced surface oscillations were observed for the air-propan-1-ol system, even at the lower temperature of 10°C. This is most likely due to the much higher gas flow rates required to produce bubbles large enough to contact as the bubble pair formed. (Recall that oscillations were also not observed in water at these higher gas flow rates). At 10°C, there is virtually no difference between the mean coalescence times measured at the two flow rates and for both flow rates, the times are considerably longer than equivalent values measured at 25°C. At the higher temperature, however, coalescence times measured at gas flow rate 50 mlmin^{-1} are almost twice as long as those measured at 10 mlmin^{-1}.

Once differences in the film areas are accounted for however, the effect of temperature is much less dramatic than the effect of gas flow rate. Coalescence rates calculated at gas flow rates of 50 mlmin^{-1} are over three times faster than those at 10 mlmin^{-1}, presumably due to the higher contact pressures which act to accelerate coalescence at 50 mlmin^{-1}. Values are slightly smaller at 10°C than at 25°C, although given the large changes in liquid viscosity between these two temperatures, this is not unexpected.

When compared to values measured under equivalent conditions in air-water systems, the only significant difference in values is seen at 10°C, Q_g = 10 mlmin^{-1}, where coalescence times are twice as long in air-propan-1-ol than in air-water. Considering that models predicted for film thinning all show the rate of film thinning to be inversely proportional to viscosity this is not unexpected, as the viscosity of propan-1-ol at 10°C is over twice as large as that of water at the same temperature. At 25°C, the difference in viscosity is much reduced

such that effects of contact pressure (due the higher gas flow rates) are the predominant influence on coalescence.

5.1.3 Discussion

Surprisingly, coalescence time measurements for bubbles in water are not widely reported in the literature, perhaps as a result of the limited practical applicability. Oolman and Blanch (1986), following Chesters and Hoffman (1982), state that 'total film-thinning times for pure liquids are predicted to be on the order of 10^{-2} to 10^{-3} seconds', although this was based on the entirely theoretical considerations of parallel-sided films between freely moving surfaces. Farooq (1972), reports experimentally measured rest times (i.e. the time a bubble remained 'resting' at a free surface prior to coalescence) of < 30 ms for air bubbles (D_b = 1 mm) approaching the air-water interface. Experimental data for coalescence times of nitrogen bubbles in water are also reported by Sagert and Quinn (1986, 1978); for an average of 10 – 15 bubbles (r_b ~ 1.4 mm) mean times of 1.5 ± 0.5 ms and 0.8 ± 0.3ms, with the data generally within two standard deviations of the mean. Interestingly, studies on the coalescence of liquid drops usually report that rest times (equivalent to the coalescence times measured in this study) for a drop coalescing with a flat interface are not constant, even under identical conditions, although reproducible distribution curves are obtained, provided sufficient drops are studied (Hodgson and Lee (1969), Lawson (1967), Charles and Mason (1960b)).

Thus, this study appears to be unique in its close scrutiny of the coalescence process of gas bubbles in pure systems, under a wide range of conditions. As mentioned previously, surface age considerations should be irrelevant in pure systems, such that the primary influences on the coalescence times and rates of film thinning will be liquid properties such as surface tension and viscosity, system properties such as temperature and as the gas flow rate increases, changing contact pressures, times and film areas.

Mean coalescence times measured at 25°C for air-water systems compare reasonably well with the literature values up to gas flow rates of 10 $mlmin^{-1}$, especially when measured from the final contact time. At gas flow rates in excess of 10 $mlmin^{-1}$, coalescence times are observed to be much longer than those reported by Sagert and Quinn (1978, 1976a), although this is most probably due to the increase in contact area that accompanies the increase in bubble size with increasing gas flow rate. However, the spread of data in the majority of cases is much wider than the ± 25 % quoted by Sagert and Quinn (1978, 1976a). Once

coalescence times have been adjusted for the different contact areas between bubble pairs, the coalescence rate remains approximately constant for gas flow rates 1 – 10 mlmin^{-1}, although there is a pronounced increase at the highest feed rate, Q_g = 50 mlmin^{-1}. As a consequence of the increased bubble volumes at higher gas flow rates, the contact area between two bubbles increases because the constraining nozzle geometry increases the degree of deformation as they are forced together. The nozzle geometry also increases the contact pressure between the bubbles, which may be reasonably expected to result in the shorter coalescence rates observed.

How do the measured values for the coalescence times compare to predictions based on theoretical considerations? Chesters and Hofman (1982) suggest that for bubbles in pure liquids, an approximate coalescence time can be given by:

$$t_c = \frac{r^2 \rho v}{\sigma} \qquad (2.11)$$

In Table 5.4, comparisons are made between the predicted coalescence times calculated using Equation 2.11 and the values measured from the high speed video studies for air-water at 25°C, over a flow rate range from 1 to 50 mlmin^{-1}. Coalescence times are those measured from the final contact. For flow rates up to 20 mlmin^{-1}, correlation between the predicted and measured values are extremely good, especially when it is recalled that the prediction is

Flow Rate, Q_g [mlmin^{-1}]	Bubble Radius, r_b [mm]	Relative Velocity, V [ms^{-1}]	Density, ρ [kgm^{-3}]	Surface Tension, σ [mNm^{-1}]	Predicted Coalescence Time, t_c [ms]	Mean Coalescence Time, $\bar{t}_c$ [ms]
1	1.6	0.015	998	71.97	0.5	1.2 ± 0.2
2	1.8	0.025	998	71.97	1.1	1.4 ± 0.3
6	1.9	0.039	998	71.97	2.0	2.0 ± 0.5
10	2.3	0.055	998	71.97	4.0	3.9 ± 1.2
20	2.4	0.116	998	71.97	9.3	9.0 ± 1.4
30	2.5	0.144	998	71.97	12.5	8.2 ± 1.7
40	3.0	0.225	998	71.97	28.1	5.3 ± 0.7
50	3.5	0.282	998	71.97	47.9	10.0 ± 1.6

Table 5.4

Comparison between predicted (calculated using Equation 2.11) and measured mean coalescence times (from final contact, with 95% confidence levels shown) for water at 25°C. Data for bubble radii and relative velocities obtained from high-speed video (2000 s^{-1}) and represent the mean of 5 measurements.

considered to give an approximate measure only. However, for flow rates in excess of 20 $mlmin^{-1}$, the correlation between the two sets of values is much less satisfactory. This is also the range of flow rates at which a substantial increase in the coalescence rate is observed (Figure 5.1 (d)), which suggests that at these gas flow rates the effects of contact pressure on the rate of film thinning become significant, hence leading to the much shorter than predicted coalescence times observed. At the highest gas flow measured, coalescence times are reduced to virtually 20 % of the predicted value as a consequence of the increased contact pressure.

The oscillation of gas bubbles during free rise is a well known characteristic of dynamic systems and has been extensively studied (Pandit, 1992). Despite this knowledge, none of the studies using visual observation to monitor coalescence, have described the surface oscillations that are seen in this work to constitute an important aspect of the contact process, especially at low flow rates. It was considered that surface oscillations would be greatest in systems with the lowest surface tensions (such as in propan-1-ol or water at 50°C) as this provides a measure of the resistance of a bubble to deformation. In practice, surface oscillations were not observed for bubbles in propan-1-ol, as at the high flow rates required to produce bubbles sufficiently large enough to contact, the rate of bubble growth far exceeds any independent movement of the surface which may arise. Significant amount of oscillation were observed for bubbles in water at 50°C (especially at Q_g = 1 $mlmin^{-1}$, where on average, bubbles contacted twice before coalescence occurred). However, by the far the greatest number of renewed contacts is seen for water at 10°C and for hydrogen-water systems. This is unexpected given that the surface tension of water at 10°C is greater than at 50°C and consequently bubbles would be expected to be more resistant to deformation.

What is the effect of gas on the coalescence behaviour observed in water? Although, it was not possible to measure the surface tension for these systems, it could be envisaged that the surface tension values would not be vastly different from those measured for air-water systems under comparable conditions. The surface tension at a gas-liquid interface is a measure of the strength of inter-molecular interactions within the liquid (alternatively, it can be viewed as a measure of the miscibility between the liquid and the gas). Although rigorously calculated from the free energies of both phases, the contribution of the gas phase is often ignored due to its low density (Vold and Vold, 1983, Hirschfelder et al., 1964) and consequently surface tension values tend to be dominated by the liquid component. The inter-molecular hydrogen bonds formed in water are extremely strong, such that the cohesive

attractions between water molecules will tend to be much greater in magnitude than the weaker dispersion forces which may form between water and gas molecules. However, Moore (1972) suggests that the 'significant solubility' of hydrogen in water (1.5 $mgkg^{-1}$ in water at 25°C) is due to "some form of specific interaction is occurring between the dissolved H_2 molecules and the liquid water structure" and speculatively proposes the possible formation of a weak H_2 bridge between two water molecules. If a significant degree of interaction does exist between hydrogen and water molecules, this could be expected to reduce the surface tension of the system and thereby the resistance of the bubbles to deformation, allowing for the increase in surface oscillations, which have been observed. In the absence of similar interactions between xenon and water, the surface tension would be considerably higher and correspondingly, the bubbles more rigid.

However, although possible reductions in surface tension may explain the large number of surface oscillations observed in hydrogen-water systems, they cannot explain why similar oscillations are so prevalent in air-water at 10°C. The increase in surface tension of water with decreasing temperature would suggest that bubbles formed in water at lower temperatures would be expected to be more rigid and less prone to oscillations, although these could be expected to be significant at 50°C. At the higher temperature, surface oscillations resulted in a number of multiple contacts for bubbles formed at gas flow rate of 1 $mlmin^{-1}$, although this was not the case at gas flow rate of 2 $mlmin^{-1}$. It appears that temperature may therefore exert influences on bubble behaviour beyond the considerations of surface tension and viscosity and which ultimately affect the nature of the bubble-bubble contacts.

5.2 Electrolyte Solutions

It is well known that in the majority of electrolyte solutions, coalescence repression occurs beyond a certain critical electrolyte concentration, as demonstrated by numerous authors (Lessard and Zieminksi, 1971, Zahradnik et al., 1998, 1995, 1987, Craig et al., 1993). However, although this appears as a well-defined step change over a small concentration range in the coalescence cell, in process systems such as agitated vessels, a more gradual change is observed (Lee and Hodgson, 1970, Calderbank, 1958). As part of this study, it was of interest to determine whether the cell could be used to generate more detailed information about the behaviour of bubble coalescence in the dynamic environment of a stirred tank or bubble column, by manipulating the conditions under which bubbles are contacted. In these

systems bubbles are likely to experience a wide variety of hydrodynamic conditions, depending on their location. The effects of surface age, for example, whilst less relevant far from the gas distributor (the bubbles having had sufficient time for the gas-liquid interfaces to have reach equilibrium) could be considered important in the zones directly adjacent to the sparger, where the bubble density is high and contacts between newly formed (and still forming) bubbles are numerous. Indeed, in Chapter 7 of this study and in the literature (Marrucci and Nicodemo, 1967), it is seen that by far the greatest amount of coalescence occurs in the zone adjacent to the gas distributor. Several authors have reported the existence of large vortices in agitated vessels (Martin, 1996), wherein entrained bubbles may be held in close proximity for extended lengths of time and in addition, subject to substantial compressive forces.

Clearly the present lack of understanding of the complete factors influencing coalescence in dynamic systems prevents accurate reproduction of conditions which may be encountered in free flow systems. However, by contacting bubbles formed over a range of gas flow rates (from 1 to 75 $mlmin^{-1}$) and over a range of nozzle spacings (4, 6 and 8 mm), factors which may be considered relevant, such as surface age, contact force and contact areas can be investigated and the influences clarified. Literature studies show different degrees of coalescence repression can be correlated well with electrolyte valency (Lessard and Zieminski, 1971, Zahradnik et al., 1998, 1987), i.e. the value of the 'transition' concentration between coalescence and non-coalescence decreases with increasing electrolyte valency. The three electrolytes chosen as the test species for the principal experiments covered a range of valence combinations; sodium sulfate, Na_2SO_4, magnesium sulfate, $MgSO_4$ and potassium iodide, KI. All data was analysed using the second definition proposed for coalescence frequency as presented in Chapter 4; i.e. coalescing events as a percentage of all contacting pairs, irrespective of the angle of contact.

5.2.1 Effects of Concentration

In Figure 5.3 the results of experiments designed to replicate those of Zahradnik et al. (1987), (Chapter 2) are shown. For these experiments the nozzle distance was set at 4 mm and a low air flow rate of ~ 1 $mlmin^{-1}$ ($f_b \sim 0.75\ s^{-1}$) was chosen. As reported in the literature, there is a distinct step change in the coalescence frequency on increasing solute concentration for each of the electrolytes. The results agree broadly with findings reported in the literature, although the 'transition' concentration value obtained for sodium sulfate in this work (0.03 M) is

significantly lower than the value quoted by Zahradnik et al. (1987, 1995 and 1999a), (0.06 M). A similar trend to that first reported by Lessard and Zieminski (1971) can be observed, with the value of the transition concentration decreasing with increasing electrolyte valency; hence $c_{trans}(KI) > c_{trans}(Na_2SO_4) > c_{trans}(MgSO_4)$.

As discussed in Chapter 4, the transition from full coalescence to coalescence repression is accompanied by a shift from fully synchronised to non-synchronous bubbling. In addition, the bubbles which form at higher electrolyte concentrations are visibly more rigid and much more resistant to the stress of continued contact than those generated in pure liquids or in solutions with concentrations below the 'transition' value. As a consequence of the increased bubble rigidity, bubbles are often observed to slip over one another, such that despite prolonged contact times (often in excess of the mean coalescence time measured for the system), no coalescence occurs.

It is not obvious why the value of the 'transition' concentration for sodium sulfate measured in this work, is approximately half that reported in previous studies (0.051 M Lessard and Zieminski (1971), 0.06 M Zahradnik et al. (1987, 1998)). Initial considerations lead to a series of experiments being carried out with solutions prepared from three different purified water sources (double distilled, ion-exchange and ion-exchange followed by reverse osmosis) and with two grades of sodium sulfate (BDH AnalaR (99.9%) and General Purpose Grade(99.5%)). However, the step change in coalescence frequency was observed to occur at

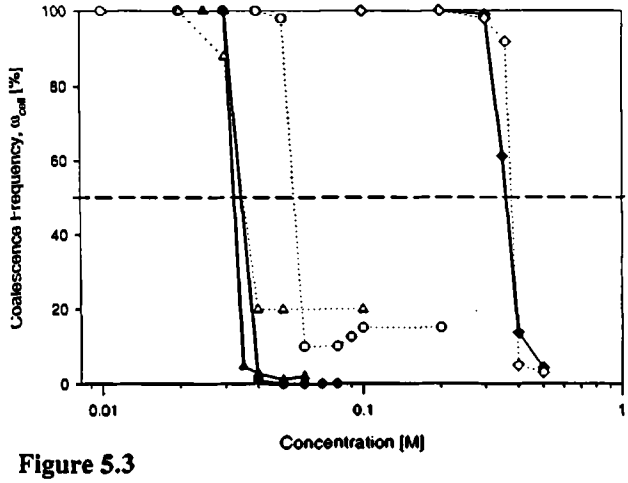

Figure 5.3

Comparing the coalescence frequencies for electrolyte solutions obtained in this study with those of Zahradnik et al., 1987. —●— Na_2SO_4, (this work, Q = 45 mlmin-1), ···○··· Na_2SO_4 (Zahradnik et al., 1987), —▲— $MgSO_4$ (this work), ···△··· $MgSO_4$ (Zahradnik et al., 1987), —◆— KI (this work), ···◇··· KI (Zahradnik et al., 1987).

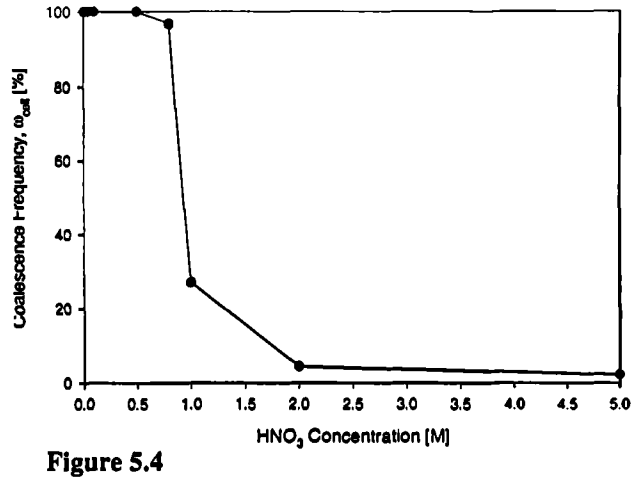

Figure 5.4

Coalescence frequencies for HNO_3, showing a step change in coalescence frequency at solution concentration ~ 0.9 M.

the same solution concentration (0.035 M) in all cases. Additional experiments, where the polypropylene nozzle inserts were removed to more closely mimic the experimental set-up used by Zahradnik et al. (1998, 1995, 1987) allowing bubbles to form directly at the stainless steel nozzles also gave a 'transition' concentration of 0.035 M Na_2SO_4. In contrast, when used in a bubble column, the same solutions demonstrated repressed coalescence at concentrations similar to the 'transition' value obtained by Zahradnik et al. (1998, 1995, 1987).

Craig et al. (1993), demonstrated that the 'transition' concentration did not exist for all electrolytes, an observation attributed to the very low values for $d\sigma/dc$ values of the 'non-transition' species, such as the mineral acids H_2SO_4, HCl and HBr, as well as electrolyte species such as CH_3COONa, CH_3COONH_4, $NaClO_4$ (Christenson and Yaminsky, 1995). However, although many of the species which were deemed to be fully coalescing were combinations of 1:1 electrolytes, the maximum concentration investigated was limited to 0.5 M, which may be considered to be on the low side, considering literature observations of high transition concentrations for other 1:1 species (e.g. 0.3 M for KI quoted by Lessard and Zieminski, 1971). As a consequence, experiments were carried out in nitric acid (HNO_3), one of the 'non-transition' species listed by Craig et al. (1993), over a much wider concentration range (0.005 to 5 M), using a gas flow rate of 1 $mlmin^{-1}$, (f_b 0.75 s^{-1}). The results are shown in Figure 5.4, wherein it can be seen that at a concentration of ~ 0.9 M there is a distinct step change in coalescence frequency. Similar experiments were attempted with solutions of sulfuric acid (H_2SO_4, another 'non-transition' species) but were abandoned at concentrations above 0.5 M due to reaction between the liquid and the stainless steel frame of the cell.

Although it is not possible to derive firm conclusions from this single experiment, the results do suggest that further work is required at concentrations above those tested by Craig et al., 1993 for those species considered to be without a 'transition' concentration. The 'transition' observed for HNO_3 is especially interesting as Christenson and Yaminsy (1995), (also Pashley and Craig, 1997) note that coalescence repression is not observed for solutes with values of $(d\sigma/dc)^2$ below ~ 1 $(mNm^{-1}M^{-1})^2$. In that work, the value quoted for $(d\sigma/dc)^2_{HNO3}$ is 0.6, well below the limiting value, which suggests that for species with $(d\sigma/dc)^2$ of similar magnitude a 'transition' concentration should exist. Craig et al. (1993) note no transition for solutions of

HCl up to concentration of 1.0 M, however the $(d\sigma/dc)^2$ value is much lower (0.1 $(mNm^{-1}M^{-1})^2$).

5.2.2 Effect of Flow on Coalescence Behaviour

The experimental results shown thus far were obtained using parameters designed to mimic the experiments of Zahradnik et al. (1998, 1995, 1987). However, the conditions represented by these parameters represent only a limited number of those which might reasonably be expected to exist in collisions between bubbles in free flow. In this section, the results of experiments carried out with much higher gas flow rates (up to 75 $mlmin^{-1}$, corresponding to bubble frequencies of ~ 23 s^{-1}) are reported. In each case the nozzle separation distance was maintained at a constant 4 mm. A small number of studies reported in the literature have reported using a variety of gas feed rates, although the bubble frequency is in all cases quite small, with a maximum of 5 s^{-1} reported by Drogaris and Weilland (1983). Adjusting the gas flow rate through the nozzles results in a number of changes to the conditions under which bubbles are formed and contacted; these are summarised in Table 5.5. As there is undoubtedly a significant degree of interplay between these effects, a series of experiments were carried out using different nozzle separations, in an attempt to separate counteracting effects; these results are presented in the Section 5.2.3.

Figures 5.5, 5.6 and 5.7 show the effects of gas flow rate on the 'transition' concentration for each of the three principal electrolytes investigated. As can be seen, the general effect of

LOW FLOW RATE	⟶	*HIGH FLOW RATE*
Slow surface expansion	⟶	Fast rate of surface expansion
Diffusion unlimited	⟶	Diffusion limited
Low bubble frequency (long contact time)	⟶	High bubble frequency (short contact time)
Small effect of contact pressure	⟶	Contact pressure significant (for face-to-face contacts)
Small bubbles (minimal deformation on contact, small area for drainage)	⟶	Larger bubbles (significant deformation on contact, increased area for film drainage)

Table 5.5

Effects of gas flow rate on condition in the coalescence cell that may be considered to affect the contact and coalescence behaviour of bubbles.

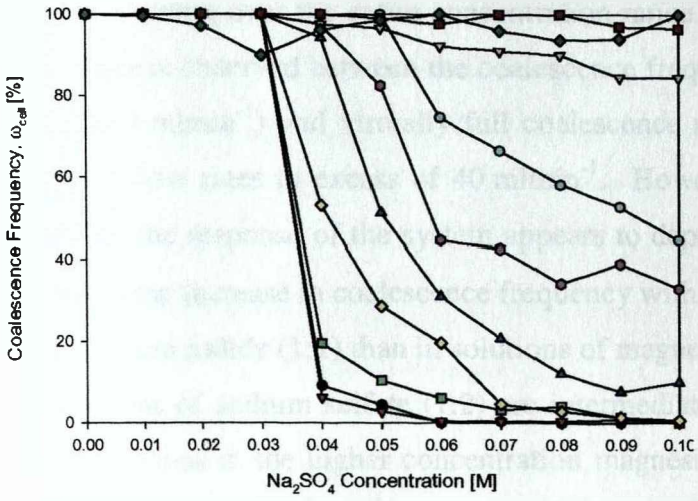

Figure 5.5

The effect of air flow rate on coalescence frequency for solutions of sodium sulfate. Q_g = 1 mlmin^{-1}, Q_g = 2 mlmin^{-1}, Q_g = 4 mlmin^{-1}, Q_g = 6 mlmin^{-1}, Q_g = 8 mlmin^{-1}, Q_g = 10 mlmin^{-1}, Q_g = 16 mlmin^{-1}, Q_g = 25 mlmin^{-1}, Q_g = 50 mlmin^{-1} and Q_g = 75 mlmin^{-1}

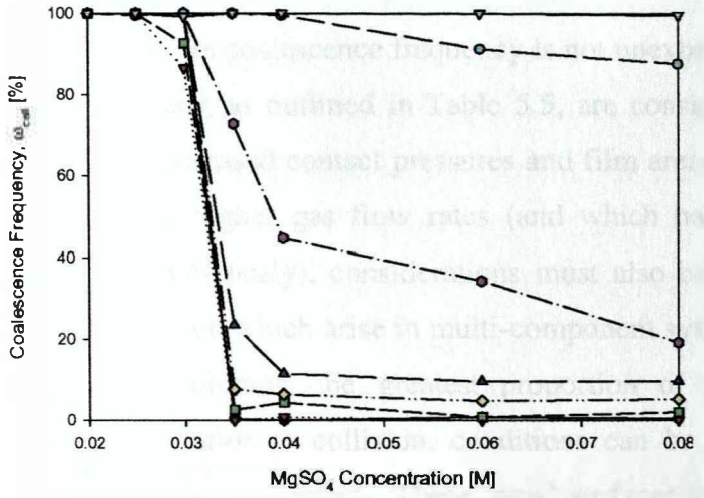

Figure 5.6

The effect of air flow rate on coalescence frequency for solutions of magnesium sulfate. Q_g = 1 mlmin^{-1}, Q_g = 2 mlmin^{-1}, Q_g = 6 mlmin^{-1}, Q_g =10 mlmin^{-1}, Q_g = 15 mlmin^{-1}, Q_g = 20 mlmin^{-1}, Q_g = 40 mlmin^{-1} and Q_g = 60 mlmin^{-1}.

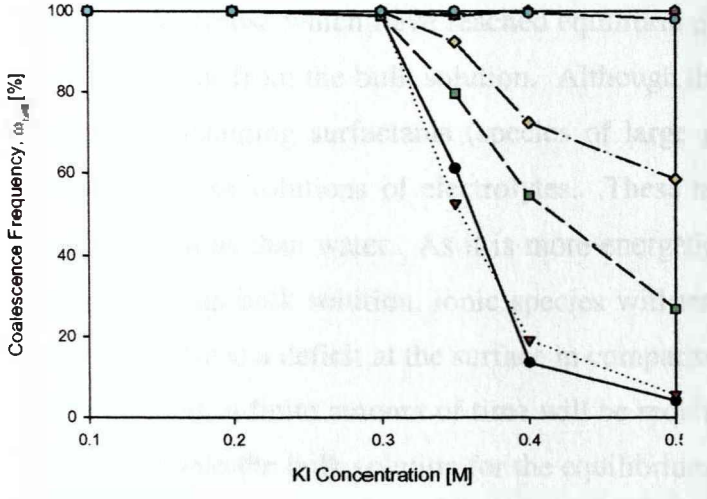

Figure 5.7

The effect of air flow rate on coalescence frequency for solutions of potassium iodide. Q_g = 1 mlmin^{-1}, Q_g = 2 mlmin^{-1}, Q_g = 6 mlmin^{-1}, Q_g =10 mlmin^{-1}, Q_g = 20 mlmin^{-1}, Q_g = 40 mlmin^{-1} and Q_g = 60 mlmin^{-1}.

increasing the gas flow rate is to increase the coalescence frequency observed in initially coalescence repressed solutions, to the extent that at above a specific flow rate, solutions are fully coalescing over the entire concentration range. For all three test electrolytes, very little difference is observed between the coalescence frequencies measured at the lowest flow rates (~1 and 2 $mlmin^{-1}$) and virtually full coalescence is observed over the entire concentration range at flow rates in excess of 40 $mlmin^{-1}$. However, at the gas flow rates between these extremes the response of the system appears to depend on valency of the electrolyte species, such that the increase in coalescence frequency with flow rate is greater and faster in solutions of potassium iodide (1:1) than in solutions of magnesium sulfate (2:2); whilst values observed in solutions of sodium sulfate (1:2) are intermediate. This is most clearly seen in the delay period obvious at the higher concentration magnesium sulfate solutions, where much higher gas flow rates (> 20 $mlmin^{-1}$) are required to increase the coalescence frequency significantly.

The increase in coalescence frequency is not unexpected when the consequences of increasing gas feed rates, as outlined in Table 5.5, are considered. In addition to the (counteracting) effects of increased contact pressures and film areas that arise from the larger bubbles which form at the higher gas flow rates (and which hold equally well in for the pure systems discussed previously), considerations must also be made of the effects of surface age and solute diffusion which arise in multi-component systems. Although in free rise systems, such as bubble columns, the greatest proportion of gas-liquid interfaces will have reached equilibrium prior to collision, conditions can be envisaged when newly formed (or still forming) surfaces contact. These 'new' surfaces formed through the rapid expansion of the gas-liquid interface will not initially display the same surface tension characteristics as much 'older' ones (those which have reached equilibrium), as a consequence of the need for solute to diffuse to or from the bulk solution. Although this phenomena is most readily observed in solutions containing surfactants (species of large molecular weight), similar considerations should apply to solutions of electrolytes. These tend to exhibit slightly higher equilibrium surface tensions than water. As it is more energetically favourable for charged species to be solvated in the bulk solution, ionic species will tend to desorb from the air-water interface, such that there is a deficit at the surface in comparison to the bulk concentration. When a new surface forms, a finite amount of time will be required before sufficient ions can diffuse from the surface into the bulk solution for the equilibrium surface tension value to be attained. This phenomenon is known as the dynamic surface tension and is demonstrated in Figure 5.8 for solutions of sodium sulfate.

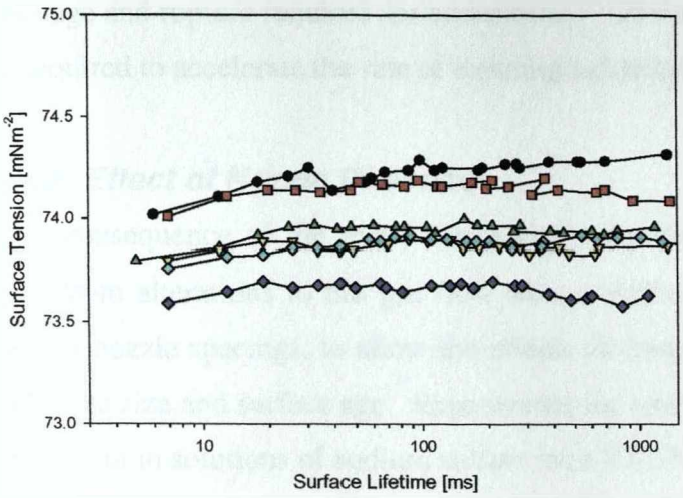

Figure 5.8

Dynamic surface tension profiles measured for solutions of sodium sulfate at concentrations ●— 0.02 M, ■— 0.03 M, ▲— 0.04 M, ▽— 0.05 M, ◆— 0.06 M and ◇— 0.08 M using Lauda Maximum Bubble Pressure meter, MPT 1

In Figure 5.8 the surface tension is shown as a function of a range of surface lifetimes comparable to those investigated in the coalescence cell (based on the mean bubble lifetime at the point of bubble pair contact, determined from the high-speed video studies). There is no consistent increase with concentration for the profiles obtained in the various solutions, as might be expected, presumably an experimental artefact. In each case however, there is an initial increase in the surface tension (until the surface age is approximately 11 ms), although this is extremely small. Indeed each profile could be reasonably approximated by a straight line and this, together with the fact that at a gas flow rate of 50 mlmin^{-1}, the mean surface age is ~50 ms at the point of contact, suggests that any effects of surface age in these electrolyte solutions can be ignored in this work.

In the absence of pronounced changes in surface tension at the rapidly expanding gas-liquid interfaces, such as produced at gas flow rates above ~ 50 mlmin^{-1}, the influence of gas flow rate reduces to considerations of contact pressures and areas as observed for pure liquids. However, differences in coalescence behaviour between the three electrolyte systems, must arise from considerations of surface phenomena. Once again, the concept of surface elasticity ($E \propto [d\sigma/dc]^2$) seems appropriate in that this determines the ability of a film to adjust its surface tension in an instant of stress and hence restore resistance to mechanical disturbances (Adamson, 1990). Literature $d\sigma/dc$ values for the three electrolytes investigated in this work are: $d\sigma/dc(Na_2SO_4) = 2.96$, $d\sigma/dc(MgSO_4) = 2.24$ (both from Weisssenborn and Pugh, 1995) and $d\sigma/dc(KI) = 1.3$ (Jarvis and Scheiman, 1968). As a consequence, the elasticity of surfaces formed in either Na_2SO_4 or $MgSO_4$ solutions will be greater than that for surfaces formed in KI solutions of comparable concentration, leading to earlier suppression of the rapid film

drainage and rupture required for coalescence. Obviously, a greater contact pressure will then be required to accelerate the rate of thinning sufficiently to force coalescence in such systems.

5.2.3 Effect of Nozzle Distance

As a consequence of the many interacting influences on the coalescence behaviour which arise from alterations to the gas flow rate, a number of experiments were carried out over various nozzle spacings, to allow the effects of contact force to be separated from the effects of bubble size and surface age. Experiments for which the nozzle separation was altered were carried out in solutions of sodium sulfate from 0.02 M to 0.1 M over a flow rate range of 10 to 75 mlmin^{-1}. Results are shown in Figure 5.9 for nozzle settings of (a) 4 mm, (b) 6 mm and (c) 8 mm.

At a nozzle separation of 4 mm, full coalescence is observed at gas flow rates of 50 mlmin^{-1} for all concentrations and even at Q_g = 25 mlmin^{-1}, systems are definitely coalescence dominated. As the gap between the nozzles is increased to 6 mm, there is a decrease in the coalescence frequency measured at a given gas flow rate for all solution concentrations in excess of the 'transition' value with the drop in ω_{cell} increasing with solution concentration. In addition, the system that was fully coalescing at a nozzle separation of 4 mm (i.e. 0.02 M), exhibited a slightly reduced coalescence frequency at the lowest gas flow rate (10 mlmin^{-1}), largely due to the small bubble diameters which just allow bubbles to contact over the increased gap width. As the air flow rate and hence the bubble size increases, full coalescence is restored in this solution. For the larger nozzle distance, full coalescence in all solutions is only achieved at the highest flow rate, 75 mlmin^{-1}. As the nozzles are moved farther apart to 8 mm, there is no longer contact between the bubbles at the lowest gas flow rate, (10 mlmin^{-1}) and over the whole range there is a sharp decrease in the coalescence frequencies compared to those measured with the previous geometries. Once again there is a decrease in the values measured in previously fully coalescent solutions (0.02 M), at the lowest flow rate for which the bubbles contact, although full coalescence is restored at gas flow rates in excess of 50 mlmin^{-1}. Coalescence frequencies appear to form two groups; for solutions below or close to the 'transition' concentration full coalescence is essentially achieved the highest gas flow, whereas for solution concentrations in excess of the 'transition' values, the measured coalescence frequencies are much lower and gas flow rates in excess of 75 mlmin^{-1} are required to force the systems to exhibit full coalescence.

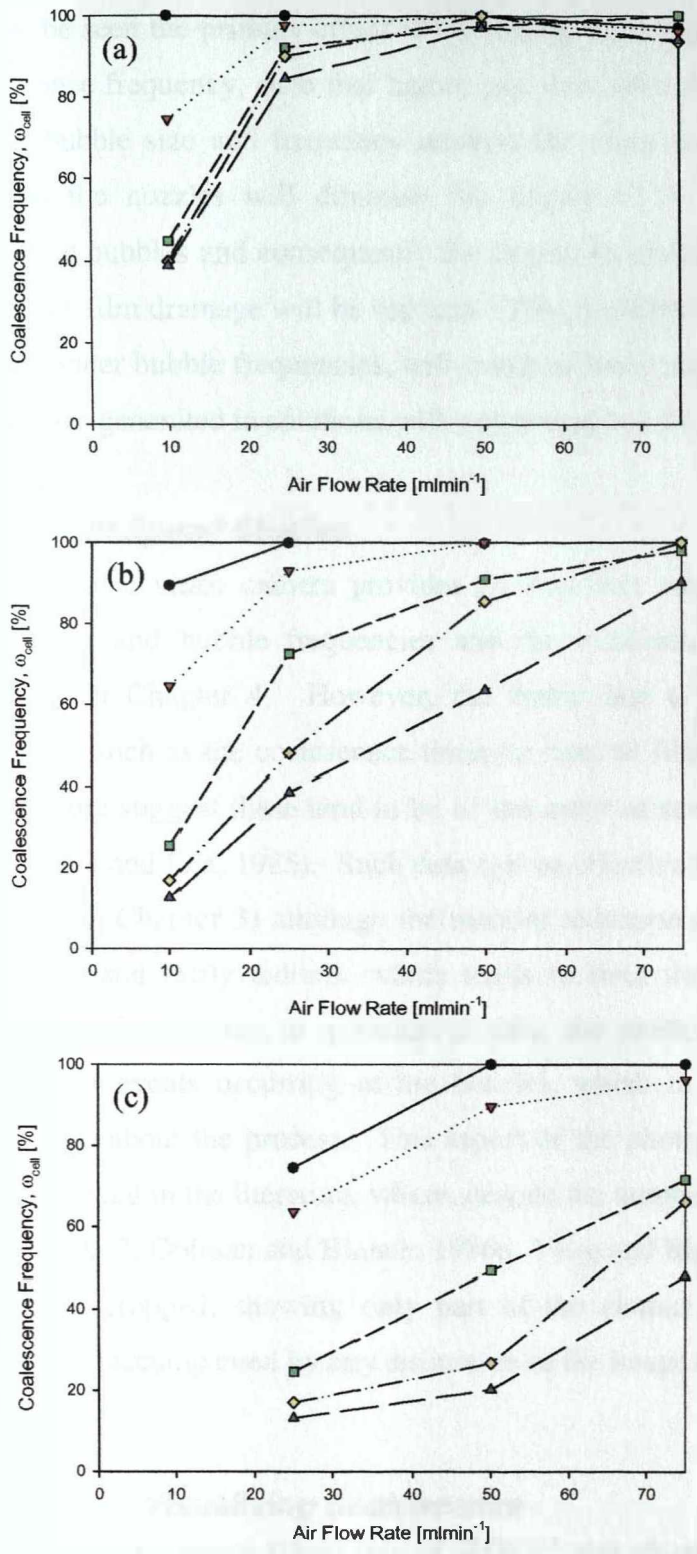

Figure 5.9

Effect of nozzle separation on coalescence frequency for flow rates from 10 to 75 mlmin^{-1}. (a) nozzle separation 4 mm, (b) nozzle separation 6 mm and (c) nozzle separation 8 mm. For all, ●— 0.02 M, ▼··· 0.04 M, ■— 0.06 M, ◇-·- 0.08 M and ▲-- 0.1 M.

As can be seen the primary effect of increasing the nozzle separation is to delay the increase in coalescence frequency, such that higher gas flow rates are required to achieve full coalescence. As the bubble size and frequency remains the same for a given flow rate, the increased gap between the nozzles will diminish the degree of deformation (and contact area) for two contacting bubbles and consequently the degree to which they are forced together. As a result, the rate of film drainage will be reduced. This, combined with the reduced contact times caused by the greater bubble frequencies, will result in fewer numbers of coalescence events, especially for bubbles generated in solutions with concentrations well beyond the 'transition' value.

5.2.4 High Speed Studies

The Panasonic video camera provides an excellent means for determining bulk data such as coalescence and bubble frequencies and the existence of macro-scale bubbling patterns, as discussed in Chapter 4. However, the frame rate of 50 s^{-1} is insufficiently fast to enable parameters such as the coalescence times or rates of film thinning to be measured, as studies in the literature suggest these tend to be of the order of several milliseconds (Oolman and Blanch, 1986a, Cain and Lee, 1985). Such data can be effectively monitored using high speed video, (as described in Chapter 3) although the manual reduction of the data following collection is time consuming and fairly tedious, which tends to limit the volume of data that can be amassed efficiently. In addition to quantitative data, the method also provides an additional level of scrutiny for events occurring at the nozzles, which in itself provides valuable, if qualitative information about the process. This aspect of the photographic approach appears to have been largely ignored in the literature, where, despite the number of studies, (Ueyama, et al., 1993, Kim and Lee, 1987, Oolman and Blanch, 1986a, Yang and Maa, 1984), the pictures presented tend to be heavily cropped, showing only part of the contact region between two bubbles and are generally unaccompanied by any discussion of the images observed.

5.2.4.1 Visualising Coalescence

In this study, a camera frame rate of 2000 s^{-1} was chosen as this offered the best compromise between frame speed and picture quality. At this speed, it was possible to view the first two steps of the coalescence process (as defined by Oolman and Blanch, 1986a), namely approach, contact and subsequent thinning of the film. However, it was not possible to capture the moment at

which the intervening film ruptured; this obviously occurs on a very small time scale (additional experiments with a camera of frame rate of 43000 s^{-1} also failed to allow this step to be visualised). As a consequence of the frame rate, the fastest coalescence time which could be measured was 0.5 ms (i.e. a difference of one frame was required between the moment of contact and film rupture). Although several events were recorded for air-water systems with coalescence times of 0.5 ms, only a very small number of events (~ 5 out of 550 events measured, i.e. < 1 %) were observed where there was less than one frame between contact and film rupture. In these cases, the coalescence time was recorded as 0.5 ms. For bubbles in solutions of electrolytes, the fastest times measured were of the order of 2 – 3 ms, such that there was usually a minimum of four frames between first contact and the frame before rupture.

Figure 5.10 shows a typical sequence of events for air bubbles coalescing in water at two different flow rates, (a) Q_g = ~ 2 $mlmin^{-1}$ and (b) Q_g = 50 $mlmin^{-1}$. The formation of bubbles at low gas flows is not a steady process; the nascent bubbles were seen to pulse at the nozzle opening until the pressure in the feed lines has increased sufficiently to allow further growth; at flow rates of ~ 1$mlmin^{-1}$, this could take up to ~ 1200 ms. After this initial pulsing, the bubble growth proceeded fairly steadily, until the point of contact was made. At higher flow rates there was no similar delay in the bubble formation, although as the bubbles approach one another, a flattening of the opposing surfaces is often observed prior to contact. Barring pronounced surface oscillations (which are a notable feature of hydrogen bubbles in water and air bubbles in water at 10°C), bubbles were always observed to coalesce very quickly after the initial contact, although at the higher flow rates, the two surfaces were observed to contact for slightly longer periods of time, perhaps as a result of the increased contact areas. Determining the exact moment of rupture was difficult, not only because of the insufficiently rapid camera frame rate, but also because two bubbles were often pressed together for some time prior to coalescence occurring; this was especially the case at high gas flow rates. The moment of film rupture is most clearly seen as a subtle but distinct change in the light reflecting from the contact area, as highlighted in Figure 5.10(a) and (b). Following the rupture of the intervening film, the newly coalesced bubble is seen to undergo considerable flexing and distortion until it obtains its final shape. This flexing and distortion is accompanied by a strange ripple or annular wave that moves rapidly away from the

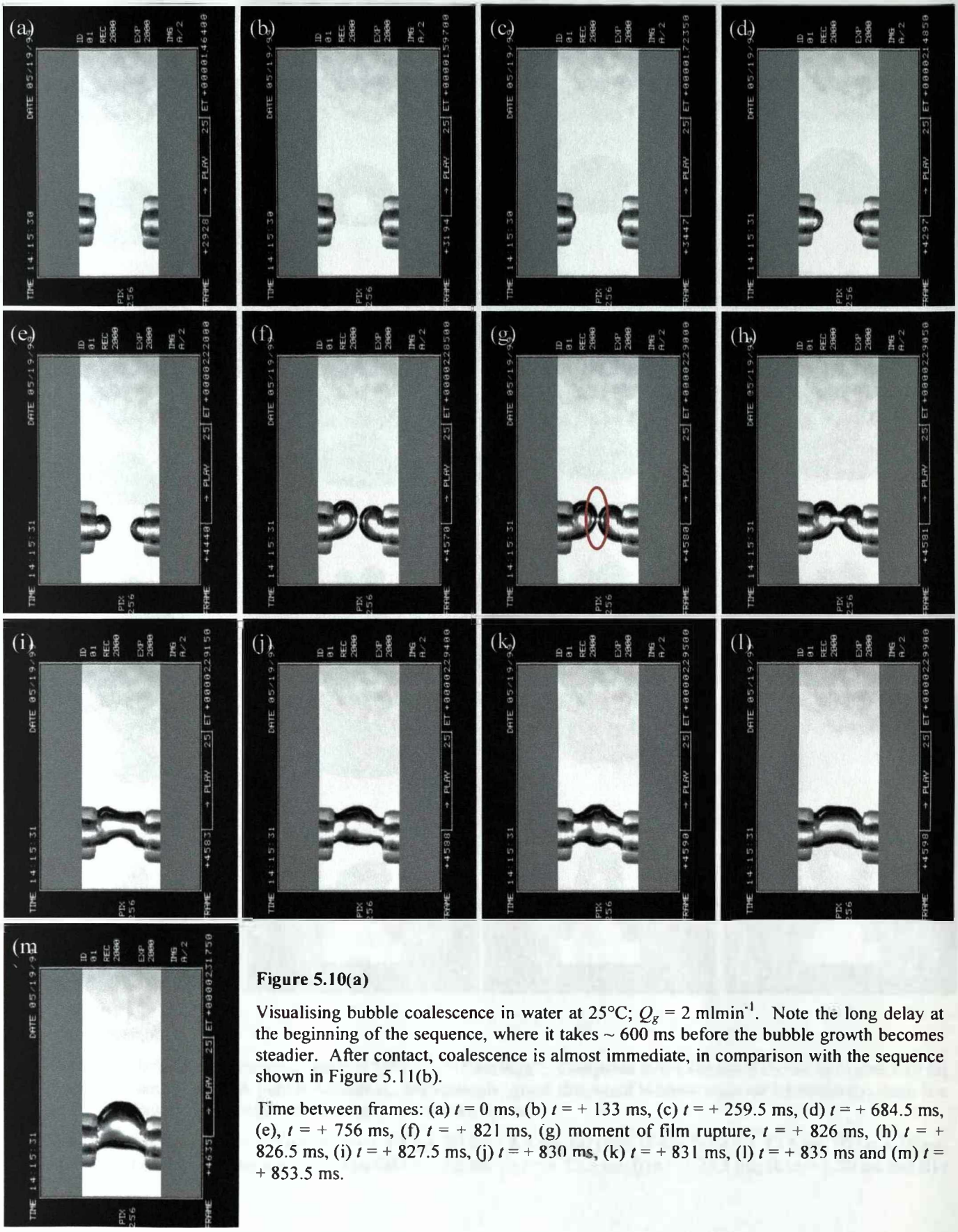

Figure 5.10(a)

Visualising bubble coalescence in water at 25°C; Q_g = 2 mlmin^{-1}. Note the long delay at the beginning of the sequence, where it takes ~ 600 ms before the bubble growth becomes steadier. After contact, coalescence is almost immediate, in comparison with the sequence shown in Figure 5.11(b).

Time between frames: (a) t = 0 ms, (b) t = + 133 ms, (c) t = + 259.5 ms, (d) t = + 684.5 ms, (e), t = + 756 ms, (f) t = + 821 ms, (g) moment of film rupture, t = + 826 ms, (h) t = + 826.5 ms, (i) t = + 827.5 ms, (j) t = + 830 ms, (k) t = + 831 ms, (l) t = + 835 ms and (m) t = + 853.5 ms.

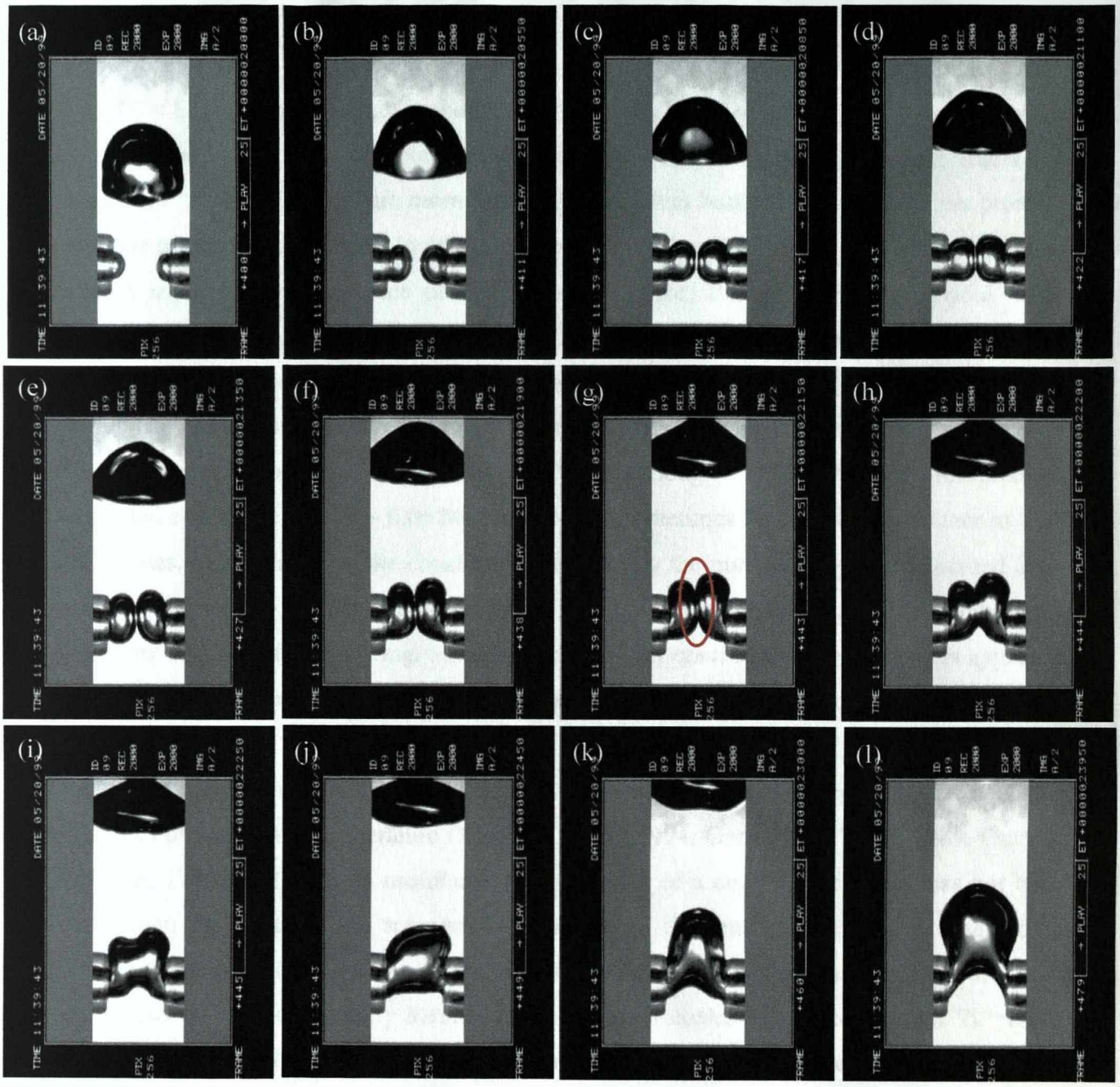

Figure 5.10(b)

Visualising bubble coalescence in water at 25°C; Q_g = 50 mlmin^{-1}. Compared to the sequence shown in Figure 5.10 (a) there is no similar delay in bubble formation. Interestingly, given that small bubbles coalesce immediately, there is a prolonged contact between the two bubbles prior to coalescence.

Time between frames: (a) t = 0 ms, (b) t = + 5.5 ms, (c) t = + 8.5 ms, (d) t = + 11 ms, (e), t = + 13.5 ms, (f) t = + 19 ms, (g) moment of film rupture, t = + 21.5 ms, (h) t = + 22 ms, (i) t = + 22.5 ms, (j) t = + 24.5 ms, (k) t = + 30 ms and (l) t = + 39.5 ms.

site of film rupture towards either end of the newly formed bubble, at which point it changes direction and returns towards the centre.

In Figure 5.11 a similar sequence of events is shown for the coalescence of air bubbles in (a) 0.02 M, ($C < C_{trans}$, Q_g = 10 mlmin^{-1}) and (b) 0.06 M ($C > C_{trans}$, Q_g = 10 mlmin^{-1}) sodium sulfate solution. Observations show that bubbles in electrolyte solution, especially at concentrations in excess of the 'transition' value, are more rigid than equivalent bubbles in water and less prone to oscillations prior to coalescence. In addition, the prolonged contact times between two bubbles indicate a much greater resistance of the surface to stress; this is especially obvious when coalescence does not follow contact and the two bubbles slide over one another, detach from the nozzles and rise independently (Figure 4.4). Following the point of rupture, the amount of distortion as the newly coalesced bubble obtains its final shape is also much reduced in comparison to those observed in air-water systems, although still present. In solutions of concentrated electrolyte (above ~ 0.06 M), bubbles can sometimes be observed to bounce at high gas flow rates, although due to the constraints provided by the nozzles, they are prevented from moving away from one another as may happen in free flow. If the bubbles are sufficiently large, they will not separate after bouncing, although directly after contact, the bubble centres appear to move in the opposite direction until impeded by the presence of the nozzle extensions.

The annular wave which immediately follows coalescence can be seen in many of the photographs presented in the literature (Tsao and Koch, 1994, Garrett and Ward, 1989, Oolman and Blanch, 1986a) although its usefulness as a indicator of a coalescence event, has not been reported upon previously. The remarkable similarity of this phenomena to that observed in pictures obtained in dynamic gas-liquid dispersions (Tse et al., 1998, Martin, 1996) enables these in-situ events to be unequivocally identified as images of coalescence (see Chapter 7). From images such as those illustrated in Figures 5.12 and 5.13, it is possible to determine the speed at which this annular wave is moving. In Figures 5.12 and 5.13, the ripple moves at a velocity of ~ 2.5 ms^{-1}. In Figure 5.12(e), after the moment of film rupture, the annular wave can be clearly seen advancing from the point of rupture. Between the lower image in Figure 5.12(e) and the upper in Figure 5.12(f), the time elapsed is 0.5 ms and the annular wave has moved a distance of approximately 1.2 mm, i.e. at a speed of 2.4 ms^{-1}. A similar value can be obtained from Figure

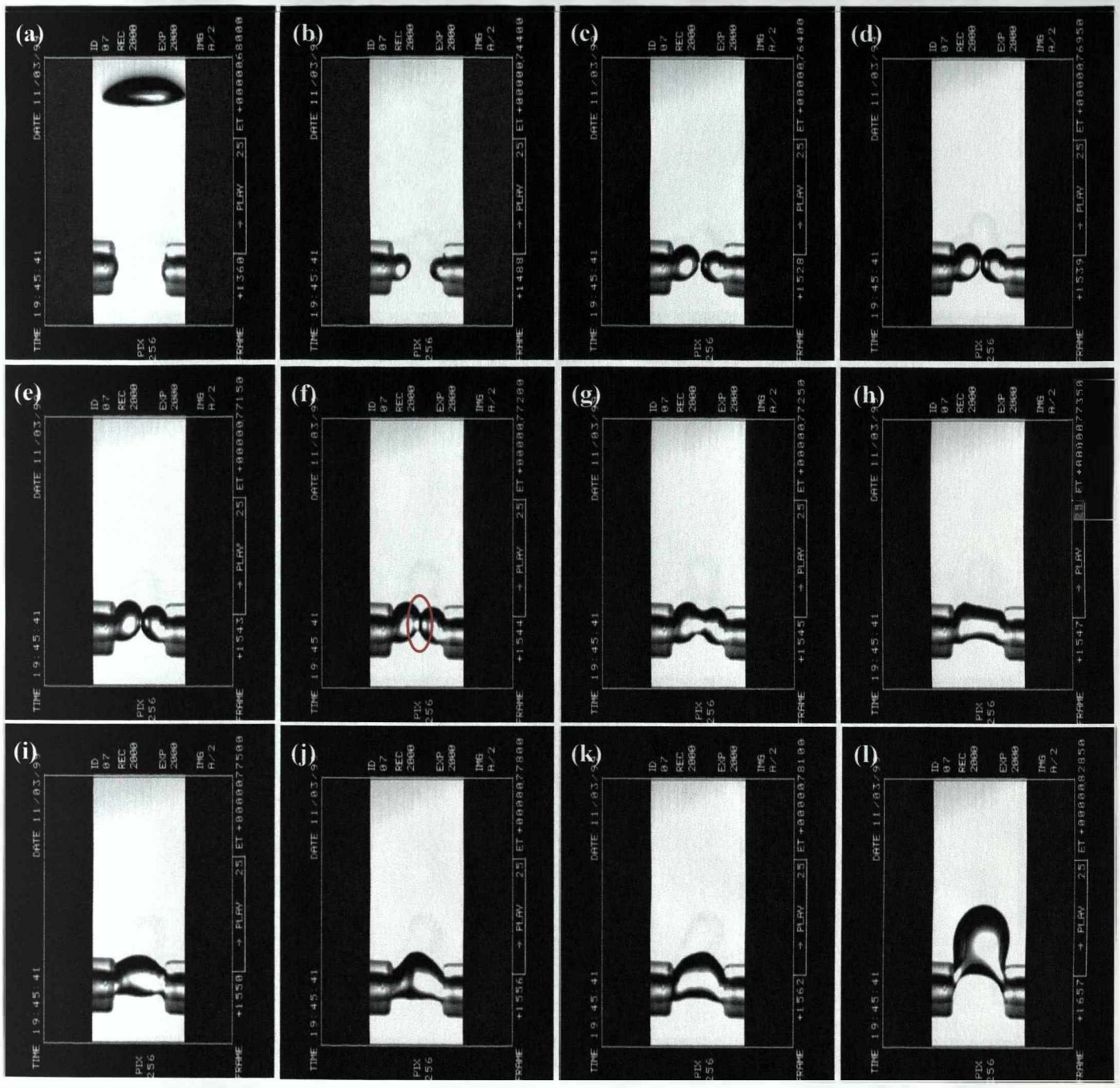

Figure 5.11(a)

A coalescence event in 0.02 M Na_2SO_4 solution at 25°C, Q_g = 10 mlmin^{-1}, nozzle separation 4 mm. Even at this low concentration, the amount of flexing and distortion following the moment of film rupture is much smaller than that observed in water. Presumably, this occurs because the presence of electrolyte species increases the resistance of the gas-liquid interface to deformation.

Time between frames: (a) t = 0 ms, (b) t = + 64 ms, (c) t = + 84 ms, (d) t = + 89.5 ms, (e), t = + 91.5 ms, (f) moment of film rupture, t = + 92 ms, (g) t = + 92.5 ms, (h) t = + 93.5 ms, (i) t = + 95 ms, (j) t = + 98 ms, (k) t = + 101 ms and (l) t = + 148.5 ms.

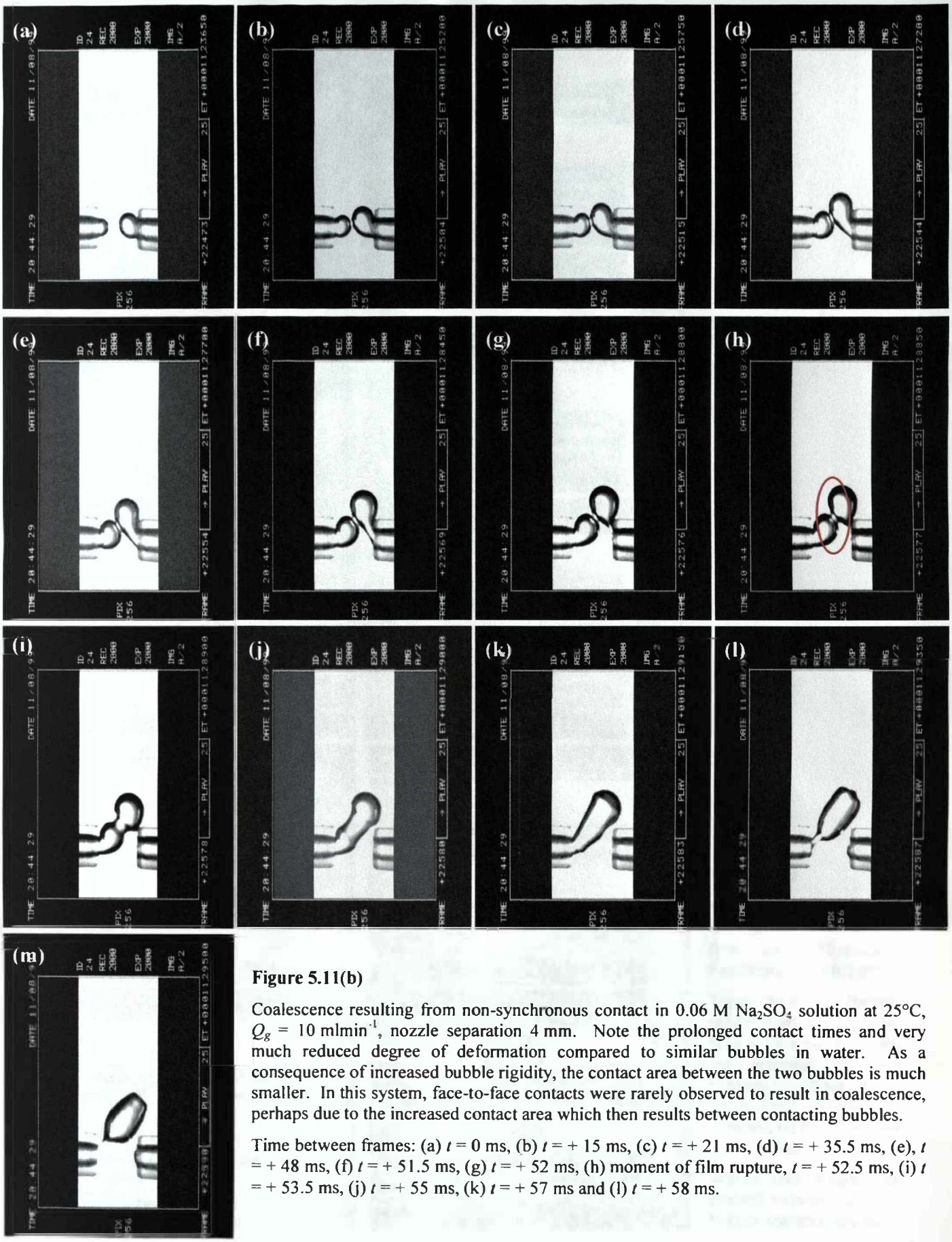

Figure 5.11(b)

Coalescence resulting from non-synchronous contact in 0.06 M Na_2SO_4 solution at 25°C, Q_g = 10 mlmin^{-1}, nozzle separation 4 mm. Note the prolonged contact times and very much reduced degree of deformation compared to similar bubbles in water. As a consequence of increased bubble rigidity, the contact area between the two bubbles is much smaller. In this system, face-to-face contacts were rarely observed to result in coalescence, perhaps due to the increased contact area which then results between contacting bubbles.

Time between frames: (a) t = 0 ms, (b) t = + 15 ms, (c) t = + 21 ms, (d) t = + 35.5 ms, (e), t = + 48 ms, (f) t = + 51.5 ms, (g) t = + 52 ms, (h) moment of film rupture, t = + 52.5 ms, (i) t = + 53.5 ms, (j) t = + 55 ms, (k) t = + 57 ms and (l) t = + 58 ms.

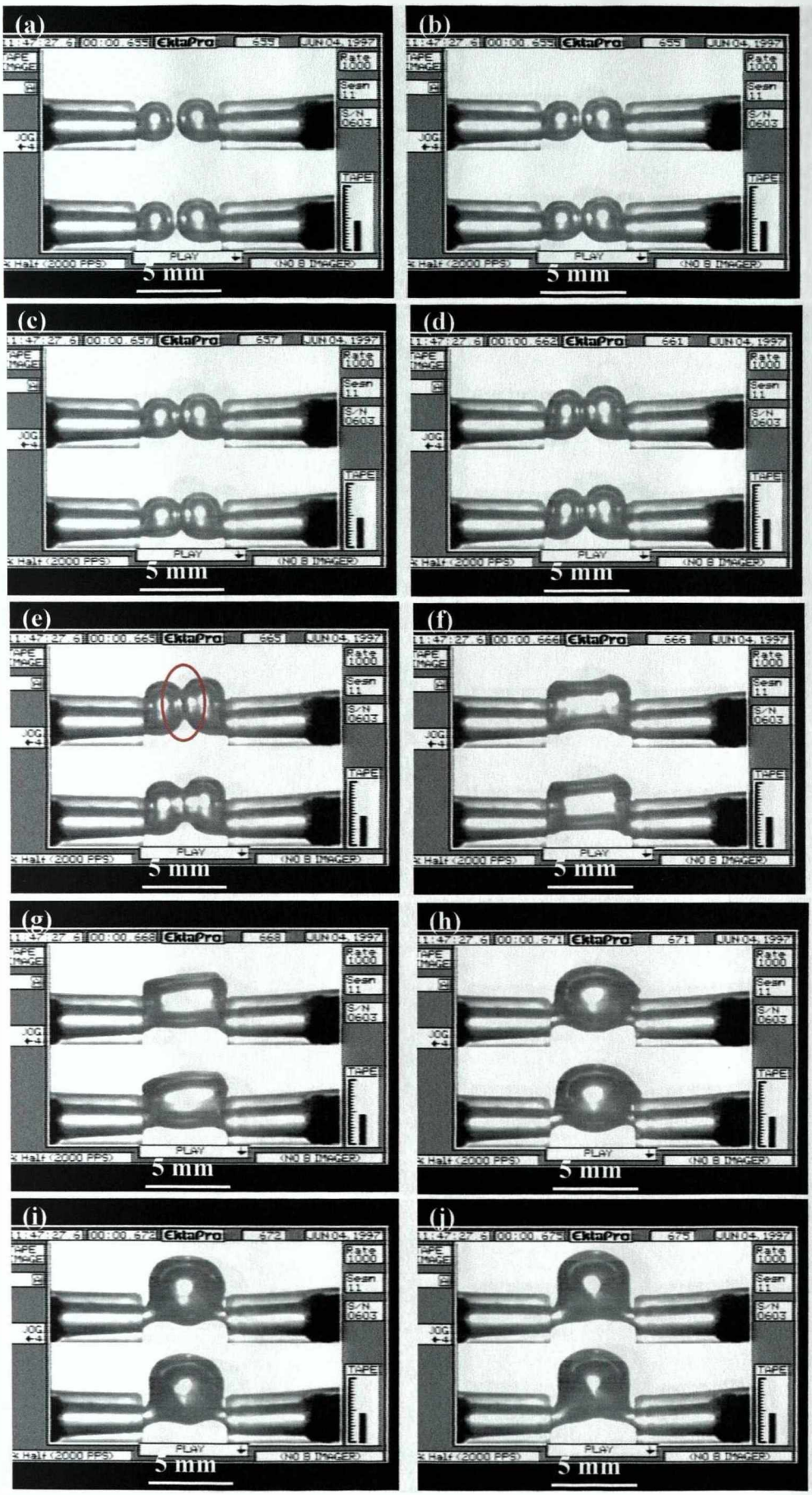

Figure 5.12

Visualising bubble coalescence in water. Air flow rate 50 mlmin^{-1}. Nozzle separation 5 mm.

Time between frames: (a) t = 0 ms, (b) t = 1 ms, (c) t = 2 ms, (d) t = 6 ms, (e) moment of film rupture, t = 10 ms, (f) t = 11 ms, (g) t = 13 ms, (h) t = 16 ms, (i) t = 17 ms and (j) t = 20 ms.

Within each image time elapsed between top and bottom frames is 0.5 ms.

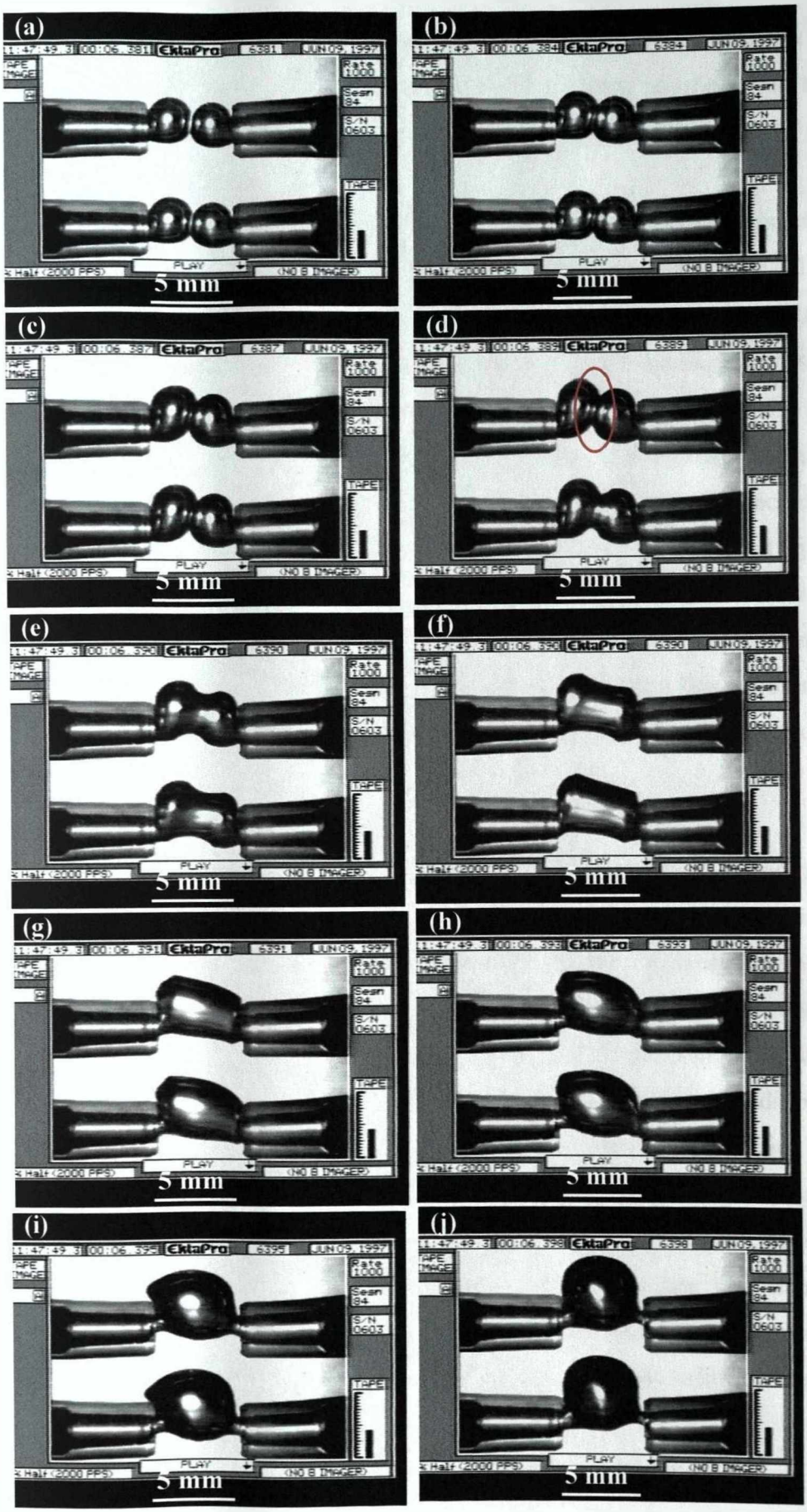

Figure 5.13

Visualising bubble coalescence in 0.08 M sodium sulfate solution. Air flow rate 50 $mlmin^{-1}$. Nozzle separation 5 mm.

Time between frames: (a) t = 0 ms, (b) t = 3 ms, (c) t = 6 ms, (d) moment of film rupture, t = 8 ms, (e) t = 9 ms, (f) t = 10 ms, (g) t = 11 ms, (h) t = 12 ms, (i) t = 14 ms and (j) t = 17 ms.

Within each image time elapsed between top and bottom frames is 0.5 ms.

5.13 where following the moment of film rupture (Figure 5.13(d)) the annular wave can be calculated to have moved approximately ~ 1.15 mm between the lower image in Figure 5.13(d) and the upper in Figure 5.13(e), a time of 0.05 ms, giving a velocity of 2.3 ms^{-1}.

There appears to be little difference between the velocity of the annular wave measured in water and that measured in electrolyte solution of various concentrations. This is not particularly surprising; the primary source of resistance to the progress of the wave arises from viscous drag and for each of these liquids, the viscosity ratio μ_g/μ_l, will be essentially the same (and very small as it is dominated by the viscosity of the liquid phase). MacIntyre (1972) has estimated a similar speed for a 'curious ripple' which moves at a velocity of ~ 2.7 ms^{-1} towards the base of a 1.7 mm diameter bubble breaking through the surface of seawater (coalescence of a bubble with a free interface). The degree of flexing and deformation will be governed by the magnitude of the forces which work to restore the bubble shape, namely the surface tension. However, as there is very little difference between the surface tension values measured over the range of sodium sulfate concentrations, the much reduced degree of distortion that is observed in the most highly concentrated electrolyte solutions may be also be due to an increased surface elasticity.

5.2.4.2 Coalescence Times

Coalescence times have been measured for air bubbles in solutions of sodium sulfate and also for air, hydrogen and xenon bubbles in solutions of magnesium sulfate; results for these latter experiments are presented in section 5.4. For the majority of these systems, when compared with the coalescence behaviour observed in water, the degree of surface oscillation was much reduced and there were no observations of the broken and renewed contacts that were so noticeable previously. Once again, coalescence rates (a/t_c) were calculated in addition to coalescence times, in order to provide a means for accounting for the differences in film area between the contacting bubbles. For coalescence time data in pure systems (and low solute concentrations), it was relatively straightforward to collect 25 measurements; however, as electrolyte solutions become increasingly concentrated and the number of coalescence events reduced, this became progressively more time-consuming. Consequently, a minimum of ten measurements for each data point was obtained. Where no data points are presented, insufficient events were recorded.

The mean coalescence times are shown as a function of the bubble lifetime in Figure 5.14 (a) and mean coalescence rates in Figure 5.14 (b) for solutions of 0.02 to 0.08 M sodium sulfate concentration. For bubbles in 0.02 M sodium sulfate ($C < C_{trans}$) the coalescence times measured remain essentially constant despite the increasing gas flow rate, although the coalescence rates show a steady increase with increasing gas flow rate (corresponding to decreasing bubble lifetimes). Coalescence times increase significantly in 0.03 sodium sulfate solution ($C \sim C_{trans}$) at the lowest gas flow rate ($t_b \sim 1000$ ms). Despite this, coalescence rates in this solution exhibit the same general increase with gas flow rate as seen for 0.02 sodium sulfate. 0.04 M sodium sulfate is beyond the 'transition' concentration as measured in this work and as for 0.03 M solution, the mean coalescence time measured at the lowest gas flow rate is very long ($\bar{t_c} = 47 \pm 27$ ms), although remaining values are not significantly different from those measured in 0.02 M solution. Both solutions at 0.06 M and 0.08 M are in excess of the 'transition' concentration and for each insufficient data was recorded at the lowest gas flow rates for mean values to be shown. However, values for the coalescence times measured over the higher flow rates are comparable with those determined in the lower concentration solutions. When the coalescence rates are considered, those for solutions 0.04 M, 0.06 M and 0.08 M are seen to follow the same general trend as the lower concentration solutions, with a significant increase in coalescence rates as the gas flow rates increase.

The substantial increase in coalescence times and decreased coalescence rates, observed between 0.02 M and 0.03 M solutions for the lowest gas flow rate, is possibly the result of the more rigid, less mobile surfaces (Chesters, 1991) that arise from surface tension gradients, as suggested by Marrucci (1969a) and which would act to slow the rate of film drainage. At the higher gas flow rates the increased contact pressure (arising from the larger bubble sizes) compensates for this reduction in the rate of film drainage, effectively accelerating the coalescence process.

It is generally considered that coalescence occurs in free flow systems when the contact time exceeds the time required for the intervening film to thin to the point of rupture. Consequently, in addition to measuring coalescence times in coalescence repressed solutions, contact times were also determined for at least ten non-coalescence events in each solution. In Figure 5.15 mean coalescence and contact times are shown for concentrations of sodium sulfate from 0.03 to

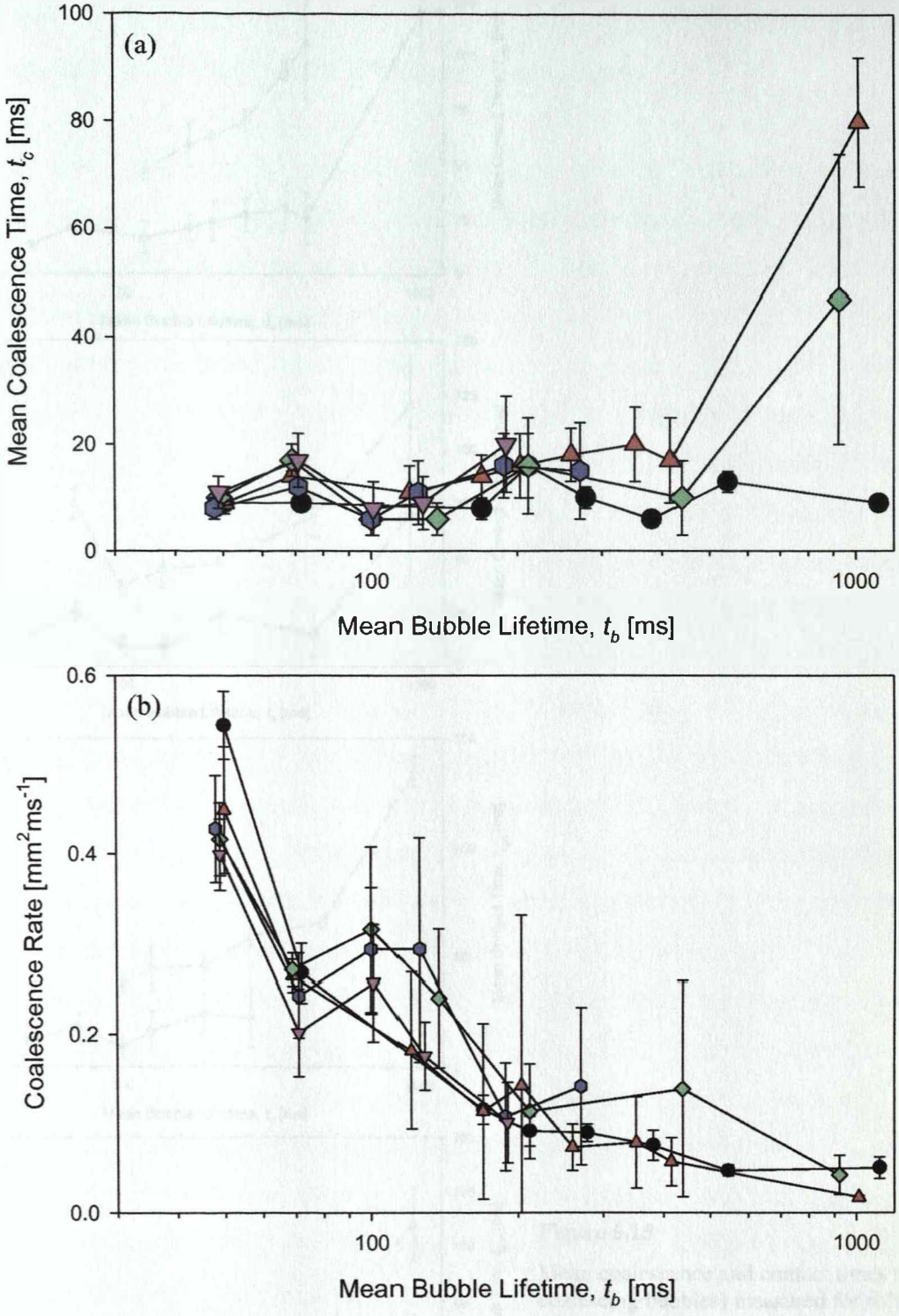

Figure 5.14

(a) Mean coalescence times measured for solutions of sodium sulfate with concentrations ranging from 0.02 M to 0.08 M. (b) Mean film drainage rates calculated for solutions of 0.02 M to 0.08 M sodium sulfate. Symbols for both are: 0.02 M, 0.03 M, 0.04 M, 0.06 M and 0.08 M. For each, error bars represent the 95% confidence intervals.

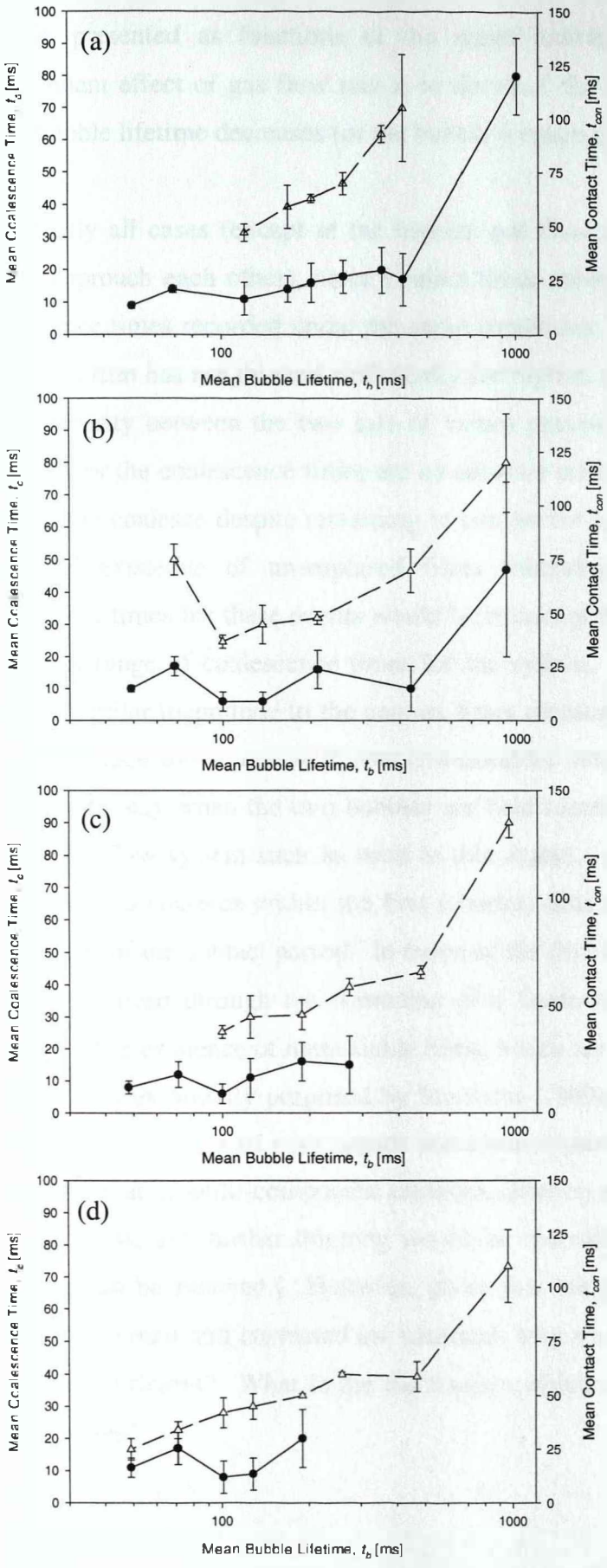

Figure 5.15

Mean coalescence and contact times (for non-coalescing bubbles) measured for solutions of sodium sulfate. Error bars in each represent 95% confidence limits. For all, symbols are: ●— mean coalescence times (n = 25) and —△— mean contact times (n = 10). (a) 0.03 M, (b) 0.04 M, (c) 0.06 M and (d) 0.08 M sodium sulfate.

0.08 M, presented as functions of the mean bubble lifetime. It is clearly seen that the predominant effect of gas flow rate is to decrease the contact time between two bubbles as the mean bubble lifetime decreases (or the bubble frequency increases).

In virtually all cases (except at the highest gas flow rates in 0.08 M solution, where the two values approach each other), mean contact times measured are significantly greater than mean coalescence times recorded under the same conditions. Although it is indisputable that in these events the film has not thinned sufficiently for rupture to occur (hence no coalescence), the very large disparity between the two sets of values provokes many questions. If the mean values recorded for the coalescence times are an accurate reflection of system behaviour, why do some films fail to coalesce despite remaining in contact for such relatively long periods of time? The continued existence of un-ruptured films following such extensive contact implies that coalescence times for these events would be excess of the contact times measured, resulting in a very wide range of coalescence times for the system. In addition, the absence of coalescence times of similar magnitude to the contact times measured suggests two separate populations for the coalescence times; one with low (measurable) values and another with much longer times (measurable only when the two bubbles are held together until coalescence occurs, i.e. not in a continuous flow system such as used in this study). Alternatively, it may suggest that if two bubbles fail to coalesce within the first (shorter) time span, then coalescence will never occur, irrespective of the contact period. In terms of the film thinning mechanism for coalescence, this may be achieved through the formation of a 'meta-stable' film, which is resistant to further thinning. [The existence of meta-stable films, which are resistant to further thinning, is not a new concept. It was initially proposed by Marrucci (1969a) to explain the differences between the coalescence behaviour of pure liquids and electrolyte/surfactant solutions. In that study, it was considered that in multi-component solutions, after an initial rapid thinning to some equilibrium film thickness, any further thinning would be controlled by the rate at which surface tension gradients can be relieved.] However, given that the conditions under which the bubble pairs have been formed and contacted are identical, why should the flow within the intervening film be so very different? What is the mechanism which determines which mode of film thinning predominates?

5.2.4.3 Comparisons with Model Predictions

There are a number of film thinning models proposed in the literature for coalescence between two fluid particles with deformable, immobile interfaces. The difficulty in applying these equations directly is that there is very little information about the degree of immobility conferred on a gas-liquid interface by the presence of electrolytic species in the bulk liquid. Generally surfaces are considered to be immobilised by the presence of small amounts of surfactants (due to the very high surface activity of these species); the comparatively smaller surface activity of electrolyte species suggests that although it may be reasonable to assume surface immobility at the higher electrolyte concentrations, this may not be the case at lower concentrations (particularly those below the 'transition' value). Even for solutions of surfactant species however, the interface may not be completely immobilised. Applying models for partially mobile interfaces is extremely difficult (unless the degree of mobility is inferred from the coalescence time measurements, as in Sagert and Quinn, 1976a) as it is not possible to accurately determine the degree of mobility possessed by a surface.

In addition, for this work the emphasis has been on measuring coalescence times and not rates of film thinning (i.e. change in film thickness with time), which limits the degree of useful comparison which can be drawn between theoretical and measured values. In order to do so, a value for the initial film thickness must be obtained. However, even with the increased resolution provided by the high-speed video camera, it was not possible to measure the thickness of the film at the point of contact, or indeed at any time during the thinning process, with any degree of accuracy. Oolman and Blanch (1986a) encountered a similar problem in their study and suggest a constant value of 10 μm be used as the standard initial film thickness. The same approach has been adopted in this work, merely as a means of allowing comparisons to be made between the predicted rates of film thinning and those measured experimentally.

The expression used to determine the theoretical rate of film thinning is that developed by Chesters (1991) for thinning between deformable, immobile surfaces:

$$-\frac{dh}{dt} \approx \frac{8\pi\sigma^2 h^3}{3\mu r_b^2 F} \qquad (2.40)$$

where the interaction force, F, can be approximated by :

Gas Flow Rate Q_g [mlmin^{-1}]	Mean Bubble Radius r_b [mm]	Mean Film Radius r_f [mm]	Surface Tension σ [mNm^{-1}]	Liquid Viscosity μ [mPas]	Contact Force F*10^4 [N]	Predicted Film Thinning Rate *10^4 [ms^{-1}]	Mean Coalescence Time $\bar{t}_c$ [ms]	'Measured' Film Thinning Rate *10^4 [ms^{-1}]
1	1.5	1.42	73.8	0.894	6.23	0.36	46.9 ± 26.9	2.13
2	1.6	0.36	73.8	0.894	0.38	5.31	10.1 ± 6.7	9.90
64	1.9	0.72	73.8	0.894	1.27	1.12	16.1 ± 5.9	6.21
10	2.1	0.54	73.8	0.894	0.64	1.80	6.0 ± 3.4	16.7
15	2.1	0.64	73.8	0.894	0.90	1.28	6.1 ± 3.1	16.4
25	2.2	0.98	73.8	0.894	2.02	0.52	16.9 ± 3.4	5.92
50	3.4	1.31	73.8	0.894	2.34	0.19	9.8 ± 1.5	10.2

Table 5.6

Comparing predicted (using Chesters (1991) equation) and measured film-thinning rates for coalescence events in 0.04 M sodium sulfate solution. Bubble and film radii and coalescence times represent the mean of not less than 10 events and are measured from high-speed video images. Surface tension data is measured from the Lauda Maximum Bubble Pressure meter and is the equilibrium surface tension value.

$$F \approx \pi r_f^2 (2\sigma / r_b) \qquad (2.41)$$

Application of this expression assumes that the fluid velocity at the gas–liquid interface is zero, due to the presence of sufficient amounts of electrolyte which immobilise the surface. Presumably, it cannot be applied to those systems which are fully coalescing as the rapid rate of thinning necessary for coalescence would suggest the absence of surface tension gradients which act to immobilise the interface. Even for those solutions beyond the 'transition' concentration, where systems are coalescence repressed, the gas-liquid interfaces for coalescence events are possibly more accurately described as partially mobile, although it is not possible to determine the degree of mobility at each event. Despite this, it was decided to apply the model of Chesters (1991) for thinning between two immobile surfaces; this should at least provide a lower bound for the predicted rate of thinning.

Values are compared in Table 5.6, which shows predicted values and then 'measured' film thinning times (calculated using the standard initial film thickness of Oolman and Blanch (1986a) and the mean coalescence times measured from this work). In each case, the thinning times calculated from parameters measured in this work are consistently greater than the values

predicted by Chesters (1991) equation. The consistently faster rates of thinning calculated from experimental measurements may arise for a number of reasons. The model assumes that the bubble-bubble collisions occur under free flow conditions and makes no allowances for situations were contact pressure is increased, such as observed in this work at the higher gas flow rates. As a result, the magnitude of the contact force is most probably greater than predicted. Surprisingly however, the fastest thinning times are not those for bubbles contacted at the highest gas flow rates (25 and 50 $mlmin^{-1}$), but for bubbles coalescing at gas feed rates of 10 and 15 $mlmin^{-1}$. This would suggest that for these gas flow rates, any enhancement of film thinning due to increased contact pressures exceeds the influence of increased contact area. At higher gas flow rates, the effects of increased contact area are more significant and partially offset the increase in thinning due to contact pressure.

However, it is not only the thinning rates at the higher gas flow rates which are much greater than predicted values, as may be expected if the increase arose solely from considerations of increased contact force. Although this may well reflect the use of a standard initial film thickness, it may also indicate that in this system, the gas-liquid interfaces are not completely immobilised. Conditions of partial mobility at the interface would result in an rate of film thinning greater than that predicted by the model as the velocity profile in the film would more closely approximate that expected for gas-pure liquid interfaces.

5.2.5 Discussion

The mechanism of coalescence repression and indeed, of the coalescence process as a whole, is still the subject of considerable debate in the literature. Although several recent studies (Christenson and Yaminsky, 1995, Hofmeier et al., 1995, Zahradnik et al., 1998, 1995) agree that the surface activity ($d\sigma/dc$) provides a good indication of the coalescence restraining ability of an electrolyte species (coalescence restraining is observed for electrolyte species where $(d\sigma/dc)^2$ in excess of ~ 1 $mNm^{-1}M^{-1}$ (Christenson and Yaminsky, 1995, Pashley and Craig, 1997), the actual mechanism of the phenomenon remains elusive. Considerations of increased surface elasticity for those solutions beyond the 'transition' concentration (Christenson and Yaminsky, 1995, Pashley and Craig, 1997) and the formation of immobilising surface tension gradients due to film stretching (Marrucci, 1969a, Sagert and Quinn, 1976a, b) are commonly discussed, as well as

effects of ion-water interactions (Marrucci and Nicodemo, 1967) and electroviscous effects at the gas-liquid interface (Lessard and Zieminski, 1971). In addition, Craig et al. (1993) proposed hydrophobic attraction as the force which acts between the two interfaces bounding the film to pull them together and lead to coalescence. For all these reasons, it is difficult to explain precisely the effect of increasing electrolyte concentration on bubble coalescence.

However, it is obvious from this study that although there may be a specific concentration over which the coalescence frequency of a system changes from 100 % to virtually zero, the actual value is strongly dependent on both the nature of the electrolyte and the force at which the two bubbles are brought together. There are a large number of studies reported in the literature which have used apparatus similar to the coalescence cell of this study, to investigate coalescence in solutions of electrolytes. However, almost without exception these studies report data gathered from only a very small range of gas flow rates (if not from a single gas flow rate); the highest bubble frequency reported is 5 s^{-1} (Drogaris and Weilland, 1983). Zahradnik et al. (1998, 1995, 1987) observe good correlation between the 'transition' concentration obtained in a coalescence cell at such low gas flow rates (45 $bubblesmin^{-1}$, nozzle separation 3.5 mm) and the concentration at which gas hold-up increases in bubble columns under the homogeneous bubbling regime. However, their study notes the correlation becomes much less definite for heterogeneous bubbling regimes, an effect which is ascribed to the dominance of macro-scale turbulence. In such systems, where coalescence is promoted by the increased bubble densities and perhaps as a result of entrainment of contacting bubbles in the macro-scale bubbling patterns, the coalescence behaviour is more closely approximated by the gradual change in coalescence frequency, observed in the cell using the higher gas flow rates of this study.

In agitated systems, the shift between coalescing and coalescence repressed systems occurs more gradually, over a wider concentration range than observed in bubble columns (Lee and Meyrick, 1970, Calderbank, 1958), especially so for higher gassing rates. Therefore, for these systems as well, the trends observed in the coalescence cell in this work, using higher gas flow rates, provide a better correlation than the sharp change over a narrow concentration range previously observed. As a consequence of the different flow patterns that result, significant influences of both impeller type and impeller speed, in addition to the effect of gassing rates, may be expected on the

coalescence behaviour. However, Martin (1996), reports similar bubble size distributions at a given gassing rate, for two different types of impeller (Rushton turbine (radial flow) and Prochem Maxflow T (axial flow)) for solutions of sodium sulfate, water and PPG, although this does not preclude influences from other types of impeller. Although perhaps a mere coincidence, (given the purely chance occurrence of such images), substantially more images of coalescence events are reported in that work for dispersions agitated with the Prochem Maxflow T, than with the Rushton turbine.

The results of experiments carried out with varying nozzle distances suggest that with minor modifications to the coalescence cell (such as the inclusion of pressure transducers to measure the bubble pressure, or the use of different diameter nozzle extensions) it should be possible to separate the effect of parameters, such as contact pressure and bubble size and thus develop a more rigorous understanding of influences on coalescence. If this could be combined with increased understanding of the nature of the bubble-bubble contacts that lead to coalescence in larger scale process, use of the coalescence cell as a diagnostic tool would be greatly enhanced.

Despite the large number of studies in the literature concerning the repression of coalescence above specific electrolyte concentrations, very few studies exist wherein measurements of the coalescence time have been made, especially over a concentration range as wide as in this study. In addition, as with coalescence times measurements in general, such measurements are made of relatively stable films, with long drainage times and in liquids which would be defined as coalescence repressed in the terms of this work. Oolman and Blanch (1986a) are the exception, although their work reports coalescence times in pure liquids (values vary from 2.7 – 100 ms) and not over a range of solution concentrations. This study appears unique therefore, in measuring coalescence times over a range of systems, (both fully coalescing and coalescence repressed) and in addition, reporting the behaviour of non-coalescent events, the results of which are surprising in light of the currently accepted mechanism for coalescence.

Cain and Lee (1985) report coalescence times for non-stable films (i.e. not those observed in foams) in KCl solutions which are much greater than those observed in this work; ~ 430 - 600 ms for bubbles in 0.5 M and 1.0 M KCl solution, respectively (making them coalescence repressed

systems, as defined in this study). The authors were not able to measure coalescence times in rapidly draining films, such as those formed in 0.3 M and 0.1 M KCl solutions, which presumably approached the fully coalescing systems of this work and thus would have enabled comparisons with the times measured here. However, their study does recognise the problems inherent in applying film thinning models to experimental data, especially in terms of interface mobility. Comparisons with predictions using the Reynolds equation for thinning (assuming immobile interfaces) predicts much slower drainage profiles (and hence longer to reach the rupture thickness) whereas application of a model developed by Radoëv et al. (1969), allowing for partially mobile interfaces, showed improved although not perfect, agreement.

Even considering the wider coalescence time literature (predominantly measured in solutions of alcohols and surfactant species), no study has previously measured bubble contact/coalescence times for coalescence and non-coalescence events. This in spite of the fact that in many cases, coalescence times are reported for seemingly coalescence repressed systems (Sagert and Quinn, 1978, 1976b, Ueyama et al., 1993) where coalescence events are not representative of the overall system behaviour. The significant differences between the coalescence and bubble contact times observed in coalescent and non-coalescent events respectively, appear to challenge the currently accepted mechanism by which bubble coalescence occurs. Although contact without coalescence is obviously the most energetically stable conformation for non-coalescent events, to determine which of the many parameters (for example, contact angle, collision velocity or perhaps size difference) confers this stability (as opposed to the more thermodynamically favoured coalescence) would require further, rigorously controlled experiments.

5.3 Solutions of A Surface Active Species

Electrolyte species are almost always negatively adsorbed from the gas-liquid interfaces (for aqueous solutions) on account of much more favourable energy considerations which arise from having charged species fully solvated in the bulk solution. In contrast, organic species such as alcohols, are positively adsorbed at such interfaces (and generally result in large reductions to the surface tension), hence the label 'surface active' species. It is well known that the addition of small amounts of alcohol will decrease the average bubble size in a gas-liquid dispersion (for

aqueous solutions) and a number of studies in the literature have confirmed the existence of 'transition' concentrations for various homologous series of organic species (Ueyama et al., 1993, Kim and Lee, 1987, Oolman and Blanch, 1986a, Yang and Maa, 1984). In comparison with electrolytes, much smaller amounts of alcohol are required to reach the 'transition' point between full coalescence and coalescence-repression and Zahradnik et al. (1999b) have demonstrated the continued efficacy of alcohols in repressing coalescence in viscous systems where electrolytes no longer display 'transition' behaviour. In this work, a limited number of experiments were carried out with a single alcohol, propan-1-ol, to investigate the response of the system to increasing air flow rate, as it was considered that the system might respond differently when compared to electrolytes on account of the different degree of interfacial activity. Whereas the surface tension of electrolyte solutions is slightly higher than that of water, that of aqueous solutions of propan-1-ol should be significantly lower, due to the affinity of the solute molecules for the gas-liquid interface. In addition, for bubbles formed in solutions of propan-1-ol, there should be a significant influence from the vapour pressure. Several authors (Oolman and Blanch, 1986a, Nicodemo et al., 1972) predict more rapid replenishment of surface tension gradients in systems with considerable vapour pressure, through diffusion from the gas phase, thus allowing for more rapid thinning and enhanced coalescence.

Experiments were carried out over a small concentration range (from 0.001 to 0.01 M) with gas flow rates from ~ 1 to 60 mlmin^{-1} and a nozzle spacing of 4 mm. Results are shown in Figure 5.16. As can be seen, increasing the gas flow rate has virtually no effect on the coalescence frequency at concentrations beyond that at which coalescence repression is observed at Q_g =

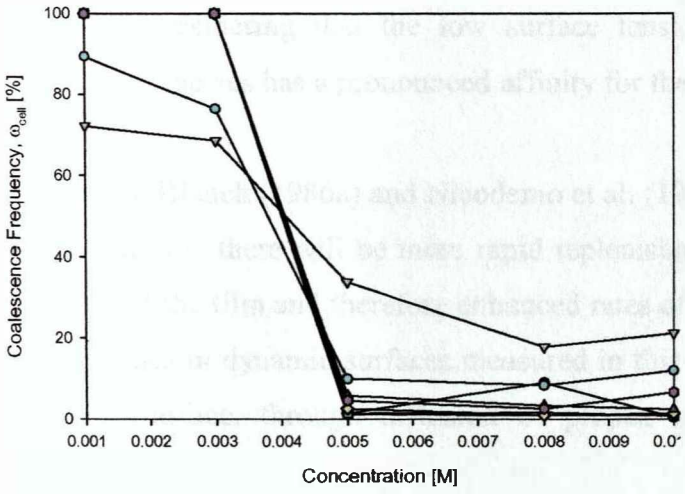

Figure 5.16

Effects of flow rate on coalescence frequencies for air and propan-1-ol solutions. ● Q_g = 1 mlmin^{-1}, ▼ Q_g = 2 mlmin^{-1}, ■ Q_g = 6 mlmin^{-1}, ◇ Q_g = 10 mlmin^{-1}, ▲ Q_g = 14 mlmin^{-1}, ● Q_g = 20 mlmin^{-1}, ○ Q_g = 40 mlmin^{-1} and ▽ Q_g = 60 mlmin^{-1}.

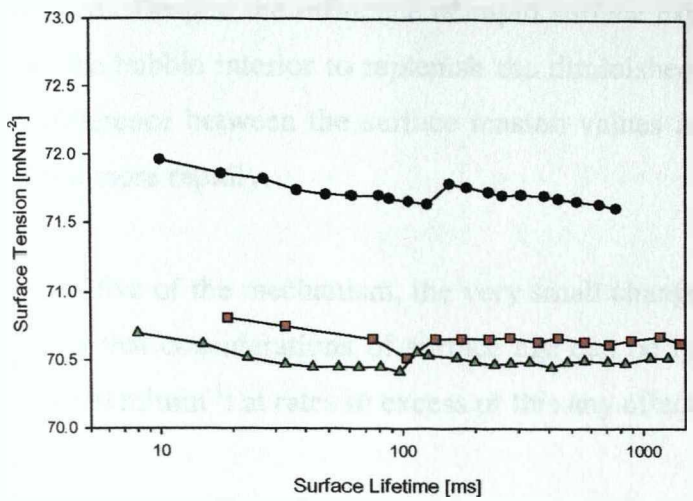

Figure 5.17

Dynamic surface tension profiles measured for solutions of propan-1-ol at concentrations —●— 0.001 M, —■— 0.005 M and —▲— 0.01 M, using Lauda Maximum Bubble Pressure meter, MPT 1

1 mlmin^{-1}. It is only when the gas flow rates are increased to the highest values (60 mlmin^{-1}) that there is a significant increase in the coalescence frequency. However, at the highest gas flow rates there is also an accompanying decrease in the coalescence frequencies measured at concentrations below the 'transition' value.

In Figure 5.17, the surface tension is shown as a function of a range of surface lifetimes, comparable to the range of mean bubble lifetimes observed in the coalescence cell for gas flow rates 2 to 50 mlmin^{-1}. When compared to the surface tension profiles obtained for solutions of sodium sulfate (Figure 5.8), it can be seen that the addition of propan-1-ol causes a decrease in the surface tension as expected, although the magnitude of the change is quite small. For all concentrations, there is a very small initial decrease in surface tension up to a surface age of ~ 100 ms (approximately equivalent to the surface ages at point of contact for bubbles formed at gas flow rates of 20 mlmin^{-1}). This very small effect on the dynamic surface tension is surprising, considering that the low surface tension of propan-1-ol (23.32 mNm^{-1} at 25°C) indicates the species has a pronounced affinity for the gas-liquid interface.

Oolman and Blanch (1986a) and Nicodemo et al. (1972) consider that in systems with significant vapour pressure, there will be more rapid replenishment of surface tension gradients formed by stretching of the film and therefore enhanced rates of thinning. Similarly, it may be that the very small changes in dynamic surfaces measured in this work, are the result of rapid renewal of the gas-liquid surface, through diffusion of propan-1-ol molecules from the gas phase to the

interface. Despite the influence of rapid surface expansion, molecules would be able to diffuse from the bubble interior to replenish the diminished surface solute concentration, thus reducing the difference between the surface tension values for bubble surfaces formed slowly and those formed more rapidly.

Irrespective of the mechanism, the very small changes in dynamic surface tension measurements suggest that considerations of surface age can be ignored for bubbles formed at gas flow rates below 20 $mlmin^{-1}$; at rates in excess of this any effect will be small.

Given that any effect of surface age appears to be very small, it must be concluded that the most significant effects of gas flow rate on coalescence in solutions of propan-1-ol are also those considered relevant for pure liquids: increasing contact pressure and contact area and decreasing contact time. However, whereas the effects of increasing contact pressure appeared to dominate in solutions of electrolytes (increasing coalescence frequency) and in pure liquids (increasing coalescence rates), in this system the predominant effect appears to be that of increased contact area or decreasing contact times. Increasing the film area between two bubbles will increase the area required to thin to the rupture thickness and (assuming that thinning occurs continuously over the total film area), lead to longer contact times. As a consequence, coalescence will not be uniformly accelerated by the increase in gas flow rate (as was the case in electrolyte solutions), rather the increase in contact areas will result in the diminished coalescence frequencies observed in previously fully coalescing solutions (0.001 and 0.003 M). However, the slight increases in coalescence frequencies observed at the highest gas flow rates suggests that the effects of contact area are not always predominant and that in some events, the increase contact pressure does accelerate the film thinning process and hence promote coalescence.

The higher gas flow rates used in this experiment generally produce synchronous bubbling in solutions of electrolytes, even at the highest concentrations. However, visual observation showed that in solutions of propan-1-ol the majority of bubbles formed at the higher gas flow rates were still non-synchronous, with a large number forming in a completely alternating manner. As a consequence, the effects of increased gas flow rate were largely restricted to increasing the size and frequency of the bubbles. Due to the limited number of face-to-face contacts (from the small

proportion of synchronously formed bubble pairs), the effects of increased contact pressure cannot be considered to play a dominant role in the coalescence of bubbles in these systems. Increasing the distance between the nozzles did not allow the formation of synchronous bubbling to be re-established, as had been observed in electrolyte solutions (at higher gas flow rates). In comparison with electrolytes where the tendency of the system to de-synchronise could be overcome when bubbles were forced towards each other at sufficiently high velocities, the presence of propan-1-ol molecules at the gas-liquid interfaces appears to be much more effective at suppressing synchronous bubbling. Increasing the velocity at which bubbles contact merely appears to increase the degree of repulsion between the bubble surfaces. This 'repulsion' cannot arise from electrostatic double layers as may be the case in electrolytes, although it may arise from changes to the water structure surrounding the bubble, where there will be a predominance of hydroxyl groups due to the preferential adsorption of propan-1-ol at the interface and subsequent orientation of the hydrocarbon chains towards the gas phase.

5.4 Effects of Gas Density

By far the majority of studies reported in the literature, have been carried out with air or nitrogen as the gas phase, the exception being a study by Sagert and Quinn (1976a) who investigated the coalescence of bubbles of carbon dioxide and hydrogen sulfide in water over a range of system pressures. However, there are a number of studies in the literature which suggests an impact of gas density on bubble size and the coalescence and break-up dynamics in agitated tanks (Takahashi and Nienow, 1993, Takahashi, McManamey and Nienow, 1992 and Hikita et al., 1980). In these reports, the numbers of smaller bubbles (< 0.2 mm diameter) were observed to increase with decreasing gas density and the coalescence rate was found to increase with gas molecular weight. Contrasting results have been reported in bubble columns (Wilkinson et al., 1994, Wilkinson and van Dierendonck, 1990) where the gas hold-up was observed to increase with increasing gas density (correspondingly, bubble sizes were observed to decrease). This was attributed to an increased propensity towards break-up at the higher gas densities, although Wilkinson and van Dierendonck (1990) state their conclusion is drawn from the results of the study by Sagert and Quinn (1976a). In addition to considerations of gas density, Craig et al. (1993), claim that for different gases, the parameter most likely to affect bubble coalescence is

	Density (gdm^{-3})	Solubility (gkg_{water}^{-1})	Viscosity (μPas)
Hydrogen	0.0898	$1.54*10^{-3}$	9.0
Nitrogen	1.2507	$1.75*10^{-2}$	17.9
Xenon	5.7168	$7.89*10^{-3}$	23.2

Table 5.7

Physical properties of gases used in experiments at 25°C, except density, taken at 0°C. Solubility and viscosity data from 'SI Chemical Data', 2nd Edition, 1971, Aylward and Findlay. Density data from Perry's Chemical Engineers Handbook, 6th Edition, 1984, Perry and Gordon.

gas solubility.

For all these reasons, it was considered useful to use the cell to investigate the effects of gas density on coalescence. These experiments were all carried out in solutions of magnesium sulfate, as a consequence of the better agreement of the 'transition' concentration value obtained at a flow rate of 1 $mlmin^{-1}$ with the observations of Zahradnik et al. (1998, 1995, 1987) and in solutions of propan-1-ol. In addition to using hydrogen and xenon, as a consequence of their widely different molecular weights, experiments were also carried out with nitrogen following the observation the brewing industry prefer to sparge the beer with nitrogen as a consequence of the more homogenous bubble size distributions and increased bubble stability (Ronteltap et al., 1991). Table 5.7 summarises the properties of the various gas species used. Experiments were carried out at four flow rates; ~ 1, ~ 2, 10 and 50 $mlmin^{-1}$ with a nozzle distance of 4 mm. Coalescence frequency data is reported for both experiments with magnesium sulfate and propan-1-ol; for experiments with magnesium sulfate coalescence time data is also reported.

5.4.1 Coalescence Frequencies

The coalescence frequencies are presented as a function of magnesium sulfate concentration for Figures 5.18, 5.19 and 5.20 for hydrogen, nitrogen and xenon bubbles respectively. At the lower gas flow rates, behaviour similar to that observed in air-magnesium sulfate solutions is seen (Figure 5.3), with a step change in the coalescence frequency occurring at a specific concentration. The values for the 'transition' concentrations (ω_{cell} = 50% for Q_g = 1 $mlmin^{-1}$) are

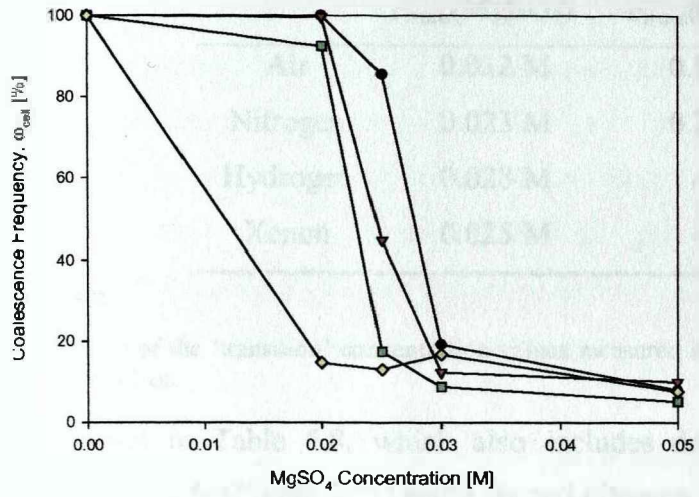

Figure 5.18

Effect of H_2 flow rate on transition concentration for solutions of $MgSO_4$. —●—, Q_g = 1 mlmin^{-1}, ▼ Q_g = 2 mlmin^{-1}, —⊡—, Q_g = 10 mlmin^{-1}, —◇— Q_g = 50 mlmin^{-1}, nozzle spacing 4 mm.

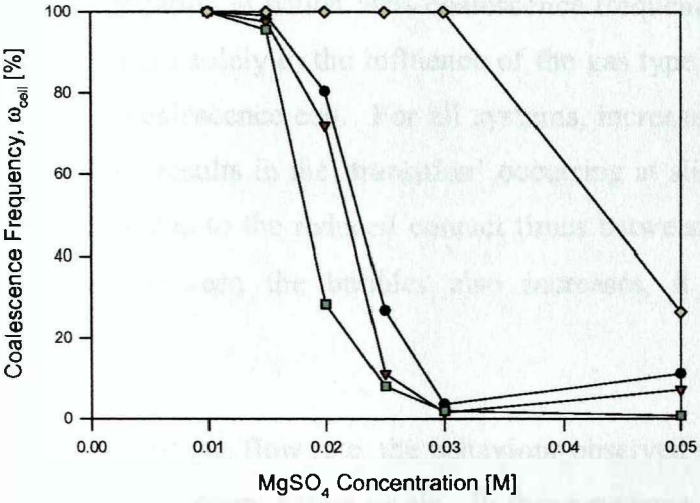

Figure 5.19

Effect of N_2 flow rate on transition concentration for solutions of $MgSO_4$. —●—, Q_g = 1 mlmin^{-1}, ▼ Q_g = 2 mlmin^{-1}, —⊡—, Q_g = 10 mlmin^{-1}, —◇— Q_g = 50 mlmin^{-1}, nozzle spacing 4 mm

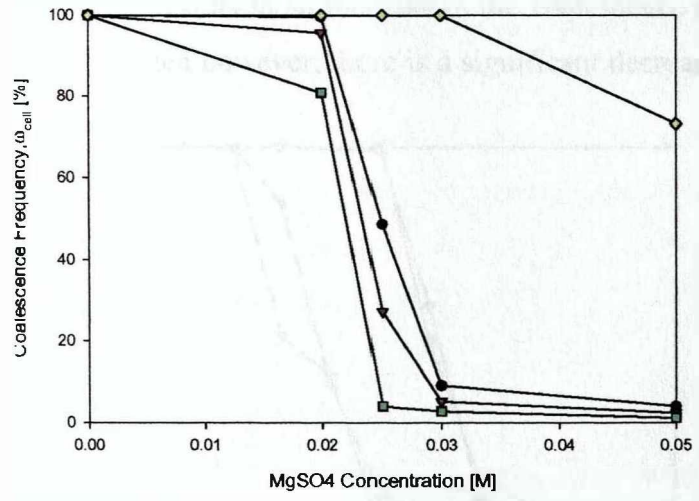

Figure 5.20

Effect of Xe flow rate on transition concentration for solutions of $MgSO_4$. —●—, Q_g = 1 mlmin^{-1}, ▼ Q_g = 2 mlmin^{-1}, —⊡—, Q_g = 10 mlmin^{-1}, —◇— Q_g = 50 mlmin^{-1}, nozzle spacing 4 mm

	$c_{trans}(MgSO_4)$	$c_{trans}(KI)$	c_{trans}(Propan-1-ol)
Air	0.032 M	0.38	0.004
Nitrogen	0.023 M	0.25	0.0075
Hydrogen	0.028 M	-	>0.01
Xenon	0.025 M	-	0.004

Table 5.8

Comparison of the 'transition' concentration values measured in solutions of magnesium sulfate, potassium iodide and propan-1-ol.

summarised in Table 5.8, which also includes data for two experiments carried out with potassium iodide (Figure 5.21) using air and nitrogen. In each case, there are small differences in the concentration at which 50% coalescence frequency is obtained, although it is not possible to attribute these solely to the influence of the gas type in light of reproducibility considerations in using the coalescence cell. For all systems, increasing the gas flow rate beyond ~1 mlmin^{-1}, to 10 mlmin^{-1}, results in the 'transition' occurring at slightly lower concentrations. Most probably this occurs due to the reduced contact times between contacting bubbles. Although the contact pressures between the bubbles also increases, it is insufficient to bring about enhanced coalescence.

At the highest gas flow rate, the behaviour observed with hydrogen is quite different to that seen with either nitrogen, xenon or air. In these systems, an increase in gas flow rate to sufficiently high values results in an increase in the coalescence frequency measured for each concentration. With hydrogen however, there is a significant decrease in coalescence frequencies for previously

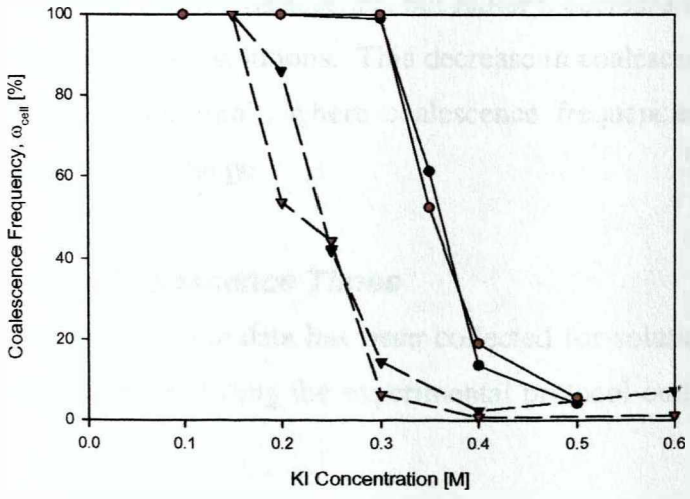

Figure 5.21

Coalescence frequency data for solutions of potassium iodide and air [Q_g ~ 1 mlmin^{-1} and Q_g ~ 2 mlmin^{-1}] and nitrogen [Q_g ~ 1 mlmin^{-1} and Q_g ~ 2 mlmin^{-1}].

fully coalescing systems and no increase in the values measured in coalescence repressed solutions. Observations of the hydrogen-magnesium sulfate systems show that once again, low values for coalescence frequency are coupled with problems in synchronisation of the bubble pairs. Whereas in the nitrogen, air or xenon systems, bubble pairs were fully synchronised at this high gas flow rate, in hydrogen, this is not the case. Bubble pairs are seen to move through periods of non-synchrony, where contacts are generally glancing and bubbles often interlaced, which are interspersed with very short periods of fully synchronised, face-to-face contacts. The behaviour is very similar to that observed in propan-1-ol solutions are higher gas flow rates.

The results of experiments in solutions of propan-1-ol are shown in Figure 5.22, 5.23 and 5.24 for hydrogen, nitrogen and xenon respectively. Unlike the small variations in 'transition' concentration observed when using air, hydrogen, nitrogen and xenon in solutions of magnesium sulfate, the coalescence frequencies measured at Q_g = 1 and 2 mlmin^{-1} for hydrogen and nitrogen are significantly greater those measured in air-propan-1-ol systems (Figure 5.16), as can be seen from Table 5.8. Although in the case of hydrogen, this difference may be ascribed to the much reduced gas density, no such explanation is possible for the results with nitrogen. The very much increased 'transition' concentrations obtained with nitrogen are very surprising, given that air comprises of approximately 70 % nitrogen.

As in magnesium sulfate solutions, increasing the gas flow rate beyond the lowest value results in a decrease in the coalescence frequencies measured for each concentration, such that the step change between full coalescence and coalescence repression occurs at progressively lower concentrations. As in air-propan-1-ol systems, at the highest flow rates there is no significant shift towards full coalescence, but rather a decrease in the coalescence frequencies for previously fully coalescing solutions. This decrease in coalescence frequencies is most significant for xenon at Q_g = 50 mlmin^{-1}, where coalescence frequencies drop to less than 50% across the entire concentration range.

5.4.2 Coalescence Times

Coalescence time data has been collected for solutions of magnesium sulfate and air, hydrogen and xenon, following the experimental protocol outlined in Chapter 3. As for experiments with

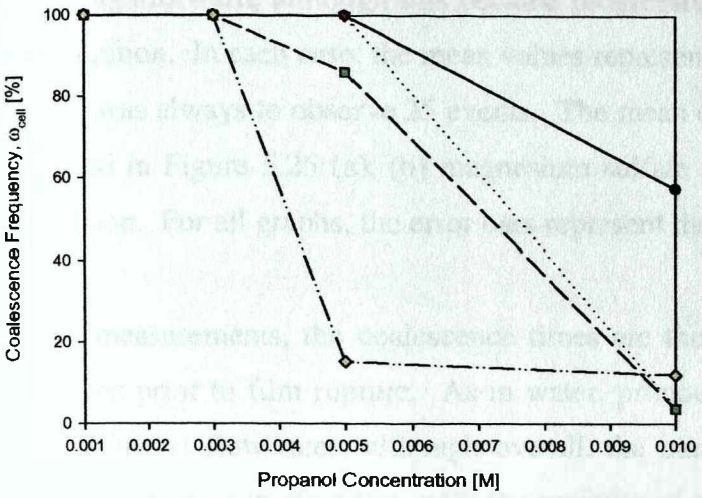

Figure 5.22

Effects of gas flow rate for hydrogen bubbles in solutions of propan-1-ol. Q_g = 1 mlmin^{-1}, Q_g = 2 mlmin^{-1}, Q_g = 10 mlmin^{-1}, and Q_g = 50 mlmin^{-1}. Nozzle separation 4 mm.

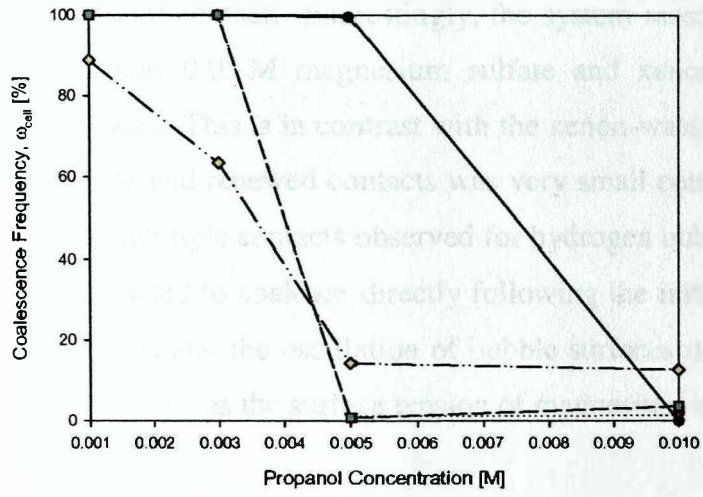

Figure 5.23

Effects of gas flow rate for nitrogen bubbles in solutions of propan-1-ol. Q_g = 1 mlmin^{-1}, Q_g = 2 mlmin^{-1}, Q_g = 10 mlmin^{-1}, and Q_g = 50 mlmin^{-1}. Nozzle separation 4 mm.

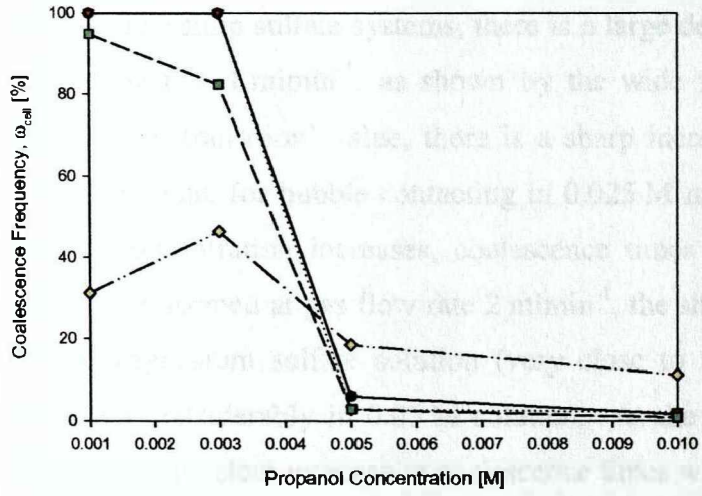

Figure 5.24

Effects of gas flow rate for xenon bubbles in solutions of propan-1-ol. Q_g = 1 mlmin^{-1}, Q_g = 2 mlmin^{-1}, Q_g = 10 mlmin^{-1}, and Q_g = 50 mlmin^{-1}. Nozzle separation 4 mm.

sodium sulfate, measuring 25 events in solutions with concentrations below the 'transition' value was straightforward, although this became progressively more difficult with increasing solution concentration. In each case, the mean values represent a minimum of 10 measurements, although the aim was always to observe 25 events. The mean coalescence times and coalescence rates are presented in Figure 5.25 (a), (b) magnesium sulfate and air, (c), (d) with hydrogen and (e), (f) with xenon. For all graphs, the error bars represent the 95% confidence limits.

For all measurements, the coalescence times are those measured from the final contact to the frame just prior to film rupture. As in water, pronounced surface oscillations were observed at the two lowest flow rates; although overall, the number of broken and renewed contacts was much smaller than in air-water, with the majority of coalescence occurring after the initial (or at most second) contact. Interestingly, the system most prone to surface oscillations and multiple contacts was 0.05 M magnesium sulfate and xenon (an average of three contacts prior to coalescence). This is in contrast with the xenon-water experiments, where the number of surface oscillations and renewed contacts was very small compared to hydrogen–water systems. Unlike the many multiple contacts observed for hydrogen bubbles in water, hydrogen-magnesium sulfate systems tended to coalesce directly following the initial contact. Once again (see Section 5.1.3) this suggests that the oscillation of bubble surfaces is not solely dependent on considerations of surface tension, as the surface tension of magnesium sulfate solutions will be slightly greater than that of water.

For air-magnesium sulfate systems, there is a large degree of scatter for the measurements taken at gas flow rate 1 $mlmin^{-1}$, as shown by the wide 95 % confidence intervals. Even prior to reaching the 'transition' value, there is a sharp increase in coalescence times measured at the lowest flow rate, for bubble contacting in 0.025 M magnesium sulfate solution, although as the solution concentration increases, coalescence times are seen to decrease progressively. For bubble pairs formed at gas flow rate 2 $mlmin^{-1}$, the sharp increase in coalescence times occurs at 0.03 M magnesium sulfate solution (very close to the 'transition' value of 0.032 M), before decreasing considerably in 0.05 M solution. At the higher gas flow rates, 10 and 50 $mlmin^{-1}$, there is no equivalent increase in coalescence times with increasing solution concentration; rather coalescence times are very similar in all solutions.

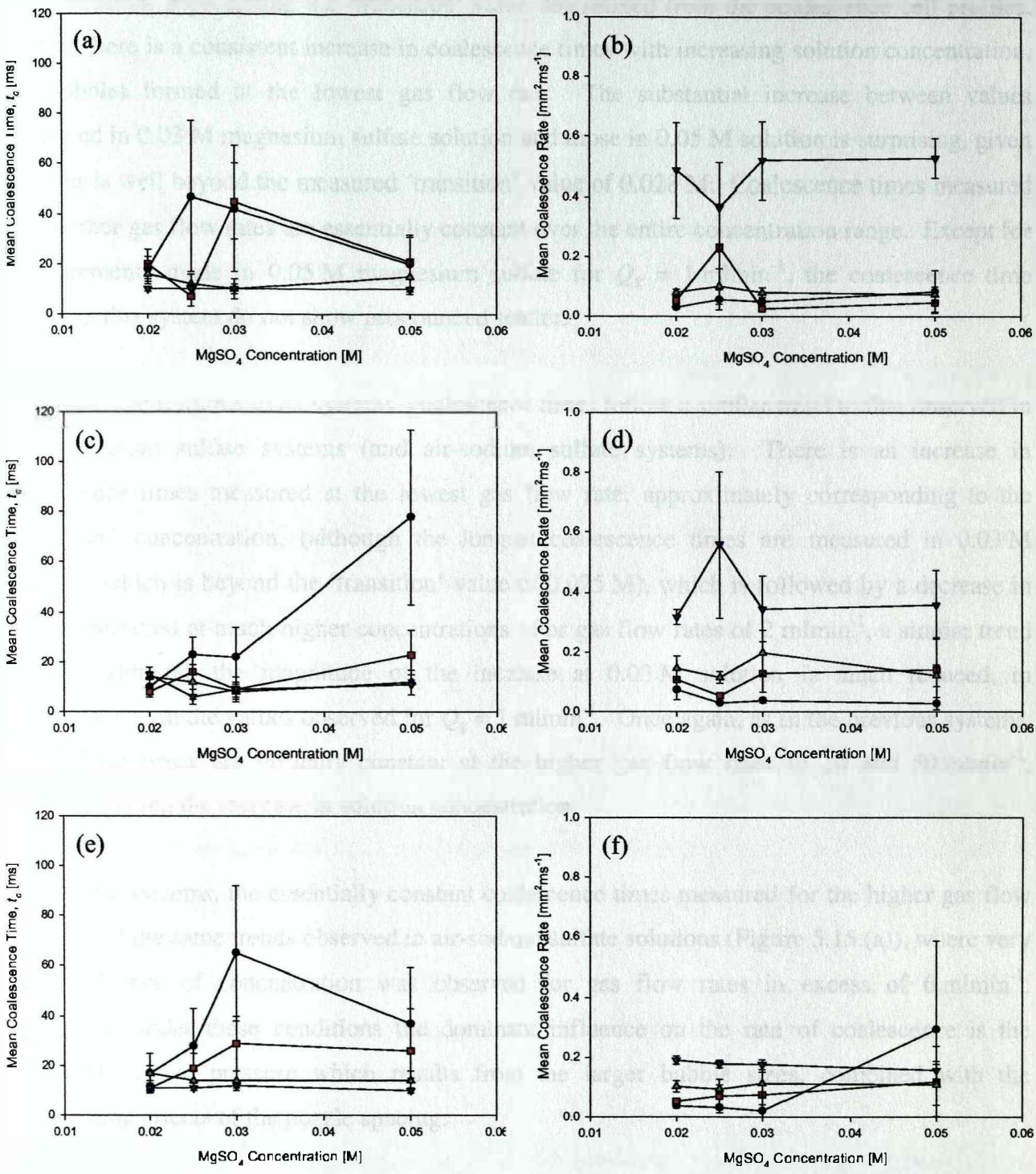

Figure 5.25

Mean coalescence times and film drainage rates for solutions of magnesium sulfate and (a), (b) air, (c), (d) hydrogen and (e), (f) xenon. Error bars show 95% confidence level. Values are mean of not less than 10 measurements. For all; ● $Q_g = 1$ mlmin^{-1}, ■ $Q_g = 2$ mlmin^{-1}, ▲ $Q_g = 10$ mlmin^{-1} and ▼ $Q_g = 50$ mlmin^{-1}.

For hydrogen-magnesium sulfate solutions however, there is no increase in coalescence times for concentrations approaching the 'transition' value determined from the coalescence cell profiles. Rather, there is a consistent increase in coalescence times with increasing solution concentration, for bubbles formed at the lowest gas flow rate. The substantial increase between values measured in 0.03 M magnesium sulfate solution and those in 0.05 M solution is surprising, given that this is well beyond the measured 'transition' value of 0.028 M. Coalescence times measured at the other gas flow rates are essentially constant over the entire concentration range. Except for measurements made in 0.05 M magnesium sulfate for Q_g = 1 mlmin^{-1}, the coalescence time values in this system do not show pronounced scatter.

In xenon-magnesium sulfate systems, coalescence times follow a similar trend to that observed in air-magnesium sulfate systems (and air-sodium sulfate systems). There is an increase in coalescence times measured at the lowest gas flow rate, approximately corresponding to the 'transition' concentration, (although the longest coalescence times are measured in 0.03 M solution, which is beyond the 'transition' value of 0.025 M), which is followed by a decrease in values measured at much higher concentrations. For gas flow rates of 2 mlmin^{-1}, a similar trend is seen, although the magnitude of the increase at 0.03 M solution is much reduced, in comparison with the values observed for Q_g = 1 mlmin^{-1}. Once again, as in the previous systems, coalescence times are virtually constant at the higher gas flow rates of 10 and 50 mlmin^{-1}, notwithstanding the increase in solution concentration.

In all these systems, the essentially constant coalescence times measured for the higher gas flow rates, recall the same trends observed in air-sodium sulfate solutions (Figure 5.15 (a)), where very little influence of concentration was observed for gas flow rates in excess of 6 mlmin^{-1}. Obviously, under these conditions the dominant influence on the rate of coalescence is the increased surface pressure which results from the larger bubble sizes, combined with the constraining effects of the nozzle spacing.

As coalescence times do not allow for differences between contact films areas, mean coalescence rates (a/t_c) are useful as they do account for differences which might arise due to difference in contact angle, degree of synchronisation or gas flow rate. In air-magnesium sulfate and

hydrogen-magnesium sulfate solutions, the values can be separated into two distinct groups. The first consists of coalescence times measured for gas flow rates 1, 2 and 10 $mlmin^{-1}$, where, generally, values are very similar over the concentration range. Values are more closely grouped in air-magnesium sulfate solutions (with the exception of the higher values measured at 0.025 M magnesium sulfate solution for Q_g = 2 $mlmin^{-1}$ and for which there is a large amount of scatter) than for hydrogen-magnesium sulfate solutions, where coalescence rates increase gradually with increasing flow rate, for much of the concentration range. The second group of coalescence rates consists of those measured at the highest gas flow rate, 50 $mlmin^{-1}$ which are significantly greater, although similar over the concentration range (considering the wide 95 % confidence intervals). Similar behaviour is observed in Figure 5.15 (b) for solutions of sodium sulfate, where there is a progressive increase with gas flow rate, although as measurements were made over a greater range of flow rates, the change is more gradual than the step change observed in air and hydrogen-magnesium sulfate solutions.

In contrast, mean coalescence rates measured for xenon-magnesium sulfate solutions, are all closely grouped and with the exception of values for 0.05 M solution, all show a progressive increase with increasing gas flow rate. In the most concentrated solution, 0.05 M, coalescence rates calculated for the lowest gas flow rate, 1 $mlmin^{-1}$, are higher than for the remaining gas flow rates, although the 95 % confidence intervals are extremely broad. Whereas in the previous two systems, there is a significant increase between coalescence rates measured at the lower flow rates and those at 50$mlmin^{-1}$, in xenon-magnesium sulfate, the difference between values calculated at the lowest and highest gas flow rates is much diminished. The small increase between coalescence rates with increasing flow rate suggests that in this system, the increased contact pressures, that accompany the higher gas flow rates, are not able to accelerate the rate of thinning as rapidly as in air or hydrogen systems. This is surprising given that the coalescence cell profiles for air and xenon-magnesium sulfate solutions both show an increase in the coalescence frequency for a given concentration as the gas flow rate (and thus contact pressure) increases, whereas for hydrogen-magnesium sulfate solutions, the coalescence frequency at a given concentration is much reduced at gas flow rate 50 $mlmin^{-1}$.

5.4.3 Discussion

As observed previously, studies in the literature report conflicting results for experiments designed to investigate the influence of gas density on bubble sizes in process systems (Wilkinson et al., 1994, Takahashi and Nienow, 1993, Takahashi, McManamey and Nienow, 1992, Clark, 1990 and Wilkinson and van Dierendonck, 1990). In addition to those studies, which correlate results in terms of gas density (analogous to system pressure), several works propose correlations between gas solubility and the influence on bubble coalescence (Pashley and Craig, 1997, Weissenborn and Pugh, 1995).

Wilkinson and van Dierendonck (1990) report that bubble sizes are more homogeneous and much reduced at higher gas densities (and increased gas pressures) and conclude the primary effect of higher gas density is to promote bubble break-up, through the greater propagation of Rayleigh-Taylor instabilities at the gas-liquid interfaces. The authors dismiss any effect of gas density on coalescence, following on from the study of Sagert and Quinn (1976a, b). However, as can be seen from this work, this is not strictly accurate. Although there is little difference between the coalescence behaviour of the different gas-magnesium sulfate solutions at low gas feed rates, at the highest gas flow rates, there is a significant difference between the different gas systems. It may be that this difference in behaviour will become significant for systems operated under high gas flow rates (for example bubble columns operated in the heterogeneous regime) or in systems where bubbles collide with substantial forces and are held in contact for prolonged time periods (such as in the vortices sometimes observed in agitated vessels, Martin (1996)). Under these conditions, the cell profiles suggest that the coalescence rates would increase with increasing gas density (or system pressure), a scenario which correlates well with the observations of Takahashi and Nienow (1993) and Takahashi et al., (1992), who report an increase in coalescence rates and a decrease in bubble sizes in agitated vessels, as the gas density increases.

An alternative explanation is that in dynamic systems, any effect of gas density on coalescence is very small, compared to its influence on the bubble break-up process. It is not possible to draw conclusions on this matter from these coalescence cell experiments, as the cell does not provide any mechanism for investigating bubble break-up (except for that associated with coalescence, see Chapter 7). Certainly, Wilkinson et al. (1994) report that the effect of electrolyte and gas

density on gas hold-up are synergistic, a conclusion which is not supported by the coalescence cell profiles obtained in this work, where coalescence is more repressed in hydrogen than in xenon-magnesium sulfate systems, especially at the highest gas flow rates.

In addition to changing the gas density, altering the gas type will introduce influences of differing gas solubilities and perhaps changing surface tension values. Pashley and Craig (1997) propose that at high gas diffusivities, there is a more rapid growth of the surface waves which cause film rupture and that the increased amount of gas in solution help to fuse the surface waves and thus accelerate rupture. Weissenborn and Pugh (1995) speculate that the inhibition of bubble coalescence is also linked to a decrease in the dissolve gas concentration in electrolyte solutions. Indeed, in this work the order of gas solubilties is nitrogen > xenon > hydrogen, (Table 5.7) which correlates with the coalescence cell profiles observed at the highest gas flow rates. Profiles obtained at flow rates up to 10 $mlmin^{-1}$, however, show very little difference between the three gases, (accounting for the experimental error inherent in the equipment), under conditions where the influence of the gas-liquid interface should dominate the film thinning process (at higher gas flows, the effects of increased contact pressure will be much greater).

With solutions of propan-1-ol, the effects of gas density are much more significant than in magnesium-sulfate solution. In these experiments, increasing the gas density significantly reduces the concentration at which the system switches from being fully coalescing to coalescence repressed. Coalescence appears to be promoted in hydrogen-propan-1-ol systems, in comparison with the behaviour observed for xenon-propan-1-ol. However, the significantly increased 'transition' concentration obtained in nitrogen-propan-1-ol, as compared to that in air-propan-1-ol suggests that the effect is not primarily dependent on the gas density. This is supported by the fact that the coalescence cell profiles in air-propan-1-ol and xenon-propan-1-ol systems are not dissimilar (similar values for the 'transition' concentration at Q_g = 1 $mlmin^{-1}$), despite the significant differences in gas density. It is also not possible to ascribe the effects to differences in gas solubility, as suggested by Pashley and Craig (1997) or Weissenborn and Pugh (1995), as this would predict a consistent pattern in the coalescence behaviour, which is not observed. No studies are reported in the literature, in which coalescence (or even bubble size distributions) is investigated in solutions of alcohols or other organic species for different gas

species, which would enable comparison to be drawn with the results of this work. Further work is obviously required to extend the range of organic species investigated and to extend the range of gas types, which should be chosen on the basis of very different chemical properties (such as solubility and diffusivity).

5.5 Conclusions

Investigations into coalescence behaviour have been carried out in pure liquids and solutions of various electrolyte and *n*-alcohol species and for a range of gas types. Experiments were designed to assess the impact of parameters such as gas flow rate, bubble frequency and nozzle separation distance on both bulk (coalescence frequency) and small-scale (coalescence times) system behaviour.

- As expected, pure systems of water and propan-1-ol are fully coalescing over a range of gas flow rates from 1 – 50 $mlmin^{-1}$. This is attributed to the lack of a third component which slows the rate of film thinning and hence retards coalescence.

  Coalescence times have been measured for air-water systems for a range of temperatures and gas flow rates; values are observed to decrease with increasing temperature, although the predominant effect is that of gas flow rate and the resulting increased contact pressure. Similarly, for hydrogen-water and xenon-water systems, the effect of gas type is much smaller than the effect of gas flow rate.

  Coalescence times measured in propan-1-ol, at temperatures of 10°C and 25°C, clearly show the influence of liquid viscosity following comparison with values obtained for water. Experimental values compare reasonably with predictions from the model of Chesters and Hofman, 1982, although the greatest deviations occur at the high gas flow rate. The increased deviations are due to the influence of increased contact pressure, as the model considers only unconstrained contacts between bubbles.
- Coalescence behaviour in electrolyte solutions is heavily dependent on the gas flow rate at which bubbles are formed and the nozzle separation distance.

  At low gas flow rates (~ 1 – 2 $mlmin^{-1}$) and for small nozzle separations (4 mm) a distinct step change in coalescence frequency, the 'transition' concentration, is observed for

solutions of Na_2SO_4, $MgSO_4$ and KI. In addition, for the first time, a 'transition' concentration has been observed in solutions of HNO_3.

Coalescence frequencies are seen to increase with gas flow rate, such that for all electrolytes studied, there is a gas flow rate at which systems becomes fully coalescing. As the valence combinations of the electrolytes increase, the shift towards full coalescence occurs at progressively higher concentrations and consequently higher flow rates are required to force the system to become fully coalescing. The increase in coalescence frequency observed is attributed to the increased contact pressure, which results at high gas flow rates from the combination of increased bubble size and geometrical constraints from the nozzles.

For a given flow rate and solution concentration, an increase in the distance between the nozzles shifts the observed coalescence cell profile to the right, such that a higher gas flow rate is required to achieve a similar coalescence frequency values. This is due to the reduced contact pressure between the contacting bubbles.

- High-speed video studies have been used to visualise the coalescence process in detail, in addition to allowing parameters such as the coalescence time, coalescence rate and contact times to be measured. Film rupture is too rapid to be observed, but bubble pair formation, approach and contact, as well as confluence following the actual coalescence event, can all be observed in detail.

  A coalescence event can be characterised by the presence of an annular wave, which is triggered by the film rupture and can be seen to move rapidly away from the site of rupture, causing considerable distortion and flexing of the newly coalesced bubble. It has been calculated that the annular wave moves at a speed of ~ 2.5 ms^{-1}, irrespective of the type of liquid (water, electrolyte solution).

  Coalescence times have been measured in a range of electrolyte concentrations and at the lowest gas flow rate, there is a large increase in coalescence time values as the solution concentration approaches the 'transition' value. Coalescence rates, which allow for effects of contact area, show a rapid increase with increasing gas flow rate, confirming the significant influence of this parameter on the nature of the coalescence event.

  For bubbles in sodium sulfate, contact times, measured between non-coalescing but contacting bubble pairs, are significantly longer than coalescence times under the same

conditions, provoking questions about the mechanism of coalescence, particularly the film thinning step.

Comparison of experimental values with those predicted by a film thinning model show the model consistently over predicts thinning times, especially at higher gas flow rates. This is presumably a result of increased contact pressures in the experiments, where the model assumes free unconstrained contact, although it also reflects the fact that the interfaces in these systems are not completely immobile as assumed in the model.

- The coalescence behaviour of solutions of propan-1-ol does not show the same dependence on gas flow rate as electrolyte solutions. As in electrolyte solutions, a distinct step change in coalescence frequency values is observed at low gas flow rates, with increasing concentration. However, there is no similar shift towards full coalescence with increasing gas flow rate, even at high gas feed rates. In addition, in solutions of propan-1-ol beyond the 'transition' value, bubbling remains non-synchronised, even at high gas flow rates.
- The results of experiments designed to elucidate the influence of gas density on coalescence behaviour are not conclusive.

  Increasing the gas density (from hydrogen to xenon) causes a small decrease in the 'transition' concentrations measured for magnesium sulfate solutions at low gas flow rates ($1 - 2$ mlmin^{-1}). However, experiments with nitrogen give significantly different values for the 'transition' concentration than obtained in air-magnesium sulfate solutions, despite similar densities.

  At the higher gas flow rates, behaviour with hydrogen is significantly different from that observed with air, nitrogen or xenon. This is tentatively attributed to the differences in gas solubility, although it is observed that in similar systems, this is the region at which the influence of gas flow rate is observed to dominate.

  Coalescence times and rates measured for air and hydrogen-magnesium sulfate solutions show similar trends, whereas different trends are observed for xenon-magnesium sulfate systems. Although results suggests that for increased gas densities, the effects of contact pressure are less important, it is difficult to correlate the trends observed for coalescence times measurements, with the coalescence cell profiles obtained in the same system.

Experiments with propan-1-ol show very different coalescence behaviour with different gases, but correlations with gas density or solubility cannot be drawn, as consistent trends are not observed.

Chapter 6
The Coalescence Cell and Viscosity Modified Solutions

This chapter reports the results of experiments using the coalescence cell to investigate the effects of increasing liquid viscosity on bubble coalescence. Initially, the results of previously published studies are briefly reviewed, together with the predictions from some of the film thinning models found in the literature, to provide an indication of the expected effects of viscosity on coalescence behaviour. The results from initial experiments are presented in Section 6.2, where the coalescence behaviour of bubbles generated in a pure liquid of slightly greater viscosity than water (3 mPas silicone fluid) is examined. Following this, Section 6.3 describes coalescence behaviour observed in solutions prepared with two different viscosity modifiers (sucrose and glycerol), at two identical viscosities and with further viscosity modification provided through temperature changes. Finally, in Section 6.3, the results of an extended investigation into coalescence over a wide range of viscosities are reported for glycerol solutions, where both coalescence frequencies and coalescence times (from high-speed video studies) have been determined.

6.1 Literature: The Effect Of Viscosity

6.1.1 Experimental Evidence

Although there is a significant body of work in the literature investigating the effects of viscosity on coalescence, the vast majority of these studies have focussed on coalescence following wake-induced collisions, with bubbles rising in-line (De Kee et al., 1986, Crabtree and Bridgwater, 1971, de Nevers and Wu, 1971). However, in these systems the primary focus is not the rate of film thinning between two contacting bubbles. Rather, the studies focus on the distance over which the wake effects of the leading bubble are able to influence the behaviour of the trailing bubble and the subsequent change in velocities of the trailing bubble following entrainment. Although it can be concluded that for Newtonian liquids, an increase in the liquid viscosity promotes coalescence through extended wake effects, this really only applies to the initial approach phase of two bubbles (under specific geometrical arrangements) and cannot be considered to hold for the whole of the coalescence process (contact, film formation and film thinning to a critical thickness followed by rupture, Oolman and Blanch, 1986a).

A much smaller number of studies have been carried out with bubbles formed simultaneously, at either adjacent or opposing nozzles, such as used in this work. Oolman and Blanch (1986a) measured coalescence times for bubbles generated at vertically adjacent nozzles in glycerol (μ = 1500 mPas) and Carbopol™ solution. [Despite being a shear thinning fluid with a yield stress, only a viscosity value is quoted for Carbopol™ solution (μ = 30 mPas).] Values were much greater for bubbles in glycerol (t_c ~ 100 ms) compared to those in Carbopol™ solution (t_c ~ 21 ms). In both cases, the measured values were larger than those calculated from either the authors' model or the equation of Chesters and Hofman (1982) for coalescence times in pure liquids, (Equation 2.40 of this work). However, as neither model allows for the influence of viscosity on the coalescence time (indeed Chesters and Hofman (1982) restrict their analysis to bubbles in liquids of low viscosity), the poor agreement is not surprising.

Zahradnik et al. (1987) carried out experiments in solutions of glycerol over a range of concentrations and linked coalescence frequencies obtained to the gas hold-up measured in a bubble column. Coalescence frequencies approached 0.1 % for those solutions with maximum hold-up (solutions of 8 and 39 %w/w glycerol (μ = 3.4 mPas)), whereas values approached 100 % in 'strongly diluted solutions' ($\leq$ 1 % w/w) and very much higher concentrations (68 and 84 %w/w), correlating with low hold-up values observed in the bubble column. The drop in coalescence frequencies observed at intermediate glycerol concentrations was attributed to the 'hindered bubble motion in viscous fluids' combined with insufficiently large drag forced to promote coalescence; surface effects were considered negligible as glycerol has 'virtually negligible surface activity'. However, given that in these experiments bubble pairs were released simultaneously from opposing nozzles, it is difficult to appreciate that the hindered bubble motion, which may be observed in dynamic systems, would be instrumental in promoting coalescence in a geometrical arrangement where the rate of film thinning must dominate the coalescence process.

Craig et al. (1993) report a 'transition' concentration in sucrose solutions over a concentration range 0.001 to 0.5 M but do not consider any effects of increasing viscosity which may be considered important in such systems. In solutions above 0.08 M there is a distinct decrease in the amount of light transmitted, suggesting a significant decrease in the amount of coalescence occurring. The experiments were carried out in a simple bubble column, a system in which the hindered rise velocities suggested by Zahradnik et al. (1987) would be

expected to lead to significant amounts of coalescence as bubble-bubble contacts are promoted through wake capture mechanisms which subsequently allow two bubbles to remain in contact for an extended period of time. Such a phenomenon may explain the relatively smaller decrease in coalescence observed in sucrose solutions compared to that measured in electrolyte systems. Craig et al. (1993) quote a percentage coalescence of 30 % for coalescence repressed sucrose solutions as opposed to the almost zero values quoted for coalescence repressed electrolyte solutions.

6.1.2 Predictions from Film Thinning Models

In terms of the three step mechanism that is generally used to describe the coalescence process, the rate determining step (and hence, the most significant contributor to the coalescence time) is the time required for the intervening film to drain to the critical thickness at which rupture can occur. In addition to the nature of the interfaces bounding the liquid film (fully mobile, partially mobile or immobile), the rate at which the liquid drains from between two bubbles will be significantly affected by the viscosity of the liquid (in liquid-liquid systems the rate of drainage will also be affected by the viscosity of the dispersed phase, although in gas-liquid systems, because $\mu_g << \mu_l$, any effect should be very small). As discussed in Chapter 2, many film thinning models have been proposed in the literature for the coalescence of fluid particles, (both drops and bubbles) either at an interface or with a similar particle; all the models, irrespective of the underlying assumptions, consistently predict the rate of film thinning to vary inversely with continuous phase viscosity.

As discussed in Chapter 2, the classical approach to film thinning between two plane parallel surfaces is expressed by the Reynolds equation:

$$V_R = -\frac{dh}{dt} = \frac{8h^3\Delta P}{3\mu r_d^{\,2}} \qquad (2.39)$$

Application of this expression to film drainage assumes the film thinning occurs between two immobile (but deformable) interfaces, where the velocity at the interface is zero; such as those containing surfactant, or where the dispersed phase viscosity is very large (not applicable to this study). For those systems where the interfaces are fully mobile, (such as pure liquids) Chesters (1991) has developed an expression which in viscous dominated systems becomes:

$$-\frac{dh}{dt} = \frac{2\sigma h}{3\mu r_b} \qquad (2.44)$$

Both these expression, although developed to determine the rate of thinning in two very different systems, show the inverse dependency on bulk viscosity that is predicted to apply in almost all the models proposed in the literature.

6.2 Pure Liquids

Considering the predictions of the various film thinning models, even a small increase in liquid viscosity should result in greater drainage times. As a result, it was decided to begin the investigation using a pure liquid of relatively low viscosity. Although it was originally hoped to investigate coalescence in a series of hydrocarbons, as a means of providing a range of liquid viscosities without additional complications from concentration related effects, these proved incompatible with the materials used in the construction of the coalescence cell and consequently experiments were only carried out in Dow Corning 200 3 mPas Silicone Fluid. Details on materials and methods are given in Chapter 3.

Bubble pairs were formed at gas flow rates of 1,2 10 and 50 $mlmin^{-1}$, for a fixed nozzle distance of 4 mm, at temperatures of 25 °C. In comparison with equivalent bubbles in water, those formed in the silicone fluid were much smaller (approximately half the diameter), such that for the two lowest flow rates there was no contact between opposing bubbles in a pair. In contrast with the situation in water, bubbles were not always synchronised and bubble-bubble contacts were most often observed to be skew. Any coalescence events that were observed occurred between non-synchronised bubbles, where the leading bubble was fully formed and rising at the moment of contact. A typical event is shown in Figure 6.1. Unlike water (or propan-1-ol) systems, the majority of bubble-bubble contacts in silicone fluid did not result in coalescence. Even when opposing bubbles were sufficiently large enough to contact; values for the coalescence frequency were always less than 10 % at air flow rates of 10 $mlmin^{-1}$. At gas flow rates 50 $mlmin^{-1}$, bubbling patterns were observed which were very similar to those seen at higher flow rates in electrolyte solutions. Bubbles were observed to rise in groups of four (two pairs) and the few coalescence events that were observed, were wake mediated. The existence of the cluster bubbling patterns is most probably due to the increased liquid viscosity; certainly the accelerated bubble rise as a consequence of preceding wakes was seen to be much more pronounced in this system than in water.

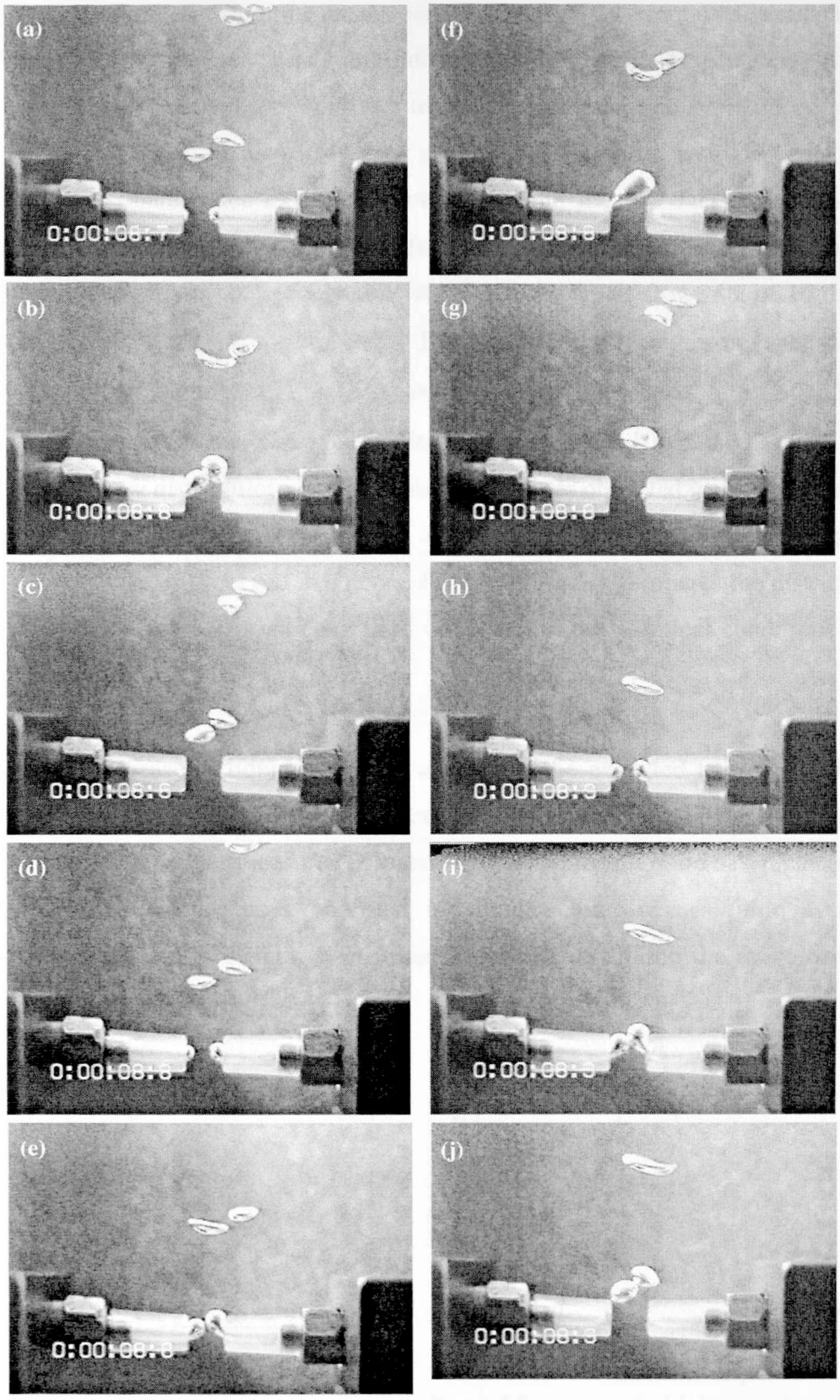

Figure 6.1

A typical bubbling sequence observed in 3 mPas silicone fluid. As can be seen bubble pairs are not well synchronised and contact tends to occur between rising bubbles. All coalescence events were observed to occur as seen in frames (d) to (g), skew contact, followed by coalescence just prior to the detachment of the leading bubble. Air flow rate 10 $mlmin^{-1}$. Nozzle separation 4 mm.

High speed video was used to determine mean coalescence (from 25 events) and contact times (from 10 events) for typical coalescence and non-coalescence events respectively, at a gas flow rate of 10 mlmin^{-1}. Due to the rapid rate of bubble formation, no pronounced surface oscillations were observed, with all coalescence events occurring after a single contact. As discussed previously, coalescence events did not occur from the few face-to-face contacts between bubble pairs; when observed, they followed the skew contacts between non-synchronous pairs. The mean coalescence time measured for an air flow rate of 10 mlmin^{-1} was 6 ± 0.6 ms (for air-water, $\overline{t_c} = 4 \pm 1$ ms). The contact areas for these events were all very similar (0.5 – 0.75 mm^2), giving rise to a mean 'coalescence rate' of 0.106 ± 0.008 mm^{2}s^{-1} (very similar to that observed in air-water systems, 0.105 ± 0.022 mm^{2}s^{-1}). In Figure 6.2, the frequency distributions for the coalescence times observed in silicone fluid and water (Q_g = 10 mlmin^{-1}) are compared. In addition, the graph shows the frequency distribution of contact times observed in silicone fluid. Figure 6.3 compares the distributions of coalescence rates calculated for silicone fluid and water under identical conditions (Q_g = 10 mlmin^{-1}, T = 25 °C).

Despite a threefold increase in liquid viscosity, which may be expected to slow the rate of film thinning proportionally, the mean coalescence times measured for silicone fluid are only half as slow as equivalent values measured in water. However, from Figure 6.2, it can be seen that whereas the coalescence times observed in silicone fluid occur within a narrow distribution, the shape of the distribution in water is quite different and the range of values

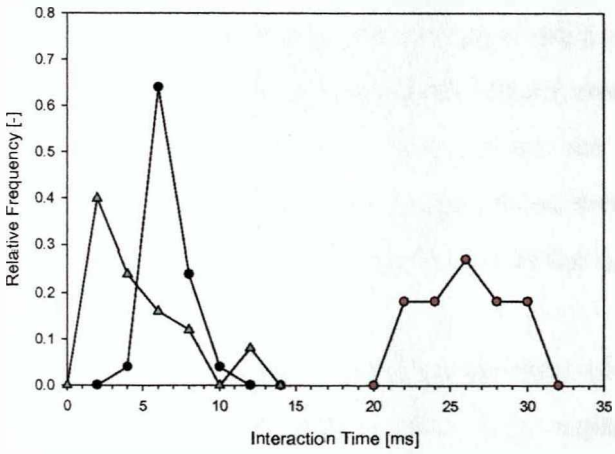

Figure 6.2

Frequency distributions for coalescence and contact times in 3 mPas silicone fluid and water. Q_g = 10 mlmin^{-1}, nozzle separation 4 mm. Coalescence time, silicone fluid —●—, coalescence time, water —▲— and contact time for silicone fluid, —●—.

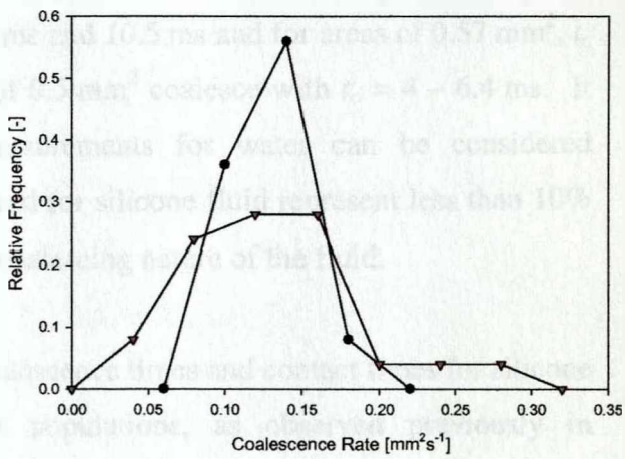

Figure 6.3

Frequency distributions for coalescence rates in 3 mPas silicone fluid, —●— and water, —▼—. Q_g = 10 mlmin^{-1}, nozzle separation 4 mm.

somewhat greater. In water, the modal value is around 2 ms after the initial contact, whereas in silicone fluid, the modal value has shifted to 6 ms and the very rapid coalescence events observed in water are absent. When compensation is made for the size of the intervening film between two contacting bubbles by calculating the corresponding 'coalescence rates', a similar situation is observed. 'Coalescence rates' for silicone fluid all fall within a narrow distribution, reflecting the narrow range of coalescence times and contact areas observed. Values for water show a much wider distribution, although it is interesting to observe that the greatest proportion occur within the same range as for silicone fluid. This was unexpected given the predicted influence of liquid viscosity on film thinning rates. A three-fold increase in the liquid viscosity, such as investigated here, would be expected to generate coalescence times approximately one third as fast. One possible explanation for the results observed is that the thinning is not continuous over the contact area, but occurs in random locations within the film. Coalescence would only require one of these random locations to thin sufficiently and reach a thickness at which rupture can occur. If thinning does occur discontinuously over the film area, this would account for the similar coalescence rates observed for water and silicone fluid, despite the differences in viscosity.

The main difference between the two systems appears to be in the degree of deformation that occurs between two contacting bubbles. This appears to be much more variable in water than in the more viscous silicone fluid, leading to a much greater range in contact areas (from 0.09 to 1.11 mm^2). From analysis of the raw data, even for events where the contact areas are comparable, no distinct trend in coalescence times is obvious. In water, coalescence times recorded for contact areas of 0.46 mm^2 are t_c = 3 ms and 10.5 ms and for areas of 0.57 mm^2, t_c = 3 ms; whereas in silicone fluid contact areas of 0.5 mm^2 coalesce with t_c = 4 – 6.4 ms. It must be recalled though that whilst the measurements for water can be considered representative of the whole system, those measured for silicone fluid represent less than 10% of events observed, as a consequence of the non-coalescing nature of the fluid.

Once again, comparison between the range of coalescence times and contact times for silicone fluid (Figure 6.2) shows two very separate populations, as observed previously in concentrated electrolyte solutions. It is difficult not to conclude that the generally accepted maxim that coalescence occurs when two bubbles remain in contact for sufficiently long for the intervening film to thin, is somewhat oversimplified. In this system, where the only influence on coalescence is the liquid viscosity (solute effects such as the formation of surface

tension gradients being absent), the existence of separate populations is particularly difficult to understand. Observations showed that contact areas were similar in both coalescent and non-coalescent events; as a consequence, it cannot be said that bubble pairs failed to coalesce due substantially greater contact areas (and hence prolonged thinning times). It is important to recall that the system was essentially non-coalescing, hence the contact times measured are much more representative of the system as a whole than the coalescence times. As a result it may be that all the bubble pairs would coalesce if held together for a sufficiently long period of time, in which case the coalescence times measured in this system represent only the lower end of a distribution. Alternatively, it may be that coalescence will not occur despite prolonged contact times. In either case, the question of interest now becomes, how is the film thinning environment different between bubble pairs generated under identical conditions? Is this difference due to hydrodynamic considerations (i.e. different contact forces arising from slightly different angles) or to surface phenomena?

Whilst there are obvious differences in the coalescence times measured in silicone fluid and water, it is not possible to conclude that the rate of film thinning is significantly slower in a liquid of increased viscosity. This is especially true when coalescence rates for the two systems are compared. Certainly, increasing the liquid viscosity by a small amount does seem to result in much more reproducible coalescence time, with consistent contact areas between bubble pairs. However, whether the increase in viscosity alone is responsible for the most obvious difference between the two systems (one coalescing, the other significantly coalescence repressed) cannot be determined from this work. In order to do so, experiments with 1 mPas silicone fluid would be needed to eliminate differences in surface phenomena, which may be expected to influence the coalescence process.

6.3 Effects Of Different Viscosity Modifiers

6.3.1 Modifying Viscosity through Solute Concentration

Following the initial experiments with silicone fluid, experiments were carried out using two low viscosity solutions with target viscosities of ~ 2.8 mPas and ~ 5.7 mPas. Solutions were prepared with two different viscosity modifiers, sucrose and glycerol, which, it was hoped, would generate information about the effects of different molecular structures on interfacial behaviour, in addition to investigating the effect of liquid viscosity.

Solution (Conc^{n}, [M])	Viscosity, μ [mPas]	Density, ρ [kgm^{-3}]	Surface Tension, σ [mNm^{-1}]
Glycerol (1.6)	2.5	1.059	72.61
Glycerol (5.0)	5.8	1.077	71.02
Sucrose (0.5)	2.7	1.059	72.83
Sucrose (1.2)	5.7	1.112	73.38

Table 6.1

Physical properties for glycerol and sucrose solutions.

Both sucrose and glycerol are commonly used to alter liquid viscosity and have the advantage of producing transparent liquids (important in this work), with Newtonian flow characteristics. The concentrations required to produce solutions of appropriate viscosity were determined by trial and error. The physical properties for each of the solutions finally used are outlined in Table 6.1. Both molecules are non-polar, hydrophilic species with the primary difference being size: glycerol is relatively small, (molecular weight 92.09 gmol^{-1}) whereas sucrose is over three times larger (342.3 gmol^{-1}). In addition to influencing physical properties such as the diffusivity, the difference in molecular size should also affect the behaviour of each species at the gas-liquid interface. As a consequence of molecular structure, both solutes will be readily solvated in the aqueous bulk and show only a small degree of surface activity, as seen in Table 6.1, although it may be expected that when considering expanding surfaces, such as in measurements of dynamic surface tension, the behaviour of the two solutes will differ. In addition, as the solute concentrations increase, the differences in interfacial behaviour are exacerbated. Sucrose, as evidenced by the increase in surface tension with concentration, exhibits a small preference for the liquid bulk. In contrast, glycerol shows a decrease in surface tension with increasing concentration suggesting a slight preference for the interface over the bulk. In each case, however, the orientation preferences are small.

The results of the initial experiments carried out at 25°C are shown in Figure 6.4(a) for the two solutions of viscosity ~ 2.8 mPas over a air flow range of 2 to 50 mlmin^{-1}. Initially, both solutions are non-coalescing with approximately one in five contacts leading to a coalescence event. As the gas flow rate increases, however, the coalescence frequency is seen to increase with increasing gas flow rate, such that at $Q_g > 30$ mlmin^{-1}, both solutions are essentially fully coalescing systems. As previously noted for experiments in electrolyte solutions, this

increase in coalescence frequency is also accompanied by a simultaneous move towards the fully synchronous bubbling which characterises a fully coalescent system. Very little difference can be found between the coalescence frequencies measured for the two solutions (recalling the considerations of experimental error discussed in Chapter 4).

The results of the initial experiments with solutions of higher viscosity (~5.6 mPas) are shown in Figure 6.4(b). Once again, an increase in the coalescence frequency is observed with increasing gas flow rate, such that the originally non-coalescing solutions are seen to become fully coalescing at sufficiently high gas flow rates. However, whereas very similar responses were observed for the sucrose and glycerol solutions in the lower viscosity solutions, the differences between the values measured for the coalescence frequencies are greater. Except at the lowest flow rates, the coalescence frequencies measured in 1.2 M sucrose solution are consistently higher than for 5 M glycerol, such that full coalescence is achieved earlier (~20 $mlmin^{-1}$ compared to > 40 $mlmin^{-1}$).

Figures 6.5(a) and (b) allow the effects of viscosity to be compared directly for the same solute, presenting the data from the initial experiments for solutions of glycerol and sucrose, respectively over a flow range 2 to 50 $mlmin^{-1}$. Despite the increase in viscosity, the coalescence frequencies observed in 5 M glycerol solution are not dissimilar to those measured in 1.6 M glycerol, over the range of gas flow rates (recalling experimental errors of the order of ± 15 % for flow rates between 10 and 50 $mlmin^{-1}$). Considering that there is over a two-fold increase in solution viscosity between the two glycerol solutions, this similarity of responses is surprising. Provided the increased viscosity is the predominant difference between the two solutions (this ignores any significant contribution from the increased solute concentration), from film thinning models the rate of film drainage should be expected to be approximately half as fast.

In contrast, there is a significant difference between the values measured in the two sucrose solutions, with the higher viscosity solution showing consistently higher value of coalescence frequency over the air flow range investigated. The difference between the two solutions is especially notable over the lower range of flow rates, up to Q_g ~ 20 $mlmin^{-1}$, when there is a much faster increase towards fully coalescence behaviour for the 1.2 M (~5.6 mPas) sucrose solutions. Once again, this is an unexpected result since the effects of increased viscosity would be expected to lead to longer film thinning times in solutions of 1.2 M sucrose.

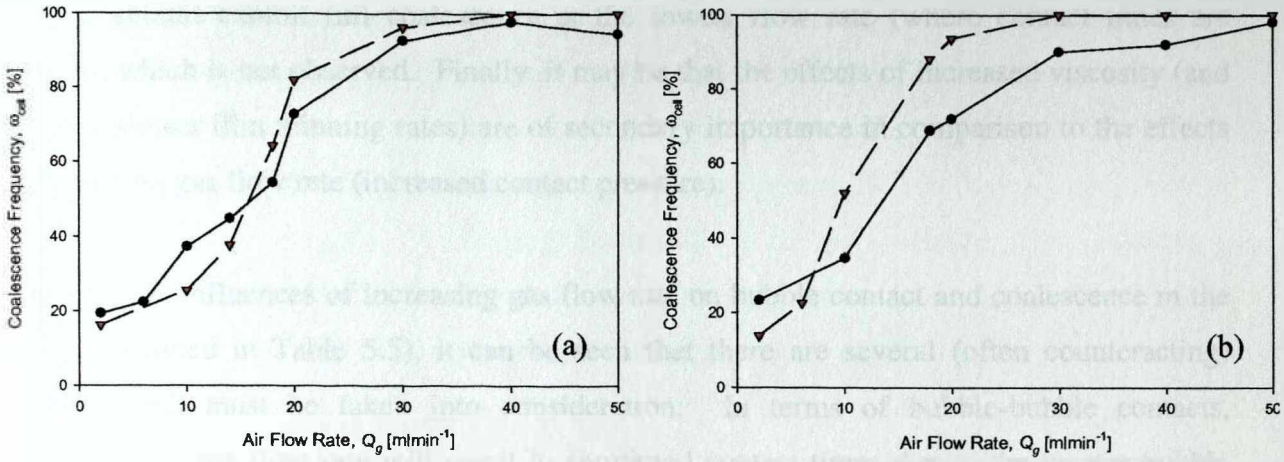

Figure 6.4

Effect of viscosity modifier on coalescence frequency over flow range Q_g = 2 - 50 mlmin^{-1} for solutions of viscosity (a) ~ 2.8mPas and (b) ~5.6mPas. For both, —●— glycerol and —▼— sucrose and nozzle separation 4 mm.

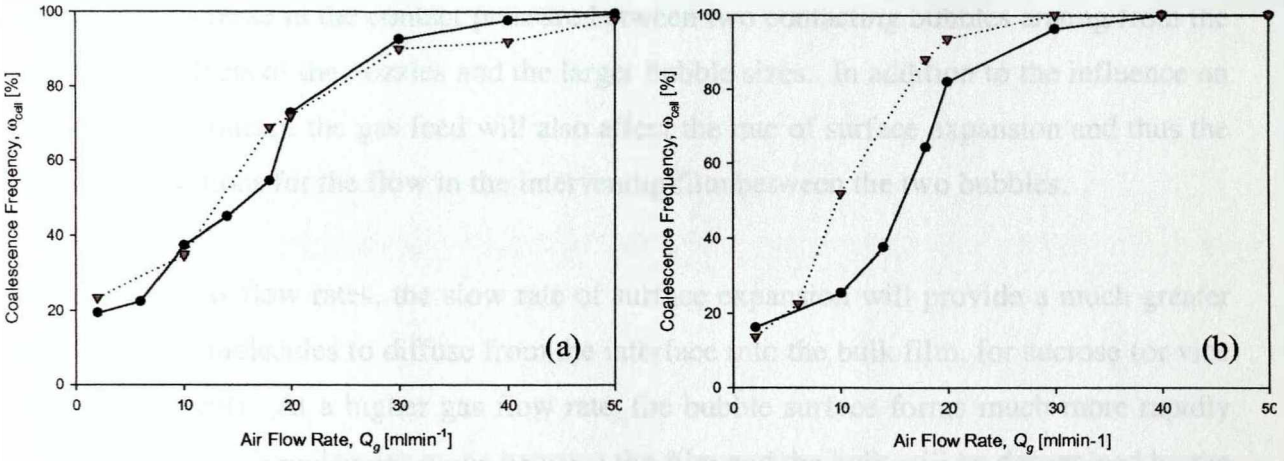

Figure 6.5

Comparing the effect of viscosity for solutions of (a) glycerol; —●— 1.6 M and —▼— 5 M and (b) sucrose; —■— 0.5 M and —▼— 1.2 M. For both air flow range Q_g = 2 - 50 mlmin^{-1} and nozzle separation 4 mm.

There are a number of possible explanations for the results obtained in these initial experiments. It may be that it is the increase in the solute concentration, rather than viscosity, which is the dominant feature in these systems. Certainly the non-coalescing behaviour of the solutions at low flow rates may be due to coalescence repression as a consequence of the presence of solute (as in electrolyte concentrations beyond the 'transition' value). The concentrations of sucrose solutions here are beyond the 'transition' value determined by Craig et al. (1993) which suggests a definite influence of concentration. However, the very similar responses for the two different glycerol concentrations suggest this is not the complete explanation. Alternatively, it may be that these solutions of relatively low viscosity, rates of film thinning are not significantly reduced, such that drainage times are still much smaller than the period for which two bubbles remain in contact. This would tend to suggest the

systems should exhibit full coalescence at the lowest flow rate (where contact times are longest), which is not observed. Finally, it may be that the effects of increased viscosity (and possibly slower film thinning rates) are of secondary importance in comparison to the effects of increasing gas flow rate (increased contact pressure).

Recalling the influences of increasing gas flow rate on bubble contact and coalescence in the cell (as outlined in Table 5.5), it can be seen that there are several (often counteracting) factors which must be taken into consideration. In terms of bubble-bubble contacts, increasing the gas flow rate will result in shortened contact times due to the greater bubble frequency, thus limiting the time available for the film to thin to the point of rupture. Opposing this tendency to reduce the coalescence frequency, however, will also be a concomitant increase in the contact pressure between two contacting bubbles arising from the constraining effects of the nozzles and the larger bubble sizes. In addition to the influence on bubble-bubble contact, the gas feed will also affect the rate of surface expansion and thus the boundary conditions for the flow in the intervening film between the two bubbles.

At the lowest gas flow rates, the slow rate of surface expansion will provide a much greater opportunity for molecules to diffuse from the interface into the bulk film, for sucrose (or vice versa for glycerol). At a higher gas flow rate, the bubble surface forms much more rapidly and the rate at which molecules move between the film and the bulk will be determined by the diffusion constant, D. As expected from the differences in molecular size, the diffusion coefficient for glycerol in water ($D_{Gly} = 1.06*10^{-5}$ cm^2s^{-1}[+]) is much larger than the equivalent value for sucrose ($D_{Suc} = 0.52*10^{-5}$ cm^2s^{-1}[+]). Consequently, a longer time will be required for sucrose molecules to diffuse from the interface into the bulk film (as preferred) and the interface will require longer to reach the equilibrium value. The effect will be exaggerated as the rate of surface expansion increases (i.e. with increasing gas flow rate), such that at high gas flow rates, the surface tension may be expected to be quite different from the equilibrium values, perhaps leading to the increased coalescence frequencies measured. However, as shown in Figure 6.7, the difference in surface tension with bubble lifetime is not greater than 1 mNm^{-1}, and for lifetimes greater than ~100 ms (corresponding to flow rates less than ~30 $mlmin^{-1}$) the dynamic surface tension becomes essentially constant.

[+] Data from Handbook of Chemistry and Physics, 74th Edition, Ed: Lide, D.

[+] Data from Handbook of Chemistry and Physics, 74th Edition, Ed: Lide, D.

In contrast, if significant surface tension gradients are established at the boundaries of the film, thus slowing the rate of thinning, replenishment will be slower in sucrose solutions. As a consequence of the smaller diffusion gradients, more time will be required for sucrose molecules to move from the interface into the bulk, in order to relieve the gradients formed and thereby allow the rate of thinning to increase. In this instance, the coalescence frequencies measured in sucrose solution would be expected to be lower than equivalent values measured in glycerol solution, although this is not observed.

Whilst it is not possible to determine unequivocally the cause for the increase in coalescence frequencies with gas flow, it is likely that this can be attributed primarily to two interacting effects; the more rapid rate of surface expansion (and diffusion limited interfacial effects) and the increased contact pressure between the bubbles which accelerates the film thinning process.

6.3.2 Modifying Viscosity through Temperature

In addition to preparing solutions with differing solute concentration, the continuous phase viscosity was further modified by carrying out experiments at three different temperatures; 15°C, 25°C ('standard') and 50°C. This aspect of the study was developed following a set of experiments investigating the effect of temperature on the coalescence behaviour of solutions of polypropylene glycol (PPG, see Appendix E). Although in these experiments changes in temperature were used primarily to alter liquid viscosity, the work in Appendix E suggests that this is not the only effect. In addition to viscosity, changing the system temperature may be expected to affect surface tension values. At each temperature, measured values (shown in Table 6.2) are very close and the overall change from 15°C to 50°C is within ± 8 mNm^{-1} (the

Solution (Conc^{n}, [M]	Viscosity at 15°C, μ_{15} [mPas]	Surface Tension, σ_{15} [mNm^{-1}]	Viscosity at 25°C, μ_{25} [mPas]	Surface Tension, σ_{25} [mNm^{-1}]	Viscosity at 50°C, μ_{50} [mPas]	Surface Tension, σ_{50} [mNm^{-1}]
Glycerol (1.6)	3.3	72.78	2.5	72.61	1.6	68.07
Glycerol (5)	7.6	72.20	5.8	71.02	1.8	66.09
Sucrose (0.5)	4.2	74.05	2.7	72.83	1.7	67.60
Sucrose (1.2)	7.6	75.92	5.7	73.38	2.2	69.23

Table 6.2

Viscosity and surface tension data for solutions of glycerol and sucrose at temperatures 15°C, 25°C and 50°C.

effect of temperature on water is similar, σ_{15} = 73.5 mNm^{-1}, σ_{25} = 72.05 mNm^{-1}, σ_{50} = 67.9 mNm^{-1}). Measurement techniques are described in Chapter 3.

The coalescence frequencies measured in each of the four solutions are presented in Figure 6.6 as a function of the air flow rate for each of the three different temperatures. In all cases, there is a general increase in the coalescence frequency measured for a specific flow rate as the temperature increases, with the 1.6 M glycerol solution in particular, being fully coalescent over the entire flow range at 50°C. For those solutions which are initially non-coalescing at the lower flow rates, there is a consistent increase in coalescence frequency with air flow rate, as observed previously.

In solutions of 1.6 M glycerol the coalescence frequencies measured at 25°C are slightly higher than equivalent value measured at 10°C (μ_{15} = 3.3 mPas), over most of the flow rate range. Given that similar responses were observed for the 5 M solution at 25 °C (where the difference in viscosity was greater), it seems unlikely that the effect is due solely to viscous influences. Likewise the full coalescence observed in 1.6 M at 50°C, but not in 5 M solution at the same temperature, is unlikely to be the result of viscous influence, as both solutions have very similar viscosities ($\mu_{1.6}$ = 1.6 mPas and $\mu_{5.0}$ = 1.8 mPas). In the 5 M solution, the coalescence frequencies observed at 10°C (μ_{15} = 7.6 mPas) are once again lower than equivalent values at 25°C, except at the very highest flow rates, where they are essentially identical.

The responses of both the 0.5 M and 1.2 M sucrose solutions at 10°C and 25°C are very similar over much of the flow rate range, although the move towards full coalescence occurs at slightly lower flow rates in the higher viscosity solutions. Indeed it is noticeable that full coalescence is never completely achieved in 0.5 M solution at 10°C. Increasing the temperature to 50°C, does not result in the full coalescence across the entire flow range as seen for solutions of glycerol (despite the similar viscosities for 0.5 M sucrose solution), although the coalescence frequencies are much higher than equivalent values at either 10°C or 25°C. In addition, full coalescence is achieved at lower flow rates (~ 20 mlmin^{-1}) than for either solution at the lower temperatures.

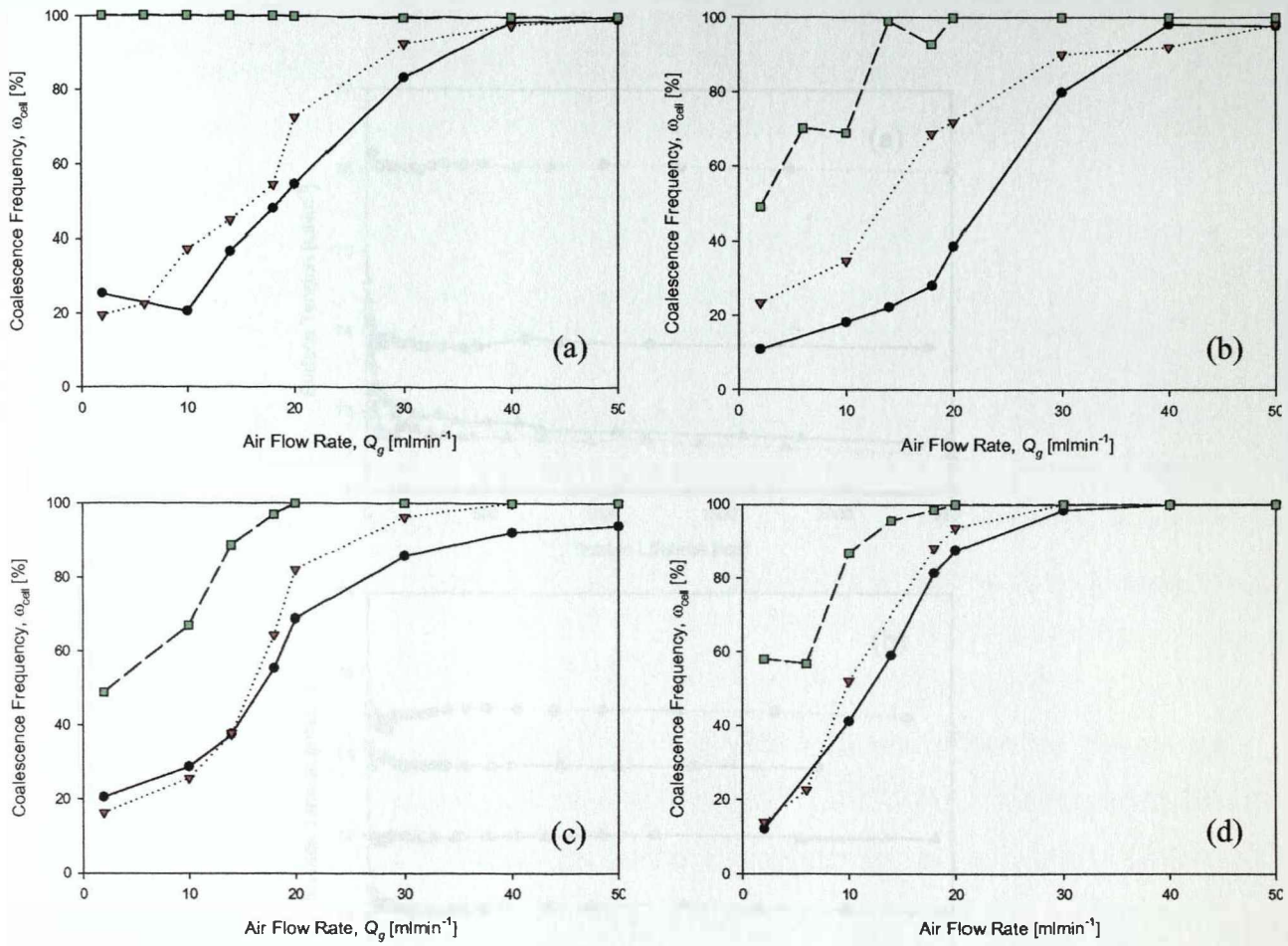

Figure 6.6

Effect of temperature on coalescence frequency over air flow rate 2 to 50 mlmin^{-1} for solutions of (a) 1.6 M, (b) 5 M glycerol and (c) 0.5 M and (d) 1.2 M sucrose solutions. For all, —●— T = 10°C, ···▼··· T = 25 °C and —□— T = 50°C. Nozzle separation 4 mm.

Despite the marked increases in coalescence frequency observed with increasing temperature, it is not possible to attribute the behaviour solely to a reduction of viscosity and enhanced rate of film thinning. Quite different behaviour is observed for solutions with similar viscosity (1.6 M and 5 M glycerol and 0.5 M sucrose solution, all at 50°C, for example) which suggests that there are other factors influencing the coalescence process. In addition to the effects of gas flow rate previously considered, the effects of temperature must now also be examined; factors which may be considered to affect the nature of the gas-liquid interface and hence impact on coalescence are summarised in Table 6.3. As well as the effects on viscosity, interfacial phenomena such as surface tension and surface excess will be affected, as will the rate of solute diffusion. Although dependent on molecular size, the diffusivity of a solute is also directly proportional to the system temperature. Consequently, increasing the system temperature should also increase the rate at which molecules can move between the gas-liquid interface and the bulk. If the interface has become immobilised through the formation of

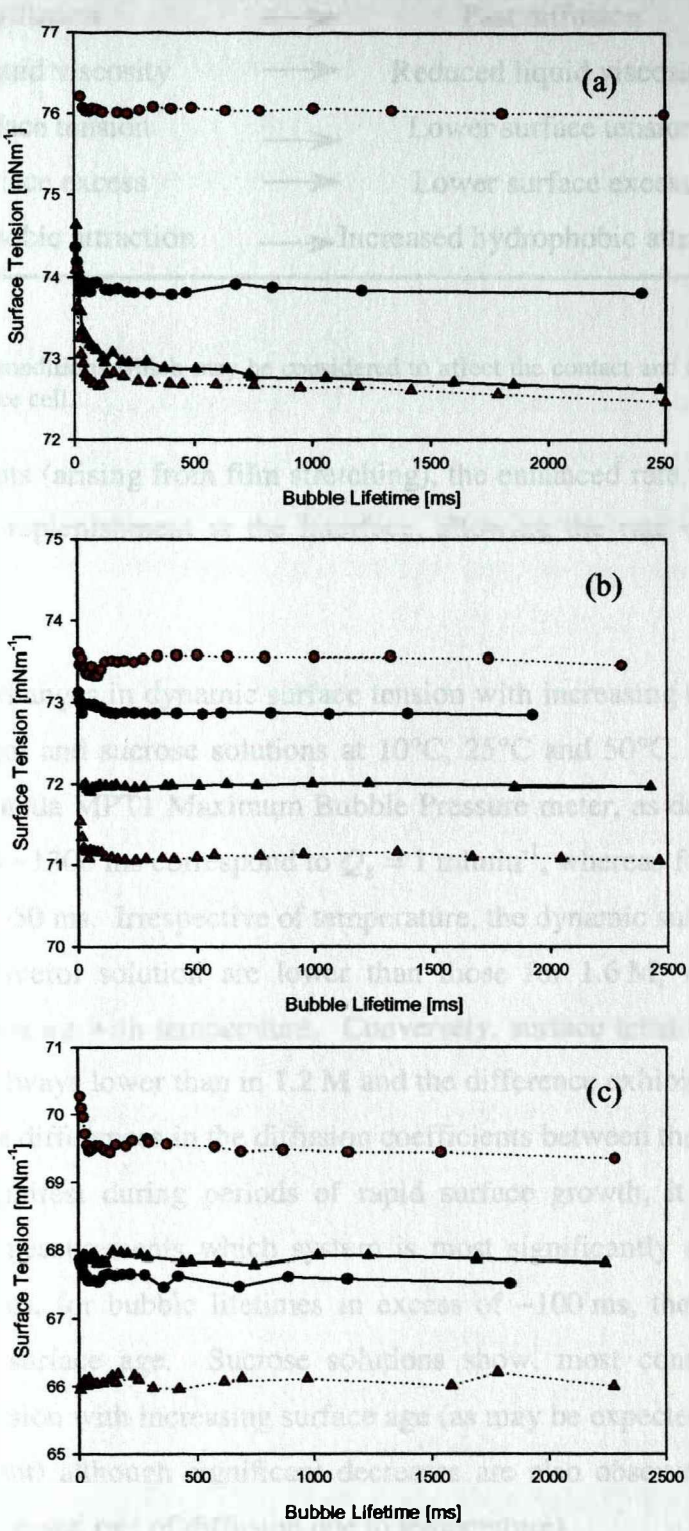

Figure 6.7

Changes in dynamic surface tension with bubble lifetime over the three temperatures (a) 15°C, (b) 25°C and (c) 50°C for 0.5 M sucrose —●— , 1.2 M sucrose ···●··· , 1.6 M glycerol —▲— and 5 M glycerol ···▲··· solutions. Measurements were made using the Lauda MPT1 Maximum Bubble Pressure meter, as outlined in Chapter 3.

LOW TEMPERATURE	⟶	*HIGH TEMPERATURE*
Slow diffusion	→	Fast diffusion
Increased liquid viscosity	→	Reduced liquid viscosity
Higher surface tension	→	Lower surface tension
Higher surface excess	→	Lower surface excess
Small hydrophobic attraction	→	Increased hydrophobic attraction

Table 6.3

Effects of temperature on conditions which may be considered to affect the contact and coalescence behaviour of bubbles in the coalescence cell.

surface tension gradients (arising from film stretching), the enhanced rate of diffusion should allow for more rapid replenishment at the interface, allowing the rate of film thinning to increase.

Figure 6.7 shows the changes in dynamic surface tension with increasing bubble lifetime, for the two sets of glycerol and sucrose solutions at 10°C, 25°C and 50°C. All measurements were made with the Lauda MPT1 Maximum Bubble Pressure meter, as described in Chapter 3. Bubble lifetimes of ~1300 ms correspond to Q_g = 1 mlmin^{-1}, whereas for Q_g = 50 mlmin^{-1}, the bubble lifetime is ~50 ms. Irrespective of temperature, the dynamic surface tension values measured for 5 M glycerol solution are lower than those for 1.6 M, with the difference between the two increasing with temperature. Conversely, surface tension values for 0.5 M sucrose solutions are always lower than in 1.2 M and the difference exhibits little temperature dependence. Although differences in the diffusion coefficients between the two solutes would be expected to be manifest during periods of rapid surface growth, it is not possible to conclude from these measurements which system is most significantly affected by surface expansion. In all cases, for bubble lifetimes in excess of ~100 ms, there is no change in surface tension with surface age. Sucrose solutions show, most consistently, the rapid decrease in surface tension with increasing surface age (as may be expected from the value of the diffusion coefficient) although significant decreases are also observed in both glycerol solutions at 10°C (decreased rate of diffusion due to temperature).

Also summarised in Table 6.3 is the effect of temperature on the hydrophobic attraction. The decrease in hydrophobic attraction between bubbles in concentrated electrolyte solution was proposed by Craig et al. (1993) as a possible explanation for the repression of coalescence in

such systems. Ruckenstein (1997) reports a threefold increase in the hydrophobic force measured in air-water systems as the temperature is increased from 20°C to 40 °C, which would suggest coalescence is promoted at higher temperatures. Although no studies exist at present which have made a substantial link between bubble coalescence and the decrease in hydrophobic attraction in the presence of significant amounts of electrolytes, it remains an intriguing possibility.

From these initial experiments although it can be concluded that viscosity does have some effect on coalescence, it is difficult to ascribe the definite area of influence due to the many interacting factors which also impact upon the coalescence process. Likewise, although differences can be observed between the behaviour of solutions of glycerol and sucrose, correlating these differences with definite explanations is not possible from this study.

6.4 Experiments With Glycerol Solutions

Following the results of initial experiments, it was decided to investigate coalescence behaviour over a much wider range of viscosities, in an attempt to determine clearly the effect of viscosity. The range of viscosities was provided by using glycerol solutions of concentration from 0.02 M to 12.0 M (viscosity range from ~ 1 to ~ 160 mPas), which requires the results to be interpreted considering the combined influences of both solute concentration and viscosity. Attempts to use a range of hydrocarbons to provide pure liquids of varying viscosity were abandoned when it became obvious they were incompatible with the construction materials of the coalescence cell.

6.4.1 Modifying Viscosity through Glycerol Concentration

In Figure 6.8, the coalescence frequencies are presented as a function of glycerol concentration (and also on the secondary x-axis as a function of solution viscosity) for a range of air flow rates. At a gas flow rate ~ 1 mlmin^{-1} (conditions equivalent to those investigated by Zahradnik et al. (1987), i.e. horizontally opposing nozzles, at a separation of 3.5 mm and bubbling frequency of 45 min^{-1}) there is a step decrease in coalescence frequency at glycerol concentration ~ 1.3 M (corresponding to viscosity 1.3 mPas). This is much smaller than the critical viscosity value reported by Zahradnik et al. (1987) (μ = 3.4 mPas) and in contrast with that study, this work finds no return to full coalescence as solution viscosity increases. There is however a gradual increase in the coalescence frequency as the solution concentration (and

viscosity) increases, although this does not rise above ~ 20%. As the gas flow rate is increased to ~ 2 mlmin^{-1}, the step decrease in coalescence frequency is seen to reduce in magnitude and is followed by a more rapid recovery towards full coalescence with increasing solution viscosity. This trend is continued as the gas flow rates increase, until by 30 mlmin^{-1}, there is only a slight drop in the coalescence frequency and solutions are essentially fully coalescing over the concentration range.

The significant decrease in coalescence frequencies observed consistently at all but the highest gas flow rates, is quite remarkable, especially recalling the experimental error inherent in this system (± 15 % for flow rates between ~10 and 50 mlmin^{-1} and increasing to ± 30 % for flow rates below 12 mlmin^{-1}). The low viscosity of this 'transition' solution precludes considerations of viscous effects and suggests that the effect is primarily the result of solute concentration. Whether the 'transition' arises as a result of surface tension gradients which act to immobilise the gas-liquid interface and thus prevent the rapid film thinning required for coalescence, as commonly considered for electrolyte solutions, cannot be concluded from this study.

The increase in coalescence frequency observed for the intermediate flow rates in the higher viscosity solutions is surprising, despite the similar observations made by Zahradnik et al., 1987. Considerations of film thinning theory all predict the increased liquid viscosity will reduce the rate of thinning. Under the experimental geometry used in this study, wake assisted coalescence was not observed, although it may be that increasing the liquid viscosity

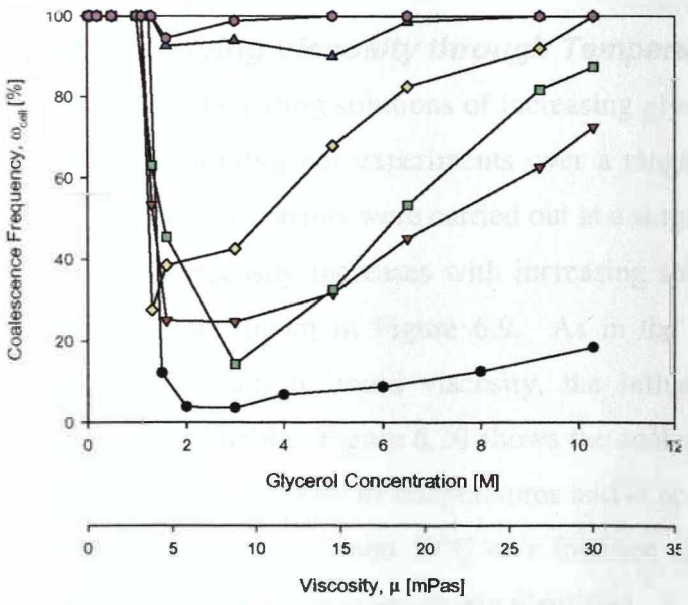

Figure 6.8

Effect of air flow rate on coalescence frequency for glycerol solutions. ● Q_g = 1 mlmin^{-1}, ▼ Q_g = 2 mlmin^{-1}, □ Q_g = 6 mlmin^{-1}, ◇ Q_g = 10 mlmin^{-1}, ▲ Q_g = 30 mlmin^{-1} and ● Q_g = 50 mlmin^{-1}. Nozzle separation 4 mm.

extended contact times for the contacting bubbles as a result of increased drag forces. At a flow rate of 1 mlmin^{-1}, high speed video of bubbles formed in concentrations beyond ~ 4 M show them to be much more rigid and resistant to deformation upon contact, than those formed in lower concentration solutions. It may be then, that there is a reduction in the area of the film between two bubbles contacting in the more viscous solutions, thereby decreasing the thinning time required. Alternatively, the increased viscosity may promote dimple formation at the point of contact, which would lead to an enhanced rate of thinning as film drainage can occur in two direction simultaneously, thus enhancing coalescence. The formation of a dimple between two contacting bubbles was first identified by Allan et al. (1961) for coalescence of a gas bubble with an interface. Even in their studies of nitrogen bubbles in glycerol solutions however, the rate of film thinning was observed to increase with decreasing film viscosity, in line with predictions from the film thinning models considered previously.

Literature evidence for enhanced coalescence in concentrated mixtures of glycerol and water generally relies on the promotion of bubble-bubble contacts through wake capture of a trailing bubble by a leading one. In contrast to this approach, Andrews, 1960 developed a method to predict the frothing ability of two-component mixtures, based on the difference in surface tension between the two constituents, $\Delta\sigma$. The non-frothing behaviour observed for mixtures of glycerol and water was ascribed to the low $\Delta\sigma$ value (9 mNm^{-1}) for this system. However, as the experiments were carried out in a simple bubble column, it is probable that there was also a significant influence of wake assisted coalescence.

6.4.2 Modifying Viscosity through Temperature

In addition to preparing solutions of increasing glycerol concentration, the viscosity was also adjusted by carrying out experiments over a range of temperatures: 10°C, 25°C, 50°C and 75°C. These experiments were carried out at a single flow rate, Q_g = 1 mlmin^{-1}. As expected, the solution viscosity increases with increasing solute concentration and decreasing system temperature, as shown in Figure 6.9. As in the previous set of experiments which used temperature to adjust liquid viscosity, the influence of a number of other factors was considered inevitable. Figure 6.10 shows the coalescence frequency as a function of glycerol concentration for a range of temperatures and is accompanied by Figure 6.11 which presents the data for 10°C, 25°C and 50°C as a function of bubble Reynolds number, to enable the effects of viscosity to be more clearly identified.

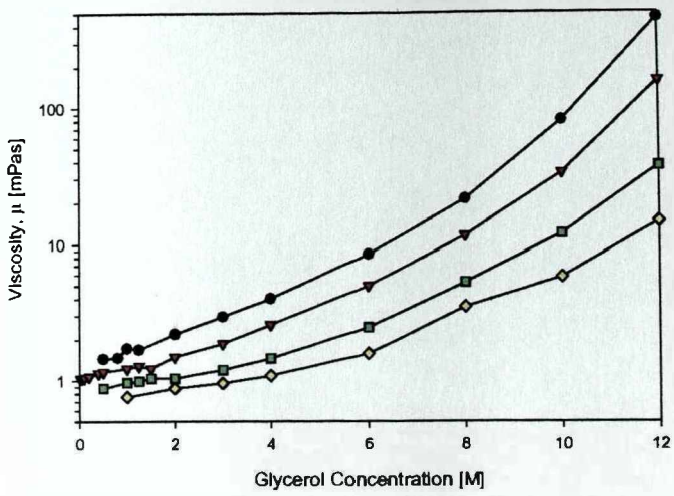

Figure 6.9

Change in viscosity with temperature for range of glycerol concentrations used in this work. ●— T = 10 C, ▼— T = 25 C, □— T = 50 C, ◇— T = 75 C. All measurements as outlined in Chapter 3.

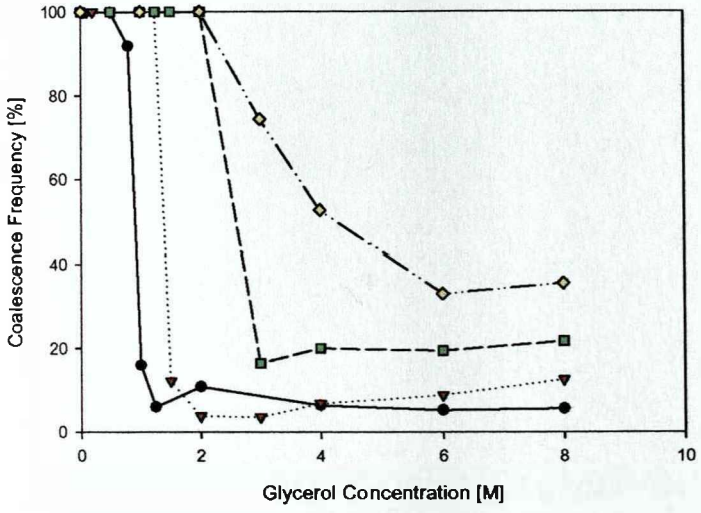

Figure 6.10

Effect of temperature on the 'transition' concentration for glycerol. ●— T = 10 C, ▼— T = 25 C, □— T = 50 C, ◇— T = 75 C. Q_g = 1 mlmin^{-1}, nozzle separation 4 mm.

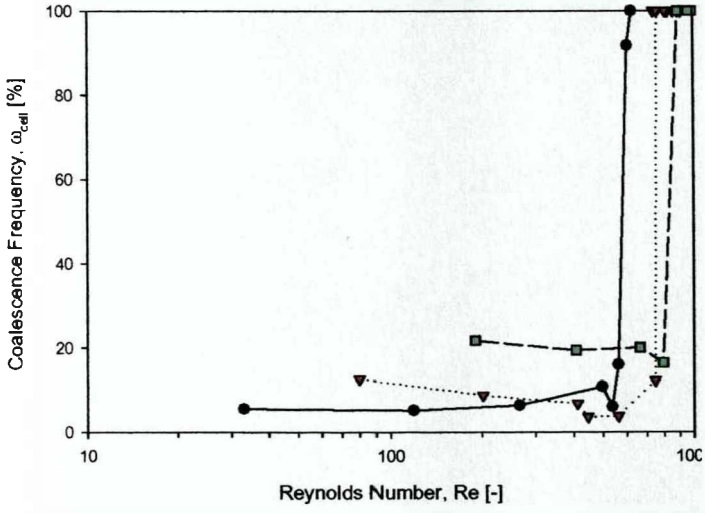

Figure 6.11

Coalescence frequency presented as function of Reynolds number for glycerol. ●— T = 10 C, ▼— T = 25 C and □— T = 50 C. Q_g = 1 mlmin^{-1}, nozzle separation 4 mm.

The bubble Reynolds number was defined as:

$$\mathrm{Re}_b = \frac{\rho U_b D_b}{\mu} \qquad (6.1)$$

where ρ is the liquid density (determined using a density bottle as described in Chapter 3); U_b is the bubble rise velocity, determined from high speed video studies; D_b is the diameter of a bubble formed at the nozzle (also measured from the high-speed video images) and μ is the liquid viscosity, measured from the graph in Figure 6.9.

As can be seen clearly from Figure 6.10, the concentration at which the system switches from being fully coalescing to coalescence repressed is different at each of the four temperatures investigated. This 'transition' concentration increases with temperature, as does the degree of coalescence following the step change, such that at 75°C, the decrease in viscosity is much more gradual than at 10°C.

Is this change in 'transition' concentration with temperature solely due to the reduced liquid viscosity (and subsequently an enhanced rate of film drainage)? When the data is re-presented in terms of Reynolds number (Figure 6.11), it can be seen in fact, that the 'transition' occurs over a range of viscosities, which suggests the influence of additional factors. In fact, the 'transition' for 50°C can be seen to occur at a lower viscosity (higher Reynolds number), than that at 10°C. As the 'transition' concentration is higher at 50°C than 10°C, this suggests that the reduction in coalescence frequency arises from a combined viscosity and concentration effect. Although liquid viscosity controls that nature of the flow within the film, the nature of the gas-liquid interface (which provide the boundaries of the film) will be influenced primarily by the number (and type) of solute molecules adsorbed and consequently the influence of concentration is not unexpected. From Figure 6.11, it would appear that in this system, solute concentration and the subsequent changes at the bubble surface, are the dominant influences on coalescence.

6.4.3 High Speed Studies

To provide a greater level of detail about the coalescence process, the high-speed video camera was used to measure coalescence (and contact) times for bubbles formed at a gas flow rate of ~1 $\mathrm{mlmin^{-1}}$ in solutions from 0.02M to 8.0M for three temperatures 10°C, 25°C and 50°C. Once again, coalescence rates have been calculated for each set of data to compensate for the differences in film area between contacting bubbles. In addition, to

Conc^{n} (10°C) [M]	Re [-]	Conc^{n} (25°C) [M]	Re [-]	Conc^{n} (50°C) [M]	Re [-]
0.5	629	0.02	912	0.5	1081
0.8	608	0.05	891	1.0	990
1.0	562	0.1	862	1.25	964
1.25	537	0.2	826	1.5	898
2.0	497	0.5	812	2.0	891
4.0	266	1.0	787	3.0	793
6.0	119	1.25	772	4.0	664
8.0	33	1.5	718	6.0	408
		2.0	562	8.0	191
		3.0	446		
		4.0	412		
		6.0	202		
		8.0	80		

Table 6.3

Bubble Reynolds numbers for glycerol solutions used at the three temperatures.

enable the effect of viscosity to be determined, measurements of bubble rise velocity and diameter were also made for use in calculating the Reynolds number. Data for each of the solutions at the three temperatures is summarised in Table 6.3. As can be seen, Reynolds number varies inversely with solution concentration, as a consequence of the associated increase in viscosity. The Reynolds numbers for solutions at 10°C are much smaller than those for equivalent solutions at 50°C, due to the substantial decrease in viscosity at the higher temperatures.

The surface oscillations which are such a predominant feature of air-water systems, leading to many broken and renewed contacts prior to coalescence, are not generally observed in glycerol solutions. Only in 0.8 M glycerol solution at 10°C were the surface oscillations sufficiently pronounced to result in a large number of renewed contacts, leading to significantly different coalescence times when measured from the initial and final contacts. For all other solutions of low viscosity (concentration), although the surface was occasionally seen to flex, this was to a much smaller degree and did not usually cause a complete break in the contact between two bubbles. For bubbles formed in solutions with viscosity in excess of

~ 4 mPas, the effects of surface oscillation were negligible, despite the slow rate of bubble growth. The lack of surface flexing was undoubtedly due to an increased rigidity of the bubble surfaces, which could be quite clearly seen. Presumably, this increased rigidity is due to the greater liquid viscosity which acts to damp out any flexing of the bubble surfaces, thus preventing surface oscillations. As a consequence of the more rigid surfaces, colliding bubbles showed almost no deformation upon contact and were instead, observed to slide over one another in a manner similar to that previously seen for bubbles in concentrated electrolyte solution.

In Figure 6.12, the mean coalescence times and coalescence rates are shown as a function of the system Reynolds number for 10°C, 25°C and 50°C. Once again, it was aimed to collect 25 measurements and data is not shown for conditions where it was not possible to obtain a minimum of 10 measurements. Measurements at all conditions show a considerable degree of scatter, as evidenced by the wide 95% confidence limits; this is especially true for measurements made in the higher viscosity solutions, approaching or just in excess of the 'transition' concentration. At the two highest temperatures, there is a sharp increase in the coalescence time with decreasing Reynolds number, for bubbles formed in solutions of concentration approaching the 'transition' value (as previously observed in solutions of sodium sulfate under similar conditions, Figure 5.14). The fully coalescing solutions measured at 25°C have viscosities approaching that of water and show coalescence times of a similar magnitude (< 5 ms).

The trend at 10°C is somewhat less well defined. There is a large degree of scatter in many of the measurements made under these conditions, but the pronounced increase observed at 25°C and 50°C is noticeably absent. Instead, at all but the highest Reynolds number, there appears to be a slight decrease with decreasing Reynolds number (and hence increasing concentration). The decrease is particularly pronounced for coalescence times measured in solutions with concentration in excess of the 'transition' value. Clearly, as these systems are coalescence repressed, coalescence events are not representative of the overall behaviour. Therefore, those contacts which result in coalescence will represent only the shortest times in the coalescence time distribution. (Measurements of longer coalescence times would not be possible in this system, as the continuous gas flow will result in bubbles rising and separate following a discrete contact time.) However, at 10°C the glycerol concentration in the non-

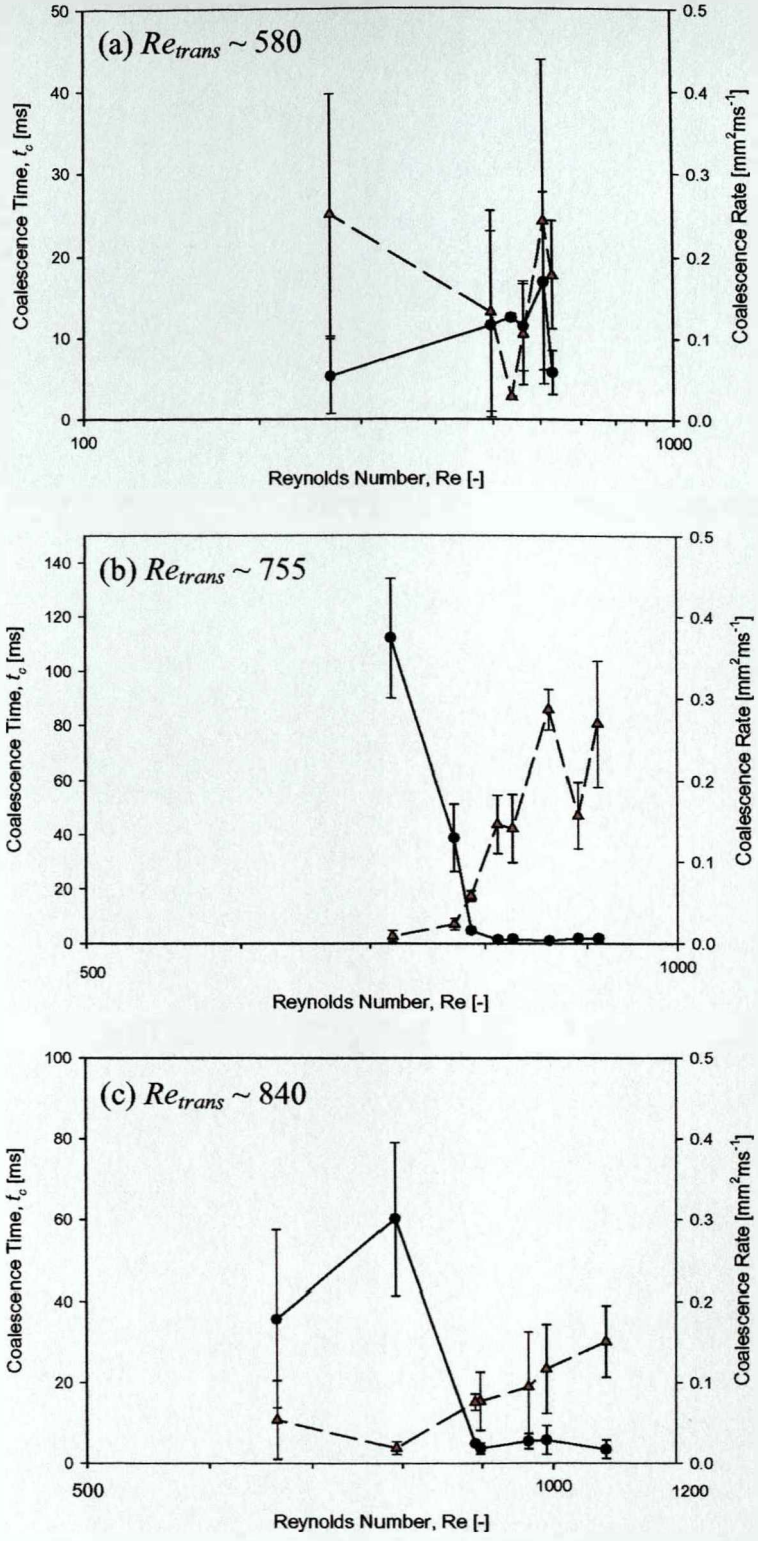

Figure 6.12

Mean coalescence times, ⊸● and coalescence rates, ▽ measured at (a) 10°C, (b) 25°C and (c) 50°C for solutions of glycerol. Error bars give 95% confidence limits. Re_{trans} is Reynolds number of the 'transition' concentration solution. Note that graphs are not directly comparable, as scales have been chosen to enable data to be displayed most clearly.

coalescing solutions is lower than in solutions which exhibit similar behaviour at the higher temperatures. Therefore the seemingly contrary trend may reflect the lower solute concentration present in these systems and consequently a decreased contribution to the mechanism of coalescence repression.

Measurements of the overall coalescence times do not account for any differences in the film area between various events; rather this can be done by determining the 'coalescence rate'. As all experiments were carried out at the same low air flow rate, the pronounced increases in contact area typically seen at the higher gas flow rates are not observed, although variations from event to event occur, arising from factors such as synchronisation and bubble rigidity. Once again, the trends observed at 25°C and 50°C are similar. Associated with the large increase in the overall coalescence time with decreasing Reynolds number (corresponding to increasing solution viscosity), there is a sharp decrease in the 'coalescence rate'. This decrease may be considered to arise from a reduction in the rate of film thinning due to increased liquid viscosities. However, when it is considered that the 'transition' viscosities measured at 25°C (~1.3mPas) and 50°C (~1.2 mPas) are not significantly greater than that of water (~1.3 mPas), a reduction in film thinning entirely due to viscous influences becomes most unlikely. Rather the synergistic effects of increasing solute concentration must also be considered.

As for the measured coalescence times, the coalescence rates calculated for solutions at 10°C appear to follow a reverse trend to those seen at the higher temperatures. As there was a slight decrease in overall coalescence time with decreasing Reynolds number (i.e. increasing solution concentration and viscosity), the coalescence rate shows a related overall increase. How could an increase in liquid viscosity result in an increase in the rate of thinning? To answer this, the dominant influence on the rate of film drainage must be determined: is it liquid viscosity or solute concentration? As can be seen from Figures 6.10 and 6.11, the 'transition' at 10°C actually occurs at a higher viscosity (compared to that at 50°C), but at a lower concentration (~0.9 M glycerol). Due to the lower solute concentration, the film thinning process is not impeded to the same extent, perhaps as a result of the diminished numbers of solute molecules at the interface. Together with the significant increases observed at 25°C and 50°C, for solutions with viscosity approaching ~1mPas, this suggests that coalescence repression in these systems is largely a concentration dependent effect. However,

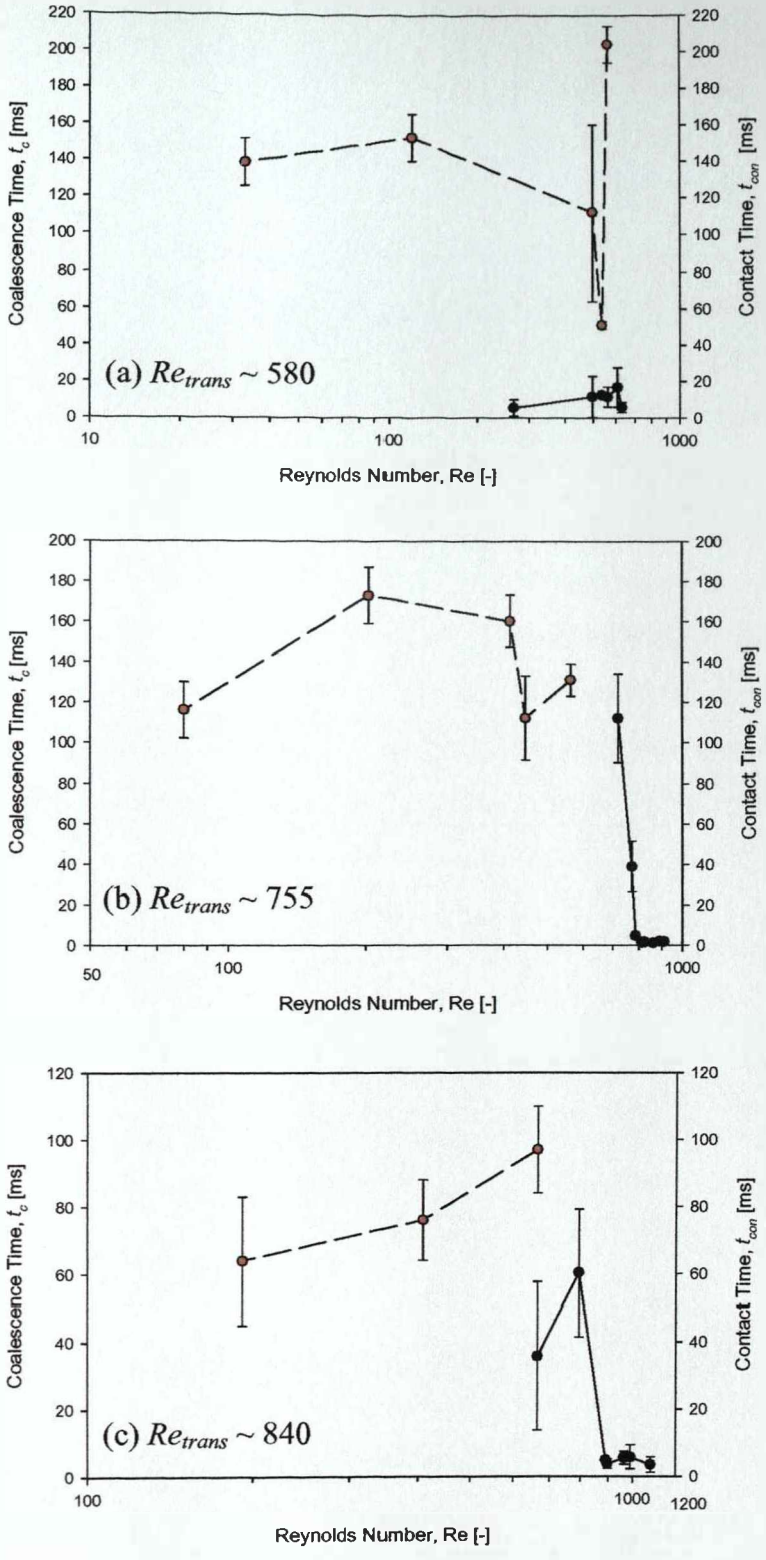

Figure 6.13

Mean coalescence times, —●— and contact times (for events where no coalescence was observed), ▼ measured at (a) 10°C, (b) 25°C and (c) 50°C for solutions of glycerol. Error bars give 95% confidence limits. Re_{trans} is Reynolds number of the 'transition' concentration solution. Note that graphs are not directly comparable, as scales have been chosen to enable data to be displayed most clearly.

it is not clear why, if solute concentration is the predominant influence, the 'transition' at 10°C does not occur at a higher value.

In Figure 6.13, the mean coalescence times and contact times are shown as functions of the system Reynolds number. The contact times represent the mean of ten non-coalescence events and can be used to provide an indication of the duration of a typical contact (irrespective of the degree of synchronisation). Between the two sets of values, the entire range of experimental observations can be represented. The data measured at 25°C appears to support the general maxim that two bubbles will coalesce provided they remain in contact for sufficiently long for the film to drain to the point of rupture. Following the very large increase in coalescence times measured in 1.25 M and 1.5 M solution, the contact times recorded in more concentrated solutions are of a similar magnitude. Provided coalescence times in these more concentrated solutions are at least as long as those measured in solutions approaching the 'transition' value, two bubbles will separate before coalescence can occur. Hence, a diminished number of coalescence events will be observed in these systems. A similar approach can be considered for the data recorded at 50°C; although there is a greater difference between the two sets of values, moderate increases in the coalescence times for contacting bubbles in solution concentrations in excess of the 'transition' value would approach the values measured for contact times.

In contrast, data recorded at 10°C does not appear to support this approach. Rather, as previously observed in electrolyte solutions, there is a very large difference between contact and coalescence times, which appears to suggest that coalescence is not necessarily the outcome of sufficiently long contact times. The existence of two very separate populations may suggest that if coalescence does not occur within a specified time, it will not occur. In terms of film drainage this could be envisaged as the formation of a 'meta-stable' film which oscillates in thickness and does not proceed to drain continuously to the rupture thickness.

In literature studies, this discrepancy between coalescence and contact times has not been previously observed. This may be because of the nature of the apparatus, or because of the focus of the study. The first category includes studies by Farooq (1972), Lee and Hodgson (1968), Allan et al. (1961) which involved observing the time required for bubbles to coalesce with a gas-liquid interface. In such systems, the contact time is much greater than in this system, such that bubbles still remain in contact until coalescence occurs. However, even in

such systems, results from this study tend to suggest that bi-modal coalescence time distributions should result; these are not reported in the literature. The second category includes coalescence time studies carried out in two-bubble apparatus, such as used in this work. Sagert and Quinn (1978, 1976a, b) report coalescence times measured a two-bubble coalescence cell, but although results are presented as the mean of approximately 25 measurements, no mention is made of whether these events are representative of the overall system behaviour (i.e. coalescing or coalescence repressed). No measurements are made of contact times for non-coalescence events.

6.5 Conclusions

- Coalescence behaviour has been investigated in 3 mPas silicone fluid to assess the effect of a small increase in viscosity on coalescence. Although a pure liquid, it is a coalescence repressed system with non-synchronised bubbling, even at the highest gas flow rates which were required to produce bubbles large enough to contact at the smallest nozzle separation of 4 mm.

  Coalescence times have been measured using a high-speed video camera. Values are significantly greater than equivalent values measured in water, although the coalescence times distributions are much narrower than those observed in water. This is surprising, given the models in the literature (Chesters, 1991, Reynolds, 1886 amongst others) predict that film thinning rates are inversely proportional to liquid viscosity, such that coalescence times increase with increasing viscosity.

  As in electrolyte solutions, contact times, measured for contacting but non-coalescing events are seen to be significantly greater than coalescence times measured under the same conditions.

- Experiments have been carried out in two equal viscosity (2.6 mPas and 5.8 mPas) solutions of sucrose and glycerol to further investigate the effects of viscosity on coalescence behaviour and also to provide information about the effects of molecular structure on the coalescence process.

  Despite interfacial differences, which could be expected to arise as a result of structural differences, solutions of the same viscosity showed similar behaviour over the gas flow rate range 1 to 50 $mlmin^{-1}$.

  Increasing the viscosity in glycerol solution had very little effect on the coalescence cell profiles observed. Greater differences were observed in solutions of sucrose, although

once again, the trend did not correlate with the predicted effect of viscosity, perhaps as a result of the greater influence of solute concentration on interfacial behaviour.

Investigations carried out over a range of temperatures, showed a definite increase in coalescence frequency with increasing temperature for a given flow rate. Although this corresponds with decrease in liquid viscosity, it is likely that there are a number of interacting influences which contribute, primarily those which would affect the nature of the gas-liquid interface (such as solute diffusivity and dynamic surface tension).

- The coalescence behaviour has been investigated for solutions of glycerol, from 0.02 M to 12 M (viscosity range ~1 ~ 160 mPas), over a range of temperatures.

  At 25°C, for a gas flow rate of 1 $mlmin^{-1}$ and nozzle separation of 4 mm, there is a 'transition' concentration at 1.3 M, which is accompanied by/precipitated by a simultaneous loss in synchrony as seen in all solutions. This cannot be due to the influence of viscosity, as values at this concentration are not significantly different from those in water (~1 – 1.3 M) and consequently the coalescence repression must arise from the influence of solute molecules at the interface.

  With a progressive increase in gas flow there is a decrease in the magnitude of the step change observed at glycerol concentration 1.3 M, such that at the higher gas flow rates (> 30 $mlmin^{-1}$) systems are essentially fully coalescing over the entire concentration range.

  At flow rates in excess of 1 $mlmin^{-1}$, there is an observed increase in the coalescence frequency as the solution viscosity (and concentration) increases. This is contrary to all expectations from models discussed in the literature. Explanations based on improved conditions for wake capture must be discounted on the basis of experimental geometry.

- In glycerol solutions, the 'transition' concentration observed at a gas flow rate 1 $mlmin^{-1}$ and nozzle spacing of 4 mm can be shifted from ~ 1 M to ~ 4.5 M by increasing the temperature of the solution from 10°C to 75°C.

  Graphs of coalescence frequency against bubble Reynolds number show that the shift in 'transition' concentration does not occur at a specific Reynolds value and that the effect is more dependent on solute concentration.

- Coalescence time measurements have been made for bubbles in glycerol solutions of concentration 0.02 M to 8 M, at three temperatures (10°C, 25°C and 50°C).

  Measurements made at 25°C and 50°C show the same trend with coalescence time increasing (coalescence rate decreasing) for solution concentrations approaching the 'transition' value. At 10°C, the trend is much less distinct, with the pronounced

increase in coalescence time values being noticeably absent. This is attributed to the reduced solute concentration and consequently smaller influence on interfacial behaviour, at the lower temperature.

Contact times have been measured for non-coalescing events. Whilst those at 25°C and 50°C, approach the coalescence time values measured in the same systems, those observed at 10°C are significantly greater than equivalent coalescence time measurements.

Chapter 7
Coalescence in Bubble Columns

This chapter investigates bubble coalescence in small-scale bubble columns and attempts to link the behaviour observed in-situ with that observed in the controlled environment of the coalescence cell. At first coalescence is observed indirectly, through the use of bubble size distributions and average bubble sizes, in order to quantify the effects of initial bubble size, gas flow rate and liquid phase on bubble coalescence. This data is used to estimate the coalescence frequency for each system. Later, direct observations of bubble coalescence, made possible through the use of high-speed video, are discussed and attempts made to quantify the interactions observed. The results obtained provide insight into the behaviour of both coalescing and coalescence-inhibited systems as the method allows bubble-bubble interactions prior to and following on from coalescence, in addition to the coalescence events themselves to be monitored.

All experiments were carried out in the small bubble columns fitted with porous plate distributors described in Chapter 3. The degree of coalescence occurring within the column was determined by measuring bubble size distributions at the distributor plate and then following the change in size distribution over the height of the column. It is assumed that the generation of larger bubbles over the height of the column is solely due to bubble coalescence and not to any increase in size as a consequence of the decrease in hydrostatic pressure. Bubble size distributions were measured in water and sodium sulfate solutions and the results reported in section 7.1. Using mean bubble sizes and the method adapted from Howarth (1967), the coalescence frequencies for each of these systems are then compared in section 7.2. To investigate the effects of gas density experiments were carried out with magnesium sulfate solutions, the results of which are presented in section 7.3. Finally, direct observations of bubble coalescence in water and 0.06 M sodium sulfate are reported in section 7.6.

Experimental data in the following sections was analysed using mean bubble diameters and number and volume probability density and cumulative distribution functions, all of which were obtained using a program developed by Pacek et al. (1994). The probability and distribution functions provide details about the changes in the bubble size distributions with changing column height. The cumulative distribution functions have been used to present

most of the experimental results as they allow for clear comparisons between the behaviour of several distributions, although the probability density functions have been used when considering the details of the bubble distributions. A standard geometric series has been used to define the interval sizes for the distributions (with the value of the constant set at 1.22) and all graphs have been constructed using a logarithmic scale to represent the bubble diameters. These measures were taken on account of the very wide range of bubble sizes observed; in some experiments (especially those in water) the smallest and largest bubble diameters measured differed by almost two orders of magnitude.

To generate the number probability density function, $q(x)$, the number of bubbles in each interval is divided by the total number of bubbles and the interval width:

$$q(x) = \frac{\Delta n}{N} \frac{1}{\Delta x} \tag{7.1}$$

where Δn is the number of bubbles in the interval of width, Δx and N is the total number of bubbles in the distribution. Similarly, the volume probability distribution function is generated by dividing the volume of the bubbles over an interval by the total volume of all bubbles and the interval width.

Provided that the value of the interval is sufficiently small ($\Delta x \rightarrow 0$) then Δx can be replaced with dx and the number [volume] probability density function can then be integrated over the entire size range to give the cumulative number [volume] distribution function, $Q(x)$. The value of the integral is by definition 1 and it describes the number [volume] of all bubbles of size less than or equal to x:

$$Q(x) = \int_{x_{min}}^{x_{max}} q(x)dx \tag{7.2}$$

In addition to the frequency and cumulative distributions, bubble populations measured under different conditions can be compared by considering mean bubble diameters. Three different mean bubble diameters have been used in this work; the number length mean, the surface volume mean and the volume moment mean.

The arithmetic or number length mean diameter, d_{10} is weighted over the total number of bubbles in the sample, with equal contribution irrespective of bubble size:

$$d_{10} = \frac{\sum n_i d_i}{\sum n_i} \tag{7.3}$$

The surface volume or Sauter mean value is defined as the ratio of the third to the second moment of the probability density function:

$$d_{32} = \frac{\sum n_i d_i^3}{\sum n_i d_i^2} \tag{7.4}$$

It is commonly used to characterise gas-liquid (and liquid-liquid) dispersions as it links the interfacial area to the volume of the dispersed phase, making it especially useful in determining mass transfer phenomena. Sanchez (1996) has observed that in a coalescence dominated system, d_{32} increases monotonically with time as the generation of larger drops is accompanied by a decrease in interfacial area resulting from the consumption of smaller drops. As a consequence, the Sauter mean diameter is a good indicator of the degree of coalescence occurring in a system.

The volume moment mean diameter, d_{43} is based on the fourth to the third moment of the distribution and as such, is weighted towards the larger drop sizes in the sample:

$$d_{43} = \frac{\sum n_i d_i^4}{\sum n_i d_i^3} \tag{7.5}$$

As a result, in a coalescing system where larger bubbles are generated over the height of the column, the value of d_{43} would be expected to increase more quickly than either d_{10} or d_{32}.

7.1 Bubble Size Distributions

7.1.1 Air-Water Systems

Each set of data comprises of four measurements, made at intervals over the column height: at the distributor plate, 2 cm above, 10 cm above and 20 cm above (corresponding to 5 cm below the level of the unaerated liquid). Consequently, in a fully coalescing system such as water, the generation of larger bubbles over the height of the column would be expected to shift the distribution to the right. By measuring at four points over the height of the column, it was hoped to confirm the observations of Marrucci and Nicodemo (1967) who reported that coalescence occurred primarily in the zone adjacent to the distributor plate and to a much lesser extent in the remainder of the column. This would imply that the greatest changes in

the bubble size would be observed within the first two measuring points and (in the absence of significant bubble break-up) any further increase over the remainder of the column will occur to a much smaller extent.

7.1.1.1 Observations

The most noticeable aspect of bubbles is water is the very wide range of bubble sizes observed and which is seen to increase with the column height. At the distributor plate, the bubbles formed are approximately the same size, although very tiny bubbles can occasionally be observed, which do not appear to be generated at the sparger. Close to the top of the column, the average bubble size is seen to increase dramatically, such that it is not uncommon for bubbles to be too large to fit within the screen. However, very small bubbles persist even at this level (Figure 7.1). A significant number of bubbles are neither spherical nor ellipsoidal in shape, with the larger bubbles particularly prone to extreme irregularity (Figures 7.2 – 7.4) and often showing pronounced surface corrugations and rippling. Similar pictures have been obtained by Martin (1996) for bubbles in stirred tanks, wherein it was suggested the 'jagged or pitted' surface may be caused by small eddies impacting on the bubble surface. However, as large bubbles coalescing and rising in the quiescent coalescence cell have been seen to show similar deformations, the corrugations may simply be a consequence of the extremely mobile air-water interface and the increased tendency of large bubbles towards deformation. Bubbles of the order of 2 mm are seen to be spherical and do not show such pronounced surface deformations.

The wide size range observed in these systems present a number of difficulties in accurately applying the image analysis technique. As discussed in Chapter 3, consecutive frames were not used in this study to avoid double counting and further, images which contained bubbles larger than the screen were ignored as it was not possible to determine the size with any degree of accuracy. In addition, as the analysis program assumed spherical fluid particles, the degree of error tended to increase with bubble size, as the bubble shapes became more irregular. For the extremely irregular (very large) bubbles, sizing was carried out by estimating an equivalent spherical diameter; for those bubbles which approximated a prolate spheroid, the two axes were measured and then a volume equivalent diameter estimated (see Appendix D for further discussion). Overall, the effect will be to underestimate the size of the largest bubbles such that the size distributions discussed in the following sections represent the maximum measurable diameters, not the maximum diameters observed. However, the

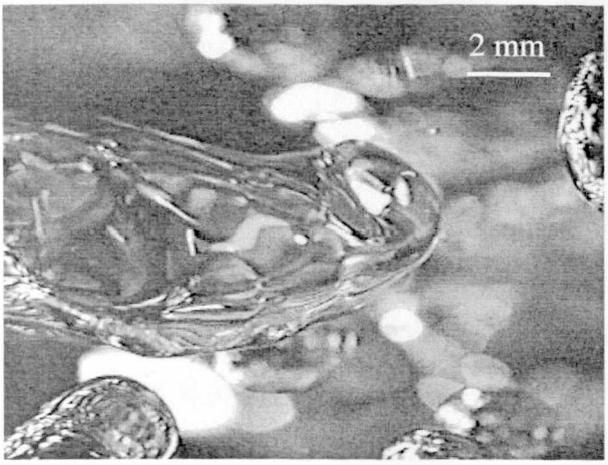

Figure 7.1

Large bubble in water, showing surface characteristic corrugations. Note also very small bubble in upper right hand quadrant. Water, 20 cm from distributor plate, u_s = 1 cms^{-1}, plate pore size 160 – 250 μm.

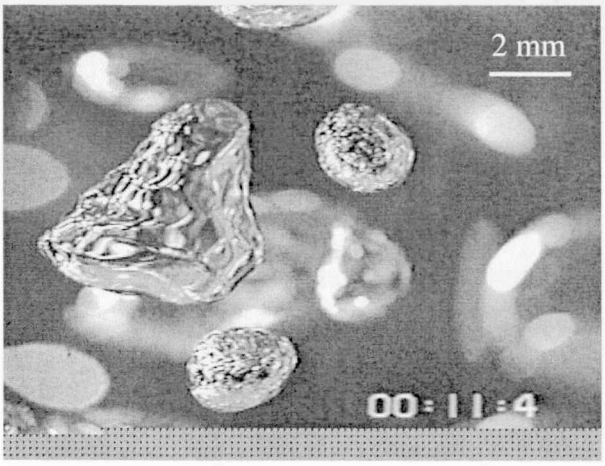

Figure 7.2

Large irregular bubble showing pronounced surface rippling; water, 10 cm above plate, u_s = 1 cms^{-1}, plate pore size 160 – 250 μm.

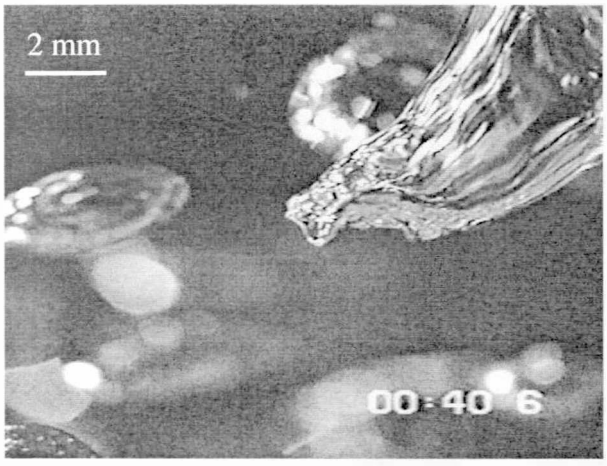

Figure 7.3

Bubble in water showing extreme irregularity at extremity and significant surface corrugations; u_s = 1 cms^{-1}, 10 cm above plate, plate pore size 160 – 250 μm.

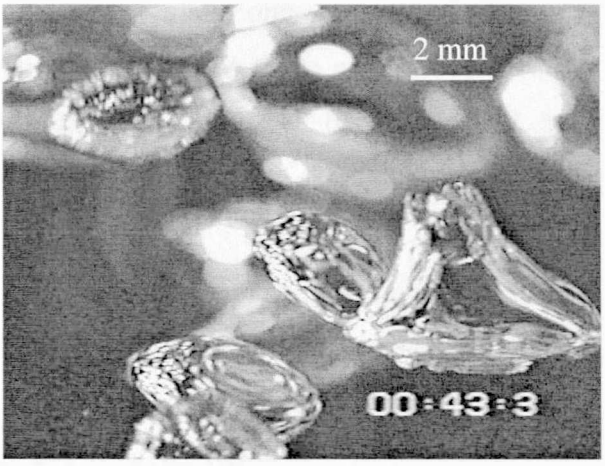

Figure 7.4

Irregularly shaped bubble in water, 2 cm above distributor plate, u_s = 1 cms^{-1}, plate pore size 160 – 250 μm.

limitations of the analytical techniques should not compromise the validity of using the distributions as a basis for comparison between systems.

7.1.1.2 Bubble Size Distributions in Water

Figures 7.5 and 7.6 show the number and volume probability density functions measured in water, at a superficial gas velocity of 1 cms^{-1} and with plate pore sizes from 160 to 250 μm. Probability density functions have been chosen to present the data for these initial experiments as they allow the change in bubble diameter with column height to be followed in greater detail. Accompanying the distributions, Figures 7.7 (a) to (d) show typical images

obtained at each measurement height for this experiment and which illustrate quite clearly an increase in bubble diameter with column height.

The number probability density function clearly shows a bimodal bubble size distribution existing at the distributor plate, which continues over the height of the column. At the distributor plate the distribution consists of two, virtually separate populations; a group of larger bubbles, with a modal value of ~ 2.5 mm and then a group of much smaller bubbles between ~ 150 and 250 μm. As they rise up the column, the larger bubbles increase slightly in size (the modal peak shifts to ~ 3 mm at 20 cm above the plate) but decrease slightly in number. In contrast, the population of smaller bubbles increases in number over the height of the column, although the modal size remains virtually constant, with the distribution measured 20 cm from the sparger plate showing a very pronounced peak of small bubbles (~ 200 μm) and the tail of much larger bubbles. As at the plate, only a small number of intermediate size bubbles are observed. Since water is considered to be a fully coalescing liquid this observation is surprising; the number proportion of larger bubbles would be expected to increase steadily with distance from the distributor plate.

The expected steady increase in bubble diameter with column height is seen quite clearly in the volume probability density function; the modal size of the single population of bubbles increases progressively from ~ 2.5 mm at the distributor plate to ~ 4.5 mm at the highest measuring point with a concomitant decrease in the relative frequency of events. The difference between the two functions arises from the different contributions of the bubble classes to the parameter of interest. The volume probability density function is inherently biased towards the larger sizes of a distribution, as the contribution of very small bubbles is virtually negligible when compared to that of larger ones. As a measure of the amount of coalescence occurring in a system therefore, it is considerably more useful as it shows clearly the generation of larger bubbles which result from a coalescence event. The number probability density function however is determined by dividing the relative number frequency by the interval width, leading to significant compression of he larger bubble classes. Consequently, although useful for observing detail about a distribution, it is of limited use as an indicator of the degree of coalescence occurring in a system, when measured by monitoring the increase in bubble size.

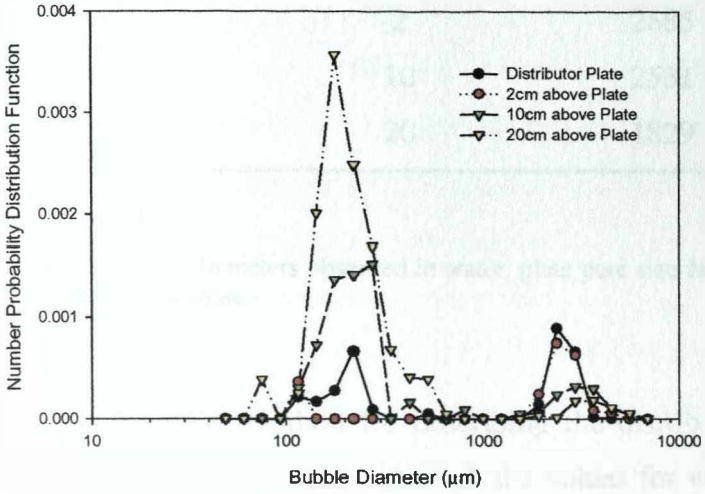

Figure 7.5

Change in number probability density function with column height; water; u_s = 1 cms^{-1}, plate pore size 160 – 250 μm.

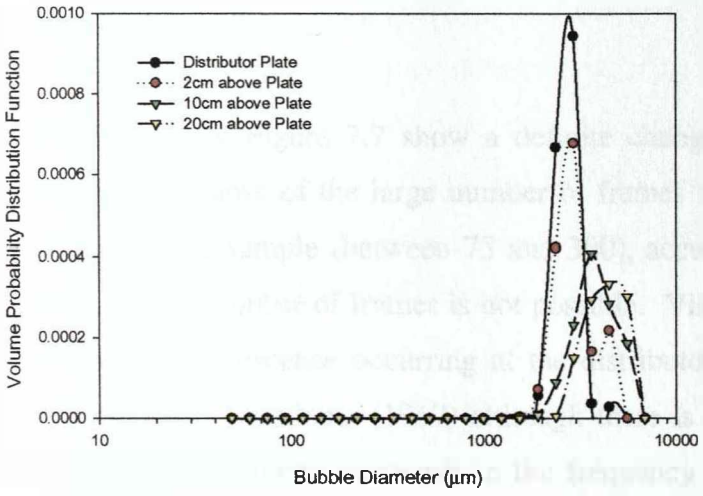

Figure 7.6

Change in volume probability density function with column height; water; u_s = 1 cms^{-1}, plate pore size 160 – 250 μm.

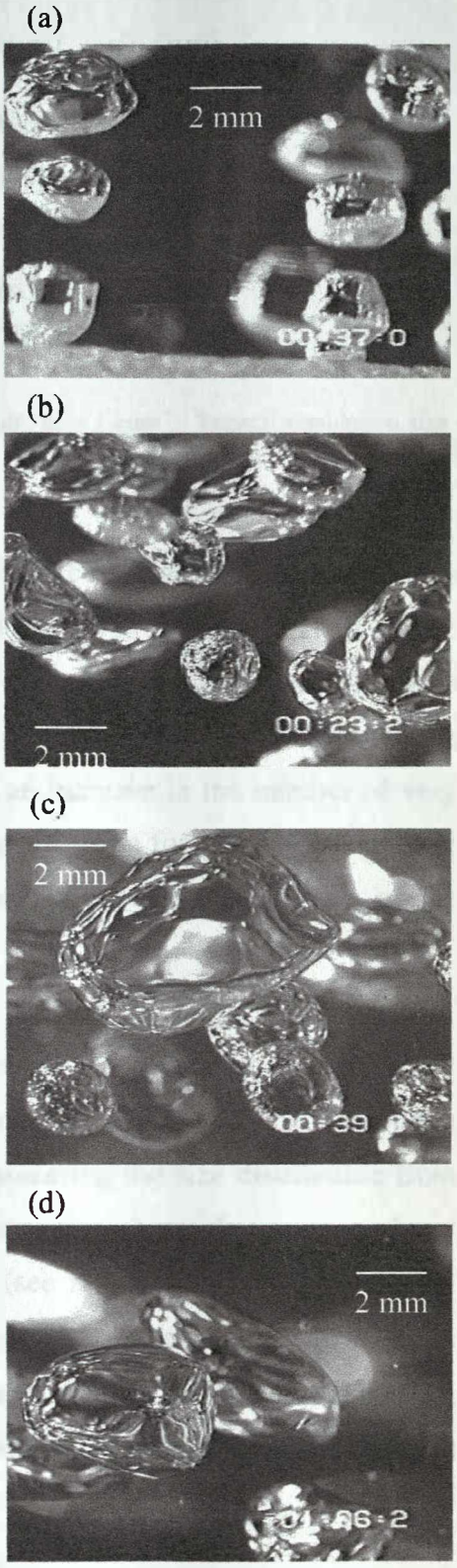

Figure 7.7

Images of bubbles in water; u_s = 1 cms^{-1}, plate pore size 160 – 250 μm. (a) at distributor plate, (b) 2 cm above, (c) 10 cm above, (d) 20 cm above plate.

Distance from Distributor Plate (cm)	d_{10} (μm)	d_{32} (μm)	d_{43} (μm)
0	2441	2695	2756
2	2685	2997	3172
10	2531	2845	4097
20	1829	4265	4495

Table 7.1

Mean bubble diameters observed in water, plate pore size 160 – 250 μm, u_s = 1 cms^{-1}. Typical population size ~ 350 – 400 bubbles.

An alternative method for describing the distributions observed is to consider the various mean bubble diameters obtained, the values for which are displayed in Table 7.1. It can be seen that for the distribution obtained at the sparger plate (where the majority of bubbles were of similar sizes), all three mean values are quite close. However, at the top of the column, the d_{43} value is almost three times larger than d_{10}, reflecting an increase in the number of very large bubbles as a result of coalescence. In addition, the small value for d_{10}, when compared to those obtained for the Sauter mean and d_{43}, indicates the pronounced width of the dispersion.

The images of Figure 7.7 show a definite change in bubble size over the column height although, because of the large number of frames which must be viewed in order to count a representative sample (between 75 and 300), accurately assessing the size distribution from such a small number of frames is not possible. Visual observation shows that there is a large amount of coalescence occurring at the distributor plate (see section 7.5), as suggested by Marrucci and Nicodemo (1967) although there is also considerable bubble growth over the height of the column, as shown in the frequency distributions. The change in bubble size distribution is much more pronounced when the initial bubble size is reduced, as considered below.

7.1.1.3 Effect of Distributor Plate Pore Size

Varying the pore size range of the distributor plate allows the effect of initial bubble size on coalescence to be investigated. Studies in the literature indicate that for a coalescing system

the equilibrium bubble size in a system should be independent of the initial bubble size. Rather, it will be determined by the dynamic equilibrium between coalescence and break-up such that all bubbles will coalesce to a maximum size and those larger than the maximum bubble diameter will tend to break up very quickly. Little work consequently has directly investigated the effect of bubble size on coalescence. Theoretical considerations may tend to suggest that larger bubbles tend to coalesce more readily, as smaller bubbles (< 1 mm) are more rigid. However, as larger bubbles deform more easily (the excess pressure required for deformation being $2\sigma/r$), this implies a larger contact area will result, with a consequent increase in the volume of film required to drain. The coalescence cell studies do not provide any definitive indications of the effect of bubble size on coalescence due to the difficulty of separating the effects of bubble size from the increased contact pressure the bubbles experience (arising from the constraints of nozzle separation) and the effects of surface age.

The cumulative number and volume distribution functions for the three sets of experiments carried out in water are shown in Figures 7.8 to 7.10. In each case the superficial gas velocity remains constant (1 cms^{-1}) and the pore size of the sparger plate reduced. All the cumulative volume distributions show the expected generation of larger bubbles up the column, with the maximum diameter measured at the top of the column similar for all systems (between ~ 6 and 7 mm). The width of the distributions measured at the distributor plate increases with decreasing pore size; the maximum diameter observed at this point is similar in all three columns (~ 2.5 – 3 mm), but obviously much smaller bubbles are observed for the smallest plate (~ 800 μm, Figure 7.10(b)) than with the largest (~ 2 mm, Figure 7.8 (b)). Only in the column with the smallest plate is there a significant amount of coalescence occurring between the plate and 2 cm above, whereas for all columns there is a significant increase in bubble size between 2 and 10 cm from the plate followed by a smaller increase in the distributions measured at 10 and 20 cm from the plate.

The cumulative number distributions show that very small bubbles (< 300 μm) are present in all columns at the distributor plate. It is in fact, the intermediate size bubbles (between ~ 500 and 1500 μm) which are absent for the largest sparger and which increase in number as the pore size decreases. This trend is continued in the distributions measured 2 cm from the plate. Most noticeably, the cumulative number distributions indicate the presence of a bimodal population for all the distributions measured at 10 and 20 cm from the sparger, as evidenced

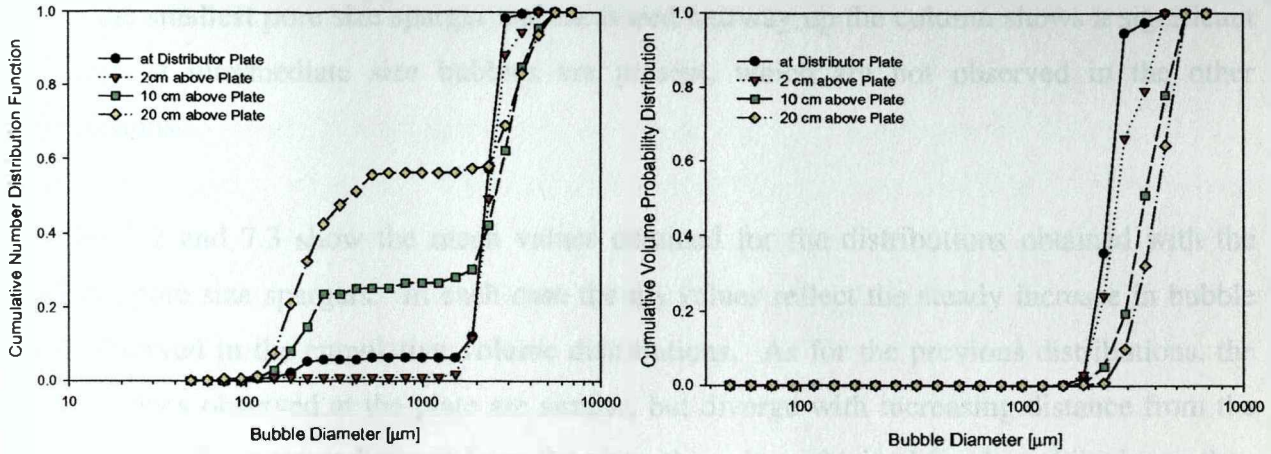

Figure 7.8 (a) and (b)

Change in (a) cumulative number distribution and (b) cumulative volume distribution with column height; water; u_s = 1 cms^{-1}, plate pore size 160 – 250 μm.

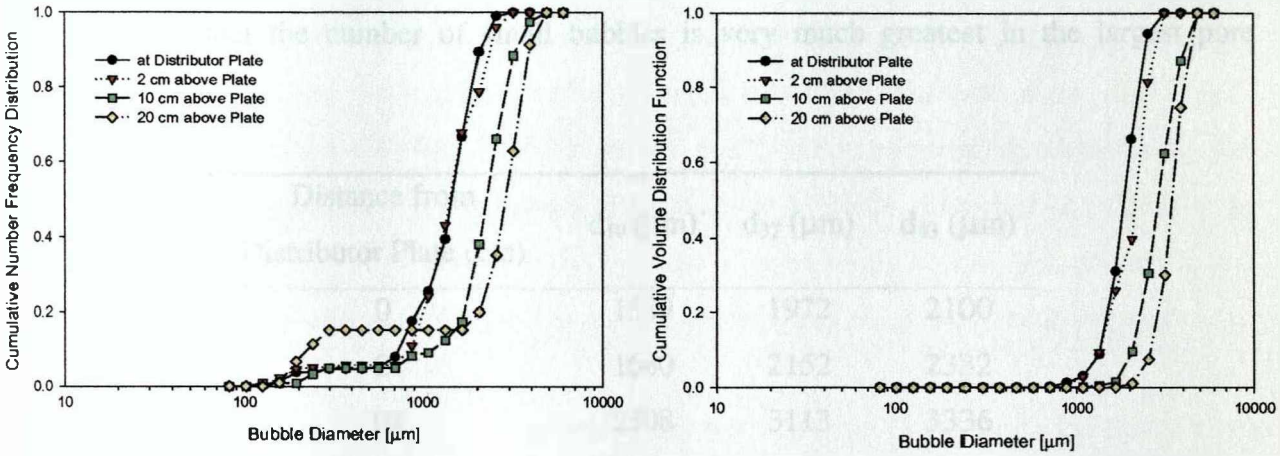

Figure 7.9 (a) and (b)

Change in (a) cumulative number distribution and (b) cumulative volume distribution with column height; water; u_s = 1 cms^{-1}, plate pore size 100 – 160 μm.

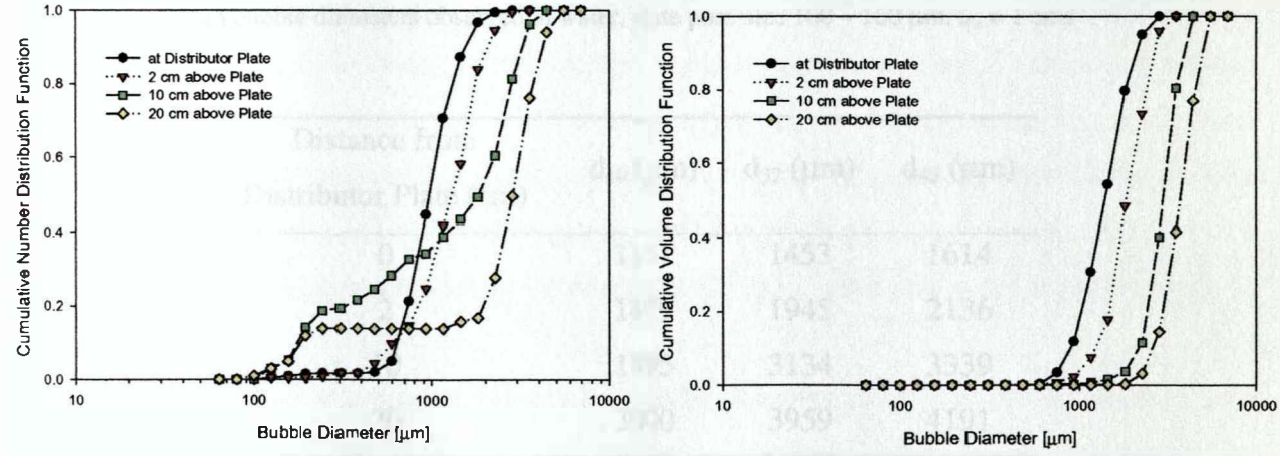

Figure 7.10 (a) and (b)

Change in (a) cumulative number distribution and (b) cumulative volume distribution with column height; water; u_s = 1 cms^{-1}, plate pore size 40 – 100 μm.

by the abrupt change in slope seen for all the curves. In addition, the distribution generated from the smallest pore size sparger and measured halfway up the column shows a significant number of intermediate size bubbles are present, which are not observed in the other populations.

Tables 7.2 and 7.3 show the mean values obtained for the distributions obtained with the smaller pore size spargers. In each case the d_{32} values reflect the steady increase in bubble size observed in the cumulative volume distributions. As for the previous distributions, the mean values observed at the plate are similar, but diverge with increasing distance from the sparger. At the greatest distance from the plate, the values obtained for d_{10}, whilst lower than either d_{32} or d_{43} (as expected) are much larger than the value obtained with the largest pore size sparger. This is reflected in the cumulative number distributions, in which it can be clearly seen that the number of small bubbles is very much greatest in the largest pore column.

Distance from Distributor Plate (cm)	d_{10} (μm)	d_{32} (μm)	d_{43} (μm)
0	1589	1972	2100
2	1660	2152	2332
10	2508	3113	3336
20	2942	3745	3892

Table 7.2

Mean bubble diameters observed in water, plate pore size 100 – 160 μm, u_s = 1 cms^{-1}.

Distance from Distributor Plate (cm)	d_{10} (μm)	d_{32} (μm)	d_{43} (μm)
0	1151	1453	1614
2	1479	1945	2136
10	1895	3134	3339
20	3000	3959	4191

Table 7.3

Mean bubble diameters observed in water, plate pore size 40 - 100 μm, u_s = 1 cms^{-1}.

7.1.1.4 Discussion

As water is considered to be a fully coalescing liquid the volume probability distributions, which for all distributor plates show a steady increase in bubble size over column height, are exactly as expected. The similar values for d_{32} measured 20 cm above the plate in all three systems are also as expected, reflecting the existence of a maximum bubble diameter beyond which further coalescence does not occur (or if it does occur, generates a large, unstable bubble which rapidly breaks up again). In fully coalescing systems, the bubble size is generally accepted to be determined by the dynamic equilibrium between bubble break-up and coalescence and not by the initial bubble size (as seen in this work).

In contrast, the number probability distributions showing the significant population of small bubbles (< 300 μm) were not as expected. In a system where the amount of coalescence occurring is significant, how are these small bubbles formed? Although break-up mechanisms have been proposed where very small bubbles are shed from the rim of very large unstable bubbles (Walters, 1983), these have been considered important only for bubbles much larger than the maximum reported here (bubble diameters 2 - 5 cm). In addition, the consistent increase of bubbles over the column height would indicate that in this system coalescence is the dominant mechanism in determining the dynamic equilibrium.

Bubble size distributions in air-water bubble columns are not commonly reported in the literature, with the majority of studies quoting gas hold-up data. Of those that can be found (Prince and Blanch, 1989, Lee and Patel, 1983), most have reported data for a single height in the column. Bimodal distributions as observed in this work, have not been reported before, with the smallest bubble sizes quoted usually of the order of 1 – 2 mm (Prince and Blanch (1989) report a smallest bubble class of 2.6 mm). This may be due to limitations arising from the measurement techniques used (often capillary suction or photographic without the use of a stereo-microscope, as used here), although to some extent they may also reflect the fact that previous studies have generally used much larger distributor plate pore sizes than this work.

Colella et al. (1999) measured at various column heights (though not at the distributor plate) and report single peak distributions showing decreasing bubble size up the column (to an asymptotic value) for the case of bubbles formed at large sparger pore sizes (3 and 10 mm) and no change with height for bubbles formed at smaller orifice sizes (0.2 mm, similar to this work). The trend towards smaller bubbles is ascribed to the dominance of bubble break-up

over coalescence; the lack of change in size with height is explained in terms of the resistance of smaller bubbles to break-up. None of their distributions show the pronounced peak due to small bubbles (> 300 μm) seen in this work. Only at low superficial gas velocity (0.75 cms^{-1}) with the 0.2 mm sparger, can a very broad bimodal distribution be observed, although this becomes unimodal (with a shift to larger bubble sizes) as the superficial gas velocity increases. As the smallest bubble class reported is 0 – 40 μm, the absence of a similar peak > 300 mm, cannot be ascribed to limitations of the measurement technique. In addition, as the maximum bubble size reported (300 μm) is considerably smaller than the value observed in this work, significantly greater amounts of bubble break-up must be occurring in the column. In this study, visual observation shows that the small bubbles are not generated directly at the sparger plate, suggesting the most obvious mode of formation is through bubble break-up, perhaps through the formation of daughter bubbles at coalescence. Consequently, in a system where considerable amounts of break-up are occurring, one would expect a significant population of these smaller bubbles.

Measurements of bubble sizes distributions in agitated vessels using the same image analysis technique as in this study (Machon et al., 1997 and Martin, 1996) have also shown pronounced bimodal distribution frequencies in air-water systems, which had not previously been reported. Machon et al. (1997) assert that it is due to the technique itself, which enables detection of bubbles below the limits of sensitivity of other measurement techniques (primarily capillary suction) and suggest that in water, bubble coalescence and break-up are equally significant. Martin (1996) observed a large number of small bubbles, similar in size to the ones reported in this study (< 0.5 mm) and proposed that they are "generated either by the strong vortices of the impeller and survive coalescence because of their small size amongst much larger ones; or by re-shedding from the rim of very large bubbles." Obviously the first mechanism proposed does not apply to this system and the second has been considered already. Considering the significant amounts of coalescence observed in this work, an alternative explanation, independent of bubble-break-up, is required to elucidate the mechanism by which the small bubbles observed are formed.

Irrespective of the formation mechanism, the question remains as to why these smallest bubbles are seen to persist over the height of the column and do not simply grow in size through coalescence. Size is a critical factor in determining the amount of excess force

required for deformation (applied force must exceed $2\sigma/r$) which is the reason smaller bubbles in the column are observed to be less prone to distortion. Consequently, the smallest bubbles require a very large pressure to deform and in the absence of constraints (such as in the free flow conditions of the column) may bounce following a bubble-bubble collision, rather than coalesce. Bouncing of bubbles has been studied in the literature, although the focus has usually been on the effect of approach velocity (Kumaran and Koch, 1993, Kirkpatrick and Lockett, 1983). However, it has been demonstrated that for low Weber numbers ($We = \rho U^2 r_b/\sigma$), which would apply here, bubbles tend not bounce but coalesce immediately following collision (Chesters and Hofman, 1982).

In addition, the high speed video studies of bubbles in columns (Section 7.6) show that the very smallest bubbles are readily affected by the flow-fields generated by surrounding bubbles, which may include both wake vortices and a boundary layer close to the surface of the larger bubbles. As a result, they do not rise vertically but are easily entrained in the macro-circulation patterns observed to exist in the column. Despite an extended residence time in the column, collisions with larger bubbles are observed to be uncommon; the smaller bubbles often appear to be swept around the periphery of the larger bubbles without coming into close proximity. This is not reported in many of the literature studies (Stewart, 1995, Miyhara, et. al., 1991, Otake et al., 1977) which predict that small bubbles will be captured in the wake vortex of a large preceding bubble, accelerate and consequently coalesce, although the majority of these studies have been carried out in quiescent systems, observing bubbles rising directly in-line.

7.1.2 Air-Sodium Sulfate Solutions

7.1.2.1 Observations

Sodium sulfate solutions were prepared over a wide concentration range, to measure bubble sizes in both fully coalescing and coalescence-inhibited solutions. The effect of initial bubble size was examined through the use of three sparger plates with different pore sizes and constant superficial gas velocity (1 cms^{-1}) for solution concentrations from 0.02 M to 1.0 M. In addition, the effect of gas flow rate was investigated using superficial gas velocities of 1 cms^{-1}, 2 cms^{-1} and 3 cms^{-1}.

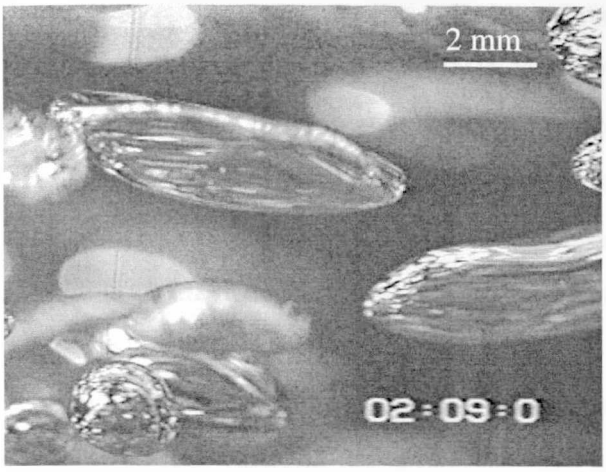

Figure 7.11

Oblate disc-shaped bubble, typical of larger bubbles observed in low concentration electrolyte solution; 0.04 M sodium sulfate, 20 cm above plate, u_s = 1 cms^{-1}, plate pore size 160 – 250 μm.

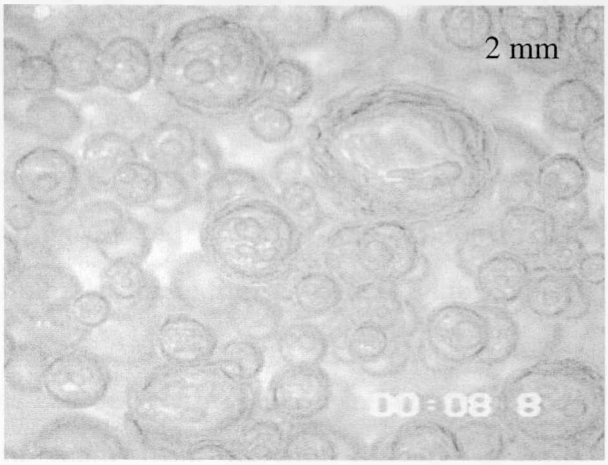

Figure 7.12

Large bubbles in 0.06 M sodium sulfate, 20 cm above plate, u_s = 3 cms^{-1}, plate pore size 40 – 100 μm.

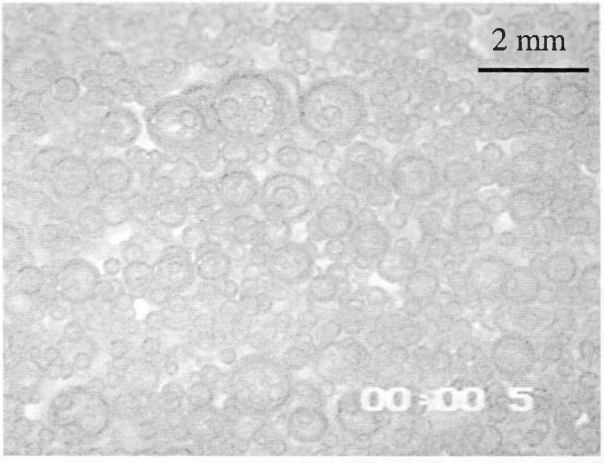

Figure 7.13

Typical picture obtained at high sodium sulfate concentration showing uniformity of bubble size; 1.0 M $NaSO_4$, u_s = 2 cms^{-1}, 20 cm above distributor, plate pore size 40 – 100 μm.

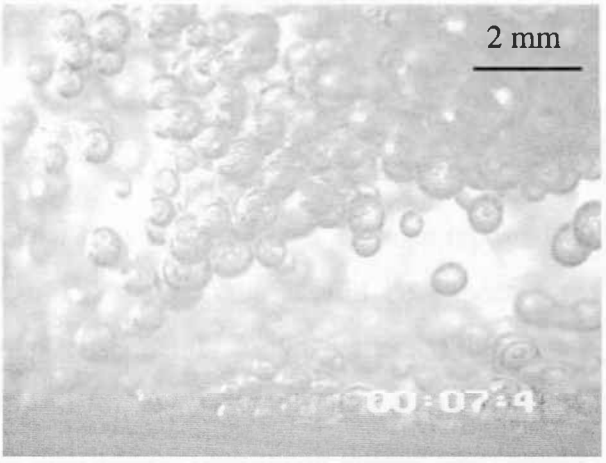

Figure 7.14

Re-circulated bubble cloud at distributor plate, due to macro-scale bubbling patterns in column; 0.06 M $NaSO_4$, u_s = 2 cms^{-1}, plate pore size 40 – 100 μm.

Even in low concentration sodium sulfate solutions (0.02 M), a discernible difference is observed upon comparing with bubbles in water. Although large bubbles are generated up the column as in water, the numbers of very irregularly shaped bubbles are reduced, with the largest bubbles being elongated ellipsoids with a significant proportion appearing oblate and disc-shaped (Figure 7.11). Most noticeably, there was a complete absence of bubbles larger than the frame and the numbers of very small bubbles were much reduced. The surface corrugations and rippling which are predominant features of larger bubbles in air-water systems are rarely seen although the smaller bubbles show surfaces similar to those in water. Although sizes observed at the plate are similar across the concentration range (at low gas velocities), away from the sparger bubbles become progressively more spherical and the

overall size diminishes as the solution concentration increases and plate pore size decreases. At intermediate concentrations (0.04 M, 0.06 M), bubbles are generally spherical in shape and large bubbles are only seen at the highest superficial gas velocities where they are observed to be essentially spherical and not prone to deformation or surface corrugations as in water (Figure 7.12). At the highest concentrations investigated (0.1M, 1.0M), bubble sizes throughout the column are very uniform and large bubbles are extremely rare (Figure 7.13).

At high gas flow rates, macro-circulation patterns can be seen to exist at all concentrations, which entrain groups of bubbles and prevent them from moving directly upwards, transporting groups in swirling eddies around the column. The effect is particularly pronounced at the distributor plate, where often a cloud of larger bubbles from the zone immediately above, is re-circulated into the image frame (Figure 7.14). Consequently, the distributions obtained at the plate will tend to overestimate the initial bubble size due to the presence of these larger bubbles.

7.1.2.2 Effect of Concentration

From studies in the coalescence cell carried out at low flow rates, as well as those reported in the literature, the amount of coalescence occurring in the column would be expected to decrease with increasing electrolyte concentration. Consequently, it was expected that when compared to the distributions measured in water and for low concentration sodium sulfate solutions, no significant increase in the bubble size distribution (and mean bubble size) would be observed over the height of the column for the coalescence repressed systems. Figures 7.15 (a) and (b) summarise the change in number probability and volume probability density functions with sodium sulfate concentration. The size distributions presented are those measured at the level farthest from the distributor plate (20 cm), for a superficial gas velocity of 1 cms^{-1} and the smallest plate pore size (between 40 – 100 μm).

The volume densities clearly show a steady decrease in the bubble size with increasing concentration, up to 0.06 M sodium sulfate solution. For solution concentrations between 0.06 M and 0.1 M, the measured distributions are almost identical, save for the small but consistent broadening of the distribution towards the smallest bubble sizes observed as the concentration increases. However, the population measured in 1.0 M sodium sulfate shows a pronounced increase in the number of small bubbles (~0.5 mm), although a tail of larger bubbles still remains. It appears that at this high sodium sulfate concentration, the distribution

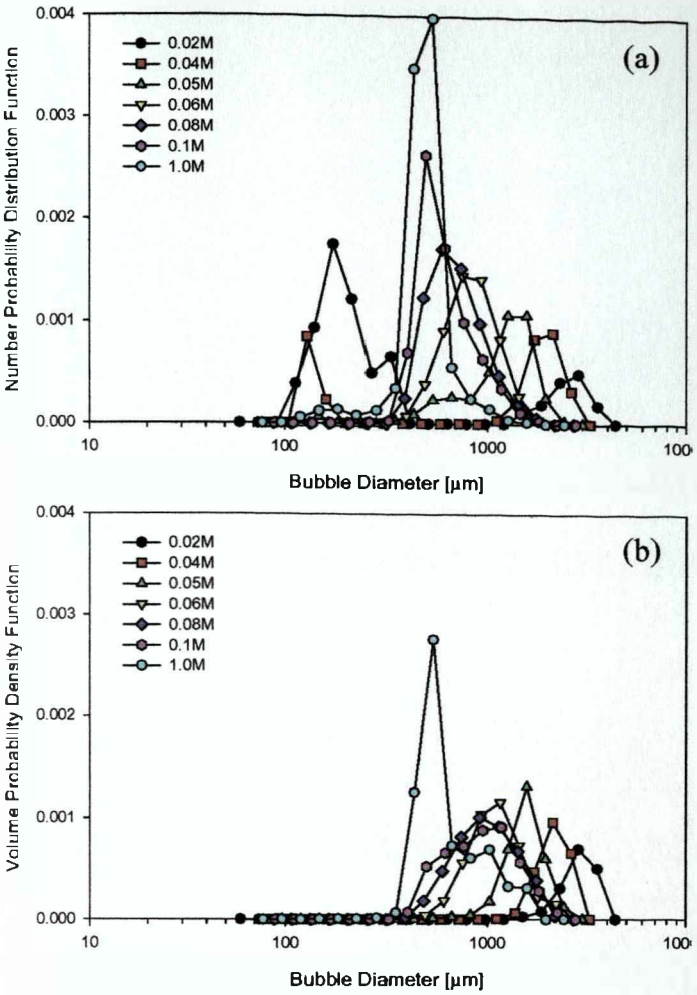

Figure 7.15 (a) and (b)

(a) Number probability and (b) volume probability density functions for sodium sulfate solutions, measured 20 cm above the distributor plate; u_s = 1 cms^{-1}; plate pore size 40 – 100 µm.

is tending towards bi-modality, with the population consisting of a large fraction of small bubbles (diameters less than ~ 0.4 mm) and a fraction of larger bubbles (diameters between ~ 0.4 and 1 mm).

The number density distributions are quite interesting. A conspicuous feature of the distributions obtained in 0.02 M sodium sulfate is the significant number of small bubbles present (diameters less than 0.3 mm), in addition to the large bubbles expected of a coalescing solution. The same feature can be observed, although to a lesser extent in 0.04 M, again a system wherein a significant amount of coalescence is occurring. However, in those solutions where the largest bubble size is much smaller (at concentrations of 0.06 M and above), there is no significant contribution to the distribution from similarly sized small bubbles. As observed in the cumulative volume distributions, the populations measured in 0.06 M, 0.08 M and 0.1 M sodium sulfate are all somewhat similar. In comparison with the volume density distribution, the number density distribution observed for 1.0 M solution, shows only a single peak (~ 0.5 mm), with very small shoulders towards both the lower and higher bubble classes.

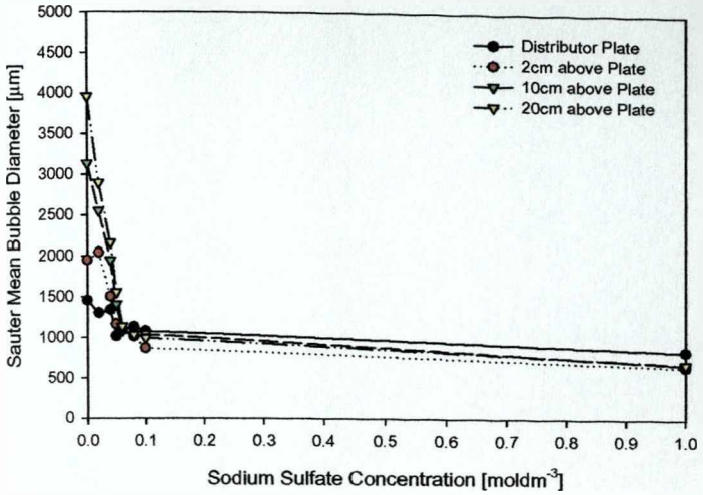

Figure 7.16

Effect of sodium sulfate concentration on Sauter mean diameter for u_s = 1 cms^{-1}, plate pore size 40 – 100 µm.

The effects of concentration on the bubble size are most clearly shown by considering the change in Sauter mean bubble diameter over a concentration range, as shown in Figure 7.16, (Figure 7.22(a) shows the same data over the smaller concentration range of 0.02 M to 0.1 M sodium sulfate). Significant increases in the mean bubble size are measured in water over the height of the column and to a systematically decreasing extent in low concentration sodium sulfate solutions. However, at concentrations above 0.06 M no change in bubble size is observed, with the mean value at the distributor plate similar to that measured close to the top of the column. The concentration at which no further change in bubble size is observed (0.06 M), corresponds very well with the value of the transition concentration demonstrated by Zharadnik et al. (1987) and Lessard and Zieminski (1971) using the coalescence cell. Correlation with the coalescence cell data obtained in this study is less favourable, largely as a result of the low 'transition value' obtained for sodium sulfate (0.03 M, see Chapter 5).

7.1.2.3 *Effect of Distributor Plate Pore Size*

In section 7.1.1.1, the effect of increasing the pore size of the distributor plate in water was investigated. A similar set of experiments was carried out over a range of sodium sulfate concentrations, in order to investigate the effect of initial bubble size on coalescence. The cumulative volume distributions for experiments with 0.02 M and 0.06 M sodium sulfate solutions are presented in Figures 7.17 and 7.18, which are used to represent coalescing and coalescence repressed systems, respectively.

The distributions obtained for bubble sizes in 0.02 M sodium sulfate are similar to those measured in water, although the maximum bubble size observed can be seen to decrease slightly with decreasing plate pore size (from ~ 6.5 mm for the largest distributor plate, to

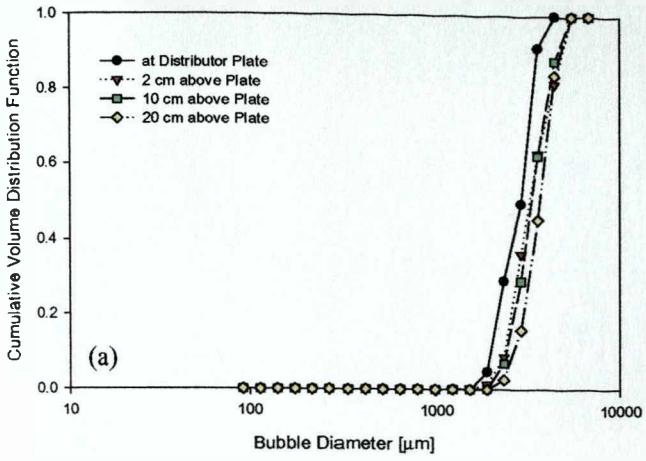

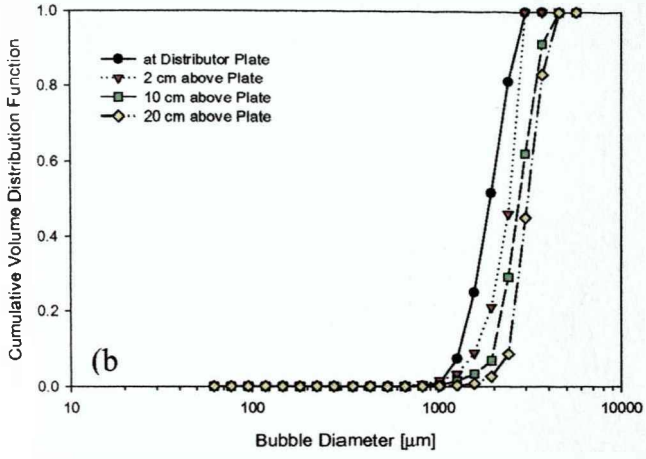

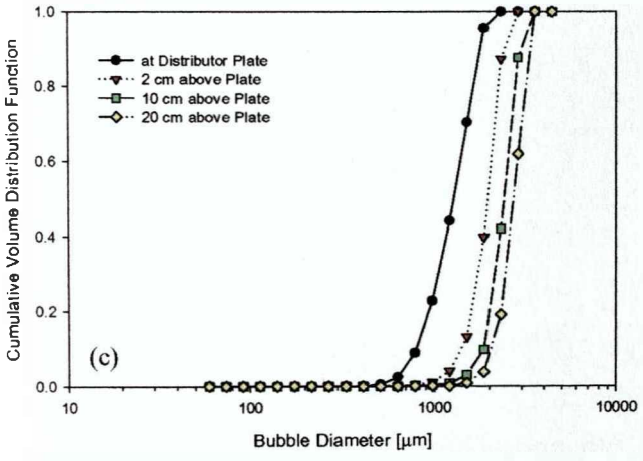

Figure 7.17

Effective of initial bubble size on cumulative volume distribution function over height of column for 0.02M sodium sulfate solution; u_s = 1 cms^{-1}. (a) Plate pore size 160 – 250 μm, (b) Plate pore size 100 – 160 μm, (c) Plate pore size 40 – 100 μm.

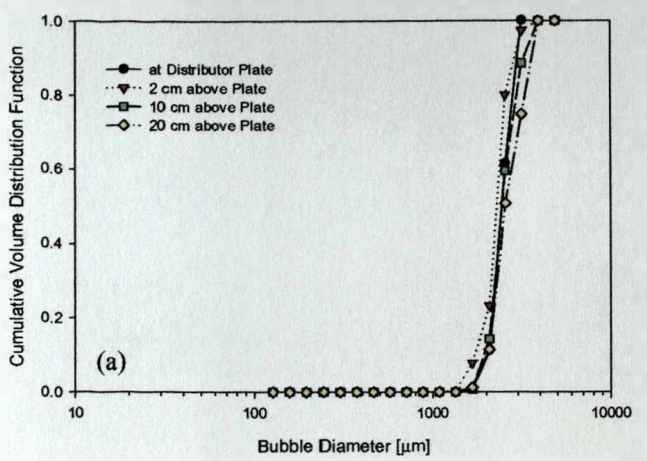

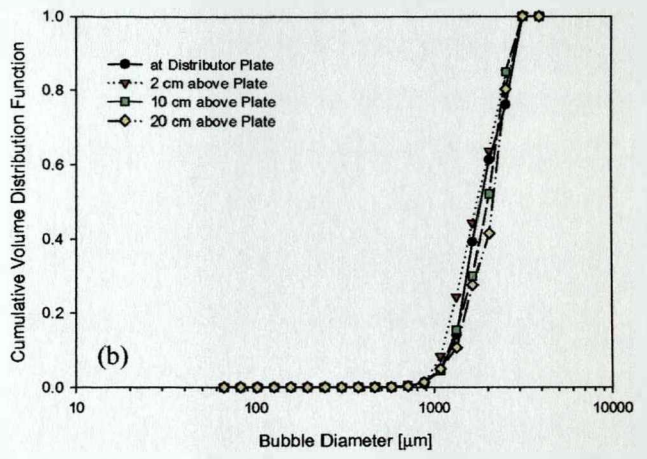

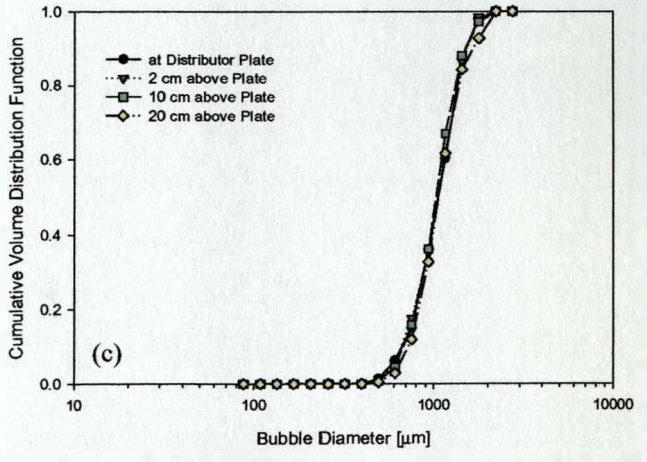

Figure 7.18

Effective of initial bubble size on cumulative volume distribution function over height of column for 0.06M sodium sulfate solution; u_s = 1 cms^{-1}. (a) Plate pore size 160 – 250 μm, (b) Plate pore size 100 – 160 μm, (c) Plate pore size 40 – 100 μm.

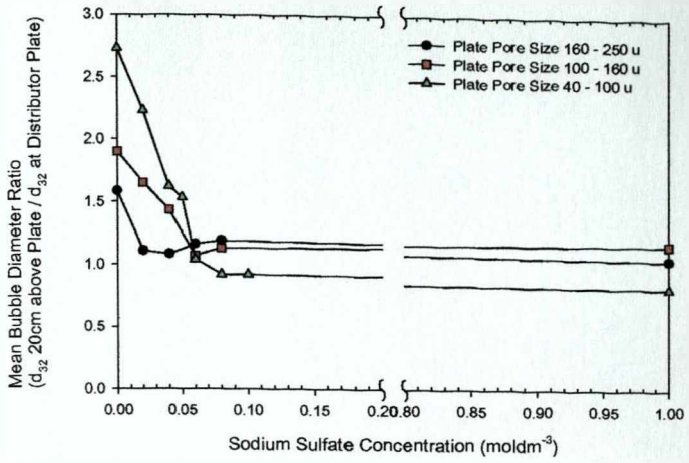

Figure 7.19

Effect of distributor plate pore size on ratio of final to initial bubble diameters.

~ 4.5 mm for the smallest). As in water, the greatest increase in bubble size is obtained with the smallest sparger and the amount of coalescence occurring between the sparger plate and the population 2 cm above it, increases significantly with decreasing plate pore size. Although further bubble growth occurs up the column in all cases, it is to a much diminished extent.

In complete contrast, the distributions measured in 0.06 M sodium sulfate show that for a coalescence repressed system (at low gas velocity), the only effect of decreasing initial bubble size is to decrease the largest bubble size observed (from ~ 4.5 mm (Figure 7.18 (a)) with the largest pore size plate, to ~ 2.5 mm (Figure 7.18 (c)) with the smallest). Very little change in the size distributions is observed over the column height in all cases. This is exactly as expected for a coalescence repressed system, where the initial bubble size governs to bubble size in the remainder of the system (in the absence of significant bubble break-up).

Figure 7.19 summarises the effect of distributor plate pore size over the concentration range investigated with the ratio of the final to initial bubble diameter shown as a function of concentration for the three plate pore sizes. As the size of the bubbles generated at the plate decreases, the influence of solution concentration is magnified. For the smallest pore size plate, the mean bubble size observed in water is over twice that measured in 0.06 M sodium sulfate, whereas for the largest pore plate it is only half as large. The differences between the mean bubble sizes measured in low and high sodium sulfate concentrations also increase as the initial bubble size decreases. For all plate pore sizes virtually no increase in mean bubble diameter is observed beyond a concentration of 0.06 M.

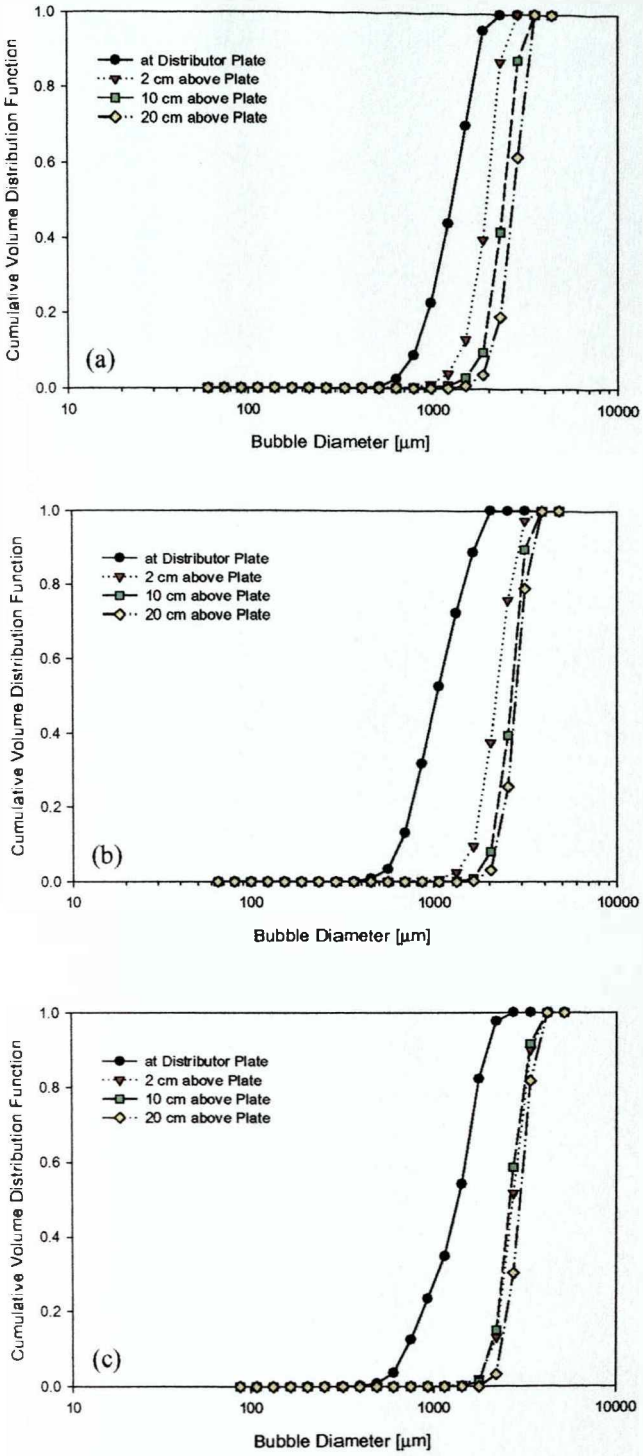

Figure 7.20

Effective of superficial gas velocity on change in cumulative volume distribution function over height of column for 0.02M sodium sulfate solution; plate pore size 40 – 100 μm. (a) $u_s = 1$ cm^{-1}, (b) $u_s = 2$ cm^{-1}, (c) $u_s = 3$ cm^{-1}.

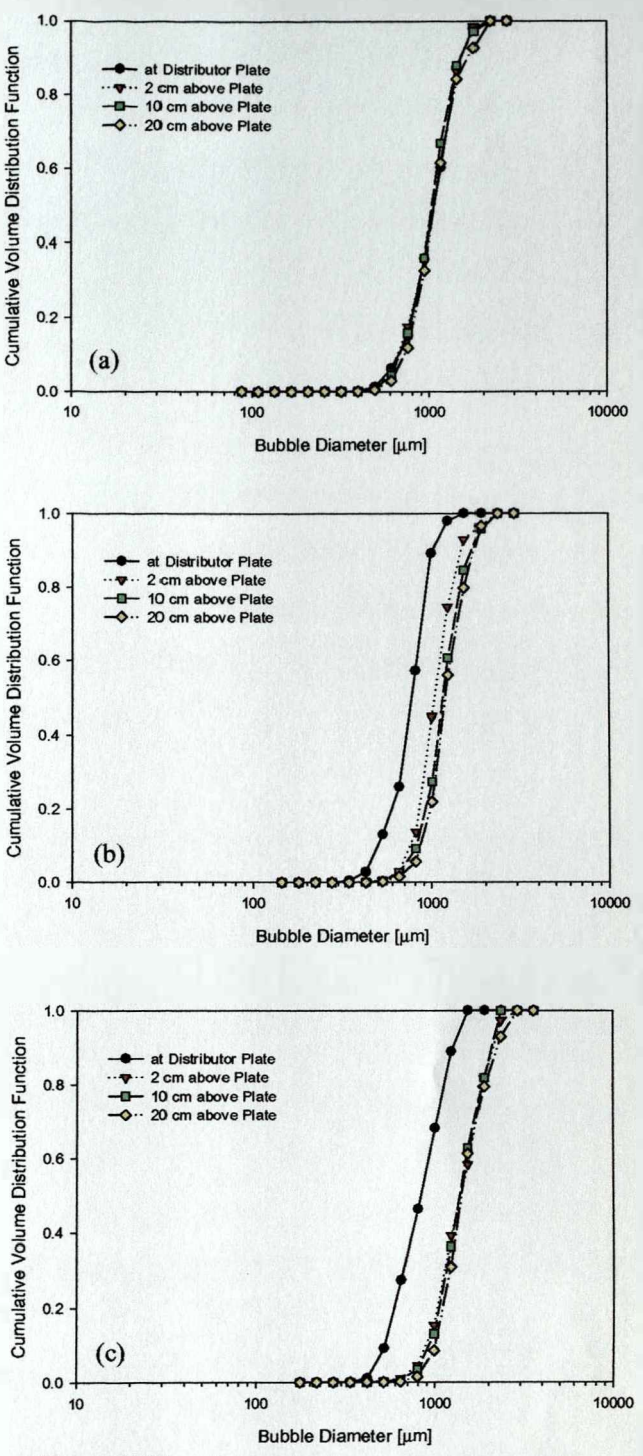

Figure 7.21

Effective of superficial gas velocity on change in cumulative volume distribution function over height of column for 0.06M sodium sulfate solution; plate pore size 40 – 100 μm. (a) $u_s = 1$ cm^{-1}, (b) $u_s = 2$ cm^{-1}, (c) $u_s = 3$ cm^{-1}.

7.1.2.4 Effect of Gas Flow Rate

The increase of gas hold-up with gas flow rate is widely known, although experiments to investigate coalescence in dynamic systems have been usually restricted to investigating low flow-rates, over which there is no change in the bubbling regime of the system, (Oolman and Blanch (1986b) are an exception). However, the increase in bubble density with gas flow rate (as the flow regime moves from homogeneous to heterogeneous) should promote the number of bubble-bubble collisions, which may lead to increased coalescence. In addition, the macro-scale eddies which are observed at the highest gas flows to entrain groups of bubbles, may result in prolonged contact times, potentially promoting conditions for coalescence. Consequently, coalescence rates may be expected to increase with superficial gas velocity.

Figures 7.20 and 7.21 present the results of experiments in 0.02 M and 0.06 M sodium sulfate, as being representative of the behaviour of the two different types of system. The experiments have been carried out for a fixed pore size (40 – 100 μm, the smallest plate used in this study and the system in which the influence of concentration is greatest, see Figure 7.19) and for superficial gas velocities of 1, 2 and 3 cms^{-1}.

The most immediately noticeable effect of increasing superficial gas velocity in 0.02 M sodium sulfate, is to greatly compress the total increase in bubble size occurring over the column height into the zone immediately adjacent to the sparger (between the plate and 2 cm above). Indeed, the intensification of coalescence in this zone has been observed visually as a bubble front that rapidly approaches the plate as the gas flow rate is increased. At u_s = 1 cms^{-1}, the shift in the cumulative distribution is slightly greater between the plate and 2 cm above, than between the remaining distributions measured further up the column. However, at u_s = 2 cms^{-1} the differences between the distribution measured 10 cm above the plate and that measured 20 cm above are very small. At the highest gas flow rate investigated (3 cms^{-1}), there is no discernible difference between the bubble size distributions observed at 2 cm, 10 cm and 20 cm above the plate.

The secondary effect of increasing the superficial gas velocity is to increase the overall bubble size observed; in both the coalescing and coalescence repressed systems. In 0.06 M sodium sulfate, whereas no change in size distribution is measured over the column for a superficial gas velocity of 1 cms^{-1}, there is a significant increase between the bubble size observed at plate and near the top of the column for values of 2 and 3 cms^{-1}. As observed in 0.02 M

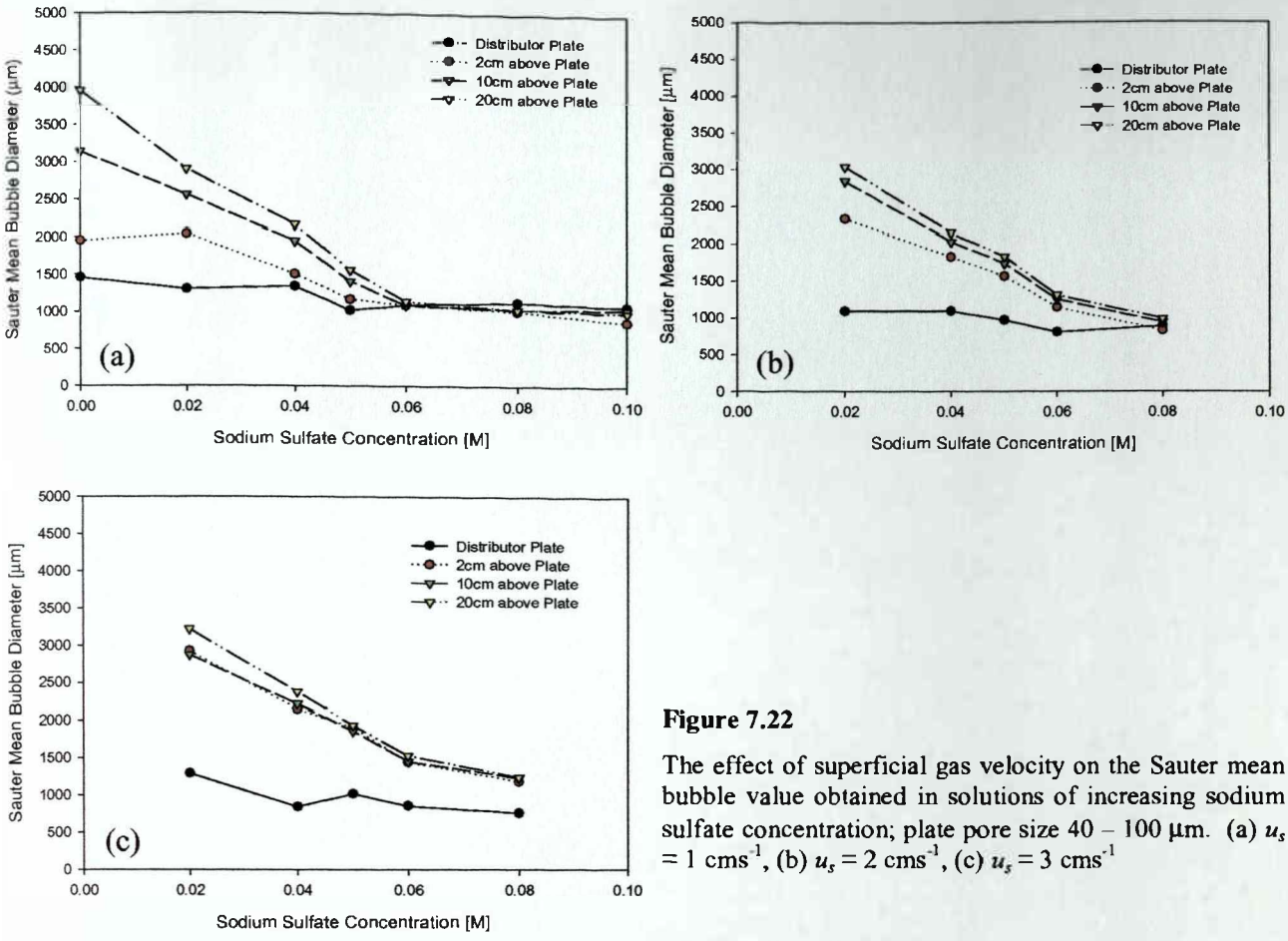

Figure 7.22

The effect of superficial gas velocity on the Sauter mean bubble value obtained in solutions of increasing sodium sulfate concentration; plate pore size 40 – 100 µm. (a) u_s = 1 cms^{-1}, (b) u_s = 2 cms^{-1}, (c) u_s = 3 cms^{-1}

solution, the primary zone for coalescence is between the plate and 2 cm above. Virtually no further change is observed over the column height, beyond this initial zone.

The Sauter mean diameters provide a useful method for assessing the overall impact of superficial gas velocity, as shown in Figure 7.22 (Sauter mean diameters are summarised in Tables 7.4, 7.5 and 7.6). Notwithstanding the consistent reduction in the final d_{32} value with increasing concentration, as the gas flow increases the difference between the mean bubble size at the distributor plate and that measured at the top of the column increases. Additionally, the sodium sulfate concentration at which bubble growth up the column is suppressed, shifts to a higher value; from 0.06 M at u_s = 1 cms^{-1} to 0.08 M at u_s = 2 cms^{-1}. For a superficial gas velocity of 3 cms^{-1} there is a significant increase in the mean bubble diameter over the column height, which suggests a further shift in the concentration at which coalescence is fully repressed.

Na_2SO_4 Conc^n [M]	Distance from Distributor Plate (cm)	d_{10} (μm)	d_{32} (μm)	d_{43} (μm)
0.02	0	2626	2946	3104
	2	3017	3487	3756
	10	3160	3557	3764
	20	3487	3884	4066
0.04	0	2676	2809	2868
	2	2785	2999	3095
	10	2794	3170	3374
	20	2777	3241	3487
0.06	0	2573	2697	2754
	2	2270	2482	2572
	10	2531	2739	2840
	20	2602	2873	3012
0.08	0	2722	2819	2872
	2	2383	2647	2706
	10	2619	3091	3340
	20	2690	3158	3388
1.0	0	2664	2828	2875
	2	2192	3008	3088
	10	2545	2939	3088
	20	2427	3161	3322

Table 7.4

Mean bubble diameters observed in sodium sulfate solutions, plate pore size 160 - 250 μm, u_s = 1 cms^{-1}.

Na_2SO_4 Conc^n [M]	Distance from Distributor Plate (cm)	d_{10} (μm)	d_{32} (μm)	d_{43} (μm)
0.02	0	1695	2009	2151
	2	1642	2411	2566
	10	2052	2901	3305
	20	2643	3305	3454
0.04	0	1277	1590	1699
	2	1427	1845	2039
	10	1742	2160	2326
	20	2000	2279	2404
0.06	0	1548	1976	2191
	2	1443	1844	2061
	10	1584	2017	2214
	20	1592	2108	2318
0.08	0	1430	1773	1928
	2	1353	1867	2106
	10	1434	1971	2249
	20	1492	2004	2260
1.0	0	1030	1376	1517
	2	947	1474	1670
	10	993	1591	1870
	20	1044	1604	1910

Table 7.5

Mean bubble diameters observed in sodium sulfate solutions, plate pore size 100 - 160 μm, u_s = 1 cms^{-1}.

Na_2SO_4 Conc^n [M]	Distance from Distributor Plate (cm)	d_{10} (μm)	d_{32} (μm)	d_{43} (μm)
0.02	0	1015	1298	1427
	2	1597	2037	2139
	10	2055	2550	2659
	20	2095	2898	2999
0.04	0	1045	1336	1455
	2	1250	1500	1603
	10	1712	1945	2024
	20	1969	2160	2222
0.05	0	814	1017	1138
	2	938	1164	1257
	10	1196	1407	1491
	20	1367	1558	1633
0.06	0	876	1091	1202
	2	875	1088	1200
	10	900	1085	1187
	20	944	1137	1251
0.08	0	808	1128	1262
	2	749	1006	1146
	10	788	1031	1168
	20	810	1033	1158
0.1	0	809	1075	1222
	2	679	864	982
	10	743	1035	1202
	20	732	992	1151
1.0	0	553	839	1080
	2	526	649	765
	10	537	676	813
	20	544	689	818

Table 7.6(a)

Mean bubble diameters observed in sodium sulfate solutions, plate pore size 40 - 100 μm, u_s = 1 cms^{-1}.

Na_2SO_4 Conc^n [M]	Distance from Distributor Plate (cm)	d_{10} (μm)	d_{32} (μm)	d_{43} (μm)
0.02	0	844	1086	1228
	2	1958	2230	2458
	10	2651	2839	2925
	20	2869	3037	3117
0.04	0	858	1086	1212
	2	1558	1821	1907
	10	1863	2026	2094
	20	2024	2147	2209
0.05	0	779	965	1050
	2	1351	1559	1642
	10	1556	1743	1807
	20	1693	1827	1890
0.06	0	1067	802	866
	2	986	1137	1225
	10	1047	1247	1352
	20	1116	1305	1402
0.08	0	737	883	946
	2	654	823	922
	10	709	935	1066
	20	743	983	1118

Table 7.6(b)

Mean bubble diameters observed in sodium sulfate solutions, plate pore size 40 - 100 μm, $u_s = 2$ cms^{-1}.

Na_2SO_4 Conc^n [M]	Distance from Distributor Plate (cm)	d_{10} (μm)	d_{32} (μm)	d_{43} (μm)
0.02	0	905	1291	1492
	2	2646	2920	3034
	10	2675	2870	2971
	20	3051	3220	3304
0.04	0	690	843	947
	2	2014	2149	2218
	10	2045	2114	2303
	20	2239	2378	2451
0.05	0	867	1016	1106
	2	1733	1905	1993
	10	1727	1859	1921
	20	1812	1934	2000
0.06	0	695	854	949
	2	1154	1442	1601
	10	1198	1452	1585
	20	1297	1529	1673
0.08	0	586	760	865
	2	791	1185	1430
	10	779	1232	1532
	20	815	1242	1523

Table 7.6(c)

Mean bubble diameters observed in sodium sulfate solutions, plate pore size 40 - 100 μm, $u_s = 3$ cms^{-1}.

Why does an increase in superficial gas velocity result in an increase in the amount of coalescence occurring in the column? From the graphs shown in Figure 7.22, it can be seen that the mean bubble size remains essentially constant (1 – 1.5 mm), irrespective of the gas flow rate, which suggests that the primary effect of increasing the gas flow rate is to increase the number of bubbles being formed at the sparger. Of the three steps in the coalescence process, the film thinning and rupture steps will be controlled primarily by the nature of the gas-liquid interface, which will not be in any way influenced by an increase in the local bubble density. Rather, it will be the initial step in the process, the rate at which two bubbles contact, which will be enhanced by an greater bubble density. For a given coalescence frequency, increasing the number of bubble-bubble contacts will result in a greater amount of coalescence and hence an increase in mean bubble size. As the distance from the distributor plate increases, the bubble density will decrease due to differing rates of rise velocity (arising from the range of bubble sizes).

7.1.2.5 Discussion

Measuring bubble sizes at various levels over the column height provides valuable insight into the coalescence process over the column as a whole. Many systems have reported mean bubble sizes in either columns or agitated vessels in previous studies, but these have rarely been taken at more than a single level. The results provide a useful means for drawing comparisons between systems but limited insight into the actual system dynamics in terms of the coalescence process. Likewise, although gas hold-up studies are useful indicators of overall system behaviour, they provide only limited information about the coalescence process.

The clear increases in bubble size observed over the column height for water and the lower concentrations of sodium sulfate solutions are exactly as one would expect for a fully coalescing liquid. In these systems, it is expected that the final bubble diameter will be determined by the equilibrium between bubble coalescence and break-up, with little influence from the pore sizes in the distributor plate. For the higher concentration solutions, however, the initial bubble diameter is expected to exert a significant influence on the mean bubble diameter observed in the system. This is evident from Figure 7.18, wherein it can be seen that the bubble sizes measured at the plate and at the top of the column are identical. This influence of concentration is well documented in the literature with many studies observing the dramatic reduction in mean bubble size upon the addition of electrolytes to air-water

systems (Jamialahmadi and Müller-Steinhagen, 1995, Zahradnik et al., 1985, 1987, Keitel and Onken, 1982, Lee and Meyrick, 1970, Marrucci and Nicodemo, 1967). As discussed in Chapter 5, the mechanism of coalescence repression is not well understood, with studies suggesting the effects of surface tension gradients (Lee and Meyrick, 1970, Marrucci, 1969), reduction of hydrophobic attraction (Craig et al., 1993) and viscous effects arising from the presence of electrolytes at the interface (Zieminski and Whittemore, 1971), amongst others.

It is generally considered that in coalescence repressed solutions, the most important determinant of the mean bubble diameter is the gas dispersion device, which is the only influence on the initial bubble size. However, as seen in this work, there is a small, but definite increase in the efficacy of solute to induce coalescence repression as initial bubble sizes decrease. The reasons for this are not conclusive. Larger bubbles are generally considered less rigid as a consequence of the decreased Laplace pressure required to cause deformation ($2\sigma/r$). This decrease in rigidity may result in increased contact areas between coalescing bubbles, thereby increasing the size of the film required to drain to the rupture thickness. However, an increase in contact area may not necessarily be detrimental. If it is considered that only a portion of the film is required to drain to the point of rupture and that localised film thinning occurs at various positions in the film, increasing the contact area may increase the number of sites at which the film thinning process can occur, thereby increasing the probability of coalescence. Alternatively, increasing the size of the bubbles will increase the bubble rise velocity and increase the collision force between bubbles (thereby increasing coalescence frequencies as seen in the coalescence cell). Literature studies predict, however, that for freely rising bubbles, an increase in contact velocity results in bubble bouncing rather than coalescence; in addition, macro-scale bubbling patterns, which may be considered to hold colliding bubbles together for a prolonged contact time are absent from the experiments carried out for $u_s = 1$ cms^{-1}, under which conditions the observation was made.

The importance of the zone adjacent to the distributor plate was first observed by Marrucci and Nicodemo (1967), who carried out one of the defining studies in terms of bubble sizes in air-electrolyte solution dispersions. This study confirms their observation and re-emphasises the importance of the initial zone for determining the final bubble size at higher gas flow rates. In their study, 'continuous but much less important' coalescence was present through the remainder of the column. However, in this study any additional coalescence beyond the initial zone, in either coalescing or coalescence repressed solutions, is found to be negligible,

especially as the superficial gas velocity increases. In contrast with the findings of this work, Marrucci and Nicodemo, 1967, report a constant asymptotic bubble diameter, irrespective of increasing gas velocity, although it must be noted that their experiments were conducted over a low range of superficial gas velocities (0.1 to 1.5 cms^{-1}), the maximum being half the highest value investigated in this study. Koide et al. (1968), measuring 'at a position slightly removed from the distributor plate' report a definite effect of gas velocity on bubble size for coalescing solutions, as in this study but no effect in coalescence repressed solutions, contrary to this work, despite comparable systems and superficial gas velocities. Parthasarathy and Ahmed (1996) report size distributions for bubbles formed at porous plate spargers (identical to this work) in non-coalescing solution. A small effect of gas velocity is observed on the bubble sizes, although the mean diameters reported (d_{10}) were smaller than those measured in this study, most probably a reflection of the much reduced range of gas flow rates (0.25 to 1.25 mms^{-1}). Oolman and Blanch (1986b) measured bubble diameters at the top and bottom of a bubble column, in solutions of 0.15 M sodium chloride. No change in diameter was observed between the two over a range of superficial gas velocities. However, in this study, air was dispersed through large diameter orifices such that bubbles broke up directly at the sparger zone and before the initial measurement was made. In the absence of a zone with increased bubble density directly above the distributor, the increase in final bubble diameter with gas velocity is not surprising.

By far the most conspicuous feature of the distributions measured in this work is the significant number of small bubbles generated in water and low concentration salt solutions, despite the overall increase in mean bubble size. This was quite unexpected, given the fully coalescing nature of these systems. In contrast, Solanki et al. (1992) report uni-modal size distributions for bubbles in water and bimodal bubble size distributions in aqueous electrolyte solutions, especially at the higher gas velocities used. Likewise, Pohorecki and Nowosielski (1986), report a separate population of much smaller 'ionic' bubbles in the froth formed from aqueous electrolyte solutions, but absent in equivalent air-water systems. In their study, the failure to observe small bubbles in fully coalescing systems, as in this work, cannot be ascribed to limitations in the analytical technique, as the smallest bubble classes reported is 0.1 mm. Koide et al. (1968) report the presence of small bubbles (diameter ~ 300 μm) generated at a porous plate in concentrated electrolyte solutions, but not in pure water or organic solutions. Similar sized bubbles are observed in this work, in 1.0 M sodium sulfate solution (Figure 7.15) although this is not unexpected given that this represents

a strongly coalescence repressed liquid. However, Machon et al. (1997) and Martin (1996), apply the same image analysis technique as in this work to dispersions in agitated tanks, and report similarly sized small bubbles in supposedly fully coalescing systems (water and 0.02 M sodium chloride). Explanations are based on break-up and coalescence together with considerations that coalescence in pure systems may not be as rapid as indicated by coalescence cell studies. This study considers an alternative explanation for the presence of these small bubbles, as discussed in Section 7.6.

7.2 Sauter Mean Bubble Sizes and the Coalescence Frequency

In order to be able to assess how well the results generated in the coalescence cell mimic the behaviour of a dynamic system, a single measure for the amount of coalescence occurring in the column must be obtained. The majority of previous studies which have taken measurements at a single level in the column, have relied on comparisons with mean bubble diameters as indicators of system behaviour. However, a major advantage of the interval measurements carried out in this study, is that they enable the amount of coalescence occurring over the column height to be quantified for each solution concentration and superficial gas velocity.

Initially it was proposed to use a Sauter mean bubble size ratio (see Figure 7.19), which was determined as the ratio of the d_{32} value obtained at the top of the column to that measured at the plate. The size ratio would consequently be much greater in a system where significant coalescence was occurring, than for a coalescence repressed system where the value should approach unity.

Following on from this initial simple definition for the degree of coalescence, it was decided to adapt the model of Howarth (1967) as a measure for the coalescence frequency in a system. The method was originally developed to measure the coalescence frequency of drops in an agitated tank where a reduction in impeller speed was used to promote coalescence and the new, larger, steady-state mean drop size which resulted was then related to the coalescence frequency of the system. The method assumes the turbulent flow field in the tank is homogeneous and isotropic, that drops will coalesce until a maximum stable size is exceeded, at which point break-up occurs and that decay of the turbulence, following the impeller step change, is virtually immediate. The coalescence frequency derived was based on the change

in Sauter mean diameter occurring after the impeller speed step change and is given by the equation:

$$\varpi = \frac{\left(\frac{dd_{32}}{dt}\right)_{t=0}}{\left[2 - 2^{\frac{2}{3}}\right]\left[d_{32}\right]_{t=0}} \tag{7.1}$$

where t refers to the time from the impeller step change.

In applying this method to determine coalescence frequencies in a bubble column it is necessary to convert the original data, collected as a function of column height, into a measure of change of mean bubble diameter with time. This was calculated by determining the average bubble rise velocity in each system and using this to convert the distance from the distributor plate into a measure of time elapsed (measurements at the distributor plate are taken as time zero). The average bubble rise velocity, U_b (ms^{-1}) can be calculated as follows:

$$\varepsilon_g = \frac{u_s}{U_b} \tag{7.6}$$

where ε_g is the gas hold-up, determined from the heights of the gassed and ungassed systems and u_s is the superficial gas velocity (ms^{-1}). As the smallest bubbles in a distribution will make only a limited contribution to the gas hold-up measured for a system, the average bubble rise velocity will tend to emphasise the larger bubbles thus giving a conservative estimate for the change in size with time. Smaller bubbles (and the smallest bubbles especially, as a consequence of entrainment in the macro-scale flow patterns) will reside in the system for longer, increasing the probability of bubble-bubble contact and eventual coalescence. An alternative approach would be to use the correlations available in the literature to determine the bubble rise velocity for the average size bubble (taken as d_{32}).

Once the average bubble rise velocity has been determined, the time elapsed can then be calculated and the coalescence frequency determined between each measurement level as:

$$\varpi_z = \frac{\left[\frac{d_{32,(z+1)} - d_{32,z}}{t_{(z+1)} - t_z}\right]}{\left[2 - 2^{\frac{2}{3}}\right]\left[d_{32,z}\right]} \tag{7.7}$$

where the subscript z refers to the measurement height up the column, and t refers to the time required for the bubble to rise this distance (s). Using this modified Howarth equation, it is

then possible to determine the coalescence frequencies for each of the sections in the column, or over the column as a whole.

The coalescence frequency determined for each of the sections in the column (distributor plate to 2 cm above, between 2 and 10 cm above and between 10 and 20 cm above) are shown in Figure 7.23 for the experiments carried out with the smallest pore size sparger and superficial gas velocities 1, 2 and 3 cms^{-1}. Also shown on the graphs are the coalescence frequencies measured in the coalescence cell at four selected gas flow rates, 1, 15, 20 and 40 $mlmin^{-1}$.

As expected from comparison of the bubble size ratios of Figure 7.22, the coalescence frequencies decrease with increasing electrolyte concentration. The lower values observed for water at superficial gas velocities of 1 and 2 cms^{-1} reflect the larger mean bubble diameters measured at the distributor plate in these systems and will also be influenced by the difficulty in accurately measuring the large bubbles commonly observed in water. As can be seen from these graphs, the coalescence frequency is consistently much greater in the initial section of the column, than over the remainder of the column. The difference is intensified as the superficial gas velocity increases, under which conditions the coalescence frequencies in each of the two remaining sections is negligible, even for the fully coalescing 0.02 M sodium sulfate solution. Qualitatively, the results are supported by the images of coalescence, which although random, show significantly greater numbers of coalescence events in the region adjacent to the sparger than at the remaining three measurement levels. Indeed, for coalescence repressed solutions, images of coalescence at positions removed from the distributor plate are extremely rare.

There are two possible reasons for the higher hold-up observed in this initial zone, both of which are related to a reduced average bubble rise velocity in this section. At the distributor plate, the rise velocities of the bubbles will be slower than at other points in the column, as bubbles will not reach their terminal velocity immediately after leaving the plate. Although bubbles require only a very short distance to achieve the steady state rise velocity, the effect of this delay will be magnified in this section as it is very small. In addition, for coalescing systems the initial Sauter mean bubble diameter is the smallest in the system, which will also mean a smaller average bubble rise velocity and consequently, a relatively greater bubble density just above the sparger plate. The increased bubble density obviously increases the

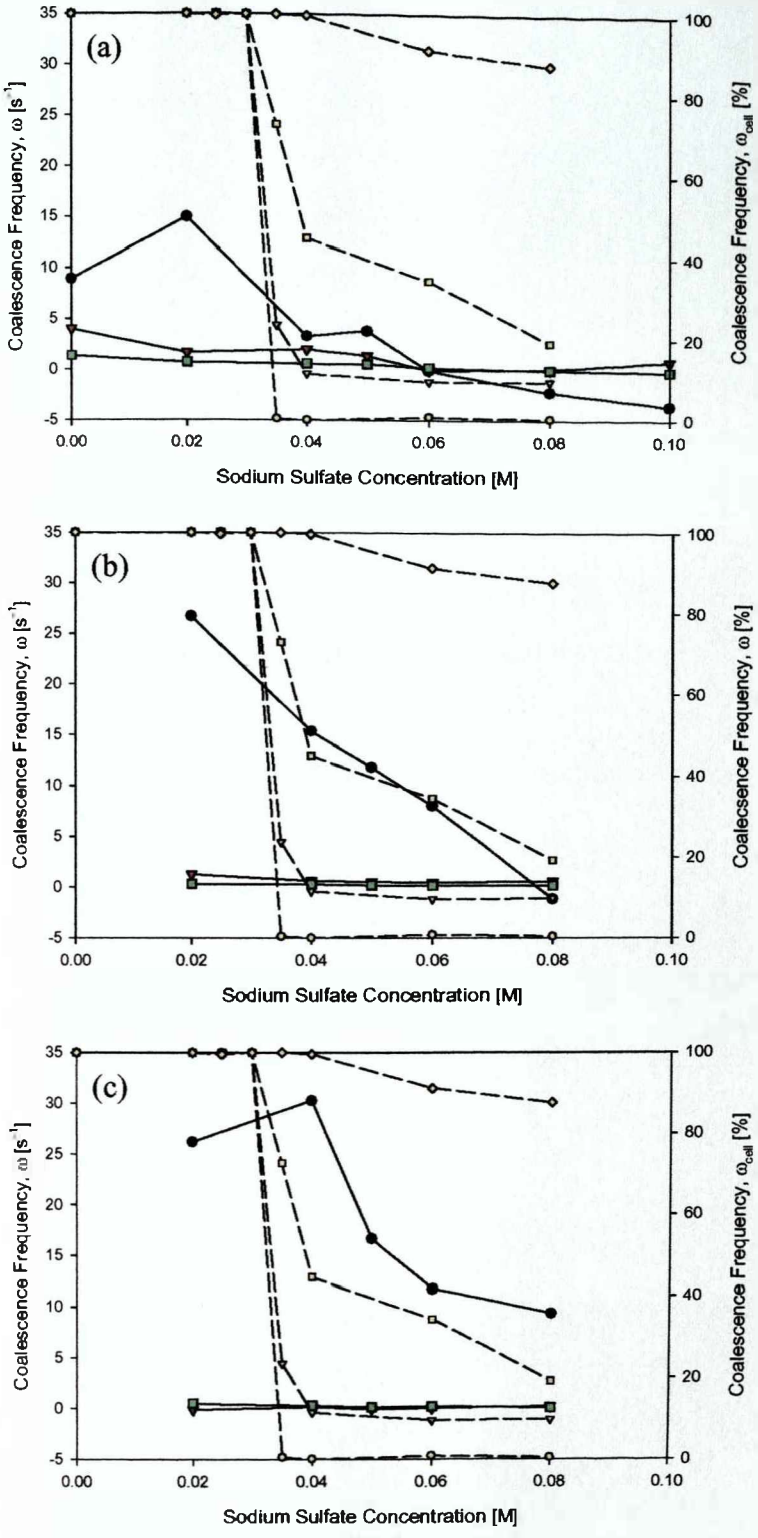

Figure 7.23

Effect of sodium sulfate concentration on coalescence frequencies measured in the column, ϖ, and in the cell, ϖ_{cell}, for the three sections of the column.

(a) u_s = 1 cms^{-1}, (b) u_s = 2 cms^{-1}, (c) u_s = 3 cms^{-1}, plate pore size 40 – 100 µm.

For column: —●— ϖ 0 – 2 cm above plate, —▼— ϖ 2 – 10 cm above plate and —■— ϖ 10 – 20 cm above plate.

For cell, —○— Q_g = 1 mlmin^{-1}, —▽— Q_g = 15 mlmin^{-1}, —□— Q_g = 20 mlmin^{-1} and —◇— Q_g = 40 mlmin^{-1}.

probability of bubble-bubble contacts, leading to increased coalescence. As the gas flow rate increases, a larger volume of gas must be dispersed, resulting in an increase in the rate of bubble formation at the distributor plate and consequently increasing the bubble density in this section. The very large values obtained at the higher gas velocities may also reflect the re-circulation that was observed to occur just above the sparger plate, with group of bubbles being transported in eddies around the column.

In the remaining sections of the column, the very low values of the coalescence frequencies reflect the much larger area under scrutiny, combined with the effect of larger mean bubble diameters which will result in increased rise velocities. As a consequence, although the coalescence probability of a bubble-bubble contact resulting in coalescence will remain unchanged, the number of collisions will be reduced, thereby decreasing the number of coalescence events.

Coalescence frequencies are not generally reported in the literature for gas-liquid dispersion, although they are often quoted for liquid-liquid systems. When compared to values measured in agitated liquid-liquid dispersions, (Man, 1999, Franklin, 1997), the coalescence frequencies obtained in this study are very much greater (generally by three orders of magnitude). Whilst direct comparisons are necessarily limited, this undoubtedly reflects the influence of the impeller together with the much increased time scales for the experiments. In a study of coalescence frequencies in bubble columns, Oolman and Blanch (1986b), measured the rate at which tracer gases (helium and neon) were mixed and obtained values in both water and for a set of sodium chloride concentrations, using a range of superficial gas velocities. As in this study, the coalescence frequencies were observed to decrease with increasing electrolyte concentration and increase with increasing gas velocity. Direct comparison between the two sets of value is not possible as their study defines coalescence frequency as the number of coalescence events per unit length; the maximum value measured corresponds to three coalescence events per metre, (for water at the highest superficial gas velocity). Comparisons with coalescence observed in a stagnant liquid (using a coalescence cell) show a decrease in the same concentration range, although the typical step change observed in the cell is not mirrored in the coalescence frequencies measured in the column. Takahashi and Nienow (1993) measured coalescence rates (number of events per unit time) in agitated vessels and report an increase in coalescence rate with increasing gas flow rate and decreasing impeller speed. The values quoted for their study are quite small ($1 - 5\ s^{-1}$), similar to the very low

values obtained in this work, for the upper regions of the column. The fact that the values are much lower than those determined in this work for the initial section of the column most probably reflects the influence of the impeller on the bubble size distribution.

Also shown in Figure 7.23, are the coalescence cell profiles for a range of gas flow rates. None of the profiles predict the essentially zero coalescence frequencies measured in the two upper regions of the column, even for the lowest electrolyte concentrations. For the frequencies measured between the plate and 2 cm above, there is a reasonable correlation between the cell profiles obtained at the two lower flow rates (1 and 15 $mlmin^{-1}$) and the coalescence frequencies measured in the initial section of the column for u_s = 1 cms^{-1}. Both cell profiles predict a reduction in the degree of coalescence at a concentration value similar to that indicated by the coalescence frequencies measured in the column. In addition, the virtually zero coalescence frequencies observed in the column at high electrolyte concentration are well indicated by similarly low cell values.

As the superficial gas velocity increases, the most reasonable correlation between column and cell behaviour is given by the cell profile obtained at Q_g = 20 $mlmin^{-1}$. At u_s = 2 cms^{-1}, the correlation between the two is particularly good; in place of the step change in behaviour observed in the cell for Q_g = 1 or 15 $mlmin^{-1}$, the cell profile now suggests a continual decrease in coalescence probability with concentration which is mirrored in the steady reduction in coalescence frequency values measured in the column. The essentially fully coalescing behaviour of the cell profile at Q_g = 40 $mlmin^{-1}$ is not reflected in the coalescence frequencies obtained, even at the highest flow rates used in this study. Rather, for coalescence frequencies measured at u_s = 3 cms^{-1}, the best correlation is still given by the cell profile obtained with Q_g = 20 $mlmin^{-1}$, as this once again predicts the consistent reduction in values with increasing electrolyte concentration. However, Zahradnik et al. (1995) observe that coalescence repression due to electrolytes is much diminished in heterogeneous flow regimes (obtained at very high gas flow rates). Combined with the observations from this work, this suggests that at sufficiently high gas velocities, the coalescence frequencies measured in the initial section of a bubble column, could approximate the trend displayed in the coalescence cell at the higher flow rates.

The correlation between the cell profiles and the coalescence frequencies measured in the column is surprising given that there the reasons for enhanced coalescence in the two systems

are unlikely to be similar. In the column, the increase with superficial gas velocity can be attributed to increased bubble density in the zone adjacent to the distributor, which increases the total number of coalescence events. In the cell, however, the increase observed with gas flow rate arises through complex series of interactions between the contact pressure, bubble size and perhaps increased contact areas. However, despite the different mechanisms determining behaviour in the two systems, initial indications from this part of the study are that the coalescence cell could be successfully manipulated to provide accurate indications of coalescence processes in larger systems, beyond the basic coalescing/non-coalescing boundaries already defined. Whether this in indeed the case will require a great deal more work to firstly assess the relevance of parameters such as coalescence frequencies in process systems, as well as studies to accurately correlate conditions in the cell with column behaviour.

7.3 Bubble Size Distributions in Magnesium Sulfate Solutions: The Effects of Gas Density

The aim of this set of experiments was to determine whether the very small shifts in 'transition concentration' observed in the coalescence cell for increasing gas density, would be reflected in the bubble size distributions measured in the column. Studies were carried out with magnesium sulfate as a result of the improved correlation between the 'transition' concentration obtained in this work and those reported in the literature. The work was carried out using the smallest distributor plate (pore size 40 – 100 μm), over a range of superficial gas velocities (u_s = 1 – 3 cms^{-1}). Measurements are reported at three different heights: at the distributor plate, 10 cm above the plate and 20 cm above the plate (again corresponding to 5 cm below the unaerated liquid surface). Due to practical constraints, experiments were not conducted with xenon.

For a given solute concentration, no differences were visibly observed between the three different gas dispersions. As noted in the experiments with sodium sulfate, bubbles became smaller and more spherical in shape with increasing solute concentration, despite the formation of similar sized bubbles at the distributor plate for all solutions. Once again the primary reason for this decrease in bubble size was ascribed to a decrease in the amount of coalescence occurring in the higher concentration solutions. For the lowest concentration solutions, large bubbles (much smaller than for water) were observed at the highest point in

the column and tended to be oblate ellipsoids. In the higher concentration solutions, larger bubbles were only seen for the highest gas velocities and were generally spherical (or slightly flattened) in shape. As in sodium sulfate, the surface corrugations readily seen in water were not observed.

7.3.1 Air

The number probability density functions obtained for air sparged systems are shown in Figure 7.24 for magnesium sulfate concentrations 0.02, 0.03, 0.04 and 0.06 M. In 0.02 M solution, a distinctly bimodal distribution is measured at the sparger plate, (modal peaks at ~ 130 μm and ~ 780 mm). These small bubbles persist as the distance from the plate increases, (secondary modal peak at ~ 160 μm) whereas there is a significant increase in the number of larger bubbles (primary modal peak shifts to ~ 1900 μm).

With increasing solution concentration, the distribution measured at the plate is no longer so clearly bimodal; although the single peak exhibits the same broad base as the larger in 0.02 M solution, it moves from being significantly skewed to the right (indicating the presence of large bubbles) in 0.03 M solution, to approximating normal in 0.04 M and finally becomes slightly skewed to the left in 0.06 M (indicating the presence of a large number of smaller bubbles). Over the height of the column, the distributions measured in intermediate concentrations show a increase in the number of larger bubbles. This does not happens at the highest concentration solution (0.06 M), where the single peak is conserved over the column height, although there is a small broadening of the tail in this system, which indicates that coalescence is still occurring to some degree. In each case, the modal bubble size measured at the top of the column, decreases with increasing concentration (from ~ 1900 μm in 0.02 M and 0.03 M, to ~ 1280 μm in 0.03 M and then significantly smaller, to ~ 550 μm in 0.06 M). As observed for water and sodium sulfate solutions in which the degree of coalescence was notable, there is an unexpected generation of a significant number of small bubbles (~ 100 – 200 μm) over the column height, for those solutions in which the modal shift is most pronounced (0.03 M and 0.04 M), which leads to a bimodal distribution.

7.3.2 Nitrogen

Figure 7.25 shows the number probability density functions measured in the nitrogen-magnesium sulfate solutions. Once again, the distributions measured in the lower

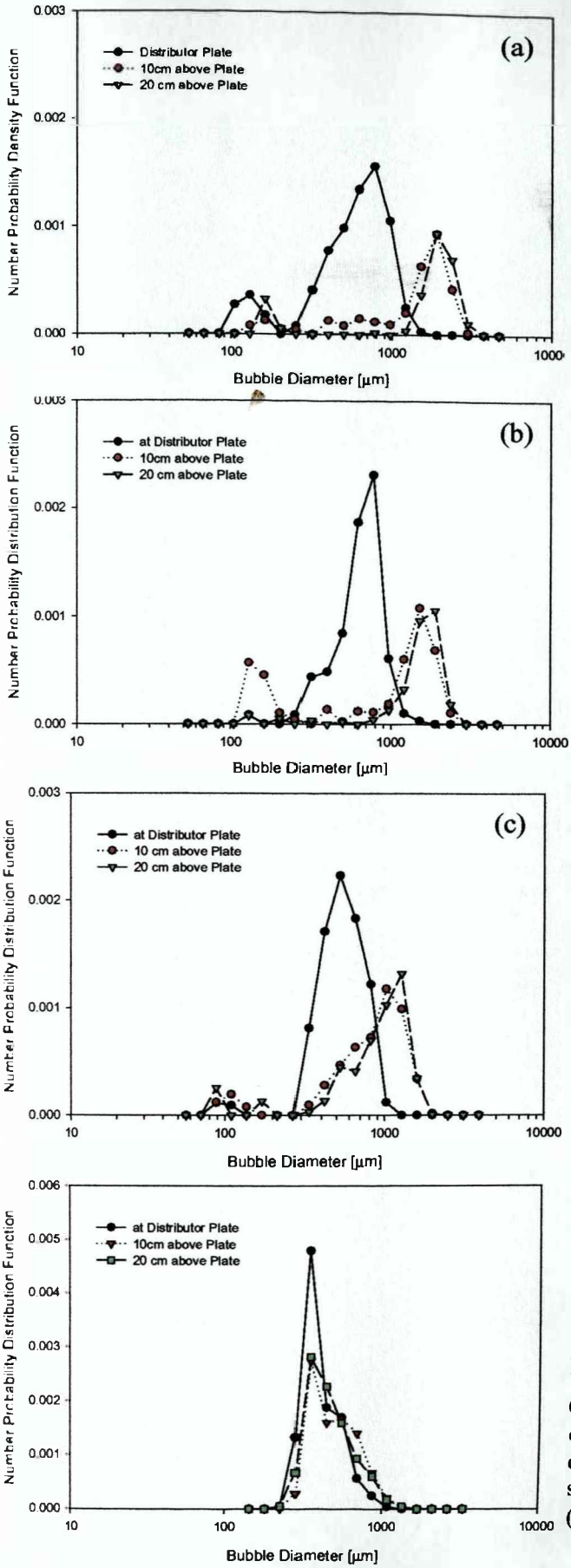

Figure 7.24

Change in number probability density functions with concentration showing evolution of bubble size from distributor plate to top of column for air-magnesium sulfate systems (a) 0.02M, (b) 0.03M, (c) 0.04M and (d) 0.06M. u_s = 1 cms-1, plate pore size 40 – 100 μm.

concentration solutions show a clearly bimodal population at the sparger plate (with modal peaks occurring at ~ 150 μm for the smaller secondary populations). A extremely broad primary peak is observed in 0.02 M magnesium sulfate solution (modal value ~ 900 μm) in comparison to the much narrower primary peak (mode ~ 650 μm) seen for 0.03 M; however, both show a similarly broad base. Once again the smaller secondary peak is conserved over the column height, whereas the primary peaks shifts to larger bubble classes (to ~ 2000 μm in 0.02 M and to ~ 1600 μm in 0.03 M) at the top of the column. In contrast, the distributions obtained in 0.05 M show a single population of bubbles, which do not change significantly in size with column height. The secondary peak of smaller bubbles, present in the distributions measured at lower solute concentration is completely absent. However, the small shift in the modal peak (from ~ 400 μm to500 μm) between the distributions measured at the distributor plate and towards the top of the column, coupled with the slight broadening of the distribution near the top of the column, suggests that some degree of coalescence is still occurring in the system.

7.3.3 Hydrogen

Number density functions for hydrogen-magnesium sulfate experiments show similar trends similar to those observed in the air and nitrogen systems, as seen in Figure 7.26. Once again, a bimodal distribution is observed at the sparger plate in the lower concentrations consisting of a primary peak of larger bubble sizes (modal peaks ~ 590 μm in 0.02 M and ~ 710 μm in 0.03 M solution) and secondary peak of smaller bubble classes (mode at ~ 160 μm in 0.02 M and ~ 120 μm 0.03 M solution). Moving away from the distributor plate the secondary peak is conserved at both concentrations, whereas the primary peak shifts to a larger bubble class (at the top of the column, modal peaks at ~ 2260 μm in 0.02 M and ~ 1740 μm 0.03 M solution). The distributions measured in 0.05 M solution again show a unimodal distribution at the sparger plate which continues over the height of the column (modal peak at ~ 690 μm).

7.3.4 Comparison of Sauter Mean Bubble Diameters

Clearly, the number density functions show similar trends for all three gas dispersions. As previously observed in water and sodium sulfate solutions, in systems where there is considerable coalescence occurring, the (expected) generation of larger bubbles is always accompanied by the formation of a significant number of very small bubbles. Beyond a certain concentration, no further increase in bubble size is measured between the distributor

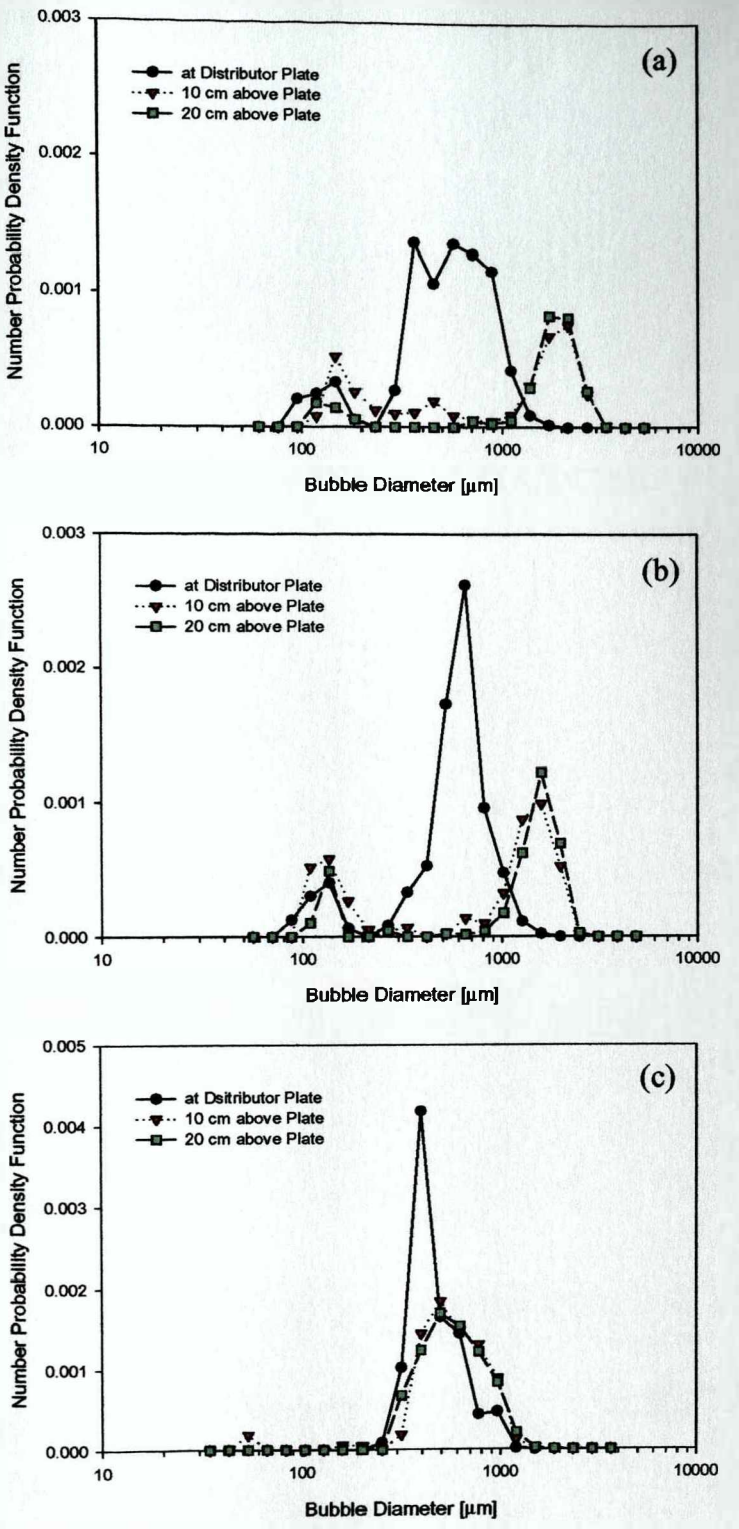

Figure 7.25

Effect of concentration on distributions measured for nitrogen-magnesium sulfate solutions, showing change in bubble size with column height, (a) 0.02 M, (b) 0.03 M and (c) 0.05 M. u_s = 1cms^{-1}, plate pore size 40 – 100 µm.

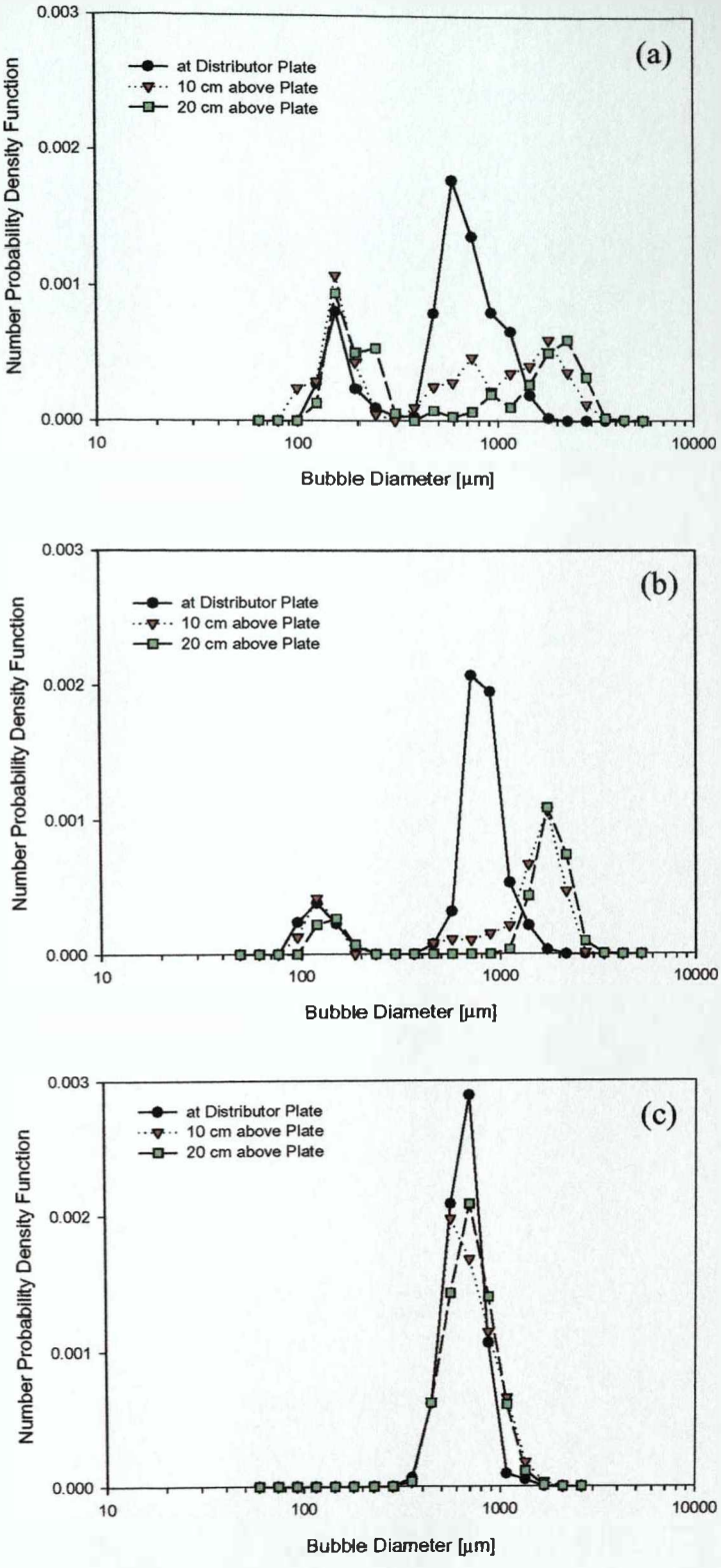

Figure 7.26

Effect of concentration on distributions measured for hydrogen-magnesium sulfate solutions, showing change in bubble size with column height, (a) 0.02 M, (b) 0.03 M and (c) 0.04 M. $u_s = 1 \text{cms}^{-1}$, plate pore size 40 – 100 µm.

plate and the top of the column. In addition the distributions measured in these coalescence repressed solutions show a complete absence of very small bubbles, although the overall mean bubble diameters are smaller.

In Figures 7.27, 7.28 and 7.29, the change in Sauter mean diameter over the height of the column are shown for superficial gas velocities of 1, 2 and 3 cms^{-1} (corresponding initial (at the sparger) and final (at the top of the column) d_{32} values tabulated in Tables 7.7, 7.8 and 7.9). As can be seen, for each set of experiments, the difference between the final and initial Sauter mean diameters decreases with increasing concentration. As observed previously in experiments with sodium sulfate solutions, the d_{32} values measured at the top of the column increase with increasing gas flow rate. For a given superficial gas flow rate, final d_{32} values obtained for hydrogen-magnesium sulfate systems are generally greater than observed in either air or nitrogen, for which the Sauter mean values are similar. Values measured at the distributor plate are similar in all cases, although in 0.02 M marginally larger mean diameters are observed with hydrogen.

Coalescence frequencies have not been calculated for these experiments due to the lack of bubble size data in the region just adjacent to the distributor plate. In Figure 7.30, the bubble size ratios are presented for all systems as a function of magnesium sulfate concentration and clearly indicate the extent of any increase in bubble size between the distributor plate and top of the column. At superficial gas velocity of 1 cms^{-1}, there are no discernible differences between the extent of bubble growth in any of the three gases, which all exhibit the same trend. A consistent decrease in Sauter mean diameter ratio over the height of the column. However, at the higher gas velocities, several differences can be observed between each system.

The mean values determined in experiments with nitrogen for higher superficial gas velocities exhibit the same trends as for u_s = 1 cms^{-1}; the d_{32} ratio decreases with increasing solute concentration. Moreover, it appears that rate of increase of bubble size is limited (a consequence of the maximum stable bubble size) at which point the effect of increasing gas flow becomes limited. Consequently, when the superficial gas velocity increases to 3 cms-1, the d_{32} ratio remains essentially the same in 0.02 M solution, whereas a significant increase is observed for the higher concentrations, due to the smaller final bubble diameters in these systems. Had these experiments been carried out over a sufficiently wide concentration

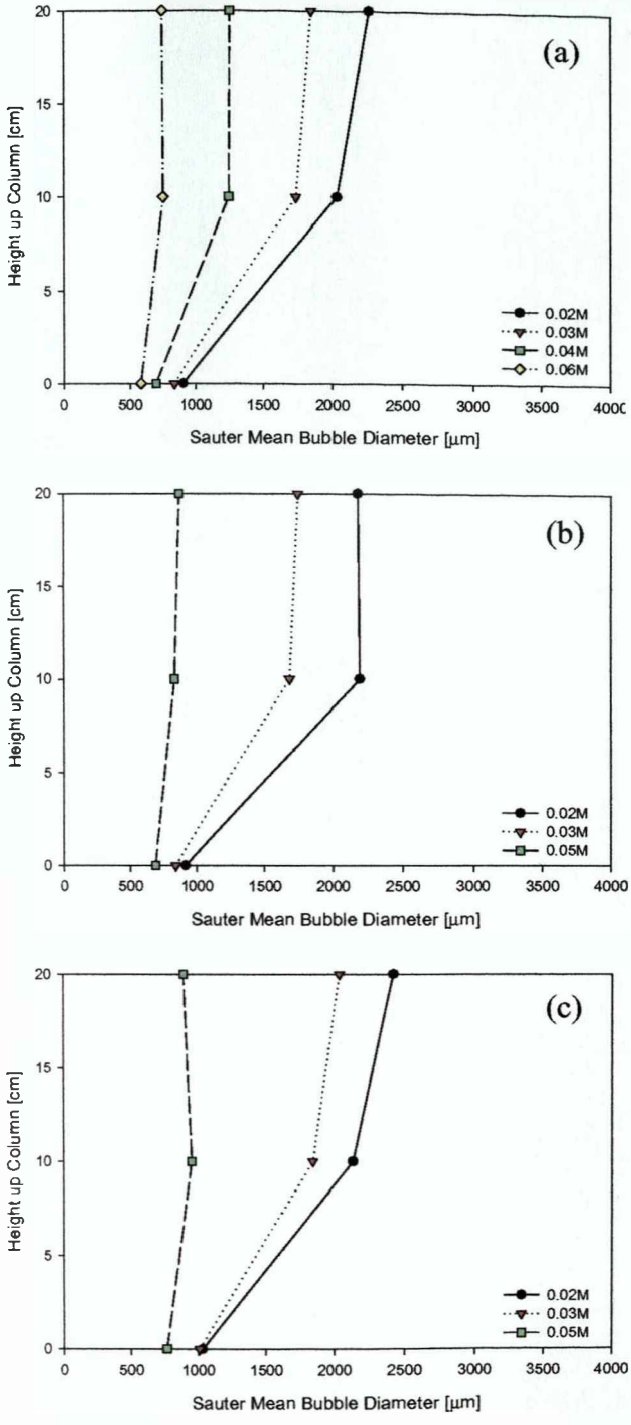

Figure 7.27

Change in Sauter mean diameter with column height for magnesium sulfate and (a) air, (b) nitrogen and (c) hydrogen. For all u_s = 1 cms^{-1}, plate pore size 40 – 100 μm.

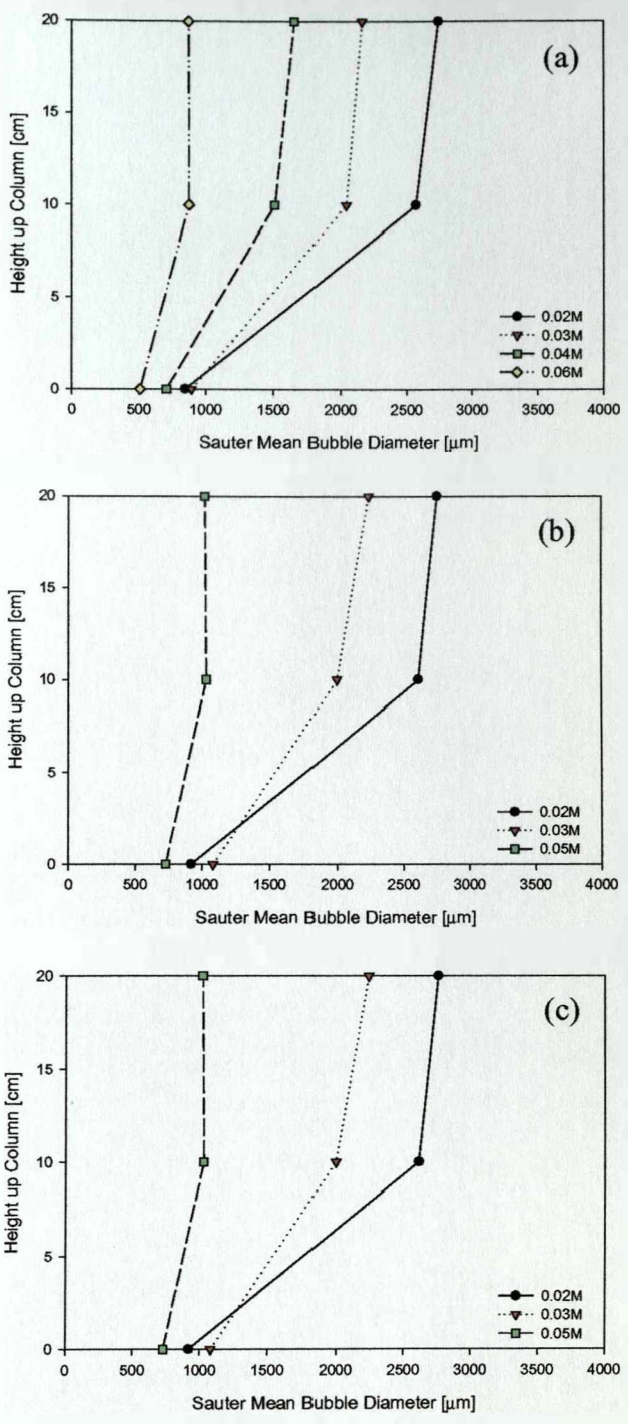

Figure 7.28

Change in Sauter mean diameter with column height for magnesium sulfate and (a) air, (b) nitrogen and (c) hydrogen. For all u_s = 2 cms^{-1}, plate pore size 40 – 100 μm.

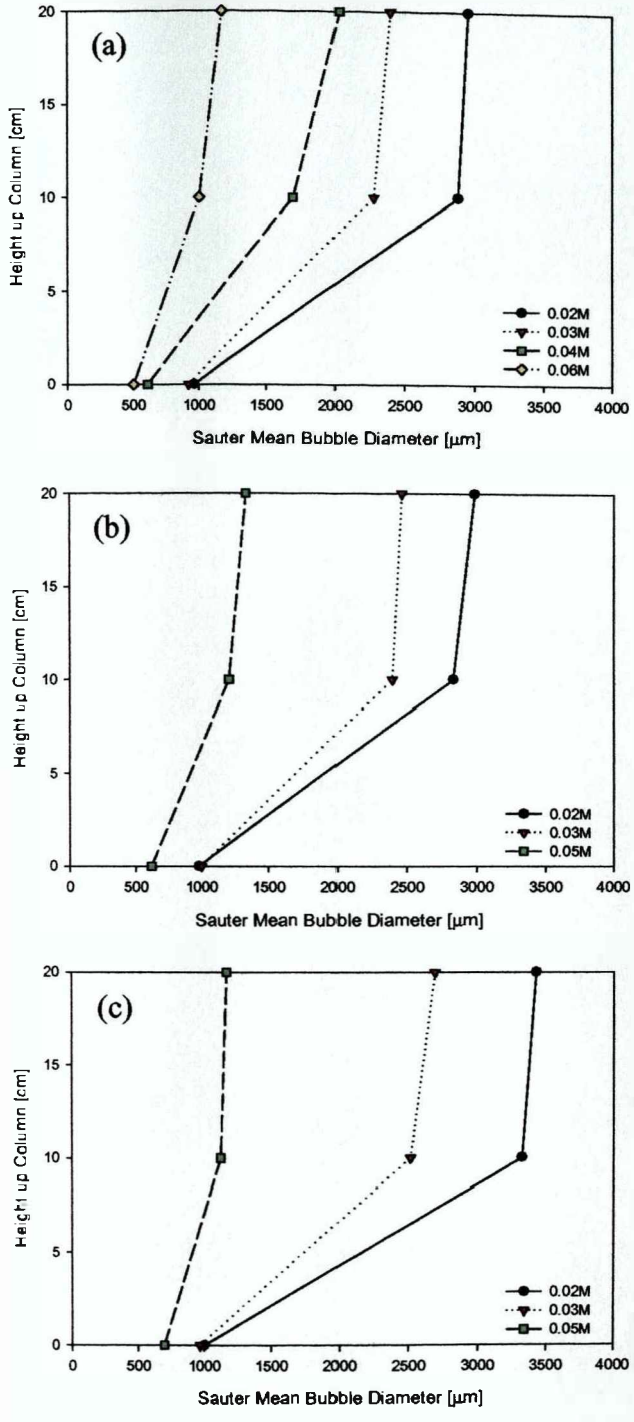

Figure 7.29

Change in Sauter mean diameter with column height for magnesium sulfate and (a) air, (b) nitrogen and (c) hydrogen. For all $u_s = 3$ cms^{-1}, plate pore size 40 – 100 μm.

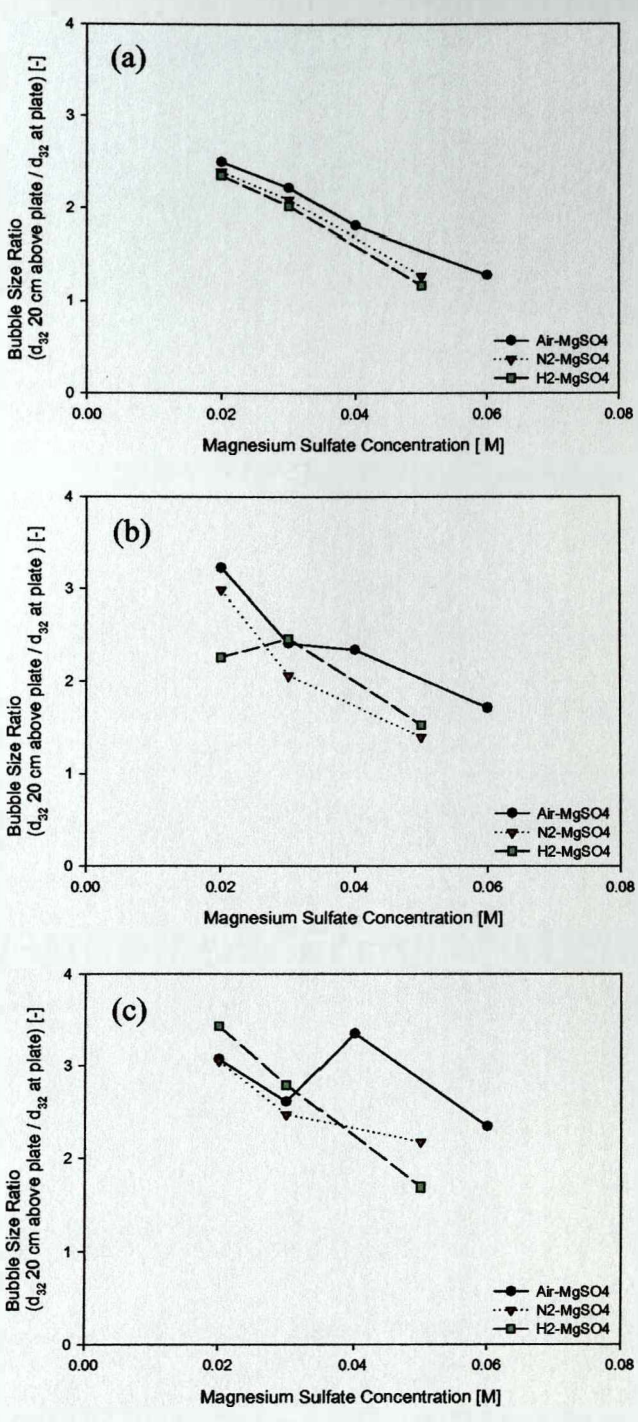

Figure 7.30

Change in dimensionless Sauter mean diameter with $MgSO_4$ concentration (a) $u_s = 1$ cms^{-1}, (b) $u_s = 2$ cms^{-1} and (c) $u_s = 3$ cms^{-1}; plate pore size 40 – 100 μm.

$MgSO_4$ Conc^n	Air		Nitrogen		Hydrogen	
	d_{32} (Initial) [mm]	d_{32} (Final) [mm]	d_{32} (Initial) [mm]	d_{32} (Final) [mm]	d_{32} (Initial) [mm]	d_{32} (Final) [mm]
0.02 M	905	2266	914	2185	1034	2429
0.03 M	834	1853	839	1750	1011	2042
0.04 M	697	1262	-	-	-	-
0.05 M	-	-	687	873	768	898
0.06 M	581	746	-	-	-	-

Table 7.7

Sauter mean diameters at distributor plate (initial) and top of column (final) for air, N_2 and H_2 – $MgSO_4$ solutions; $u_s = 1$ cms^{-1}, plate pore size 40 – 100 μm.

$MgSO_4$ Conc^n	Air		Nitrogen		Hydrogen	
	d_{32} (Initial) [mm]	d_{32} (Final) [mm]	d_{32} (Initial) [mm]	d_{32} (Final) [mm]	d_{32} (Initial) [mm]	d_{32} (Final) [mm]
0.02 M	848	2742	920	2752	1356	3062
0.03 M	897	2162	1083	2233	1026	2519
0.04 M	708	1659	-	-	-	-
0.05 M	-	-	729	1017	665	1015
0.06 M	510	871	-	-	-	-

Table 7.8

Sauter mean diameters at distributor plate (initial) and top of column (final) for air, N_2 and H_2 – $MgSO_4$ solutions; $u_s = 2$ cms^{-1}, plate pore size 40 – 100 μm.

$MgSO_4$ Conc^n	Air		Nitrogen		Hydrogen	
	d_{32} (Initial) [mm]	d_{32} (Final) [mm]	d_{32} (Initial) [mm]	d_{32} (Final) [mm]	d_{32} (Initial) [mm]	d_{32} (Final) [mm]
0.02 M	964	2962	980	2987	1002	3432
0.03 M	920	2405	999	2467	968	2697
0.04 M	608	2040	-	-	-	-
0.05 M	-	-	618	1339	696	1180
0.06 M	502	1179	-	-	-	-

Table 7.9

Sauter mean diameters at distributor plate (initial) and top of column (final) for air, N_2 and H_2 – $MgSO_4$ solutions; $u_s = 3$ cms^{-1}, plate pore size 40 – 100 μm.

range, one would expect to see, as in air-sodium sulfate, an progressive delay in the concentration at which coalescence is suppressed as the superficial gas flow rate increases.

For both experiments with air and hydrogen, trends are somewhat less conclusive. Although experiments with both gases broadly show the same general increase in Sauter mean ratio with gas flow rate, for a particular concentration, there are some deviations. For experiments with air in 0.02 M and 0.03 M magnesium sulfate solution, the degree of bubble growth is similar for both u_s = 2 cms^{-1} and 3 cms^{-1}. The d_{32} ratio is observed to increase consistently with gas flow rate in air-0.06 M magnesium sulfate, however the increase observed in air-0.04 M $MgSO_4$ for increasing the superficial gas velocity to 3 cms^{-1} appears extremely large. Conversely, for experiments with hydrogen, the value determined in 0.02 M for u_s = 2 cms^{-1}, appears quite small in relation to values obtained in the same solution for air and nitrogen experiments.

One disadvantage in using bubble size ratios as a means of comparison is to magnify the effects of inconsistencies in the original data. Consequently, it may be that the values obtained for air-0.04 M and hydrogen-0.02 M magnesium sulfate deviate from the expected as a result of final or initial d_{32} values which are unrepresentative. From Table 7.8 it can be seen that in comparison with equivalent values, the initial d_{32} values appear unexpectedly large and small for H_2-0.02 M and air-0.04 M, respectively. Why might these values be considered unrepresentative? At the higher gas flow rates (u_s = 2 - 3 cms^{-1}) the flow patterns in the column can be seen to change from pure bubbly flow to almost churn-turbulent, where groups of bubbles are transported around the column in swirling eddies. Consequently, images taken of the distributor plate at these gas velocities often contain bubbles that have re-circulated from the zone directly above, where the greatest amount of coalescence occurs (Figure 7.14). Therefore, it may be that the images used to calculate the bubble size distributions do not accurately reflect the actual bubbles sizes formed at the distributor, but rather the mean bubble size near the plate.

7.4.2 Discussion

It is not possible to draw definite conclusions from this set of experiments as to the precise influence of gas type on the coalesce behaviour of a dynamic system. Certainly the behaviour observed does not provide any evidence of correlation with the very small differences in 'transition' concentration observed in the coalescence cell profiles. Whilst this may be due to

the limited number of concentrations investigated in the column (and given that experiments were not conducted with xenon), it must also be considered that in sodium sulfate solutions (investigated over a much wider concentration range), the behaviour in the column was much less well defined than for equivalent systems in the cell. Consequently, it may be that the cell profiles are much more sensitive to weak influences on coalescence, whereas in the much more diverse environment of a bubble column, such influences are subordinated. Alternatively, it may be that the principle effect of gas type is on the rate of bubble break-up and not coalescence, an influence which would not be observed in the cell but may dominate in dynamic systems.

Indeed, Wilkinson et al. (1994, 1990), investigating effects of gas density and pressure in bubbles columns, observed that gas hold-up increased with increasing gas density, especially for the higher superficial gas velocities and conclude that gas density influences bubble break-up and not coalescence. Instrumental to drawing this conclusion were the studies of Sagert et al. (1978, 1977) who measured the coalescence times of CO_2, H_2S and N_2 bubbles in water over a range of systems pressures. [In that work, coalescence times for CO_2 bubbles were found to remain unchanged below pressures of 2 MPa, for N_2 bubbles no influence was observed below pressures of 2.7 MPa, although those measured for H_2S bubbles showed consistent increase with increasing system pressure.] Bubble break-up was postulated to arise from critical instabilities at the gas-liquid interface, the growth rates of which were considered to increase in systems with a combination of high gas density and high relative velocities at the interface (high superficial gas velocity). In contrast, Takahashi and Nienow (1993, 1992) and Takahashi et al. (1992), investigated the effect of gas density on bubble sizes in agitated tanks and report significantly greater number of smaller bubbles (< 0.2 mm) for hydrogen-water, than in either air or xenon-water systems. Correspondingly, in their measurements of coalescence rate (number of events per unit time), Takahashi and Nienow (1993), observe this increases with gas molecular weight (and hence density). In each case, the results were tentatively explained on the basis of an increased surface area of the vortex cavities issuing from the impeller blades, as the gas density decreased.

It would appear therefore that further work is required to elucidate the influence of gas type on the equilibrium between bubble coalescence and break-up in dynamic systems. Additional

experiments using the coalescence cell are unlikely to provide useful information in this respect as the set-up allows only one aspect of the equilibrium process to be investigated. However, it may be that the multi-level measurement technique followed in this study will provide the answer as it allows for the necessary close scrutiny of the bubble size distributions within the vessel.

7.4 Images of Coalescence

Although the progress of a bubble can occasionally be traced over sequential frames (this applies especially for the smallest bubbles, which become entrained in the flow and can often occupy a sequence of up to about 10 frames), the standard video camera and stereo microscope equipment is too slow to follow the process of coalescence in-situ. However, as noted by Tse et al. (1998) and Martin (1996), the experimental set-up does occasionally provide (entirely fortuitous) snap-shots of the coalescence process between two bubbles. Relative to the large numbers of frames viewed, coalescence events are rarely captured, rising from about one frame in fifty for systems where a larger amount of coalescence occurs, to less than one in a thousand for coalescence repressed systems. In both cases, the majority of coalescence events are observed at the distributor plate where it can be divided into two types: coalescence at the plate of a still forming (or newly formed) bubble with the preceding bubble generated from the same pore (Figure 7.31), or at some distance above the plate between two freely moving bubbles formed from different streams (Figure 7.32). In coalescence events between newly formed/still-forming bubbles with those in the stream directly above, the characteristic annular wave (see below) is often compressed by the lower surface of the bubble retracting rapidly which appears to accelerate the progress of the bubble away from the plate.

In terms of the three step mechanism for coalescence, these images are more accurately defined as images of confluence, as they generally show the steps immediately following the point of film rupture, before the newly generated composite bubble has regained its more regularly observed spherical (or ellipsoidal) shape. Indeed, this irregularity of shape, combined with the presence of a characteristic annular wave (see Martin, 1996) are generally very reliable indicators of the occurrence of a coalescence event. The annular wave can be clearly seen to move outward (in pairs) from the site of film rupture to each end of the bubble, appearing as a well-defined edge

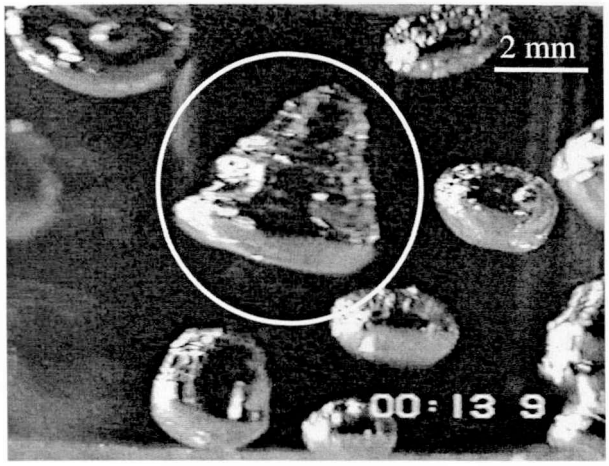

Figure 7.31

A newly coalesced bubble at the distributor plate showing the annular wave with an irregular compressed shape; water, u_s = 1 cms^{-1}, plate pore size 160 – 250 μm.

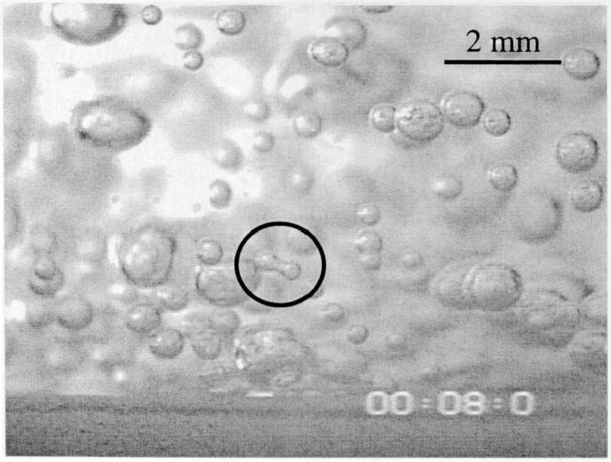

Figure 7.32

Coalescence between two freely moving small bubbles at the distributor plate in H_2 – 0.02 M MgSO4; u_s = 2 cms^{-1}, plate pore size 40 – 100 μm.

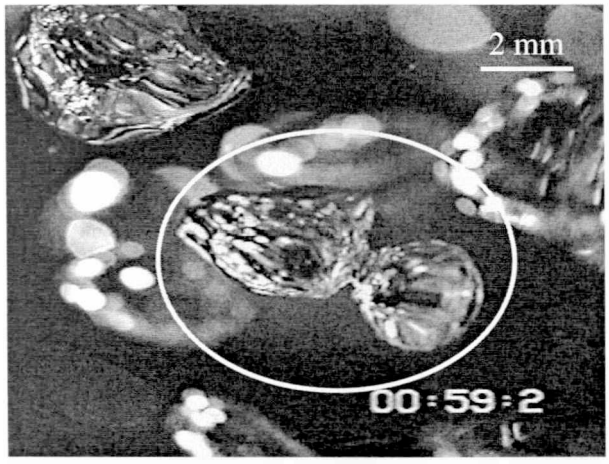

Figure 7.33

Coalescing bubbles ~ 14 ms after the moment of film rupture, as evidenced by narrow bridging neck and short distance between pairs of annular waves. Water; 10 cm above plate; u_s = 1 cms^{-1}; plate pore size 160-250 μm.

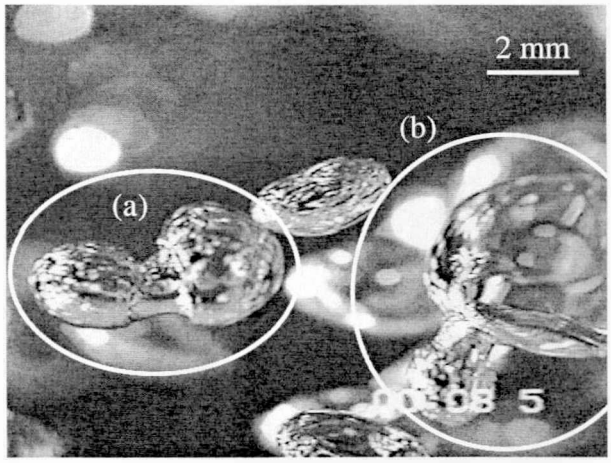

Figure 7.34

Bubble pairs in the final stages of confluence with the annular wave still visible at each end. Note surface corrugations. (a) ~ 0.6 ms and (b) ~ 0.25 ms after film rupture. Water; 2 cm above plate; u_s = 1 cms^{-1}; plate pore size 160- 250 μm.

between the concave bubble neck and the convex bubble surface. It results from the very rapid expansion of the hole following the instant of film rupture and as it moves down the length of the bubble causes the rippling effect. As noted by Martin (1996), similar events have been described in the literature for the coalescence of a liquid drop with a liquid interface (Charles and Mason, 1960) and for a bubble at the gas-liquid interface (MacIntyre, 1972). The images are extremely similar to those observed with the high-speed video camera in the coalescence cell and which

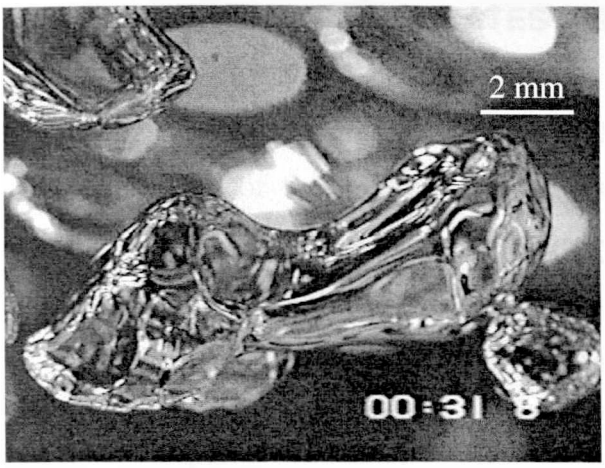

Figure 7.35

Advanced coalescence between two very large bubbles in water; 10 cm above plate; u_s = 1 cms^{-1}, plate pore size 160 – 250 μm. Note the very large, deformed bridging neck and surface corrugations which almost obscure the characteristic annular wave.

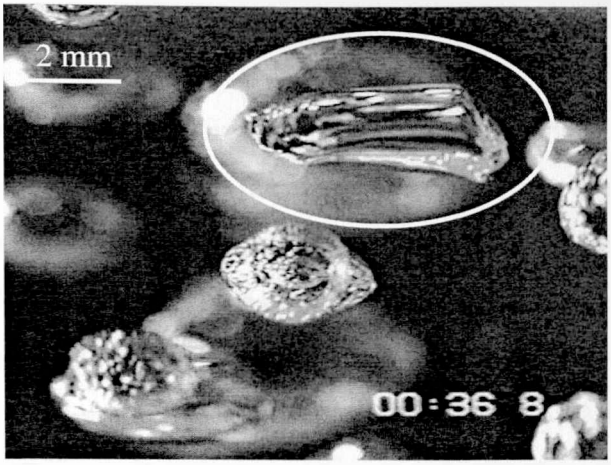

Figure 7.36

Coalesced bubble in the final stages of confluence with the annular wave still visible at each end (~ 0.9 ms after film rupture). Note stretched surface corrugations. Water; 2 cm above plate; u_s = 1 cms^{-1}; plate pore size 160- 250 μm.

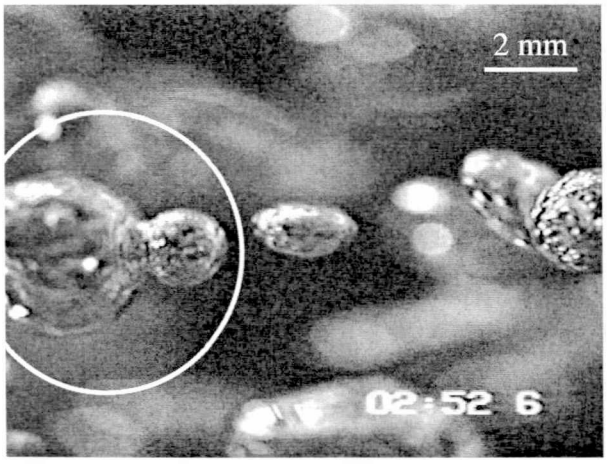

Figure 7.37

Rare image of coalescence between two differently sized bubbles in 0.08 M Na_2SO_4, ~ 0.18 ms after film rupture; 20 cm above plate, u_s = 1 cms^{-1}, plate pore size 160 – 250 μm.

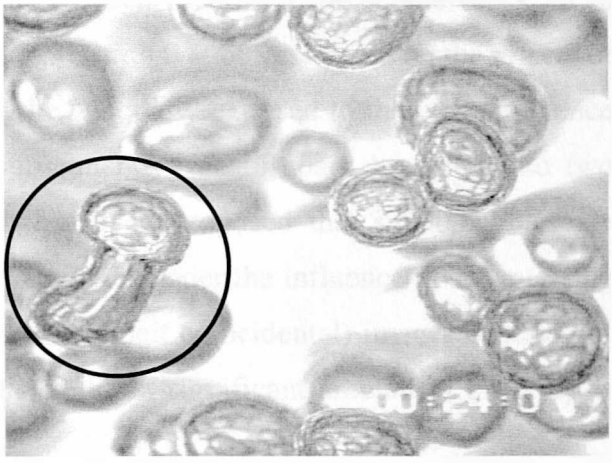

Figure 7.38

Coalescence in N2-0.02 M $MgSO_4$ between two approximately equal sized bubbles, possibly through a wake-assisted interaction; 20 cm above plate, u_s = 2 cms^{-1}, plate pore size 40 – 100 μm.

showed a 'strange ripple' in the frames directly following film rupture. Comparisons of these images with those obtained in the free flow conditions of the column suggest the 'strange ripple' is analogous to the annular wave reported here. Given that the 'strange ripple' was calculated to move at a speed of approximately 2.5 ms^{-1} (Chapter 5), it is then possible to determine how long film rupture and consequently, coalescence occurred before image capture (Figures 7.37, 7.38).

7.5 COALESCENCE GENERATES VERY SMALL BUBBLES

In systems where there is a large increase in the bubble size distribution between the distributor plate and the top of the column, a most conspicuous feature of the distributions is that the generation of larger bubbles is almost always accompanied by a significant increase in the number of very small bubbles (~100 - 200 μm diameter). In each case, these small bubbles are not present in the distributions obtained at the sparger plate in any great number and consequently cannot be said to have persisted over the height of the column. In addition, the number of small bubbles appears to decrease as the difference between the distributions is reduced (i.e. moving up the column, as the coalescence rate decreases).

The obvious explanation is that the small bubbles are the result of bubble break-up over the height of the column. Two primary mechanisms have been identified for bubble break-up in columns (Prince and Blanch, 1989, Miyahara et al., 1991, amongst others) based on the effects of wake vortices. A bubble rising up the column may be unequally exposed to the wake influence of a preceding bubble, becomes elongated and subsequently shears apart, breaking into two daughter bubbles, (Figure 7.39). Alternatively, it has been proposed that small bubbles are generated by shedding from the rim of large unstable bubbles under the influence of shear arising from wake vortices (Figure 7.40). However, for all the (albeit coincidental) images obtained of coalescence, no images have been seen which indicate that a significant amount of break-up is

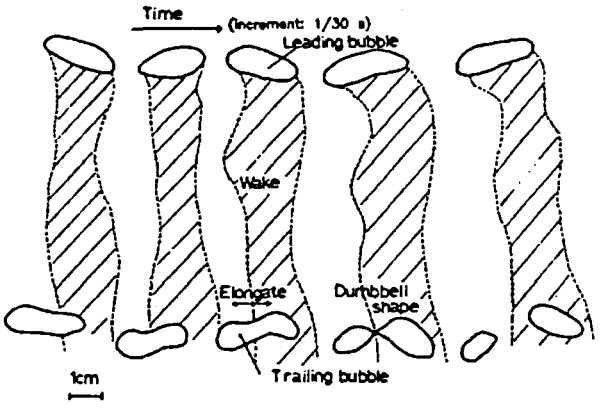

Figure 7.39

Sequence of break-up of trailing bubble due to the turbulent shear created by the wake of the leading bubble (from Miyahara et al., 1991).

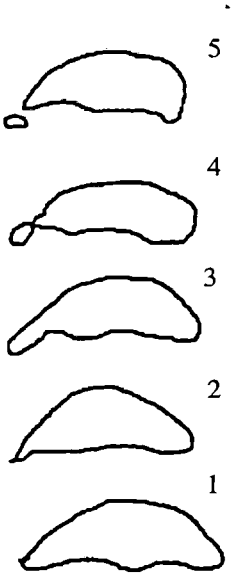

Figure 7.40

Break-up occurring as rising bubble is exposed to the high shear created by wake vortices which pinch off small bubbles at the rim (schematic drawn from Walter and Blanch, 1983).

Time scale for schematic is 50 milliseconds.

Bubble volume: 50cm^{-3}.

occurring in these systems. This absence of common break-up events is also noticeable in the high-speed video studies which have been carried out (see Section 7.7), wherein coalescence events are numerous.

Martin (1996) and Machon et al. (1997) have both used the same video camera-stereo microscope as used in this study to observed bubble sizes in stirred vessels and both have noted the presence of significant numbers of very small bubbles in air-water systems. Martin (1996) suggests that after these smaller bubbles are generated in the strong vortices of the impeller zone, they fail to coalesce further either as a result of the low bubble density observed in water, or perhaps due to the presence of an unfavourable flow-field around larger bubbles, which prevents close approach. In this system, the absence of an impeller to generate high shear fields implies that the generation of smaller bubbles must then arise from break-up events, perhaps the results of unequal entrainment in bubble wakes. However, it seems particularly significant that the greatest numbers of small bubbles are observed in systems with the largest increase in overall bubble size over the column height. Although counter-intuitive, the evidence suggests a strong link between the generation of larger bubbles and the increase in much smaller bubbles. It appears that the coalescence process itself generates these small bubbles. The question then becomes, by what mechanism could coalescence result in the formation of much smaller bubbles?

The answer to the question is provided in Figure 7.41, which was obtained in 0.03 M magnesium sulfate and nitrogen (u_s = 2 cms^{-1}, 20 cm from the distributor plate). The image very clearly

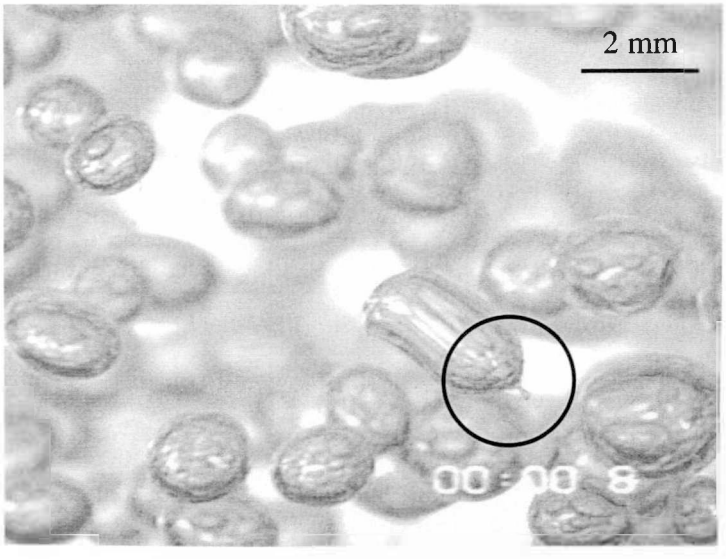

Figure 7.41

Coalescence leading to the simultaneous formation of a very small bubble. The annular wave characteristic of coalescence can be clearly seen at either end of the newly coalesced bubble.

shows the generation of a small bubble as the annular wave, which characterises a coalescence event, travels the length of the newly coalesced bubble, pinching off a small bubble at the extremity. In addition, many images have been obtained which show either a recently coalesced bubble shortly before the break-up event occurs (Figure 7.42 and 7.43) or just after, before the very small bubble has left the immediate vicinity of the newly coalesced bubble (Figure 7.44 and

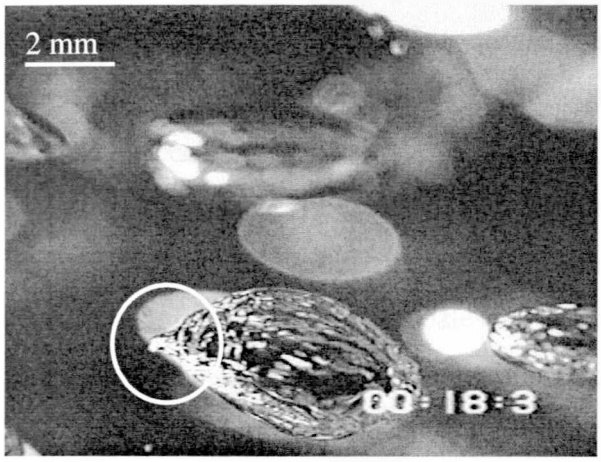

Figure 7.42

A newly coalescence bubble just prior to forming the very small secondary bubble, as indicated by the protruding column. Water; 20 cm above plate, us = 1 cms-1, plate pore size 100 – 160 μm.

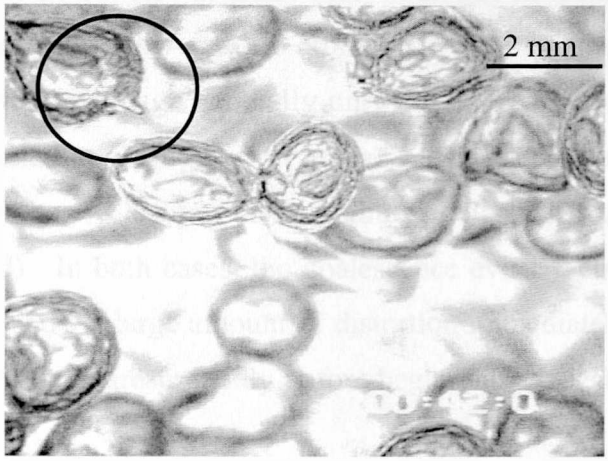

Figure 7.43

Similar image clearly showing the annular wave characteristic of coalescence and the column from which the secondary bubble is formed. 0.02M $MgSO_4$ – N_2, 20 cm above plate, u_s = 3 cms^{-1}, plate pore size 40 - 100 μm.

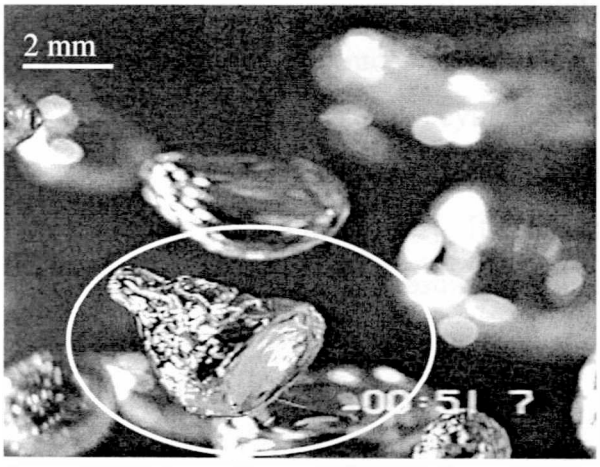

Figure 7.44

Image taken immediately following secondary bubble formation. Water, 2 cm above plate, u_s = 1 cms^{-1}, plate pore size 160 - 250 μm.

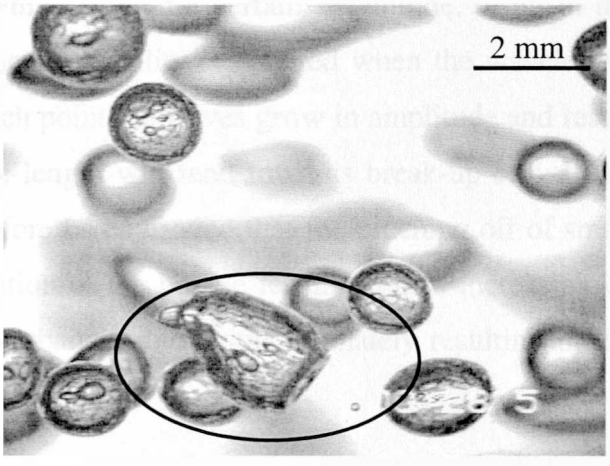

Figure 7.45

Secondary bubble formation, showing annular wave and very small bubble. Possible pinching off at opposite end to generate a second daughter bubble? 0.02M $MgSO_4$ – Air, 20 cm above plate, u_s = 1 cms^{-1}, plate pore size 40 - 100 μm.

7.45). In the many thousands of frames screened, Figure 7.40 is the only image captured which so clearly illustrates the process, a consequence surely of the very short time frame of the event.

Similar events have also been observed in the coalescence cell, where the coalescence of two bubbles has resulted in the simultaneous formation of a much smaller one. Figures 7.47 and 7.48 show sequences for the process occurring between air bubbles in water (very high gas flow rate 400 $cmmin^{-1}$) and 0.04 M sodium sulfate solution (gas flow rate 30 $cmmin^{-1}$). Simultaneous coalescence and break-up is not an uncommon event, although generally only observed in water for coalescence between very large bubbles (formed at high gas flow rates) and in electrolyte solutions between poorly synchronised bubbles (where a leading bubble, almost detached from the nozzles 'captures' a bubble still being formed). In both cases, the coalescence event seems extremely violent as the newly coalesced bubbles show a large amount of distortion immediately after the event, with the whole bubble appearing to flex unrestrainedly before beginning to regain the 'regular' ellipsoidal shape.

The mechanism leading to the formation of these daughter bubbles appears similar to the mechanism of capillary break-up in liquid cylindrical columns, as first considered by Rayleigh (1897). In this case (Figure 7.46), as the diameter of the cylinder decreases, the growth of capillary waves introduces critical instabilities which beyond a certain magnitude, result in the break-up of the cylinder into droplets. The critical instability is reached when the wavelength exceeds the circumference of the cylinder, at which point the waves grow in amplitude and result in break-up. This means that a column of finite length will tend towards break-up only if the length exceeds the circumference. It could therefore be envisaged that the pinching off of small bubbles by the annular wave results from elongation of the bubble terminus, thus increasing its susceptibility towards the effect of capillary disturbances and result ultimately resulting in the formation of secondary bubbles.

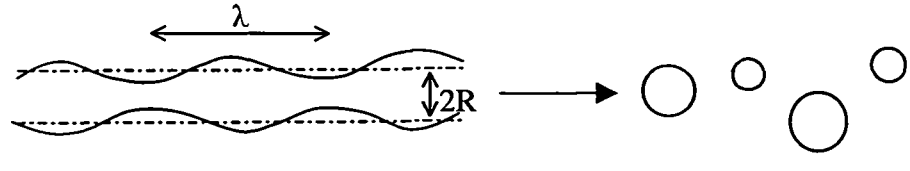

Figure 7.46

Formation of droplets from a cylinder of liquid, caused by the growth of instabilities

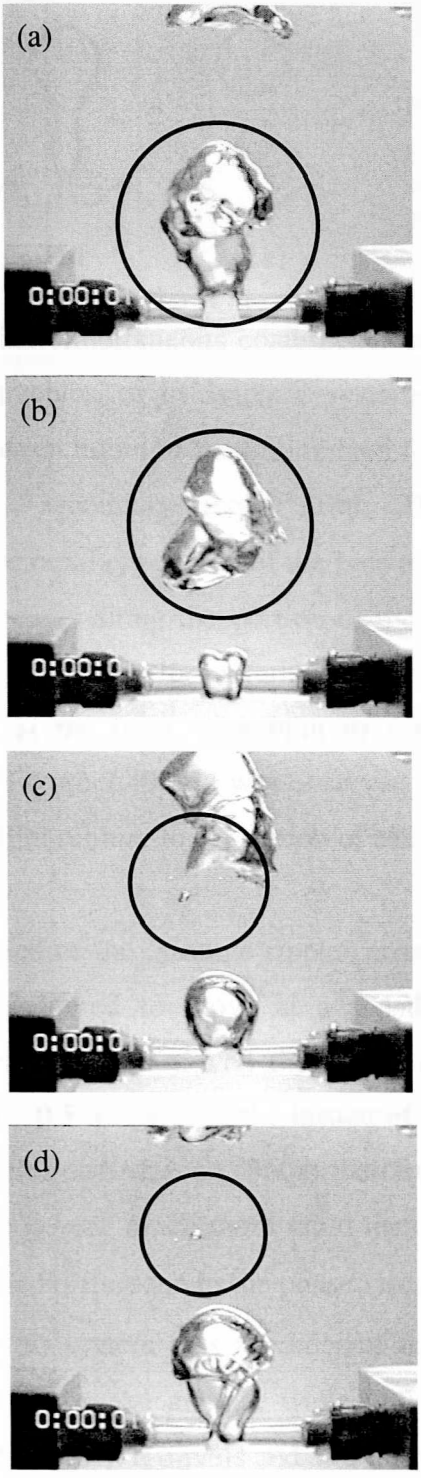

Figure 7.47

Coalescence in cell, in air - water between two previously coalesced bubbles pairs, resulting in further (in-line) coalescence and generation of four secondary bubbles. Nozzle distance 4 mm, gas flow rate = 400 $cmmin^{-1}$.

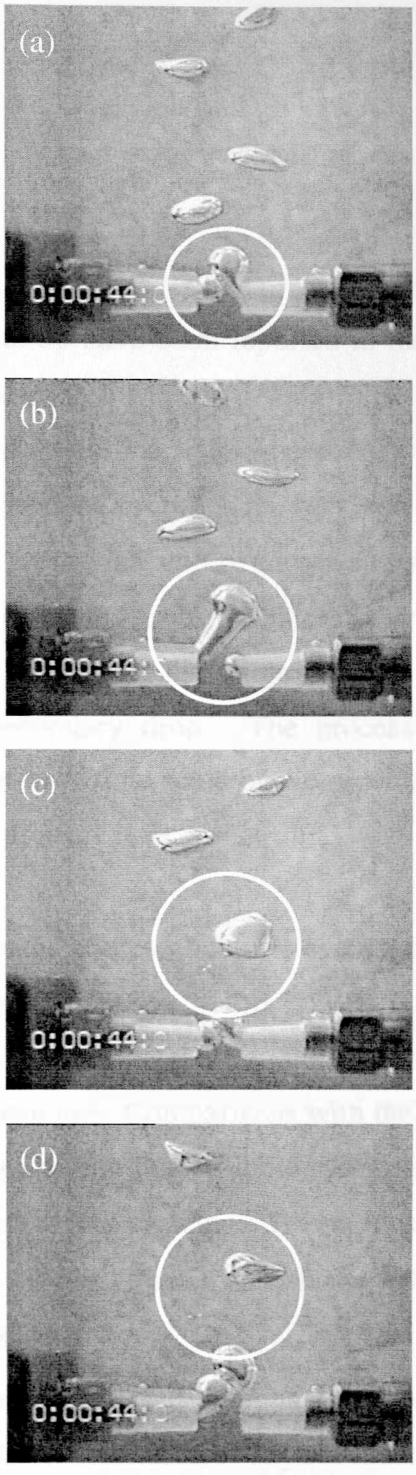

Figure 7.48

Coalescence in cell, in air - 0.04 M $MgSO_4$ between two non-synchronised bubbles, resulting in formation of two secondary bubbles. Nozzle distance 4 mm, gas flow rate = 30 $cmmin^{-1}$.

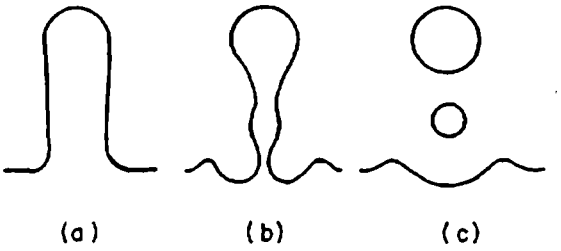

Figure 7.49

Schematic diagram of simultaneous formation of two large secondary drops during partial coalescence (from Charles and Mason, 1960).

Instances of similar simultaneous coalescence and break-up have been reported in the literature but not for gas bubbles, or in dynamic systems. Charles and Mason (1960a) observe 'partial coalescence' between liquid drops falling on a flat liquid–liquid interface where the primary drop is succeeded by a secondary smaller drop. The mechanism proposed is very similar to that observed here: the rapid expansion of the hole resulting from film rupture causes a "shock-wave" which travels upwards along the portion of the drop protruding from the interface creating "an unstable bulge on reaching the summit". As drainage proceeds, the bulge becomes a column which contracts at the base, detaching to form a secondary drop. The process is shown schematically in Figure 7.49 and was observed to occur on a time scale of the order of ~150 ms (from instant of film rupture to separation of secondary drop).

Based on the speed of the 'strange ripple' observed in the coalescence cell events, the annular wave can be considered to move at a speed of approximately 2.5 ms^{-1}. In Figure 7.40, consequently, where it has moved the length of the bubble (~ 2.5 mm), the moment of film rupture occurred ~ 0.5 ms prior to the instant of image capture. Comparisons with the time scale observed by Charles and Mason (1960a) therefore, suggests that in gas-liquid systems secondary bubble formation is very much more rapid than in liquid-liquid systems. This is most probably due to the increased difference in the phase viscosity ratios (for Charles and Mason (1960a) μ_d/μ_c ~ 4, whereas in this system it is an order of magnitude less (μ_g/μ_l ~ 0.2)). Consequently in a liquid-liquid dispersion the annular wave will encounter increased viscous forces which will reduce the speed at which it travels and as a result the rate of formation of any secondary drops.

The number distributions which show the greatest population of small bubbles are those measured in water, where the final bubble size distribution is clearly bimodal. For the three different porous plates, the greatest number of small bubbles is observed in the experiments with

the largest pore size (160 – 250 μm) where the initial bubble size is large (d_{32} ~ 4 mm). In electrolyte solutions, the distributions which show significant numbers of smaller bubbles are also those which are obtained using the large pore size plate (see Figure 7.5). As seen in the sequences from the coalescence cell, small bubbles are only generated when the newly coalescence bubble is subject to a considerable amount of distortion. The increased flexibility of larger bubbles, especially those formed in water, may make them more susceptible to large amounts of distortion as the annular wave caused by the rapid expansion of the hole, moves rapidly away from the point of coalescence, thus facilitating the formation of secondary bubbles. In electrolyte solutions, even at concentrations where significant amounts of coalescence occur, bubbles of all sizes appear much less flexible, less prone to undulation as they rise and more spherical in shape. Consequently, bubbles should be less prone to severe distortion from the annular wave, thereby decreasing the number of coalescence events that give rise to secondary bubbles.

In addition to the formation of very small bubbles in fully coalescing systems, it is important to note that they are seen to persist over the height of the column. As discussed previously, the lack of further coalescence and consequent bubble growth may be due to bubble bounce following collisions or to an inability to approach larger bubbles sufficiently close for coalescence to occur. It is well known that in viscous systems, bimodal bubble distributions exist where the small bubbles, as a consequence of excessive drag force remain in the dispersion after they have become exhausted. Although in inviscid systems, such as considered here, the bubbles do not experience such an impediment to free rise, it is possible that they will fail to disengage readily, due to entrainment in the flow fields of the larger bubbles.

7.6 High Speed Video Studies of In-Situ Behaviour

In order to carry out simplified coalescence studies (such as in the cell) which will generate useful information about coalescence in dynamic systems, it is necessary to characterise the mechanisms by which bubbles contact in situ. Many questions remain to be answered about the influences of system hydrodynamics on bubble behaviour; what is the effect of the various flow regimes on bubble-bubble interactions and to what extent does coalescence arise from turbulent

collisions or due to bubble entrainment in the vortices or eddies observed in bubble columns (and agitated vessels)? It would be useful to know what types of bubble-bubble contacts occur; what are the typical contact times (and contact forces) for bubbles in a free system; and which contact orientations give rise to coalescence, for example. High-speed camera studies such as those used by Walter and Blanch (1986), Prince and Blanch (1989b) and Stewart (1995) to follow bubble-bubble interactions, could provide a useful tool in resolving some of these questions. In this work high speed video studies have been carried out to observe bubble-bubble interactions in water and coalescence inhibited solutions of sodium sulfate (0.06 M). Observations were made using a frame rate of 1000 s^{-1} and images were taken at a distance 10 cm above the distributor plate for superficial gas velocities of 1 to 4 cms^{-1}.

It is extremely difficult to obtain sharp images of in-situ coalescence using the high-speed video camera. Images obtained with the Panasonic camera (frame speed 50 s^{-1}) were taken using a strobe flashing at 50 s^{-1} to enable bubbles in the column to be clearly resolved. However, despite the much faster frame speed of the high speed video camera (1000 s^{-1}), images are not of comparable quality, as can be seen in Figures 7.50 to 7.53. In part this was due to the difficulty of providing suitable lighting, in solutions of 0.06 M sodium sulfate especially, the increased number of bubbles significantly reduced the amount of light transmitted. However, the focal depth of the fast camera was also much greater than that of the Panasonic, which made it more difficult to focus exclusively on a single plane of interest. Additionally, increasing the frame speed of the camera did in some cases provide improved pictures, although a frame speed of 1000 s^{-1} was chosen as it offered the best compromise between lighting requirements, image size and image quality.

7.6.1 Water

The most conspicuous feature of bubbles rising in distilled water is the free form nature of the bubbles, which appear to continuously oscillate whilst rising up the column. The centre of a bubble is seen to move slowly in a random manner through the image frame, while the outer portions of the bubble undergo rapid oscillations, which consistently alter the bubble shape. At a superficial gas velocity of 1 cms^{-1}, the bubbles do not move directly upwards but rather in a poorly defined manner through the column. Consequently, the bubbles appear to rise very slowly

up the column. Increasing the superficial gas velocity causes the bubbles to move more directly upwards, with the random linear motion observed at lower gas flow much reduced. In addition, the amount of oscillation observed appears substantially decreased at the higher gas flow rates. The random linear motion of the bubbles appears different from the zigzag rise path which has been reported for rising single bubbles (Tsuge and Hibino, 1977) as those in the column are seen to move primarily in a single direction until a collision results in a change of direction.

Visual observations appear to suggest that the bubbles interact with each other beyond simple physical contact; the oscillations of one bubble can be seen to induce similar oscillations in a neighbouring bubble as a result of their close presence and not through direct contact. Contacts between bubbles are frequent, although only a small proportion lead to coalescence. More often bubbles contact, deform to accommodate the obstacle (suggesting a large area for film drainage) and then separate, all whilst continuing to oscillate. In other contact events, the bubbles are seen to collide, immediately contract in the direction of the collision and separate without coalescing. Collisions between very small bubbles and substantially larger ones are the only type in which bubbles are obviously seen to bounce apart. This is most probably as result of the increased rigidity of the very small bubbles, which also has the effect of making them spherical and not prone to shape oscillations. As noted by Stewart (1995), coalescence events are only ever observed to be binary processes. In Figure 7.50, a seeming three-bubble coalescence event is shown, although closer scrutiny disproves this. [Initially the two right most bubbles coalesce, followed (1 ms later) by the coalescence of the new bubble (still distorted from the first event) with that on the left side.]

When viewed at high speed, the presence of the annular wave, which is so characteristic of coalescence in pictures taken at slower speeds, is not obvious. Rather, the most reliable indication of a coalescence event when viewed at high speed, is the systematic cycle of diminishing latitudinal contractions and longitudinal expansions that the newly coalesced bubble undergoes before it regains its more regular shape. However, shape distortions can be seen following coalescence events which, when the image is frozen, are identical to those obtained with the 50 frames^{-1} camera. Although some of the coalescence events can be viewed in light of the three step mechanism of approach, film drainage and rupture, a considerable number of

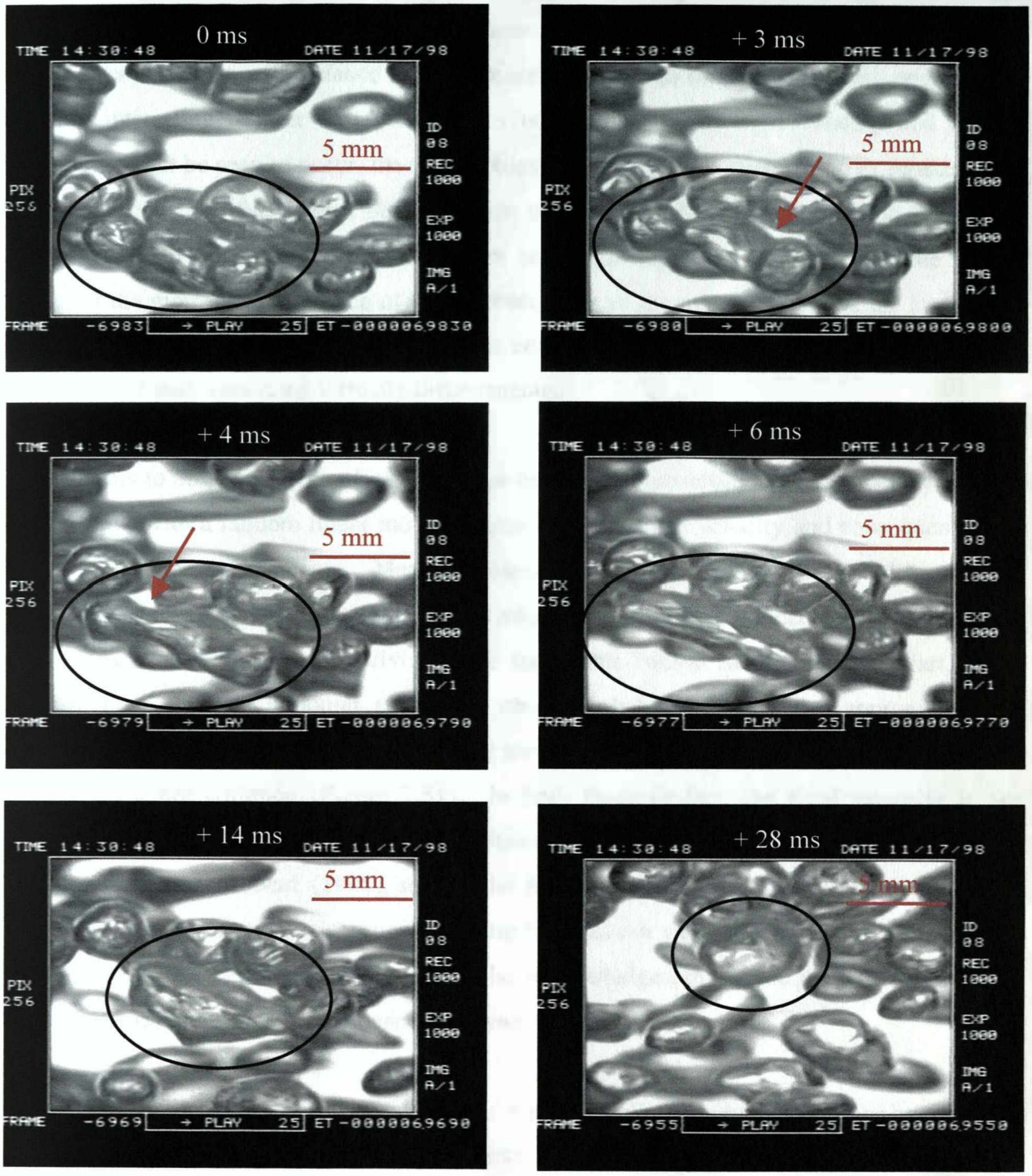

Figure 7.50

Series of frames showing binary coalescence in water: 0 ms: three bubbles approach and contact, 3 ms: film rupture between bubbles on right, 4 ms: coalescence between bubbles on left, 6 – 28 ms: confluence of newly coalesced bubble. u_s = 1 cms^{-1}, plate pore size 40 – 100 μm. (Arrows denote point of film rupture).

events are seen to occur without the two bubbles appearing to approach sufficiently close enough for contact. In these instances, the bubble surfaces appear to experience some form of attraction to each other and at a small distance apart coalescence occurs as the two move into one another. It is also interesting to note that in the cases where the contact, film thinning and rupture mechanism might be seen to occur, the two bubbles are often seen to slide over one another, such that a new contact surface forms between them over time. In all cases, the probability of a coalescence event appears to decrease if there is a high degree of movement at the bubble surfaces at the moment of approach of two bubbles. For all the events observed, the moment of film rupture (as suggested by the studies in the coalescence cell) occurred within the time of a single frame (1 ms), appearing virtually instantaneous.

There appears to be no one type of contact event that leads to coalescence. As stated earlier, the bubbles move with a random linear motion at low superficial gas velocity and consequently can contact in various arrangements. Many coalescence events occur between bubbles colliding horizontally or on an inclined plane (diagonally adjacent). The wake induced collisions that have been reported to be the primary driving force for bubble-bubble interactions (Stewart, 1995, Miyahara et al., 1991), although sometimes observed (when two bubbles approach in the horizontal plane, the smaller one is occasionally seen to accelerate rapidly as it is swept in behind the larger) are not common (Figure 7.51). In both these studies, the fluid viscosity is not substantially greater than used in this study (Stewart (1995) uses fluids with viscosity ranging from 1 to 8 mPas). Stewart (1995), reports the bubble wake to be the 'sole mechanism' for bubble interaction, with no coalescence occurring that was not wake-mediated. This is certainly not observed in this system, although it must be acknowledged that there is some difficulty in determining the extent of wake influence in a dynamic system.

In these high speed video studies no evidence of bubble break-up is observed, either by shedding of small bubbles from the rim of larger unstable ones or through the wake-induced breakage mechanisms suggested by Prince and Blanch (1989b) and Miyahara et al. (1991). Although this may reflect a reduced overall bubble size as compared to those observed in larger scale systems, it may also suggest that the mechanism is not valid in low viscosity liquids (such as water) where the wake structure is much less well defined (Narayanan et al., 1974). No definitive images were

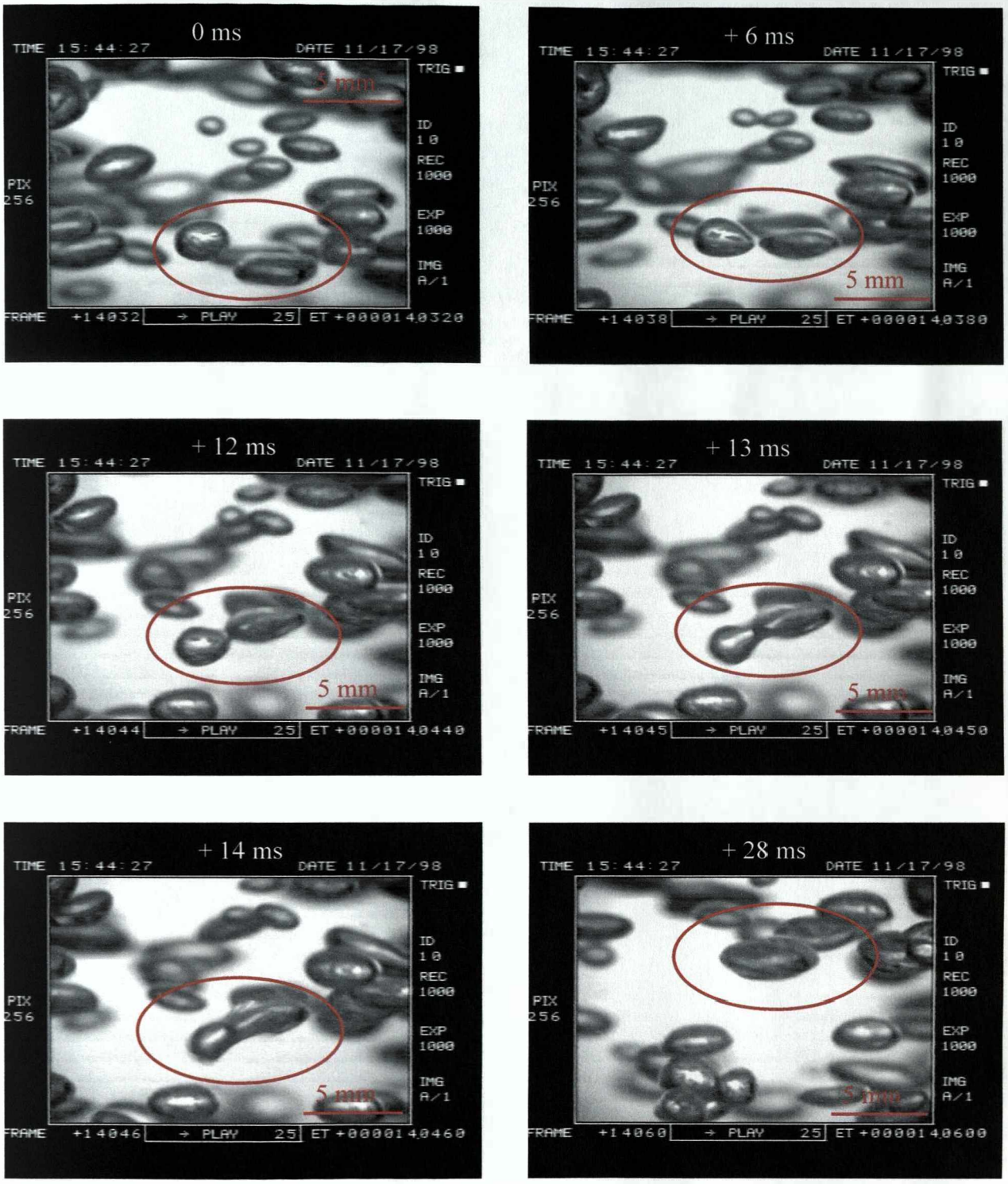

Figure 7.51

Possible wake-mediated coalescence between two similar sized bubbles in water. Leading bubble at t = 0 ms, is drawn into wake of trailing bubble (t = 6 ms, 12 ms). Coalescence follows rapidly, t = 13 ms. 14 – 28 ms: confluence of newly coalesced bubble. u_s = 1 cms^{-1}, plate pore size 40 – 100 μm.

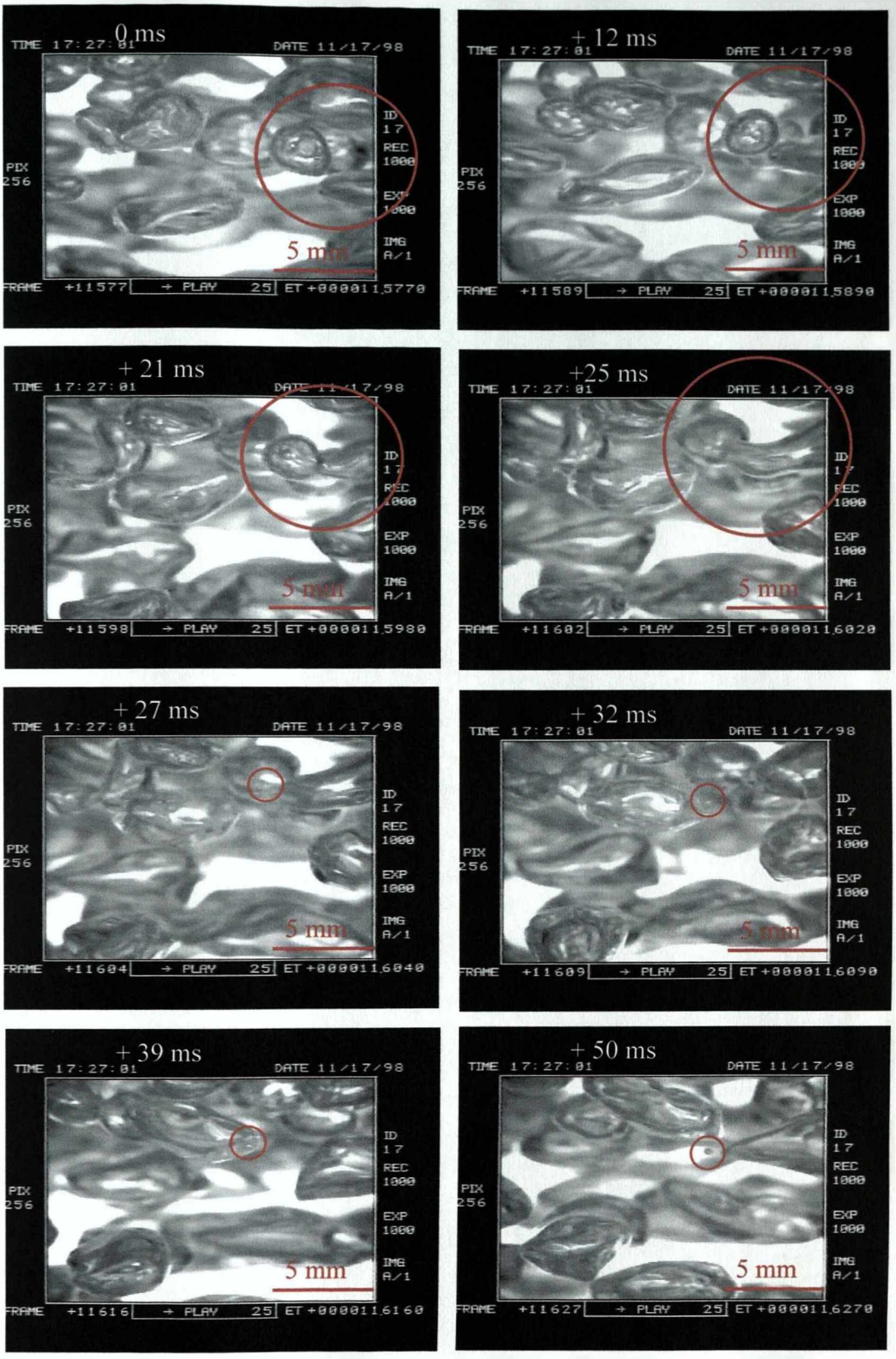

Figure 7.52

Possible formation of daughter bubbles following a coalescence event, although not clearly visible due to position background obscuration. No evidence of small bubble prior to t = 32 ms, observation at t = 32 ms follows coalescence event between two bubbles of disparate size. Water, u_s = 1 cms^{-1}, plate pore size 40 – 100 μm.

obtained to confirm the mechanism proposed for the formation of the very small bubbles so evident in the bubble size distributions. However, several images were observed where a coalescence event was rapidly followed by the presence of a small bubble in the same frame, Figure 7.52. In each of these images, the pinching off of the small bubble was obscured from view, either by the orientation of the coalescing bubble or due to the presence of another bubble.

In Table 7.10 the times are evaluated from initial contact to coalescence in water at the three gas flow rates. As can be seen, a considerable range of times is observed for all the flow rates, although this is largely a reflection of the difficulty in determining the exact moment of contact between two bubbles, due to viewing constraints. This is especially the case for bubbles which approach each other in the plane of the screen, in which case the time is measured from the last moment the bubbles appear as separate entities and will contain the greatest degree of error.

u_s (cms^{-1})	$\bar{t}_c$ (ms)	CV (%)	*n (No. Coalescence Events)*	*Range*
1	6.4	53	100	1 - 15
2	10.0	68	56	2 - 36
3	11.0	54	36	3 - 25

Table 7.10

Times from initial contact to coalescence in water for superficial gas velocities 1, 2 and 3 cms^{-1} for plate pore size 40 – 100 μm.

7.6.2 0.06 M Sodium Sulfate Solution

Bubbles in 0.06 M sodium sulfate solution appear quite different from those observed in water, not only in terms of shape (the majority are seen to be spherical, with larger bubbles tending to be flattened spheroids) but in that there is a complete absence of constantly oscillating shapes, with the bubbles appearing quite rigid and similar to hard spheres. In addition, they appear to rise much more directly and faster than in water, with very little random linear motion. Following collisions, which are considerably less frequent than observed for water, bubbles can be seen to bounce with little deformation (only the largest bubbles appear to quiver as they move away). As the superficial gas velocity increases, the bubbles can be seen to jostle with one another as they

rise, increasing the number of contacts and subsequently, the number of coalescence events. The larger bubbles formed at greater superficial gas velocities, are seen to show surface oscillation, although they still retain the ellipsoidal shape, appearing to wobble more (like gelled solids). At higher gas velocities, collisions occur with much greater force, giving bubbles which are often flattened as they collide, as proposed by the three step mechanism.

Coalescence is often seen to occur within a few frames, with a typical sequence shown in Figure 7.53. The bubbles appear just to touch and then film rupture occurs, in contrast to the long coalescence times measured in the coalescence cell. As observed for bubbles coalescing in water, for a large number of events there is no distinct contact, deformation and film thinning process as the accepted mechanism might suggest. Following a coalescence event, the newly coalesced bubble is subject to pronounced distortions, as in water. However, due to the increased bubble rigidity, this distortion occurs over a much shorter time scale and the protracted cycle of

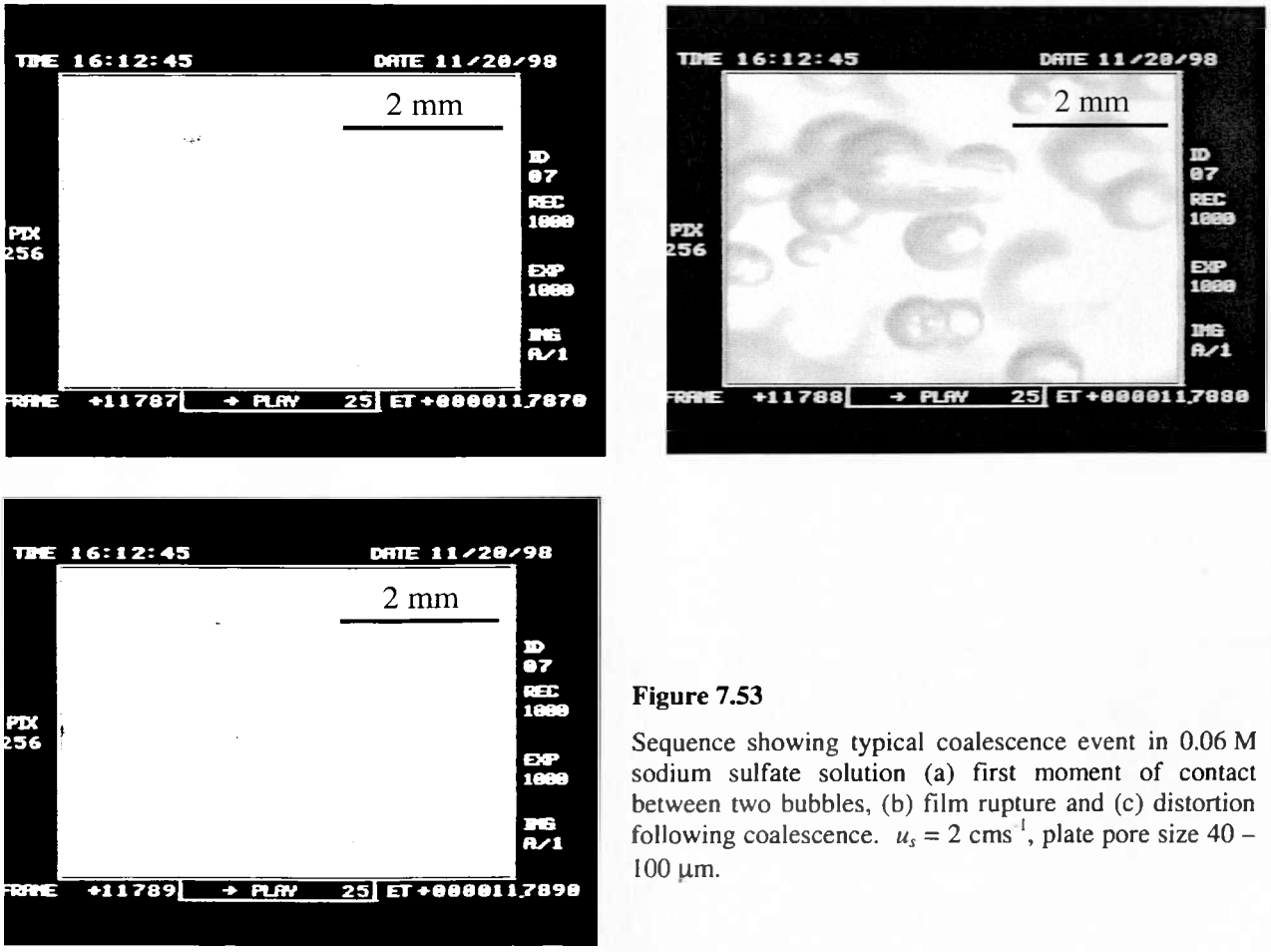

Figure 7.53

Sequence showing typical coalescence event in 0.06 M sodium sulfate solution (a) first moment of contact between two bubbles, (b) film rupture and (c) distortion following coalescence. u_s = 2 cms^{-1}, plate pore size 40 – 100 μm.

u_s (cms^{-1})	$\bar{t}_c$ (ms)	CV (%)	*n (No. Coalescence Events)*	*Range*
1	5.6	47	9	1 - 10
2	6.9	63	10	2 - 14
3	3.9	65	15	1 - 9

Table 7.11

Times from initial contact to coalescence in 0.06 M sodium sulfate solution for superficial gas velocities 1, 2 and 3 cms^{-1} for plate pore size 40 – 100 μm.

flexing and stretching does not usually exceed 10 ms (compared with > 24 ms required in Figure 7.50). In Table 7.11 the time between initial contact and coalescence is presented for each of the three superficial gas velocities. Data for these measurements was obtained from a much smaller population than the equivalent data in water, although evaluated over the same time frame (19 s), which reflects the much decreased coalescence frequency in these systems. It can be seen that the coalescence times are in fact of a similar order to those in water. This is not completely unexpected; given that coalescence times generally tend to be distributed about some mean values (Chapter 5), the coalescence times measured here most probably represent those at the lower end of the distribution. Collisions which do not lead to coalesce, therefore, will be those for which the film drainage time exceeds the limited contact time available in the dynamic system.

As in water, no instances of bubble break-up were observed, although the rigidity of the bubbles would suggest they are more resistant to the shape distortions that may result from partial entrainment in bubble wakes. A number of very small bubbles were observed in the column, although these were quite rare and much less numerous than in water. From visual comparison of bubbles in water and 0.06 M sodium sulfate solution it is easier to understand why very few daughter bubbles form following coalescence in the electrolyte solution. The much smaller degree of flexing and stretching which follows a coalescence event in electrolyte solution, significantly reduces the chance of forming an unstable extension, which will be prone to disruption from instabilities (as discussed in Section 7.6), thus breaking into daughter bubbles.

7.7 Conclusions

- Bubble size distributions have been measured at four different levels over the height of a small bubble column, to investigate bubble coalescence in-situ. Effects of original bubble size and superficial gas velocity have been assessed, in addition to the effects of electrolyte concentration and gas density.

  Bubbles sizes were measured using an advanced image analysis technique where a stereomicroscope is couple to a high-resolution video camera. Distributions have been characterised using number and volume probability density and cumulative functions, in addition to three mean values, d_{10}, d_{32} and d_{43}.

- The diameters of bubbles in water were observed to span two orders of magnitude. Bubbles occurred in a wide variety of shapes, from very small spherical bubbles to large irregularly shaped ones.

  Number probability distributions were bi-modal, due to the presence of significant populations of very small bubbles (< 0.3 mm) as well as the expected very large bubbles, coupled with an pronounced absence of intermediate sized bubbles. The degree of bi-modality was observed to increase with distance from the distributor plate and was largest for the large pore size plate (largest initial bubble sizes).

- In sodium sulfate solutions, number distributions were originally bi-modal at low concentrations but were observed to become progressively more uni-modal and much narrower with increasing concentration.

  The largest and smallest bubble sizes were measured in dilute sodium sulfate solutions, where as in water, significant numbers of small bubbles (< 0.3 M) were observed, which increase in number up the column.

  For a given position in the column, mean bubble sizes were observed to decrease with increasing solute concentration. At low solute concentrations, the mean bubble size increased progressively up the column. However, at concentrations beyond 0.06 M sodium sulfate, for superficial gas velocity of 1 cms^{-1}, any change in bubble size over the column height was very small.

As the initial bubble size decreases, the coalescence repression due to electrolyte concentration becomes more effective, such that for the smallest pore size plate, there is no change in bubble size over the column height.

With increasing superficial gas velocity, there is an increase in the mean bubble size. In all solutions, the greatest amount of coalescence was observed to occur in the zone directly adjacent to the distributor plate. In dilute electrolyte solutions, very small changes in bubble size are observed in regions further up the column; this is not the case in concentrated solutions, where all coalescence is compressed into this initial zone.

A secondary effect of increasing the superficial gas flow rate is to delay the concentration at which an increase in bubble size is not observed over the height of the column, i.e. prolong the concentration range over which significant bubble coalescence occurs.

- Coalescence frequencies have been calculated from mean bubble sizes measured in solutions of sodium sulfate with the smallest pore size plate and for superficial gas velocities 1, 2 and 3 cms^{-1}. This was achieved by modifying the method of Howarth, 1967 to allow the coalescence frequency to be determined for each of the three regions in the column.

  For all superficial velocities, coalescence frequencies were greatest in the initial part of the column, adjacent to the sparger plate and essentially zero in the regions beyond. This was not surprising given the much greater bubble density which my be expected in the initial part of the column, due to a combination of smaller mean bubble diameters and consequently, reduced average rise velocities.

  Good correlation was observed with coalescence cell profiles obtained at higher gas flow rates, which were able to predict the shape of the coalescence frequency curves for the initial region in the column, together with the delayed coalescence repression that results from increasing the superficial gas velocities in the column.

- Experiments were carried out to assess the impact of gas density on the coalescence behaviour in small bubble columns, using solutions of magnesium sulfate and air, nitrogen and hydrogen. Experiments were not conducted with xenon due to practical constraints.

  For all systems, at concentrations which were fully coalescing in the coalescence cell, bubble sizes were seen to increase over the height of the column.

Number probability density functions measured in dilute solutions were observed to be bi-modal, especially those observed at the greatest distance from the distributor plate. Once again, these distributions contained a significant number of very small bubbles (< 0.3 mm), in addition to the large bubbles expected in coalescing systems.

For increasing solution concentration uni-modal distributions were observed at all measurement points over the column and bubbles sizes were intermediate, when compared to equivalent values in dilute solutions.

To allow comparison between the three systems, mean bubble size ratios were calculated, by comparing values measured at the distributor plate with those values obtained close to the top of the column. Trends in all systems are similar and show a reduction in the mean bubble size ratio with increasing solution concentration. No significant differences were observed between the three systems, although this may reflect the small concentration range investigated. Comparisons with results from the coalescence cell, indicate that the influence of gas type on bubble coalescence is complex and in need of further investigation.

- Images of in-situ coalescence have been obtained which show the same features as coalescence events in the coalescence cell, namely the presence of an annular wave formed due to the energy released by film rupture. This can be used as a good indicator of coalescence in dynamic systems. Combined with estimations of the speed of the annular wave from high-speed video studies in the coalescence cell, the time from the moment of rupture of such coalescence events can be determined.
- The presence of very small bubbles in systems where a significant amount of coalescence is occurring (water, dilute electrolyte solutions) is attributed entirely to the formation of daughter bubbles following a coalescence event.

  Visual evidence has been obtained to support the mechanism of secondary bubble formation, whereby the annular wave pinches off an extension of the bubble, caused by the distortion and flexing of the bubble after coalescence and before it regains its usual spherical (ellipsoid) shape.
- High-speed video studies of air-water and air-0.06 M sodium sulfate solution, over a range of superficial gas velocities, show pronounced differences between the appearance of the bubbles in each system.

Bubbles in water are seen to oscillate continuously, which results in the irregular shapes observed in studies with the slower frame rate camera. The amount of oscillation slows the rise of the bubbles, which appear to move in a random linear manner. Although considered a fully coalescing liquid, coalescence events are few compared to the large number of bubble-bubble contacts. Such coalescence events are always binary, can be seen to occur between bubbles of very different sizes and are followed by extensive flexing and stretching before the bubble regains its more usual shape. There appears to be no preference for wake mediated coalescence.

Bubbles in sodium sulfate solution are much smaller, more spherical and less prone to shape deformations arising from oscillations. They appear more rigid and often bounce following contact. Coalescence events are observed to be very rapid and are followed by a much reduced amount of flexing. The number of events observed increases with superficial gas flow rate.

Chapter 8
Conclusions and Recommendations for Further Work

8.1 Summary

This study presents results from a thorough investigation of a coalescence cell, which aimed to assess its use as a potential tool for determining the coalescence behaviour in larger scale process apparatus. Within the cell, conditions can be manipulated to control the various influences on the coalescence process, thereby allowing their individual effects to be examined. The coalescence behaviour was investigated in a range of well defined model fluids of differing viscosities, including several pure liquids, solutions of various electrolyte, *n*-alcohol and non-polar solute species and for a range of gas types. The response of each gas-liquid system to a wide range of experimental parameters, including gas flow rate, bubble frequency and nozzle separation distance has been examined for both bulk (coalescence frequency) and small-scale (coalescence times) behaviour. To enable comparisons with the coalescence cell results, coalescence in a dynamic system has been investigated by measuring bubble size distributions and mean bubble diameters in a number of laboratory-scale bubble columns. Responses observed in the coalescence cell were seen to approach trends observed in the small-scale systems, despite being attributed to very different influences. As an analytical tool, the cell shows potential for advancing the current state of knowledge, although its use as a general diagnostic tool is disadvantaged by the degree of rigour which must be applied to both experiments and the subsequent interpretation of results.

8.1.1 Using the Coalescence Cell

An in-depth assessment of the coalescence cell has shown that its use is not as simple and straightforward as may be assumed from literature studies. Operational experience is required to ensure the results obtained are an accurate reflection of system behaviour and free from experimental artefact. In addition, clear and explicit definitions are required for parameters such as the coalescence frequency to allow unambiguous interpretation of coalescence cell data. Results obtained are strongly influenced by the degree of synchrony between bubble pairs, which the analysis of coalescence patterns, has demonstrated to be a system dependent variable, rather than experimental artefact. Synchronous bubbling is influenced by the nature of the liquid phase, gas flow rate and rate of bubble formation and nozzle separation distance

for two equal gas feed rates; it significantly impacts on the degree of experimental reproducibility with which the system can be operated.

8.1.2 The Coalescence Cell and Inviscid Liquids

Operation of the coalescence cell with inviscid liquids has demonstrated that by adjusting operational parameters, a much broader range of behaviour has been observed, than previously reported in the literature. As expected, pure liquids (water and propan-1-ol) are observed to be fully coalescing over the range of operating conditions and show the synchronous bubbling typical of such systems. Coalescence times values measured in water and porpan-1-ol clearly demonstrate the significant impact of increased contact pressures arising from high gas flow rates, although smaller effects of temperature and gas type are also observed.

Coalescence behaviour in electrolyte solutions is observed to be heavily dependent on the operating conditions of the coalescence cell, with the most significant influences being that of gas flow rate and nozzle separation distance. Although the step change in coalescence frequency ('transition' concentration), is observed at low gas flow rates and for small nozzle separations, values for the coalescence frequency increase with gas flow rate, such that for all electrolytes studied, there is a gas flow rate at which systems becomes fully coalescing. This is attributed to the increased contact pressure which results at high gas flow rates due to the combination of increased bubble size and geometrical constraints from the nozzles.

High-speed video studies have enabled the coalescence process to be visualised in detail. Although film rupture is too rapid to be observed, bubble pair formation, approach and contact, as well as confluence following the actual coalescence event, can all be clearly seen. Coalescence time values measured for a range of electrolyte concentrations show a large increase as the solution concentration approaches the 'transition' value. Coalescence rates, which allow for effects of contact area, show a rapid increase with increasing gas flow rate, confirming the significant influence of this parameter on the nature of the coalescence event. Interestingly, contact times measured between non-coalescing but contacting bubble pairs in sodium sulfate, are significantly longer than coalescence times under the same conditions, provoking questions about the mechanism of coalescence, particularly the film thinning step.

The coalescence behaviour of solutions of propan-1-ol does not show the same dependence on gas flow rate as electrolyte solutions. As in electrolyte solutions, a distinct step change in coalescence frequency values is observed at low gas flow rates, with increasing concentration. However, there is no similar shift towards full coalescence with increasing gas flow rate, even at high gas feed rates. Importantly, in solutions of propan-1-ol beyond the 'transition' value, bubbling remains non-synchronised, even at high gas flow rates.

Experiments carried out to elucidate the influence of gas density on coalescence behaviour are inconclusive, although a definite influence of gas type can be observed. Differences in system behaviour are observed, but cannot be ascribed solely to the effects of gas density. Experiments with propan-1-ol show very different coalescence behaviour with different gases, but correlations with gas density or solubility cannot be drawn, as consistent trends are not observed.

8.1.3 The Coalescence Cell and Viscosity Modified Solutions

Coalescence behaviour determined in liquids of viscosities slightly greater than water do not correlate with predictions of literature models (Chesters, 1991, Reynolds, 1886 amongst others) which suggest film thinning rates to be inversely proportional to liquid viscosity, such that coalescence times increase with increasing viscosity. For solutions of modified viscosity (not pure liquids), the predominant influence appears to be that of solute concentration and the subsequent impact on gas-liquid surface phenomena.

Although a pure liquid, 3 mPas silicone fluid, is a coalescence-repressed system which exhibits non-synchronous bubbling. Coalescence times values are slightly greater than equivalent values measured in water, although the coalescence times distributions are significantly narrower. As in electrolyte solutions, contact times are seen to be significantly greater than coalescence times measured under the same conditions.

Results of experiments with equal viscosity solutions of sucrose and glycerol follow broadly similar trends, despite interfacial differences, which may be expected to arise as a result of structural differences. Trends observed in all systems did not correlate with the predicted effect of viscosity, perhaps as a result of the greater influence of solute concentration on interfacial behaviour. Investigations over a range of temperatures show a definite increase in coalescence frequency with increasing temperature for a given flow rate. Although this

corresponds with decrease in liquid viscosity, it is likely that there are a number of interacting influences which contribute, primarily those which would affect the nature of the gas-liquid interface (such as solute diffusivity and dynamic surface tension).

The coalescence behaviour of glycerol solutions was investigated, where solution viscosity was modified through concentration and temperature. Although 'transition' behaviour is observed at all temperatures, this is found to occur at different solution viscosities. As a consequence, it is concluded that the coalescence repression is most likely to arise from the influence of solute molecules at the interface and not the effect of liquid viscosity. Surprisingly, an increase in the coalescence frequency is observed with increasing gas flow rate and increasing solution viscosity (and concentration) for experiments carried out at 25°C, which is contrary to all expectations from models discussed in the literature. The predominant influence of solute concentration is also demonstrated in coalescence and contact time measurements.

8.1.4 Coalescence in Bubble Columns

Bubble size distributions and mean bubble sizes have been measured in laboratory bubble columns, to allow for comparison with data obtained in the coalescence cell. Bubble size distributions, measured over the height of the column, are observed to change from being broadly bi-modal in water and dilute electrolyte solutions to being much narrower, single peak distributions in solutions with increased concentration. Interestingly, in solutions where there is a greater degree of coalescence over the column height, significant populations of very small bubbles were observed as well as the expected very large bubbles; notably, there is a pronounced absence of intermediate sized bubbles.

As the electrolyte concentration increases, the progressive increase in mean bubble size with column height decreases, such that at concentrations beyond 0.06 M, any change in bubble size over the column height is very small. For a given solution concentration, values for mean bubble sizes were observed to be strongly influenced by initial bubble size and superficial gas velocity. Coalescence repression arising from the presence of electrolyte becomes more effective as the initial bubble size decreases. Increasing the superficial gas flow rate increase the mean bubble size and prolongs the concentration range over which significant bubble coalescence occurs.

Coalescence frequencies have been determined for each of the three regions in the column. For all superficial velocities, frequencies are greatest in the initial part of the column, adjacent to the sparger plate and essentially zero in the regions beyond. This was not surprising given the much greater bubble density which may be expected in the initial part of the column, due to a combination of smaller mean bubble diameters and consequently, reduced average rise velocities. Good correlation was observed with coalescence cell profiles obtained at higher gas flow rates, which were able to predict the shape of the coalescence frequency curves for the initial region in the column, together with the delayed coalescence repression that results from increasing the superficial gas velocities in the column.

Experiments to assess the impact of gas density on coalescence behaviour do not show pronounced differences between the trends observed in three different systems. Comparisons with results from the coalescence cell indicate that the influence of gas type on bubble coalescence is complex and in need of further investigation.

Video observation has been used to increase the level of scrutiny of coalescence occurring in dynamic systems. Captured images of in-situ coalescence show the same features as coalescence events observed in the coalescence cell, namely the presence of an annular wave formed due to the energy released by film rupture. Visual evidence has been obtained to explain the presence of very small bubbles in systems where a significant amount of coalescence is occurring (water, dilute electrolyte solutions) and which is attributed to the formation of daughter bubbles following a coalescence event. A mechanism is proposed for the secondary bubble formation whereby the annular wave pinches off an extension of the bubble, caused by the distortion and flexing of the bubble after coalescence and before it regains its usual spherical (ellipsoid) shape. High-speed video studies show pronounced differences between the appearance of the bubbles in air-water and air-0.06 M sodium sulfate solution which may quantitatively explain the differences observed between the coalescence behaviour of each system.

8.1.5 Overall Conclusion

At present, this study cannot recommend the use of a coalescence cell apparatus as a predictive tool to assess the coalescence behaviour of larger scale dynamic systems. This is in spite of the fact that the study has ascertained a much wider range of coalescence behaviour can be investigated in the cell, beyond the simple step change behaviour often reported in the

literature. Although trends observed in the cell for high bubble frequencies were observed to correlate well with coalescence frequencies measured in small-scale bubble columns, the degree of applicability to larger scale systems still remains to be determined. However, when used within well-defined operational limits, which includes the need for rigorously defined analytical parameters, the cell provides a valuable method of investigating gas, liquid and hydrodynamic effects on the bubble coalescence process. This is largely a reflection of the equipment versatility, which allows the influence of discrete operating variables to be examined, in addition to system effects, such as the nature of the gas-liquid interface. Whilst the mechanism of coalescence and indeed, coalescence repression, remains to be elucidated, such information on the degree of influence of such variables, provides a clear step forward in improving understanding of the coalescence process and thus developing strategies to exploit or avoid its influence in process operations.

8.2 Recommendations for Future Work

This study has highlighted several interesting areas for future work, which may provide increased insight into the coalescence process.

- The results of all the experiments carried out suggest that contact pressure exerts a significant influence on the coalescence behaviour of a system. With only minor modifications to the existing coalescence cell, pressure transducers could be introduced across the nozzle extensions to allow this effect to be quantified. This would have the additional benefit of enabling closer comparison with values from model predictions, as the current study has shown the degree of deviation between measured and predicted values increases with increasing gas flow rate (and hence contact pressure).
- Following investigations into the effect of viscosity, it has become apparent from this study that in order to draw accurate conclusions as to the nature and degree of influence, contributing effects from solute concentration must be eliminated. Consequently, it is recommended that the cell be reconstructed to allow experiments to be carried out in a range of pure liquids with increasing viscosities (such as hydrocarbons). In addition, such experiments would allow the effects of temperature on the coalescence process to be more clearly understood.

- Despite thorough investigation into the effects of gas density on coalescence, this study has been unable to identify either a controlling mechanism or a well-defined influence on the coalescence behaviour in a variety of liquids. This reflects the current state of the literature where conflicting experimental results are reported and suggests that a comprehensive investigation is required to elucidate fully the influence of gas type on coalescence behaviour of a system.
- The association of fully coalescent behaviour and bubble synchronicity has not been fully resolved in this study. The bubbling geometries used in the cell may be expected to display similarities with the systems observed by Ruzicka et al. (2000, 1999), to exhibit chaotic behaviour over a range of increasing gas flow rates. In addition, bubbling from the horizontally opposing nozzles could de considered to be approach that of the classically chaotic, double oscillatory system. Consequently, it would be intriguing to assess coalescence behaviour in terms of a similar chaotic analysis, which may provide greater insight into the seemingly coupled phenomenon of reduced coalescence frequencies and the loss of synchronous bubbling in the cell.
- The use of chaos analysis is also recommended for the film thinning and rupture steps in the coalescence process, which, through measurements of coalescence times and coalescence rates, have been observed in this work, to suggest the currently accepted mechanism is perhaps oversimplified. Pronounced differences between coalescence and contact times measured for coalescing and non-coalescing events in the same environment, are one of the most intriguing observations in the study. The present explanations for coalescence and coalescence repression are not able to explain the existence of two such very different states, in systems subject to (seemingly) the same external influences. Certainly, the application of such techniques to investigations of the coalescence process should provide a fresh approach to the complex study of coalescence behaviour.

References

A

Adamson, A. W., 1990, Physical Chemistry of Surfaces, John Wiley & Sons, Inc., ISBN 0-0471-61019-4.

Akita, K., 1989, Effect of the Electrolyte on the Mass Transfer Characteristics of a Bubble Column, *Int. Chem. Eng.*, **29** 127-135.

Akita, K. and Yoshida, F., 1973, Gas Hold-up and Volumetric Mass Transfer Coefficient in Bubble Columns, *Ind. Eng. Chem. Proc. Des. Dev.*, **12** 76-80.

Allan, R. S., Charles, G. E. and Mason, S. G., 1961, The Approach of Gas Bubbles to a Gas/Liquid Interface, *J. Cool. Sci.*, **16** 150-165.

Andrew, S. P. S., 1960, Frothing in Two-Component Liquid Mixtures, *Int. Symp. on Distillation*, Rottenburg, P. A. (ed), Institution of Chem Engrs., London, 73-78.

Aylward, G. H. and Findlay, T. J. V., 1974, SI Chemical Data, 2nd Edition, John Wiley & Sons, ISBN 0-471-03851-2.

B

Bach H. F. and Pilhofer, Th., 1978, Variation of Gas Hold-up in Bubble Columns with Physical Properties of Liquids and Operating Parameters of Columns, *Ger. Chem. Eng.*, **3**, 270–275.

Barber, A. D. and Hartland, S., 1976, The Effects of Surface Viscosity on the Axisymmetric Drainage of Planar Liquid Films, *Can. J. Cham. Eng.*, **54**, 279-284.

Bhaga, D., Pruden, B. B. and Weber, M. E., 1971, Gas Holdup in a Bubble Column Containing Organic Liquid Mixtures, *Can. J. Chem. Eng.*, **49** 417-420.

Bisgaard, C., 1983, Velocity fields around Spheres and Bubbles Investigated by Laser-Doppler Anemometry, *J. Non-Newtonian Fluid Mech.*, **12** 283-302.

C

Cain, F. W. and Lee, J. C. Lee, 1985, A Technique for Studying the Drainage and Rupture of Unstable Liquid Films Formed between Two Captive Bubbles: Measurements on KCl Solutions, *J. Coll. Int. Sci.*, **106**, 1, 70-85.

Calderbank, P. H., 1967, Mass Transfer in Fermentation Equipment in '*Biochemical and Biological Engineering Science*', Vol. 1, Ed. N. Blakeborough, Academic Press, 102 - 180.

Calderbank, P. H., Moo-Young, M. B., and Bibby, R., 1965, Coalescence in Bubble Reactors and Absorbers, *Proc. 3rd Europ. Conf. Chem. React. Eng.*, Pergamon Press Ltd, 91-111.

Cattaneo, R., 1995, Bubble Coalescence Behaviour in Stagnant Liquids, *Final Year Project*, University of Birmingham, UK.

Charles, G. E. and Mason, S. G., 1960a, The Mechanism of Partial Coalescence of Liquid Drops at Liquid-liquid Interfaces, *J. Coll. Sci.*, **15** 105-122.

Charles, G. E. and Mason, S. G., 1960b, The Coalescence of Liquid Drops with Flat Liquid-liquid Interfaces, *J. Coll. Sci.*, **15** 236-254.

Chaudhari, R. V. and Hofman, H., 1994, Coalescence of Gas Bubbles in Liquids, *Reviews in Chem. Eng.*, **10** 131–190.

Chen, J., Hahn, P. S. and Slattery, J.C., 1988, Effects of Electrostatic Double-Layer Forces on Coalescence, *AIChE J.*, **34** 140–143.

Chen, J., Hahn, P. S. and Slattery, J.C., 1984, Coalescence Time for a Small Drop or Bubble at a Fluid-Fluid Interface, *AIChE J.*, **30** 622-630.

Chesters, A. K., 1991, The Modelling of Coalescence Processes in Fluid-Liquid Dispersions: A Review of Current Understanding, *Trans. IChemE Part A*, **69** 259–270.

Chesters, A. K. and Hofman, G., 1982, Bubble Coalescence in Pure Liquids, *Appl. Sci. Res.*, **38** 353–361.

Christenson, H. K., and Yaminsky, V. V., 1995, Solute Effects on Bubble Coalescence, *J. Phys. Chem.*, **99** 10420.

Clark, K. N., 1990, The Effect of High Pressure and Temperature on Phase Distributions in a Bubble Column, *Chem. Eng. Sci.*, **45** 2301-2307.

Clift, R., Grace, J. R. and Weber, M. E., 1978, *Bubbles, Drops and Particles*, Academic Press, Inc., ISBN 0-12-176950-X.

Colella, D., Vinci, D., Bagatin, R., Masi, M. and Abu Bakr, E., 1999, A Study on Coalescence and Breakage Mechanisms in Three Different Bubble Columns, *Chem. Eng. Sci.*, **54** 4767-4777.

Coulaloglou, C. A. and Tavlarides, L. L., 1977, Description of Interaction Processes in Agitated Liquid-Liquid Dispersions, *Chem. Eng. Sci.*, **32** 1289-1297.

Crabtree, J. R. and Bridgwater, J., 1971, Bubble Coalescence in Viscous Liquids, *Chem. Eng. Sci.*, **26** 839-851.

Craig, V. S. J., Ninham, B. W. and Pashley, R. M., 1993a, The Effect of Electrolytes on Bubble Coalescence in Water, *J. Phys. Chem.*, **97** 10192–10197.

Craig, V. S. J., Ninham, B. W. and Pashley, R. M., 1993b, Effect of Electrolytes on Bubble Coalescence, *Nature*, **364** 317-319.

D

Davies J. T. and Rideal, E. K., 1961, Interfacial Phenomena, Academic Press Inc., London.

De Kee, D., Carreau, P. J. and Mordarski, J., 1986, Bubble Velocity and Coalescence in Visco-elastic Liquids, *Chem. Eng. Sci.*, **41** 2273-2283

Doubliez, L., 1991, The Drainage and Rupture of a Non-Foaming Liquid Film Formed upon Bubble Impact with a Free Surface, *Int. J. Multiphase Flow*, **17** 783-803.

Drogaris, G. and Weilland, P., 1983, Coalescence Behaviour of Gas Bubbles in Aqueous Solutions of n-Alcohols and Fatty Acids, *Chem. Eng. Sci.*, **38** 1501-1506

Duineveld, P. C., 1994, Bouncing and Coalescence of Two Bubbles in Water, *PhD Thesis*, Twente University.

E

Edwards, D. A., Bremer, H. and Wasan, D. T., 1991, Interfacial Transport Processes and Rheology, Butterworth-Heinemann, ISBN 0-7506-9185-9.

F

Farooq, S. Y., 1972, Bubble Coalescence, *PhD Thesis*, University College of Swansea, University of Wales, UK.

Franklin, R., 1997, Coalescence in Dispersions Containing Solid Particles, *PhD Thesis*, University of Birmingham, UK.

G

Garrett, P. R. and Ward, D. R., 1989, A Re-Examination of the Measurement of Dynamic Surface Tensions Using the Maximum Bubble Pressure Method, *J. Coll. Sci.*, **132** 475-490.

Gezork, K. M., 1999, Personal communication.

Grace, J. R. and Wairegi, T., 1992, Shapes of Fluid Particles, Chapter 6 from *Transport Processes in Bubbles, Drops and Particles*, Ed. Chhabra, R. P. and De Kee, D., Hemisphere Publishing Corporation, ISBN 0-89116-999-7.

Grienberger, J. and Hofman, H., *Preprints of 2nd Japanese/German Symp. on 'Bubble Columns', Kyoto*, 99-104 (1991) [from Chaudhuri and Hofman, 1994]

Grover, G. S., Rode, C. V. and Chaudhari, R. V., 1986, Effect of Temperature on Flow Regimes and Gas Hold-up in a Bubble Column, *Can. J. Chem. Eng.*, **64** 501-504.

H

Hahn, P. S. and Slattery, J. C., 1986, Effects of Surface Viscosities on the Thinning and Rupture of a Dimpled Liquid Film as a Small Bubble Approaches a Liquid-Gas Interface, *AIChE Symp. Ser.*, **82** 100-118.

Hahn, P.S., Chen, J. D. and Slattery, J. C., 1985, Effects Of London-Van Der Waals Forces on the Thinning and Rupture of a Dimpled Liquid Film as a Small Drop or Bubble Approaches a Fluid-Fluid Interface, *AIChE J.*, **31** 2026-2038.

Hahn, P. C. and Slattery, J. C., 1985, Effects of Surface Viscosities on the Stability of a Draining Plane Parallel Liquid Film as a Small Bubble Approaches a Liquid-Gas Interface, *AIChE J.*, **31** 950-956.

Harnby, N., Edwards, M. F. and Nienow, A. W., 1992, Mixing in the Process Industries, Butterworth-Heinemann Ltd, ISBN 0-7506-1110-3.

Hikita, H., Asai, S., Tanigawa, K., Segawa, K. and Kitao, M., 1980, Gas Hold-up in Bubble Columns, *Chem. Eng. J.*, **20** 59-67.

Hirschfelder, J. O., Curtiss, C. F. and Bird, R. B., 1964, Molecular Theory of Gases and Liquids, John Wiley & Sons, Inc.

Hodgson, T. D. and Lee, J. C., 1969, The Effect of Surfactants on the Coalescence of a Drop at an Interface I., *J. Coll. Int. Sci.*, **30** 94-108.

Hofmeier, U., Yaminsky, V. V. and Christenson, H. K., 1995, Observations of Solute Effects on Bubble Formation, *J. Coll. Int. Sci.*, **174** 199-210.

J

Jamialahmadi, M. and Müller-Steinhagen, H., 1992, Effect of Alcohol, Organic Acid and Potassium Chloride Concentration on Bubble Size, Bubble Rise Velocity and Gas Hold-Up in Bubble Columns, *Chem. Eng. J.*, **50** 47-56.

Jamialahmadi, M. and Müller-Steinhagen, H., 1991, Effect of Solid Particles on Gas Hold-Up in Bubble Columns, *Can. J. Chem. Eng.*, **69** 390-393.

Jamialahmadi, M. and Müller-Steinhagen, H., 1990, Effect of Electrolyte Concentration on Bubble Size and Gas Hold-Up in Bubble Columns, *Trans. IChemE*, **68** 202-204.

Jamialahmadi, M. and Müller-Steinhagen, H., 1989, Bubble Formation and Coalescence in Bubble Columns, *Chem. Ing. Tech.*, **61** 715-718.

Jarvis N. L. and Scheiman, M. A., 1968, Surface Potentials of Aqueous Electrolyte Solutions, *J. Phys. Chem.*, **72**, 1, 74-78.

Jeelani, S. A. K., and Hartland, S., 1994, Effect of Interfacial Mobility on Thin Film Drainage, *J. Coll. Int. Sci.*, **164** 296-308.

Jeelani, S. A. K., and Hartland, S., 1991, Effect of Approach Velocity in Binary and Interfacial Coalescence, *Trans. IChemE., Part A*, **69** 271-281.*

Jiang, P., Lin, T. S., Luo, X. and Fan, L. S., 1995, Flow Visualization of High Pressure (21 MPa) Bubble Column: Bubble Characteristics, *Trans IChemE*, **73** Part A 269-274.

K

Katz, J. and Meneveau, C., 1996, Wake-Induced Relative Motion of Bubbles Rising In Line, *Int. J. Multiphase Flow*, **22** 239-258.

Keitel, G. and Onken, U., 1982a, Inhibition of Bubble Coalescence by Solutes in Air/Water Dispersions, *Chem. Eng. Sci.*, **37** 1635-1638.

Keitel, G. and Onken, U., 1982b, The Effect of Solutes on Bubble Size in Air-Water Dispersions, *Chem. Eng. Comm.*, **17** 85-98.

Kim, J. W. and Lee, W. K., 1987, Coalescence Behaviour of Two Bubbles in Stagnant Liquids, *J. Chem. Eng. Japan*, **20** 448-453.

Kirkpatrick. R. D. and Lockett, M. J., 1974, The Influence of Approach Velocity on Bubble Coalescence, *Chem. Eng. Sci.*, **29** 2363-2373.

Koide, K., Shinji, K., Tanaka, Y and Kubota, H., 1968, Bubble Generated from a Porous Plate, *J. Chem. Eng. Jap.*, **1** 51-56.

Krishna, R., de Swart, J. W. A., Hennephof, D. E., Ellenberg, J. and Hoefsloot, H. C. J., 1994, Influence of Increased Gas Density on Hydrodynamics of Bubble-Column Reactors, *AIChE J.*, **40** 112-119.

Kuncova, G. and Zahradnik, J., 1995, Gas Hold-up and Bubble Frequency in a Bubble Column Reactor Containing Viscous Saccharose Solutions, *Chem. Eng. Proc.*, **34** 25-23.

L

Lawson, G. B., 1967, Coalescence Processes, *Chem. Proc. Eng.*, **May**, 45-63.

Lee, C. H., Erickson, L. E. and Glasgow, L. A., 1987, Bubble Break-up and Coalescence in Turbulent Gas-Liquid Dispersions, *Chem. Eng. Commun.*, **59** 65-84.

Lee, C. H. and Patel, S. A., 1983, Dynamics of Bubble Size Distributions in Air-Lift Fermentors, *Annucal Biochem. Eng. Symp.*, 81-90.

Lee, C. H., Hodgson, T. D., 1968, Film Flow and Coalescence (I) Basic Relations, Film Shape and Criteria for Interface Mobility, *Chem. Eng. Sci.*, **23** 1375–1397.

Lee, J. C. and Meyrick, D. L., 1970, Gas-Liquid Interfacial Areas in Salt Solutions in an Agitated Tank, *Trans. Inst. Chem. Engr.*, **48** T37-45

Lessard, R. R. and Zieminski, S. A., 1971, Bubble Coalescence and Gas Transfer in Aqueous Electrolytic Solutions, *Ind. Eng. Chem. Fund.*, **10** 260–269.

Li, D., 1996, Coalescence between Small Bubbles: Effects of Surface Tension Gradients and Surface Viscosities, *I. Coll. Int. Sci.*, **181** 34-44.

Li, D., 1996, Coalescence Between Small Bubbles: Effects of Bulk and Surface Diffusion, *Chem. Eng. Sci.*, **51** 3623–3630.

Li, D. and Slattery, J. C., 1988, Experimental Support for Analyses of Coalescence, *AIChE J.*, **34** 862–862.

Li, H. Z., 1999, Bubbles in Non-Newtonian Fluids: Formation, Interactions and Coalesce, *Chem. Eng. Sci.*, **54** 2247-2254.

Li, H. Z., 1998a, Chaotic Behaviour of Bubble Coalescence in Non-Newtonian Fluids, *Chem. Eng. Technol..*, **21** 12-985.

Li, H. Z., Mouline, Y., Funfschilling, D., Marchal, P., Choplin, L. and Midoux, N., 1998b, Evidence for In-Line Bubble Interactions in Non-Newtonian Fluids, *Chem. Eng. Sci.*, **53** 2219-2230.

Li, H. Z., Mouline, Y., Choplin, L. and Midoux, N., 1997a, Chaotic Bubble Coalescence in Non-Newtonian Fluids, *Int. J. Multiphase Flow*, **23** 713-723.

Li, H. Z., Mouline, Y., Choplin, L. and Midoux, N., 1997b, Rheological Simulation of In-Line Bubble Interactions, *AIChE J.*, **43** 265-267.

Lide, D. R., 1993, Handbook of Chemistry and Physics 74th Edition, ISBN 0-8493-0474-1

Lin, C. Y. and Slattery, J. C., 1982, Thinning of a Liquid Film as a Small Drop or Bubble Approaches a Fluid-Fluid Interface, *AIChE J.*, **28** 786-792.

Lin, T. J., Tsuchiya, K. and Fan, L. S., 1998, Bubble Flow Characteristics in Bubble Columns at Elevated Pressure and Temperature, *AIChE J.*, **44** 545-560.

Lloyd, E., Ed., 1980, Handbook of Applicable Mathematics Volume II: Probability, John Wiley & Sons, ISBN 0-471-27821-1.

M

MacIntyre, F., 1972, Flow Patterns in Breaking Bubbles, *J. Geophysical Res.*, **77** 5211-5228.

Mackay, G. D. M. and Mason, S. G., 1963, *J. Can. J. Chem. Eng.*, **41** 203-212

Machon, V., Pacek, A. W. and Nienow, A. W., 1997 Bubble Sizes in Electrolyte and Alcohol Solutions in a Turbulent Stirred Vessel, *Trans IChemE*, **75** Part A 339-348.

Machon, V., Vleck, J., Zahradnik, J. and Fialova, M., 1996, The Effect of Surface Active Substances on Hydrodynamics and Mass Transfer in Aerated Stirred Tank Reactors, *12th International Congress CHISA 96, August 1996, Prague.*

Machon, V., Vleck, J. and Kudrna V., 1977, Gas Hold-Up in Agitated Aqueous Solutions of Strong Inorganic Salts, *Second European Conference on Mixing*, **F2** 17-34.

Man, C.C., 1998, Drop Sizes and Coalescence Rates in Oil-in-Aqueous and Aqueous-in-Oil Dispersions in Stirred Vessels, *PhD Thesis,* University of Birmingham, UK.

Mao, Z. and Core, K. L., 1993, Visualization of the Coalescence Process in Dispersed Multi-Phase Systems, *Gas Liquid Flows, ASME*, **165** 3-11, ISBN 0-7918-0973-0.

Marrucci, G., 1969, A Theory of Coalescence, *Chem. Eng. Sci.*, **24** 975–985.

Marrucci, G. and Nicodemo, L., 1967, Coalescence of Gas Bubbles in Aqueous Solutions of Inorganic Electrolytes, *Chem. Eng. Sci.*, **22** 1257–1265.

Martin, T., 1996, Gas Dispersion with Radial and Hydrofoil Impellers in Fluids with Different Coalescence Characteristics, *PhD Thesis*, University of Birmingham, UK.

Martin, T., McFarlane, C. M. and Nienow, A. W., 1994, The Influence of Liquid Properties and Impeller Type on Bubble Coalescence Behaviour and Mass Transfer in Sparged, Agitated Reactors, *IChemE Symp. Series. No. 136*, 57–64.

Martin, T., Attempt of Determining the Coalescence Probability of Hydrogen Bubbles in an Acidic Salt Solution, *unpublished results*

Miyhara, T., Tsuchiya, K and Fan, L - S., 1991, Effect of Turbulent Wake on Bubble-bubble Interaction in a Gas-Liquid-Solids Fluidized Bed, *Chem. Eng. Sci.*, **46** 9 2368-2373.

Miyhara, T. and Takahasi, T., 1986, Coalescence Phenomena at the Moment of Bubble Formation at Adjacent Holes, *Chem. Eng. Res. Des.*, **64** 320–323.

Miyhara, T., Haga, N. and Takahasi, T., 1983, Bubble Formation from an Orifice at High Gas Flow Rates, *Int. Chem. Eng.*, **23** 524-531.

Moore, W. J., 1972, Physical Chemistry, 5th Edition, Prentice-Hall, Inc, New Jersey, ISBN 0-582-44234-6.

N

Narayanan, S., Goossens, L. H. J. and Kossen, N. W. F., 1974, Coalescence of Two Bubbles Rising in Line at Low Reynolds Numbers, *Chem. Eng. Sci.*, **29**, 2071-2082

Nicodemo, L., Marrucci, G. and Acierno, D., 1972, Bubble Pair Coalescence in Electrolyte Solution, *Quad. Ing. Chim. Ital.*, **8**, 1–7.

Nienow, A. W., 1991, *Kirk Othmer, Enc. Chem. Tech.*, 4th Ed., John Wiley & Sons, New York, pp645

Nienow, A. W., Pacek, A. W., Moore, I. P. T. and Homer, J., 1994, Fundamental Studies of Phase Inversion in a Stirred Vessel, *IChemE Symp. Series. No. 136*, 171–178.

O

Oels, U., Lucke, J., Buchholz, R., and Schugerl, K., 1978, Influence of Gas Distributor Type and Composition of Liquid on the Behaviour of a Bubble Column Bioreactor, *Ger. Chem. Eng.*, **1** 115-129

Oolman, T. O. and Blanch, H. W., 1986a, Bubble Coalescence in Stagnant Liquids, *Chem. Eng. Commun.*, **43** 237-261.

Oolman, T. O. and Blanch, H. W., 1986b, Bubble Coalescence in Air-Sparged Bioreactors, *Biotech. & Bioeng.*, **28** 578-584.

Otake, T., Tone, S., Nakao, K. and Mituhashi, Y., 1977, Coalescence and Breakup of Bubbles in Liquids, *Chem. Eng. Sci.*, **32** 377-383.

P

Pacek, A. W., Moore, I. T. P. and Nienow, A. W., 1994, Video Technique for Measuring Dynamics of Liquid-Liquid Dispersion During Phase Inversion, *AIChE J.*, **40** 1940-1949.

Palermo, T., 1991, Le Phénomène de Coalescence, *Revue de l'Institute François.*, **46**, 3, 325-360.

Parker J. L., Claesson, P. M. and Attard, P., 1994, Bubbles, Cavities and the Long-Ranged Attraction between Hydrophobic Surfaces, J. *Phys. Chem.*, **98** 8468-8480.

Parthasarathy, R., Ahmed, N., 1996, Size Distribution of Bubbles Generated by Fine-Pore Spargers. *J. Chem. Eng. Jap.*, **29** 1030-1034.

Pashley, R. M. and Craig, V. S. J., 1997, Effect of Electrolytes on Bubble Coalescence, *Langmuir*, **13** 4772-4774.

Pashley, R. M., 1981, Hydration Forces between Mica Surfaces in Aqueous Electrolyte Solutions, *J. Coll. Int. Sci.*, **80** 153-162.

Perry, R. H., Green, D. and Maloney, J. O., 1984, Perry's Chemical Engineering Handbook, McGraw-Hill, ISBN 0-07-049479-7

Prince, M. J. and Blanch, H. W., 1990a, Transition Electrolyte Concentrations for Bubble Coalescence, *AIChE J.*, **36** 1425-1429.

Prince, M. J. and Blanch, H. W., 1990b, Bubble Coalescence and Break-up in Air-Sparged Bubble Columns, *AIChE J.*, **36** 1485-1499.

Pohorecki, R. and Nowosielski, J., 1986, Interfacial Area Generated in Aqueous Electrolyte Solutions on a Sieve Plate, *AIChE J.*, **32** 632–639.

Pulda, J., Vleck, J. and Machon, V., The Influence of Surface Active Agents on Oxygen Transfer in Stirred Tank Reactors, *9th International Congress CHISA 93, September 1993, Prague*

R

Radoëv, B. P., Dimitrov, D. S. and Ivanov, I. B., 1974, Hydrodynamics of thin liquid films, Effect of the surfactant on the rate of thinning, *Coll. Pol. Sci.*, 50–55.

Ronteltap, A. D., Hollemans, M., Bisperink, C. G. J. and Prins, A., 1991, Beer Foam Physics, *MBAA Tech. Quart.*, **28** 25-32.

Ruckenstein, E. and Jain, R. K., 1973, Spontaneous Rupture of Thin Liquid Films, *J. Chem. Soc. Faraday II*, **70** 132-147.

Ruzicka, M., Drahos, J., Zahradnik, J. and Thomas, N. H., 2000, Structure of Gas Pressure Signal at Two-Orifice Bubbling from a Common Plenum, *Chem. Eng. Sci.*, **55**, 421-429.

Ruzicka, M., Drahos, J., Zahradnik, J. and Thomas, N. H., 1999, Natural Modes of Multi-Orifice Bubbling from a Common Plenum, *Chem. Eng. Sci.*, **54**, 5223-5229.

S

Sagert, N. H. and Quinn, J. H., 1978, The Coalescence of Gas Bubbles in Dilute Aqueous Solutions, *Chem. Eng. Sci.*, **33** 1087-1095.

Sagert, N. H. and Quinn, J. H., 1977, Influence of High-Pressure Gases on Stability of Thin Aqueous Films, *J. Coll. Int. Sci.*, **61** 279-286.

Sagert, N. H. and Quinn, J. H., 1976a, The Coalescence of H_2S and CO_2 Bubbles in Water, *Can. J. Chem. Eng.*, **54** 392-398.

Sagert, N. H., Quinn, J. H., Cribbs, S. C. and Rosinger E. L. J., 1976b, Bubble Coalescence in Aqueous Solutions of *n*-Alcohols, in *Foams*, Akers, R. J. (Ed.) Academic Press, London 147-162 (1976)

Sanchez, G. A., 1996, Coalescence Phenomena in Liquid-liquid Dispersions, PhD Thesis, University of Birmingham, UK.

Scheludko, A. *Proc. K. Ned. Akad. Wet.*, **B65** 76 (1962) [from Chaudhuri and Hofman, 1994]

Scheludko, A. *Adv. Colloid Int. Sci.*, **1** 391 (1967) [from Chaudhuri and Hofman, 1994]

Solanki, M. K. S., Mukherjee, A. K. and Das, T. R., 1992, Bubble Formation at Closely Spaced Orifices in Aqueous Solutions, *Chem. Eng. J.*, **49** 65–71.

Stewart, C. W., 1995, Bubble Interaction in Low-Viscosity Liquids, *Int. J. Multiphase Flow.*, **21** 1037–1046.

Stewart, C. W., Crowe, C. T. and Saunders, S. C., 1993, A Model for Simultaneous Coalescence of Bubble Clusters, *Chem. Eng. Sci.*, **48** 3347–3354.

T

Takahashi, K. and Nienow, A. W., 1993, Bubble Sizes and Coalescence Rates in an Aerated Vessel Agitated by a Rushton Turbine, *J. Chem. Eng. Jap.*, **26** 5 536-542.

Takahashi, K., McManamey, W. J. and Nienow, A. W., 1992, Bubble Sizes Distributions in Impeller Region in a Gas-Sparged Agitated by a Rushton Turbine, *J. Chem. Eng. Jap.*, **25** 4 427-432.

Takahashi, K. and Nienow, A. W., 1992, Effect of Gas Density on Power Consumption in Aerated Vessel Agitated by a Rushton Turbine, *J. Chem. Eng. Jap.*, **25** 4 432-434.

Thomas, R. M., 1981, Bubble Coalescence in Turbulent Flows, *Int. J. Multiphase Flow*, **7** 709–717.

Tsao, H. K. and Koch, D. L., 1994, Collisions of Slightly Deformable High Reynolds Number Bubbles with Short Range Repulsive Forces, *Phys. Fluids*, **6** 2591-2605.

Tsao, Y. H., Fennell Evans, D. and Wennerstrom, H., 1993, Long Range Attraction between a Hydrophobic Surface and a Polar Surface is Stronger than that between 2 Hydrophobic Surfaces, *Langmuir*, **9** 779-785.

Tse, K. L., Martin, T. M., McFarlane C. M. and Nienow, A. W., 1998, Visualisation of Bubble Coalescence in a Coalescence Cell, a Stirred Tank and a Bubble Column, *Chem. Eng. Sci.*, **53** 23 4031-4036.

U

Ueyama, K., Saeki, M. and Matsukata, M., 1993, Development of System for Measuring Bubble Coalescence Time by Using a Laser, *J. Chem. Eng. Japan*, **26** 308–314.

V

Viswanath, D. S., Narajan, G., 1989, Data Book on Viscosity of Liquids, Hemisphere Publishing Company, ISBN 0-89116-778-1.

Vold, R. D. and Vold, M. J., 1983, Colloid and Interface Chemistry, Addison-Wesley Publishing Company, Inc, ISBN 0-201-08195-4.

Vrij, A. and Overbeek, J. T. G., 1968, Rupture of Thin Liquid Films due to Spontaneous Fluctuations in Thickness, *J. Am. Chem. Soc.*, **90** 3074–3078.

W

Weinberg, M. C., 1981, Surface Tension Effects in Gas Bubble Dissolution and Growth, *Chem. Eng. Sci.*, **36** 137–141.

Weissenborn, P. K. and Pugh, R. J., 1996, Surface Tension if aqueous Solutions of Electrolytes: Relationship with Ion Hydration, Oxygen Solubility and Bubble Coalescence, *J. Coll. Int. Sci.*, **184** 550-563.

Weissenborn, P. K. and Pugh, R. J., 1995, Surface Tension and Bubble Coalescence Phenomena of Aqueous Solutions of Electrolytes, *Langmuir*, **11** 1422-1426.

Weyl, W. A., 1951, Surface Structure of Water and Some of its Physical and Chemical Manifestations, *J. Coll. Sci*, **6** 389-405.

Wilkinson, P. M., Haringa, H. and van Dierendonck, L. L., 1994, Mass Transfer and Bubble Size in a Bubble Column Under Pressure, *Chem. Eng. Sci.*, **49** 1417-1427.

Wilkinson, P. M. and van Dierendonck, L. L., 1990, Pressure and Gas Density Effects on Bubble Break-up and Gas Hold-up in Bubble Columns, *Chem. Eng. Sci.*, **45** 2309-2315.

Wood, J. and Sharma, R., 1995, How Long is the Long-Range Hydrophobic Attraction?, *Langmuir*, **11** 4797-4802.

X – Z

Yang, Y. M. and Maa, J. R., 1984a, Bubble Coalescence in Dilute Surfactant Solutions, *J. Coll. & Int. Sci.*, **98** 120-125.

Yang, Y. M. and Maa, J. R., 1984b, Dynamic Surface Effect on the Boiling of Mixtures, *Chem. Eng. Comm.*, **25** 47–62.

Zahradnik, J., Kuncova, G. and Fialova, M., 1999b, The Effect of Surface Active Additives on Bubble Coalescence in Aqueous Media, *Chem. Eng. Sci.*, **54** 4757-4766.

Zahradnik, J., Kuncova, G. and Fialova, M., 1999a, The Effect of Surface Active Additives on Bubble Coalescence and Gas Hold-up in Viscous Aerated Batches, *Chem. Eng. Sci.*, **54** 2401-2408.

Zahradnik, J., Kuncova, G. and Linek, V., 1998, The Effect of Surface Active Additives on Bubble Coalescence in Aqueous Media, *Proc. CHISA 98, Prague, August* 1998, P7.47-59, ISBN 80-86059-26-X 0823.

Zahradnik, J. and Fialova, M., 1996, The Effect of Bubbling Regime on Gas and Liquid Phase Mixing in Bubble Column Reactors, *Chem. Eng. Sci.*, **51** 2491–2500.

Zahradnik, J., Fialova, M., Kastanek, F., Green, K. D. and Thomas, N. H., 1995, The Effect of Electrolytes on Bubble Coalescence and Gas Holdup in Bubble Column Reactors, *Trans. IChemE Part* A,**73** 341–346.

Zahradnik, J., Peter, R. and Kastanek, F., 1987, The Effect of Liquid Phase Properties on Gas Holdup in Bubble Column Reactors, *Coll. Czech. Chem. Comm.* **52** 335–347.

Zahradnik, J., Peter, R. and Kastanek, F., 1982, Hydrodynamics and Mass Transfer in Uniformly Aerated Bubble Column Reactors, *Coll. Czech. Chem. Comm.* **52** 262–276.

Zieminski, S. A. and Whittemore, R. C., 1971, Behaviour of Gas Bubbles in Aqueous Electrolyte Solutions, *Chem. Eng. Sci.*, **26** 509–520.

Zieminski, S. A. and Raymond, D. R., 1968, Experimental Study of the Behaviour of Single Bubbles, *Chem. Eng. Sci.*, **23** 17–28.

Zou, R., Jang, X., Li, B., Zu, Y. and Zhang, L., 1988, Studies on Gas Holdup in a Bubble Column Operated at Elevated Temperatures, *Ind. Eng. Chem. Res.*, **27** 1910-1916.

Appendix A
Tables of High-Speed Video Data

In the following tables, mean data acquired using the high-speed video is summarised. Measurements were made according to the experimental protocol outlined in Chapter 3.

- Table A.1 summarises the data obtained for air, hydrogen and xenon-water systems. Air water systems have been investigated at temperatures of 10°C, 25°C and 50°C.
- Table A.2 summarises data for air-propan-1-ol systems at 10°C and 25°C.
- Table A.3 contains coalecsence time, coalecsence rate and contact time measurements for air-sodium sulfate solutions, at 25°C.
- Table A.4 summarises data for air, hydrogen and xenon-magnesium sulfate experiments at 25°C.
- Table A.5 summarises data for air-glycerol solution experiments at temperatures of 10°C, 25°C and 50°C.

A.1 Symbols

$\bar{t}_{ci}$	Mean coalescence time measured from initial contact	[ms]
$\bar{t}_{cf}$	Mean coalescence time measured from final contact	[ms]
$\bar{a}$	Mean contact area	[mm]
$\bar{a}/t_{cf}$	Mean coalescence rate (determined using the coalescence time from final contact)	[mm^2ms^{-1}]
$\bar{t}_{con}$	Mean contact time	[ms]

Symbols in red indicate data points not represented on graphs due to small number of events observed.

System	Temperature [°C]	Flow Rate, Q_g [mlmin^{-1}]	Number of Events, n	Mean Coalescence Time $\bar{t}_{ci}$ [ms]	Mean Coalescence Time $\bar{t}_{cf}$ [ms]	Mean Contact Area $\bar{a}$ [mm]	Mean Coalescence Rate $\overline{a/t_{cf}}$ [mm^{2}ms^{-1}]
Air/Water	10	1	25	42.6 ± 11.9	13.1 ± 6.0	0.576 ± 0.144	0.093 ± 0.32
		2	25	21.5 ± 5.5	6.0 ± 2.2	0.655 ± 0.153	0.195 ± 0.069
		10	25	12.6 ± 1.9	6.4 ± 1.2	0.865 ± 0.074	0.165 ± 0.066
		50	25	-	9.7 ± 1.4	3.05 ± 0.421	0.325 ± 0.023
Air/Water	25	1	25	3.1 ± 2.7	1.5 ± 0.8	0.125 ± 0.028	0.141 ± 0.045
		2	25	-	1.4 ± 0.3	0.171 ± 0.039	0.141 ± 0.027
		6	25	-	2.0 ± 0.5	0.238 ± 0.053	0.131 ± 0.023
		10	25	-	3.9 ± 1.2	0.606 ± 0.082	0.105 ± 0.022
		20	25	-	9.0± 1.4	1.01 ± 0.213	0.109 ± 0.017
		30	25	-	8.2 ± 1.7	1.86 ± 0.426	0.238 ± 0.050
		40	25	-	5.3 ± 0.7	1.37 ± 0.129	0.272 ± 0.028
		50	25	-	10.0 ± 1.6	2.90 ± 0.479	0.317 ± 0.051
Air/Water	50	1	25	9.0 ± 4.1	2.5 ± 0.9	0.337 ± 0.097	0.197 ± 0.079
		2	25	5.6 ± 2.1	2.2 ± 0.8	0.188 ± 0.047	0.123 ± 0.030
		10	25	8.8 ± 1.5	8.2 ± 1.6	0.676 ± 0.116	0.107 ± 0.039
		50	25	-	8.2 ± 1.9	3.77 ± 0.572	0.707 ± 0.234
H_2/Water	25	1	25	24.4 ± 5.8	6.6 ± 2.4	0.519 ± 0.126	0.148 ± 0.064
		2	25	14.9 ± 3.9	5.4 ± 2.2	0.654 ± 0.138	0.196 ± 0.050
		10	25	n/m	n/m	n/m	n/m
		50	25	-	7.1 ± 0.9	2.73 ± 0.168	0.424 ± 0.095
Xe/Water	25	1	25	3.9 ± 2.1	2.0 ± 0.8	0.224 ± 0.041	0.183 ± 0.046
		2	25	1.9 ± 0.6	1.7 ± 0.5	0.224 ± 0.031	0.172 ± 0.043
		10	25	-	2.3 ± 0.7	0.301 ± 0.061	0.151 ± 0.032
		50	25	-	7.2 ± 1.4	1.168 ± 0.369	0.252 ± 0.131

Table A.1

Data for coalescence time and coalescence rates for air, hydrogen and xenon-water systems. Air-water systems measured at temperatures of 10°C, 25°C and 50°C.

System	Temperature [°C]	Flow Rate, Q_g [mlmin^{-1}]	Number of Events, n	Mean Coalescence Time $\overline{t_{ci}}$ [ms]	Mean Coalescence Time $\overline{t_{cf}}$ [ms]	Mean Contact Area $\overline{a}$ [mm]	Mean Coalescence Rate $\overline{a/t_{cf}}$ [mm^{2}ms^{-1}]
Air/ Propan-1-ol	10	10		42.6 ± 11.9	13.1 ± 6.0	0.576 ± 0.144	0.093 ± 0.32
		50		21.5 ± 5.5	6.0 ± 2.2	0.655 ± 0.153	0.195 ± 0.069
Air/ Propan-1-ol	25	10		3.1 ± 2.7	1.5 ± 0.8	0.125 ± 0.028	0.141 ± 0.045
		50		-	1.4 ± 0.3	0.171 ± 0.039	0.141 ± 0.027

Table A.2

Data for coalescence times, coalescence rates and contact times for air-propan-1-ol systems measured at 10° and 25°C.

System	Flow Rate, Q_g [mlmin^{-1}]	Number of Events, n	Mean Coalescence Time $\overline{t_{cf}}$ [ms]	Mean Contact Area $\overline{a}$ [mm]	Mean Coalescence Rate $\overline{a/t_{cf}}$ [mm^{2}ms^{-1}]	Mean Contact Time, $\overline{t_{con}}$ [ms]
Air/0.02 M Na_2SO_4	1	22	8.5 ± 1.2	0.379 ± 0.074	0.050 ± 0.0121	-
	2	25	13.3 ± 1.6	0.586 ± 0.070	0.047 ± 0.006	-
	4	20	6.4 ± 1.2	0.415 ± 0.041	0.075 ± 0.017	-
	6	25	9.7 ± 2.4	0.787 ± 0.174	0.089 ± 0.010	-
	8	20	16.4 ± 9.5	1.05 ± 0.264	0.091 ± 0.017	-
	10	20	8.2 ± 2.0	0.861 ± 0.186	0.115 ± 0.066	-
	25	25	9.2 ± 1.4	2.19 ± 0.240	0.267 ± 0.033	-
	50	25	8.6 ± 1.6	4.37 ± 0.676	0.544 ± 0.038	-
Air/0.03 M Na_2SO_4	1	25	79.7 ± 12.0	1.21 ± 0119	0.017 ± 0.002	-
	2	10	16.9 ± 8.3	0.699 ± 0.436	0.057 ± 0.027	-
	4	20	20.0 ± 7.1	0.786 ± 0.102	0.078 ± 0.051	-
	6	20	17.9 ± 4.6	0.851 ± 0.149	0.073 ± 0.026	-
	8	20	16.2 ± 5.8	0.825 ± 0.151	0.142 ± 0.098	-
	10	20	13.5 ± 4.2	0.985 ± 0.267	0.113 ± 0.051	-
	15	20	10.7 ± 4.8	0.908 ± 0.364	0.181 ± 0.087	-
	25	20	14.0 ± 1.4	3.61 ± 0.381	0.264 ± 0.018	-
	50	20	7.9 ± 1.4	3.15 ± 0.339	0.449 ± 0.071	-
Air/0.04 M Na_2SO_4	1	11	46.9 ± 26.9	1.42 ± 0.920	0.042 ± 0.022	120 ± 23
	2	11	10.1 ± 6.7	0.355 ± 0.120	0.138 ± 0.120	70.2 ± 10.0
	6	22	16.1 ± 5.9	0.721 ± 0.164	0.113 ± 0.053	47.9 ± 2.8
	10	24	6.0 ± 3.4	0.538 ± 0.180	0.239 ± 0.077	44.8 ± 9.1
	15	25	6.1 ± 3.1	0.636 ± 0.137	0.315 ± 0.093	37.5 ± 3.4
	25	19	16.9 ± 3.4	0.977 ± 0.111	0.071 ± 0.018	74.9 ± 6.8
	50	25	9.8 ± 1.5	1.31 ± 0.069	0.163 ± 0.041	-

Table A.3

Data for coalescence times, coalescence rates and contact times for air-sodium sulfate solutions, all at 25°C.

System	Flow Rate, Q_g [mlmin^{-1}]	Number of Events, n	Mean Coalescence Time $\overline{t_{cf}}$ [ms]	Mean Contact Area $\overline{a}$ [mm]	Mean Coalescence Rate $\overline{a/t_{cf}}$ [mm^{2}ms^{-1}]	Mean Contact Time, $\overline{t_{con}}$ [ms]
Air/0.06 M Na_2SO_4	1	-	-	-	-	135 ± 7
	2	-	-	-	-	66.0 ± 2.8
	4	10	15.4 ± 9.1	0.799 ± 0.346	0.141 ± 0.088	59.1 ± 3.7
	6	15	15.7 ± 6.5	0.794 ± 0.146	0.107 ± 0.060	46.2 ± 7.1
	10	18	11.1 ± 6.3	0.580 ± 0.140	0.293 ± 0.125	44.7 ± 10.1
	15	25	5.8 ± 3.3	0.663 ± 0.236	0.293 ± 0.069	37.5 ± 3.1
	25	25	11.8 ± 4.4	0.698 ± 0.136	0.142 ± 0.047	-
	50	25	7.6 ± 2.0	1.15 ± 0.114	0.228 ± 0.060	-
Air/0.06 M Na_2SO_4	1	-	-	-	-	110 ± 17
	2	-	-	-	-	58.5 ± 6.6
	4	-	-	-	-	60.1 ± 0.8
	6	15	17.9 ± 4.6	0.851 ± 0.149	0.073 ± 0.026	50.2 ± 1.3
	10	24	13.5 ± 4.2	0.985 ± 0.267	0.113 ± 0.051	44.8 ± 5.6
	15	26	10.7 ± 4.8	0.908 ± 0.364	0.181 ± 0.087	41.8 ± 7.3
	25	25	14.0 ± 1.4	3.61 ± 0.381	0.264 ± 0.018	34.4 ± 4.2
	50	26	7.9 ± 1.4	3.15 ± 0.339	0.449 ± 0.071	25.2 ± 5.5

Table A.3 (continued).

Data for coalescence times, coalescence rates and contact times for air-sodium sulfate solutions, all at 25°C.

System	Flow Rate, Q_g [mlmin^{-1}]	Number of Events, n	Mean Coalescence Time $\overline{t_{ci}}$ [ms]	Mean Coalescence Time $\overline{t_{cf}}$ [ms]	Mean Contact Area $\overline{a}$ [mm]	Mean Coalescence Rate $\overline{a/t_{cf}}$ [mm^{2}ms^{-1}]	Mean Contact Time, $\overline{t_{con}}$ [ms]
Air/0.02 M $MgSO_4$	1	25	23.0 ± 6.3	18.3 ± 4.8	0.515 ± 0.139	0.030 ± 0.005	-
	2	25	22.0 ± 7.1	20.0 ± 6.4	0.884 ± 0.221	0.053 ± 0.012	-
	10	25	-	15.8 ± 3.7	1.18 ± 0.261	0.080 ± 0.012	-
	50	25	-	10.3 ± 1.3	3.92 ± 0.385	0.487 ± 0.159	-
Air/ 0.025 M $MgSO_4$	1	17	63.0 ± 32.2	46.8 ± 30.0	0.683 ± 0.177	0.056 ± 0.035	108.8 ± 46.1
	2	11	21.6 ± 10.5	7.4 ± 3.8	0.769 ± 0.256	0.234 ± 0.144	48.8 ± 28.8
	10	11	16.1 ± 4.4	12.2 ± 3.5	0.909 ± 0.274	0.101 ± 0.060	44.7 ± 12.4
	50	25	-	9.9 ± 2.4	2.64 ± 0.466	0.365 ± 0.147	36.6 ± 7.6
Air/0.03 M $MgSO_4$	1	21	55.5 ± 26.8	42.3 ± 24.5	0.627 ± 0.152	0.049 ± 0.152	144.6 ± 32.0
	2	12	-	45.4 ± 15.2	0.897 ± 0.271	0.025 ± 0.011	74.6 ± 2.3
	10	14	-	9.6 ± 3.5	0.660 ± 0.191	0.080 ± 0.017	34.2 ± 8.4
	50	25	-	9.8 ± 1.8	3.98 ± 0.666	0.520 ± 0.129	-
Air/0.05 M $MgSO_4$	1	11	23.6 ± 10.1	19.5 ± 11.0	0.383 ± 0.146	0.083 ± 0.072	120.4 ± 5.1
	2	11	24.4 ± 12.6	20.9 ± 10.6	0.481 ± 0.192	0.046 ± 0.031	36.5 ± 8.5
	10	12	-	15.4 ± 7.2	0.632 ± 0.182	0.073 ± 0.027	46.4 ± 5.2
	50	25	-	10.3 ± 1.2	5.00 ± 0.499	0.527 ± 0.067	-
H_2/0.02 M $MgSO_4$	1	25	12.9 ± 3.3	9.8 ± 2.6	0.468 ± 0.115	0.074 ± 0.033	-
	2	25	9.3 ± 2.6	7.8 ± 2.4	0.505 ± 0.101	0.108 ± 0.040	-
	10	25	-	13.9 ± 3.7	1.46 ± 0.330	0.146 ± 0.042	-
	50	25	-	14.9 ± 1.1	4.85 ± 0.661	0.318 ± 0.025	-

Table A.4

Data for coalescence times, coalescence rates and contact times for air, hydrogen and xenon-magnesium sulfate solutions, all at 25°C.

System	Flow Rate, Q_g [mlmin^{-1}]	Number of Events, n	Mean Coalescence Time $\bar{t}_{ci}$ [ms]	Mean Coalescence Time $\bar{t}_{cf}$ [ms]	Mean Contact Area $\bar{a}$ [mm]	Mean Coalescence Rate $\overline{a/t_{cf}}$ [mm^{2}ms^{-1}]	Mean Contact Time, $\bar{t}_{con}$ [ms]
H_2/0.025 M $MgSO_4$	1	25	-	22.7 ± 6.7	0.620 ± 0.152	0.030 ± 0.004	-
	2	25	-	16.2 ± 6.7	0.670 ± 0.109	0.054 ± 0.008	-
	10	25	-	11.5 ± 2.8	1.15 ± 0.249	0.116 ± 0.020	37.8 ± 2.8
	50	25	-	6.3 ± 2.5	1.61 ± 0.487	0.558 ± 0.243	33.2 ± 3.3
H_2/0.03 M $MgSO_4$	1	12	24.8 ± 12.6	22.1 ± 12.3	0.614 ± 0.128	0.038 ± 0.008	-
	2	16	-	8.9 ± 5.1	0.546 ± 0.143	0.129 ± 0.063	94.0 ± 29.3
	10	25	-	7.7 ± 3.2	0.650 ± 0.156	0.199 ± 0.076	44.1± 13.4
	50	25	-	9.0 ± 2.9	1.96 ± 0.785	0.345 ± 0.108	25.5 ± 3.7
H_2/0.05 M $MgSO_4$	1	16	81.2 ± 38.4	78.1 ± 34.7	0.800 ± 0.187	0.028 ± 0.021	145 ± 93.5
	2	14	24.2 ± 9.4	22.8 ± 10.1	1.07 ± 0.294	0.142 ± 0.109	75.6 ± 21.7
	10	16	-	11.5 ± 5.2	0.818 ± 0.238	0.122 ± 0.037	39.4 ± 1.4
	50	25	-	10.3 ± 4.2	1.20 ± 0.430	0.359 ± 0.113	31.9 ± 3.7
Xe/0.02 M $MgSO_4$	1	23	81.2 ± 38.4	78.1 ± 34.7	0.800 ± 0.187	0.028 ± 0.021	-
	2	26	24.2 ± 9.4	22.8 ± 10.1	1.07 ± 0.294	0.142 ± 0.109	114 ± 14.3
	10	25	-	11.5 ± 5.2	0.818 ± 0.238	0.122 ± 0.037	-
	50	25	-	10.3 ± 4.2	1.20 ± 0.430	0.359 ± 0.113	-
Xe/0.025 M $MgSO_4$	1	22	31.5 ± 15.3	28.0 ± 15.0	0.611 ± 0.168	0.031 ± 0.005	-
	2	21	20.1 ± 6.1	19.3 ± 6.1	0.731 ± 0.206	0.070 ± 0.056	116.4 ± 10.9
	10	24	14.0 ± 4.0	13.6 ± 4.1	1.60 ± 0.323	0.093 ± 0.015	66.7 ± 2.3
	50	25	-	10.5 ± 0.8	1.91 ± 0.264	0.178 ± 0.013	-

Table A.4 (continued).

Data for coalescence times, coalescence rates and contact times for air, hydrogen and xenon-magnesium sulfate solutions, all at 25°C.

System	Flow Rate, Q_g [mlmin^{-1}]	Number of Events, n	Mean Coalescence Time $\bar{t}_{ci}$ [ms]	Mean Coalescence Time $\bar{t}_{cf}$ [ms]	Mean Contact Area $\bar{a}$ [mm]	Mean Coalescence Rate $\overline{a/t_{cf}}$ [mm^{2}ms^{-1}]	Mean Contact Time, $\bar{t}_{con}$ [ms]
Xe/0.03 M $MgSO_4$	1	15	74.6 ± 26.4	65.1 ± 26.7	0.953 ± 0.239	0.020 ± 0.005	207 ± 11
	2	16	37.0 ± 10.1	29.1 ± 11.2	0.774 ± 0.198	0.074 ± 0.076	82.0 ± 11.3
	10	17	-	13.7 ± 4.3	0.824 ± 0.208	0.112 ± 0.071	48.2 ± 4.6
	50	25	-	11.8 ± 0.6	2.12 ± 0.267	0.176 ± 0.016	-
Xe/0.05 M $MgSO_4$	1	17	58.4 ± 23.3	37.4 ± 21.6	0.813 ± 0.225	0.294 ± 0.292	209 ± 11.0
	2	11	35.8 ± 17.4	26.4± 17.3	0.513 ± 0.128	0.117 ± 0.121	82.0 ± 11.3
	10	11	-	14.4 ± 4.2	0.886 ± 0.155	0.108 ± 0.068	48.2 ± 4.6
	50	25	-	10.2 ± 0.9	1.44 ± 0.126	0.156 ± 0.031	-

Table A.4 (continued).

Data for coalescence times, coalescence rates and contact times for air, hydrogen and xenon-magnesium sulfate solutions, all at 25°C.

System	Temperature [°C]	Number of Events, n	Mean Coalescence Time $\overline{t_{ci}}$ [ms]	Mean Coalescence Time $\overline{t_{cf}}$ [ms]	Mean Contact Area $\overline{a}$ [mm]	Mean Coalescence Rate $\overline{a/t_{cf}}$ [mm^2ms^{-1}]	Mean Contact Time, $\overline{t_{con}}$ [ms]
Air / 0.5 M Glycerol	10	16	10.2 ± 0.9	5.8 ± 2.7	0.52 ± 0.18	0.177 ± 0.065	-
Air / 0.8 M Glycerol	10	12	40.3 ± 16.6	16.9 ± 10.8	0.77 ± 0.32	0.241 ± 0.197	-
Air / 1.0 M Glycerol	10	11	12.9 ± 5.6	11.5 ± 5.5	0.57 ± 0.12	0.105 ± 0.062	204 ± 10
Air / 1.25 M Glycerol	10	14	-	12.6 ± 0.4	0.36 ± 0.02	0.028 ± 0.001	51.0 ± 2.5
Air / 2.0 M Glycerol	10	5	18.8 ± 16.8	11.6 ± 11.3	0.70 ± 0.20	0.132 ± 0.122	112 ± 48
Air / 4.0 M Glycerol	10	6	28.7 ± 13.3	5.3 ± 4.6	0.64 ± 0.18	0.249 ± 0.147	-
Air / 6.0 M Glycerol	10	-	-	-	-	-	153 ± 13
Air / 8.0 M Glycerol	10	-	-	-	-	-	139 ± 13
Air / 0.02 M Glycerol	25	16	1.9 ± 1.3	1.2 ± 0.2	0.30 ± 0.04	0.286 ± 0.070	-
Air / 0.05 M Glycerol	25	12	-	2.0 ± 0.5	0.25 ± 0.03	0.157 ± 0.041	-
Air / 0.1 M Glycerol	25	17	-	1.0 ± 0.1	0.22 ± 0.01	0.286 ± 0.025	-
Air / 0.2 M Glycerol	25	12	-	1.6 ± 0.3	0.19 ± 0.03	0.141 ± 0.042	-

Table A.5

Data for coalescence times, coalescence rates and contact times for air-glycerol solutions at temperatures of 10°C, 25°C and 50°C..

System	Temperature [°C]	Number of Events, n	Mean Coalescence Time $\overline{t_{ci}}$ [ms]	Mean Coalescence Time $\overline{t_{cf}}$ [ms]	Mean Contact Area $\overline{a}$ [mm]	Mean Coalescence Rate $\overline{a/t_{cf}}$ [mm^2ms^{-1}]	Mean Contact Time, $\overline{t_{con}}$ [ms]
Air / 0.5 M Glycerol	25	14	-	1.4 ± 0.3	0.18 ± 0.02	0.146 ± 0.036	-
Air / 1.0 M Glycerol	25	18	-	4.8 ± 1.0	0.26 ± 0.03	0.058 ± 0.006	-
Air / 1.25 M Glycerol	25	15	-	38.8 ± 12.5	0.64 ± 0.03	0.024 ± 0.007	-
Air / 1.5 M Glycerol	25	10	-	112 ± 22	0.73 ± 0.26	0.009 ± 0.007	150 ± 101
Air / 2.0 M Glycerol	25	-	-	-	-	-	131 ± 8
Air / 3.0 M Glycerol	25	-	-	-	-	-	112 ± 21
Air / 4.0 M Glycerol	25	-	-	-	-	-	160 ± 13
Air / 6.0 M Glycerol	25	-	-	-	-	-	173 ± 14
Air / 8.0 M Glycerol	25	-	-	-	-	-	116 ± 14
Air / 0.02 M Glycerol	50	14	4.4 ± 2.5	3.5 ± 2.3	0.28 ± 0.06	0.151 ± 0.044	-
Air / 0.02 M Glycerol	50	15	-	5.8 ± 3.6	0.28 ± 0.06	0.117 ± 0.055	-
Air / 0.02 M Glycerol	50	15	6.1 ± 1.9	5.5 ± 1.9	0.22 ± 0.04	0.095 ± 0.068	-
Air / 0.02 M Glycerol	50	11	-	3.7 ± 1.4	0.18 ± 0.02	0.077 ± 0.076	-

Table A.5 (continued)

Data for coalescence times, coalescence rates and contact times for air-glycerol solutions at temperatures of 10°C, 25°C and 50°C..

System	Temperature [°C]	Number of Events, n	Mean Coalescence Time $\overline{t_{ci}}$ [ms]	Mean Coalescence Time $\overline{t_{cf}}$ [ms]	Mean Contact Area $\overline{a}$ [mm]	Mean Coalescence Rate $\overline{a/t_{cf}}$ [mm^{2}ms^{-1}]	Mean Contact Time, $\overline{t_{con}}$ [ms]
Air / 2.0 M Glycerol	50	15	-	4.9 ± 0.5	0.36 ± 0.03	0.076 ± 0.010	-
Air / 3.0 M Glycerol	50	6	-	60.3 ± 18.8	0.98 ± 0.26	0.019 ± 0.008	-
Air / 4.0 M Glycerol	50	6	-	35.7 ± 21.9	0.91 ± 0.42	0.054 ± 0.049	96.8 ± 12.9
Air / 6.0 M Glycerol	50	-	-	-	-	-	76.4 ± 11.5
Air / 8.0 M Glycerol	50	-	-	-	-	-	64.3 ± 15.1

Table A.5 (continued)

Data for coalescence times, coalescence rates and contact times for air-glycerol solutions at temperatures of 10°C, 25°C and 50°C..

Appendix B
Cleaning Procedure for Experimental Equipment

The importance of complete cleanliness in experiments investigating interfacial phenomena is well known as the presence of very small amounts of impurities can greatly alter the events observed. The cleaning procedure adopted in this work was developed from the experience of previous workers (Cattaneo, 1995, Man, 1998).

B.1 Cleaning the Coalescence Cell

Prior to each experiment (or set of experiments for a single set of test fluids) the coalescence cell was dismantled and thoroughly cleaned using the following 'standardised' procedure.

1. The cell and frame were rinsed thoroughly with hot tap water.
2. The glass cell was then filled with a hot (~ 50°C) solution of ≤ 5 % by volume Decon-75 ™ (Decon Laboratories ltd., England) and scrubbed thoroughly with a stiff bristle brush. Particular care was taken to ensure the silicone sealant in the corners and the rear (ground glass) face of the cell were both well scrubbed.
3. The stainless steel frame was dismantled and the constituent parts soaked in a hot (~ 50°C) solution of ≤ 5 % by volume Decon-75 ™. All components were brushed thoroughly with a soft bristle brush. Special care was paid to the polypropylene nozzle extensions and the vertical winding thread and also to ensure that the two nozzle mountings were completely submerged in the cleaning fluid.
4. Both the cell and the stainless steel frame were left to stand for not more than 30 minutes before being rinsed with a jet of hot tap water. The internal surfaces of the cell and the constituent parts of the stainless steel frame were then brushed and rinsed with hot water for about 5 minutes.
5. The cell was then scrubbed with double distilled water and rinsed several times (no less than five) with more double distilled water.
6. The components of the stainless steel frame were also scrubbed with double distilled water and then rinsed well. Using clean hands the frame was reassembled: the nozzles were aligned vertically with the nozzle extensions touching before the horizontally

adjustable nozzle was bolted into position at a set nozzle spacing, measured using Vernier calipers (see Figure 3.5 for schematic diagram).

7. The cell was then completely filled with double distilled water, the frame was inserted and both left overnight to soak, thereby removing any water-soluble impurities.
8. Before use the cell was emptied, re-filled with double distilled water and shaken. This rinse step was then repeated no less than three times. This step was designed as a crude measure of the cleanliness of the cell: formation of bubbles on the glass surfaces indicated the cell was not clean and the cleaning procedure was repeated. As a secondary measure a visual check was made on the rate at which bubbles coalesced with the surface: in a clean system large bubbles formed which collapsed rapidly upon reaching the surface, if however a number of little bubbles were created which persisted at the surface, the system was considered unclean and the cleaning procedure had to be repeated.

B.2 Cleaning the Bubble Column

As for the two-bubble experiments, it was considered critical that the bubble column and all glassware used in the test rig was cleaned thoroughly prior to each experiment (or set of experiments for a single set of test fluids). This was done according to the following procedure.

1. The column was rinsed with hot tap water, filled with a hot (~ 50°C) solution of $\leq 3\%$ by volume Decon-75 ™ and then scrubbed thoroughly with a stiff bristle and left to soak for not more than 30 minutes.
2. After soaking, the column was rinsed with hot tap water for about 5 minutes.
3. The column was then rinsed thoroughly with double distilled water, which was allowed to drain away through the porous plate sparger and stood overnight in a 2 dm^3 beaker of double distilled water to remove any remaining water soluble residues.
4. Before use the column was filled with double distilled water and shaken. A quick check was made to note whether any of the bubbles formed adhered to the column walls, if so, the cleaning procedure was repeated. If not, the column was considered to be ready for use.

Appendix C
Method of Data Acquisition for Bubble Size Distributions

This section describes in greater detail the method used to acquire, analyse and reduce the data used in producing the bubble size distributions which form the basis of results presented in Chapter 7.

C.1 Image Selection

In applying the method developed by Pacek et al. (1994) it was decided not to follow their approach of basing the distributions on data collected from consecutive images; rather images were selected by choosing the first frame in every minute for the analysis. The method was initially developed to investigate drop size distributions in a stirred vessel, where the energy dissipated by the impeller made it almost impossible to track a single bubble from one frame to the following. In this system however, where bubble motion is determined solely by bubble rise velocities and bubble-bubble interactions, it was not uncommon for the bubbles to be followed over a number of consecutive frames. This was especially the case for the very smallest bubbles which become entrained in the flow and tend to persist over a greater number of frames. Consequently, by altering the method it was hoped to avoid the double counting of drops that may have otherwise occurred.

Obviously it was not possible to accurately determine the size of bubbles which were larger than the frame size, a concern which was particularly relevant in determining the bubble size distributions in air-water systems. Consequently these images were not chosen for analysis; they were replaced by the closest image which contained bubbles of a size which could be more accurately determined.

C.2 Acquiring the Digital Image

The frame-by frame control on the Panasonic AG-5700 SVHS video recorder was used to choose the image for analysis, which was then converted into a digital image using the screen capture software, Screen Machine II, a Windows™ based software package. Image capture is made in SM TV II mode, which produces a default image size of 736 by 560 pixels. The

stilled frame from the videotape appears in the SM TV II window and adjustments to image intensity, contrast and brightness can be made to ensure the image was of maximum clarity for accurate analysis. The full-sized, black and white optimised image is saved as a "*.dib*" file format, with the image resolution set to 8 bit and 256 greyscales. The process is then repeated until sufficient frames have been collected.

C.3 Measuring the Bubble Size

After the images have been converted to digital format, they can be analysed using a Windows™ based program developed by Jadayel et al. (1995), Droplet Detection System, Version 1.5. The appropriate *.dib* file is opened from within Droplet Detection System and appears in the counting window. The program requires that the bubbles be analysed manually, with size determination based on approximation to a sphere. Three, preferably equidistant, points on the perimeter of the bubble are selected using the mouse, which then enables the program to construct a coloured circle around the bubble perimeter, based on the lengths of the sides of the triangle subsequently formed. After the perimeter has been identified, corresponding information about the type of fluid particle (liquid, gas or other), the number and the radius in pixels appears for each bubble in the associated 'Bubble Details' window. If the perimeter constructed does not accurately represent the bubble of interest, it can be removed and redrawn until satisfactorily representative. Only those bubbles which are clearly in focus should be chosen for analysis. Once all the in-focus bubbles in the image frame have been counted and size, the data can be saved as "*.bbl*" format. The counted image can then be closed and the next image opened for analysis.

As this technique was initially used to measure the diameters of liquid-liquid drops in a stirred tank, the correlation between spherical requirements of the software and the shapes of the fluid particles to be measured was excellent. In this study, many bubbles in air-water systems and in solutions with low electrolyte concentration (particularly at the highest superficial gas velocity) were often observed to deviate significantly from spherical. The technique has been successfully applied to air-water systems, albeit in stirred tanks by Martin (1996) and Machon et al. (1997) although in these systems very large, non-spherical bubbles have also been encountered. Martin (1996), in particular has considered the problem in some detail and concludes that the technique can be successfully applied by assuming the non-spherical

bubbles to be either prolate or oblate spheroids. In this study, the diameter of non-spherical bubbles has been approximated through one of two methods. In addition to constructing circle around a bubble from the three triangulated pints, the program also contains a function to measure the distance between two points. For those bubbles which could be approximated as a ellipsoid, i.e. the shape can be defined with major and minor axes, a and b respectively, then the diameter of the equivalent spherical body, d_e is:

$$d_e = \left[4a^2b\right]^{\frac{1}{3}} \qquad \text{(D.1)}$$

as given by Grace and Wairegi (1992). Trial and error was then used to define a bubble of the same radius. However, if the bubble could not be consider as an ellipsoid, then it was necessary to approximate the shape to spherical, using personal judgement. As a consequence it was not possible to determine the size of the very largest and most irregular bubbles with any great degree of accuracy. The diameter thus 'measured' provided only an order of magnitude estimation of bubble size.

C.4 Obtaining the Size Distributions

Once a representative number of bubbles had been counted, a file was created to compile the *.bbl* data files for each data point into a single set. This was achieved using the Windows™ 'Notepad' text editor. Following this, the data was analysed using a DOS based program, developed in-house by A. W. Pacek ('DropDis') which calculated mean diameters, probability density functions and cumulative functions. This data could then be imported into Windows™ 'Excel' program for further analysis.

Appendix D
Coalescence in Solutions of Polypropylene Glycol

The overall aim of this study was to determine whether the coalescence cell could be used as a predictive tool for the coalescence behaviour of larger scale gas-liquid dispersions. The equilibrium between bubble coalescence and break-up is the primary mechanism which determines the bubble size distribution in a system and subsequently, the bubble gas-hold up. When large volumes of gas are dispersed in strongly coalescence repressed solutions, such as concentrated solutions of electrolytes, alcohols or other surface active species, regions of very low liquid, but high gas content, may form as either froth or foam towards the upper levels of the dispersion. The lifetime of such a froth or foam is strongly dependent on the lifetime of the component bubbles and hence on the amount of coalescence occurring.

D.1 Motivation

The series of experiments reported here were carried out following observations made during studies into high gas hold-ups in a stirred tank, which showed a strong dependency of gas hold-up, in particular foam height, on system temperature (Gezork, 1999). The work was carried out in a baffled, stirred tank fitted with a standard 6-blade Rushton turbine. Compressed air was dispersed into aqueous solutions of 20 ppm polypropylene glycol (PPG), a strongly coalescence repressed liquid. Typical hold-up values for this system were of the

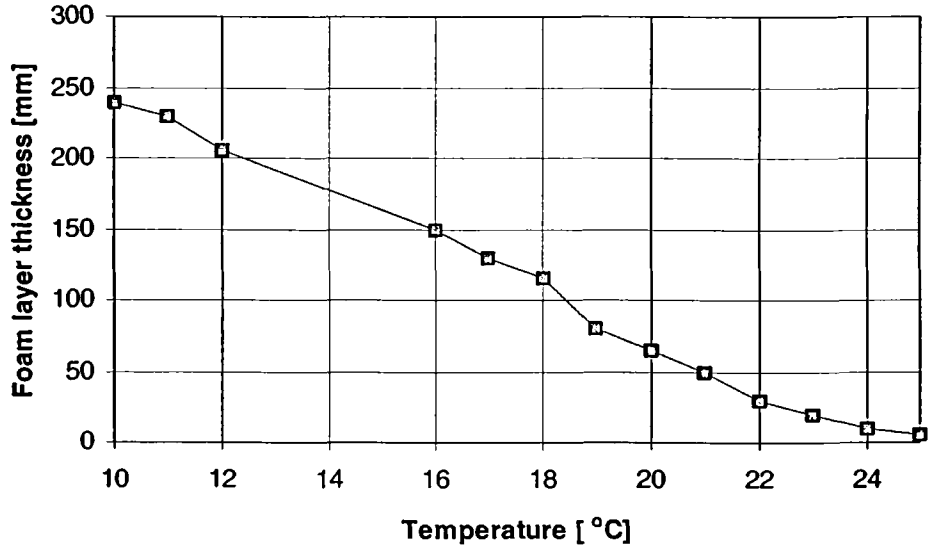

Figure D.1

Foam layer thickness as a function of temperature in 20 ppm PPG. Rushton turbine at: H/T=0.5, v_S=0.3125ms^{-1}, N=400 rpm (this is approx. an energy dissipation rate of 1.9 kWm^{-3}). (from Gezork, 1999).

order of 30 %. At low temperatures this value included a significant contribution from a layer of foam at the top of the dispersion; however, the height of this layer was observed to decrease rapidly in height with increasing temperature, until completely absent. Figure E.1 shows very clearly the steady decrease in foam height as the system temperature increased from 10 to 25°C. It was considered that the very strong link between temperature and coalescence made this system an excellent test case for assessing the predictive capabilities of the coalescence cell.

D.2 Coalescence Cell Studies

Studies were carried out following the experimental method outlined in Chapter 3, using a nozzle separation of 4 mm and gas flow rates from 2 to 60 mlmin^{-1}. The PPG solution used in the experiments was prepared in 20 dm^3 aquilots, as for the agitated vessel experiments. This ensured consistency between the cell and stirred tank solutions, and reduced errors due to the very small volumes of polypropylene glycol which were required to make accurate preparation of small test volumes. Experiments were carried out at three different temperatures: 10°C, 18°C and 25°C. Results were analysed with the Panasonic video camera (50 frames s^{-1}); coalescence frequencies at each of the test temperatures are shown in Figure E.2 as a function of the gas flow rate.

An immediate assessment of Figure E.2 suggests that the profiles obtained in the coalesce cell in no way correlate with the consistent decrease in foam height with increasing temperature, observed in the stirred tank. It appears that the graph can be divided into two distinct regions. At gas flow rates below ~ 20 mlmin^{-1}, systems at all temperatures are essentially fully coalescing and the lower the temperature the longer the period of full coalescence. For gas

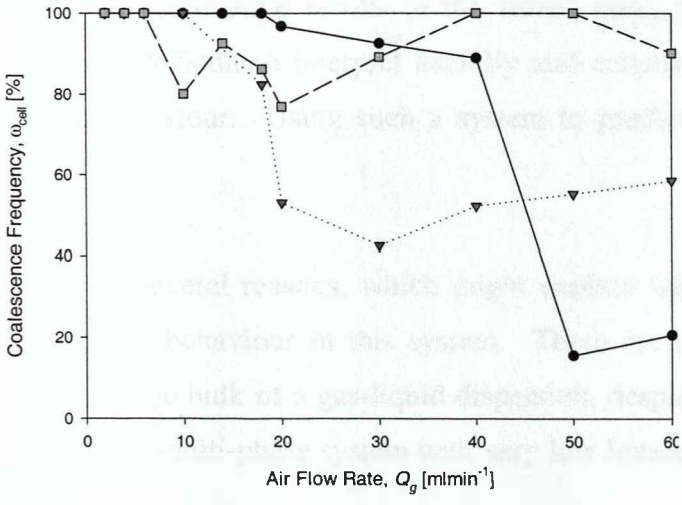

Figure D.2

Coalescence cell profiles obtained at three different temperatures for solutions of 20 ppm PPG. —●— 10°C, ···▼··· 18°C and —□— 25°C. Nozzle distance 4 mm.

flow rates in excess of 30 $mlmin^{-1}$, the coalescence behaviour is much less well defined. At 25°C, although erratic, the coalescence cell profile is close to fully coalescent, as may be expected from the results of the experiments carried out in the stirred tank. However, for solutions at 10°C and 18°C there appears to be a step change in the coalescence frequency, occurring at gas flow rates of ~ 45 $mlmin^{-1}$ for solutions at 10°C and at a much lower flow rate of ~ 18 $mlmin^{-1}$ for solutions at 18°C. Only at the very highest flow rates is a trend similar to that observed in the stirred tank seen, with reduced coalescence frequencies measured with decreasing system temperature.

Studies in the literature have shown that for solutions of electrolytes in stirred tanks, there is a much broader transition between coalescing and non-coalescing systems, than that observed for equivalent systems in homogeneously operated bubble columns (Lee and Meyrick, 1970, Calderbank, 1965). For this reason, earlier in this study it was considered that such behaviour is best approximated by coalescence cell profiles obtained for intermediate to high gas flow rates (thus avoiding the sharp step changes in coalescence frequency observed at the lowest gas flow rates). In addition, the very high superficial gas velocity used in the stirred tank experiments, would suggest that in this system, coalescence behaviour is best approximated by measuring coalescence cell profiles at the higher gas flow rates. Under these conditions it can be seen the cell does begin to approximate the coalescence behaviour observed in the agitated vessel.

However, the aim of this project was to assess the suitability of the coalescence cell as a predictive tool for determining the coalescence behaviour observed in dynamic systems. In light of this consideration, it must be concluded that the cell is not an accurate diagnostic tool. Irrespective of the 'correct' trends observed at the highest gas flow rates (i.e. able to correlate with the experimental results in the stirred tank), the overall coalescence cell profiles are extremely difficult to interpret usefully and certainly do not appear to approach the known system behaviour. Using such a system to predict behaviour for unknown systems is not possible.

There are several reasons, which might explain why the cell profiles so poorly predict the coalescence behaviour in this system. There are significant differences between foam (or froth) and the bulk of a gas-liquid dispersion, despite the fact that foam can be considered to be merely a multi-phase system with very low levels of liquid hold-up. In foam, the effects of

system hydrodynamics are likely to be of reduced importance, as the bubbles are not able to move freely, forming instead a well-ordered structure. Consequently, contact times between two bubbles are much greater than they would be for bubbles contacting during free rise, in a gas-liquid dispersion. As a result of the close packed structure of foam, contact areas between bubbles are also much larger than equivalent values in dynamic dispersions. In the coalescence cell used in this study, it is not possible to observe larger contact areas and prolonged contact times simultaneously. Similar larger contact areas will only be observed for deformable bubbles contacting face-to-face at high gas flow rates, although such high gas flow rates are also associated with shorter contact times due to the continuous flow aspects of the experimental equipment.

The stable structure of a foam arises from the resistance of the constituent bubbles to coalescence. This resistance is conferred by the presence of surfactants, which as a result of the prolonged bubble lifetimes are able to adopt the most energetically favourable conformation at the gas-liquid surface. In addition, a significant feature of a foam is the existence of Plateau borders. These are tetrahedral shaped reservoirs which form at the junctions between bubbles and provide a means of rapidly replenishing areas of the interface which are depleted in surfactant species and hence may be prone to rupture. In comparison with bubbles formed in the coalescence cell at high gas flow rates (rapid surface expansion rates), bubbles in a foam will be surfactant enriched, which should significantly alter the systems tension and prevent the rapid film thinning required for coalescence.

To investigate the effect of the rate of surface expansion on the dynamic surface tension, experiments were carried out with the Lauda MPT1 Maximum Bubble Pressure meter at the three temperatures of interest, 10°C, 18°C and 25°C. Results are shown in Figure E.3, where

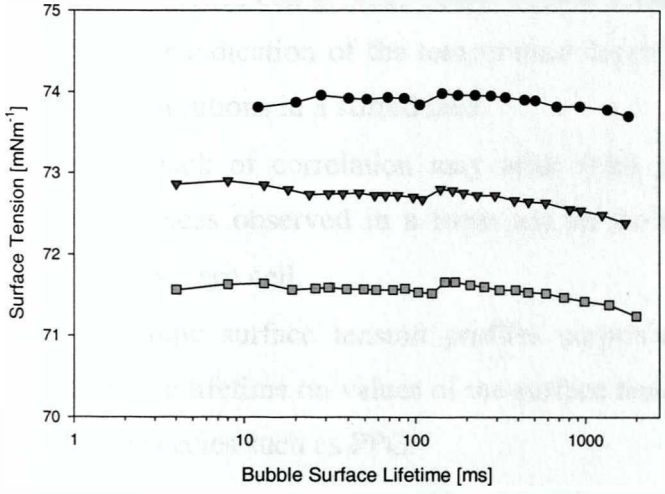

Figure D.3

Dynamic surface tension profiles as a function of bubble surface lifetime for bubbles formed in solutions of 20 ppm PPG at temperatures of ⊸● 10°C, ⊸▼ 18°C and ⊸□ 25°C. Profiles measured using Lauda MPT1 Maximum Bubble Pressure meter, as outlined in Chapter 3.

a log scale has been chosen to allow the effects at short bubble surface lifetimes to be closely scrutinised. Surprisingly, given that solutions of low concentration PPG, such as the 20 ppm concentration investigated in this study, have such pronounced effects on the gas hold-up and bubble size (Martin, 1996) of a system, little difference is observed for surface tension values over a wide range of surface lifetimes. The results are more surprising when the molecular structure of PPG is considered. As a large molecular weight polymeric species containing separate hydrophobic and hydrophilic regions, not only should it exhibit a definite preference for orientation at the surface, but also a finite amount of time will be required for it to adopt the most energetically favourable conformation at the interface. Consequently, one would expect to see a definite decrease in surface tension as the bubble surface lifetime increases. It may be that even at bubble surface lifetimes of 2 s, the amount of time has been insufficient for the molecule to adopt the most favourable orientation. Despite this consideration, it is surprising that no effects of surface lifetime are observed.

In terms of the coalescence process as it is currently understood, the effects of increasing systems temperature will be to decrease the liquid viscosity and surface tension values. For such small concentrations of solute, the viscosity can be considered to be that of water. In water, the change in viscosity as temperature increases from 10°C to 25°C is very small (see Table 5.1) and it is unlikely this will significantly affect the rate of film thinning. Surface tension values, as shown in Figure E.3, are also only slightly affected by the increasing system temperature; from 10°C to 25°C, the average values decreases from ~ 74 mNm^{-1} to ~ 71.5 mNm^{-1} and must be discounted as the reason for the changes in coalescence behaviour observed.

D.4 Conclusions

- Coalescence cell profiles observed over a range of gas flow rates are not able to provide a clear indication of the temperature dependency of foam heights observed in 20 ppm PPG solutions in a stirred tank.
- This lack of correlation may arise from pronounced differences in the coalescence influences observed in a foam and in the continuously renewing environment of the coalescence cell.
- Dynamic surface tension profiles surprisingly show very little influence of bubble surface lifetime on values of the surface tension, despite the pronounced surface activity of a species such as PPG.

Appendix E

Publication from this Project

Visualisation of bubble coalescence in a coalescence cell, a stirred tank and a bubble column

Chemical Engineering Science, 1998

Vol. 53, No. 23, pp 4031-4036

Pergamon

Chemical Engineering Science, Vol. 53, No. 23, pp. 4031–4036, 1998

Printed in Great Britain
PII: S0009-2509(98)00182-1
0009-2509/98/$-See front matter

Visualisation of bubble coalescence in a coalescence cell, a stirred tank and a bubble column

(Received 6 February 1998; in revised form 5 May 1998; accepted 11 June 1998)

INTRODUCTION

There are a number of reports in the literature wherein coalescence between two bubbles in a controlled environment has been studied with the use of either high-speed photographic methods or high-speed video/motion picture cameras (Ueyama *et al.*, 1993; Kim and Lee, 1987; Oolman and Blanch, 1986; Yang and Maa, 1984). In all cases, however, the quality of the pictures in those papers has been rather poor. This poor quality may have been because of the difficulty of obtaining such pictures or possibly because, in general, they have been used either for determining the coalescence time; or merely that the authors were more interested only in whether coalescence occurred or not. For the process engineer, studies in these idealised configurations have been undertaken in order to gain an understanding of coalescence in equipment such as stirred tanks and bubble columns. However, to the authors knowledge, pictures of such events in these types of equipment have never been published in the open literature, even though photographic techniques have often been used to obtain bubble sizes in them. Again, one can speculate on the reasons for this. Possibly it is because such events are rare; possibly because they are so fast that they do not get captured; and possibly because, even if they are, they are difficult to recognise unequivocally as such. Probably, it is all of these.

Such difficulties in visualising coalescence are not surprising given its complexity. The event consists of four stages. Firstly, the external flow governs whether the bubbles collide, the force of the collision and the contact time (Chesters, 1991). This initial step is followed by coalescence itself which involves three steps as summarised by Oolman and Blanch (1986):

1. Two bubbles contact each other within the liquid phase. Upon impact, there is a flattening of the bubble surfaces in contact, leaving a thin liquid film separating them. This film is typically 10^{-3}–10^{-4} cm in thickness.
2. The film drains until it is approximately 10^{-6} cm thick. Coalescence will only occur if the two bubbles are in contact for longer than is required for the film to thin.
3. Once the film is sufficiently thin, an instability mechanism will result in film rupture and formation of a coalesced bubble. Marrucci (1969) proposed that the entire process occurs on a millisecond time-scale, the rate determining step being film drainage. Once the film reached the critical thickness, film rupture is almost instantaneous.

In this note, we begin by showing coalescence in a coalescence cell in which bubble collision is highly controlled, the event being recorded by high-speed video images. These pictures are then used to show convincing, magnified images of bubbles at various stages during the coalescence event in a pilot scale stirred tank and a bubble column, in both of which the bubbles are carried by a free external flow.

EXPERIMENTAL

The studies of two-bubble coalescence were carried out in the controlled environment of a coalescence cell, the design of which is similar to that used by Zahradnik *et al.* (1987). The bubbles were formed at two polypropylene nozzles of internal diameter 2 mm, facing each other in a glass tank of dimensions, height = 277 mm, width = 110 mm and depth = 71 mm. The nozzles were held in position by means of a stainless-steel frame which fits inside the cell and which allowed a variety of geometrical configurations to be investigated. One such configuration at a spacing of 5 mm is shown in Fig. 1. Air was supplied continuously at a constant absolute pressure of 1.22×10^5 Pa and the flow rate was controlled by a series of rotameters and needle valves in order to synchronise the bubbles being produced at the nozzles. A Kodak Ekta-Pro high-speed video camera was used to record the coalescence events, at a frame speed of $2000\,s^{-1}$ using a split screen ($1000\,s^{-1}$ frame speed for full screen). These images could also be used to check the synchronisation. Water and a range of sodium sulphate solutions up to 0.08M, a concentration well beyond that considered to prevent coalescence (Lessard and Zeminski, 1971), were used as the fluids.

The observations of coalescence in a stirred tank were made in a baffled, cylindrical Perspex tank 0.56 m in diameter and agitated with either a standard 6-blade Rushton turbine (RT) or a 5-blade, down-pumping Prochem Maxflo T impeller (PMD). An advanced video technique developed in-house (Pacek *et al.*, 1995) consisting of a stereo-microscope attached to a video recorder (frame speed $50\,s^{-1}$) was used to record the coalescence events. A strobe light was placed inside the vessel, 1.5 cm in from the wall and just in front (relative to the rotation of the impeller) of a baffle in order to minimise the bubble distortion due to the flow. The strobe provided suitable lighting conditions for filming with its frequency synchronised to the frame speed of the camera. Pictures were taken at the impeller mid-plane, and water and 0.05 M sodium sulphate were used whilst the agitator speeds

(a)0.0sec

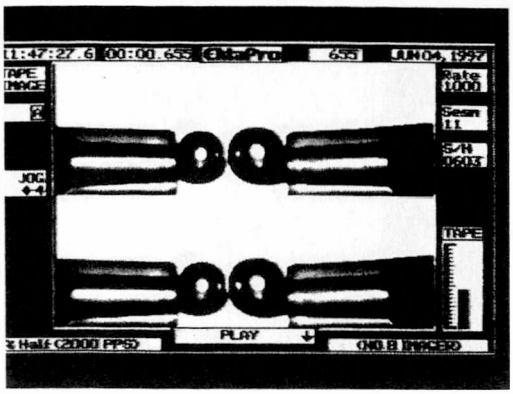

(b)0.002sec

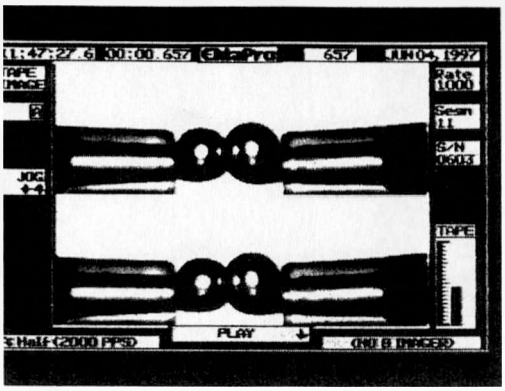

(c)0.01sec

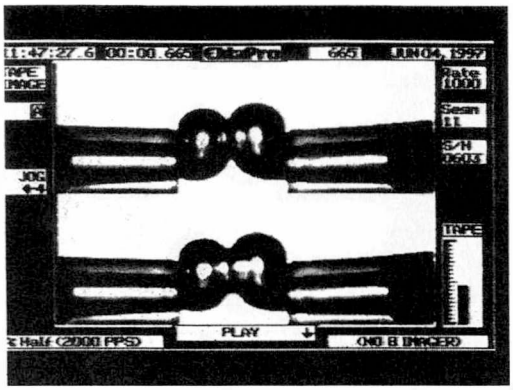

(d)0.012sec

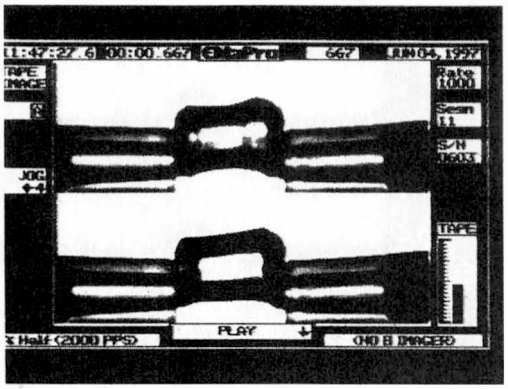

(e)0.013sec

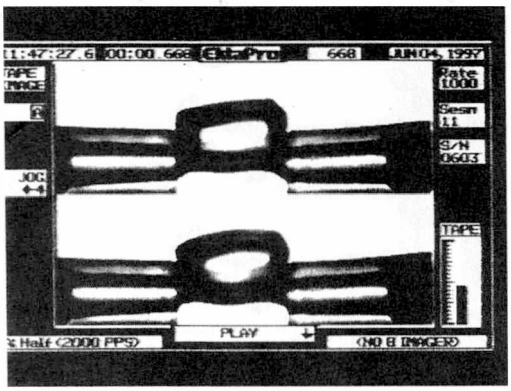

(f)0.017sec

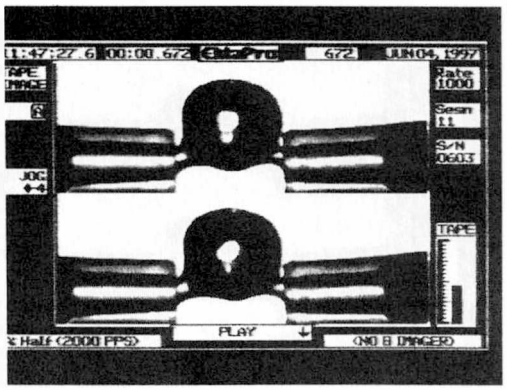

(g)0.028sec

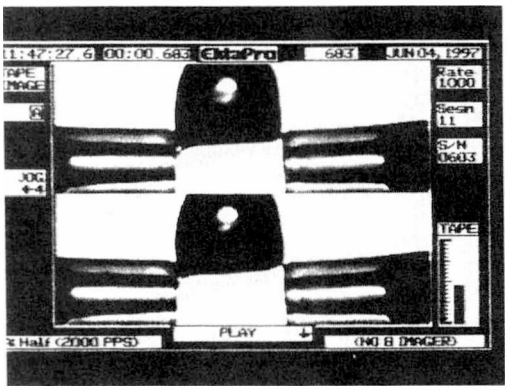

Fig. 1. Two bubble coalescence in distilled water: nozzle spacing 5 mm; air flow rate 50 $cm^{-1} min^{-1}$ (equivalent to bubble frequency 23 s^{-1}); bubble volume ~140 μl.

(a)0.0sec

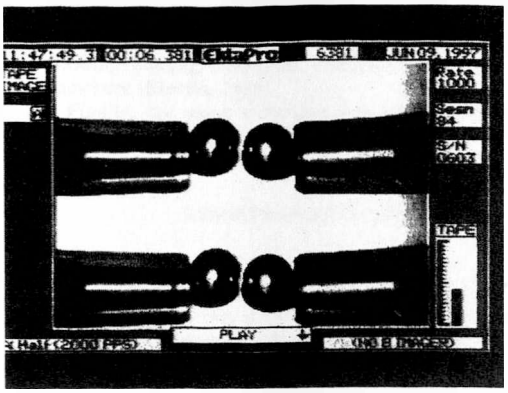

(b)0.003sec

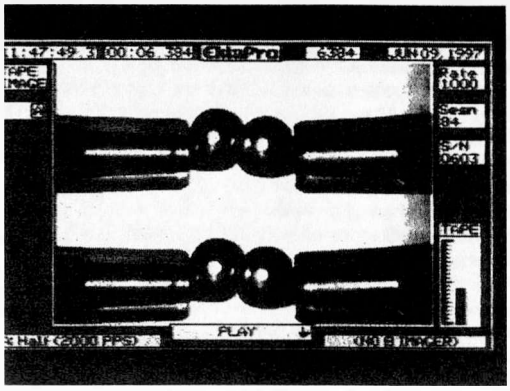

(c)0.008sec

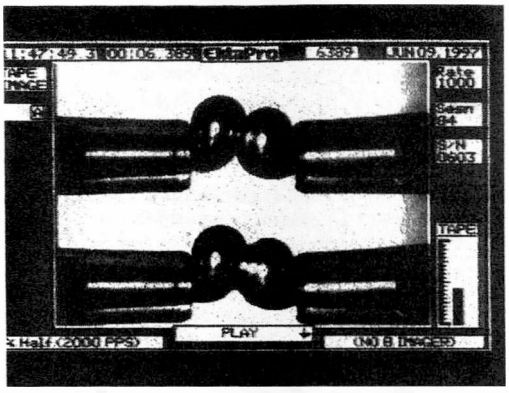

(d)0.009sec

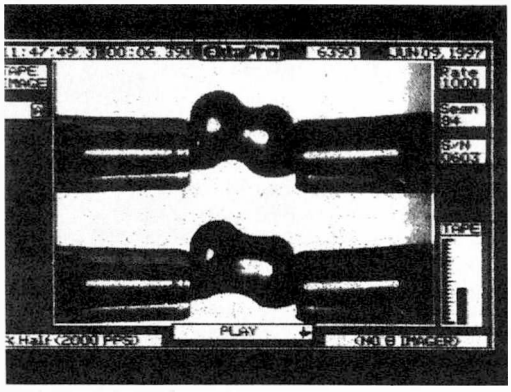

(e)0.01sec

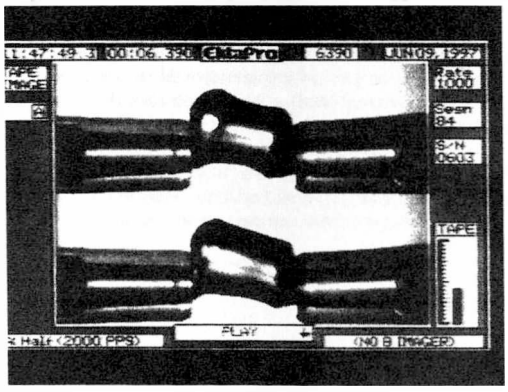

(f)0.013sec

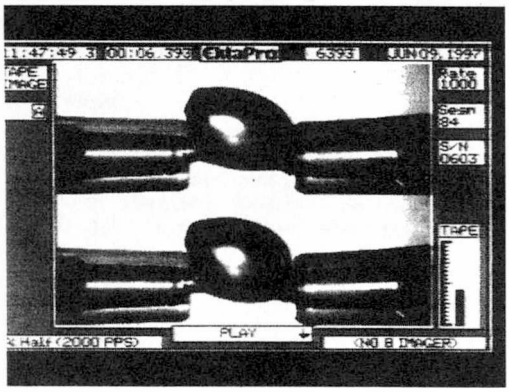

(g)0.02sec

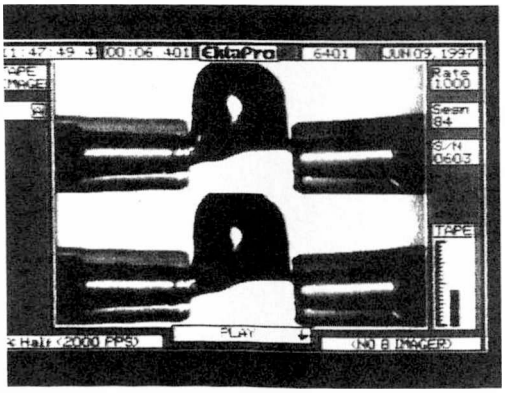

Fig. 2. Two bubble coalescence in 0.08 M sodium sulfate solution: nozzle spacing 5 mm; air flow rate 50 $cm^3 min^{-1}$ (equivalent to bubble frequency 23 s^{-1}); bubble volume ~140 μl.

were always high enough to ensure operation well above the flooding–loading transition. Further details are available elsewhere (Martin, 1996).

Finally, the same technique was used to obtain video pictures of bubbles in a 46 mm diameter bubble column, typically at 5 cm above its porous plate distributor.

RESULTS AND DISCUSSION

Coalescence cell

By using the high-speed video camera, it was possible to observe the first two stages of the coalescence process (according to Oolman and Blanch). However, it is not possible to capture precisely the point of rupture of the intervening film, which obviously occurs on an even shorter time scale than the frame rate of the camera. It is also difficult to detect because the bubbles are already pressed together for some time before coalescence occurs. Figure 1 clearly shows the sequence of events recorded for a coalescence event in water: the moment of contact between the two bubbles; the period in which the bubbles are in contact and the film is draining; and following the rupture of the intervening film, flexing of the newly coalesced bubble with an annular wave or discontinuity in the surface initially, until a spherical shape has been obtained.

In Fig. 2, a similar sequence shows the coalescence process for two bubbles in a solution of 0.08M sodium sulphate. Though not apparent in these stills, observation of the video film suggested that the bubbles are more rigid since they were less prone to fluctuating deformations prior to coalescence compared to water. In addition, following the point of film rupture, the amount of distortion is decreased as the newly coalesced bubble obtains its final shape. This solution concentration is well beyond the transition concentration determined by Lessard and Zieminski (1971) and consequently represents, in their terms, a 'non-coalescing' situation. This tendency for coalescence to occur well above the transition concentration has been seen regularly in this work (data not shown) at the higher bubbling rates of the order of that used in the experiments leading to Figs 1 and 2. Under the conditions pertaining in these figures, it can be seen from them that the time required for the film to drain to the point of rupture is similar for both solutions.

In summary, clear pictures of much of the coalescence event have been obtained in water and in Na_2SO_4 solution at electrolyte concentrations which have traditionally been defined as 'non-coalescing' (Lessard and Zieminski, 1971). However, in that definitive study of Lessard and Zieminski, the bubbling rate was much lower than here. In addition, the bubbles were brought gently together as they emerged from two almost vertical nozzles rather than being pushed together at a relatively high velocity by opposed nozzles as in this case. Interestingly, at lower bubbling rates than those used in Figs. 1 and 2 but which approach those used by Lessard and Zieminski, the time between the bubbles touching to the point at which rupture occurs is significantly longer in the electrolyte (on average 0.013 s) than in water (0.0045 s) (data not shown). It is postulated that this longer time is due to slower drainage of the liquid film because of the more rigid, less mobile interfaces (Chesters, 1991), arising from surface tension gradients (Marrucci and Nicodemo, 1967). It is concluded that whether coalescence occurs or not depends not only on the hydrodynamics of drainage and the surface properties but also on the external flow. Thus, the more vigorously bubbles are driven together by that flow, the more rapidly the film drains and the more likely they are to coalesce, especially if, as here, they are prevented from bouncing apart.

From Fig. 1(c) (bottom) to Fig. 1(d) (top), the time elapsed is 1/2000 s and the annular wave in the coalescing bubbles can be clearly seen on the right hand side [and also in Fig 2d]. Given that the nozzle spacing is 5 mm, it can be estimated that, since the ripple arises from the coalescence event, it has moved about 1.5 mm in 1/2000 s, i.e., at a speed of about 2.5 $m\,s^{-1}$. A very similar speed can be estimated from Fig. 3 provided by MacIntyre (1972) for what he called a 'curious ripple', moving at about 2.7 $m\,s^{-1}$ towards the base of a 1.7 mm diameter bubble breaking through the surface of seawater, i.e. the coalescence of a bubble with a free surface. Similar waves or ripples, though not so clear, are shown in the work of Garrett and Ward (1989) for two very different size bubbles coalescing in water after leaving a capillary tube; and for bubbles coalescing in 0.4M NaCl solution in which one bubble is allowed to rise up into a trapped bubble above it (Tsao and Koch, 1994).

Stirred vessel

In contrast with unequivocal recorded images of coalescence in a controlled environment, the pictures of coalescence in the stirred vessel must be considered as obtained by a fortunate coincidence. Relative to the number of frames taken at 50 s^{-1}, large numbers of which were also used to

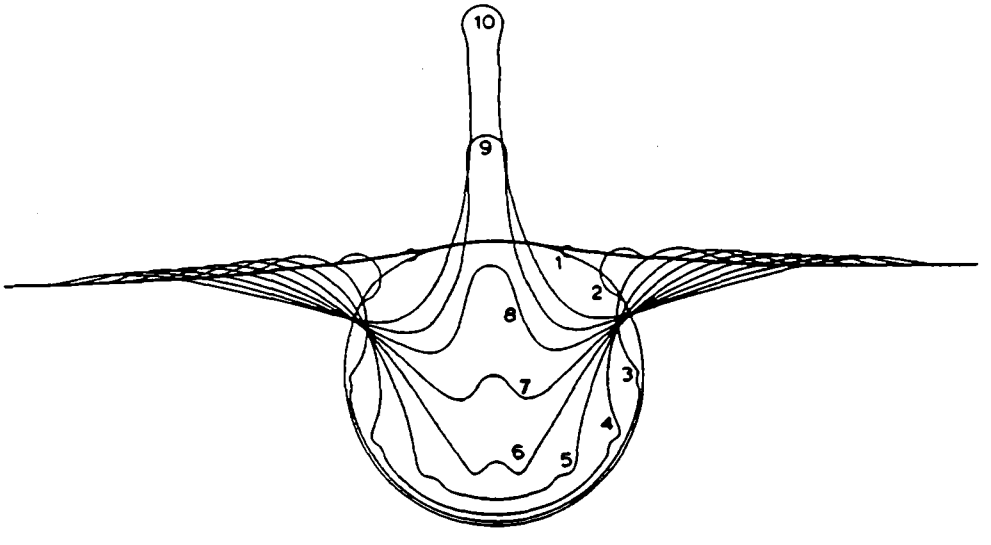

Fig. 3. Time sequence of rupture of a 1.7 mm diameter, 2.57 μl bubble in sea water. Profiles are ~1/6000 sec apart (MacIntyre (1972)).

obtain size distributions (Martin, 1996), the pictures shown here represent less than one in a thousand. Thus, very few images were obtained. Comparison of Fig. 4 with the high-speed video film of bubble coalescence in Fig. 1c.(water) and Fig. 2c (0.08M Na_2SO_4) clearly shows the early stages of coalescence in water, arising from the chance encounter of two approximately equal-sized bubbles in an uncontrolled manner in the turbulent external flow field close to the vessel wall. Figure 5 by comparison with Figs 1(e) and 2(e) shows a later stage of the event, again probably with initially equal-sized bubbles. Figures 6–8 show different-sized bubbles just after coalescence in water has commenced, i.e. equivalent to Fig 1(d). The annular waves or 'strange ripples' can be clearly seen as sharp edges between the two convex bubble surfaces and the concave neck.

Figure 9 is one of the rare pictures obtained in the agitated 0.05M Na_2SO_4 solution, i.e. equivalent to Fig. 2(d). Though it is not obvious in this single frame, on average, the bubble sizes were much smaller in the electrolyte solution than in water under equivalent agitation and aeration conditions (Martin, 1996). The rarity of the pictures and the smaller bubble size is due to the low coalescence rate found in these conditions of external flow and interfacial properties (Machon *et al.*, 1997).

Bubble columns

Figures 10 and 11 show pictures of bubbles in water, immediately after coalescence (Fig. 10) and a little later (Fig. 11), equivalent to Fig 1(d). In the electrolyte solution above the critical concentration (Lessard and Zieminski, 1971), coalescence events were almost never observed on video and as expected, bubble sizes were much smaller (Marrucci and Nicodemo, 1967).

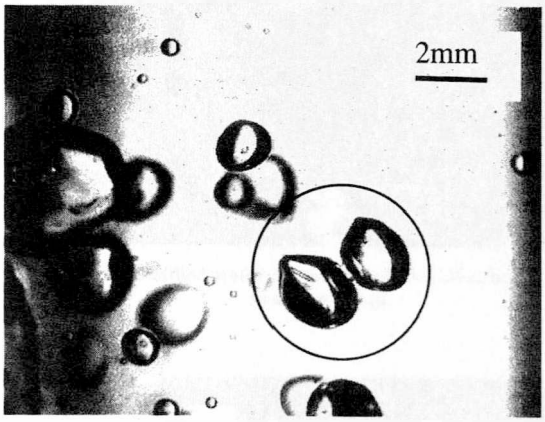

Fig. 4. Stirred tank; deionised water; PMD impeller; N = 500 rpm; Q_G = 1.0 vvm.

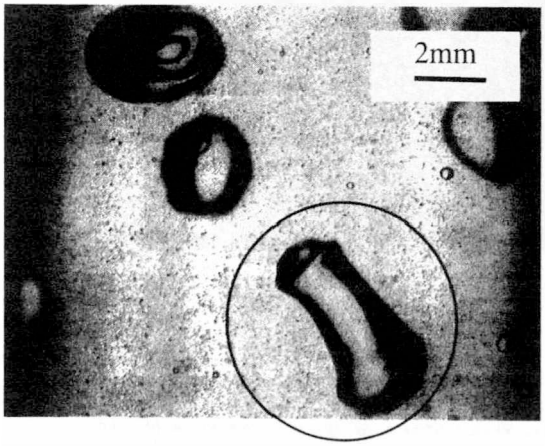

Fig. 5. Stirred tank; water and MnO_2; PMD impeller, N = 350 rpm; Q_G = 1.4 vvm.

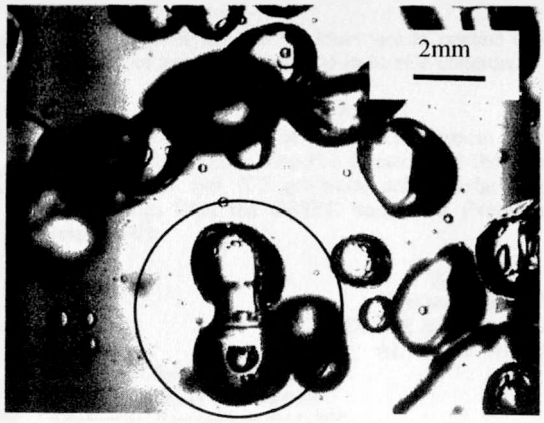

Fig. 6. Stirred tank; deionised water; PMD impeller, N = 400 rpm; Q_G = 1.0 vvm.

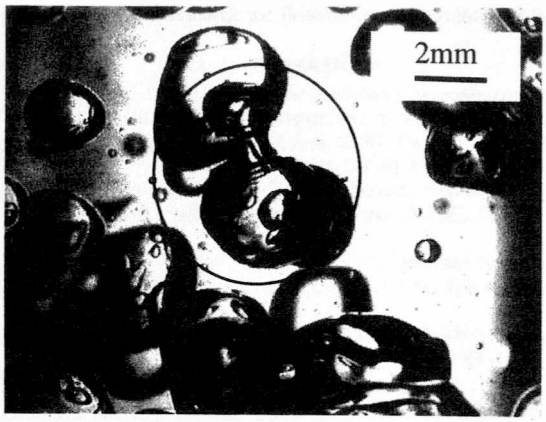

Fig. 7. Stirred tank; deionised water; PMD impeller, N = 400 rpm; Q_G = 1.0 vvm.

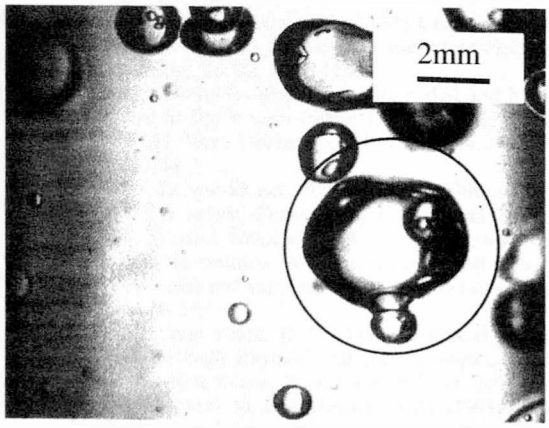

Fig. 8. Stirred tank; deionised water; PMD impeller, N = 300 rpm; Q_G = 0.8 vvm.

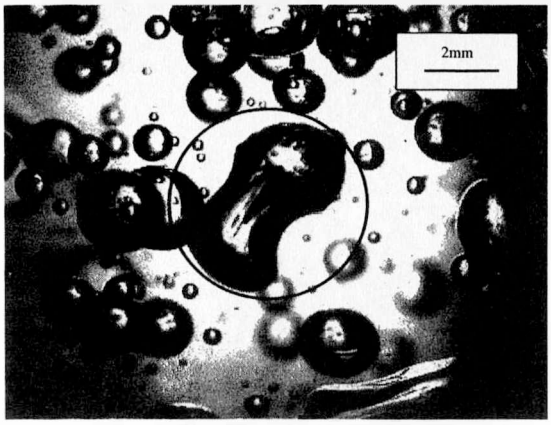

Fig. 9. Stirred tank; 0.05M Na_2SO_4 solution: RT impeller, $N = 250$ rpm; $Q_G = 1.6$ vvm.

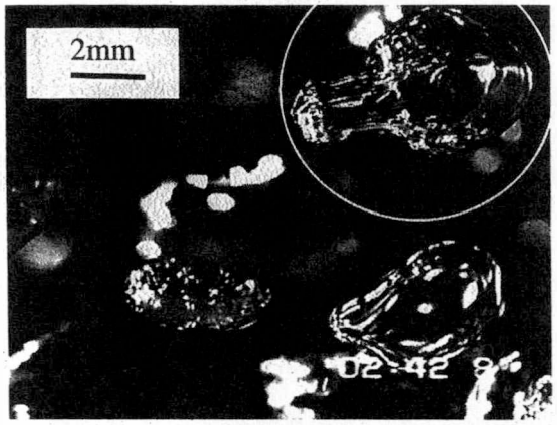

Fig. 10. Distilled water in bubble column; distributor pore size 160–250 μl.

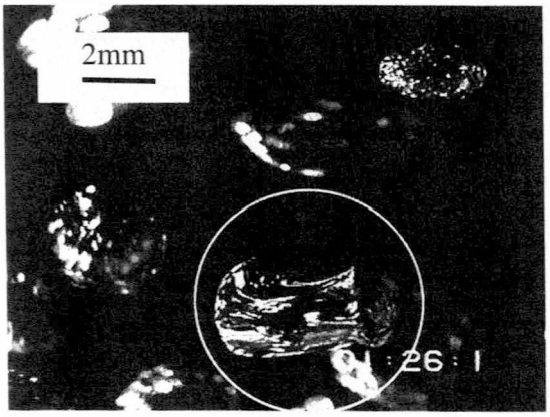

Fig. 11. Distilled water in bubble column; distributor pore size 160–250 μl.

CONCLUSIONS

Clear pictures of coalescence events are presented for the first time in a coalescence cell, in a stirred tank and in a bubble column. These pictures also show that coalescence can occur when a pair of bubbles are forced together as they emerge from opposing horizontal nozzles even in electrolyte solutions at concentrations which are normally considered to be 'non-coalescing' in the more 'gentle' contact found in the bulk of agitated vessels and in bubble columns.

Acknowledgements

Thanks are due to the EPSRC Instrument Pool for providing the Kodak Ekta-Pro Camera and the technical support; TM and KT gratefully acknowledge research studentships from the BBSRC and DSM (Netherlands), respectively.

KATHRYN TSE
THOMAS MARTIN*
CAROLINE M. McFARLANE
ALVIN W. NIENOW†

School of Chemical Engineering
The University of Birmingham
Edgbaston, Birmingham B15 2TT
U.K.

NOTATION

N	agitator speed
Q_G	volumetric air flow rate
vvm	volumetric air flow/minute per volume of liquid

REFERENCES

Chesters, A. K. (1991) The modelling of coalescence processes in fluid–liquid dispersions: a review of current understanding. *Trans. I. Chem. E.* **69**, Part A, 259–270.

Garrett, P. R. and Ward, D. R. (1989) A re-examination of the measurement of dynamic surface tensions using the maximum bubble pressure method. *J. Coll. Int. Sci.* **132**, 475–490.

Kim, J. W. and Lee, W. K. (1987) Coalescence behaviour of two bubbles in stagnant liquids. *J. Chem. Engng Japan* **20**, 448–453.

Lessard, R. R. and Zieminski, S. A. (1971) Bubble coalescence and gas transfer in aqueous electrolytic solutions. *Ind. Engng Chem. Fund* **10**, 260–269.

Machon, V., Pacek, A. W. and Nienow, A. W. (1997) Bubble sizes in electrolyte and alcohol solutions in a turbulent stirred vessel. *Trans. I. Chem. E.* **75**, Part A, 339–348.

MacIntyre, F. (1972) Flow patterns in breaking bubbles. *J. Geophysical. Res.* **77**, 5211–5228.

Marrucci, G. (1969) A Theory of Coalescence, *Chem. Engng Sci.* **24**, 975–985.

Marrucci, G. and Nicodemo, L. (1967) Coalescence of gas bubbles in aqueous solutions of inorganic electrolytes, *Chem. Engng Sci.* **22**, 1257–1265.

Martin, T. (1996) Gas dispersion with radial and hydrofoil impellers in fluids with different coalescence characteristics. PhD thesis, University of Birmingham, 1996. ISBN 3-89675 104 2.

Oolman, T. O. and Blanch, H. W. (1986) Bubble coalescence in stagnant liquids. *Chem. Engng Commun* **43**, 237–261.

Pacek, A. W. and Nienow, A. W. (1995) Measurement of drop size distribution in concentrated liquid liquid dispersions: video and capillary techniques. *Trans. I. Chem. E* **73**, Part A, 512–517.

Tsao, H. K. and Koch, D. L. (1994) Collisions of slightly deformable, high Reynolds number bubbles with short-range repulsive forces. *Phys. Fluids* **6**, 2591–2605.

Ueyama, K., Saeki, M. and Matsukata, M. (1993) Development of system for measuring bubble coalescence time by using a laser. *J. Chem. Engng Jap.* **26**, 308–314.

Yang, Y. Y. and Maa, J. R. (1984) Bubble coalescence in dilute surfactant solutions. *J. Coll. Int. Sci.* **98**, 120–125.

Zahradnik, J., Peter, R. and Kastanek, K. D. (1987) The effect of liquid phase properties on gas hold-up in bubble column reactors. *Coll. Czech. Chem. Commun* **52**, 335–347.

*Now at: DSM Research, Geleen, The Netherlands.
†Corresponding author. Tel.: 0121 414 5325; fax: 0121 414 5324; e-mail: a.w.nienow@bham.ac.uk.